# A Numerical Investigation into the Potential to Enhance Natural Gas Recovery in Water-drive Gas Reservoirs through the Injection of $CO_2$

**Myles L. M. Regan**

**A thesis submitted for the degree of**

**Doctor in Philosophy in Petroleum Engineering**

**Australian School of Petroleum**

**The University of Adelaide**

**December 2010**

# Abstract

The injection of carbon dioxide ($CO_2$) into oil reservoirs for the purpose of enhancing recovery has been performed for decades. Conversely, the injection of $CO_2$ into natural gas reservoirs has received very little attention, primarily due to the typically high recovery achievable under primary depletion. This high recovery is however associated with volumetric gas reservoirs only. If the reservoir is in the presence of an active water-drive, recovery can be considerably lowered. This is caused by pressure maintenance and the trapping of gas, rendering a volume of gas immobile. Consequently, any technique that reduces reservoir pressure and/or retards the influx of the aquifer will enable natural gas recovery to be enhanced.

In this thesis, the injection of $CO_2$ has been proposed as a method of retarding the influx of the aquifer. Favourable fluid properties between the injected $CO_2$ and natural gas also allow the displacement of natural gas towards the production wells with minimal mixing. This thesis investigates the nature of the effects of a number of parameters deemed potentially influential on the displacement of natural gas by $CO_2$ and the ability to produce and enhance recovery with as low a producing $CO_2$ concentration as possible. Parameters chosen include uncontrollable reservoir and fluid properties such as permeability, thickness, diffusion coefficients and salinity. Controllable factors are also investigated, such as the timing of injection, production and injection rates and the type of wells employed. This investigation was conducted through the use of numerical simulation. Simulations were first performed on a simple, conceptual model in order to understand the key processes involved in the $CO_2$ enhanced gas recovery process. The results of these studies were then applied to a more complex numerical investigation involving a model of the Naylor gas field.

The results of the initial studies found that the parameters which determined the extent of viscous and gravity forces, such as permeability, thickness and formation dip, were the most influential in determining the stability of the displacement, and consequently the recovery achievable at the breakthrough of $CO_2$ at the production well. The fluid properties, such as water salinity and the diffusion coefficient, were found to have less of an impact than the reservoir properties. Efficient displacement in a non-dipping reservoir was possible with either viscous or gravity dominated displacement, while only gravity stable displacement was preferred in a dipping reservoir. The primary recovery efficiency did however dictate where the injection of $CO_2$ should be targeted in order to achieve incremental recovery with the lowest producing $CO_2$ concentration. Due to the low primary recovery efficiency, the injection of $CO_2$ should be targeted in high permeability, non-dipping reservoirs.

The presence of heterogeneity accelerated the breakthrough of $CO_2$, and so it was shown that delaying the injection of $CO_2$ was beneficial in maximising the recovery at the initial breakthrough of $CO_2$. However, once $CO_2$ had reached the production well, the rate of increase in $CO_2$ production was considerably more rapid if injection was delayed. The choice of the timing of injection and the ability to maximise incremental recovery is therefore heavily influenced by the maximum allowable producing $CO_2$ concentration, which will be determined by the economics of the project. The investigation into the other controllable parameters showed that the operational strategies which either lowered the susceptibility for $CO_2$ to cone into the production well, or which mitigated against the uneven advancement of $CO_2$ due to heterogeneity were preferred.

Ultimately this study showed that the injection of $CO_2$ can effectively retard the influx of the aquifer and efficiently displace natural gas towards the production well. By understanding the mechanisms involved in this displacement process, operational parameters can be optimised accordingly to maximise natural gas recovery with the lowest producing $CO_2$ concentration. The extent of incremental recovery is subsequently determined by the maximum producing $CO_2$ concentration allowable, as determined by the economics of the project.

# Declaration

This work contains no material which has been accepted for the award of any other degree or diploma in any university or other tertiary institution.

To the best of my knowledge and belief, it contains no material previously published or written by another person, except where due reference has been made in the text.

I give consent to this copy of my thesis, when deposited in the University Library, being made available for loan and photocopying, subject to the provisions of the Copyright Act 1968.

I also give permission for the digital version of my thesis to be made available on the web, via the University's digital research repository, the Library catalogue, the Australasian Digital Theses Program (ADTP) and also through web search engines, unless permission has been granted by the University to restrict access for a period of time.

Signature:

Date:

# Acknowledgements

Firstly, after the bumpy start to my PhD studies, I would like to thank my two supervisors, **Prof. Richard Hillis** and **Dr. Geoff Weir**. Amongst other things, Richard assisted me in setting the foundations to successfully conduct my studies, while Geoff provided excellent and extremely valuable technical knowledge which assisted me greatly, at times under very trying conditions. I would particularly like to thank Geoff and of late Richard for taking time out of their day jobs to supervise my studies and assist me in being able to complete my studies.

I would also like to thank my two previous supervisors, Hemanta Sarma and Seung Ihl Kam for their supervision and guidance during the initial stages of my studies, and for laying the foundations during my undergraduate days. I would particularly like to thank Hemanta Sarma for introducing the idea of furthering my studies with an option to conduct a PhD and assisting in the realisation of this.

I would like to thank the Co-operative Research Centre for Greenhouse Gas Technologies (CO2CRC) for both the financial support they have given me to complete my studies, as well as providing a broad range of experiences and opportunities within and outside of my studies. I would like to thank all my colleagues within the CO2CRC (too many to name) for making my time within the CO2CRC fun, interesting and a very worthwhile experience. In particular I would like to thank Prof. John Kaldi for providing the opportunity to be a part of the CO2CRC and for the guidance and support during my time with the organisation.

I would like to acknowledge Fiona Johnston for providing professional editing services for the preparation of this thesis.

I would like to thank all of the staff and students, both past and present, from the Australian School of Petroleum for providing the necessary support to complete both my undergraduate and now postgraduate studies. Without their expertise and support, my task of completing would have been made considerably harder, if not impossible.

Last but not least, I would like to thank my family and friends. In particular I would like to thank my mum and dad for all of the love, help and support they have given me and for the sacrifices they have made to give me all of the opportunities I have had. I can never repay the debt I owe you but I will give it a go. I would like to thank my brohan, Courtney, for all the help he has given me and for all of the shenanigans we have got up to, and for being considerably shorter than me. I would like to thank the female one, Nina, for all of the love and support she has given me over these long, long 8 years and also to the rest of the Rudduck family for making me feel very welcome. Finally I would like to thank all of my friends, one is not going to name you all as the list would be super massive

because one is so popular, but without them I would not have received as many scars and injuries as I have through various, at times drunken, escapades and for providing much needed stress relief, andy how.

# Table of Contents

**ABSTRACT** ..... **I**

**DECLARATION** ..... **III**

**ACKNOWLEDGEMENTS** ..... **IV**

**TABLE OF CONTENTS** ..... **VI**

**LIST OF FIGURES** ..... **X**

**LIST OF TABLES** ..... **XVII**

**NOMENCLATURE** ..... **XIX**

**1 INTRODUCTION** ..... **1**

1.1 BACKGROUND ..... 1

1.2 RESEARCH OBJECTIVES ..... 4

1.3 METHODOLOGY ..... 5

1.4 REVIEW OF CHAPTERS ..... 5

1.5 SIGNIFICANCE ..... 6

**2 LITERATURE REVIEW** ..... **7**

2.1 FLUID PROPERTIES OF $CO_2$ AND $CH_4$ ..... 7

2.2 NATURAL GAS RESERVOIRS ..... 13

2.3 ENHANCED GAS RECOVERY ..... 21

*2.3.1 Accelerated Gas Production* ..... *22*

*2.3.2 Co-production of Gas and Water* ..... *25*

2.4 LABORATORY AND NUMERICAL STUDIES INTO $CO_2$ EGR ..... 27

2.5 FIELD TRIALS OF $CO_2$ EGR ..... 36

2.6 SUMMARY ..... 37

**3 GEOLOGICAL $CO_2$ STORAGE CODE COMPARISON STUDY** ..... **38**

3.1 INTRODUCTION ..... 38

3.2 LBNL CODE COMPARISON STUDY: PROBLEM 1 ..... 39

*3.2.1 Discussion of Results* ..... *40*

3.3 LBNL CODE COMPARISON STUDY: PROBLEM 2 ..... 44

*3.3.1 Discussion of Results* ..... *46*

3.4 LBNL CODE COMPARISON STUDY: PROBLEM 3 ..... 47

3.5 CONCLUSION ..... 64

**4 EXPERIMENTAL DESIGN METHODOLOGY AND ITS USE IN THE OIL AND GAS INDUSTRY** ..... **66**

4.1 INTRODUCTION ..... 66

*Screening Designs* ..... *67*
*Two-level Full Factorial Designs* ..... *67*
*Two-level Fractional Factorial Designs* ..... *67*
*Three-level Full Factorial Design* ..... *68*
*Central Composite Design (CCD)* ..... *68*
*Box-Behnken Design* ..... *69*
*Computer Generated Designs* ..... *70*
*Analysis of Experimental Designs* ..... *70*
4.2 The Use of Experimental Design in the Oil and Gas Industry ..... 70
**5 STUDY 1: THE INJECTION OF $CO_2$ AT THE COMMENCEMENT OF $CH_4$ PRODUCTION ..... 74**
5.1 Introduction ..... 74
5.2 Model Description ..... 75
5.3 Experimental Design Study ..... 79
*5.3.1 Design Selection* ..... *79*
*5.3.2 Parameter and Range Selection* ..... *79*
5.4 Study 1 Responses (Metrics) ..... 83
*5.4.1 Response 1: $CH_4$ Recovery Efficiency at a $CO_2$ Breakthrough Limit of 10%* ..... *83*
*5.4.2 Response 2: Minimum producing $CO_2$ concentration required to achieve incremental $CH_4$ recovery* *83*
5.5 Study 1 D-Optimal Design ..... 84
5.6 Results and Discussion of Response 1: $CH_4$ Recovery Efficiency at a $CO_2$ Breakthrough Limit of 10% ..... 85
5.7 Results and discussion of Response 2: Minimum producing $CO_2$ concentration required to achieve incremental recovery. ..... 102
5.8 Summary of the Experimental Design ..... 111
*5.8.1 Response 1* ..... *111*
*5.8.2 Response 2* ..... *111*
5.9 Follow-up Simulations ..... 112
*5.9.1 Impact of Heterogeneity* ..... *112*
*5.9.2 Impact of Operational Strategy* ..... *115*
*5.9.3 Summary* ..... *123*
**6 STUDY 2: THE EFFECT OF DELAYING $CO_2$ INJECTION ..... 125**
6.1 Introduction ..... 125
6.2 Study 2A: The Injection of $CO_2$ into an Anisotropic, Homogenous Reservoir ..... 126
*6.2.1 Design, Parameter and Range Selection* ..... *126*
*6.2.2 Study 2A Responses* ..... *127*
*6.2.3 Response 1 Results and Discussion* ..... *128*
*6.2.4 Response 2 Results and Discussion* ..... *139*

*6.2.5 Response 3: Results and Discussion* ..... *147*
*6.2.6 Summary* ..... *155*
6.3 STUDY 2B: THE COMPARISON OF THE TIMING OF $CO_2$ INJECTION INTO A SIMPLE, HETEROGENEOUS RESERVOIR ..... 156
*6.3.1 Reservoir Model* ..... *156*
*6.3.2 Design, Parameter and Range Selection* ..... *157*
*6.3.3 Study 2B Responses (Metrics)* ..... *158*
*6.3.4 Response 1 Results and Discussion* ..... *158*
*6.3.5 Response 2 Results and Discussion* ..... *167*
*6.3.6 Response 3 Results and Discussion* ..... *173*
*6.3.7 Summary* ..... *179*
**7 CASE STUDY: THE NAYLOR GAS FIELD, OTWAY BASIN, VICTORIA ..... 181**
7.1 FIELD LOCATION AND BACKGROUND ..... 181
7.2 RESERVOIR MODEL CHARACTERISATION ..... 184
7.3 INITIAL INVESTIGATIONS ..... 187
7.4 EXPERIMENTAL DESIGN STUDY ..... 193
*7.4.1 Results and discussion for Response 1: Natural Gas Recovery Efficiency at a 10% $CO_2$ Breakthrough Limit* ..... *195*
*7.4.2 Results and discussion of Response 2: Natural Gas Recovery Efficiency at a 50% $CO_2$ Breakthrough Limit 205*
*7.4.3 Results and Discussion of Response 3: Minimum Production Stream $CO_2$ Concentration Required to Achieve Incremental Natural Gas Recovery.* ..... *212*
*7.4.4 Optimisation of the Responses* ..... *222*
7.5 COMPOSITION OF THE INJECTION GAS ..... 223
7.6 SUMMARY OF RESULTS ..... 225
**8 SCREENING CRITERIA ..... 227**
8.1 CRITERIA FOR AN EFFICIENT DISPLACEMENT OF $CH_4$ BY $CO_2$ ..... 227
*8.1.1 Fluid properties* ..... *228*
*8.1.2 Non-dipping reservoirs* ..... *228*
*8.1.3 Dipping reservoirs* ..... *229*
8.2 THE EFFECT OF THE TIMING OF $CO_2$ INJECTION ..... 230
8.3 KEY CRITERIA TO MAXIMISE THE BENEFIT OF $CO_2$ INJECTION OVER PRIMARY DEPLETION ..... 231
**9 CONCLUSIONS AND FUTURE WORK ..... 233**
9.1 CONCLUSIONS ..... 233
9.2 FUTURE WORK ..... 237
**REFERENCES ..... 239**

**APPENDIX A – REGRESSION ANALYSIS ..... 250**

**APPENDIX B – ANOVA TABLES ..... 260**

**APPENDIX C – EXPERIMENTAL DESIGN DATA FOR PRIMARY DEPLETION RESPONSES FOR STUDY 1, 2A AND 2B ..... 271**

# List of Figures


FIGURE 2.1: $CO_2$ PHASE DIAGRAM. 8

FIGURE 2.2: DENSITY OF $CO_2$ AND $CH_4$ AS A FUNCTION OF PRESSURE AND TEMPERATURE (DATA SOURCED FROM LEMMON, MCLINDEN, AND FRIEND). 8

FIGURE 2.3: VISCOSITY OF $CO_2$ AND $CH_4$ AS A FUNCTION OF PRESSURE AND TEMPERATURE (DATA SOURCED FROM LEMMON, MCLINDEN, AND FRIEND). 9

FIGURE 2.4: SOLUBILITY OF $CO_2$ IN PURE WATER AS A FUNCTION OF PRESSURE AND TEMPERATURE (MODIFIED FROM CHANG ET AL. 1998). 11

FIGURE 2.5: $CO_2$ SOLUBILITY AS A FUNCTION OF TEMPERATURE AND PRESSURE, INDICATING THE VARIABLE TRENDS WITH RESPECT TO TEMPERATURE. 11

FIGURE 2.6: SOLUBILITY OF $CH_4$ IN PURE WATER AS A FUNCTION OF TEMPERATURE AND PRESSURE (MODIFIED FROM CULBERSON & MCKETTA 1951). 12

FIGURE 2.7: SOLUBILITY OF $CO_2$ AS A FUNCTION OF SALINITY (MODIFIED FROM BACHU & ADAMS 2003). 12

FIGURE 2.8: A PHASE DIAGRAM. 13

FIGURE 2.9: P/Z VERSUS GP PLOT FOR A VOLUMETRIC RESERVOIR, INDICATING THE LINEAR RELATIONSHIP BETWEEN P/Z AND GP. 16

FIGURE 2.10: P/Z VERSUS GP GRAPH FOR A GAS RESERVOIR WITH VARYING STRENGTH WATER-DRIVES. 18

FIGURE 2.11: SCHEMATIC OF GAS TRAPPING IN A SINGULAR CAPILLARY. 19

FIGURE 2.12: SCHEMATIC OF GAS TRAPPING IN A PORE DOUBLET MODEL 19

FIGURE 2.13: P/Z VS CUMULATIVE GAS PRODUCTION ($G_p$) PLOT INDICATING THE EFFECT OF VARIABLE PRODUCTION RATES ON THE RECOVERY OF NATURAL GAS UNDER WATER-DRIVE CONDITIONS (MODIFIED FROM AGARWAL ET AL. 1965). 23

FIGURE 2.14: TYPICAL GAS FIELD DEVELOPMENT RATE-TIME PROFILE WHEN UNDER CONTRACTUAL OBLIGATIONS 24

FIGURE 2.15: SCHEMATIC OF THE CONING OF WATER DUE TO INSTABILITY AT THE GWC 24

FIGURE 3.1: INITIAL FLUID DISTRIBUTION (PROBLEM 1) 39

FIGURE 3.2: GRAPH OF CO2 MOLE FRACTION AS A FUNCTION OF DEPTH FOR FOUR CODES PRESENTED IN LBNL REPORT (PRUESS ET AL. 2002. REPRINTED WITH PERMISSION) 43

FIGURE 3.3: GRAPH OF CO2 MOLE FRACTION AS A FUNCTION OF DEPTH FOR THE E300 SIMULATION CODE 43

FIGURE 3.4: INITIAL FLUID DISTRIBUTION (PROBLEM 2) 44

FIGURE 3.5: $CO_2$ MOLE FRACTION AT A DEPTH OF 50 METRES WITH RESPECT TO TIME FOR THE FOUR CODES PRESENTED IN THE LBNL REPORT (PRUESS ET AL. 2002. REPRINTED WITH PERMISSION) 44

FIGURE 3.6: $CO_2$ MOLE FRACTION AT A DEPTH OF 50 METRES WITH RESPECT TO TIME FOR THE E300 CODE 45

FIGURE 3.7: $CO_2$ DENSITY AFTER 365 DAYS PREDICTED BY THE GEM CODE (PRUESS ET AL. 2002. REPRINTED WITH PERMISSION) 45

FIGURE 3.8: $CO_2$ DENSITY AFTER 365 DAYS PREDICTED BY THE E300 CODE 46

FIGURE 3.9: PROBLEM 3 48

FIGURE 3.10: PRESSURE VERSUS THE SIMILARITY VARIABLE FOR THE 6 CODES PRESENTED IN THE LBNL REPORT (PRUESS ET AL. 2002. REPRINTED WITH PERMISSION) 50

FIGURE 3.11: PRESSURE VERSUS THE SIMILARITY VARIABLE FOR THE E300 CODE 50

FIGURE 3.12: GAS SATURATION VERSUS THE SIMILARITY VARIABLE FOR THE 6 CODES PRESENTED IN THE LBNL REPORT (PRUESS ET AL. 2002. REPRINTED WITH PERMISSION) ..... 51
FIGURE 3.13: GAS SATURATION VERSUS THE SIMILARITY VARIABLE FOR THE E300 CODE ..... 52
FIGURE 3.14: DISSOLVED $CO_2$ MASS FRACTION VERSUS THE SIMILARITY VARIABLE FOR THE 6 CODESPRESENTED IN THE LBNL REPORT (PRUESS ET AL. 2002. REPRINTED WITH PERMISSION) ..... 52
FIGURE 3.15: DISSOLVED $CO_2$ MASS FRACTION VERSUS THE SIMILARITY VARIABLE FOR THE E300 CODE ..... 53
FIGURE 3.16: COMPARISON OF $H_2O$ DENSITY AS A FUNCTION OF PRESSURE (ZERO SALINITY) FOR E300 AND THE CODES PRESENTED IN THE LBNL REPORT (MODIFIED FROM PRUESS ET AL. 2002) ..... 55
FIGURE 3.17: COMPARISON OF $H_2O$ VISCOSITY AS A FUNCTION OF PRESSURE (ZERO SALINITY) FOR E300 AND THE CODES PRESENTED IN THE LBNL REPORT (MODIFIED FROM PRUESS ET AL. 2002)..... 55
FIGURE 3.18: COMPARISON OF $CO_2$ DENSITY AS A FUNCTION OF PRESSURE FOR E300 AND THE CODES PRESENTED IN THE LBNL REPORT (MODIFIED FROM PRUESS ET AL. 2002)..... 56
FIGURE 3.19: COMPARISON OF $CO_2$ VISCOSITY AS A FUNCTION OF PRESSURE FOR E300 AND THE CODES PRESENTED IN THE LBNL REPORT (MODIFIED FROM PRUESS ET AL. 2002)..... 56
FIGURE 3.20: COMPARISON OF AQUEOUS ($H_2O + CO_2$) DENSITY AS A FUNCTION OF PRESSURE (ZERO SALINITY) FOR E300 AND THE CODES PRESENTED IN THE LBNL REPORT (MODIFIED FROM PRUESS ET AL. 2002) ..... 57
FIGURE 3.21: COMPARISON OF AQUEOUS ($H_2O + CO_2$) VISCOSITY AS A FUNCTION OF PRESSURE (ZERO SALINITY) FOR E300 AND THE CODES PRESENTED IN THE LBNL REPORT (MODIFIED FROM PRUESS ET AL. 2002) ..... 57
FIGURE 3.22: COMPARISON OF DISSOLVED $CO_2$ MASS FRACTION IN LIQUID PHASE AS A FUNCTION OF PRESSURE (ZERO SALINITY) FOR E300 AND THE CODES PRESENTED IN THE LBNL REPORT (MODIFIED FROM PRUESS ET AL. 2002) ..... 58
FIGURE 3.23: PRESSURE VERSUS SIMILARITY VARIABLE FOR THE 4 CODES PRESENTED IN THE LBNL REPORT (PRUESS ET AL. 2002. REPRINTED WITH PERMISSION) ..... 59
FIGURE 3.24: PRESSURE VERSUS SIMILARITY VARIABLE FOR THE E300 CODE ..... 59
FIGURE 3.25: $CO_2$ MASS FRACTION IN THE LIQUID PHASE FOR THE 4 CODES PRESENTED IN THE LBNL REPORT (PRUESS ET AL. 2002. REPRINTED WITH PERMISSION) ..... 60
FIGURE 3.26: $CO_2$ MASS FRACTION IN THE LIQUID PHASE FOR THE E300 CODE..... 60
FIGURE 3.27: COMPARISON OF BRINE DENSITY AS A FUNCTION OF PRESSURE (15 WEIGHT PERCENT SALINITY) FOR E300 AND THE CODES PRESENTED IN THE LBNL REPORT (MODIFIED FROM PRUESS ET AL. 2002) ..... 62
FIGURE 3.28: COMPARISON OF BRINE VISCOSITY AS A FUNCTION OF PRESSURE (15 WEIGHT PERCENT SALINITY) FOR E300 AND THE CODES PRESENTED IN THE LBNL REPORT (MODIFIED FROM PRUESS ET AL. 2002) ..... 62
FIGURE 3.29: COMPARISON OF AQUEOUS (BRINE + $CO_2$) DENSITY AS A FUNCTION OF PRESSURE (15 WEIGHT PERCENT SALINITY) FOR E300 AND THE CODES PRESENTED IN THE LBNL REPORT (MODIFIED FROM PRUESS ET AL. 2002) ..... 63
FIGURE 3.30: COMPARISON OF AQUEOUS (BRINE + $CO_2$) VISCOSITY AS A FUNCTION OF PRESSURE (15 WEIGHT PERCENT SALINITY) FOR E300 AND THE CODES PRESENTED IN THE LBNL REPORT (MODIFIED FROM PRUESS ET AL. 2002) ..... 63
FIGURE 3.31: COMPARISON OF DISSOLVED $CO_2$ MASS FRACTION IN THE LIQUID PHASE AS A FUNCTION OF PRESSURE (15 WEIGHT PERCENT SALINITY) FOR E300 AND THE CODES PRESENTED IN THE LBNL REPORT (MODIFIED FROM PRUESS ET AL. 2002) .... 64
FIGURE 4.1: GRAPHICAL REPRESENTATION OF THE CENTRAL COMPOSITE DESIGN (CCD)..... 69
FIGURE 4.2: GRAPHICAL REPRESENTATION OF THE BOX-BEHNKEN DESIGN..... 70

FIGURE 5.1: RELATIVE PERMEABILITY DATA USED IN MODEL ..... 75
FIGURE 5.2: SCHEMATIC OF NON-DIPPING MODEL ..... 76
FIGURE 5.3: MOLE FRACTION OF $CO_2$ IN PRODUCTION STREAM FOR VARIABLE GRID BLOCK SIZES ..... 78
FIGURE 5.4: DISPLACEMENT PROFILES FOR (TOP) DOMINANT GRAVITY FORCES CAUSING GRAVITY UNDER-RIDE, AND (BOTTOM) DOMINANT VISCOUS FORCES. ..... 81
FIGURE 5.5: RESULTS FOR EACH DESIGN RUN AND THE AVERAGE OF ALL RUNS (BLACK LINE) FOR RESPONSE 1 ..... 85
FIGURE 5.6: NORMAL PROBABILITY PLOT FOR RESPONSE 1 ..... 87
FIGURE 5.7: EFFECT GRAPH FOR THE PERMEABILITY - FORMATION DIP INTERACTION FOR RESPONSE 1 ..... 88
FIGURE 5.8: SIDE-VIEW OF $CO_2$ SATURATION AFTER 2620 DAYS IN A NON-DIPPING RESERVOIR WITH A PERMEABILITY OF 10MD. INJECTION WELLS LOCATED ON THE LEFT WITH THE PRODUCTION WELL ON THE RIGHT ..... 89
FIGURE 5.9: SIDE VIEW OF $CO_2$ SATURATION AFTER 2620 DAYS IN A NON-DIPPING RESERVOIR WITH A PERMEABILITY OF 100MD .. 89
FIGURE 5.10: SIDE-VIEW OF $CO_2$ SATURATION ONCE THE 10% $CO_2$ LIMIT HAS BEEN REACHED IN AN 11° DIP RESERVOIR. PERMEABILITY IS EQUAL TO 10MD ..... 90
FIGURE 5.11: SIDE-VIEW OF $CO_2$ SATURATION ONCE THE 10% $CO_2$ LIMIT HAS BEEN REACHED IN AN 11° DIP RESERVOIR. PERMEABILITY IS EQUAL TO 100MD ..... 91
FIGURE 5.12: EFFECT GRAPH FOR THE PERMEABILITY - $K_V/K_H$ RATIO INTERACTION FOR RESPONSE 1 ..... 91
FIGURE 5.13: EFFECT GRAPH FOR THE $K_V/K_H$ RATIO – FORMATION DIP INTERACTION FOR RESPONSE 1 ..... 93
FIGURE 5.14: $CO_2$ SATURATION AFTER 2276 DAYS IN A NON-DIPPING RESERVOIR. THE VERTICAL TO HORIZONTAL PERMEABILITY RATIO IS EQUAL TO 100% ..... 94
FIGURE 5.15: $CO_2$ SATURATION AFTER 2276 DAYS IN A NON-DIPPING RESERVOIR. THE VERTICAL TO HORIZONTAL PERMEABILITY RATIO IS EQUAL TO 1% ..... 94
FIGURE 5.16: $CO_2$ SATURATION AFTER THE 10% $CO_2$ LIMIT HAS BEEN REACHED. FORMATION DIP IS EQUAL TO 21° WITH THE VERTICAL TO HORIZONTAL PERMEABILITY RATIO EQUAL TO 1% ..... 95
FIGURE 5.17: $CO_2$ SATURATION AFTER THE 10% $CO_2$ LIMIT HAS BEEN REACHED. FORMATION DIP IS EQUAL TO 21° WITH THE VERTICAL TO HORIZONTAL PERMEABILITY RATIO EQUAL TO 100% ..... 95
FIGURE 5.18: EFFECT GRAPH FOR THE MAIN EFFECT OF THICKNESS FOR RESPONSE 1 ..... 96
FIGURE 5.19: EFFECT GRAPH FOR THE THICKNESS - FORMATION DIP INTERACTION FOR RESPONSE 1 ..... 97
FIGURE 5.20:SCHEMATIC OF DISPLACEMENT PROFILES BETWEEN $CO_2$ AND $CH_4$ IN A NON-DIPPING RESERVOIR WITH INCREASING THICKNESS ..... 98
FIGURE 5.21: RESULTS OF STAND ALONE SIMULATIONS WHERE THICKNESS WAS ALTERED WITH PERMEABILITY IN A 21° DIP RESERVOIR ..... 99
FIGURE 5.22: SCHEMATIC OF THE PROGRESSION OF THE DISPLACEMENT PROFILE IN LOW PERMEABILITY, DIPPING RESERVOIR WITH RESPECT TO THICKNESS ..... 99
FIGURE 5.23: EFFECT GRAPH FOR THE MAIN EFFECT OF THE AQUIFER SIZE FOR RESPONSE 1 ..... 100
FIGURE 5.24: RESULT FOR EACH DESIGN RUN AND THE AVERAGE FOR ALL RUNS (BLACK LINE) FOR RESPONSE 2 ..... 102
FIGURE 5.25: NORMAL PROBABILITY PLOT FOR RESPONSE 2 ..... 103
FIGURE 5.26: EFFECT GRAPH FOR THE MAIN EFFECT OF FORMATION DIP FOR RESPONSE 2 ..... 104

FIGURE 5.27: EFFECT GRAPH OF THE MAIN EFFECT OF FORMATION DIP FOR THE THIRD RESPONSE: $CH_4$ RECOVERY UNDER CONVENTIONAL PRIMARY DEPLETION (AT WATER BREAKTHROUGH) ..... 105
FIGURE 5.28: SCHEMATIC OF THE DIFFERENCE IN SWEEP EFFICIENCY BETWEEN (A) NON-DIPPING AND (B) DIPPING RESERVOIRS..... 105
FIGURE 5.29: EFFECT GRAPH FOR THE MAIN EFFECT OF FORMATION DIP FOR RESPONSE 1 ..... 106
FIGURE 5.30: EFFECT GRAPH FOR THE PERMEABILITY - FORMATION DIP INTERACTION FOR RESPONSE 2..... 106
FIGURE 5.31: EFFECT GRAPH FOR THE PERMEABILITY - $K_V/K_H$ RATIO INTERACTION FOR RESPONSE 2 ..... 108
FIGURE 5.32: SCATTER PLOT OF THE RESULTS FROM THE ED FOR RESPONSE 2 FOR A NON-DIPPING AND DIPPING RESERVOIR WITH RESPECT TO ISOTROPIC PERMEABILITY..... 109
FIGURE 5.33: EFFECT GRAPH FOR THE MAIN EFFECT OF PERMEABILITY FOR RESPONSE 2..... 110
FIGURE 5.34: PERMEABILITY DISTRIBUTION SHOWING THE HIGH PERMEABILITY LAYER (1000MD) IN A LOW PERMEABILITY RESERVOIR (10MD)..... 113
FIGURE 5.35: $CO_2$ SATURATION OF THE HIGH PERMEABILITY HETEROGENEITY MODEL DISPLAYING THE POOR SWEEP EFFICIENCY AT THE 10% $CO_2$ BREAKTHROUGH LIMIT ..... 114
FIGURE 5.36: $CO_2$ SATURATION AT THE 10% $CO_2$ BREAKTHROUGH LIMIT FOR A MEDIUM PERMEABILITY (100MD) RESERVOIR WITH A HIGH PERMEABILITY (1000MD) LAYER ..... 115
FIGURE 5.37: $CO_2$ SATURATION FOR A LOW PERMEABILITY DIPPING RESERVOIR WITH RATES EQUAL TO 1 MMSCF/DAY..... 117
FIGURE 5.38: SCHEMATIC OF THE INJECTION WELL COMPLETION LOCATION, WHERE RED INDICATES THE DEFAULT LOCATION AND BLACK REPRESENTS THE ALTERED LOCATION..... 118
FIGURE 5.39: $CO_2$ SATURATION FOR THE LOW PERMEABILITY (10MD) MODEL WITH INJECTION WELL COMPLETIONS LOCATED AT THE BOTTOM OF THE RESERVOIR ..... 119
FIGURE 5.40: $CO_2$ SATURATION FOR THE DEFAULT LOW PERMEABILITY (10MD) MODEL WITH INJECTION WELL COMPLETIONS LOCATED AT THE TOP OF THE RESERVOIR..... 119
FIGURE 5.41: $CO_2$ SATURATION FOR RATES EQUAL TO 2.5 MMSCF/DAY ..... 120
FIGURE 5.42: $CO_2$ SATURATION FOR RATES EQUAL TO 10 MMSCF/DAY ..... 121
FIGURE 5.43: SCHEMATIC OF HORIZONTAL WELL LOCATION. INJECTION WELLS LOCATED ON THE EDGE, WITH THE PRODUCTION WELL LOCATED IN THE MIDDLE OF THE RESERVOIR..... 122
FIGURE 5.44: $CO_2$ SATURATION WHERE INJECTION AND PRODUCTION OCCUR THROUGH HORIZONTAL WELLS ..... 123
FIGURE 6.1: RESPONSE 1 RESULTS FOR EACH DESIGN RUN. THE AVERAGE OF ALL RUNS IS SHOWN AS THE BLACK LINE. ..... 128
FIGURE 6.2: THE NORMAL PROBABILITY PLOT FOR RESPONSE 1. ..... 129
FIGURE 6.3: THE EFFECT GRAPH FOR THE THICKNESS FORMATION DIP INTERACTION FOR RESPONSE 1 ..... 130
FIGURE 6.4: SCHEMATIC OF THE DISPLACEMENT PROCESS WHEN THE INJECTION OF $CO_2$ IS DELAYED IN A NON-DIPPING RESERVOIR. ..... 131
FIGURE 6.5: SCREENSHOTS OF A THIN (50M), NON-DIPPING RESERVOIR AT THE POINT OF 10% $CO_2$ BREAKTHROUGH SHOWING $CO_2$ SATURATION (TOP) AND $CH_4$ SATURATION (BOTTOM). INJECTION HAS BEEN DELAYED..... 132
FIGURE 6.6: $CO_2$ SATURATION FOR A THIN (50M) DIPPING RESERVOIR (TOP) AND A THICK (150M) DIPPING RESERVOIR (BOTTOM), DISPLAYING SIMILAR DISPLACEMENT PROFILES IN THE FREE GAS ZONE, BUT WITH GREATER OVER-RIDE OF THE INVADED ZONE AS THICKNESS INCREASES. ..... 133
FIGURE 6.7: THE EFFECT GRAPH FOR THE PERMEABILITY THICKNESS INTERACTION FOR RESPONSE 1 ..... 134

FIGURE 6.8: THE EFFECT GRAPH FOR THE MAIN EFFECT OF THICKNESS FOR RESPONSE 1 ..... 135
FIGURE 6.9: THE EFFECT GRAPH FOR THE $K_V/K_H$ RATIO INJECTION RATE INTERACTION FOR RESPONSE 1 ..... 136
FIGURE 6.10: THE EFFECT GRAPH FOR THE QUADRATIC EFFECT OF FORMATION DIP FOR RESPONSE 1 ..... 137
FIGURE 6.11: SUMMARY OF THE RESULTS FOR EACH RUN FOR RESPONSE 1 AS A FUNCTION OF FORMATION DIP AND THICKNESS. NOTE THE OPPOSING TRENDS FOR THE LEVELS OF THICKNESS AS FORMATION DIP INCREASES. ..... 138
FIGURE 6.12: THE EFFECT GRAPH FOR THE THICKNESS TIMING OF INJECTION INTERACTION FOR RESPONSE 1 ..... 138
FIGURE 6.13: RESPONSE 2 RESULTS FOR EACH DESIGN RUN. THE AVERAGE OF ALL RUNS IS SHOWN AS THE BLACK LINE. ..... 140
FIGURE 6.14: THE NORMAL PROBABILITY PLOT FOR RESPONSE 2. ..... 141
FIGURE 6.15: THE EFFECT GRAPH FOR THE MAIN EFFECT OF TIMING OF INJECTION FOR RESPONSE 2. ..... 141
FIGURE 6.16: THE COMPARISON OF PRODUCING $CO_2$ CONCENTRATION PROFILES WHERE THE INJECTION OF $CO_2$ HAS EITHER BEEN DELAYED OR NOT DELAYED. ..... 142
FIGURE 6.17: THE $CH_4$ SATURATION FOR TWO MODELS WHERE INJECTION HAS NOT BEEN DELAYED (TOP), AND WHERE INJECTION HAS BEEN DELAYED (BOTTOM). THE REDUCTION IN THE THICKNESS OF THE FREE GAS ZONE (AND THEREFORE EFFECTIVELY THE RESERVOIR) IS CLEARLY VISIBLE. ..... 144
FIGURE 6.18: THE EFFECT GRAPH FOR THE THICKNESS FORMATION DIP INTERACTION FOR RESPONSE 2. ..... 145
FIGURE 6.19: THE EFFECT GRAPH FOR THE PERMEABILITY THICKNESS INTERACTION FOR RESPONSE 2. ..... 146
FIGURE 6.20: THE EFFECT GRAPH FOR THE $K_V/K_H$ RATIO INJECTION RATE INTERACTION FOR RESPONSE 2. ..... 146
FIGURE 6.21: THE EFFECT GRAPH FOR THE MAIN EFFECT OF FORMATION DIP FOR RESPONSE 2. ..... 147
FIGURE 6.22: RESPONSE 3 RESULTS FOR EACH DESIGN RUN. THE AVERAGE OF ALL RUNS IS SHOWN AS THE BLACK LINE. ..... 148
FIGURE 6.23: THE NORMAL PROBABILITY PLOT FOR RESPONSE 3. ..... 149
FIGURE 6.24: THE EFFECT GRAPH FOR THE MAIN EFFECT OF FORMATION DIP FOR RESPONSE 3. ..... 149
FIGURE 6.25: THE EFFECT GRAPH FOR THE MAIN EFFECT OF PERMEABILITY FOR RESPONSE 3. ..... 150
FIGURE 6.26: THE EFFECT GRAPH FOR THE PERMEABILITY $K_V/K_H$ RATIO INTERACTION FOR RESPONSE 3. ..... 151
FIGURE 6.27: THE EFFECT GRAPH FOR THE MAIN EFFECT OF $K_V/K_H$ RATIO FOR RESPONSE 3. ..... 152
FIGURE 6.28: THE EFFECT GRAPH FOR THE PERMEABILITY FORMATION DIP INTERACTION FOR RESPONSE 3. ..... 152
FIGURE 6.29: THE EFFECT GRAPH FOR THE $K_V/K_H$ RATIO FORMATION DIP INTERACTION FOR RESPONSE 3. ..... 153
FIGURE 6.30: THE EFFECT GRAPH FOR THE FORMATION DIP TIMING OF INJECTION INTERACTION FOR RESPONSE 3. ..... 154
FIGURE 6.31: RESPONSE 1 RESULTS FOR EACH DESIGN RUN. THE AVERAGE OF ALL RUNS IS INDICATED BY THE BLACK LINE. ..... 159
FIGURE 6.32: THE NORMAL PROBABILITY PLOT FOR RESPONSE 1. ..... 160
FIGURE 6.33: THE EFFECT GRAPH FOR THE MAIN EFFECT OF THICKNESS FOR RESPONSE 1. ..... 160
FIGURE 6.34: THE EFFECT GRAPH FOR THE THICKNESS TIMING OF INJECTION INTERACTION FOR RESPONSE 1. ..... 161
FIGURE 6.35: SCHEMATIC OF THE INFLUENCE OF GRAVITY FORCES ON MITIGATING AGAINST THE NEGATIVE EFFECTS OF THE HIGHER PERMEABILITY LAYER IN A NON-DIPPING RESERVOIR. ..... 162
FIGURE 6.36: SCHEMATIC OF THE EFFECT OF VISCOUS AND GRAVITY FORCES ON THE DISPLACEMENT IN A DIPPING RESERVOIR. STRONGER VISCOUS FORCES (TOP) LEAD TO MORE SEVERE UNEVEN ADVANCEMENT OF THE DISPLACEMENT FRONT. INCREASED GRAVITY FORCES (BOTTOM) ACT TO SUPPRESS THE UNEVEN ADVANCEMENT. ..... 162
FIGURE 6.37: THE EFFECT OF GRAVITY OVER-RIDE IN A NON-DIPPING RESERVOIR WITH HETEROGENEITY. OVER-RIDING OF THE INVADED ZONE DIRECTS THE $CO_2$ TOWARDS THE HIGHER PERMEABILITY LAYER. ..... 163

FIGURE 6.38: THE EFFECT GRAPH FOR THE PERMEABILITY MULTIPLIER TIMING OF INJECTION INTERACTION FOR RESPONSE 1..... 164
FIGURE 6.39: THE EFFECT GRAPH OF THE THICKNESS FORMATION DIP INTERACTION FOR RESPONSE 1. ..... 165
FIGURE 6.40: SCHEMATIC OF THE EFFECT OF THICKNESS IN A NON-DIPPING RESERVOIR. DISPLACEMENTS CONTROLLED BY VISCOUS FORCES (TOP) LEAD TO MAXIMUM CONTACT WITH THE HETEROGENEITY, LEADING TO THE SEVERE UNEVEN ADVANCEMENT OF THE DISPLACEMENT FRONT. INCREASING THICKNESS AND ALLOWING FOR GRAVITY TO INFLUENCE THE DISPLACEMENT (BOTTOM) ENSURES THE RESERVOIR FILLS FROM THE BOTTOM UP (INDICATED BY THE DASHED LINES), NEGATING THE EFFECT OF THE HETEROGENEITY. ..... 166
FIGURE 6.41: THE EFFECT GRAPH FOR THE MAIN EFFECT OF TIMING OF INJECTION FOR RESPONSE 1. ..... 166
FIGURE 6.42: RESPONSE 2 RESULTS FOR EACH DESIGN RUN. THE AVERAGE FOR ALL RUNS IS INDICATED BY THE BLACK LINE..... 167
FIGURE 6.43: THE NORMAL PROBABILITY PLOT FOR RESPONSE 2. ..... 168
FIGURE 6.44: THE EFFECT GRAPH FOR THE MAIN EFFECT OF TIMING OF INJECTION FOR RESPONSE 2. ..... 169
FIGURE 6.45: THE EFFECT GRAPH FOR THE MAIN EFFECT OF THICKNESS FOR RESPONSE 2..... 170
FIGURE 6.46: THE EFFECT GRAPH FOR THE THICKNESS FORMATION DIP INTERACTION FOR RESPONSE 2. ..... 171
FIGURE 6.47: THE EFFECT GRAPH FOR THE PERMEABILITY MULTIPLIER TIMING OF INJECTION INTERACTION FOR RESPONSE 2..... 172
FIGURE 6.48: THE EFFECT GRAPH FOR THE THICKNESS TIMING OF INJECTION INTERACTION FOR RESPONSE 2. ..... 173
FIGURE 6.49: RESPONSE 3 RESULTS FOR EACH DESIGN RUN. THE AVERAGE OF ALL RUNS IS INDICATED BY THE BLACK LINE. ..... 174
FIGURE 6.50: THE NORMAL PROBABILITY PLOT FOR RESPONSE 3. ..... 175
FIGURE 6.51: THE EFFECT GRAPH FOR THE MAIN EFFECT OF FORMATION DIP FOR RESPONSE 3. ..... 175
FIGURE 6.52: THE EFFECT GRAPH FOR THE FORMATION DIP TIMING OF INJECTION INTERACTION FOR RESPONSE 3. ..... 176
FIGURE 6.53: THE EFFECT GRAPH FOR THE MAIN EFFECT OF THE PERMEABILITY MULTIPLIER FOR RESPONSE 3. ..... 178
FIGURE 6.54: THE EFFECT GRAPH FOR THE PERMEABILITY MULTIPLIER FORMATION DIP INTERACTION FOR RESPONSE 3..... 178
FIGURE 7.1: LOCATION OF THE NAYLOR FIELD IN SOUTH-WESTERN VICTORIA, AUSTRALIA..... 181
FIGURE 7.2: PLAN VIEW OF THE MODEL OF THE NAYLOR FIELD. THE GAS RESERVOIR (RED) IS ENCLOSED BY THREE BOUNDING FAULTS. ..... 182
FIGURE 7.3: HISTORICAL GAS PRODUCTION RATE FOR THE NAYLOR FIELD..... 183
FIGURE 7.4: RELATIVE PERMEABILITY DATA USED FOR THE DYNAMIC MODEL. ..... 185
FIGURE 7.5: LOCATION OF THE NUMERICAL AQUIFERS USED TO HISTORY MATCH THE HISTORICAL PRODUCTION. ..... 186
FIGURE 7.6: LOCATION OF THE CRC-1 WELL DRILLED BY THE CO2CRC FOR USE IN A $CO_2$ STORAGE PILOT PROJECT. ..... 187
FIGURE 7.7: CROSS-SECTION OF THE RESERVOIR SHOWING THE FLAT NATURE OF THE GAS ZONE. ..... 188
FIGURE 7.8: CROSS-SECTION OF THE RESERVOIR DISPLAYING THE PERMEABILITY HETEROGENEITY PRESENT IN THE MODEL. ..... 189
FIGURE 7.9: PLAN VIEW OF THE RESERVOIR INDICATING THE LOCATION OF THE FIVE INJECTION WELLS. ..... 190
FIGURE 7.10: COMPARISON OF $CO_2$ CONCENTRATION FOR A PRODUCTION/INJECTION RATE OF 100,000 SM3/DAY (TOP) AND 250,000 SM3/DAY (BOTTOM) WHEN THE PRODUCING $CO_2$ CONCENTRATION REACHES 5 MOLE PERCENT..... 192
FIGURE 7.11: THE RESULT FOR INDIVIDUAL DESIGN RUNS WITH REGARD TO RESPONSE 1. THE AVERAGE OF ALL RUNS IS SHOWN IN BLACK. ..... 196
FIGURE 7.12: THE NORMAL PROBABILITY PLOT FOR THE ANALYSIS OF RESPONSE 1. ..... 197
FIGURE 7.13: EFFECT GRAPH FOR THE MAIN EFFECT OF THE TIMING OF $CO_2$ INJECTION. ..... 197
FIGURE 7.14: EFFECT GRAPH FOR THE MAIN EFFECT OF THE PRODUCTION RATE. ..... 198

Figure 7.15: Effect graph for the interaction between the timing of $CO_2$ injection and the Y location of the injection well. ..... 199
Figure 7.16: Cross-section from the production well to the injection well located in the south of the reservoir. The continuous higher permeability streak can be seen in green in the lower section of the cross-section. ..... 200
Figure 7.17: Schematic of the effect of the high permeability layer when (a) injection is not delayed (top) and (b) injection is delayed (bottom) where the invaded zone is represented in blue. If injection is delayed, gravity segregation leads to the bypassing of the high permeability layer. ..... 200
Figure 7.18: Effect graph for the interaction between the timing of $CO_2$ injection and the production rate. ..... 201
Figure 7.19: Effect graph for the interaction between the Y location of the injection well and the production rate. ..... 202
Figure 7.20: Effect graph for the main effect of the X location of the injection well. ..... 203
Figure 7.21: The result for individual design runs with regard to Response 2. The average of all runs is shown in black. ..... 206
Figure 7.22: The normal probability plot from the analysis of Response 2. ..... 207
Figure 7.23: The effect graph for the main effect of the production rate for Response 2. ..... 207
Figure 7.24: The effect graph for the main effect of the timing of $CO_2$ injection for Response 2. ..... 208
Figure 7.25: The effect graph for the main effect of the Y location for Response 2. ..... 209
Figure 7.26: The effect graph for the interaction between the timing of $CO_2$ injection and the production rate for Response 2 ..... 210
Figure 7.27: The result for individual design runs with regard to Response 3. The average of all runs is shown in black. ..... 212
Figure 7.28: The normal probability plot displaying the deviation from the normality assumption, requiring a transformation. ..... 213
Figure 7.29: A graph of the residuals versus the predicted values, with the funnel pattern indicating non-constant variance. ..... 214
Figure 7.30: Box-Cox diagnostic plot indicating a transform would improve the fit of the regression model to the input data. ..... 215
Figure 7.31: The normal probability plot after the transformation to the data has been applied. ..... 215
Figure 7.32: The plot of residuals versus the predicted values after the transformation to the data has been applied, displaying no obvious pattern ..... 216
Figure 7.33: The effect graph for the main effect of the production rate for Response 3. ..... 216
Figure 7.34: The effect graph for the main effect of the Y location of the injection well for Response 3. ..... 218
Figure 7.35: The effect graph for the main effect of the timing of $CO_2$ injection for Response 3. ..... 219
Figure 7.36: The effect graph for the interaction between the timing of $CO_2$ injection and the production rate for Response 3 ..... 220
Figure 7.37: A comparison of the $CO_2$ production profiles where the injection gas composition is being tested. ..... 224

# List of Tables


TABLE 3-1: PARTICIPATING ORGANISATIONS AND THE NUMERICAL CODES EMPLOYED IN THE CODE COMPARISON STUDY. ..... 39

TABLE 3-2: MODEL PROPERTIES (PROBLEM 1) ..... 40

TABLE 3-3: PROPERTIES OF $CO_2$ – $CH_4$ MIXTURES AND AQUEOUS SOLUBILITY AT A PRESSURE OF 40 BAR ..... 41

TABLE 3-4: PROPERTIES OF CO2 – CH4 MIXTURES AND AQUEOUS SOLUBILITY AT A PRESSURE OF 100 BAR ..... 42

TABLE 3-5: MODEL PROPERTIES (PROBLEM 3) ..... 48

TABLE 4-1: USE OF THE ED METHODOLOGY IN THE OIL AND GAS INDUSTRY ..... 72

TABLE 5-1: BASE CASE MODEL PROPERTIES ..... 75

TABLE 5-2: COMPUTATIONAL TIME REQUIRED TO COMPLETE EACH SIMULATION RUN FOR VARIABLE GRID BLOCK SIZES ..... 78

TABLE 5-3: EXPERIMENTAL DESIGN PARAMETERS AND RANGES ..... 79

TABLE 5-4: EXPERIMENTAL DESIGN MATRIX AND RESULTS ..... 84

TABLE 5-5: RANKING OF STATISTICALLY SIGNIFICANT COEFFICIENTS FROM THE ANALYSIS OF RESPONSE 1 ..... 86

TABLE 5-6: $CO_2$ BREAKTHROUGH TIMES AND CORRESPONDING $CH_4$ RECOVERY EFFICIENCIES FOR VARIABLE, ISOTROPIC PERMEABILITY MODELS IN AN 11° DIPPING FORMATION ..... 92

TABLE 5-7: COMPARISON OF THE EFFECT OF THE $K_V/K_H$ RATIO AND THE DIFFUSION COEFFICIENT ON THE $CH_4$ RECOVERY FACTOR AT A 10% $CO_2$ BREAKTHROUGH LIMIT ..... 101

TABLE 5-8: RANKING OF STATISTICALLY SIGNIFICANT COEFFICIENTS FROM THE ANALYSIS OF RESPONSE 2 ..... 103

TABLE 5-9: RESULTS OF SIMULATIONS INVESTIGATING THE IMPACT OF A HIGH PERMEABILITY (1000MD) LAYER IN A LOW PERMEABILITY (10MD) RESERVOIR ..... 114

TABLE 5-10: RESULTS OF SIMULATIONS INVESTIGATING THE IMPACT OF A HIGH PERMEABILITY (1000MD) LAYER IN A MEDIUM PERMEABILITY (100MD) RESERVOIR ..... 115

TABLE 5-11: RESULTS OF SIMULATIONS INVESTIGATING VARIABLE RATES IN A LOW PERMEABILITY (10MD) DIPPING RESERVOIR ..... 117

TABLE 5-12: RESULTS OF SIMULATIONS INVESTIGATING THE LOCATION OF COMPLETIONS IN A LOW PERMEABILITY (10MD) DIPPING RESERVOIR ..... 118

TABLE 5-13: RESULT OF SIMULATIONS INVESTIGATING VARIABLE RATES AND THE USE OF HORIZONTAL WELLS IN A THIN, NON DIPPING RESERVOIR ..... 120

TABLE 5-14: RESULTS OF SIMULATIONS COMPARING THE USE OF VERTICAL AND HORIZONTAL WELLS ..... 122

TABLE 6-1: PARAMETER AND RANGE SELECTION FOR STUDY 2A ..... 126

TABLE 6-2: D-OPTIMAL DESIGN FOR STUDY 2A ..... 127

TABLE 6-3: RANKING OF STATISTICALLY SIGNIFICANT COEFFICIENTS FOR RESPONSE 1 ..... 129

TABLE 6-4: RANKING OF STATISTICALLY SIGNIFICANT COEFFICIENTS FOR RESPONSE 2 ..... 140

TABLE 6-5: ANOVA TABLE FOR RESPONSE 3 ..... 148

TABLE 6-6: DESIGN PARAMETERS AND THE CORRESPONDING LOW, MID AND HIGH VALUES. ..... 157

TABLE 6-7: D-OPTIMAL DESIGN FOR STUDY 2B ..... 157

TABLE 6-8: ANOVA TABLE FOR RESPONSE 1 ..... 159

TABLE 6-9: ANOVA TABLE FOR RESPONSE 2 ..... 168

TABLE 6-10: ANOVA TABLE FOR RESPONSE 3 ..... 174

TABLE 6-11: COMPARISON OF RESULTS BETWEEN EQUIVALENT NON-DIPPING MODELS, INVESTIGATING THE DIFFERENCE BETWEEN THE TIMING OF INJECTION. ..... 177
TABLE 6-12: COMPARISON OF RESULTS BETWEEN EQUIVALENT DIPPING MODELS, INVESTIGATING THE DIFFERENCE BETWEEN THE TIMING OF INJECTION. ..... 178
TABLE 7-1: BASIC PROPERTIES OF THE NAYLOR FIELD. ..... 182
TABLE 7-2: THE RESULTS FROM THE TESTING OF THE INJECTION WELL LOCATION. ..... 191
TABLE 7-3: THE RESULTS OF THE TESTING OF THE INJECTION AND PRODUCTION RATES. ..... 191
TABLE 7-4: PARAMETERS AND THE CORRESPONDING LEVELS FOR THE EXPERIMENTAL DESIGN. ..... 193
TABLE 7-5: EXPERIMENTAL DESIGN RUNS INDICATING PARAMETER LEVEL COMBINATIONS. ..... 194
TABLE 7-6: RANKING OF STATISTICALLY SIGNIFICANT COEFFICIENTS FROM THE ANALYSIS OF RESPONSE 1. ..... 196
TABLE 7-7: THE PARAMETER LEVEL COMBINATION WHICH OPTIMISES RESPONSE 1. ..... 204
TABLE 7-8: THE COMPARISON OF THE ERROR BETWEEN PREDICTED AND SIMULATED (CALCULATED) RESULTS FOR RESPONSE 1. ..... 205
TABLE 7-9: RANKING OF STATISTICALLY SIGNIFICANT COEFFICIENTS FROM THE ANALYSIS OF RESPONSE 2. ..... 206
TABLE 7-10: THE PARAMETER LEVEL COMBINATION WHICH OPTIMISES THE NATURAL GAS RECOVERY FOR RESPONSE 2. ..... 211
TABLE 7-11: THE PARAMETER LEVEL COMBINATION THAT MINIMISES THE NATURAL GAS RECOVERY FOR RESPONSE 2. ..... 211
TABLE 7-12: THE COMPARISON OF THE ERROR BETWEEN PREDICTED AND SIMULATED (CALCULATED) RESULTS FOR RESPONSE 2. .. 212
TABLE 7-13: RANKING OF STATISTICALLY SIGNIFICANT COEFFICIENTS FROM THE ANALYSIS OF RESPONSE 3. ..... 213
TABLE 7-14: PRIMARY RECOVERY EFFICIENCIES FOR PRODUCTION RATES EMPLOYED IN THE EXPERIMENTAL DESIGN ..... 217
TABLE 7-15: THE PARAMETER LEVEL COMBINATION THAT OPTIMISES RESPONSE 3. ..... 221
TABLE 7-16: THE COMPARISON OF THE ERROR BETWEEN THE PREDICTED AND SIMULATED (CALCULATED) RESULTS FOR RESPONSE 3. ..... 222
TABLE 7-17: COMPARISON OF CALCULATED AND PREDICTED RESULTS FOR THE OPTIMISED MODEL ..... 223
TABLE 8-1: SUMMARY OF KEY CRITERIA TO MAXIMISE THE EFFICIENCY OF THE DISPLACEMENT OF $CH_4$ BY $CO_2$. ..... 229

# Nomenclature

| Symbol | Description |
|---|---|
| $\phi$ | porosity |
| $\lambda$ | mobility of the fluid |
| $\lambda$ | exponent (relative permeability correlation) |
| $\mu$ | viscosity |
| $\rho$ | density |
| A | area |
| $B_g$ | formation volume factor |
| $B_{gi}$ | initial formation volume factor |
| $B_{ga}$ | formation volume factor at abandonment conditions |
| C | concentration |
| C | Land's trapping constant |
| $c_t$ | total aquifer compressibility |
| D | diffusion coefficient |
| E | expansion factor |
| g | gravity constant |
| G | gas volume initially in place |
| $G_p$ | gas volume produced |
| h | thickness |
| k | permeability |
| $k_r$ | relative permeability |
| $k_{rg}$ | gas relative permeability |
| $k_{rl}$ | liquid relative permeability |
| l | length |
| M | mobility ratio |
| n | number of moles |
| p | pressure |
| $P_c$ | capillary pressure |
| $P_0$ | strength coefficient |
| q | flow rate |
| R | universal gas constant |
| $R^2$ | correlation coefficient |
| $R^2_{adjusted}$ | adjusted correlation coefficient |

| | |
|---|---|
| $R_{v/g}$ | viscous to gravity ratio |
| sc | standard conditions |
| $S_g$ | gas saturation |
| $S_{gr}$ | residual gas saturation |
| $S_{gt}$ | trapped gas saturation |
| $S_{lr}$ | residual liquid saturation |
| $S_w$ | water saturation |
| $S_{wi}$ | initial water saturation |
| $S_{wir}$ | irreducible water saturation |
| t | time |
| T | temperature |
| u | Darcy velocity |
| V | volume |
| W | total water volume |
| $W_e$ | cumulative volume of water influx |
| x | distance |
| $x_g$ | gas phase concentration |
| $x_l$ | aqueous phase concentration |
| Z | compressibility factor |

| Acronyms | Description |
|---|---|
| ANOVA | ANalysis Of VAriance |
| CCD | Central Composite Design |
| CCS | Carbon Capture and Storage |
| $CH_4$ | Methane |
| $CO_2$ | Carbon dioxide |
| CO2CRC | Co-operative Research Centre for Greenhouse Gas Technologies |
| CSEGR | Carbon Sequestration with Enhanced Gas Recovery |
| ED | Experimental Design |
| EGR | Enhanced Gas Recovery |
| EOR | Enhanced Oil Recovery |
| GWC | Gas Water Contact |
| HCPV | Hydrocarbon Pore Volume |
| MM | Million |

| | |
|---|---|
| NPV | Net Present Value |
| OBPP | Otway Basin Pilot Project |
| OGIP | Original Gas in Place |
| PDE | Partial Differential Equations |
| PVT | Pressure Volume Temperature |
| RF | Recovery Factor |
| RMSE | Root Mean Square Error |
| Scf | Standard Cubic Feet |
| SGS | Sequential Gaussian Simulation |
| STB | Stock Tank Barrel |

# CHAPTER 1

# 1 Introduction

## 1.1 Background

Gas reservoirs generally fall into two categories, volumetric and water-drive gas reservoirs. Volumetric gas reservoirs are characterised by being a completely enclosed system, which during production experiences no pressure support. The production of gas is derived purely through the expansion of gas, which is a very efficient process. The recovery efficiency in a volumetric gas reservoir is inversely proportional to the reservoir pressure. Consequently, the lower the reservoir pressure the greater the natural gas recovery. This is purely an economic criterion which can lead to recovery efficiencies of up to 80 – 90% of the original gas in place (OGIP) (Ahmed 2000).

On the other hand, such high recovery efficiencies are not achievable in water-drive gas reservoirs. Recovery efficiencies in this type of gas reservoir can be considerably lower, generally of the order of 50 – 80% of the OGIP (Ahmed 2000). This considerable reduction in recovery is attributable to two main processes. Firstly, the immobilisation of gas pockets through the process of capillary trapping. The influx of the aquifer in response to the production of gas leads to the uneven advancement of the aquifer into the gas zone, both at a microscopic and macroscopic level. This uneven advancement isolates pockets of gas, rendering them immobile and creating a trapped or residual gas saturation. Note that gas saturation in a volumetric reservoir does not change, only the number of moles changes. Research has shown that trapped gas saturations can be as high as 50% (Geffen et al. 1952; Chierici et al. 1963; Katz et al. 1966; D. Keelan & Pugh 1975). Secondly, recovery is reduced through the restriction of gas expansion caused by the pressure support provided by the aquifer responding to production. The residual gas saturations can be trapped at pressures up to the original reservoir pressure. The pressure at which the residual gas saturation is trapped will determine the number of moles that is trapped and therefore the reduction in the recovery.

It follows that any technique that can restrict the influx of the aquifer and/or reduce reservoir pressure will enhance the recovery of natural gas from water-drive gas reservoirs. Two operational techniques that have been implemented in the field are accelerated gas production and the co-production of gas and water. Argawal et al (1965) noted that the recovery in water-drive gas reservoirs is rate dependent. It was shown that accelerated production, or the production of gas at higher rates, can be implemented to take advantage of the transient behaviour of the aquifer. At the commencement of production, there can exist a period of time where the pressure transient has not

reached the aquifer, and so the aquifer will not immediately respond to production and advance into the gas reservoir. This will allow a greater drawdown of reservoir pressure. This technique does have its drawbacks however. Firstly, gas fields are commonly developed under long term (20+ years) contracts, which specify a certain volume of gas to be delivered in a particular time frame (e.g. a minimum daily quota). Unless the use of gas storage is available, accelerated gas production will violate the conditions of the contract, with much greater volumes of gas being produced than are contractually required. Secondly, heterogeneity present in the reservoir could lead to the channelling of water due to the high rates employed, which could result in the premature breakthrough of water at the production wells.

Another technique to enhance natural gas recovery is the co-production of water and gas, in an effort to reduce the reservoir/abandonment pressure. Implementation of this technique can occur early in the field life to limit the influx of the aquifer. This is achieved by placing water producers into the aquifer, reducing the pressure gradient induced by gas production. This technique can also be implemented after water has invaded the reservoir, by converting watered-out gas wells to water producers, to reduce reservoir pressure and re-mobilise trapped gas. This technique does however require the ability to handle and dispose of the produced water, the volume of which can be significant.

Another potential technique to limit the influx of the aquifer is through the injection of $CO_2$. Rather than reducing reservoir pressure, the injection of $CO_2$ will maintain reservoir pressure retarding the influx of the aquifer. Consequently, this will limit the volume of gas residually trapped. Additionally, fluid properties of both natural gas and $CO_2$ at typical reservoir conditions are potentially conducive to the displacement of natural gas by $CO_2$ with minimal mixing. At typical reservoir conditions, the density and viscosity of $CO_2$ are considerably greater than natural gas (dry gas). The greater density will aid in minimising the mixing between the two fluids as well as cause the $CO_2$ to flow beneath the natural gas column creating a barrier between the aquifer and the natural gas. A greater viscosity leads to a favourable mobility ratio which will assist in a stable displacement process without the formation of viscous fingering.

The favourable fluid properties between natural gas and $CO_2$ have led to a handful of laboratory and numerical studies investigating the injection of $CO_2$ into volumetric gas reservoirs (Clemens & Wit 2002; Mamora & Seo 2002; C.M. Oldenburg 2003; Seo & Mamora 2003; Al-Hashami et al. 2005; Sim et al. 2008). Unfortunately, the laboratory studies have led to conflicting ideas on the degree of mixing between $CO_2$ and $CH_4$. Mamora and Seo (2002) state that the displacement process is very efficient with low dispersion coefficients. Sim *et al* (2008) state that the mixing between $CO_2$ and $CH_4$

by diffusion can be significant, especially in scenarios involving low pressure and low flow rates. These studies also found that the solubility of $CO_2$ in water has the potential to delay the breakthrough of $CO_2$, improving the recovery of $CH_4$ if a $CO_2$ production limit is in place. The numerical studies investigated the effect of both controllable factors (i.e. operational parameters) and uncontrollable factors (i.e. reservoir properties) on the displacement of $CH_4$ by $CO_2$. The investigations into the uncontrollable factors demonstrated predictable results. A larger diffusion coefficient resulted in greater mixing and earlier breakthrough of $CO_2$ at the production wells (Al-Hashami et al. 2005). Earlier $CO_2$ breakthrough also resulted from the introduction of permeability heterogeneity into the model (C.M. Oldenburg & Benson 2001). Reflecting the results of the laboratory studies, the breakthrough of $CO_2$ was delayed when the dissolution of $CO_2$ into the formation water was enabled in the model (Al-Hashami et al. 2005).

The investigations into the effect of controllable factors involved testing operational strategies such as the timing of $CO_2$ injection (C.M. Oldenburg et al. 2001; Clemens & Wit 2002; Al-Hashami et al. 2005) and injection rates (Al-Hashami et al. 2005). It was found that the recovery of natural gas at a particular $CO_2$ breakthrough limit was reduced compared to the no injection scenario, the earlier the injection of $CO_2$ occurred. Early injection provided the greatest time for $CO_2$ to mix with the natural gas. While no agreement was found on the optimal time to inject $CO_2$, the consensus was that it should occur late in the life of the field, near the time of abandonment. The injection of $CO_2$ would raise reservoir pressure, enhancing the deliverability and allowing production rates to be maintained in a period where under normal circumstances production rates would be declining. This period would therefore enhance natural gas recovery over what would be achievable if no injection occurred. The testing of rates showed that higher injection rates enhanced the deliverability, but it was noted that higher rates might also correspond to greater mixing between the two fluids. It has been noted by a number of authors that $CO_2$ enhanced gas recovery (EGR) could be used as method to offset the costs of carbon capture and storage (CCS) projects. Injection into a nearly depleted gas field could assist in the recovery of an extra volume of natural gas which could assist in covering the costs of the CCS project.

There exist two known (published) field pilots of $CO_2$ EGR, these pilots being located in the Szintfeletti XVL reservoir in Hungary (Papay 1999a; Papay 1999b) and the K12-B field in the Dutch sector of the North Sea (van der Meer et al. 2005). Only the results for the Szintfeletti XVL pilot have been published however. Injection occurred after this reservoir had undergone traditional primary depletion followed by use as a natural gas storage facility. Interestingly, injection occurred in the top of the structure, which would lead to a gravity unstable displacement. It was however stated that

34% of the gas that remained in place following the gas storage operations was recovered from the $CO_2$ injection operation whereby production was terminated once a $CO_2$ breakthrough limit of 20 mole percent was reached.

A key issue with the injection of $CO_2$ into a volumetric gas reservoir nearing abandonment conditions is the current reservoir pressure. Typical abandonment pressures equate to $CO_2$ being in a gaseous state in the reservoir. Although $CO_2$ will still be denser and more viscous than natural gas at these pressures, the difference in these fluid properties between the two fluids is considerably less than if $CO_2$ is in a supercritical state. With $CO_2$ in a gaseous state, mixing by diffusion will be considerably faster. Injection into a water-drive gas reservoir has the benefit of reservoir pressure being maintained regardless of when $CO_2$ is injected. This will ensure that mixing by diffusion will be minimised and the stability of the displacement process will be maximised. Coupled with the reduction/elimination of the trapped gas saturations by the advancing aquifer, injecting $CO_2$ in water-drive gas reservoirs has the potential to significantly enhance the recovery of natural gas.

## 1.2 Research Objectives

The specific objectives of this thesis are:

1. To evaluate the potential for $CO_2$ injection to enhance natural gas recovery in a water-drive reservoir compared to conventional primary depletion.

2. To evaluate the impact of selected rock, fluid and operational properties on the effectiveness of increasing the recovery of natural gas through $CO_2$ injection.

3. To investigate the influence of timing of $CO_2$ injection on the ability to enhance natural gas recovery.

4. To apply the results of the initial investigations to a case study involving a depleted gas field, the Naylor field, in an effort to maximise incremental recovery based upon historical production.

5. To develop screening criteria, indicating the reservoir and/or fluid properties which are more favourable to the application of $CO_2$ injection to enhance recovery.

## 1.3 Methodology

The thesis comprises three main sections. All sections involve the investigation of $CO_2$ injection into water-drive gas reservoirs using the experimental design (ED) methodology. This methodology allows for the simultaneous investigation of a number of parameters in order to determine their effect on chosen responses, such as natural gas recovery efficiency.

The first section (Chapter 5) involves the investigation of $CO_2$ injection at the commencement of $CH_4$ production. Reservoir and fluid properties considered potentially influential have been chosen to determine their effect on the efficiency of the displacement of $CH_4$ by $CO_2$, and the ability to maximise $CH_4$ recovery with as low a producing $CO_2$ concentration as possible. The effect of operational parameters and the influence of heterogeneity are also investigated in this section.

The second section (Chapter 6) investigates the effect of the timing of $CO_2$ injection. Research into the injection of $CO_2$ into volumetric reservoirs showed that delaying the injection decreased the time available for the two fluids to mix and consequently increased natural gas recovery when $CO_2$ production limits were imposed. Delaying the injection of $CO_2$ in this instance could limit the degree of mixing, but it will allow the aquifer to advance into the reservoir.

The final section (Chapter 7) determines whether the results of the previous sections involving simple models can be applied to a more complex case study, involving the modelling of $CO_2$ injection in the depleted Naylor gas field. The knowledge gained from the previous studies is used to maximise natural gas recovery with the lowest producing $CO_2$ concentration possible in an effort to achieve incremental recovery over the historical production.

## 1.4 Review of Chapters

This thesis is organised as follows:

Chapter 2 presents a literature review of the fluid properties of $CO_2$ and $CH_4$, the theory of gas reservoirs and their production, and the methods currently employed to enhance gas recovery in water-drive reservoirs. A review of current research and knowledge of the topic of $CO_2$ EGR is also presented.

Chapter 3 reports on a code comparison study performed by leading researchers in the field in order to confirm that the simulator employed in this study can accurately model the processes expected when $CO_2$ is injected into a water-drive gas reservoir.

Chapter 4 provides a review of experimental design and how this methodology has been used in the oil and gas industry.

Chapter 5 presents a study of the $CO_2$ EGR process and the effect of a selection of parameters on the efficiency of the displacement process when injection of $CO_2$ commences at the beginning of $CH_4$ production. Following this is a section on the effect of operational parameters and the impact of heterogeneity.

Chapter 6 presents a study investigating the effect of the timing of $CO_2$ injection in both a homogeneous and heterogeneous reservoir model.

Chapter 7 presents the results of a case study involving the modelling of $CO_2$ injection into the Naylor field. This study aims to determine if the results of the previous study correlate to a more realistic, more complex scenario and can result in the successful enhancement of natural gas recovery over the historical recovery.

Chapter 8 outlines screening criteria developed from the results of the three main studies of this thesis. It outlines the properties that are the most conducive to maximising natural gas recovery with the lowest producing $CO_2$ concentration.

Chapter 9 summarises the research conducted in this thesis and presents recommendations for future work.

## 1.5 Significance

This thesis presents an initial investigation into the possible technique of $CO_2$ injection in a water-drive gas reservoir. Unlike volumetric gas reservoirs, where recovery efficiencies of up to 80 – 90% can be achieved, the recovery from water-drive gas reservoirs can be significantly lower, requiring techniques to counter the negative effect of the water drive. No published study into the injection of $CO_2$ into water-drive gas reservoirs can be found in the literature, and so this thesis provides an initial insight into the mechanisms involved in the $CO_2$ EGR process. This thesis presents findings on influential parameters, both controllable (e.g. operational parameters such as injection rates) and uncontrollable (reservoir properties such as permeability), and which reservoirs would be best suited to the $CO_2$ EGR process. In addition, based upon the effects of the uncontrollable parameters, suggestions are given on what operational techniques can be applied to improve the stability of the displacement and maximise natural gas recovery. These findings can therefore be used as an initial guide to determine whether a particular reservoir would be suitable for a $CO_2$ EGR project.

# CHAPTER 2

# 2 Literature Review

## 2.1 Fluid Properties of $CO_2$ and $CH_4$

The mixing of carbon dioxide and methane ($CH_4$), and hence the contamination of the natural gas with $CO_2$ is a primary concern with injecting $CO_2$ into a natural gas reservoir in order to enhance recovery (Blok et al. 1997; C.M. Oldenburg et al. 2001; Al-Hashami et al. 2005). Contamination of natural gas with $CO_2$ degrades the quality of the natural gas, requiring extra facilities to separate the $CO_2$ from the gas stream to meet pipeline specifications. Corrosion resistant facilities are also required with the presence of $CO_2$, increasing the cost of the development. Although $CH_4$ and $CO_2$ are miscible, the fluid properties of $CO_2$ and $CH_4$ do suggest that the displacement of $CH_4$ by $CO_2$ is possible with minimal mixing over the relevant time scales typical in petroleum operations.

Figure 2.1 displays the phase diagram for $CO_2$. The critical pressure of $CO_2$ is 73.8 bar (7.38 MPa) and $CO_2$ has a critical temperature of 30.978°C (304.1282 K) (Span & Wagner 1996). $CH_4$ on the other hand has a critical pressure of 46 bar (4.6 MPa), and a critical temperature of -82.6°C (190.6 K) (Setzmann & Wagner 1991). At typical reservoir conditions, both fluids are in a supercritical state. The transitioning of these fluids to a supercritical state does not have the same effect however.

Figure 2.2 and Figure 2.3 present the density and viscosity of both $CO_2$ and $CH_4$ as a function of pressure and temperature. As $CO_2$ transitions from a gaseous to a supercritical state, a significant change in both the density and viscosity of $CO_2$ occurs. Over an equivalent temperature and pressure range, $CH_4$ exhibits no such dramatic change in density and viscosity. It is this contrast in the change of fluid properties that the $CO_2$ enhanced gas recovery process aims to take advantage of. At typical reservoir conditions, the density and viscosity of $CO_2$ is substantially greater than that of $CH_4$. It is these favourable fluid properties which have the potential to enable the stable displacement of $CH_4$ by $CO_2$ with minimal mixing over the typical field development timeframes.

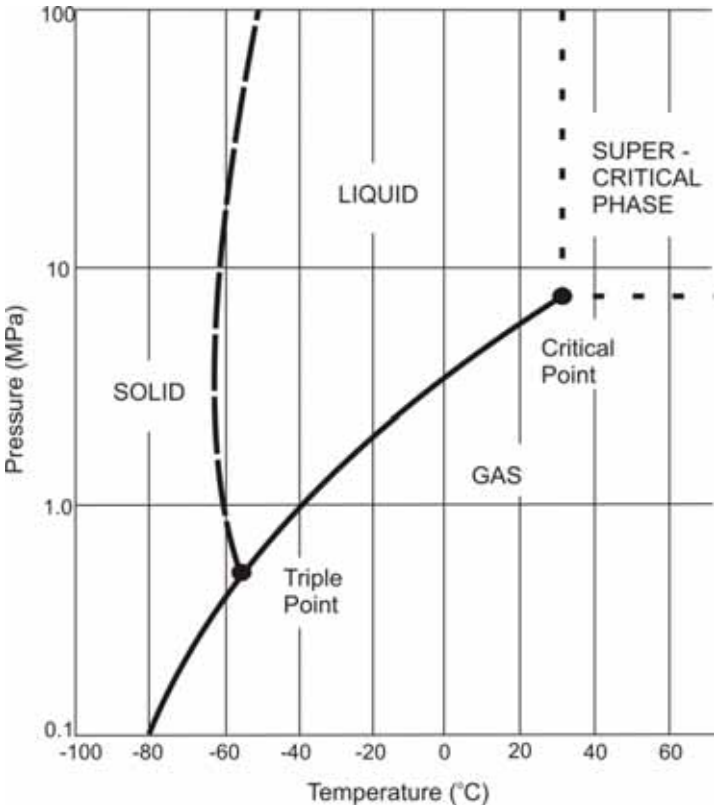


**Figure 2.1: $CO_2$ phase diagram.**

NOTE:
This figure is included on page 8 of the print copy of the thesis held in the University of Adelaide Library.

**Figure 2.2: Density of $CO_2$ and $CH_4$ as a function of pressure and temperature (data sourced from Lemmon, McLinden, and Friend).**

NOTE:
This figure is included on page 9
of the print copy of the thesis held in
the University of Adelaide Library.

**Figure 2.3: Viscosity of $CO_2$ and $CH_4$ as a function of pressure and temperature (data sourced from Lemmon, McLinden, and Friend).**

Specifically, these fluid properties induce the following effects. When injected into a natural gas reservoir, the larger density of $CO_2$ will result in preferential flow beneath the $CH_4$ column. Additionally, the density of $CO_2$ is less than that of formation waters. At a depth of around 1000 metres, the density of $CO_2$ plateaus to a value between 600 – 700 kg/m$^3$. Typical formation brines under similar conditions are 30 – 40% denser than $CO_2$ (Ennis-King & Paterson 2002). This is ideal for the use of $CO_2$ to enhance recovery as the $CO_2$ will preferentially flow between the natural gas column and the aquifer. In addition to displacing $CH_4$ towards the production well, the $CO_2$ is essentially replacing the $CH_4$ at the gas-water contact (GWC). This will reduce the volume of $CH_4$ that can be residually trapped, and from a CCS perspective, will enable a portion of the injected $CO_2$ to be residually trapped instead, an important storage mechanism in CCS (Flett et al. 2004; Kumar et al. 2005; Spiteri et al. 2005).

The greater viscosity of $CO_2$ compared to $CH_4$ is also an important aspect beneficial to the stable displacement of $CH_4$ by $CO_2$. The stability of a displacement process is a strong function of the mobility ratio, M. The mobility ratio is defined as

$$M = \frac{\lambda_{di}}{\lambda_{dp}} = \frac{(k_r/\mu)_{di}}{(k_r/\mu)_{dp}} \qquad (2.1)$$

where $\lambda$ = mobility of the fluid

$di$ = displacing fluid

$dp$ = displaced fluid

$k_r$ = relative permeability

$\mu$ = viscosity

For miscible displacements, the ease of flow of both the displacing and displaced phases in the rock is equal, and so the corresponding relative permeability terms in Equation 2.1 are equal. Therefore the mobility ratio is just a function of the viscosity ratio. If the mobility ratio is greater than one, the displacement process is unstable. This is due to the displacing fluid having a lower viscosity, and therefore being more mobile than the displaced fluid. This therefore leads to processes such as viscous fingering occurring, which can result in the bypassing of displaced fluid reducing the effectiveness of the displacement process. The establishment of viscous fingering in the case of $CH_4$ displacement by $CO_2$ would be extremely unwanted as the formation of these fingers enhances the contact area between the two fluids, increasing the potential for mixing. A mobility ratio equal to or less than one is favoured as this would eliminate viscous fingering, enhancing the stability of the displacement process. As shown in Figure 2.3, $CO_2$ at all relevant reservoir conditions will have a greater viscosity than $CH_4$, leading to a favourable mobility ratio.

Another favourable fluid property with respect to using $CO_2$ to enhance gas recovery is the solubility of both $CO_2$ and $CH_4$ in water. Figure 2.4 and Figure 2.6 display the solubilities of $CO_2$ and $CH_4$ in water. Comparison of these two Figures highlights the substantially higher solubility of $CO_2$ in water. For example, at a pressure and temperature of 10,000 psia and 100°F respectively, solubility of $CO_2$ is 230 scf/STB compared with just 34 scf/STB for $CH_4$, an order of magnitude difference. This higher solubility is a potential benefit if a $CO_2$ production constraint is placed on the project. A portion of the injected $CO_2$ will be dissolved into the formation water, with less volume of $CO_2$ remaining in a free state, and able to mix with the resident gas. This has the potential to delay the breakthrough of $CO_2$ at the production well which, if a $CO_2$ production constraint is in place, will enable a greater recovery of natural gas. In addition to pressure and temperature, the solubility of $CO_2$ is a function of salinity (Chang et al. 1998). In Figure 2.4, it can be seen that solubility increases with increasing pressure. The effect of temperature on solubility is dependent upon the pressure of the system, as seen in Figure 2.5. At low pressures (50 bar), an increase in reservoir temperature will reduce the solubility of $CO_2$ in water. However, at high pressures (1500 bar), curvature is observed as temperature is increased. The same effect is seen in the solubility of $CH_4$ in water (Figure 2.6).

NOTE:
This figure is included on page 11 of the print copy of the thesis held in the University of Adelaide Library.

**Figure 2.4: Solubility of $CO_2$ in pure water as a function of pressure and temperature (modified from Chang et al. 1998).**

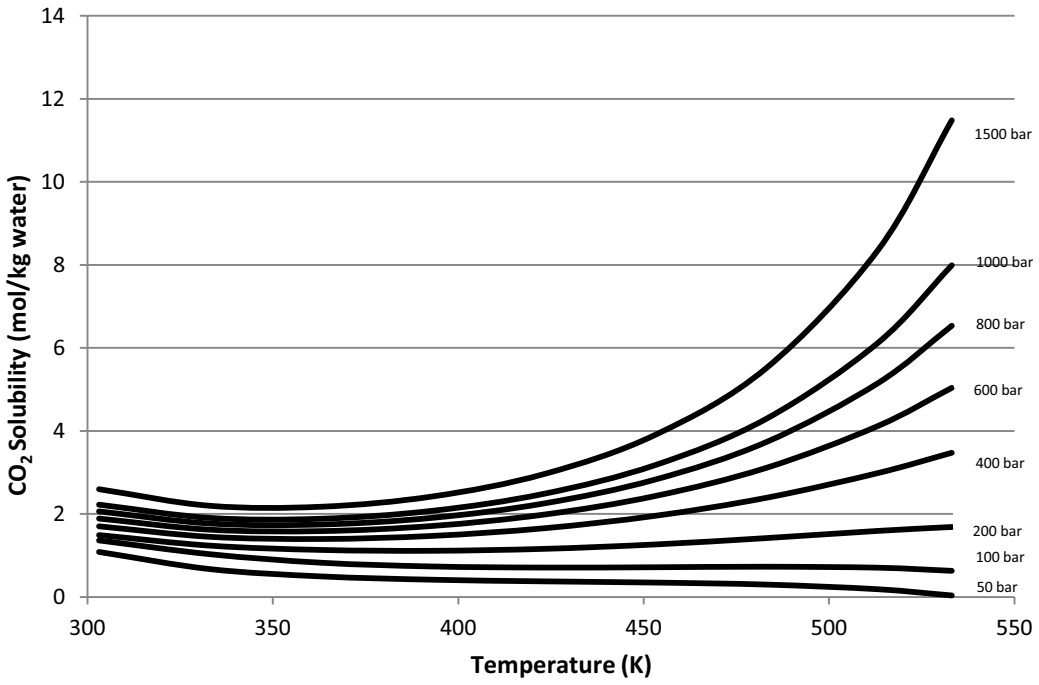


**Figure 2.5: $CO_2$ solubility as a function of temperature and pressure, indicating the variable trends with respect to temperature.**

NOTE:
This figure is included on page 12 of the print copy of the thesis held in the University of Adelaide Library.

**Figure 2.6: Solubility of $CH_4$ in pure water as a function of temperature and pressure (modified from Culberson & McKetta 1951).**

Salinity in the formation water serves to reduce the solubility of $CO_2$, as indicated by Figure 2.7. A study conducted by Enick and Klara (1990) calculated a five-fold decrease in the solubility of $CO_2$ as salinity varied from 0 – 30%.

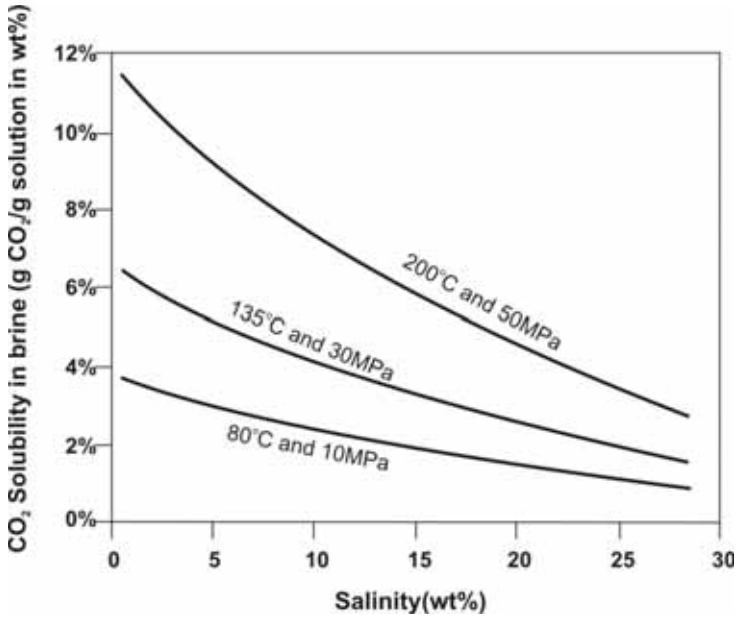


**Figure 2.7: Solubility of $CO_2$ as a function of salinity (modified from Bachu & Adams 2003).**

## 2.2 Natural Gas Reservoirs

Reservoirs that contain only free gas are known as gas reservoirs. These reservoirs contain a mixture of hydrocarbon gases which exist at reservoir conditions in a wholly gaseous state. The gaseous mixtures are termed based on the hydrocarbon composition, either being a dry, wet or retrograde gas. To assist in the description of these gases, Figure 2.8 presents a phase diagram.

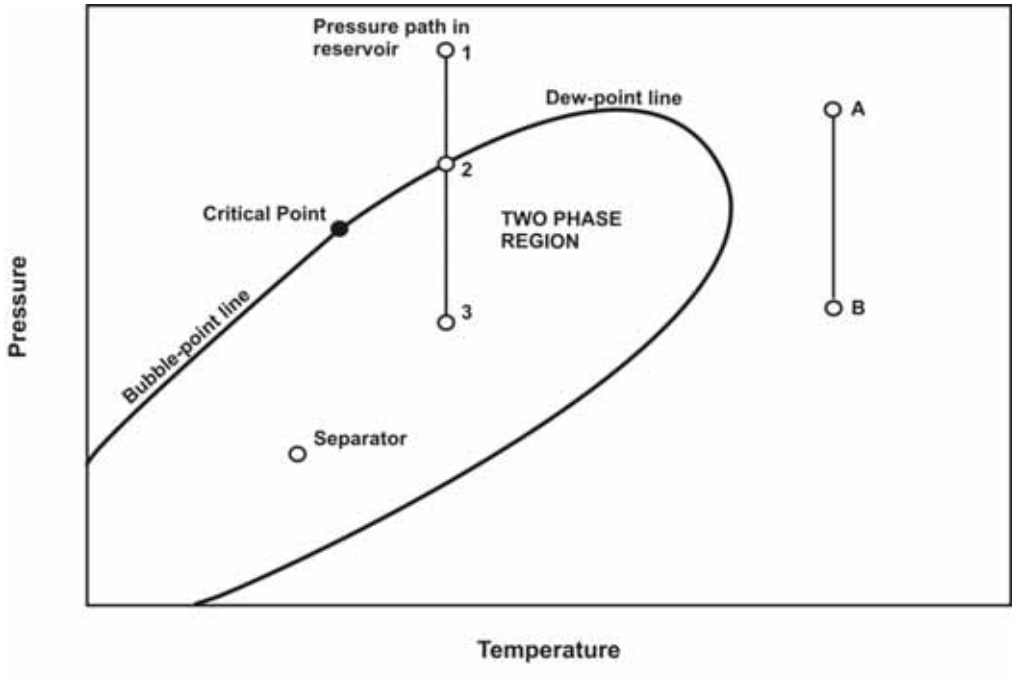


**Figure 2.8: A phase diagram.**

A dry gas consists of mainly methane with some intermediate hydrocarbons. The term dry gas relates to the fact that the gas does not form a liquid at surface conditions (typically 60°F and 14.7 psi) due to the absence of heavier hydrocarbons. Referring to the phase diagram, from the initial reservoir conditions (A), pressure will decrease (B) as production commences. Note, for a dry gas the separator conditions would be to the right of the dew-point line (not located in the two phase region as pictured). Consequently, as the dew-point line is never intersected, no condensation of liquids occurs at all conditions. This thesis will only concentrate on dry gas reservoirs.

A reservoir fluid is termed a wet gas due to the formation of a liquid at separator conditions. The pressure reduction in the reservoir due to production does not result in the formation of a liquid in the reservoir (A to B). However, the pressure and temperature reduction once at separator conditions is sufficient for condensation of the heavier hydrocarbons (B to separator). Consequently, a hydrocarbon liquid exists at surface/separator conditions, hence the term ‘wet’.

Retrograde gas is best described with the aid of the phase diagram (Figure 2.8). At initial reservoir conditions, the fluid is in a gaseous state (1). However as pressure is reduced through production (with constant temperature in the reservoir), the retrograde gas exhibits a dew point (2). With further pressure reduction, liquid condenses from the gas to form a free liquid (3) in the reservoir (liquid drop-out). This liquid is usually immobile and cannot be produced.

Gas reservoirs exist in two forms, volumetric and water-drive gas reservoirs. A volumetric gas reservoir is completely enclosed with no external pressure support. Using the volumetric method for reserves calculation, the gas recovery equation is given by

$$G_p = 43{,}560\ A\ h\ \phi\ (1 - S_{wi}) \left(\frac{1}{B_{gi}} - \frac{1}{B_{ga}}\right) \tag{2.2}$$

where $G_p$ = gas produced (scf)

$A$ = area of reservoir (acres)

$h$ = average reservoir thickness (ft)

$\varphi$ = porosity

$S_{wi}$ = initial water saturation

$B_{gi}$ = initial gas formation volume factor ($ft^3$/scf)

$B_{ga}$ = gas formation volume factor evaluated at abandonment conditions ($ft^3$/scf)

The gas formation volume factor ($B_g$) is defined as the volume (v) occupied by *n* moles of gas at a specified temperature and pressure divided by the volume occupied by the same mass of gas at standard conditions ($v_{sc}$).

$$B_g = \frac{V}{V_{sc}} \tag{2.3}$$

The volume of *n* moles of gas at a specified temperature is obtained from the real gas law.

$$V = \frac{znRT}{p} \tag{2.4}$$

where $z$ = compressibility factor

n = number of moles

$R$ = universal gas constant

$T$ = temperature

$p$ = pressure

At standard conditions (sc), the volume of the same number of moles of the gas is

$$V_{sc} = \frac{z_{sc} nRT_{sc}}{p_{sc}} \tag{2.5}$$

The gas formation volume factor is subsequently

$$B_g = \frac{V}{V_{sc}} = \frac{\frac{znRT}{p}}{\frac{z_{sc}nRT_{sc}}{p_{sc}}} = \frac{zTp_{sc}}{z_{sc}T_{sc}p} \quad (2.6)$$

For isothermal conditions (an assumption made for hydrocarbon reservoirs), it can be seen from Equation 2.6 that the formation volume factor is a function of reservoir pressure only. It follows that, in a volumetric gas reservoir, the recovery efficiency is a function of the formation volume factor at abandonment conditions, and hence is a function of abandonment pressure.

This can also be demonstrated graphically using material balance. Again, a volumetric reservoir infers that there is insignificant water influx into the reservoir. Subsequently, the volume occupied by hydrocarbons remains unchanged during depletion. An expression for hydrocarbon pore volume (HCPV) can be obtained from equation 2.7.

$$HCPV = V\phi(1 - S_{wc}) = G/E_i \quad (2.7)$$

where *G* = gas volume initially in place expressed at standard conditions (sc)

*E* = gas expansion factor (= $1/B_g$)

The material balance for a given volume of production, $G_p$, and subsequent drop in average reservoir pressure is

$$Production\ (sc) = OGIP\ (sc) - Unproduced\ Gas\ (sc) \quad (2.8)$$

$$G_p = G - (HCPV)E \quad (2.9)$$

$$G_p = G - \frac{G}{E_i}E \quad (2.10)$$

which can be expressed as

$$\frac{p}{Z} = \frac{p_i}{Z_i}\left(1 - \frac{G_p}{G}\right) \quad (2.11)$$

using

$$E = 35.37\frac{p}{zT} \quad (2.12)$$

Equation 2.11 demonstrates that there is a linear relationship between p/Z and the recovery efficiency $G_p/G$, as well as cumulative gas production $G_p$. This is demonstrated graphically in Figure 2.9, whereby a straight line through successive measurements of pressure and gas compressibility (black dots) can be extrapolated to determine the OGIP. It can be seen from this graph that the

lower the abandonment pressure, the greater the gas recovery (Gp). The abandonment pressure is dictated by both technical and economic criteria. The abandonment pressure is greatly influenced by the nature of the gas contract, be it gas sold at a specified rate or constant surface pressure (pressure at the delivery point) (L. Dake 2001). Abandonment pressure has been reached once this specified rate or surface pressure can no longer be sustained. Recovery can be enhanced by producing the reservoir at lower pressures with the addition of compression at the surface. The increase in gas recovery naturally has to compensate for this increase in capital and operating costs. Recovery efficiencies of the order of 80 – 90% of the OGIP are common for volumetric gas reservoirs (Ahmed 2000).

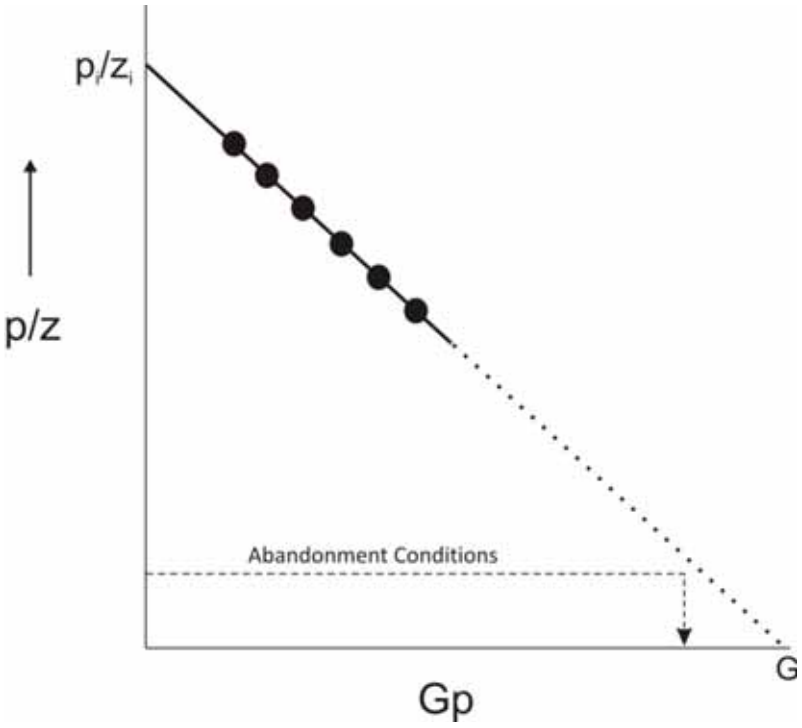


**Figure 2.9: p/Z versus Gp plot for a volumetric reservoir, indicating the linear relationship between p/Z and Gp.**

Unlike a volumetric gas reservoir, the recovery efficiency of a water-drive gas reservoir is not solely dependent upon the lowest abandonment pressure obtainable. The addition of a water-drive to a gas reservoir results in a reduction in ultimate gas recovery for two reasons, pressure support and residual gas trapping.

To demonstrate the negative effect of aquifer influx on pressure maintenance and hence gas recovery, the material balance method is again used. Gas production in a water-drive gas recovery reservoir causes a pressure drop in the reservoir. This pressure drop leads to an expansion of the

adjacent aquifer, leading to the influx of water into the gas bearing formation. This influx must be accounted for in the material balance equation,

$$Production\ (sc) = OGIP\ (sc) - \ Unproduced\ Gas\ (sc) \tag{2.8}$$

$$G_p = G - \left(\frac{G}{E_i} - W_e\right) E \tag{2.13}$$

where $W_e$ is the cumulative volume of water influx resulting from the pressure drop. This influx of water in turn causes a reduction in the hydrocarbon pore volume. This equation assumes no difference in water volumes at both surface and reservoir conditions, and ignores connate water expansion and pore volume reduction.

Equation 2.14 can be transformed using equation 2.12,

$$\frac{p}{Z} = \frac{p_i}{Z_i}\left(1 - \frac{G_p}{G}\right)/\left(1 - \frac{W_e E_i}{G}\right) \tag{2.14}$$

where $W_eE_i$ / G represents the fraction of the initial hydrocarbon pore volume flooded by water, and is always less than unity. Comparison of Equation 2.14 with Equation 2.10 indicates that for an equivalent volume of gas produced, reservoir pressure is maintained at a higher level when a water-drive is present. A typical p/Z vs. $G_p$/G plot is shown in Figure 2.10. The points, A, B and C are indicative of the size, and hence strength of the aquifer showing that as the size of the aquifer increases the degree of pressure maintenance is enhanced. The circles featured on Figure 2.10 represent the maximum achievable gas recovery, which is a strong function of reservoir pressure. As will be described later, the immiscible displacement of one fluid by another does not result in 100% displacement efficiency. A residual saturation of the displaced fluid remains behind the displacement front. This residual gas saturation is largely independent of the pressure at which the gas is trapped (L. Dake 2001). Applying the equation of state (Equation 2.4) to the trapped, or residual, gas saturation gives

$$\frac{p}{Z} S_{gr} = nRT \tag{2.15}$$

and with residual gas saturation being independent of pressure, for isothermal conditions

$$n\ \alpha\ \frac{p}{Z} \tag{2.16}$$

Therefore, at higher abandonment pressures, a greater quantity of natural gas is trapped.

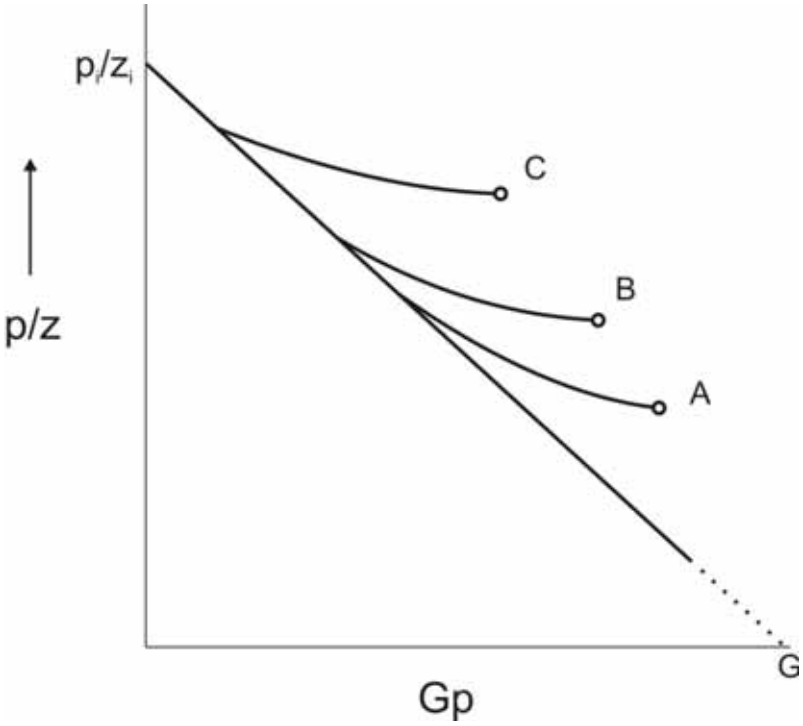


**Figure 2.10: p/Z versus Gp graph for a gas reservoir with varying strength water-drives.**

As mentioned briefly, the immiscible displacement of one fluid (i.e. natural gas) by another (i.e. water) results in a displacement efficiency less than 100%. The influx of the aquifer due to gas production results in the trapping of natural gas, introducing a residual gas saturation. This residual gas saturation is immobile, leaving a volume of gas unable to be produced, with the exact volume determined by the pressure at which it was trapped. Whilst not completely understood, the trapping of fluids is known to depend on the pore structure, fluid/rock interactions related to wettability, and fluid/fluid interactions (Green & Willhite 1998). Mathematical models have been unable to describe the phenomenon of phase trapping in porous media, however there are models that partly describe the processes involved in phase trapping, including the Jamin effect and the pore doublet model.

The Jamin effect describes the trapping and mobilisation of a phase in a singular capillary (Bethel & Calhoun 1953; Taber 1969; Muskat 1981). Consider the situation shown in Figure 2.11. This figure depicts a situation where a gas droplet is contacted on both sides by water and is static. To initiate flow, the static pressure difference at points A and B, $p_B - p_A$, must be overcome. The pressure difference required to overcome this static pressure difference can be quite high. Obviously, if this pressure difference cannot be overcome, the gas droplet will remain static forming a residual saturation.

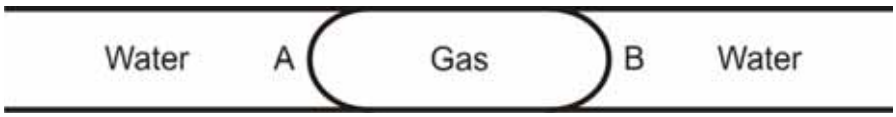


**Figure 2.11: Schematic of gas trapping in a singular capillary.**

The pore doublet model (Stegemeier 1977; Willhite 1986), which considers flow through two connected parallel capillaries, is shown in Figure 2.12. This model introduces the concept of differential flows in multiple flow channels, and aids in the description of how phases become isolated and trapped in porous media. The model describes the displacement of oil (assumed the non-wetting fluid) by water (assumed the wetting fluid), but the model can also be applied to the displacement of gas by water. The model depicts water displacing oil from two pores with differing radii. Oil will be trapped if the displacement proceeds faster in one pore, and if the pressure difference between points A and B is insufficient to displace the isolated oil drop with the slower displacement rate. From the pore doublet model, it has been shown that displacement of oil by water will occur primarily in the smaller pore, with residual trapping of oil occurring in the larger pore once the water has reached point B (Willhite 1986). In a gas-water environment, the gas is assumed to be the non-wetting fluid.

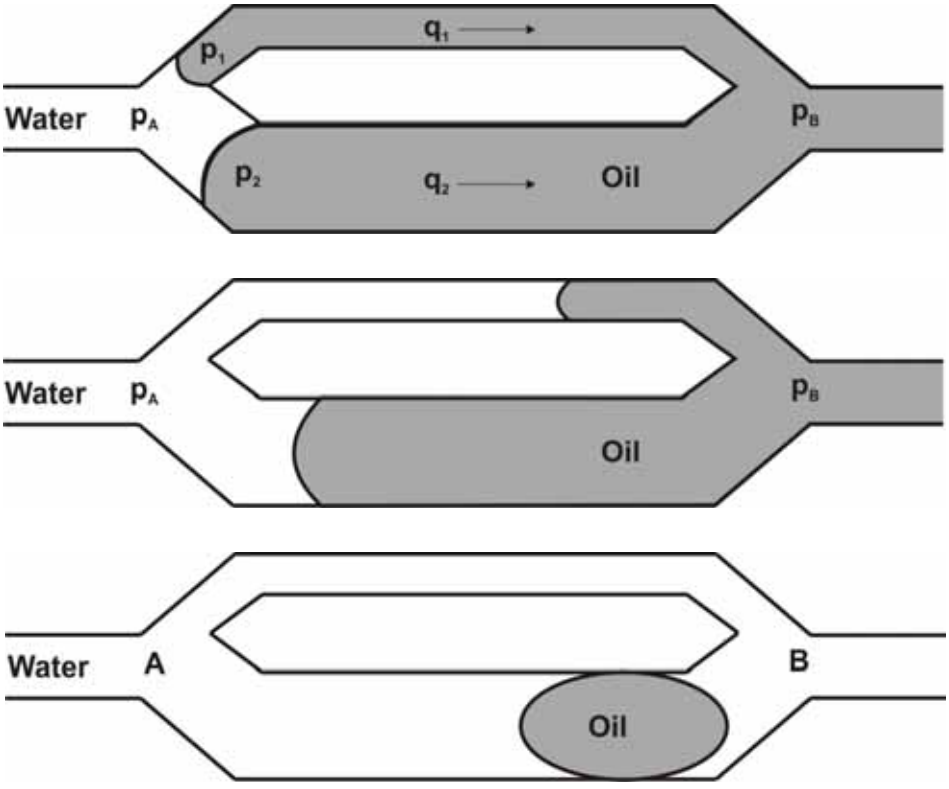


**Figure 2.12: Schematic of oil trapping in a pore doublet model**

Numerous studies have been conducted on residual hydrocarbon saturations through the imbibition of water, however the majority of studies have focused on residual oil saturations. A renewed interest in residual gas saturation has occurred with the rapidly increasing attention to carbon capture and storage (CCS) (Flett et al. 2004; Kumar et al. 2005; Spiteri et al. 2005; Juanes et al. 2006; Ghomian et al. 2008; Nattwongasem & Jessen 2009; Nghiem et al. 2009). Residual trapping is a relatively fast and effective method of $CO_2$ immobilisation. The permanent trapping of injected $CO_2$ is a primary concern in carbon storage projects, and so quantifying the volumes of $CO_2$ able to be residually trapped and the factors affecting this trapping is important.

Experimental studies have been performed in an attempt to understand the mechanisms of gas trapping. Geffen *et al* (1952) found that residual gas saturations measured under laboratory conditions corresponded to the residual gas saturations found in the field. The results of laboratory studies could therefore be applied to much larger scales (i.e. field scale) confidently. Residual gas saturations were found to be independent of pressure, temperature and the flooding rate (Geffen et al. 1952).

Crowell *et al* (1966) proposed that a relationship exists between residual gas saturation and initial gas saturation, with Land (1968) developing an empirical relationship between the initial ($S_{gi}$) and trapped ($S_{gt}$) gas saturations.

$$C = \frac{1}{S_{gt}^*} - \frac{1}{S_{gi}^*} \tag{2.17}$$

where *C* is Land's (1968) trapping constant which is a characteristic of the formation. Land's equation uses normalised saturations, denoted by the superscript (*). The normalised saturations refer to the saturation space that does not contain irreducible water ($S_{wir}$), and is calculated as follows

$$S_w^* = \frac{S_w - S_{wir}}{1 - S_{wir}} \tag{2.18}$$

$$S_g^* = \frac{S_g}{1 - S_{wir}} \tag{2.19}$$

Numerous attempts at correlating residual gas saturation with reservoir characteristics have been performed (Chierici et al. 1963; Katz et al. 1966; D. Keelan & Pugh 1975; D.K. Keelan 1976; McKay 1977; Delclaud 1991; Jerauld 1997; Suzanne et al. 2003; Ding & Kantzas 2004). Most attempts at seeking a correlation of residual gas saturation with permeability have failed, although Keelan (1976) concluded in one study that a slight increase in residual gas saturation occurred with decreasing permeability. There has been mixed success in showing a correlation between porosity and residual

gas saturation. Chierici *et al* (1963) could not identify any correlation between porosity and residual gas saturation. Other studies have identified a correlation between the two variables with residual gas saturations increasing as porosity decreases (Katz et al. 1966; D. Keelan & Pugh 1975; McKay 1977; Jerauld 1997); however these trends have only been of a very general nature. Definitive, consistent trends between reservoir characteristics and residual gas saturations have been elusive and this highlights the individual nature at which residual gas saturations need to be determined.

Most importantly, it has been experimentally determined that residual gas saturations vary from 15% up to 50% (Geffen et al. 1952; Chierici et al. 1963; Katz et al. 1966; D. Keelan & Pugh 1975). This number can be higher in carbonate reservoirs, as shown by Keelan and Paugh (1975). Consequently, this can lead to substantial volumes of natural gas remaining in the reservoir and subsequently provides a significant incentive to find methods which will limit the influx of the aquifer and reduce these trapped gas volumes.

Combining these two processes (pressure maintenance and residual trapping), the recovery efficiency possible in water-drive gas reservoirs is typically much lower than that possible in volumetric reservoirs. Typical recovery efficiencies range from 50 – 80% of the OGIP, highlighting the considerable prize that can be gained if recovery can be enhanced (Ahmed 2000).

One benefit of a water-drive is the enhanced well deliverability. From Darcy's law (2.20), it can be seen that flow rate is proportional to pressure differential. Maintaining reservoir pressure enables a specified flow rate to be maintained for a longer period. Alternatively, if a constant production pressure scheme is implemented, higher production rates will result earlier on in the life of the field. Whether this is beneficial towards the production of the field is determined by the economics of the project (net present value (NPV) versus ultimate gas recovery) as well as contractual requirements.

$$u = -\frac{k}{\mu}\frac{dp}{dl} \tag{2.20}$$

where $u$ = Volumetric rate (Darcy velocity) (cm/sec)

$k$ = permeability (Darcy)

$\mu$ = viscosity (cp)

$p$ = pressure (atm)

$l$ = length (cm)

## 2.3 Enhanced Gas Recovery

An important conclusion from the theory of natural gas reservoirs with an associated water drive is that any technique that will retard the influx of the aquifer and/or reduce reservoir pressure will

lead to an increase in natural gas recovery. Complete aquifer retardation in most cases would be preferred, however this has not yet been practically achieved. Pressure reduction has generally been the more practical option. This has been achieved by either accelerated gas production or co-production of gas and water.

### 2.3.1 Accelerated Gas Production

If the size of the aquifer is of the same order of magnitude as the reservoir, then the following simple model can be used to determine the cumulative amount of water influx.

$$W_e = c_t W \Delta p \tag{2.21}$$

where $c_t$ = total aquifer compressibility

$W$ = total volume of water

$\Delta p$ = pressure drop at the original reservoir-aquifer boundary

As the aquifer size is relatively small, this model assumes that a pressure drop is instantaneously transmitted throughout the entire reservoir-aquifer system. The p/Z vs. Gp/G plot would not however differ too much from the volumetric depletion plot (straight line plot) of Figure 2.9.

However, with a larger aquifer volume, the instantaneous response of the aquifer to the start of gas production does not occur. Consequently, there is a time lag between the start of production and full aquifer response. It is this time lag that the accelerated gas production method aims to exploit. The process is quite straightforward, involving the production of natural gas at high rates prior to the pressure transient reaching the aquifer. Once the pressure transient has reached the aquifer, the aquifer will advance into the gas reservoir, limiting the expansion of gas (i.e. reduce pressure reduction). The high gas withdrawal rates enable greater reservoir pressure reduction, thereby reducing the number of moles of gas remaining in the reservoir. An indication of the degree of influence production rates can have on ultimate gas recovery is highlighted in a study by Agarwal *et al* (1965). Figure 2.13 is modified from the Agarwal *et al* study (1965), displaying the effect of production rates on the recovery of natural gas on a p/Z versus $G_p$ plot. A greater production rate, and therefore a greater pressure drawdown can result in substantially improved recovery.

**Figure 2.13: p/Z vs cumulative gas production ($G_p$) plot indicating the effect of variable production rates on the recovery of natural gas under water-drive conditions (modified from Agarwal et al. 1965).**

Ideally one would aim to produce the reservoir at as high a rate as possible. A number of factors can however make this an unfeasible field development option. Firstly, the contractual requirements usually dictate that gas is to be supplied at either a constant rate or at a constant surface pressure. A typical gas production schedule is given in Figure 2.14. This schedule can be divided into three parts, the build-up ($t_1$), plateau production ($t_2$) and decline periods ($t_3$). Accelerated gas production would result in gas volumes produced exceeding the required contractual volumes leading to a surplus of gas at the surface which would need to be stored or sold to a separate contract. Furthermore, unless planned for, accelerated production could compromise the duration of plateau production, potentially compromising the operator's ability to meet contractual obligations.

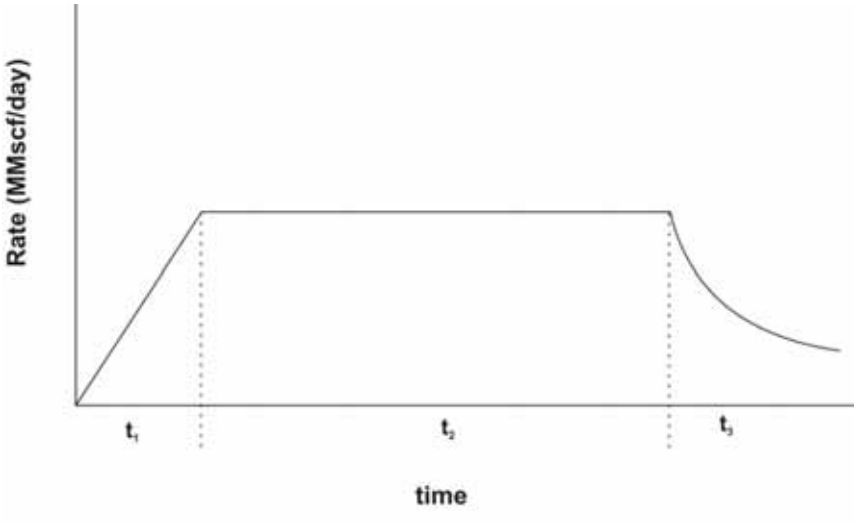


**Figure 2.14: Typical gas field development rate-time profile when under contractual obligations**

Accelerated gas production can also lead to operational problems such as water coning and sand production. Coning occurs when, locally around the production well, viscous forces at the fluid interface, induced by production, are greater than gravity which acts to stabilise the fluid interface. The fluid interface becomes unstable, and, in the case of gas-water environment, water is drawn up towards the production well, as depicted in Figure 2.15. This can significantly impact on sweep efficiency, reducing the recovery of natural gas considerably. As this phenomenon is induced by production, there exists a critical production rate whereby above this rate, viscous forces will exceed gravity forces, leading to the formation of coning. If accelerated production is initiated, then there is a substantial increase in the chance that the coning of water will occur, thereby potentially offsetting the benefits that accelerated production has for ultimate gas recovery.

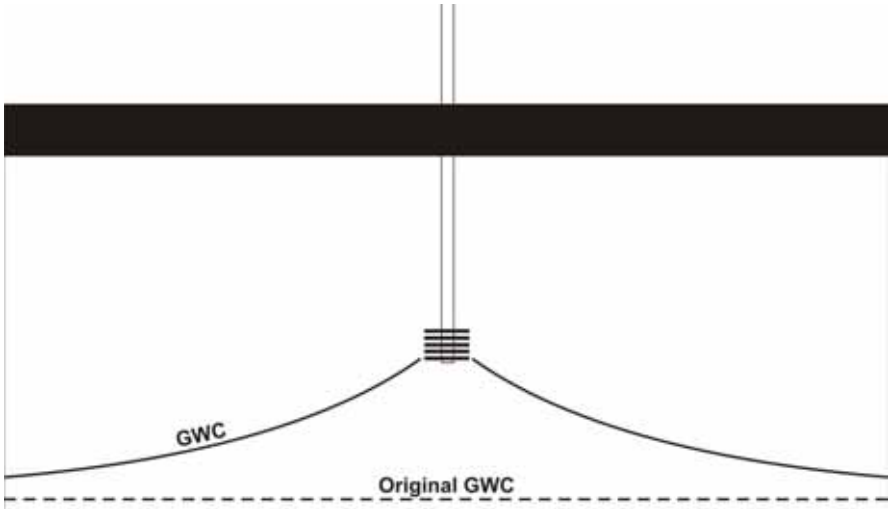


**Figure 2.15: Schematic of the coning of water due to instability at the GWC**

Other operational issues exist with attempting to accelerate gas production. Factors such as surface facilities, type of wells, and number of wells will have a direct impact on the maximum production

rate possible. The facilities, both subsurface and surface, are typically designed based upon the specified plateau production rate, and so the ability to increase production rates would be limited.

The successful field application of accelerating gas production in water-drive reservoirs has been reported (Lutes et al. 1977; Brinkman 1981; Moltz 1993; T. Brady 2002; Cook 2005). As well as being applied to dry gas reservoirs, accelerated gas production has also been applied to oil reservoirs with large gas caps, typically following the economic recovery of the oil leg. One successful application of accelerated production in a dry gas reservoir occurred in the Katy field (Lutes et al. 1977). OGIP in this field totalled 330 Bcf. Small scale gas production and gas cycling operations occurred until 1969 when an accelerated blowdown operation began. Prior to the blowdown operation, recovery had totalled 151 Bcf of gas, with reservoir pressure dropping from 3,303 psi to 2,830 psi. During the blowdown operation, the production rate was ramped up from under 15 MMscf/day prior to the blowdown operation to a maximum average of 97 MMscf/day during 1970. The reserves to production ratio (R/P) was reduced from 15 to 1.5. Reservoir pressure was able to be reduced to an average of 1,100 psi by 1972 prior to the watering out of the production wells and subsequent increase in reservoir pressure due to the aquifer influx. Ultimate gas recovery amounted to 242 Bcf (73.3% OGIP), with the blowdown operation achieving an incremental gas recovery of 91 Bcf of gas. This was estimated to be 28 Bcf greater than if production had continued at a R/P ratio of 15.

### 2.3.2 Co-production of Gas and Water

The co-production technique involves the production of both gas and water. This technique aims to both reduce the strength of the aquifer, limiting the degree of influx into the reservoir as well as reduce reservoir pressure. This technique can be performed at all stages of the field's lifecycle.

If initiated at the start of gas production, this technique aims to limit influx of the aquifer into the gas zone by placing water producing wells into the aquifer. This aims to reduce the pressure gradient induced by gas production, therefore limiting the influx of the aquifer. The limitation of the influx of the aquifer will result in the reduction of residually trapped gas. The reduction of the reservoir pressure will subsequently allow for a greater number of moles of gas to be produced.

If production has already led to the influx of the aquifer and subsequent watering out of the production wells, the production of water can be initiated to reduce reservoir pressure and re-mobilise trapped gas. Experimental studies have shown that the gas saturation required to re-mobilise the trapped gas is not equal to the trapped gas saturation (Firoozabadi et al. 1987; Fishlock et al. 1988) and that gas saturation has to increase above this trapped gas saturation before remobilisation will occur. Pressure depletion causes the expansion of gas which increases the gas

saturation. A laboratory study by Fishlock et at (1988) investigated the effect of pressure reduction using sandstone cores with permeabilities of 1,280 mD and 240 mD respectively. After waterflooding, residual gas saturations were 0.35 (1,280 mD) and 0.39 (240 mD). During the subsequent blowdown phase, it was found that the trapped gas does not immediately become mobile. Results showed that, for the 1,280 mD core, a critical gas saturation (the minimum gas saturation where remobilisation occurred) of 0.49 was required before remobilisation was observed. A critical gas saturation of 0.47 was observed for the 240 mD core. These results demonstrated that the increase in gas saturation that is required to remobilise the trapped gas can be quite substantial.

Field examples of the co-production technique have been published, with results showing varied but overall positive results from field implementation (Boyd et al. 1982; Chesney et al. 1982; Rogers 1984; Randolph & Wible 1986; Ancell & Manhart 1987; Cagle 1990). Chesney et al (1982) and Cagle (1990) reported results of the use of the co-production technique in the North Alazan H-21 gas reservoir, Texas, which was under the influence of a moderately strong water-drive. The initial focus was on the development and production of the oil leg. Following the oil production, accelerated gas production was initiated in order to "out-run" the aquifer. It was calculated that 44 billion cubic feet (Bcf) of gas was trapped in the invaded zones at an abandonment pressure of 2,200 psia (62% of the original reservoir pressure). Studies showed that with a water withdrawal rate of 30,000 barrels per day, reservoir pressure could be reduced to 500 psi, producing an incremental 22 Bcf of natural gas. Water production began in 1980 with the target withdrawal rate of 30,000 B/D being reached by mid 1981. As of the end of 1988, the co-production project had recovered an additional 5.7 Bcf of gas, 340 Mstb of oil and 90 MMbbl of water, with the project deemed an economical and technical success (note that development of the field had not ended at the end of 1988 which is the year of the last paper).

Boyd *et al* (1982) published results of a co-production project implemented in the Double Bayou field, Texas. Initial production of the field began in 1948, with primary production ceasing around 1974. Primary production recovered 19.6 Bcf (79%) of the 24.8 Bcf of gas originally in place. Studies indicated that 50% of the trapped gas could be potentially recovered with a reservoir pressure reduction of 2100 psia (3100 to 1000 psia). Initially one water production well was considered sufficient. However, the strength of the aquifer was underestimated. Consequently, two production wells were brought online to achieve the desired pressure reduction. Although production totals are not given in this publication, the success of the de-watering project is verified with remobilisation and subsequent production of trapped gas occurring. From the data given, production from the two

wells peaked at 1.1 MMscf/day in September 1981, with rates stabilising at 750 Mscf/day in the last quarter of 1981.

A key assumption in the field case publications is that residual gas saturation is independent of pressure. The implication of this assumption is that the initial trapped gas saturation is identical to the remobilisation saturation when pressure is decreased. Therefore once reservoir pressure has been reduced below the entrapment pressure (pressure at which the gas was initially trapped) and the gas saturation has expanded above the initial trapped gas saturation, remobilisation will instantly occur. However, as shown by Firoozabadi *et al* (1987) and Fishlock *et al* (1988), the remobilisation saturation is not necessarily equal to the initial trapped gas saturation. Firoozabadi *et al* (1987) suggest that this phenomenon could explain why the theoretical incremental gas recoveries have not been consistent with field results.

## 2.4 Laboratory and Numerical Studies into $CO_2$ EGR

The injection of $CO_2$ to enhance natural gas recovery is not an entirely new concept, with a small number of studies having been published (C.M. Oldenburg & Benson 2001; Clemens & Wit 2002; Mamora & Seo 2002; Jikich et al. 2003; C.M. Oldenburg 2003; Al-Hashami et al. 2005; Turta et al. 2007; Sim et al. 2008; Secklehner et al. 2010), in addition to two known field trials having been implemented (Papay 1999a; Papay 1999b; van der Meer et al. 2005). Numerical simulation and laboratory experiments have been performed, however all studies have assumed volumetric depletion conditions (no influx of water). The premise behind the research conducted on the potential of injecting $CO_2$ into volumetric gas reservoirs is due to both a primary recovery efficiency of less than 100% as well as the favourable fluid properties between $CO_2$ and $CH_4$. Although primary recovery efficiencies for volumetric gas reservoirs can reach 80 – 90% of the OGIP, the remaining 10 – 20% of gas in place can amount to significant volumes of gas. The prize could therefore warrant the cost of implementation. Additionally, as previously shown, the contrasting fluid properties of $CO_2$ and $CH_4$ have the potential to displace $CH_4$ with minimal mixing.

An issue that is apparent from the notion of $CO_2$ injection into a volumetric gas reservoir is that reservoir pressure will be increased and not decreased. For the injection of $CO_2$ to be effective in increasing natural gas recovery, the displacement process has to be efficient with minimal mixing. The research conducted, both experimental and numerical, has focussed on the processes and parameters which influence the ability to maximise natural gas recovery whilst minimising the contamination of the gas with $CO_2$.

Experimental studies have been performed investigating the extent of mixing during gas-gas displacements, as well as the effect of gas solubility on the breakthrough of $CO_2$ and therefore the natural gas recovery efficiency.

Mamora and Seo (2002) conducted coreflood experiments and analytical modelling in order to understand the displacement of natural gas by $CO_2$ in a depleted carbonate porous medium. The experiment involved the injection of $CO_2$ into a 1 ft (length) by 1 in (diameter) carbonate core saturated with $CH_4$. This was carried out over a range of pressures (500 – 3000 psig) and temperatures (68°F - 140°F) encountered in the field. Seventeen runs in total were performed. $CH_4$ recovery was calculated once $CO_2$ was detected in the outlet stream (i.e. initial $CO_2$ breakthrough). Key results from the experiments were as follows:

- The displacement of methane by $CO_2$, whether $CO_2$ be at gas, liquid or supercritical states, was a very efficient process with relatively low dispersion coefficients of $CO_2$ in $CH_4$. Mamora and Seo's use of the term dispersion coefficient corresponds to the molecular diffusion coefficient, which describes the rate of mixing due to random molecular motion. Molecular diffusion in a gas is much greater than in a liquid. For instance, a molecular diffusion coefficient of gas is around $10^{-5}$ $m^2/s$ while in a liquid a coefficient of around $10^{-10}$ can be expected. Dispersion coefficients of 0.01 – 0.12 $cm^2/min$ were calculated ($1.67 \times 10^{-8}$ – $2.0 \times 10^{-7}$ $m^2/s$).
- $CH_4$ recovery at $CO_2$ breakthrough increased as temperature increased. Recovery efficiencies ranged from 73% - 85% for runs conducted at 20°C, 83% - 86% at 40°C, and 86% - 87% at 60°C.
- A 100% recovery efficiency of $CH_4$ was achieved at the end of each run (no limit on the production of $CO_2$).

Results from these experiments suggest that, at typical reservoir conditions, the mixing between $CO_2$ and $CH_4$ is low, as indicated by the small dispersion coefficients. This result is promising in showing that the displacement of $CH_4$ by $CO_2$ can occur with minimal mixing. Mamora and Seo (2002) state that $CH_4$ recovery increases with increasing temperature because, in their own words, the "sweep of $C_1$ increases as $CO_2$ becomes more supercritical (and thus more dense)" (Mamora and Seo, 2002: 4). This statement is confusing for two reasons. The first is that a fluid cannot become more supercritical, in the same way a gas cannot become more gas-like. Secondly, at a constant pressure, an increase in temperature will cause a fluid to become less dense, not more dense. An interesting result from their experiments was that complete recovery of $CH_4$ was achievable at the end of each run. This result suggests that the maximum recovery of $CH_4$ will be heavily dependent upon the

maximum concentration of $CO_2$ that can be tolerated in the production stream, which will be an economic rather than a technical criterion.

Researchers based at the Alberta Research Council (ARC) conducted two sets of experiments investigating gas-gas displacements. Turta *et al* (2007) conducted such experiments in Berea cores with dimensions of 30cm (length) by 4cm (diameter) at a pressure of 6,200 kPa (900 psi) and 70°C. The experiments involved the displacement of $CH_4$ by $CO_2$, nitrogen ($N_2$) and mixtures of $CO_2$ and $N_2$ (simulating flue gas). Experiments were conducted in the presence and absence of connate water. A summary of the key results is as follows:

- Displacement experiments on dry core (without connate water saturation) resulted in very similar $CH_4$ recovery efficiencies for displacements involving pure $CO_2$ (67%) and $N_2$ (69%), where recovery efficiency was measured at an injectant breakthrough limit of 1%.
- Recovery efficiencies for experiments involving pure $CO_2$ were greater in cores with an irreducible water saturation compared to the experiments conducted on dry cores. It is believed that the dissolution of $CO_2$ at the leading edge of the displacement front led to a slight delay in $CO_2$ breakthrough. Additionally, it was postulated that as water is the wetting fluid it will occupy the narrower flow paths and pore spaces leaving the larger channels open to the flow of gas.
- Displacement experiments involving the injection of flue gas (combustion exhaust gas) in the presence of an irreducible water saturation resulted in improved $CH_4$ recovery when compared to the use of pure $CO_2$. The flue gas contained 14% $CO_2$ and 86% $N_2$. Recovery efficiency involving flue gas injection was 66% at the 1% breakthrough limit of $N_2$ compared to 61% where pure $CO_2$ was injected. Note that the recovery efficiency for the flue gas experiment was calculated at a breakthrough limit of 1% $N_2$. Due to the different solubilities of the two components in the flue gas, $N_2$ reached the outlet first. The higher solubility of $CO_2$ in water caused the $CO_2$ to reach the outlet much later. The authors subsequently note that allowable concentrations of $N_2$ in the production stream (i.e. sales gas) are much greater than $CO_2$. Production of $CH_4$ could therefore occur until a $CO_2$ concentration limit has been reached, and not necessarily a $N_2$ limit. This could significantly increase the potential recovery of $CH_4$ using flue gas as an injectant as opposed to pure $CO_2$.

However, the conclusions presented in Turta *et al* (2007) this paper are not always consistent with the results presented. For instance, the recovery efficiencies for two cases involving the injection of pure $CO_2$ into a dry core amounted to 48% and 67% (at the 1% breakthrough limit). By comparison, for two cases involving the injection of pure $CO_2$ in the presence of an irreducible water saturation, recovery efficiencies were 61% and 62%. The greater recovery for one of the dry core tests

contradicts the conclusion of greater recovery when in the presence of an irreducible water saturation. A difference in the density and/or viscosity could have impacted on the stability of the displacement and therefore caused the variations in the results, however the properties are almost identical. No explanation is however given for this discrepancy.

Despite the weaknesses, the underlying conclusion is still important. Namely the solubility of $CO_2$ in formation water could be an important factor in any potential EGR operation by delaying $CO_2$ breakthrough and therefore increasing $CH_4$ recovery.

Sim *et al* (2008) conducted another set of experiments with essentially the same experimental setup. The difference in this study was the use of a 2 metre long sandpack (4 cm diameter) instead of the 1 foot Berea core used in the study by Turta *et al* (2007). Again, injection fluids consisted of pure $CO_2$ and $N_2$ as well as a flue gas containing 14% $CO_2$ and 86% $N_2$. All displacement tests were conducted in the presence of an irreducible water saturation. Factors such as displacement gas composition, displacement rate and pressure were systematically varied in order to test their relationship on displacement efficiency. Numerical simulation was used to determine the relationship between the variables. A summary of the results is as follows:

- Uncontaminated $CH_4$ recovery increased as a result of increasing pressure. Breakthrough of the injection fluid occurred earlier at lower pressures, with the mixing zone (defined as the region containing 1% - 99% $CH_4$ in this study) being wider than the mixing zone at higher pressures. Sim et al conclude that this result is consistent with the finding of Sigmund (1976) that the diffusion coefficient, and hence degree of mixing, is reduced with increasing pressure.
- Tests involving variable displacement flow rates indicated that displacement efficiency was enhanced with a higher displacement rate. The authors again suggest that this result is further evidence that molecular diffusion is a significant factor in gas-gas displacements. With a lower displacement rate, the residence time of the gases is longer, allowing for greater mixing.
- Injection gas composition again showed the benefits of $CO_2$ solubility in formation water. In this instance, comparisons of pure $CO_2$ and $N_2$ were made, with displacement efficiency under $CO_2$ injection being considerably higher than $N_2$ at breakthrough. Tests involving the injection of flue gas showed equivalent results to those presented in the experiments of Turta *et al* (2007).

These results show that the effect of molecular diffusion could be a significant factor in the displacement of $CH_4$ by $CO_2$ when a breakthrough limit is applied.

All numerical simulation studies have involved the injection of $CO_2$ into a volumetric reservoir. Again, the primary concern with the injection of $CO_2$ into a gas reservoir is the contamination of the natural gas, potentially influencing contractual obligations and devaluing the natural gas. Numerical studies have therefore focused on factors which influence the degree of mixing between the $CO_2$ and natural gas, directly influencing the ability to produce uncontaminated natural gas.

Al-Hashami *et al* (2005) studied the effect of both the diffusion coefficient and the solubility of $CO_2$. The authors noted that as part of the reservoir simulation model, a value for the diffusion coefficient is required however no such reliable data exists in the literature. Four diffusion coefficients (0, $10^{-4}$, $10^{-5}$, $10^{-6}$ $m^2/s$) were chosen as a sensitivity analysis regarding the breakthrough of $CO_2$ and hence decline in $CH_4$ production, assuming a constant production rate of 15 MMscf/day. The results of this study are as follows:

- Greater mixing between $CO_2$ and $CH_4$ occurred with larger diffusion coefficients ($10^{-4}$ $m^2/s$) leading to earlier $CO_2$ breakthrough.
- The difference in results between a diffusion coefficient of $10^{-6}$ $m^2/s$ and a coefficient of zero (no mixing) was minimal, indicating that for coefficients less than $10^{-6}$ $m^2/s$, mixing due to molecular diffusion can be ignored, with mixing entirely due to convective flow.
- A comparison of two simulations, where the dissolution of $CO_2$ was either allowed or disallowed, led to a disparity in the breakthrough time of $CO_2$. The enabling of dissolution led to the breakthrough of $CO_2$ being delayed by six months.

These results again show the influence both the diffusion coefficient and the solubility of $CO_2$ into formation waters can have on the breakthrough times of $CO_2$ and the associated natural gas recovery efficiency. Strangely, no change in incremental $CH_4$ recovery was noted with the delay in the breakthrough of $CO_2$ due to the dissolution in the formation water. This suggests that incremental recovery was not calculated based upon a specified $CO_2$ breakthrough limit.

The effect of heterogeneity was studied by Oldenburg et al (2001). Simulations were performed on a 2-D model representing the Rio Vista field in California. Two permeability scenarios were considered, the first being a homogeneous anisotropic permeability field. The second model involved a statistically generated permeability field. The conclusion drawn from the results of simulations performed indicate that injected $CO_2$ travels much faster in higher permeability layers, serving to accelerate the breakthrough of $CO_2$. It was noted that faster breakthrough times occurred for models with greater permeability variations.

The controllable factors have been investigated in an effort to maximise natural gas recovery by influencing the breakthrough times of $CO_2$. Factors investigated include the timing of $CO_2$ injection, injection rates and the type of injection well (vertical versus horizontal).

Al-Hashami et al (2005) investigated the effect of both the injection rate and the timing of injection. Two scenarios involving the timing of injection were studied. The first involved the injection of $CO_2$ at the commencement of $CH_4$ production to maintain reservoir pressure, while the second involved the injection of $CO_2$ after four years of natural gas production, when the specified production rate was unable to be maintained. For both cases, a producing $CO_2$ concentration limit of 10 mole percent was imposed. The effect of the injection rate was tested by varying the rate from 2 Mscf/day to 20 MMscf/day. The results were as follows:

- Delaying the injection of $CO_2$ by four years resulted in a 20% increase in $CH_4$ recovery at the $CO_2$ production limit. Delaying the injection resulted in a recovery efficiency of 86%, compared to 66% if injection was not delayed.
- The results for the variable rates were based upon ultimate recovery after 16 years, regardless of the producing $CO_2$ concentration. It was found that increasing the injection rate led to an increase in ultimate $CH_4$ recovery.

These results show the potentially significant impact the timing of $CO_2$ injection can have on the degree of mixing and therefore the natural gas recovery efficiency at a chosen $CO_2$ breakthrough limit. With respect to the results for the variable rates, it was noted by the authors that although high rates lead to an increase in ultimate $CH_4$ recovery, implementing higher rates has the potential to increase the degree of mixing between the two fluids.

Oldenburg et al (2001) also investigated the effect of the timing of $CO_2$ injection. Two scenarios were investigated. Both scenarios involved the injection of $CO_2$ after a period of primary production matching the historical production of the Rio Vista field. The first scenario involved the injection of $CO_2$ for a 10 year period (no $CH_4$ production) followed by the recommencement of $CH_4$ production for a further 10 year period with $CO_2$ injection ceasing once $CH_4$ production recommenced. The second scenario involved the simultaneous injection of $CO_2$ with production of $CH_4$ for a 20 year period following the period of primary production. For comparison, a reference case was performed where primary production occurred without the injection of $CO_2$. $CO_2$ injection occurs at a specified rate, based upon the output of $CO_2$ from a gas-fired power plant. The results were as follows:

- The continuation of primary production in the reference case for an additional 20 year period resulted in an additional 9.4 Bcf of $CH_4$ being produced.

- In comparison, incremental $CH_4$ recovery for the first scenario amounted to 51 Bcf, while for the second scenario an additional 73 Bcf of $CH_4$ was produced.

The direct comparison of these results is difficult however. Each scenario had different production strategies implemented. Scenario one involved production at a constant rate, while scenario two involved production at a constant pressure. Additionally, the production times differed (10 years versus 20 years). The authors state that for scenario one the production of 99% pure $CH_4$ can occur for five years following $CO_2$ injection. For scenario two, production of 99% pure $CH_4$ also occurs for five years, but at a production rate that is considerably less than for scenario one. Comparisons are difficult as recovery is based upon a timeframe and not upon a maximum $CO_2$ concentration. Additionally, the timeframe is not consistent, with production occurring for 10 years in scenario one and 20 years in scenario two. The one conclusion that can be made is that the injection of $CO_2$ did increase $CH_4$ recovery over that achievable under conventional primary depletion.

Clemens and Wit (2002) conducted a simulation study investigating the effect of $CO_2$ injection at various stages of depletion for an example reservoir consisting of two compartments. A base case scenario involved 22 years of historical production (1978 – 2000) in addition to four years of forecasted production (2000 – 2004). At the end of the forecasted period (2004) a compressor was installed to reduce the tubing head pressure of the production well to increase production rates. Four scenarios pertaining to the enhancement of gas recovery (in conjunction with $CO_2$ storage) were modelled, which involved:

- Scenario 1: $CO_2$ injection at the same time as installation of the compressor (2004).
- Scenario 2: $CO_2$ injection earlier than the installation of the compressor (1999).
- Scenario 3: $CO_2$ injection early for pressure maintenance (1985).
- Scenario 4: $CO_2$ injection at the end of conventional gas production.

Results were compared to a conventional primary depletion case. The results of these simulations were as follows:

- Incremental gas recovery was achieved in three of the four cases, with greater incremental recovery as $CO_2$ injection was delayed.
- Case 4 achieved the greatest incremental recovery (706 $MMm^3$), followed by Case 1 (390 $MMm^3$) and Case 2 (260 $MMm^3$).
- The early injection of $CO_2$ for the purposes of pressure maintenance, Case 3, resulted in a reduction in ultimate gas recovery (-320 $MMm^3$) compared to the conventional primary depletion case.

Interestingly, no indication of a maximum $CO_2$ production limit is given, only an economic limit on $CH_4$ production (30,000 $m^3$/day) is mentioned, however this is for the base case (primary depletion) only. It is not clear if this limit applies to the other cases as well. The authors note that the early injection of $CO_2$ decreases the recovery efficiency. The reason given is not due to a maximum producing $CO_2$ concentration having been reached but that the recovery in the second compartment (the reservoir is split into two compartments) is reduced due to the presence of a semi-sealing fault in this compartment. According to the authors, the presence of this semi-sealing fault reduces the gas recovery by $CO_2$ displacement compared with the base case of conventional primary depletion. With no limit placed on the producing $CO_2$ concentration, it is unclear as to why early $CO_2$ injection would result in a poorer sweep efficiency when compared to the other $CO_2$ injection cases, and why recovery would be lower than the primary depletion case. Therefore the general claim that the early injection of $CO_2$ will decrease cumulative gas recovery is hard to substantiate based upon these results. It is noted by the authors that $CO_2$ injection does result in enhanced deliverability of $CO_2$, which is beneficial especially in increasing recovery in the tail gas time period as indicated in Figure 2.14.

In addition to the timing of $CO_2$ injection, a study on carbon sequestration with EGR (CSEGR) by Jikich et al (2003) also focussed on the type of injection well (vertical versus horizontal). Two injection scenarios were considered, the first involving simultaneous $CO_2$ injection and $CH_4$ production at the beginning of the field operations. The second involved the commencement of $CO_2$ injection once primary $CH_4$ production had reached the economic limit, which equated to a recovery efficiency of 73% of the OGIP. A $CO_2$ concentration limit of 10% in the production stream was set for both scenarios.

Scenario one was compared against an equivalent case under primary depletion. Key results from this comparison are as follows:

- In scenario one, the $CO_2$ breakthrough limit was reached after 233 days.
- Ultimate gas recovery for scenario one (taken at the time of $CO_2$ breakthrough) amounted to 350 MMscf.
- Incremental recovery over the primary depletion case after 233 days amounted to 70 MMscf.
- Ultimate gas recovery for the primary depletion case amounted to 448 MMscf (73% of OGIP), which was taken after an economic production limit was reached.
- The use of horizontal wells was detrimental to cumulative gas production, with gas production decreasing as horizontal injector length increased.

These results clearly show that, when a limit on $CO_2$ production is employed, the early injection of $CO_2$ enhances deliverability due to the pressure maintenance, but decreases ultimate gas recovery when compared to conventional primary depletion. A constant injection pressure was employed in all simulations and so the use of horizontal wells corresponded to higher injection rates. Without any mention of if permeability heterogeneity was included in this model, it is therefore assumed that these higher rates resulted in greater mixing between the $CO_2$ and $CH_4$.

In the second scenario, the injection of $CO_2$ followed primary production once an average reservoir pressure of 150 psi had been reached. This occurred after 730 days. Key results from this scenario are as follows

- The time taken to reach the $CO_2$ breakthrough limit was 55 days for a horizontal well, and 134 days for a vertical well.
- $CO_2$ injection following primary production resulted in an incremental recovery of just 16 MMscf and 33 MMscf for the horizontal and vertical well cases respectively.

Although the increase is only moderate, delaying the injection of $CO_2$ did result in the enhancement of $CH_4$ recovery over the conventional primary depletion case. The authors comment that the early breakthrough of $CO_2$ in this scenario is a surprising development, given that $CO_2$ at reservoir conditions should result in a fluid more dense and viscous than $CH_4$. This comment itself is surprising considering the reservoir conditions at the commencement of $CO_2$ injection. Conventional primary depletion is stated to end once an average reservoir pressure of 150 psi is reached. At this pressure, and considering the reservoir temperature of 72 °F, the $CO_2$ density and viscosity are 19.613 kg/m$^3$ and 0.014897 cP respectively while $CH_4$ density and viscosity are 6.883 kg/m$^3$ and 0.011225 cP respectively. At these conditions, the difference in density and viscosity between $CO_2$ and $CH_4$ is minimal due to the fact that both fluids are in a gaseous state. Consequently, there is minimal benefit with respect to the fluid properties, and with mixing due to diffusion enhanced when the reservoir is at low pressure and the fluids are in their gaseous state, it is not surprising that $CO_2$ rapidly reaches the production well.

This study does however highlight the influence of operational factors on the stability and effectiveness of the displacement of natural gas by $CO_2$ when a $CO_2$ production limit is in place. The strong effect of the timing of injection is clearly shown. The early injection of $CO_2$ will maximise the favourable difference in fluid properties between $CO_2$ and $CH_4$ due to the higher pressure, as well as enhance well deliverability. The early contamination of the natural gas will however reduce ultimate recovery compared to that achievable under conventional primary depletion. Injection at

abandonment conditions will result in the least favourable fluid properties, however any additional production will result in incremental recovery being achieved.

## 2.5 Field Trials of $CO_2$ EGR

The only known field application of the injection of $CO_2$ for purely enhanced gas recovery purposes occurred in the Szintfeletti XVL reservoir in Hungary (Papay 1999a; Papay 1999b). Conventional gas production commenced in 1963 and continued for five years, with a recovery efficiency of 75% of the OGIP. Following production, the reservoir was converted into a gas storage facility for 10 years until 1977. At the completion of the use of the reservoir for gas storage, 19.6 $MMm^3$ of gas remained in place. An injection gas consisting of 81 mole percent $CO_2$ was subsequently injected in an effort to recover this remaining volume of gas. Strangely, the injection of the $CO_2$ rich gas occurred at the top of the structure, with production occurring at the flanks. Reservoir pressure at the commencement of $CO_2$ injection was only 45 bar, with $CO_2$ therefore in a gaseous state. However, density and viscosity differences would still be apparent, and injection into the top of the structure would result in an unfavourable displacement profile. Nevertheless, incremental recovery was achieved with a $CO_2$ breakthrough limit of 20% in effect. The injection of $CO_2$ increased gas recovery by 6.7 $MMm^3$, amounting to 34% of the gas which remained in place after the gas storage operation or 11.6% of the OGIP. Of note was the presence of a moderate strength aquifer, however with injection chosen at the top of the structure, remobilisation of trapped gas saturations was not an aim. The efficiency of the displacement of the free gas saturation was of primary concern. In that regard, 50% of the free gas volume was recovered through the injection of $CO_2$.

The K12-B project in the Dutch sector of the North Sea is the only other known field application investigating EGR through $CO_2$ injection (van der Meer et al. 2005). However, the primary focus of this project is not on $CO_2$ EGR, but on the sequestration of $CO_2$. The K12-B field was a producing natural gas field, with a relatively high $CO_2$ content of 13%. Subsequently, for this project the $CO_2$ was stripped and re-injected rather than venting to the atmosphere which was the procedure prior to commencement of the $CO_2$ injection project. With the K12-B field nearly depleted, the aim of the project was to investigate the feasibility of $CO_2$ injection and storage into a depleted gas field. Prior to the full-scale phase of $CO_2$ injection, a desktop feasibility study and a demonstration phase were required. As part of the demonstration phase, the potential to enhance gas recovery was tested through the injection of $CO_2$ through one production well into a nearly depleted compartment, with continued gas production from two wells. Injection into the nearly depleted compartment commenced at the start of 2005, however no results have been published on the influence of $CO_2$

injection in enhancing gas recovery and as such no comment can be made on whether this pilot was successful.

## 2.6 Summary

It has been shown in this review that any technique that will limit the influx of an aquifer and/or reduce reservoir pressure will enhance recovery in a water-drive gas reservoir. Current techniques in use are accelerated gas production and the co-production of water and gas. The injection of $CO_2$ to retard aquifer influx has been suggested as another method which could enhance gas recovery in water-drive gas reservoirs.

Although research has been conducted on EGR through the injection of $CO_2$, it has only focussed on the application in volumetric reservoirs. There is therefore a gap in the knowledge of the $CO_2$ EGR process when applied to a water-drive gas reservoir.

Fluid properties suggest that at typical reservoir condition, the stable displacement of $CH_4$ by $CO_2$ is possible, more so in a water-drive reservoir as compared to a volumetric reservoir due to the pressure maintenance supplied by the aquifer. Water-drive gas reservoirs generally have considerably lower recovery efficiencies compared to volumetric reservoirs, due to the processes described in this chapter. Consequently, there is considerable potential to enhance the recovery of natural gas through the injection of $CO_2$.

# CHAPTER 3

# 3 Geological $CO_2$ Storage Code Comparison Study

## 3.1 Introduction

Numerical simulation has played an important role for many years in evaluating the feasibility of oil and gas developments. Due to the many similarities between the modelling of these developments and $CO_2$ storage projects, traditional oil and gas numerical codes are now being used to study the sub-surface sequestration of $CO_2$.

However, despite the similarities with typical oil and gas numerical modelling, the primary fluid under consideration is now, of course, $CO_2$, and this does introduce a number of different physical and chemical processes that need to be considered. The Lawrence Berkeley National Laboratory (LBNL), recognising the growing use of what is essentially a non-standard application of traditional oil and gas numerical codes, initiated a code comparison study in 2001 to test the accuracy of such codes when attempting to model the various physical and chemical processes involved in $CO_2$ injection and storage operations (Pruess et al. 2001).

In total, eight problems were posed to address a wide range of processes involved in $CO_2$ injection into depleted gas reservoirs, oil reservoirs and saline aquifers. Three of these problems are particularly relevant to the topic of this thesis on $CO_2$ enhanced gas recovery in water-drive gas reservoirs. Two of the problems investigate advective and diffusive mixing of $CO_2$ and $CH_4$, while the third investigates the injection of $CO_2$ into a saline aquifer.

Various research groups took part in the code comparison study and there are many references to this work in the literature (Pruess et al. 2001; Pruess & Garcia 2002; Pruess et al. 2002; C.M. Oldenburg et al. 2003; Pruess 2004; Pruess & Garcia 2005). One report presenting the entire results of the study (Pruess et al. 2002) refers to results submitted by a team from Los Alamos National Laboratory (LANL) using Schlumberger's compositional numerical simulation code E300, which is the code being used to generate results for this thesis. Unfortunately these results have not been made public and so it is a logical first step to repeat the three problems referred to above to build up expertise whilst confirming the accuracy of the E300 code in modelling the enhancement of gas recovery in water-drive reservoirs through the injection of $CO_2$. The results obtained from the analyses of these three problems performed for this thesis using the E300 code are compared against the published results from the original code comparison study.

The list of study participants, and the numerical codes employed by each group is outlined in Table 3-1.

**Table 3-1: Participating organisations and the numerical codes employed in the code comparison study.**

| Participating Organisations | Numerical Code |
|---|---|
| Lawrence Berkeley National Laboratory (LBNL) | TOUGH2/ECO2, THOUGHREACT, and TOUGH-FLAC |
| University of Stuttgart | MUFTE_UG |
| CSIRO Petroleum | In-house version of TOUGH2ECO2 |
| Institut Francais du Pétrole (IFP) | SIMUSCOPP |
| Stanford University | Unnamed research code |
| Alberta Research Council (ARC) | GEM |
| Los Alamos National Laboratory (LANL) | FLOTRAN and ECLIPSE300 |
| Lawrence Livermore National Laboratory (LLNL) | NUFT |
| Industrial Research Limited (IRL) | In-house version of TOUGH2 and CHEM-TOUGH |
| Pacific Northwest National Laboratory (PNNL) | STOMP |

## 3.2 LBNL Code Comparison Study: Problem 1

In the first problem $CO_2$ and $CH_4$ are placed in a one-dimensional porous medium, as shown in Figure 3.1.

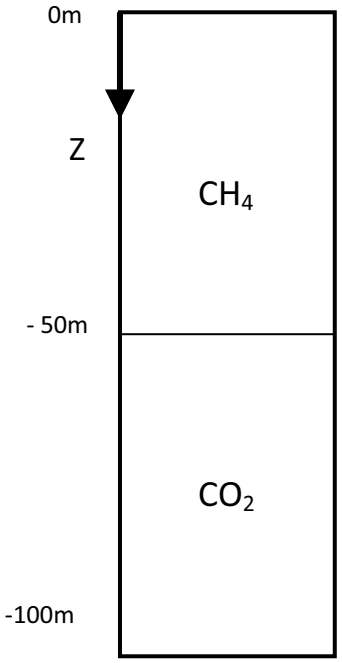


**Figure 3.1: Initial Fluid Distribution (Problem 1)**

**Table 3-2: Model Properties (Problem 1)**

| | |
|---|---|
| ***Rock and Fluid Properties*** | |
| Permeability | 10mD ($1x10^{-14}$ $m^2$) |
| Porosity | 0.1 |
| Tortuosity | 1.0 |
| Molecular Diffusivity | $1x10^{-7}$ $m^2s^{-1}$ |
| Residual Liquid Saturation | 0.1 |
| Relative Permeability of Liquid | 0 (immobile) |
| Relative Permeability of Gas ($k_{rg}$) | Linear $k_{rg}(S_g = 1) = 1$<br>$k_{rg}(S_g = 0) = 0$ |
| ***Initial Conditions*** | |
| Pressure at top of domain | 40 bars |
| Temperature | 40 °C |
| ***Boundary Conditions*** | |
| All boundaries are closed | |

Since $CH_4$ is less dense than the $CO_2$, this system is gravity stable and as such mixing is expected to be dominated, at least at early times, by diffusion at the interface. However, small advective fluxes are expected to be generated due to density changes arising from the diffusive mixing which in turn will lead to pressure changes.

Basic model properties are given in Table 3-2. Additional $CO_2$ and $CH_4$ properties are given in Table 3-3 and Table 3-4, which also report results generated by the E300 code (conducted for this thesis) and by results generated by other groups as part of the LBNL code comparison study. All simulator results are compared to experimental / reference data as reported by LBNL.

### 3.2.1 Discussion of Results

Results are shown in Table 3-3 and Table 3-4[1]. It should be noted that the E300 code is unable to calculate $CH_4$ solubilities in the aqueous phase with the particular modelling option selected in this study. The E300 code actually offers three modelling options with regards to $CO_2$ storage but only one option permits the modelling of a combined water, $CO_2$ and hydrocarbon system. This option, although designed as a three-phase compositional approach to the modelling of $CO_2$ flooding of oil reservoirs, does not permit hydrocarbon components to be present in the aqueous phase. However, the solubility of $CH_4$ in water is an order of magnitude less than that of $CO_2$ and is therefore expected to have a negligible effect on the results.

Despite this slight limitation it can be seen from the tabulated results that the various fluid properties calculated by E300 are consistent with results from the four other numerical codes for both pressure conditions considered. Furthermore, when compared to the reference values, it appears that E300 is one of the better codes in terms of its ability to reproduce experimental results.

[1] Gas phase mole fractions are based upon initial conditions (i.e. prior to dissolution of $CO_2$)

The greatest difference observed between the results calculated by E300 and the reference values, aside from the aqueous concentration of $CH_4$, is for the density and viscosity of pure $CO_2$, especially at the higher pressure. In having said that, the greatest error amongst the other codes when compared to the reference value is also for the properties of pure $CO_2$ and in fact the E300 code fairs very favourably with respect to the other codes.

**Table 3-3: Properties of $CO_2$ – $CH_4$ mixtures and aqueous solubility at a pressure of 40 bar**

| | Gas Phase | | | | Aqueous Phase | |
|---|---|---|---|---|---|---|
| **Simulation Code** | $x_g^{CH_4}$ | $x_g^{CO_2}$ | **ρ (kg m$^{-3}$)** | **μ (cP)** | $x_l^{CH_4}$ | $x_l^{CO_2}$ |
| **E300** | **0** | **1** | **86.84** | **0.0173** | **0** | **1.40 x 10$^{-2}$** |
| CHEMTOUGH | 0 | 1 | 105.39 | 0.0149 | 0 | 1.64 x 10$^{-2}$ |
| GEM | 0 | 1 | 85.41 | 0.0175 | 0 | 1.50 x 10$^{-2}$ |
| SIMUSCOPP | 0 | 1 | 85.35 | 0.0102 | 0 | 1.24 x 10$^{-2}$ |
| TOUGH2 | 0 | 1 | 85.45 | 0.0170 | 0 | 1.62 x 10$^{-2}$ |
| **Reference Values** | **0** | **1** | **83.79** (a) | **0.0173** (a) | **0** | **1.37 x 10$^{-2}$** (b) |
| **E300** | **0.5** | **0.5** | **51.99** | **0.0151** | **0** | **7.00 x 10$^{-3}$** |
| CHEMTOUGH | 0.5 | 0.5 | 46.88 | 0.0134 | 4.08 x 10$^{-4}$ | 7.45 x 10$^{-3}$ |
| GEM | 0.5 | 0.5 | 52.26 | 0.0153 | 3.82 x 10$^{-4}$ | 7.64 x 10$^{-3}$ |
| SIMUSCOPP | 0.5 | 0.5 | 52.29 | 0.0111 | 3.90 x 10$^{-4}$ | 6.20 x 10$^{-3}$ |
| TOUGH2 | 0.5 | 0.5 | 51.97 | 0.0144 | 3.73 x 10$^{-4}$ | 8.07 x 10$^{-3}$ |
| **Reference Values** | **0.5** | **0.5** | **51.33** (a) | **0.0167** (a) | **3.66 x 10$^{-4}$** (c, d, e, f) | **6.74 x 10$^{-3}$** (c, d, e, f) |
| **E300** | **1** | **0** | **26.30** | **0.0121** | **0** | **0** |
| CHEMTOUGH | 1 | 0 | 24.58 | 0.0116 | 7.49 x 10$^{-4}$ | 0 |
| GEM | 1 | 0 | 26.48 | 0.0122 | 7.51 x 10$^{-4}$ | 0 |
| SIMUSCOPP | 1 | 0 | 26.46 | 0.0126 | 7.81 x 10$^{-4}$ | 0 |
| TOUGH2 | 1 | 0 | 26.42 | 0.0121 | 7.43 x 10$^{-4}$ | 0 |
| **Reference Values** | **1** | **0** | **26.10** (a) | **0.0123** (a) | **7.22 x 10$^{-4}$** (c, d, e, f) | **0** |

**Table 3-4: Properties of CO2 – CH4 mixtures and aqueous solubility at a pressure of 100 bar**

| Simulation Code | Gas Phase | | | | Aqueous Phase | |
|---|---|---|---|---|---|---|
| | $x_g^{CH_4}$ | $x_g^{CO_2}$ | ρ (kg $m^{-3}$) | μ (cP) | $x_l^{CH_4}$ | $x_l^{CO_2}$ |
| **E300** | **0** | **1** | **585.58** | **0.0451** | **0** | **2.14 x $10^{-2}$** |
| CHEMTOUGH | 0 | 1 | 432.33 | 0.0288 | 0 | 4.09 x $10^{-2}$ |
| GEM | 0 | 1 | 564.82 | 0.0435 | 0 | 2.39 x $10^{-2}$ |
| SIMUSCOPP | 0 | 1 | 561.44 | 0.0359 | 0 | 2.30 x $10^{-2}$ |
| TOUGH2 | 0 | 1 | 566.00 | 0.0435 | 0 | 4.03 x $10^{-2}$ |
| **Reference Values** | **0** | **1** | **631.90** (a) | **0.0504** (a) | **0** | **2.19 x $10^{-2}$** (b) |
| **E300** | **0.5** | **0.5** | **159.53** | **0.0187** | **0** | **1.81 x $10^{-2}$** |
| CHEMTOUGH | 0.5 | 0.5 | 130.58 | 0.0141 | 1.14 x $10^{-5}$ | 1.61 x $10^{-2}$ |
| GEM | 0.5 | 0.5 | 158.10 | 0.0188 | 8.27 x $10^{-4}$ | 1.33 x $10^{-2}$ |
| SIMUSCOPP | 0.5 | 0.5 | 158.44 | 0.0146 | 9.08 x $10^{-4}$ | 1.15 x $10^{-2}$ |
| TOUGH2 | 0.5 | 0.5 | 155.16 | 0.0181 | 9.43 x $10^{-4}$ | 2.00 x $10^{-2}$ |
| **Reference Values** | **0.5** | **0.5** | **153.97** (a) | **0.0194** (a) | **7.95 x $10^{-4}$** (c, d, e, f) | **1.21 x $10^{-2}$** (c, d, e, f) |
| **E300** | **1** | **0** | **70.45** | **0.0137** | **0** | **0** |
| CHEMTOUGH | 1 | 0 | 61.45 | 0.0116 | 1.87 x $10^{-3}$ | 0 |
| GEM | 1 | 0 | 71.78 | 0.0139 | 1.58 x $10^{-3}$ | 0 |
| SIMUSCOPP | 1 | 0 | 71.66 | 0.0143 | 1.82 x $10^{-3}$ | 0 |
| TOUGH2 | 1 | 0 | 71.57 | 0.0141 | 1.86 x $10^{-3}$ | 0 |
| **Reference Values** | **1** | **0** | **70.03** (a) | **0.0141** (a) | **1.54 x $10^{-3}$** (c, d, e, f) | **0** |

(a) (NIST 1992) (b) (Wiebe & Gaddy 1940) (c) (Spycher & Reed 1988)

(d) (Johnson et al. 1992) (e) (Shock et al.1989) (f) (Wagmann et al. 1982)

A graphical comparison is made in Figure 3.2 of the predicted $CO_2$ mole fraction as a function of depth for the various codes used in the comparative study at a pressure of 40 bar. This Figure is taken directly from the LBNL report[2]. The results generated by the E300 code are shown in Figure 3.3.

Both figures show the $CO_2$ mole fraction versus depth after 10 and 100 years and it can be seen that the E300 results compare very favourably with the other numerical codes, particularly those generated by GEM, SIMUSCOPP and TOUGH2. All these codes indicate that after a period of 10 years, the $CO_2$ mole fraction deviates from zero at a depth of around 28 metres. Furthermore, after a period of 100 years, due to the mixing that has occurred over this period of time, the $CO_2$ mole fraction at a depth of zero metres (i.e. the top of the column) has risen from a value of zero to 0.05.

[2] The primary author of the LBNL report was contacted in an attempt to acquire the original data used to construct these graphs in order to provide graphs of greater resolution but this was unsuccessful.

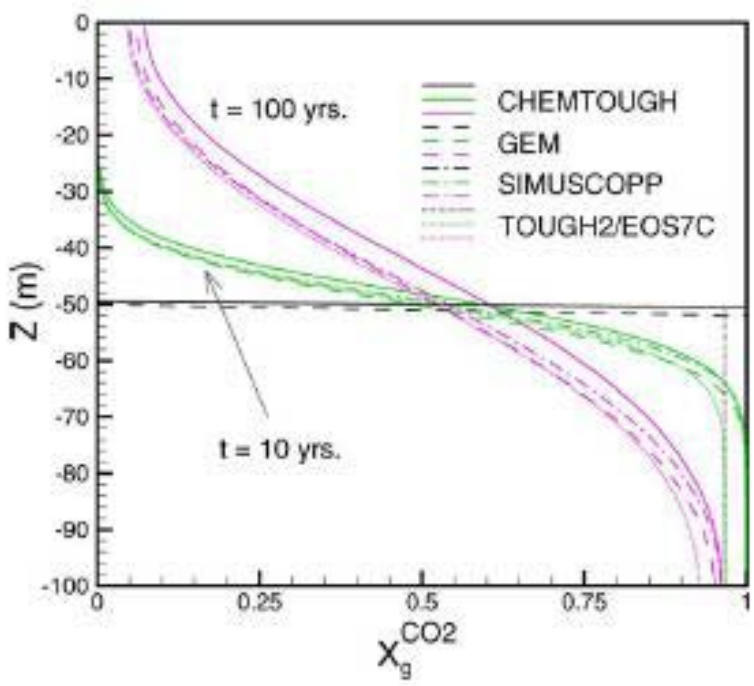


**Figure 3.2: Graph of CO2 mole fraction as a function of depth for four codes presented in LBNL report (Pruess et al. 2002. Reprinted with permission)**

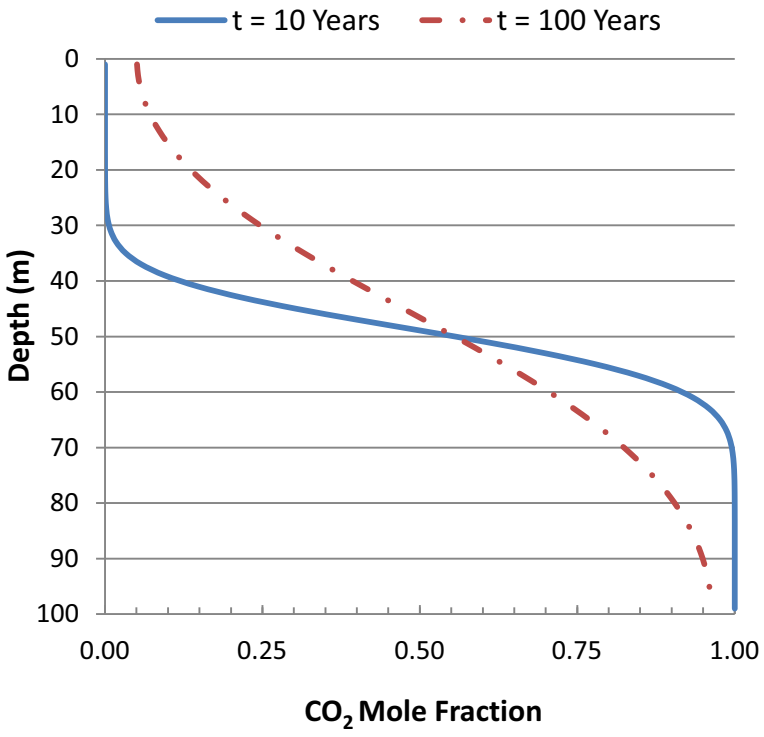


**Figure 3.3: Graph of CO2 mole fraction as a function of depth for the E300 simulation code**

## 3.3 LBNL Code Comparison Study: Problem 2

In the second problem $CO_2$ and $CH_4$ are placed in a two-dimensional porous medium, as shown in Figure 3.4, and the properties used for Problem 1 (Table 3-2) apply.

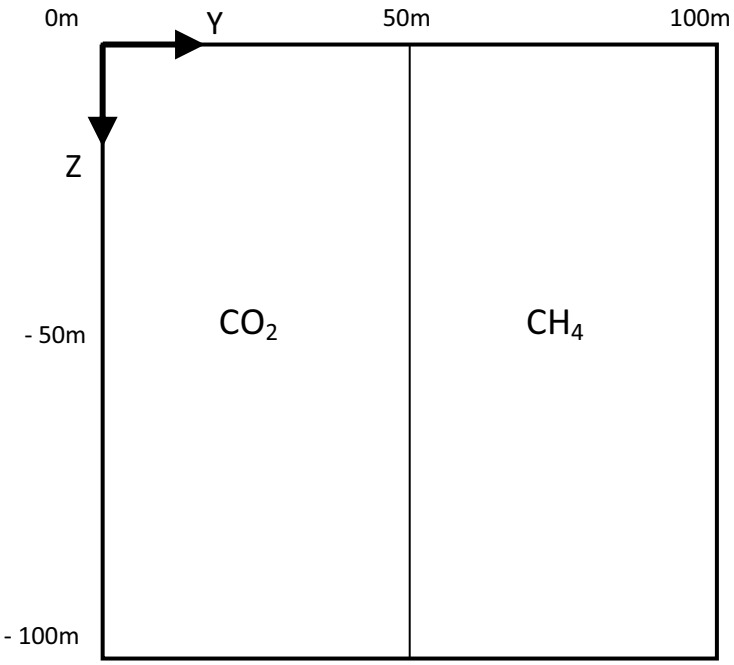


**Figure 3.4: Initial Fluid Distribution (Problem 2)**

As with Problem 1, a combination of diffusion and advective processes, stemming from gravity instabilities, determines the development of the mixing of the two gases.

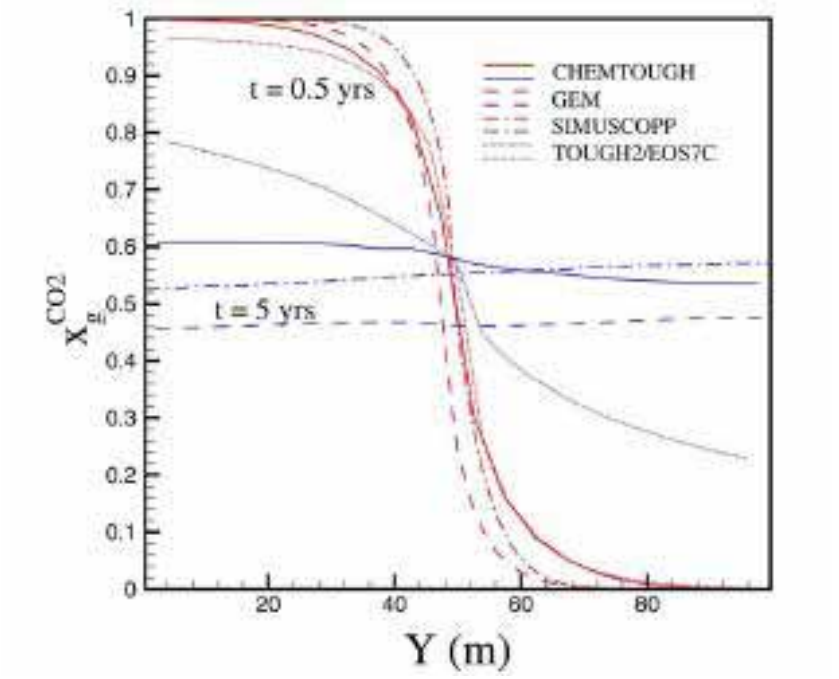


**Figure 3.5: $CO_2$ mole fraction at a depth of 50 metres with respect to time for the four codes presented in the LBNL report (Pruess et al. 2002. Reprinted with permission)**

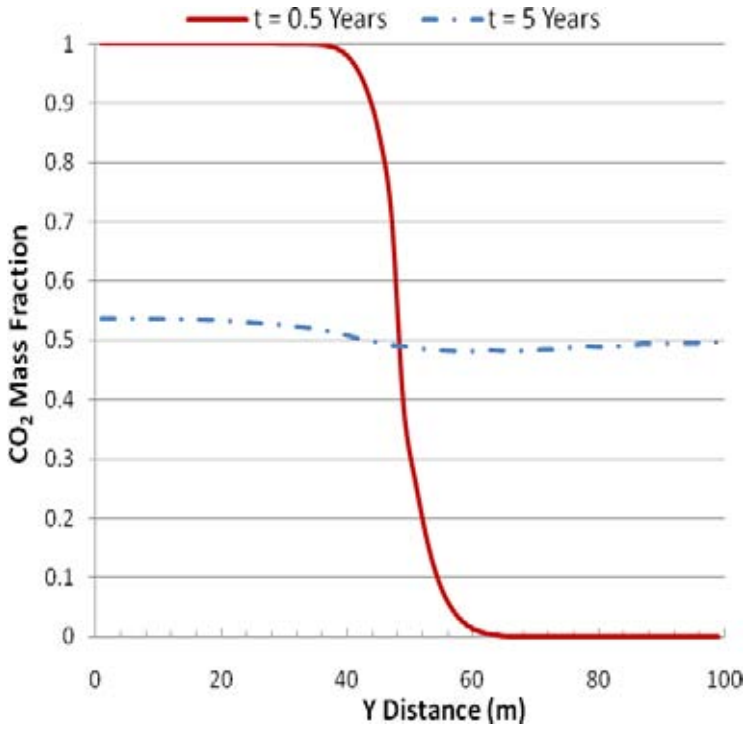


**Figure 3.6: $CO_2$ mole fraction at a depth of 50 metres with respect to time for the E300 code**

Figure 3.5 shows the predicted $CO_2$ mole fraction at a depth of 50m after six months and five years for the various codes used in the comparative study. This Figure has been taken directly from the LBNL publication. Figure 3.6 shows the E300 predictions.

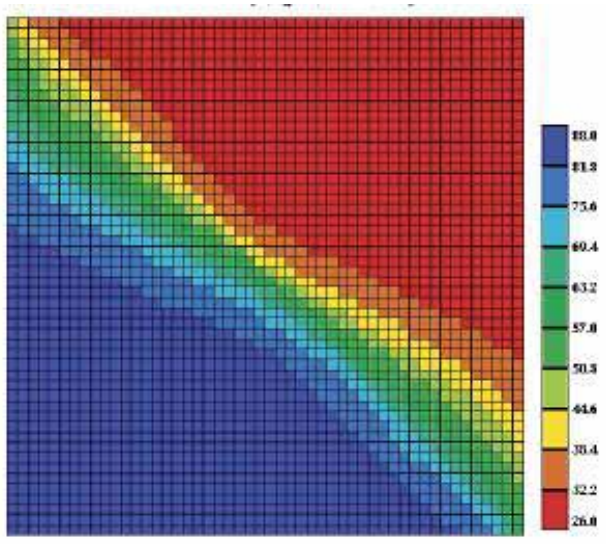

**Figure 3.7: $CO_2$ density after 365 days predicted by the GEM code (Pruess et al. 2002. Reprinted with permission)**

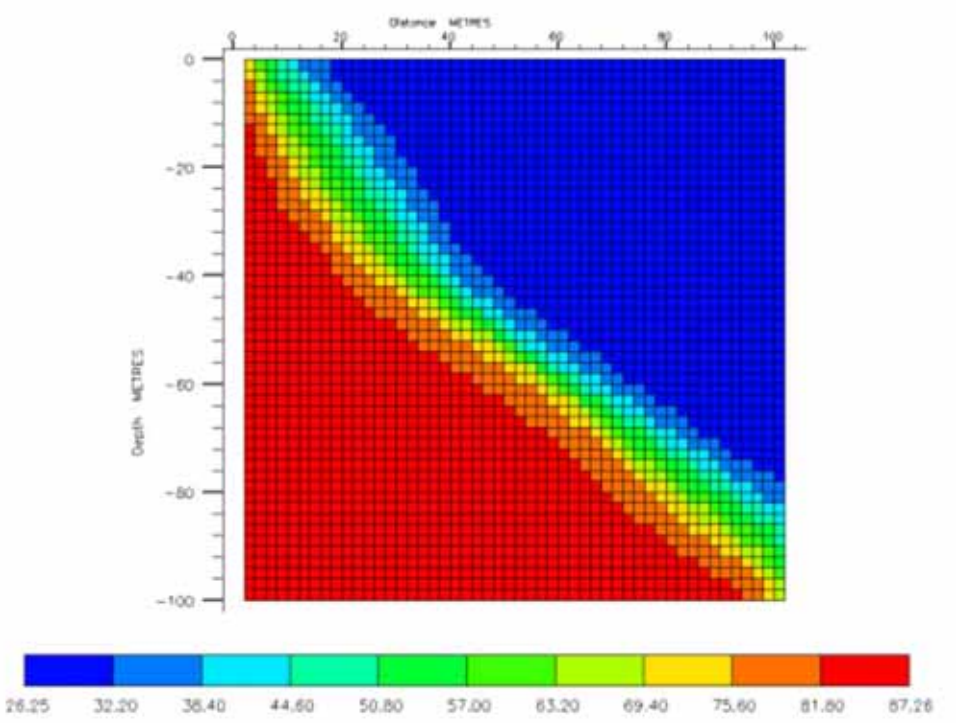


**Figure 3.8: $CO_2$ density after 365 days predicted by the E300 code**

Figure 3.7 and Figure 3.8 display a cross section of gas density after a one year period for the GEM and E300 codes respectively.

### 3.3.1 Discussion of Results

Figure 3.5 and Figure 3.6 show that after half a year the E300 code produces very similar results to those of the commercial simulator GEM and the research code SIMUSCOPP, although it does predict the least amount of mixing (steeper slope). The TOUGH2 simulator displays the most varied results. Whereas all other codes show no reduction in the $CO_2$ mass fraction after six months, the TOUGH2 code predicts a greater degree of mixing between the two fluids, with the $CO_2$ mass fraction at Y = 0 already lowering to 96%.

After a five year period, however, the TOUGH2 code demonstrates the least mixing between the two fluids, with the $CO_2$ mole fraction at Y=0 almost 80%. By comparison the range of $CO_2$ mass fractions as calculated by the other codes, including E300, range from 45 – 60%, with this range being maintained across the horizontal plane (at a depth of 50m). No explanation is given in the LBNL report as to why these differences should exist.

Figure 3.7 and Figure 3.8 show a comparison of the density distribution as predicted by the GEM and E300 models. Although qualitatively there is reasonable agreement between the two, it is clear that the GEM code predicts a wider transition zone between the $CO_2$ and $CH_4$ than the E300 code.

Again, there is no discussion of these differences in the original report, nor if they are representative of the performances of other codes. It is, however, noted in the LBNL report that larger differences in the results between the various codes are to be expected when the flow becomes more complex, as is the case when moving from Problem 1 to Problem 2.

Without a more detailed knowledge of the set up of the models for Problems 1 and 2 it is impossible to make any definitive statements regarding the reasons for differences between the results. When comparing such codes there is a range of phenomena that can impact on the output. Most notably grid size and timestep length can have a large effect on the numerical dispersion within the model and it is well known that this can often far exceed the real physical dispersion that the code is attempting to model. In the case of a displacement process this enhanced mixing tends to result in early breakthrough of the injectant and other errors in recovery.

However, one thing that is apparent from the results generated so far is that both of the commercial simulators, GEM and E300, produce similar answers and that these compare favourably with experimental measurements. Whilst this is not an assurance that they are sufficiently accurate in all respects, it does nevertheless provide some confidence that these codes have merit in modelling displacement processes involving $CO_2$ and $CH_4$.

## 3.4 LBNL Code Comparison Study: Problem 3

The third problem is a one-dimensional (line source), two-phase flow problem which investigates the effects of injecting $CO_2$ at a constant rate into a radial, homogeneous, isotropic and infinite acting aquifer. Relative permeability and capillary pressure effects are considered but gravity and inertial effects are ignored. A schematic of the problem is shown in Figure 3.9 and additional model parameter data is given in Table 3-5.

This simplified radial flow problem has a distinct advantage in that it permits a similarity solution to be formulated. Under the conditions stated for this problem, the solution only depends on radial distance *R* and time *t* through a similarity variable $\xi=R^2/t$. In other words, the governing partial differential equations in terms of *R* and *t* can be rigorously transformed into ordinary differential equations in the variable ξ. What this means is that all plots of, say, pressure versus the similarity variable will be identical over time. This holds true even when taking into account non-linearities due to the PVT properties and the two-phase flow conditions (such as relative permeability and capillary pressure).

However, the space and time discretisation used in numerical simulation to formulate a finite difference approximation to the governing equations leads to the strict invariance of the similarity

solution to be violated to some extent. What this means is that curves that previously lay on top of each other no longer do so. This effect will be discussed when presenting the results of this problem.

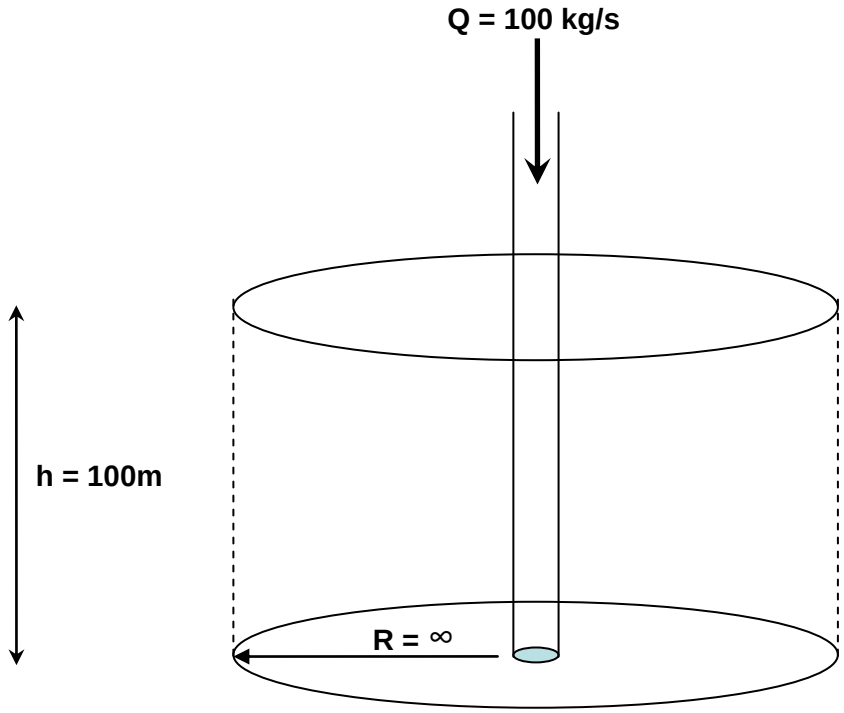


**Figure 3.9: Problem 3**

**Table 3-5: Model Properties (Problem 3)**

| | |
|---|---|
| Permeability | 100mD ($1x10^{-13}$ $m^2$) |
| Porosity | 0.12 |
| Pore Compressibility | 4.5x10-10 Pa-1 |
| Aquifer Thickness | 100 m |
| Pressure | 120 bar |
| Temperature | 45°C |
| Salinity | 0 or 15 wt% NaCl |
| Residual Water Saturation | 0.3 |
| Residual Gas Saturation | 0.05 |

Aqueous phase salinities of 0 and 15 weight percent have been considered and to ensure the aquifer is infinite acting for the time period simulated, the radial grid is extended to a radius of 100km.

The permeability, relative permeability and capillary pressure values are based on generic values and correlations for sedimentary basins.

The liquid relative permeability is calculated using the van Genuchten (1980) correlation:

$$k_{rl} = \sqrt{S^*}\left\{1 - \left(1 - [S^*]^{1/\lambda}\right)^{\lambda}\right\}^2 \quad (3.1)$$

where

$$S^* = (S_l - S_{lr})/(1 - S_{lr}) \quad (3.2)$$

The gas relative permeability is calculated using the Corey correlation:

$$k_{rg} = \left(1 - \hat{S}\right)^2 (1 - \hat{S}^2) \quad (3.3)$$

where

$$\hat{S} = \frac{(S_l - S_{lr})}{(1 - S_{lr} - S_{gr})} \quad (3.4)$$

The capillary pressure function was also calculated using a correlation proposed by van Genuchten (1980):

$$P_c = -P_0\left([S^*]^{-1/\lambda} - 1\right)^{1-\lambda} \quad (3.5)$$

where

$$S^* = (S_l - S_{lr})/(1 - S_{lr}) \quad (3.6)$$

Finally, the selected injection rate of 100 kg/s is based on the $CO_2$ emission rate of a 288 MWe (MegaWatt electric) coal-fired power plant (Pruess & Garcia 2002).

## Discussion of Results

The key processes to be investigated in this problem, as determined by the LBNL comparative study, are:

Two-phase flow of $CO_2$ and water subject to relative permeability and capillary effects.

The change in fluid density, viscosity, and $CO_2$ solubility with respect to pressure and salinity.

Formation dry-out with precipitation of salt.

Unfortunately the E300 code does not allow water to be soluble in the $CO_2$ phase, and so formation dry-out cannot be modelled. The implications of this will be discussed in due course.

The pressure profiles as a function of the similarity variable for the zero salinity case, as generated by the LBNL comparison study, are shown in Figure 3.10 and the results from the E300 code are presented in Figure 3.11. Qualitatively there is good agreement between all the codes used and, in particular, the results for the E300 code show that discretisation errors do not seem to have impacted markedly on the similarity solution, as the graphs plotted for the four times considered line up very closely.

All the results show a sharp change in slope at a similarity variable of $10^{-2}$ $m^2/s$, which indicates the point of change from a two-phase region to a single phase region (i.e. the $CO_2$ displacement front).

The E300 predicts a pressure profile comparable to all of the other codes, especially the TOUGH2 code used by the LBNL and CSIRO organisations.

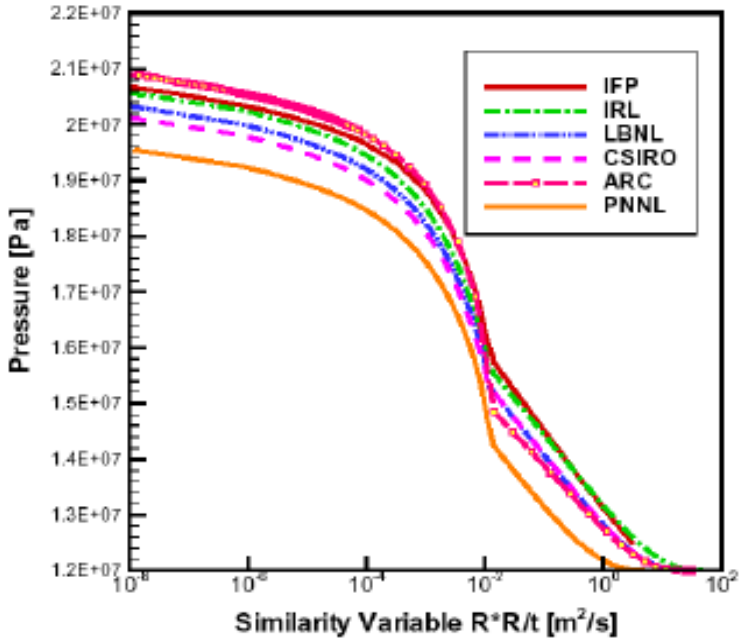


**Figure 3.10: Pressure versus the similarity variable for the 6 codes presented in the LBNL report (Pruess et al. 2002. Reprinted with permission)**

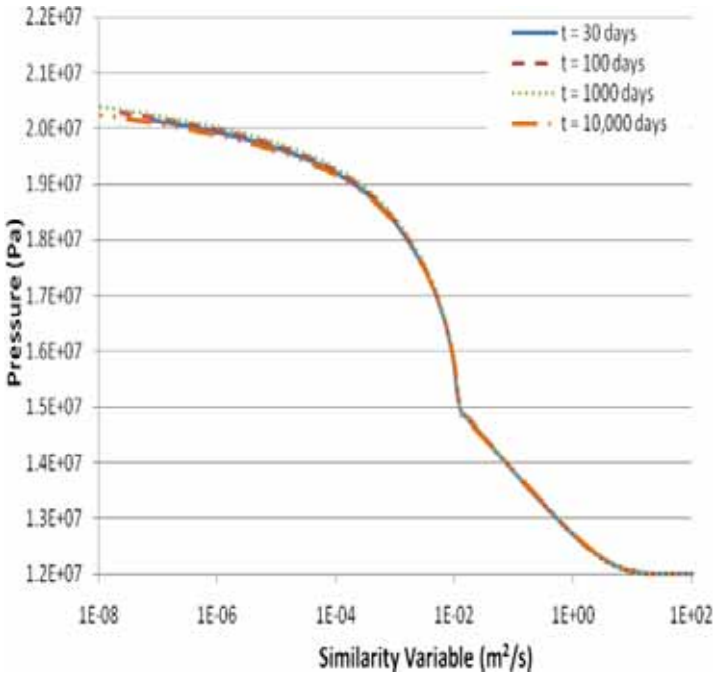


**Figure 3.11: Pressure versus the similarity variable for the E300 code**

Figure 3.12 displays the gas saturation as a function of the similarity variable, as presented in the LBNL report. The codes which predict a gas saturation of 1 in the similarity variable region of $10^{-8}$ to

$10^{-6}$ of 1.00 are those which are able to incorporate formation dry-out. In these simulation models water is evaporated in the near-wellbore region due to the injection of $CO_2$, leaving a 100% gas saturation in this region. Conversely, codes which are unable to incorporate formation dry-out, such as the GEM and E300, as shown in Figure 3.13, predict a residual water saturation in the near-wellbore region instead of a single phase gas saturation.

The E300 code calculates a maximum gas saturation in the near wellbore region of 70%. This is consistent with the relative permeability data which has a residual water saturation of 30%. It is unclear as to why the other codes unable to incorporate formation dry-out calculate such different maximum gas saturations in the near wellbore region. Results from all codes including E300 do however calculate the transition zone from two-phase to single phase (water) at a similarity variable of $10^{-2}$.

The results of the dissolved mass fraction of $CO_2$ after 10,000 days for the comparative study are shown in Figure 3.14 where it is evident there are some discrepancies between the predictions made by the various codes. In the similarity variable range of $10^{-2}$ to $10^{-6}$, the value of the dissolved mass fraction ranges between 0.044 and 0.066.The E300 code results after 10,000 days, shown in Figure 3.15, fall into the middle of this range (0.058), as does the prediction made by TOUGH2, the code used by LBNL.

Again, a code's ability to model formation dry-out causes differences in the results at low similarity variable values, typically less than $10^{-6}$. Codes able to model formation dry-out calculate zero dissolved $CO_2$ concentrations due to the fact that only a single gas phase exists in this region.

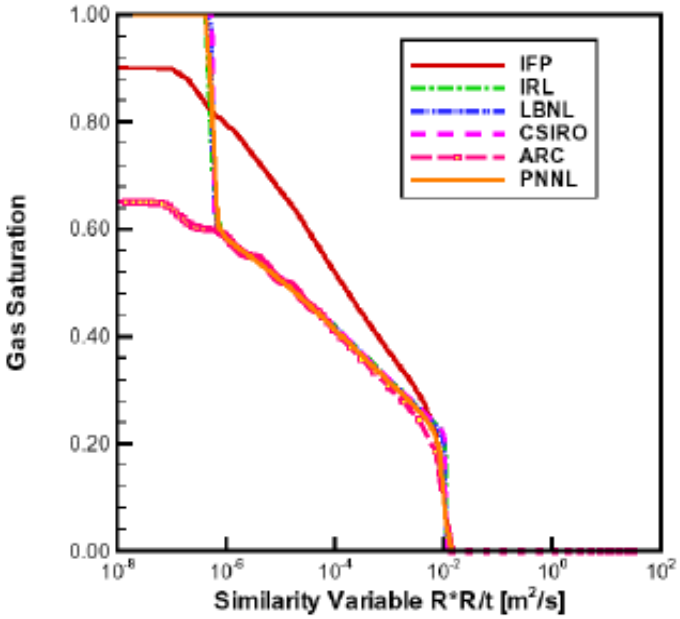


**Figure 3.12: Gas saturation versus the similarity variable for the 6 codes presented in the LBNL report (Pruess et al. 2002. Reprinted with permission)**

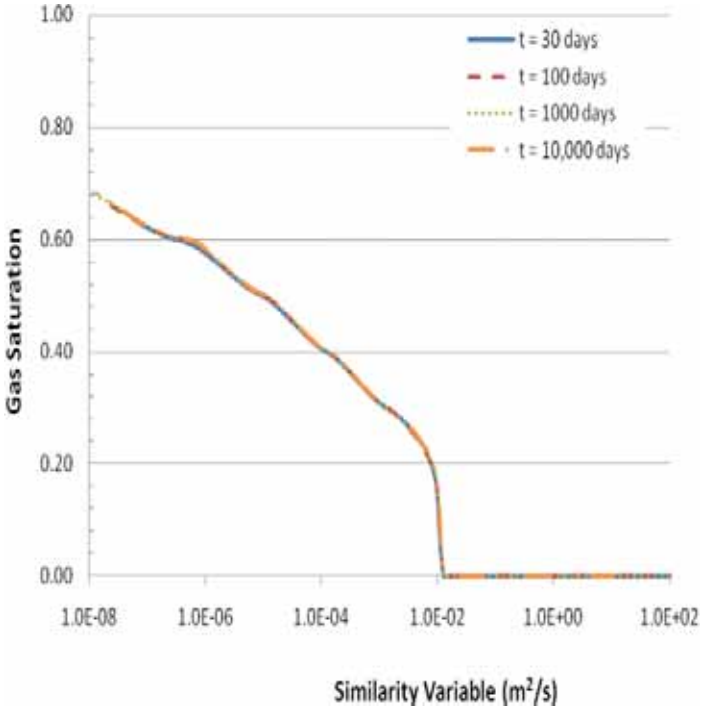


**Figure 3.13: Gas saturation versus the similarity variable for the E300 code**

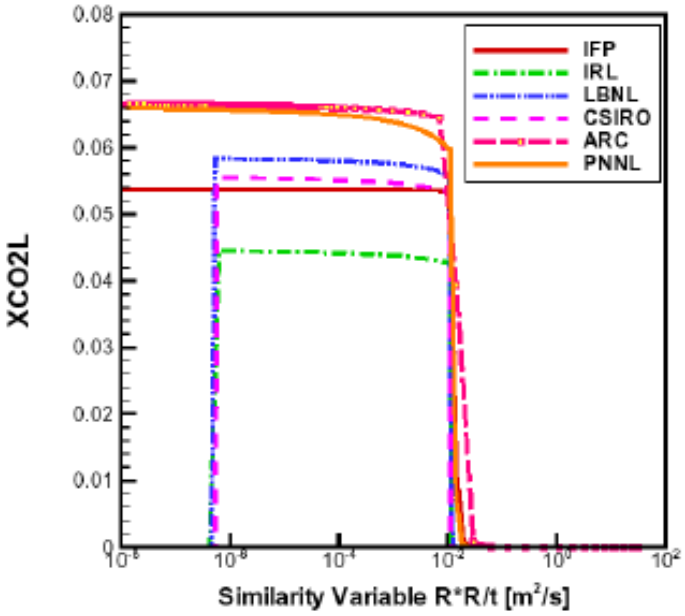


**Figure 3.14: Dissolved $CO_2$ mass fraction versus the similarity variable for the 6 codespresented in the LBNL report (Pruess et al. 2002. Reprinted with permission)**

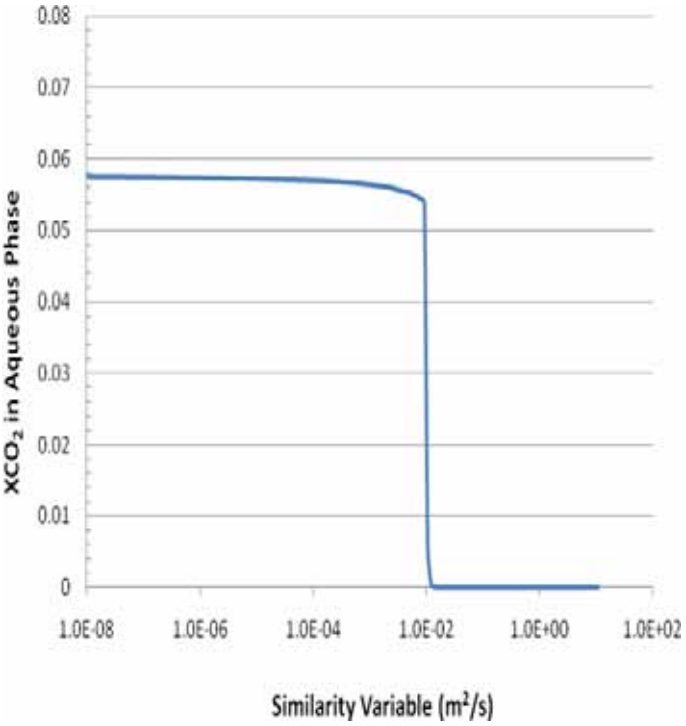


**Figure 3.15: Dissolved $CO_2$ mass fraction versus the similarity variable for the E300 code**

The comparison study also reports fluid properties calculated by each code at four different pressures. These results are shown in Figure 3.16 to Figure 3.22, for zero salinity, and are also compared with the E300 code predictions and a set of reference values[3] which are calculated based upon experimental data.

It can be seen that, in general, the E300 predicted results for water compare well with both the reference value and the results from the other codes (Figure 3.16 and Figure 3.17). The maximum difference between the E300 predicted water density and the reference value is of the order of -0.2% (at 240 bar), and all of the E300 density results are very similar to those reported by LBNL and CSIRO, using their own versions of the TOUGH2 code. With regards to viscosity E300 tends to over predict the value when compared with both the reference value and those generated by the other codes. However, since the maximum difference is of the order + 0.3% (at 160 bar) this is considered negligible.

When calculating the $CO_2$ properties (Figure 3.18 and Figure 3.19), E300 in general tends to slightly underestimate the various parameters compared to the other codes and to the reference values. It is noted that E300's calculated $CO_2$ density at lower pressures is similar to those calculated by SIMUSCOPP and GEM, the codes used by the IFP and the ARC institutions respectively. Compared to

[3] The reference values are calculated using a fluid properties calculator developed by Jonathan Ennis-King from the CSIRO.

the two TOUGH2 code calculations, E300's calculated $CO_2$ density is comparable at the lower pressures but as the pressure is increased so does the difference in density calculations amongst the codes and with the reference value. The maximum error between the E300 result and the reference value is 8.8% (at 120 bar).The prediction of $CO_2$ viscosity by the E300 code is consistently lower than the reference value, with the maximum difference of 9.6% occurring at a pressure of 160 bar. In terms of overall predictive capability of $CO_2$ properties, the E300 code compares favourably with the other commercial code, GEM.

The aqueous ($H_2O$ and $CO_2$) density is slightly overestimated at all pressures when calculated by the E300 code (Figure 3.20). In absolute values, the difference between the E300 code and the reference value is consistently around 20 kg/m$^3$ for all pressures. In percentage terms this error is relatively minor, with the maximum difference being 2.1% at a pressure of 240 bar. Interestingly, the GEM code consistently underestimates the aqueous density by almost an equivalent amount in absolute terms. The increase in density as pressure increases is relatively minor for the GEM code, and consequently the difference between the GEM calculated density and the reference value is greatest at a pressure of 240 bar (almost 30 kg/m$^3$), with an error of 3%.

Figure 3.21 shows equivalent viscosities for the aqueous solution as calculated by E300. This result mirrors that of the GEM code, and is believed to be due to the lack of correlations available for calculation of the viscosity of an aqueous solution saturated with $CO_2$. It has been experimentally shown that the effect of dissolved $CO_2$ on the viscosity of water is very small, potentially leading to the low importance being placed on the development of any such correlation (Sayegh & Najman 1987; Chang et al. 1998). This is also reflected in the results of the other codes, aside from the code used by PNNL, whereby the viscosities presented are equivalent to those of water with no dissolved $CO_2$. The reference values also follow this condition.

The calculation of dissolved $CO_2$ mass fractions by E300 show good agreement to results from both TOUGH2 codes used by LBNL and CSIRO, as well as the reference value at all pressures (Figure 3.22). The maximum difference between the E300 calculated value and the reference value is 1.24% at a pressure of 120 bar. In comparison, at the equivalent pressure, the error exhibited by the calculation of the GEM code is 19%.

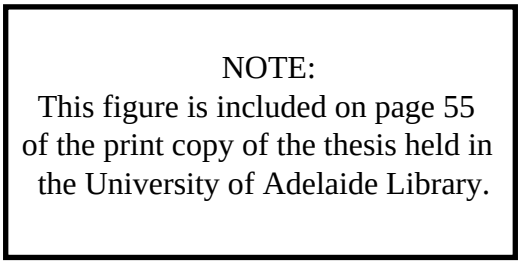


**Figure 3.16: Comparison of $H_2O$ density as a function of pressure (zero salinity) for E300 and the codes presented in the LBNL report (Modified from Pruess et al. 2002)**

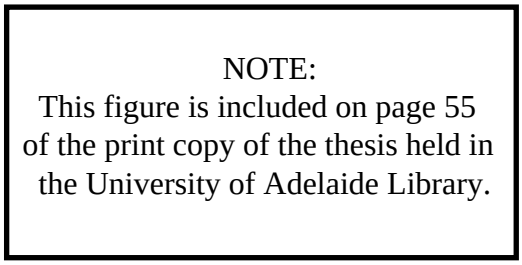


**Figure 3.17: Comparison of $H_2O$ viscosity as a function of pressure (zero salinity) for E300 and the codes presented in the LBNL report (Modified from Pruess et al. 2002)**

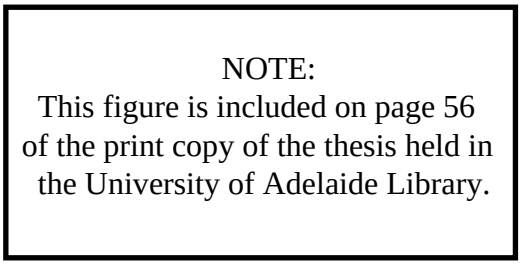


**Figure 3.18: Comparison of $CO_2$ density as a function of pressure for E300 and the codes presented in the LBNL report (Modified from Pruess et al. 2002)**

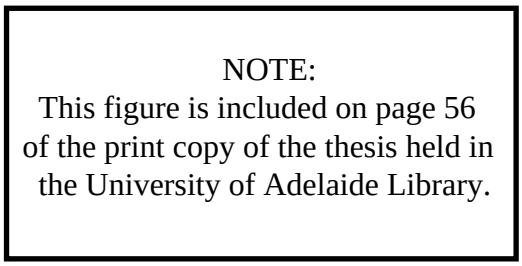


**Figure 3.19: Comparison of $CO_2$ viscosity as a function of pressure for E300 and the codes presented in the LBNL report (Modified from Pruess et al. 2002)**

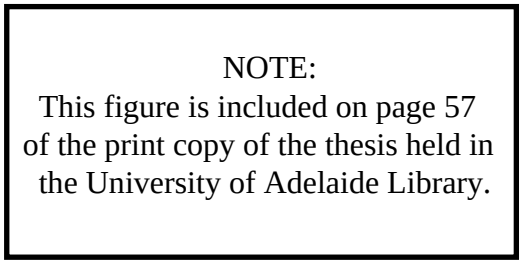


**Figure 3.20: Comparison of Aqueous ($H_2O$ + $CO_2$) density as a function of pressure (zero salinity) for E300 and the codes presented in the LBNL report (Modified from Pruess et al. 2002)**

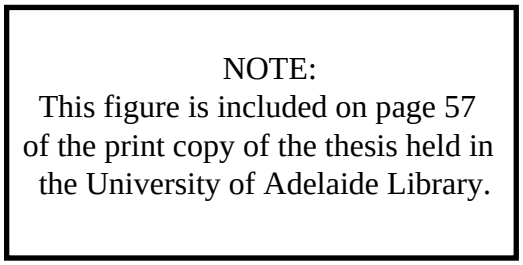


**Figure 3.21: Comparison of Aqueous ($H_2O$ + $CO_2$) viscosity as a function of pressure (zero salinity) for E300 and the codes presented in the LBNL report (Modified from Pruess et al. 2002)**

**Figure 3.22: Comparison of dissolved $CO_2$ mass fraction in liquid phase as a function of pressure (zero salinity) for E300 and the codes presented in the LBNL report (Modified from Pruess et al. 2002)**

Moving to the results where water salinity is now 15 weight percent, results of the E300 calculations are once again comparable to other numerical codes as well as the reference values.

Firstly, to the pressure profiles (Figure 3.23 and Figure 3.24), again the results from the E300 code compare favourably with the other codes, especially those of the LBNL and CSIRO organisations. Notice the increase in near wellbore pressure with the addition of salinity as compared with the case with no salinity.

There was no implication of the addition of salinity on the gas saturation profile, and so the results are equivalent to those presented in Figure 3.13. Differences were observed for the codes that could model formation dry-out due to the precipitation of salts. The presence of these salts meant that gas saturation was not 100% in the volume experiencing dry-out.

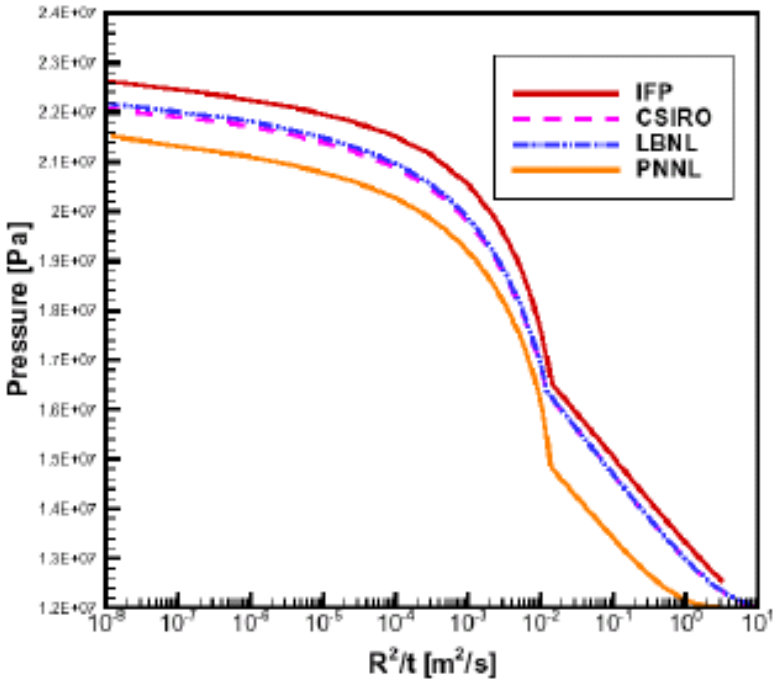


**Figure 3.23: Pressure versus similarity variable for the 4 codes presented in the LBNL report (Pruess et al. 2002. Reprinted with permission)**

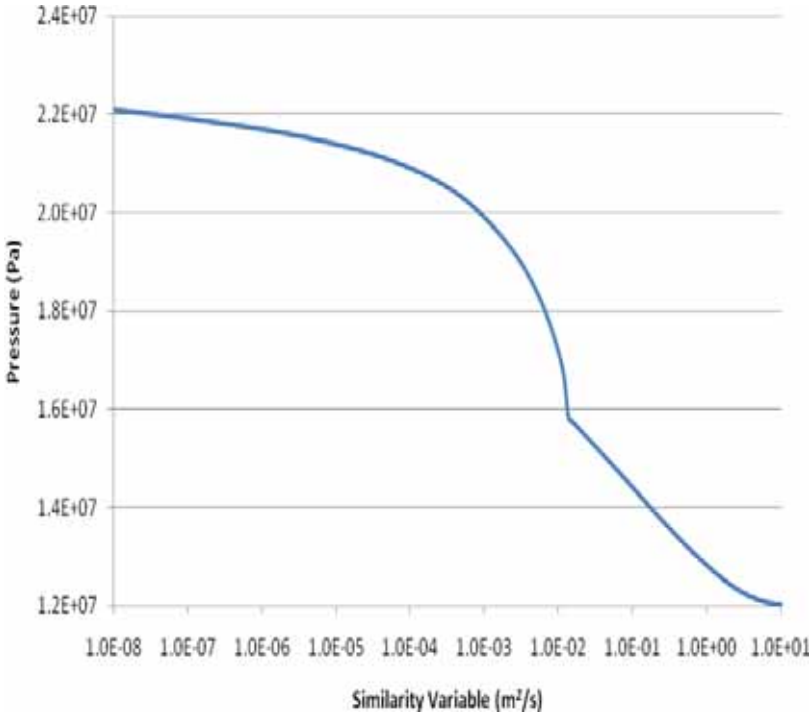


**Figure 3.24: Pressure versus similarity variable for the E300 code**

The addition of salinity to the formation water has a direct negative influence on the degree of dissolution of $CO_2$ (Figure 3.25 and Figure 3.15), with a significant decrease noticeable in the $CO_2$ mass fraction profile. Once more, for codes unable to model the evaporation of water in the near

wellbore region, dissolution of $CO_2$ is observed in the results from a similarity variable of around $10^{-6}$ and less. Aside from this characteristic, the results from the E300 code compare favourably once more with the results from the LBNL and CSIRO organisations.

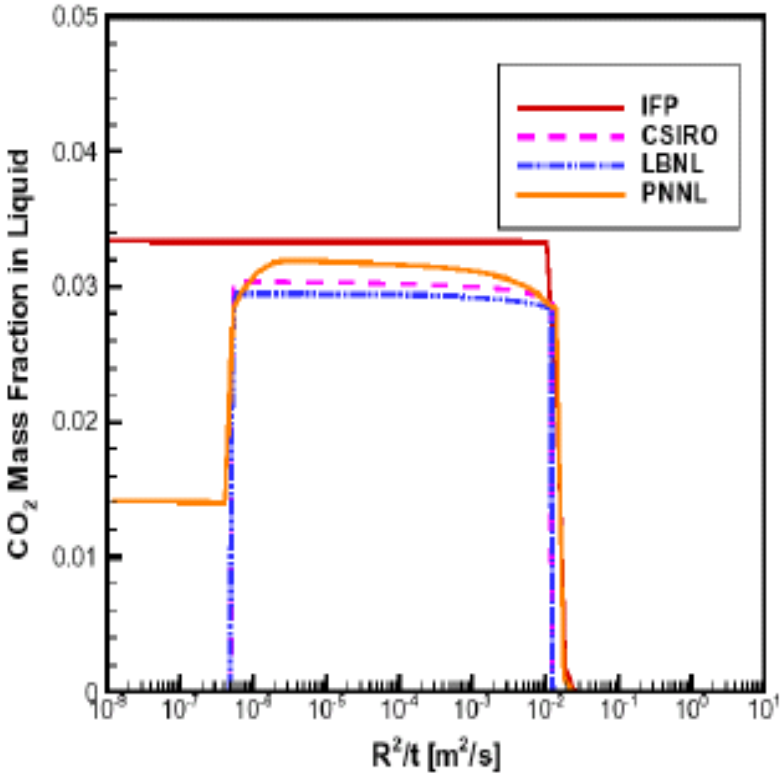


**Figure 3.25: $CO_2$ mass fraction in the liquid phase for the 4 codes presented in the LBNL report (Pruess et al. 2002. Reprinted with permission)**

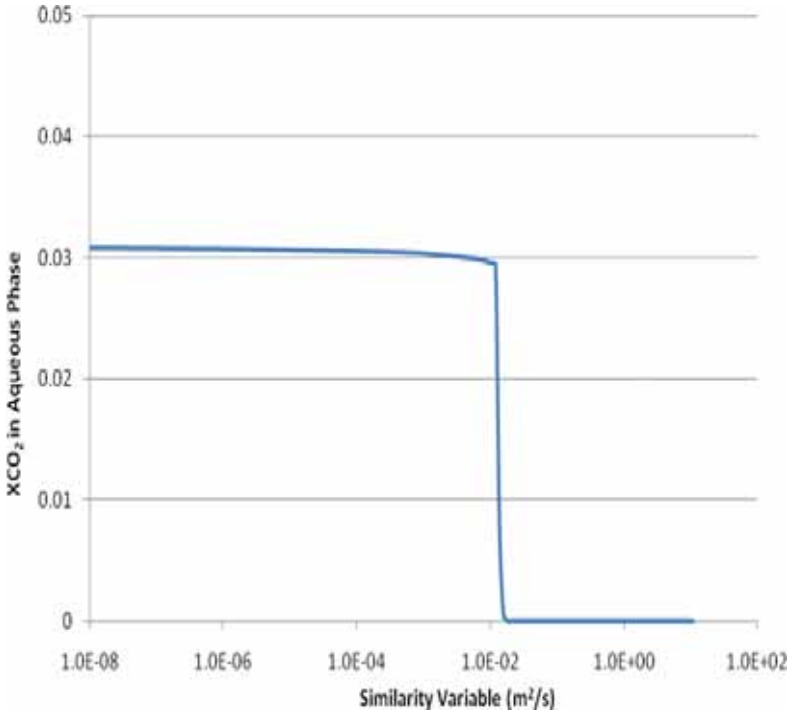


**Figure 3.26: $CO_2$ Mass fraction in the liquid phase for the E300 code**

Whereas calculated water density was slightly underestimated for a formation water with no salinity, E300 overestimates brine density at all pressures with respect to the reference value (Figure 3.27). This overestimation is small though, with a maximum error of just 0.44% at a pressure of 240 bar.

Brine viscosity is once again accurately calculated by E300 (Figure 3.28), with the maximum error of only 0.3% with respect to the reference value (at 120 bar).

The E300 code once again overestimates the aqueous density (Figure 3.29), but as was the case previously, the error is relatively minor, being 1.9% at a pressure of 240 bar.

Aqueous viscosity once again did not change with increasing pressure (Figure 3.30), due to the reasons previously stated. Of the four codes which have results presented, the E300 code matches closely with the TOUGH2 codes employed by LBNL and CSIRO for the viscosity of the aqueous solution.

The addition of salinity causes an increase in the error of the calculation of dissolved $CO_2$ mass fraction (Figure 3.31), with the largest error being 6.3% at a pressure of 200 bar, compared with 1.24% when salinity is not present. Comparing the results of the other numerical codes, it appears that the addition of salinity has a negative impact on the accuracy of calculations on dissolved $CO_2$ mass fractions, especially for the TOUGH2 code used by the CSIRO.

Overall, the E300 code models the two-phase flow of $CO_2$ and water comparatively well with respect to other numerical codes, both commercial and research. In terms of the fluid properties as a function of pressure and salinity, the E300 code did demonstrate strengths and weaknesses with certain properties, but the results compared well with both the reference values as well as the other codes, especially with respect to the other commercial code, GEM. With access only available to the commercial codes, confidence has been raised in the application of the E300 code to model the similar processes expected in this thesis.

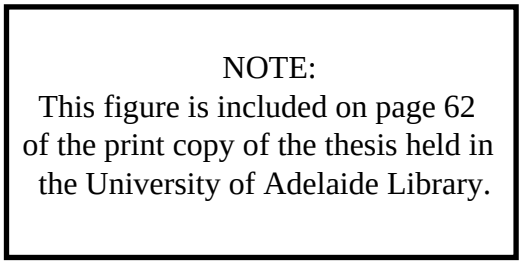


**Figure 3.27: Comparison of brine density as a function of pressure (15 weight percent salinity) for E300 and the codes presented in the LBNL report (Modified from Pruess et al. 2002)**

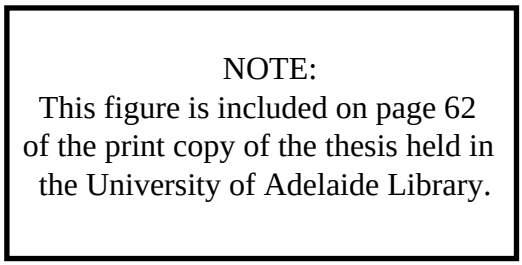


**Figure 3.28: Comparison of brine viscosity as a function of pressure (15 weight percent salinity) for E300 and the codes presented in the LBNL report (Modified from Pruess et al. 2002)**

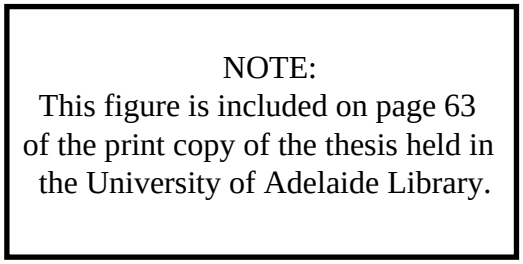


**Figure 3.29: Comparison of aqueous (brine + $CO_2$) density as a function of pressure (15 weight percent salinity) for E300 and the codes presented in the LBNL report (Modified from Pruess et al. 2002)**

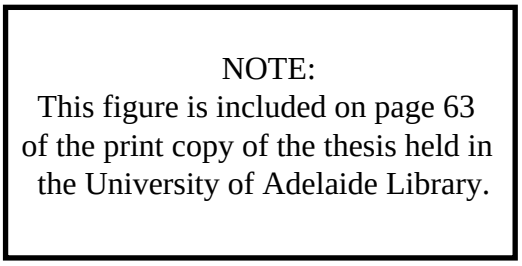


**Figure 3.30: Comparison of aqueous (brine + $CO_2$) viscosity as a function of pressure (15 weight percent salinity) for E300 and the codes presented in the LBNL report (Modified from Pruess et al. 2002)**

**Figure 3.31: Comparison of dissolved $CO_2$ mass fraction in the liquid phase as a function of pressure (15 weight percent salinity) for E300 and the codes presented in the LBNL report (Modified from Pruess et al. 2002)**

## 3.5 Conclusion

Three problems posed in a report investigating the ability of numerical codes to adequately model the processes involved in carbon storage have been modelled using the E300 numerical code. The three problems posed involve the same processes as would be expected in an enhanced gas recovery operation involving the injection of $CO_2$. To gain confidence in the application of the E300 code to model the processes important to the injection of $CO_2$ into a natural gas reservoir, the code was employed to model the three chosen problems from the code comparison study. Results from the E300 models were compared to other numerical codes, both commercial and research, as well as reference values obtained from correlations used to fit experimental data. Results obtained from the modelling of the three problems indicated the ability for the E300 code to accurately model the processes involved in each of the problems, and to obtain accurate fluid properties.

For the first problem, properties as calculated by E300 compared very well to the reference values, especially for the properties of pure $CH_4$, and of the mixed concentration gas. The greatest errors in the E300 calculations, aside from the inability to model dissolution of $CH_4$ into the aqueous phase, are the calculation of pure $CO_2$ properties. However, in comparison to the other codes, E300 is one

of the better codes in reproducing the experimental results. In terms of fluid movements spatially, the E300 code is comparable to the other codes tested.

With the second problem involving slightly more complex processes such as mixing by advection as well as diffusion, the results of all codes, including E300, demonstrated greater variability with one another. As time proceeded, and the mixing of the two fluids increased, the differences between the codes became more apparent. The $CO_2$ mole fraction profile after five years as produced by E300 was similar to all but the TOUGH2 code. The TOUGH2 code showed a dramatically different profile to the other codes, although no explanation in the original report is given as to why this is the case. The E300 code does however produce similar results to that of the other commercial code tested, the GEM code.

The investigation of two-phase flow in the third problem involved the injection of CO2 into an infinite acting saline aquifer. Of key importance was the calculation of fluid properties with respect to pressure and salinity, as well as the pressure profile and gas saturation profile with respect to the similarity variable. Variability in the results could be related to at least two factors. The first is whether the code was able to model formation dry-out due to the injection of $CO_2$. If the code is unable to model formation dry-out, then a residual water saturation is present in the near wellbore region during $CO_2$ injection. The option used for the E300 code is unable to model formation dry-out, and this is the cause of differences observed in the gas saturation and $CO_2$ dissolved mass fraction profiles. In terms of calculations of fluid properties at varying pressures and salinity, the results from the E300 code compared favourably with those of the other codes, as well as the reference values. Most properties calculated by E300 had an error margin of less than 5%, with no error greater than 10%. In comparison to the GEM code, the E300 code performed better in calculating the properties of the water and aqueous densities and dissolved $CO_2$ mass fractions, whereas the GEM code performed slightly better in calculating $CO_2$ properties.

Overall, the E300 code performs very well in simulating the key processes involved in the three problems attempted in addition to calculating fluid properties at various conditions. E300 results compare very well with respect to the other codes used in the code comparison study as well as the reference values. With no drastic errors exhibited in the calculations by E300 with respect to other codes as well as the reference values, confidence has been gained in the applicability of the E300 code in modelling the processes expected to be important in the injection of $CO_2$ into water-drive gas reservoirs.

# CHAPTER 4

# 4 Experimental Design Methodology and its Use in the Oil and Gas Industry

## 4.1 Introduction

Experimental design (ED) is a methodology which allows a selection of uncertain input variables to be simultaneously varied in a series of experimental runs according to a predefined pattern or design matrix in order to generate an experimental output relating the input variables to the response. The key feature of the methodology is that it allows the user to build up a meaningful probability distribution using a subset of possible combinations of inputs such that the resultant distribution covers the entire range of possible outcomes.

The ED methodology is widely used in many industries, including agriculture (Fisher 1971; Fisher 1973), chemical and process industries (Lazić 2004), automotive and aerospace manufacturing (Montevechi et al. 2007) and electronics (Ghaderi et al. 2005). ED is also widely used as a statistical research tool in areas such as psychology (Abdi 2009) and engineering (Sciortino 2002). One of the earliest references to the use of ED in the oil and gas industry is from Heins and Friz (1967) who applied ED methods to study the properties of rocks. ED has since been widely used in the oil and gas industry, as will be described section 4.2.

An experiment is performed in order to gain an understanding of a particular process or system. It involves a test or series of tests whereby changes are made to input variables in order to identify and understand the effect of these input parameters on the chosen process or system. It is also common for a model to be developed based on the results of the experiment, with the idea that this model can replace the need for these experiments, which can be complicated, time consuming and costly. In order to develop an accurate model, the process or system has to be sampled adequately over the operating region. The experimental design methodology utilises statistical methods to define the number and conditions (parameter levels) of experiments required to adequately cover the solution space so that meaningful conclusions can be made. The methodology aims to gain maximum information with minimal experimental cost.

There are many types of experimental designs and the selection of the design should be based upon the objectives of the study. As mentioned previously, the use of experimental designs falls into two main categories, whether the design is to be used for screening or predictive/optimisation purposes.

### Screening Designs

Screening designs generally involve a large number of parameters where the primary objective is to determine the degree of influence these parameters have on a chosen response within a less stringent confidence interval. Rather than determining the precise effect of a parameter, the use of these designs is to efficiently narrow the list of parameters for further study using higher resolution designs. Screening designs are typically two-level designs, such as the two-level full factorial and two-level fractional factorial designs.

### Two-level Full Factorial Designs

A factorial design is a design where all possible combinations of the levels of the input parameters are tested. For example, if there are *a* levels of parameter A and *b* levels of parameter B, the design contains *ab* combinations (experimental runs). Therefore, in a two-level factorial design involving two parameters there would be 2 x 2 = 4 combinations. In general, if there are *k* factors, the number of experimental runs required is $2^k$. Factorial designs are used in studies involving more than one factor where it is required to study the joint effect of parameters on the response, known as an interaction. For instance, the effect of parameter A might be dependent upon the level of parameter B, rather than the effect of A being consistent regardless of the level of parameter B. The disadvantage of this design is however immediately apparent. The number of experimental runs required increases rapidly as the number of parameters increases. For example, a design incorporating 10 parameters would require $2^{10}$ or 1024 experimental runs. Due to the inefficiency of these designs, designs which utilise a subset of all possible combinations have been developed. These designs are known as fractional factorial designs.

### Two-level Fractional Factorial Designs

With the number of runs required rapidly increasing as the number of parameters increase in a $2^k$ factorial design, the resources required rapidly become unfeasible. Additionally, a significant number of experimental runs correspond to determining the effect of three-factor or higher interactions, which are generally deemed negligible. For example, in a $2^5$ design which requires 32 experimental runs, 5 runs are required to estimate the main effects and 10 are required to estimate the effects of two-way interactions. This leaves 16 runs (one run is used to estimate the mean), over half of the design, to estimate three-way and higher interactions. If these higher order interactions can be assumed to be negligible, only half of the design is therefore required, a considerable saving in resources. Fractional factorial designs are designs which use a subset of all possible combinations to estimate the effects of interest. There are various strategies which can be employed to determine the runs chosen, the detail of which will not be discussed here but can be found in comprehensive texts on the matter (Box et al. 1978; Raymond Myers 1990; D. Montgomery 2001). Due to their efficiency, fractional designs are widely implemented.

An assumption of a two-level design is the effects of the parameters on a response are linear. Perfect linearity is not required however, with the model (a first-order model) able to adequately represent the process or system when there is some degree of curvature in the effects of the parameters. Screening designs are a good example of where some degree of curvature can be acceptable. If the curvature cannot be adequately modelled, a higher order model, such as a second-order model, should be used. Three-level (or higher level) designs are used to enable the curvature present in the parameter effects to be accurately modelled. The ability to model both linear and nonlinear effects leads to these designs being employed for predictive and optimisation purposes.

### Three-level Full Factorial Design

To incorporate the fact that a parameter might not have a linear effect on a chosen response, another level is added. As is the case with the two-level factorial design, a three-level full factorial design incorporates all combinations of the levels of the input parameters, however the number of experimental runs required as the number of parameters increases is considerably more rapid than for the two-level design. A design with five input parameters will require $3^5$, or 243, experimental runs to be performed to capture all effects in the model. The inefficiency of these designs has led to the development of a number of three-level fractional designs.

### Central Composite Design (CCD)

The CCD is a popular design for fitting second-order models. A representation of a two parameter CCD is presented in Figure 4.1. The CCD is essentially a $2^k$ factorial design with star, or axial, points (the points lying outside of the square) and centre points (Box & Wilson 1951; Box et al. 1978). Note the points in Figure 4.1 represent the parameter levels for a specific experiment. For example, the point (+1, +1) represents an experiment where both parameters are at their high level.

Each component of the design has a primary purpose. The $2^k$ factorial component provides a fit for the first-order model (main effects in interactions), while the axial and centre points make the design a three-level design, enabling quadratic effects to be incorporated and also provides an estimate of the pure error of the model.

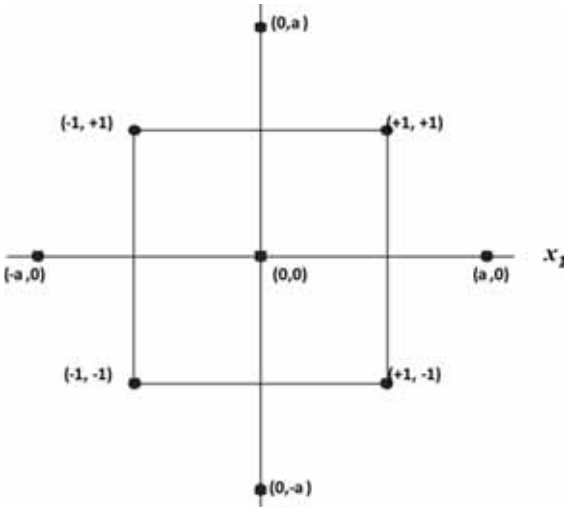


**Figure 4.1: Graphical representation of the Central Composite Design (CCD)**

## Box-Behnken Design

Another three-level design is the Box-Behnken design (Box & Behnken 1960). These designs are formed by combining a $2^k$ factorial with an incomplete block design. A block design refers to a technique where a design is altered when a known and controllable source of variation is present in an experiment. For example if an industrial experiment is to be performed where different batches of raw material with known differences in quality are used then the design can be altered accordingly to account for this known variation. Figure 4.2 displays a Box-Behnken design for three parameters. A key feature of this design is that it does not contain any points on the vertices of the cubic region (the upper and lower levels of each variable). While this may be advantageous in some instances where these combinations represent an experimental run which may be prohibitively expensive or impossible to run due to physical constraints, through experience gained through the completion of this thesis it has been found that this design does not necessarily test the design space adequately. The attractiveness of this design is however its efficiency (i.e. number of experimental runs). For example, for a 7-factor design, a Box-Behnken design requires only 57 experimental runs (with one centre point run) whereas a 3-level full factorial design requires 2187 runs. Even a 2-level full factorial design requires 128 runs.

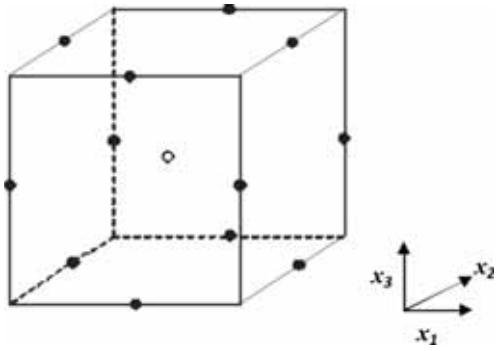


**Figure 4.2: Graphical representation of the Box-Behnken design**

### Computer Generated Designs

Computer generated designs are constructed using computer codes which search for an optimal design matrix which is for a pre-determined optimality criterion. These types of designs can be chosen based upon a number of reasons such as if the design space is of an irregular shape, there is more than three levels for input parameters, and reducing the number of experimental runs required.

One such computer generated design is the D-optimal design. The optimality criterion for this design aims to minimise the covariance of the parameter estimates, which is equivalent to maximising the determinant $|\mathbf{X'X}|$, where X is the design matrix. The benefit of the D-optimal design is versatility. It can be used for any type of the model (first-order, second-order, etc) and for any purpose (screening, prediction or optimisation).

### Analysis of Experimental Designs

Once the experiments have been completed, the data is analysed using statistical methods. There are many methods which can be employed, such as kriging or neural networks but a widely used method is the response surface methodology. Many textbooks provide a comprehensive review of this methodology, but a brief review of the important aspects can be found in Appendix A.

## 4.2 The Use of Experimental Design in the Oil and Gas Industry

One of the first uses of the ED methodology in the oil and gas industry concerned the analysis of physical experiments (Heins and Friz 1967), and subsequently by Burwell and Jacobson (1975); Gerbacia (1978) and Jacques and Bourland (1983). More recently, the greatest application of ED methodology in the oil and gas industry has been in the area of computer experiments. Major decisions in the oil and gas industry are often made based on minimal information so that great uncertainty and subsequent risk exists in oil and gas operations. Geological models and subsequent dynamic simulation models are built in order to gain a better understanding of these uncertainties. However, covering the entire range of uncertainties with these models is not practicle, both

computationally as well as with respect to time and money. The application of ED is one way to use resources more efficiently through the generation of a surrogate mathematical model to minimise the number of numerical simulation models required to characterise the problem.

The experimental design methodology has been extensively used in the oil and gas industry to achieve three main objectives:

1. Sensitivity analysis (screening studies). The purpose of these studies is to analyse the effect the input variables have on a chosen response. These studies are used to test if a factor is influential on a response and if so the magnitude of the effect. This is useful in history matching studies where the most influential parameters affecting the quality of the history match can be identified efficiently. It is also useful in studies where initially a large number of factors is considered, and the most influential parameters can be identified for further use in higher order experimental designs with the purpose of, for example, optimising a process. Note that the retainment of unnecessary (uninfluential) parameters reduces the quality of the fit of the model, which is undesirable if the model is to be used as a surrogate to reservoir simulation.
2. Predictive purposes. The surrogate equation generated from the analysis of the experimental design can become a substitute for numerical simulation. This surrogate equation can be used in conjunction with, for example, Monte Carlo simulation to generate probability distribution curves for responses such as hydrocarbon volumes in place and oil recovery relatively quickly.
3. Optimisation purposes. Experimental design methodology can also be used for optimisation of, for example, a field development plan. This can involve a range of parameters, such as the number of producers and/or injectors, well locations, and the volume of the slug used for enhanced oil recovery (EOR) purposes to name but a few.

Table 4-1 provides a summary (by no means exhaustive) of the use of experimental design methods in oil and gas industry studies.

**Table 4-1: Use of the ED methodology in the oil and gas industry**

| Use of Experimental Design Methodology | O&G Industry Application |
|---|---|
| Sensitivity/Screening Study | (Heins & Friz 1967; Torrest 1982; Jones et al. 1997; Cobianco et al. 1999; B. Corre et al. 2000; Friedmann et al. 2001; C. White et al. 2001; Kabir et al. 2002; Al Salhi et al. 2005; Cheong & Gupta 2005; Cheong et al. 2005; Esmaiel et al. 2005; Peake et al. 2005; Carreras, Turner et al. 2006; Carreras, S. Johnson et al. 2006) |
| Predictive Purposes | (Torrest 1982; Damsleth et al. 1992; Jones et al. 1997; B. Corre et al. 2000; van Elk & Guerrera 2000; Friedmann et al. 2001; C. White et al. 2001; Feng & C. White 2002; Kabir et al. 2002; Cheong & Gupta 2005; Cheong et al. 2005; Peake et al. 2005; Carreras, Turner et al. 2006; Carreras, S. Johnson et al. 2006; Lee et al. 2006; Amorim & Moczydlower 2007) |
| Optimization Purposes | Aanonsen et al. 1995b; G. Vincent et al. 1999; C. White & Royer 2003b; Carreras et al. 2006c; Kalla & C. White 2007 |

A common practice adopted in the oil and gas industry is the staged use of the experimental design methodology in order to gain a full understanding of the uncertainties associated with the chosen response(s) which can then be utilised to make accurate predictions and decisions. For example, to develop estimates of the hydrocarbon volumes in place, a screening study would be performed initially. A significant number of parameters would be tested to determine whether they have a significant influence on determining the volumes of hydrocarbons in place. Those parameters which have been identified to have a significant influence would then be incorporated into a higher level design to accurately develop a surrogate (proxy) equation which, as mentioned, can then be used to develop probability distributions for the in place volumes.

This staged approach has two benefits. The first is the reduction in resources required to test the influence of the selected input parameters. A considerable number of experimental runs would be required if all parameters under consideration were to be tested using a higher order design (e.g. a three-level design). The screening study, typically conducted using a two-level design, allows for the testing of a large number of parameters efficiently, with only the influential parameters being included in the higher order design. Secondly, the removal of uninfluential parameters in a design used for predictive or optimisation purposes can improve the capability of the surrogate equation to replicate the results of the experimental runs, as well as accurately predict the results of untested areas in the design space.

Careful consideration of a number of aspects in the implementation of ED is required to ensure the results of the analysis accurately represent the processes studied (Amudo *et al* 2009). The incorrect choice of the design, the selection of a too wide or narrow range for the parameters, and the selection of too many parameters can lead to erroneous results.

In this thesis, the ED methodology is used to both test the sensitivity of parameters on the EGR process, as well as for optimisation/predictive purposes. The successful application of the ED methodology in the oil and gas industry for these purposes has given confidence that this methodology can be employed in this thesis with success.

# CHAPTER 5

# 5 Study 1: The Injection of $CO_2$ at the Commencement of $CH_4$ Production

## 5.1 Introduction

Study 1 investigates the situation where $CO_2$ is injected at the commencement of $CH_4$ production. The advantage of the early injection is that with the pressure maintenance supplied by the injection of $CO_2$, the influx of the aquifer will be restricted. The influx of the aquifer into the gas reservoir will limit the recovery potential of $CH_4$ through pressure maintenance and gas trapping. Restriction of the influx of the aquifer will ensure minimal to no loss in recovery due to residual trapping. However, previous research has shown that the early injection of $CO_2$ into volumetric gas reservoirs has the disadvantage of allowing the maximum time for mixing between the natural gas and $CO_2$ (Clemens & Wit 2002; Jikich et al. 2003; Al-Hashami et al. 2005). With maximum benefit in restricting the influx of the aquifer occurring with the early injection of $CO_2$, it is important to gain an understanding of the properties which will stabilise the displacement, and reduce the extent of mixing between the two fluids.

In this chapter, the experimental design (ED) methodology has been utilised to study the displacement of $CH_4$ by $CO_2$. Factors investigated in the design have been chosen based upon a number of reasons. The parameters studied have been chosen based on their potential impact on the stability of the displacement process, their potential to influence the degree of mixing between the two fluids, the efficiency of the sweep of the reservoir, and the interaction between the injected $CO_2$ and the formation water. Factors were also chosen based upon the impact on recovery under primary depletion conditions, in order to compare recovery under injection conditions with conventional primary depletion.

Concluding this chapter is a section which, based upon the results of the experimental design, investigates operational strategies that can be applied to scenarios which resulted in poor sweep of the reservoir. Identifying reservoir management strategies that improve the efficiency of the displacement process is obviously of great benefit.

## 5.2 Model Description

A simple, conceptual numerical simulation model in the form of a rectangular tank was constructed in this study. This model, in the base case form, is a homogeneous, anisotropic $CH_4$ reservoir with an associated water-drive. Key properties of the model are given in Table 5-1. Relative permeability data is presented in Figure 5.1, which comprises a theoretical data set calculated from correlations presented by Standing (1974), with residual gas saturation set at 30%, and original gas saturation at 90%. The initial pressure and temperature used in the model is based on that found in the Naylor gas field ($P_i$ = 2830 psi and $T_i$ = 85°C at a depth of 2020 m (GWC)).

**Table 5-1: Base case model properties**

| | |
|---|---|
| Model Dimensions | 500m by 500m by 100m |
| Grid Block Dimensions | 50m by 50m by 2m |
| Horizontal Permeability (kh) | 100mD |
| Vertical Permeability (kv) | 10% of kh |
| Porosity (ϕ) | 15% |
| Initial Pressure at top of structure | 3000 psia / 206 bar |
| Temperature | 100 °C / 212 °F |
| Formation water salinity | 10,000 ppm |
| OGIP | 19.67 Bscf / 562 $MMsm^3$ |
| Production Rate | 5 MMscf/day / 141,500 $sm^3$/day |
| Injection Rate | 5 MMscf/day / 141,500 $sm^3$/day |
| Number of Production Wells | 1 |
| Number of Injection Wells | 2 |

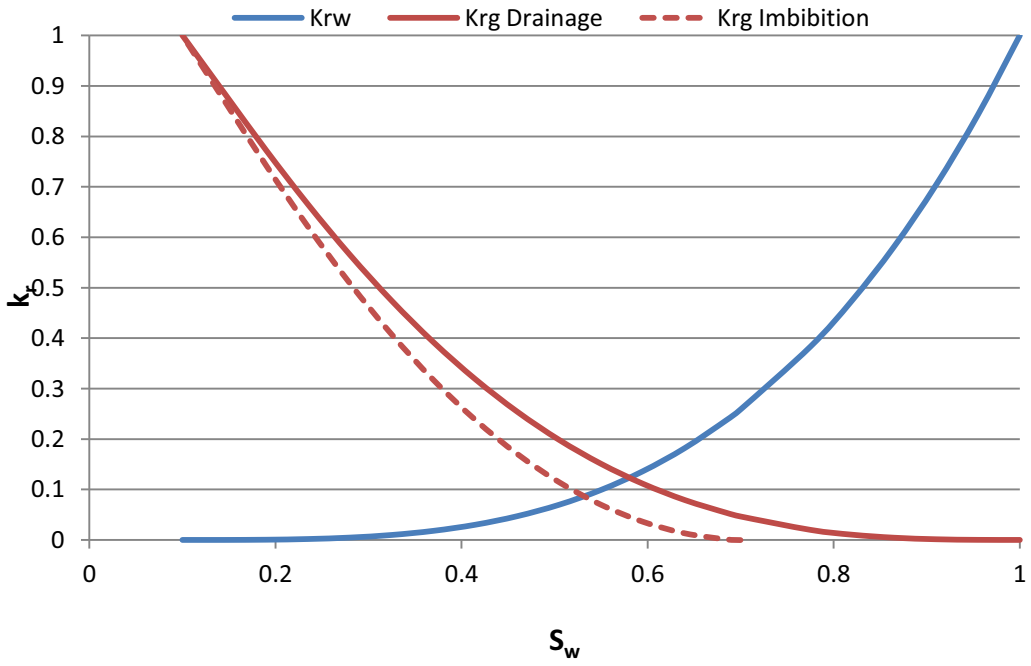


**Figure 5.1: Relative permeability data used in model**

A schematic of the field and well locations in a model with no formation dip is shown in Figure 5.2. The well pattern is a staggered line drive, with one production well and two injection wells. From the review of the fluid properties of $CO_2$ and $CH_4$, at reservoir conditions the injected $CO_2$ will under-ride the $CH_4$ column whilst over-riding the water column. The well completions for both the injection and production wells are therefore located to maximise the advantage presented by these fluid properties. The injection well completions are located at the gas-water contact (GWC) and not over the entire interval, with the production well completions located at the top of the structure to maximise stand-off from the GWC. All further diagrams and schematics in this thesis represent injection well completions at the GWC and not over the entire interval.

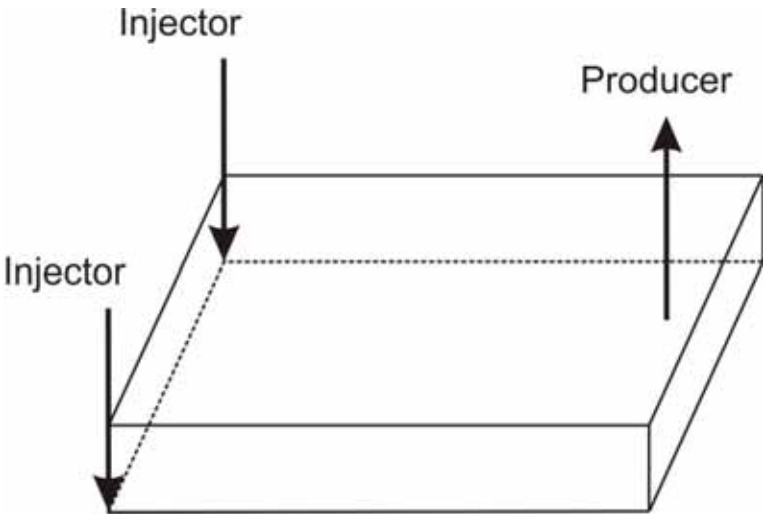


**Figure 5.2: Schematic of non-dipping model**

A simple, homogeneous model has been initially chosen for this investigation. This will enable knowledge to be developed on the important processes involved in the displacement of $CH_4$ by $CO_2$ without the added complexity of a more detailed (i.e. heterogeneous) model. Complexity in the form of heterogeneity is added with the introduction of simple permeability heterogeneity later in this chapter as well as in Chapter 6. Once a fundamental understanding of the key processes involved in the displacement of $CH_4$ by $CO_2$ is developed, the application of $CO_2$ EGR will be applied to a model of a depleted gas field in Chapter 7.

The simulations performed in this study involve the mixing of two gases. A known issue in the field of numerical simulation with respect to the displacement of one fluid by another is the effect of numerical dispersion. Before the effect of numerical dispersion is discussed, the advection-diffusion equation will be introduced. The flow of a component can be described by the advection-diffusion equation (assuming constant diffusion coefficient and advection velocity and assuming no source or sink).

$$\frac{\partial c}{\partial t} = u\frac{\partial c}{\partial x} + D\frac{\partial^2 c}{\partial x^2} \quad (5.1)$$

where $c$ = variable of interest, in this case concentration

$D$ = diffusion coefficient

$u$ = velocity

The first term on the right hand side of equation 5.1 is the advection term, with the second being the diffusion term. Diffusion describes the movement of particles through random motion, while advection describes the movement of particles due to the bulk motion in a particular direction. In most reservoir situations, the advective term is much larger than the diffusive term (Tek 1989).

It can be seen that Equation 5.1 is a partial differential equation. Due to the highly non-linear nature of partial differential equations (PDEs), numerical methods have to be implemented to convert them into algebraic equations, giving solutions (such as pressure and saturations) at discreet points. The most widely used numerical method in the oil and gas industry is the finite difference method which uses the Taylor series approximations for the discretisation of the PDEs (Abou-Kassem et al. 2006). The use of the Taylor series approximations does however introduce a truncation error, commonly known as numerical dispersion. This numerical dispersion mimics physical dispersion in that it smears saturation fronts (L.P. Dake 2001). With the advective term usually being much larger than the diffusive term, the numerical dispersion error is also generally much larger (Tek 1989). This can therefore completely mask the true extent of physical diffusion. As physical diffusion is a parameter of interest in this study, it is desirable to limit the amount of numerical dispersion arising in the model. Numerical dispersion is a function of the spatial and time discretisation, i.e. grid block and time step sizes. Decreasing the grid block sizes and/or the time steps will reduce the numerical dispersion error being introduced into the model. However, this also increases the number of calculations required in the simulation, increasing computational time, an important issue in compositional simulation. Consequently, a balance between computational time and accuracy of results is required when choosing the grid size in the model. To find this balance, a sensitivity study on the number of grid blocks used in the model was performed. As gravitational effects are expected to be important in all simulations, high resolution in the vertical direction is required. A thickness of 2 metres for each grid block was deemed acceptable in capturing these gravitational effects. The sensitivity study involved determining the size of the grid blocks in the horizontal direction. The length of the model in the X and Y directions in the non-dipping model is 500 metres. The study tested grid block sizes of 16.67 metres (30 by 30 grid in X and Y), 25 metres (20 by 20 grid) and 50 metres (10 by 10 grid). Each simulation was run for a 25 year period, with $CO_2$ injection commencing at the start of $CH_4$ production. The largest diffusion coefficient of 1 x $10^{-6}$ $m^2/s$ used in Study 1 is

chosen as this represents the greatest potential for mixing by diffusion in this study. Comparison of results was based upon the $CO_2$ production profile, indicating the breakthrough times of $CO_2$ at the production well, with these results compared to the computational time required to complete the simulation. Figure 5.3 illustrates the $CO_2$ concentration in the production well over the 25 year period, with Table 5-2 presenting the computational time required in seconds.

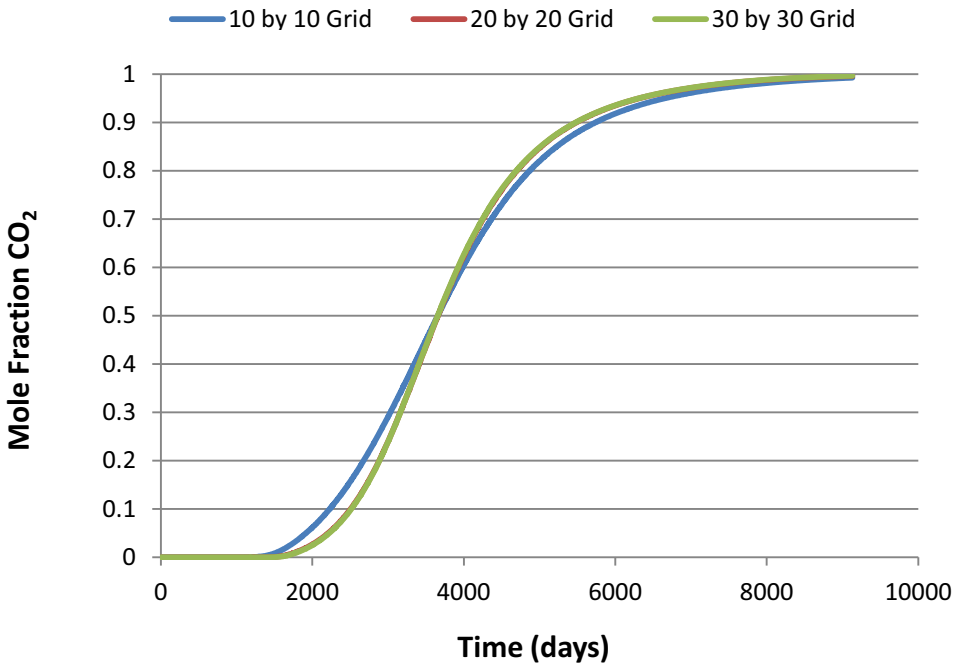


**Figure 5.3: Mole fraction of $CO_2$ in production stream for variable grid block sizes**

**Table 5-2: Computational time required to complete each simulation run for variable grid block sizes**

| X and Y Grid Dimensions | Computational Time (seconds) |
|---|---|
| 10 by 10 | 1516 |
| 20 by 20 | 4959 |
| 30 by 30 | 11,860 |

From Figure 5.3 it can be seen that there is no difference in the results of the higher resolution grids. However, a discrepancy can be seen in between the results of the 10 x 10 grid and the higher resolution grids. This discrepancy is not however considered large enough to warrant the exclusion of the use of the 10 x 10 grid. Whilst there is no difference in the $CO_2$ production profiles of the two finest grids, Table 5-2 indicates a clear difference in the computational time. Although some difference is observed in the $CO_2$ production profile of the 10 x 10 grid, the computational time was relatively short at 1,516 seconds (about 25 minutes). The 20 by 20 grid simulation run time was over three times longer than the 10 x 10 grid, with the 30 x 30 grid simulation taking 11,860 seconds (about 197 minutes) to complete. It was decided to employ the 10 by 10 grid for this study.

The decision to use the 10 x 10 grid was based upon two main reasons. Firstly, the purpose of initial studies using the simple model was for comparative purposes. There would be no adverse influence

on the comparison of the results if all models had the same/similar numerical error present, considering that from Figure 5.3 the error appears minimal. It was not the aim of this section to optimise the breakthrough time of $CO_2$, and so accurate consideration of the effect of numerical dispersion was not required. Secondly, a large number of simulations was expected to be, and in fact was, performed in this thesis (well above the number presented in this thesis). Simulations which required a computational time greater than one hour were deemed unsatisfactory.

## 5.3 Experimental Design Study

### 5.3.1 Design Selection

The selection of the experimental design was based upon experience gained in this thesis through trial and error, as well as designs employed in published oil and gas studies using ED. It was initially decided that a two-level design would not meet the aims of this study. The effect of the chosen parameters was expected to be both non-linear in some instances, due to the complexity of the processes involved, as well as strongly influenced by other parameters, i.e. interactions. A two-level design assumes that the input parameters have a linear effect on the chosen responses. Therefore, if it is believed that the effect of the input parameters will be non-linear, a two-level design would be unsatisfactory in capturing these expected effects with sufficient accuracy. A three-level design was subsequently selected due to the ability to model the expected non-linear effects.

A review of the designs used in oil and gas studies showed the successful application of the D-optimal design (Egeland et al. 1992; Aanonsen et al. 1995; Jones et al. 1997; Cobianco et al. 1999; Gilles Vincent et al. 1999; B. Corre et al. 2000; Friedmann et al. 2001; Kabir et al. 2002). Additionally, it was noted during the review of experimental design methodology that the D-optimal design can also be used for any purpose, be it for sensitivity, predictive or optimisation purposes. This versatility as well as its demonstrated use in oil and gas studies led to the selection of this design for this study.

### 5.3.2 Parameter and Range Selection

The parameters chosen in this study, and the range of values used for each parameter, are shown in Table 5-3.

**Table 5-3: Experimental design parameters and ranges**

| Parameter | Low (-1) Level | Mid (0) Level | High (+1) Level |
|---|---|---|---|
| Permeability | 10mD | 100mD | 1,000mD |
| $k_v/k_h$ Ratio | 0.01 | 0.1 | 1 |
| Aquifer Size* | 100x | 300x | 500x |
| Salinity | 1,000ppm | 10,000ppm | 100,000ppm |
| Diffusion Coefficient | $1x10^{-6}$ $m^2$ $s^{-1}$ | $1x10^{-8}$ $m^2$ $s^{-1}$ | $1x10^{-10}$ $m^2$ $s^{-1}$ |
| Thickness | 50m | 100m | 150m |
| Dip of Formation | 0° | 11° | 21° |

* Aquifer size is a multiplication of the gas pore volume

*Permeability and* $k_v/k_h$ *ratio:* the permeability of the reservoir, both horizontal and vertical, was chosen based on a number of reasons. The importance of the viscous to gravity ratio on the displacement process between fluids of differing densities was shown by Craig *et al*. (1957). The viscous to gravity ratio is defined as

$$R_{v/g} = \left(\frac{u\mu_d}{kg\Delta\rho}\right)\left(\frac{L}{h}\right) \quad (5.2)$$

where, $u$ = linear Darcy velocity

$\mu_d$ = displaced fluid viscosity

$k$ = permeability of porous media

$g$ = gravity constant

$\Delta\rho$ = density contrast between displaced and displacing fluids

$L$ = length of system

$h$ = height of system

As shown in Chapter 3, when two fluids of contrasting density interact, gravity acts to force the denser fluid below the lower density fluid. The dominant influence of gravity on the displacement process is characterised by lower viscous to gravity ratio values. Depending on the density difference between the displaced and displacing fluids, this will lead to either gravity over-ride or under-ride. In the case of $CO_2$ and $CH_4$, $CO_2$ will under-ride the $CH_4$ column, as depicted in Figure 5.4. It has been demonstrated in EOR operations involving the injection of $CO_2$ that gravity segregation leads to the channelling of $CO_2$ over the oil column. This limits the contact, and hence the degree of mixing, between the two fluids and reduces the sweep efficiency leading to the early breakthrough of $CO_2$ at the production wells. While gravity segregation can be detrimental in EOR operations, with the fluid properties of $CO_2$ and $CH_4$, and the well completion configurations it is anticipated that gravity segregation could prove beneficial in $CO_2$ EGR operations. With respect to permeability, gravity dominated displacement is characterised by high permeability.

Improvement in the vertical sweep efficiency in EOR operations involving the injection of $CO_2$ is achieved with viscous dominated flow (Figure 5.4). Viscous dominated flow is characterised by higher values of the viscous to gravity ratio. Viscous flow is achieved when forces are great enough to counter the effect of gravity, leading to a more vertically uniform displacement profile. In $CO_2$ EOR operations, viscous dominated flow leads to a much improved sweep of the reservoir. Viscous dominated flow is characterised by low permeability.

With consideration of the effect on $CO_2$ EOR operations, the viscous to gravity ratio, and therefore the permeability of the reservoir, is expected to be influential in the stability of the displacement process between $CO_2$ and $CH_4$.

In a localised sense, the permeability will affect the stability of the fluid-fluid interfaces, both $CO_2$-$CH_4$ as well as $CH_4$-$H_2O$, around the production well. In other words the permeability will influence the formation and extent of both $CO_2$ and water coning impacting on the sweep efficiency. Under primary depletion conditions, the permeability will influence the impact on the ability of the aquifer to respond to gas production and therefore the degree of pressure support provided. In addition to the $CH_4$ – $CO_2$ displacement, the permeability of the reservoir will influence the primary recovery achievable, and therefore the extent that $CO_2$ injection will enhance gas recovery.

A wide range of permeabilities was chosen for this study, in an effort to capture all of the likely effects discussed above. Horizontal permeability ranges from 10 to 1000mD, with vertical permeability (in the form of the $k_v/k_h$ ratio) ranging from 1% to 100% of the horizontal permeability.

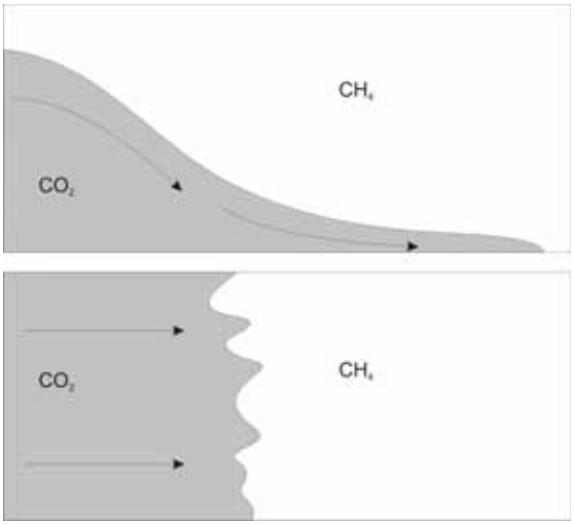


**Figure 5.4: Displacement profiles for (top) dominant gravity forces causing gravity under-ride, and (bottom) dominant viscous forces.**

*Aquifer Size:* the degree of pressure support provided by the aquifer is influenced by the size and hence strength of the aquifer. For this study, the aquifer is modelled through the use of a numerical aquifer. The size of the aquifer is based on a multiplication of the size of the gas reservoir. The range of aquifer size is based upon stand alone simulations which tested the effect of various sized aquifers on the primary recovery efficiency.The range chosen was deemed reasonable to represent a low, mid and high strength aquifer. A volumetric condition was unable to be chosen as part of the range due to the requirement of water breakthrough under primary depletion conditions. The second response for this ED study requires the calculation of primary recovery efficiency at a water production rate limit of 20 STB/day.

*Salinity:* as described in Chapter 2, the solubility of $CO_2$ is a function of the salinity of the formation water. The dissolution of $CO_2$ has the potential to delay the breakthrough of $CO_2$ at the production

well. With a $CO_2$ production limit in place, this has the potential to increase $CH_4$ recovery efficiency. Again a wide range of salinity values was chosen for the study, in order to test the effects of relatively fresh water to quite saline formation water.

*Diffusion Coefficient:* as indicated by the advection-diffusion equation, the mixing of two non-stationary fluids is comprised of two components attributable to flow (advection) and random molecular motion (diffusion). Although it is commonly believed that mixing is dominated by the advective component, Sim *et al* (2008) showed through core flood experiments that mixing by diffusion can be significant and cannot be ignored. The diffusion coefficient was subsequently chosen as a parameter for this study. Sim *et al* (2008) also stated that molecular diffusion is a function of pressure, with the magnitude of diffusion reduced at higher pressure. This influenced the selection of the range of diffusion coefficients, with the range encompassing the fact that both $CO_2$ and $CH_4$ are at supercritical conditions. In addition, the range was influenced by experimentally determined diffusion coefficients matched by numerical simulation from Seo and Mamora (2003) as well as Sim *et al* (2008). A range of diffusion coefficients from $2 \times 10^{-7}$ $m^2/s$ to $1.67 \times 10^{-8}$ $m^2/s$ was calculated in the study of Seo and Mamora (2003), while Sim *et al* (2008) matched experimental results with a numerical model utilising a diffusion coefficient of $1.67 \times 10^{-9}$ $m^2/s$. Based on these results and the fact that both fluids are in a supercritical state, the range chosen for this study utilises coefficients representing gas-like diffusion ($1 \times 10^{-6}$ $m^2/s$) through to liquid-like diffusion ($1 \times 10^{-10}$ $m^2/s$).

*Thickness:* the influence of viscous and gravity forces, both at the field scale (Figure 5.4), and the localised scale (i.e. coning), is influenced by the thickness of the reservoir. The influence of gravity increases relative to the influence of viscosity as the thickness of the reservoir increases (see Equation 5.2). As part of the development of the viscous to gravity ratio, Craig *et al* (1957) employed aspect ratios (i.e. length/thickness) ranging from 4 to 66 in their experimental models. For this study, aspect ratios ranging from 3.33 to 10 were used, corresponding to thickness ranging from 50 – 150 metres.

*Formation Dip:* in EOR operations involving the injection of a gas, preference is given for injection to occur in thin reservoirs (non-dipping) unless dipping (Taber et al. 1997a). The term “unless dipping” refers to the stabilising effect of gravity on the displacement front in dipping reservoirs. The density difference between fluids can be used to advantage if injection occurs below a critical rate, whereby the dominance of gravity will stabilise the displacement front, leading to high volumetric sweep efficiencies. If injection rates are greater than the critical rate, viscous forces can overcome the force

of gravity leading to viscous fingering and channelling. In non-dipping reservoirs, thin reservoirs are preferred to increase the likelihood of a viscous dominated displacement being achieved.

With a considerable density difference between $CO_2$ and $CH_4$, the effect of gravity and viscous forces is expected to be highly influential, as it is in $CO_2$ EOR operations. However with the density difference in $CO_2$ EGR operations ($\rho_{displacing} > \rho_{displaced}$), the opposite of $CO_2$ EOR operations ($\rho_{displaced} > \rho_{displacing}$), similar conclusions are not expected. A wide range of formation dip has been subsequently chosen to gain a comprehensive understanding of the effect of the formation dip on the displacement process, and the ability to achieve incremental recovery. The specific dip angles were chosen due to the ease of grid construction (11° and 21° rather than 10° and 20°).

## 5.4 Study 1 Responses (Metrics)

### 5.4.1 Response 1: $CH_4$ Recovery Efficiency at a $CO_2$ Breakthrough Limit of 10%

The degree of mixing between $CH_4$ and $CO_2$ is a primary concern with the injection of $CO_2$ into a gas reservoir. Consequently, it is paramount that the production of uncontaminated $CH_4$ is maximised. This response has been selected to gain an understanding of the influence the chosen parameters have on the stability of the displacement process, and the ability to maximise the production of $CH_4$ prior to the breakthrough of $CO_2$ at the production wells. In this instance, the initial breakthrough of $CO_2$ has been chosen to be once $CO_2$ production has reached 10 mole percent.

### 5.4.2 Response 2: Minimum producing $CO_2$ concentration required to achieve incremental $CH_4$ recovery

Whilst a certain reservoir situation might provide conditions suitable for the stable displacement of $CH_4$ by $CO_2$, it might not necessarily correspond to a situation where $CH_4$ production under $CO_2$ injection conditions compares favourably with the recovery under primary depletion conditions. This response therefore aims to highlight conditions which will lead to incremental recovery being achieved with the lowest producing $CO_2$ concentration. This response is calculated in a two step process:

- Firstly, under primary depletion conditions, $CH_4$ recovery is determined at a water breakthrough limit of 20 stb/day.
- Secondly, the model is re-run under conditions of $CO_2$ injection, and the producing $CO_2$ concentration is noted at the same $CH_4$ recovery determined in the primary depletion case.

This $CO_2$ concentration is therefore the minimum producing $CO_2$ concentration required to achieve incremental recovery. Any further $CH_4$ recovery beyond this point is considered incremental recovery, the extent of which would be determined by the maximum allowable producing $CO_2$ concentration.

## 5.5 Study 1 D-Optimal Design

The D-optimal design used in this study is presented in Table 5-4, specifying the parameter levels (presented in Table 5-3) for each design run. The parameter levels are displayed in their coded form (i.e., -1, 0, +1) representing the low, mid and high levels. Note that levels can also be non-integer numbers (i.e. +0.5) when a D-optimal design is implemented. The table was constructed using a commercial experimental design program (Stat-Ease 2008).

**Table 5-4: Experimental design matrix and results**

| Run | Permeability | $k_v/k_h$ ratio | Diffusion Coefficient | Salinity | Aquifer Size | Formation Thickness | Formation Dip |
|---|---|---|---|---|---|---|---|
| 1 | -1 | 0 | -1 | -1 | 1 | -1 | -1 |
| 2 | 0 | -1 | 1 | 1 | 1 | -1 | -1 |
| 3 | 1 | -1 | -1 | 1 | 1 | -1 | 0 |
| 4 | -1 | -1 | 1 | -1 | -1 | 1 | -1 |
| 5 | 0 | 1 | 1 | 1 | -1 | -1 | -1 |
| 6 | -1 | -1 | 1 | 1 | 0 | -1 | 1 |
| 7 | -1 | 1 | -1 | -1 | 0 | 1 | 1 |
| 8 | 1 | 1 | -1 | 1 | 1 | 1 | -1 |
| 9 | -1 | 0 | 1 | 1 | 1 | 1 | 1 |
| 10 | -1 | 1 | -1 | 1 | 1 | -1 | 1 |
| 11 | 0 | 0 | 0 | -1 | 0 | 0 | 0 |
| 12 | 0 | 1 | 1 | -1 | 1 | 1 | -1 |
| 13 | 1 | -1 | -1 | 0 | -1 | -1 | 1 |
| 14 | 1 | -1 | -1 | 1 | 0 | 1 | 1 |
| 15 | 0 | -1 | 1 | 1 | -1 | 1 | 1 |
| 16 | 1 | -1 | 1 | 1 | 1 | 0 | 1 |
| 17 | 0 | -1 | -1 | -1 | -1 | 1 | -1 |
| 18 | -1 | 1 | 1 | 1 | 1 | 0 | -1 |
| 19 | 1 | 1 | -1 | -1 | -1 | -1 | -1 |
| 20 | 1 | 1 | 0 | 1 | -1 | -1 | 1 |
| 21 | 1 | -1 | 1 | -1 | 0 | 1 | 1 |
| 22 | 1 | -1 | 1 | -1 | -1 | -1 | 0 |
| 23 | -1 | -1 | -1 | 1 | 1 | 1 | -1 |
| 24 | -1 | -1 | 0 | 1 | -1 | -1 | -1 |
| 25 | -1 | -1 | 0 | -1 | 1 | -1 | 1 |
| 26 | -1 | 1 | -1 | 1 | -1 | 1 | -1 |
| 27 | -1 | -1 | 0 | -1 | 1 | -1 | 1 |
| 28 | -1 | -1 | -1 | -1 | -1 | 0 | 1 |
| 29 | 1 | 1 | 1 | 0 | 1 | -1 | -1 |
| 30 | 1 | 1 | -1 | 1 | 1 | 1 | -1 |
| 31 | -1 | 1 | 1 | -1 | -1 | -1 | 1 |
| 32 | 1 | 1 | 1 | 0 | -1 | 1 | 1 |
| 33 | -1 | -1 | 1 | -1 | -1 | 1 | -1 |
| 34 | -1 | 1 | -1 | 0 | -1 | -1 | -1 |
| 35 | 1 | 1 | 0 | -1 | -1 | 1 | -1 |
| 36 | -1 | -1 | -1 | -1 | -1 | -1 | -1 |
| 37 | 1 | -1 | -1 | -1 | 1 | 1 | -1 |
| 38 | 1 | 0 | -1 | -1 | 1 | -1 | 1 |
| 39 | 1 | -1 | 1 | 1 | 0 | 1 | -1 |
| 40 | 1 | 0 | -1 | 1 | -1 | -1 | -1 |
| 41 | 1 | 1 | -1 | -1 | 1 | -1 | 0 |
| 42 | 1 | -1 | -1 | -1 | 0 | -1 | -1 |
| 43 | 0 | 0 | 0 | 0 | 0 | 0 | 0 |

## 5.6 Results and Discussion of Response 1: $CH_4$ Recovery Efficiency at a $CO_2$ Breakthrough Limit of 10%

The results for each design run are shown in Figure 5.5. This Figure shows that the average recovery efficiency of all the runs was around 63% of the OGIP. Recovery did range from as high as 80% to as low as 32%.

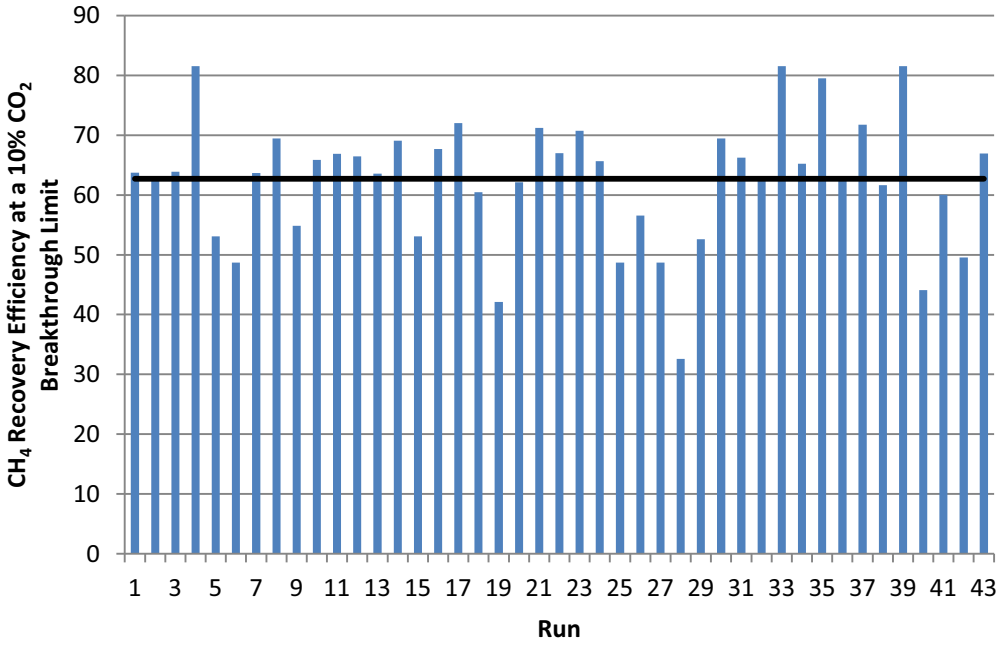


**Figure 5.5: Results for each design run and the average of all runs (black line) for Response 1**

Table 5-5 present a list of the ranking of statistically significant coefficients arising from the analysis of the experimental design. This list is constructed from the ANOVA table, which is the resultant table from the analysis of the experimental design. The ANOVA table presents a summary of the statistical significance of both the regression model as a whole, as indicated by, for example, the correlation coefficients, $R^2$, statistics, and of the individual coefficients of the model (i.e. main effects and interactions). A significance level of 0.05 was set for the analysis, which corresponds to a 95% confidence level. Step-wise regression was performed on the model to eliminate the statistically insignificant coefficients to improve the fit of the model. A more detailed description of the analysis of the experimental design can be found in Appendix A, or relevant experimental design textbooks (Box et al. 1978; Raymond Myers 1990; D. Montgomery 2001; D.C. Montgomery et al. 2006). To simplify the results presented in this thesis, the ANOVA tables for this response and all of the following responses presented in this thesis have been placed in Appendix B. A description of the meaning of the various terms in the ANOVA table (found in the Appendix), can be found in relevant texts on the theory of ED. The F-value in Table 5-5 is an indication of the relative statistical

significance of the coefficient. The higher the F-value, and consequently the lower the p-value, the greater the relative effect of the coefficient on the chosen response. For a parameter to be statistically significant with a 95% confidence level, the p-value has to be less than 0.05. In Table 5-5, a parameter listed singularly represents the main effect of that parameter. If two parameters are listed (i.e. permeability*dip), this represents an interaction meaning that the effect of one parameter is dependent upon the other. A quadratic coefficient (i.e. thickness$^2$) indicates that the main effect of this parameter on the response is not linear but has a degree of curvature.

**Table 5-5: Ranking of statistically significant coefficients from the analysis of Response 1**

| Statistically Significant Coefficient | F Value | p-value Prob > F |
|---|---|---|
| Permeability*Dip | 443.19 | < 0.0001 |
| Permeability*$k_v/k_h$ Ratio | 179.63 | < 0.0001 |
| $k_v/k_h$ Ratio*Dip | 131.79 | < 0.0001 |
| Thickness | 104.09 | < 0.0001 |
| Thickness*Dip | 100.74 | < 0.0001 |
| Aquifer Size | 100.07 | < 0.0001 |
| $k_v/k_h$ Ratio*Aquifer Size | 96.74 | < 0.0001 |
| Diffusion | 74.1 | < 0.0001 |
| Permeability*Salinity | 67.76 | < 0.0001 |
| Thickness$^2$ | 65.71 | < 0.0001 |
| Dip | 61.68 | < 0.0001 |
| $k_v/k_h$ Ratio*Diffusion | 55.59 | < 0.0001 |
| Salinity$^2$ | 48.96 | < 0.0001 |
| Aquifer Size*Thickness | 48.6 | < 0.0001 |
| Salinity*Aquifer Size | 41.54 | < 0.0001 |
| Permeability*Thickness | 37.93 | < 0.0001 |
| Permeability | 31.88 | < 0.0001 |
| Salinity | 31.62 | < 0.0001 |
| Diffusion*Thickness | 31.24 | < 0.0001 |
| Aquifer Size*Dip | 26.57 | 0.0001 |
| Diffusion*Aquifer Size | 21.67 | 0.0004 |
| Diffusion$^2$ | 18.76 | 0.0007 |
| $k_v/k_h$ Ratio*Thickness | 17.14 | 0.001 |
| Dip$^2$ | 16.67 | 0.0011 |

All of the relevant diagnostics ensuring the developed model adequately represents the data of the ED are acceptable. The correlation coefficient, $R^2$, and the adjusted $R^2$ coefficient are 0.9941 and 0.9830 respectively. The closer these coefficients are to one, the better the fit of the model to the data of the design. The normal probability plot, shown in Figure 5.6, provides a visual diagnostic tool to assess the adequacy of the model to replicate the data from the ED. Under the normality assumption, the residuals (the difference between the predicted response and the actual response in the design) should be normally and independently distributed with a mean of zero and a constant

but unknown variance. Visually, if this assumption is satisfied, the residuals in the normal probability plot should fall on a straight line. In reality the residuals do not fall perfectly on a straight line, however as long as there is no major deviation the results are acceptable. Figure 5.6 indicates no major deviation from the normality assumption.

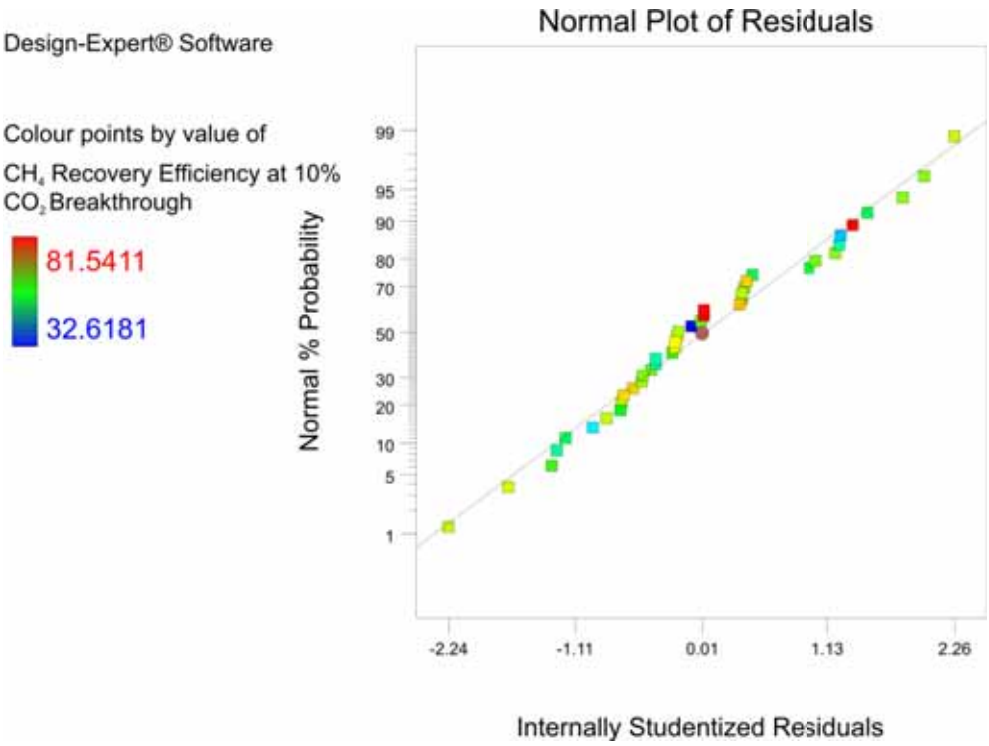


**Figure 5.6: Normal probability plot for Response 1**

The effect of the regression model coefficients on the chosen response can be represented by an effect graph. These graphs indicate the effect of varying a parameter (or parameters) from the low to high level (Table 5-3) on the response, in this instance the $CH_4$ recovery efficiency. Therefore, in Figure 5.7, it can be seen that for the low level of formation dip (i.e. a non-dipping reservoir), as permeability increases from the low (10mD) to high level (1000mD), $CH_4$ recovery efficiency at the 10% $CO_2$ limit decreases. It can also be observed to the left in Figure 5.7 that the remaining parameters in the design are at their mid (0) level. The effects of the two parameters in the effect graph, permeability and formation dip, are therefore calculated using the regression model with the remaining parameters based at the mid level. Consequently, if for example the $k_v/k_h$ ratio was increased to the high (+1) level, the effect of permeability in a non-dipping reservoir could be different to that observed in Figure 5.7. In this thesis, the effect graphs where the remaining parameters are at their mid level will be discussed.

As noted previously the statistical significance of the coefficients in Table 5-5 is a relative significance, and not an absolute significance. Therefore, while the lower ranking coefficients are statistically significant, there absolute effect on the response is likely to be minor. Consequently, only the most significant coefficients, in this case the top six, will be discussed.

Permeability – formation dip interaction

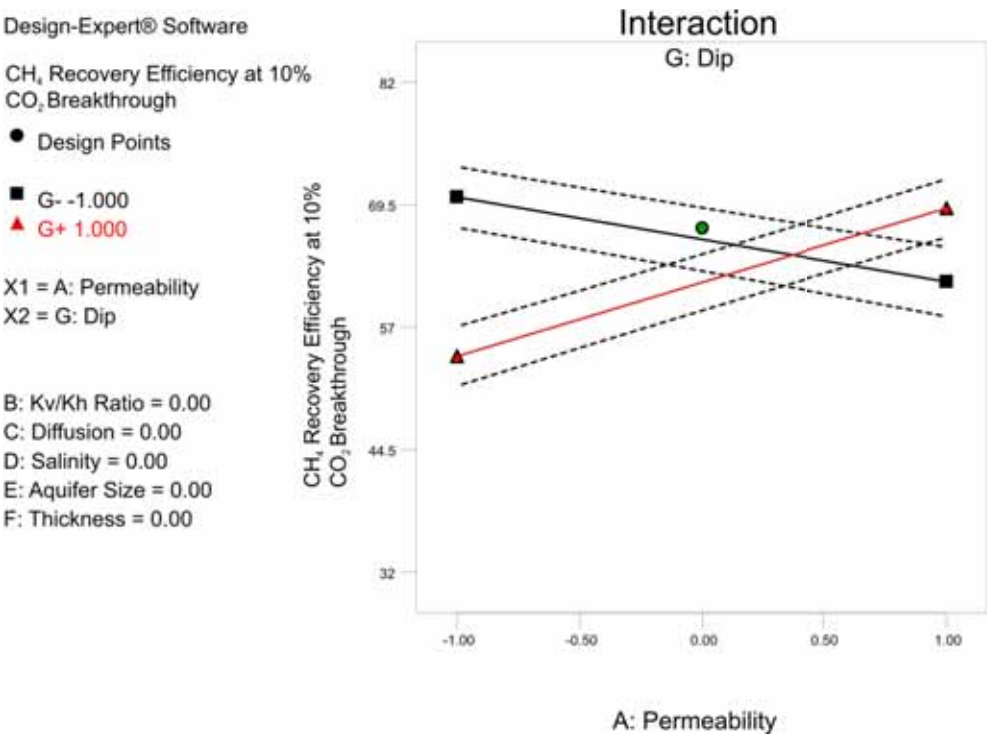


**Figure 5.7: Effect graph for the permeability - formation dip interaction for Response 1**

Figure 5.7 presents the effect graph for the permeability – formation dip interaction. Note that horizontal permeability will be called permeability from this point on in the thesis. From Figure 5.7, it can be seen that increasing permeability has opposing effects on the recovery efficiency of $CH_4$ at the 10% $CO_2$ limit depending on the degree of formation dip. In a non-dipping reservoir, increasing permeability reduces the recovery of $CH_4$ at the $CO_2$ breakthrough limit, while the opposite can be said for a dipping reservoir.

Firstly, in a non-dipping reservoir, Figure 5.8 and Figure 5.9 illustrate the effect of permeability on the displacement profile in a non-dipping reservoir. Both screenshots were taken at the equivalent time, corresponding to the time at which $CO_2$ production reaches 10% for the 100mD case. Strong, macroscopic viscous forces lead to a piston-like displacement which, similar to $CO_2$ EOR operations, can lead to an excellent sweep of the reservoir. Gravity segregation on the other hand forces $CO_2$ below the $CH_4$ column where it travels along the GWC to the area below the production well, essentially filling the reservoir from the bottom up. This then introduces the problem of $CO_2$ coning, as described in Chapter 2. If viscous forces locally are strong enough to overcome the effect of

gravity, $CO_2$ will be drawn up to the production well. The coning of $CO_2$ can lead to the premature breakthrough of $CO_2$ and severely limit the sweep of the reservoir. Although the susceptibility for coning to occur is minimised with increasing horizontal permeability, over the range tested increasing permeability has lead to the premature breakthrough of $CO_2$, limiting $CH_4$ recovery. If the permeability range used in the design was extended, it might be expected that recovery would increase with increasing permeability (i.e. curvature in the effect would be observed).

One issue that has to be considered with the low permeability case is the susceptibility of water coning prior to the breakthrough of $CO_2$. To meet a specified production rate, low horizontal permeability reservoirs require a greater drawdown which will induce greater viscous forces locally around the production well, increasing the likelihood of water coning. This could result in water production prior to the breakthrough of $CO_2$. The construction of the ED ensured this situation did not arise in any of the simulation runs, but in reality this is an issue that needs to be considered.

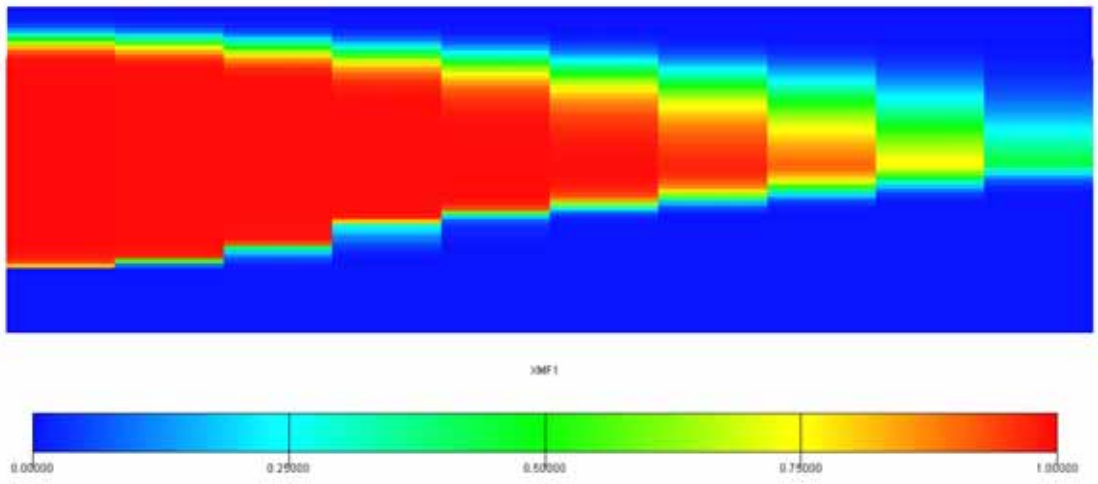


**Figure 5.8: Side-view of $CO_2$ saturation after 2620 days in a non-dipping reservoir with a permeability of 10mD. Injection wells located on the left with the production well on the right**

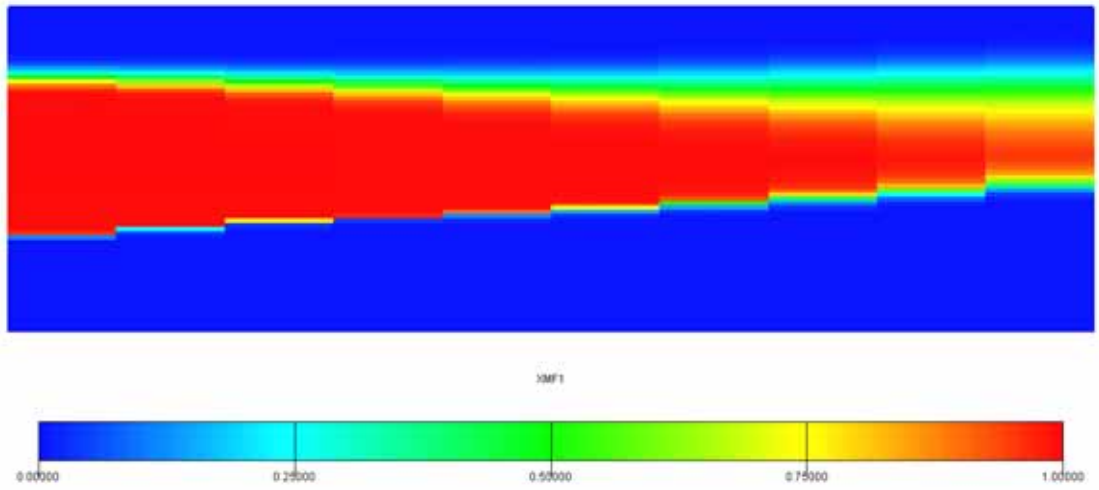


**Figure 5.9: Side view of $CO_2$ saturation after 2620 days in a non-dipping reservoir with a permeability of 100mD**

In a dipping reservoir, a positive trend is observed in Figure 5.7. The effect of permeability on the sweep of the reservoir can be observed in a comparison of Figure 5.10 and Figure 5.11, which presents two simulation screenshots of an 11° dipping scenario where only permeability has been altered. Both screenshots are taken at the time where the respective producing $CO_2$ concentrations have reached 10%. Once more, low permeability scenarios lead to a viscous dominated displacement process. It should be pointed out that when terms "viscous dominated displacement" and "gravity dominated displacement" are used, this refers to the macroscopic displacement process, unless otherwise stated. It can be seen in Figure 5.10 that viscous dominated displacement leads to the spreading of the displacement front in the vertical direction, with the flow of $CO_2$ concentrated at the top of the structure. This leads to a poor sweep of the reservoir resulting in the premature breakthrough of $CO_2$ at the production well. Increasing the permeability enables gravity to stabilise the displacement front (Figure 5.11). The stabilisation of the displacement front due to gravity leads to an improved sweep of the reservoir as $CO_2$ proceeds through the reservoir, as indicated by the reduced area of blue surrounding the production well at the top of the structure.

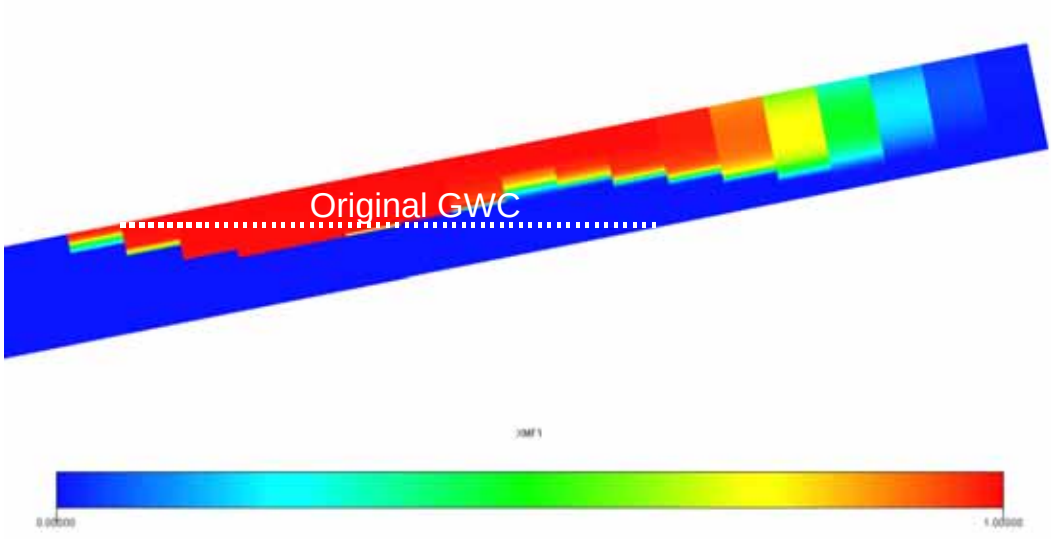


**Figure 5.10: Side-view of $CO_2$ saturation once the 10% $CO_2$ limit has been reached in an 11° dip reservoir. Permeability is equal to 10mD**

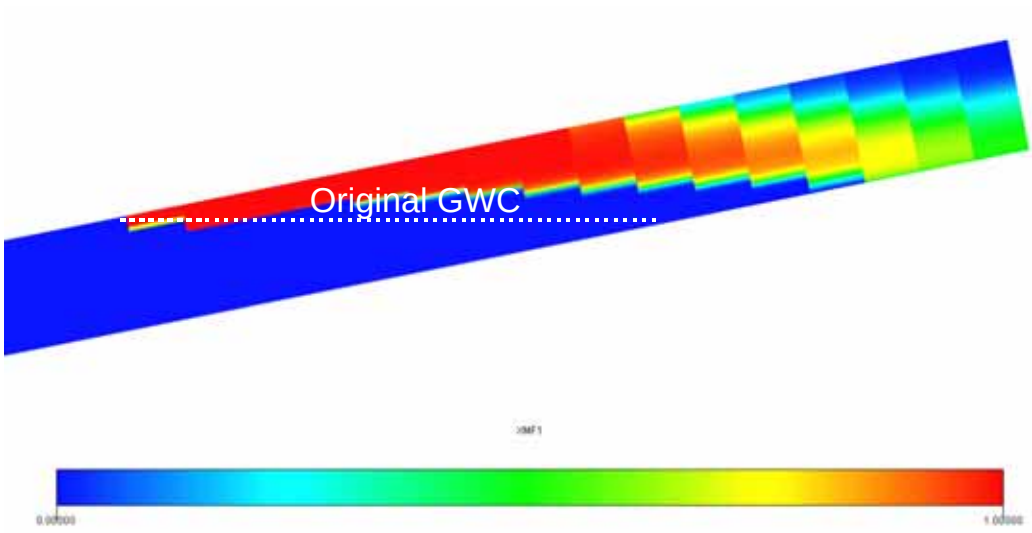


**Figure 5.11: Side-view of $CO_2$ saturation once the 10% $CO_2$ limit has been reached in an 11° dip reservoir. Permeability is equal to 100mD**

Permeability – $k_v/k_h$ ratio interaction

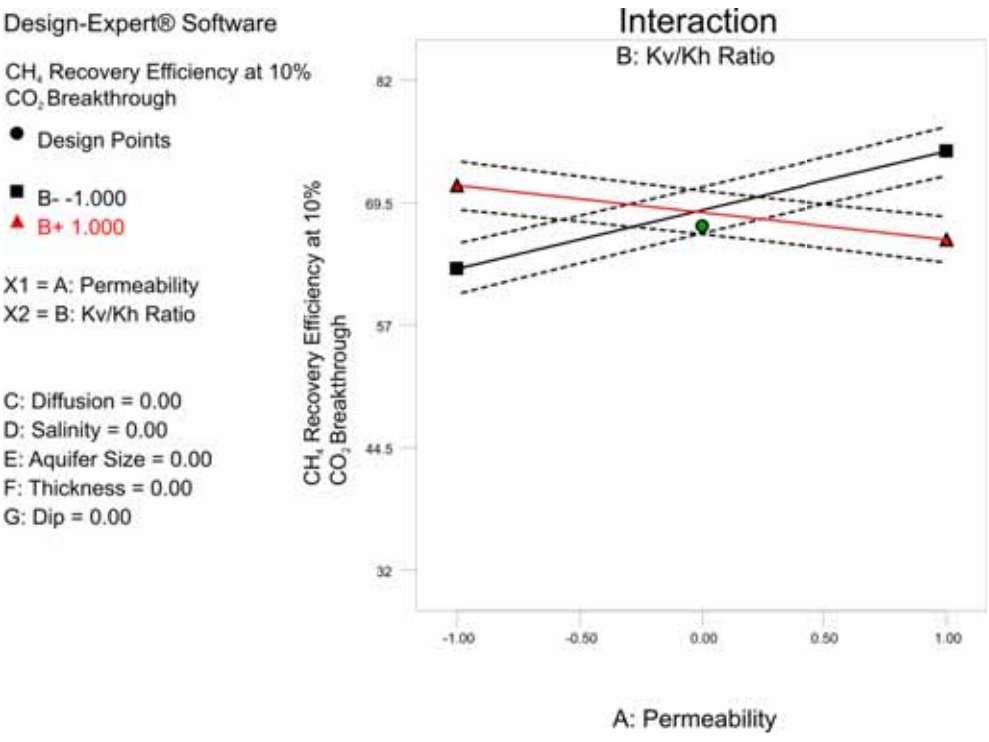


**Figure 5.12: Effect graph for the permeability - $k_v/k_h$ ratio interaction for Response 1**

Second in the ranking of significant coefficients is the permeability – $k_v/k_h$ ratio interaction (Figure 5.12). Opposing trends are again observed for the effect of permeability. At low ratio values, increasing permeability has a positive effect on $CH_4$ recovery, while the opposite is true when increasing permeability at isotropic conditions. Note that this effect graph is based on a formation

dip of 11 degrees (mid (0) level). With formation dip being such an influential parameter, this trend will differ depending upon the dip of the formation.

When the ratio is at the low level (1% of $k_h$), increasing permeability has a positive effect on the recovery of $CH_4$ at the 10% $CO_2$ limit. This is again due to the stabilising influence of gravity on the displacement front improving the sweep of the reservoir, as described in the permeability – formation dip interaction.

At isotropic conditions, a negative trend is observed in Figure 5.12 with increasing permeability. It was expected at first that increasing permeability would produce a positive trend, for the same reasons that have been described so far regarding the effect of permeability on the viscous and gravity forces. Consequently, further, stand alone simulations being performed to gain an understanding of this trend. The results of three simulations where permeability was altered are presented in Table 5-6. As expected, viscous dominated displacement was evident in low permeability situations, and gravity dominated displacement in high permeability situations. It was however the enhanced mobility attributable to the higher vertical permeability which led to the trend observed in Figure 5.12. Even with gravity dominated displacement, the enhanced mobility in both the horizontal and vertical direction led to earlier $CO_2$ breakthrough than for the low permeability case. The results did however exhibit curvature. Table 5-6 shows that the 100mD case had the earliest $CO_2$ breakthrough. This is due to the issue of $CO_2$ coning. At low permeability conditions, whilst permeability is low in the horizontal direction promoting coning, vertical permeability is also low, mitigating against the formation of coning. Likewise, at high isotropic permeability, whilst high vertical permeability promotes the formation of coning, high horizontal permeability acts to mitigate against it. Consequently, the 100 mD isotropic permeability case is the most conducive to the formation of $CO_2$ coning, and hence leads to the earliest $CO_2$ breakthrough and lower $CH_4$ recovery.

**Table 5-6: $CO_2$ breakthrough times and corresponding $CH_4$ recovery efficiencies for variable, isotropic permeability models in an 11° dipping formation**

| **Isotropic Permeability** | 10mD | 100mD | 1000mD |
|---|---|---|---|
| **10% $CO_2$ Breakthrough Time (days)** | 2634 | 2571 | 2640 |
| **Recovery Factor at 10% $CO_2$ Breakthrough Limit** | 64.7% | 62.9% | 64.8% |

$k_v/k_h$ ratio – formation dip interaction

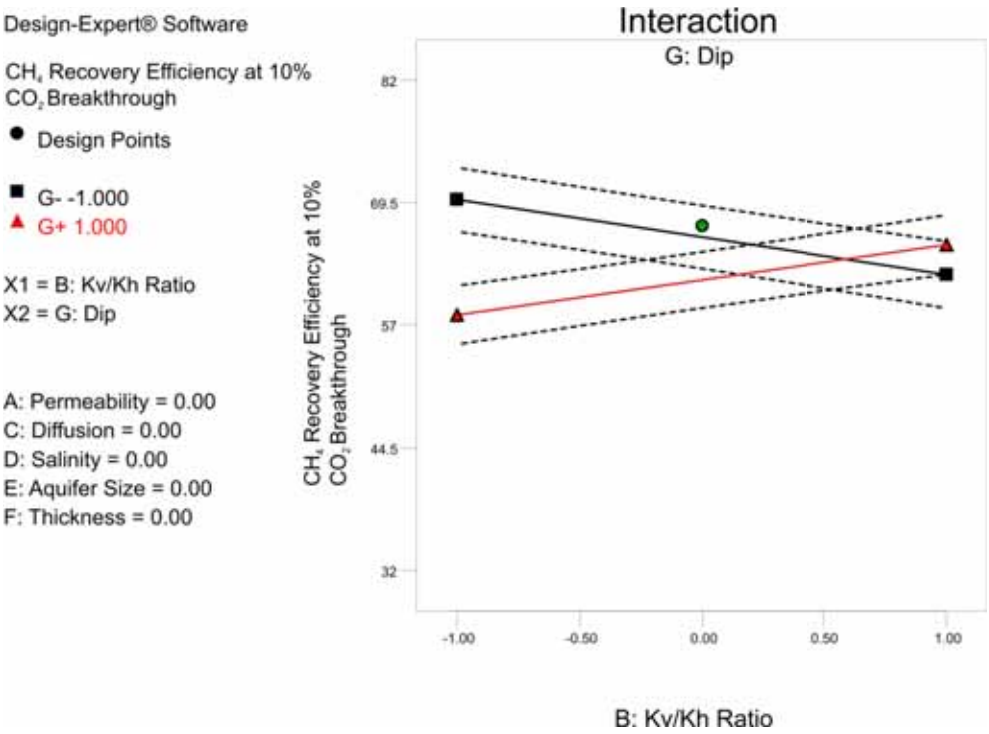


**Figure 5.13: Effect graph for the $k_v/k_h$ ratio – formation dip interaction for Response 1**

Moving to the $k_v/k_h$ ratio – formation dip interaction, Figure 5.13 shows a negative trend in $CH_4$ recovery efficiency with increasing vertical permeability in a non-dipping reservoir. Once more, the issue of $CO_2$ coning is evident in the results for a non-dipping reservoir. To demonstrate, Figure 5.15 and Figure 5.14 display the $CO_2$ saturation for two cases of differing $k_v/k_h$ ratio, 1% and 100%. Both screenshots are taken at the time where $CO_2$ production has reached 10% for the isotropic case. An increased susceptibility to fluid coning is attributable to, amongst other things, lower horizontal permeability (provided the fluid is beneath the production well) and greater vertical permeability. The enhanced mobility in the vertical direction clearly leads to the formation of $CO_2$ coning as shown in Figure 5.14. This leads to the premature breakthrough of $CO_2$ and consequently a poor sweep of the reservoir. Restricting the vertical movement of $CO_2$ reduces the potential for $CO_2$ coning and improves the sweep of the reservoir once $CO_2$ has reached the production well (Figure 5.15).

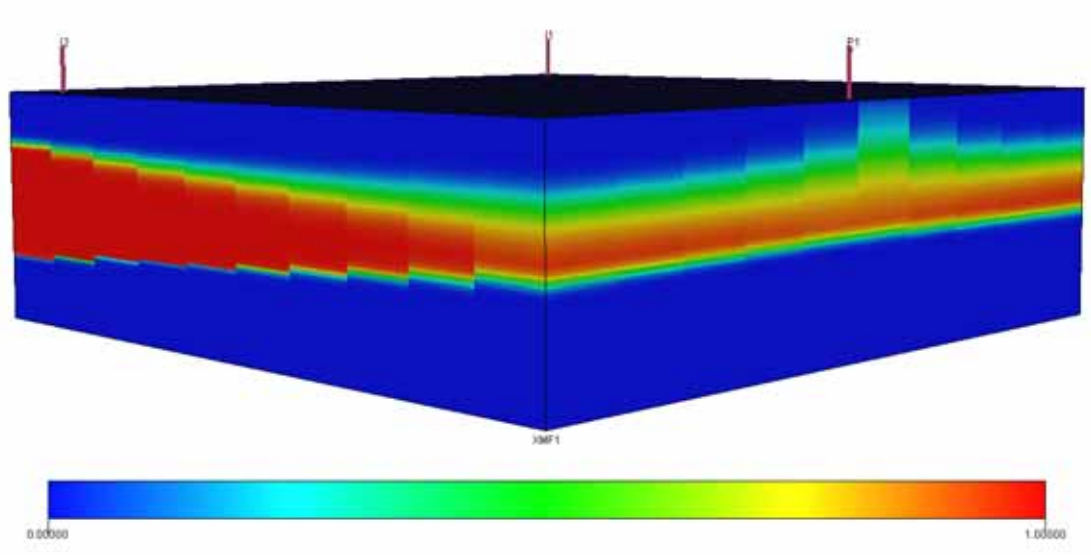


**Figure 5.14: $CO_2$ saturation after 2276 days in a non-dipping reservoir. The vertical to horizontal permeability ratio is equal to 100%**

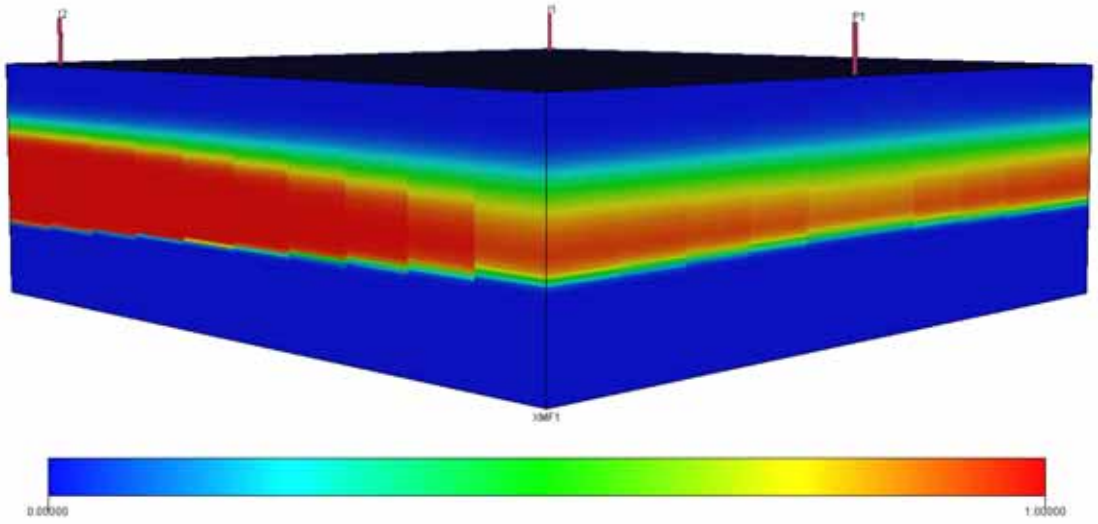


**Figure 5.15: $CO_2$ saturation after 2276 days in a non-dipping reservoir. The vertical to horizontal permeability ratio is equal to 1%**

Increasing the vertical permeability in a dipping formation of 21° meanwhile increases $CH_4$ recovery efficiency at 10% $CO_2$ breakthrough. Due to the significant component of vertical flow as $CO_2$ migrates from the injection to the production well, the vertical permeability has a similar effect to that of horizontal permeability in a dipping reservoir, as evident in Figure 5.16 and Figure 5.17. With low vertical permeability, viscous dominated displacement is once more observed (Figure 5.16), resulting in a poorer sweep of the reservoir. Increasing the vertical permeability enables gravity to have a progressively greater influence, leading to the displacement profile observed in Figure 5.17 and improving the recovery efficiency as compared to the low $k_v/k_h$ ratio scenario.

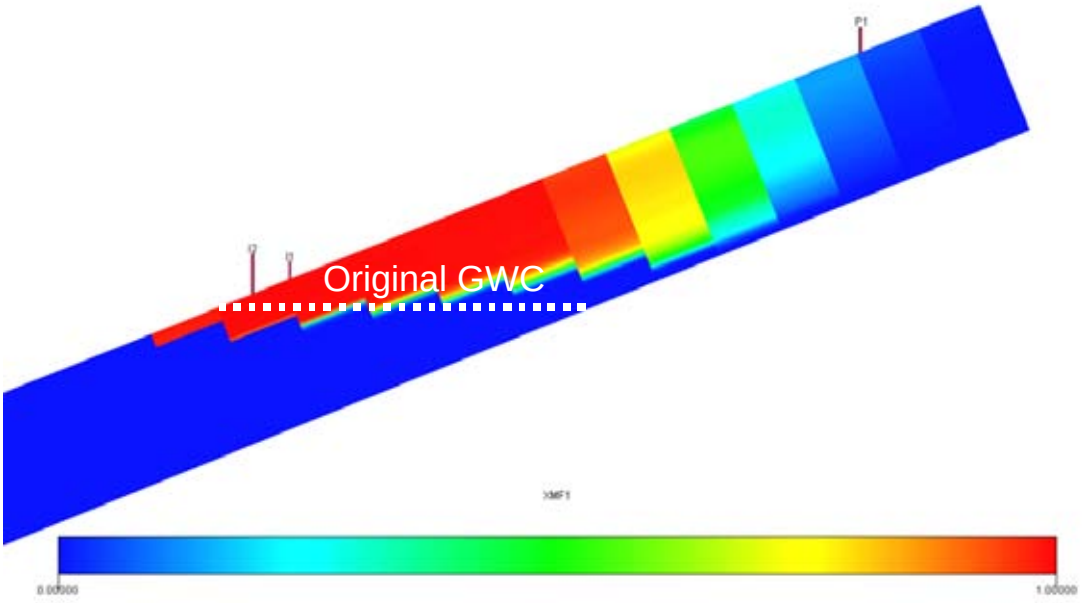


**Figure 5.16: $CO_2$ saturation after the 10% $CO_2$ limit has been reached. Formation dip is equal to 21° with the vertical to horizontal permeability ratio equal to 1%**

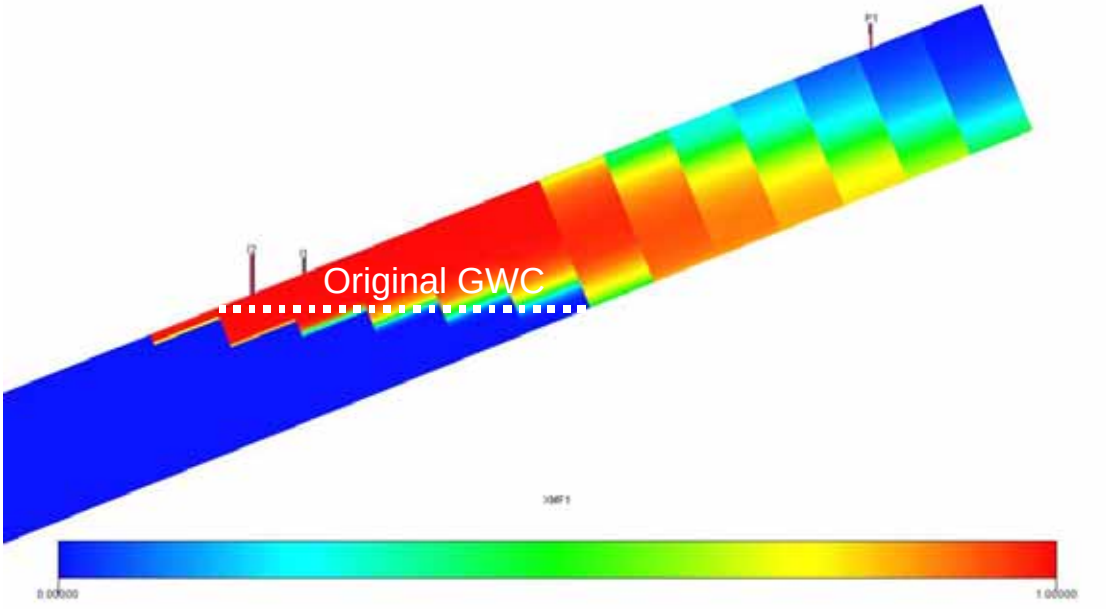


**Figure 5.17: $CO_2$ saturation after the 10% $CO_2$ limit has been reached. Formation dip is equal to 21° with the vertical to horizontal permeability ratio equal to 100%**

Main effect of thickness

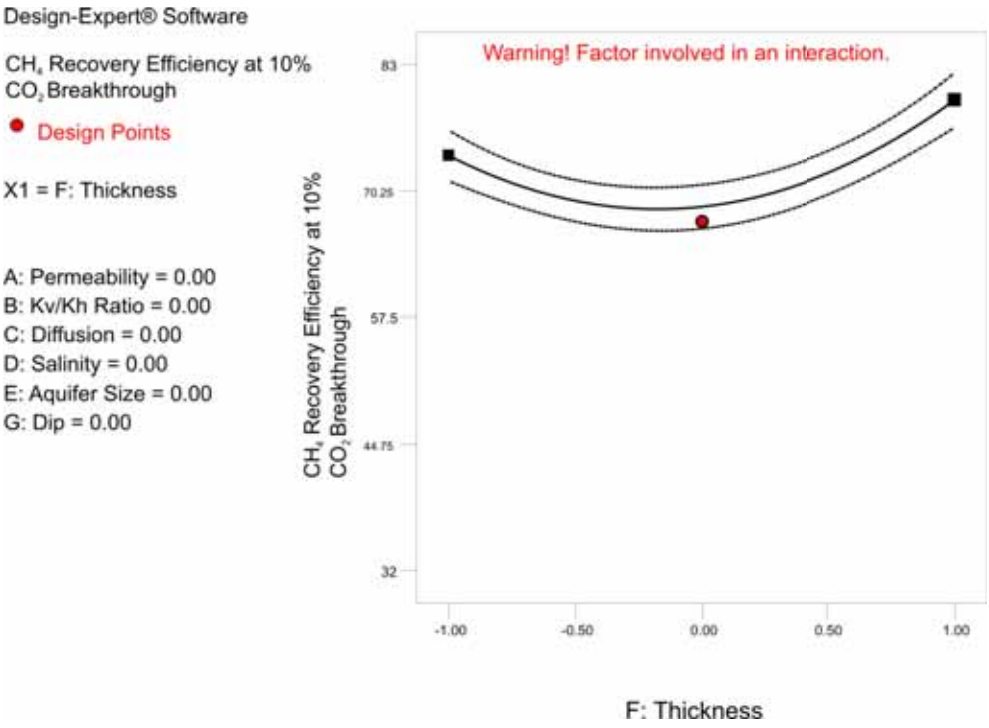


**Figure 5.18: Effect graph for the main effect of thickness for Response 1**

The main effect of thickness, as shown in Figure 5.18, indicates a degree of curvature exists with respect to $CH_4$ recovery at 10% $CO_2$ breakthrough due to the quadratic term also being statistically significant. Figure 5.18 shows that $CH_4$ recovery decreases as thickness moves from the low to mid level, with recovery increasing as thickness further increases from the mid to high level. This is however the average effect of thickness over the entire range of parameters tested, and as Figure 5.18 warns (Warning! Factor involved in an interaction), this parameter is involved in interactions with other parameters. Therefore the extent of the effect of thickness is influenced by these other parameters (such as formation dip as shown on the following page), and as such the interpretation of the effect of thickness has to be considered in conjunction with these other parameters.

Thickness – formation dip interaction

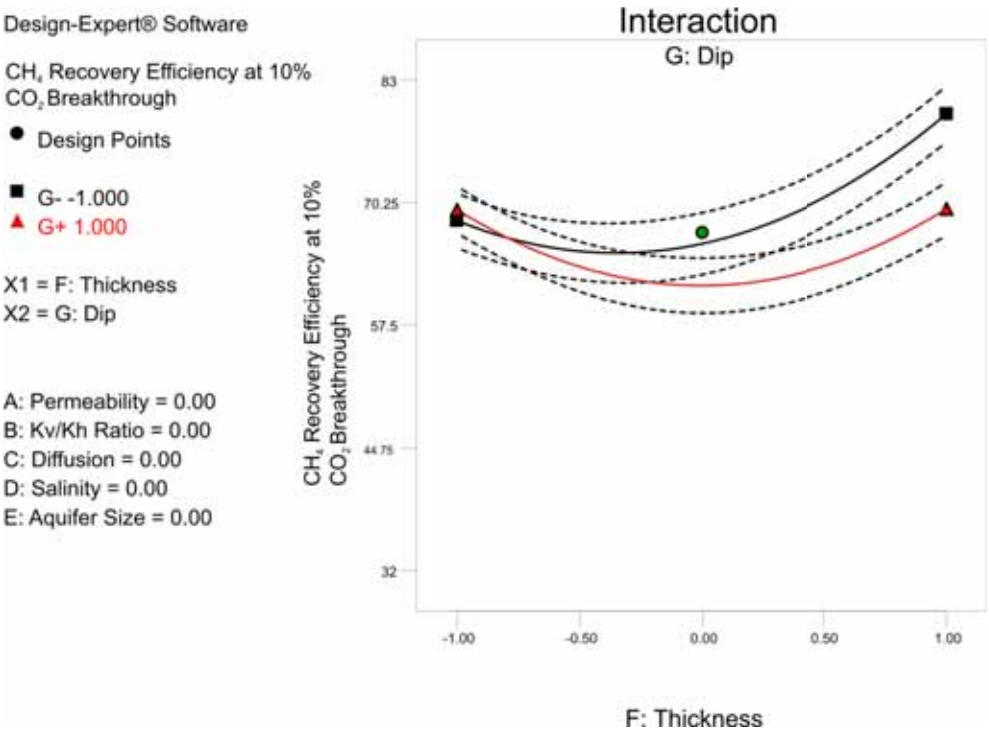


**Figure 5.19: Effect graph for the thickness - formation dip interaction for Response 1**

Figure 5.19 displays the effect graph for the interaction between the thickness of the reservoir and formation dip. It can be seen from this effect graph that in a non-dipping reservoir $CH_4$ recovery decreases as thickness is varied from the low to mid level. Eventually a minimum is reached with $CH_4$ recovery increasing sharply as thickness is further increased. Figure 5.20 provides a schematic of why this is the case. Note that this Figure presents a schematic and does not depict an exact replication of the displacement profiles that would result in these scenarios. As evident from Equation 5.2, stronger viscous forces are attributable to thinner reservoirs leading to a more piston-like displacement process (top schematic in Figure 5.20). The benefit of viscous dominated displacement in a non-dipping reservoir has been previously demonstrated. Increasing reservoir thickness leads to gravity having a progressively greater influence on the displacement causing $CO_2$ to under-ride the $CH_4$ column along the GWC. Under gravity dominated displacement, the thickness of the reservoir will influence the susceptibility of coning, with thinner reservoirs being more susceptible to coning (middle schematic in Figure 5.20). At constant rates, increasing the reservoir thickness reduces the influence of production, and consequently the susceptibility for coning leading to $CO_2$ stably displacing $CH_4$ vertically towards the production well completions (as indicated by the horizontal $CH_4$-$CO_2$ interface). It is apparent from Figure 5.19 that a gravity stable displacement in a non-dipping reservoir can lead to a significantly larger recovery efficiency than is possible with a viscous dominated displacement.

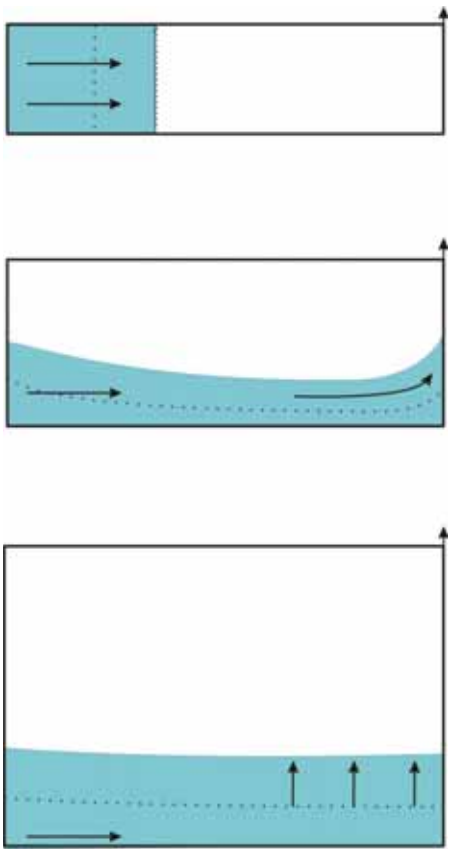

**Figure 5.20:Schematic of displacement profiles between $CO_2$ and $CH_4$ in a non-dipping reservoir with increasing thickness**

In a dipping reservoir, Figure 5.19 shows that variable thickness has minimal effect on the recovery efficiency of $CH_4$ between the low and high levels, but with curvature downwards between these levels. It was initially expected that variable thickness in a dipping reservoir would have a relatively flat trend due to the influence of gravity in stabilising the displacement profile in most instances tested in the design. The degree of curvature in the effect graph was not expected, and warranted further investigation. To test under what conditions the trend in Figure 5.19 could result, stand alone simulations were again performed. Another statistically significant coefficient involving thickness present in Table 5-5 is the permeability – thickness interaction. Consequently, stand alone simulations involving variable thickness and permeability were performed, with the results presented in Figure 5.21. This Figure presents a graph illustrating the effect of varying thickness at a permeability of 10mD and 1000mD. Opposing trends can be observed, with increasing thickness having a positive effect on the recovery efficiency at a high permeability, while at a low permeability a negative trend is apparent. When permeability is high, the dominance of gravity ensures similar sweep of the reservoir, with only the influence of production differentiating the recovery efficiency achievable. With a constant production rate employed in all cases, the influence of production is felt less in a thicker reservoir, enabling a higher recovery of $CH_4$. Conversely, at low permeability, viscous forces dominate the displacement process, with the reservoir geometry now determining the

efficiency of the sweep, as demonstrated in Figure 5.22. This Figure shows that with viscous dominated displacement in a thin reservoir, the lower boundary of the reservoir will deflect the vertical displacement front as it proceeds towards the production well. This deflection results in the displacement front now mimicking that of a gravity stable displacement. Increasing the thickness of the reservoir either delays or eliminates the contact with the lower boundary, with the injected $CO_2$ continually dispersing in the vertical direction until breakthrough at the production well. This dispersion will negatively impact on the sweep of the reservoir at the breakthrough of $CO_2$.

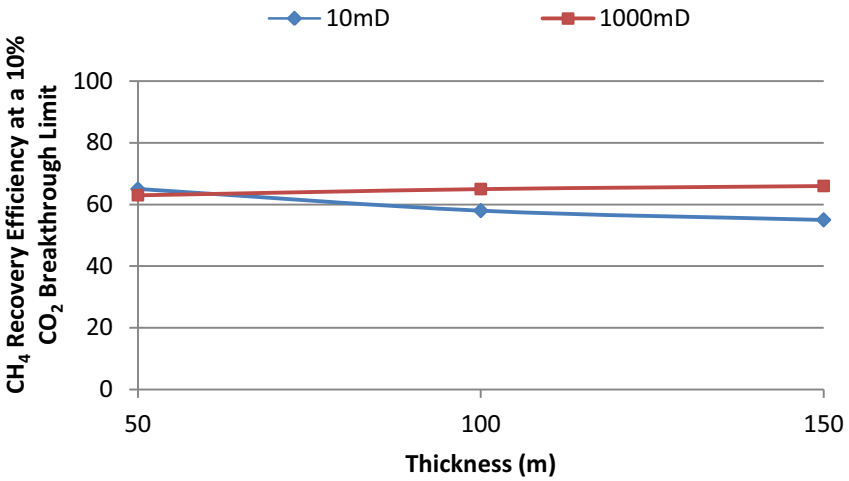


**Figure 5.21: Results of stand alone simulations where thickness was altered with permeability in a 21° dip reservoir**

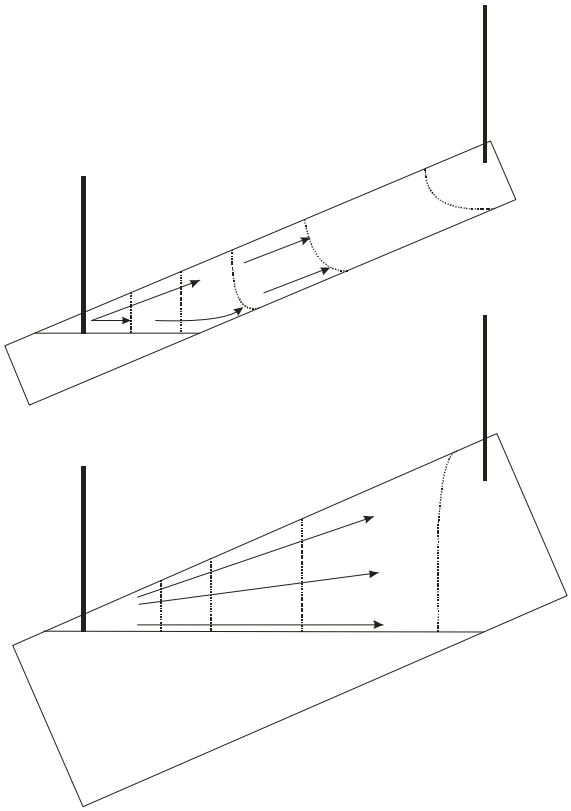

**Figure 5.22: Schematic of the progression of the displacement profile in low permeability, dipping reservoir with respect to thickness**

It is the consideration of the trends observed in Figure 5.21 that is responsible for the curvature found in the effect graph for the thickness – formation dip interaction.

Main effect of the aquifer size

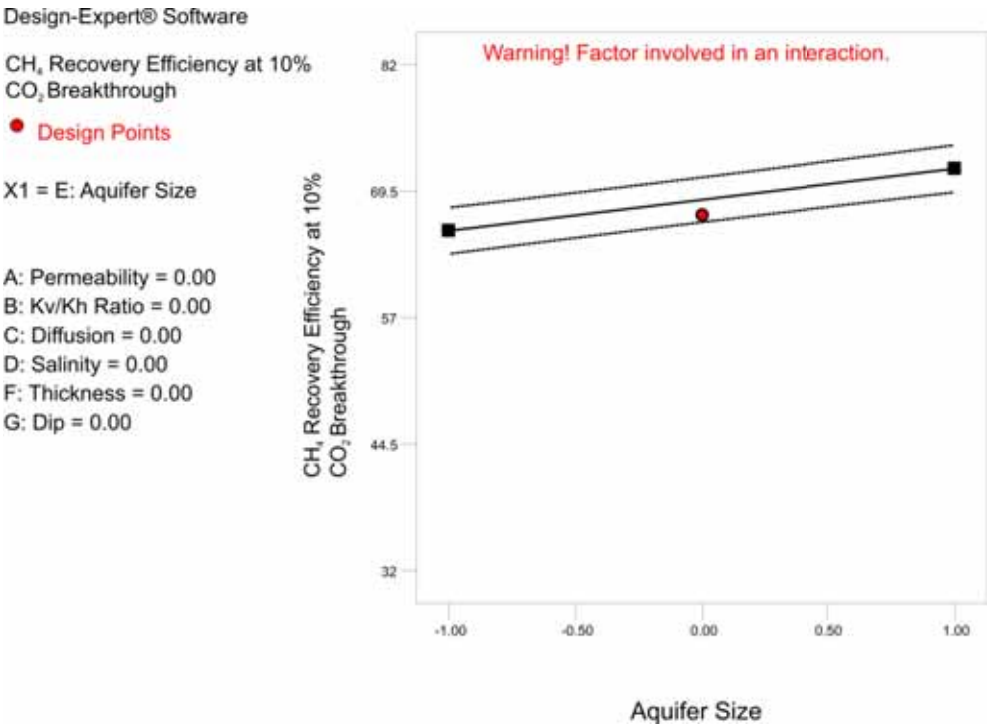


**Figure 5.23: Effect graph for the main effect of the aquifer size for Response 1**

The last of the six most influential coefficients is the main effect of the aquifer size and hence strength. With equal surface injection and production rates providing pressure maintenance to the system, the significance of the effect of the aquifer was a surprise. A minor influence was expected due to the initial discrepancy between the volumes injected and the volumes produced at reservoir conditions attributable to the different compressibilities of $CO_2$ and $CH_4$. With $CH_4$ being less compressible, initially a greater volume is being produced at reservoir conditions than is being injected. This would result in the minor influx of the aquifer which would result in a small volume of gas being residually trapped. Consequently, it was expected that if any effect was to be observed with variable aquifer sizes it would be that recovery would be decreased, not increased, as the size and hence strength of the aquifer was increased.

Stand alone simulations were again performed in an effort to mimic the positive effect displayed in Figure 5.23 in order to determine under what circumstances an increase in aquifer size resulted in a positive effect on $CH_4$ recovery efficiency. The results of these simulations were not able to produce a positive trend. The influx of the aquifer was effectively restricted through the pressure maintenance supplied by the injection of $CO_2$, with the aquifer essentially having no effect on the

recovery of $CH_4$ under conditions of $CO_2$ injection. The significance of the aquifer size is therefore believed to be a product of the ED analysis, and not a physical reality. This might suggest that the other results of the ED analysis are questionable. However, trends observed in the effects graphs of Response 1 have been able to be replicated through the mentioned stand alone simulations performed. This ability to duplicate these results provides confidence in the results of the ED analysis.

The effects of the gas diffusion coefficient and water salinity parameters

Lastly, the effects of the gas diffusion coefficient and formation water salinity were found to be statistically significant, both as a main effect as well as in interactions with other parameters. Recall however that the results of the ANOVA table indicate a relative significance with the other parameters tested. Although these parameters were found to be statistically significant, their influence in comparison to other parameters such as the $k_v/k_h$ ratio is less. For example, consider the results presented in Table 5-7. This table presents the results of two sets of simulations where the $k_v/k_h$ ratio and the diffusion coefficient were individually tested in a non-dipping model. While a considerable effect is observed between coefficients of $1x10^{-6}$ $m^2/s$ and $1x10^{-8}$ $m^2/s$, essentially no effect on the recovery is observed as the diffusion coefficient is changed to $1x10^{-10}$ $m^2/s$. The decrease in recovery factor as the diffusion coefficient is altered from $1x10^{-8}$ $m^2/s$ to $1x10^{-6}$ $m^2/s$ is due to the $1x10^{-8}$ $m^2/s$ coefficient representing liquid-like diffusion and the $1x10^{-6}$ $m^2/s$ coefficient representing gas-like diffusion. Random molecular motion is greater in a gas; hence mixing by random molecular motion (i.e. diffusion) is therefore greater, leading to a lower recovery efficiency at the 10% $CO_2$ limit. That being said, the effect of the $k_v/k_h$ ratio across the entire range of values is greater. Consequently, while it was found that the effect of the diffusion coefficient and salinity were found to be statistically significant, their relative effect in comparison to the remaining parameters in the design is not as great.

**Table 5-7: Comparison of the effect of the $k_v/k_h$ ratio and the diffusion coefficient on the $CH_4$ recovery factor at a 10% $CO_2$ breakthrough limit**

| Parameter | Parameter Level | Recovery Factor (RF) at 10% $CO_2$ limit |
|---|---|---|
| $k_v/k_h$ ratio | 0.01 | 72.2% |
| | 0.10 | 61.7% |
| | 1.00 | 56.1% |
| Diffusion Coefficient ($m^2/s$) | $1x10^{-6}$ | 55.3% |
| | $1x10^{-8}$ | 61.7% |
| | $1x10^{-10}$ | 61.8% |

## 5.7 Results and discussion of Response 2: Minimum producing $CO_2$ concentration required to achieve incremental recovery.

The individual result for each design run for Response 2 is presented in Figure 5.24 with the ranking of statistically significant coefficients presented in Table 5-8. Again, the ANOVA table from the analysis of Response 2 can be found in Appendix B. The simulation runs for this response show a wide of results, with the minimum producing $CO_2$ concentration required to achieve incremental recovery ranging from essentially zero mole percent to as high as 95 mole percent. The results of this response have to be analysed in reference to two aspects. The first is the effect of the parameters on the stability of the displacement between $CH_4$ and $CO_2$, as described in Response 1. The second is the effect of the parameters on the conventional primary recovery.

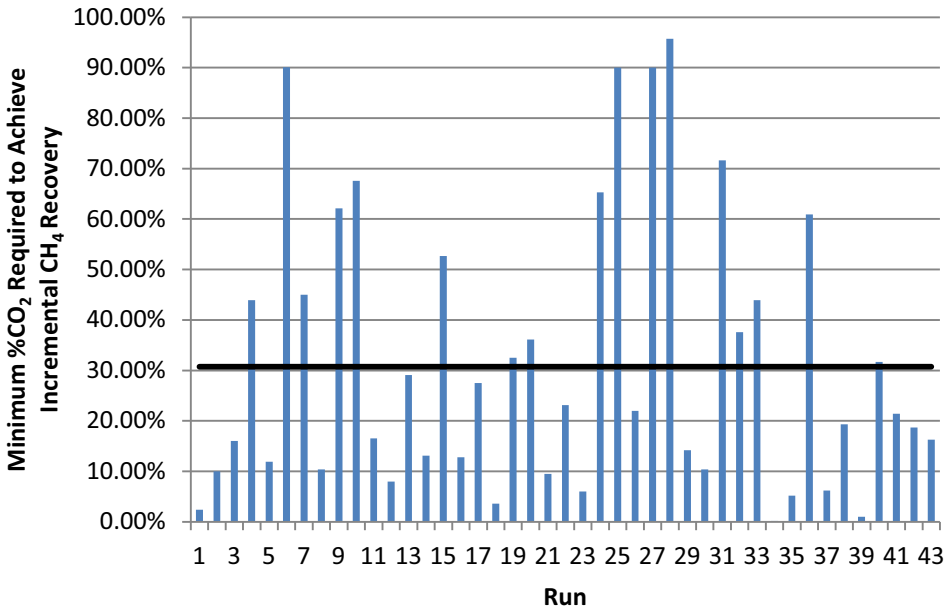


**Figure 5.24: Result for each design run and the average for all runs (black line) for Response 2**

**Table 5-8: Ranking of statistically significant coefficients from the analysis of Response 2**

| Statistically Significant Coefficient | F Value | p-value Prob > F |
|---|---|---|
| Dip | 483.48 | <0.0001 |
| Permeability*Dip | 200.13 | <0.0001 |
| Permeability*Ratio | 149.42 | <0.0001 |
| Permeability | 143.10 | <0.0001 |
| $k_v/k_h$ Ratio | 58.49 | <0.0001 |
| Thickness | 44.43 | <0.0001 |
| $k_v/k_h$ Ratio*Aquifer Size | 34.29 | <0.0001 |
| $k_v/k_h$ Ratio*Dip | 32.98 | <0.0001 |
| $k_v/k_h$ Ratio$^2$ | 22.29 | 0.0002 |
| Permeability*Diffusion | 17.65 | 0.0005 |
| Aquifer Size | 14.02 | 0.0015 |
| Aquifer Size*Thickness | 13.11 | 0.0020 |
| Permeability*Thickness | 12.13 | 0.0027 |
| Aquifer Size$^2$ | 9.85 | 0.0057 |
| Thickness*Dip | 8.55 | 0.0091 |
| Diffusion*Thickness | 7.82 | 0.0119 |
| Thickness$^2$ | 6.73 | 0.0183 |
| Aquifer Size*Thickness | 6.42 | 0.0208 |
| $k_v/k_h$ Ratio*Diffusion | 4.68 | 0.0443 |
| Dip$^2$ | 4.53 | 0.0473 |

The regression diagnostics once again indicate that the model adequately represents the results of the design. The $R^2$ and adjusted $R^2$ coefficients are 0.9887 and 0.9742 respectively, and the normal probability plot (Figure 5.25) shows no major deviation from the normality assumption.

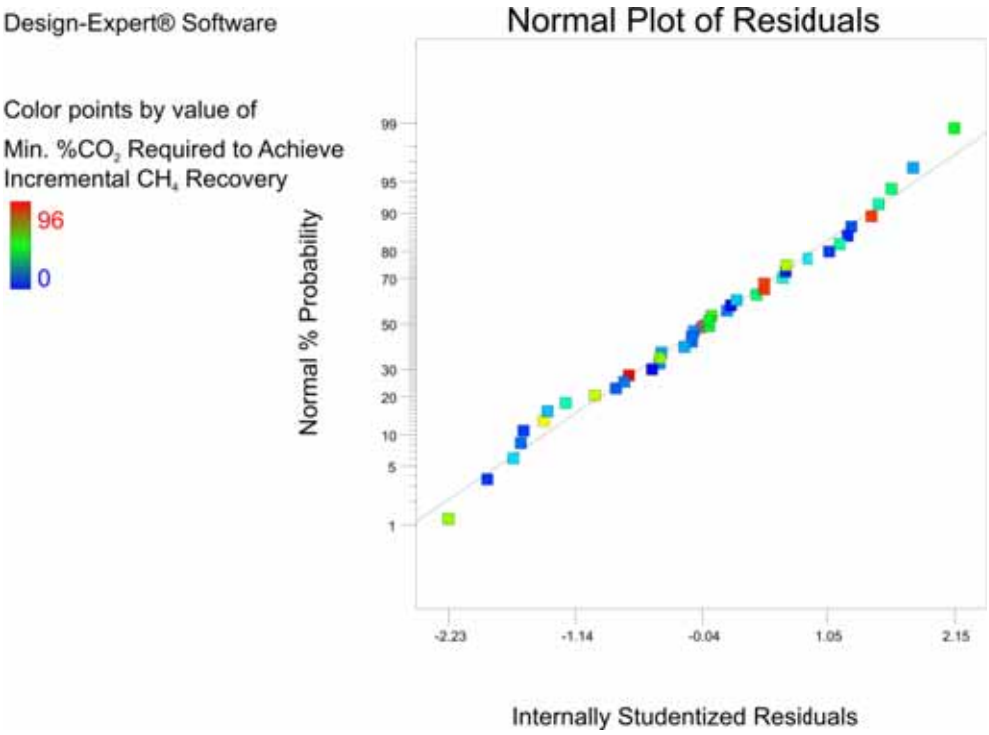


**Figure 5.25: Normal probability plot for Response 2**

Main effect of formation dip

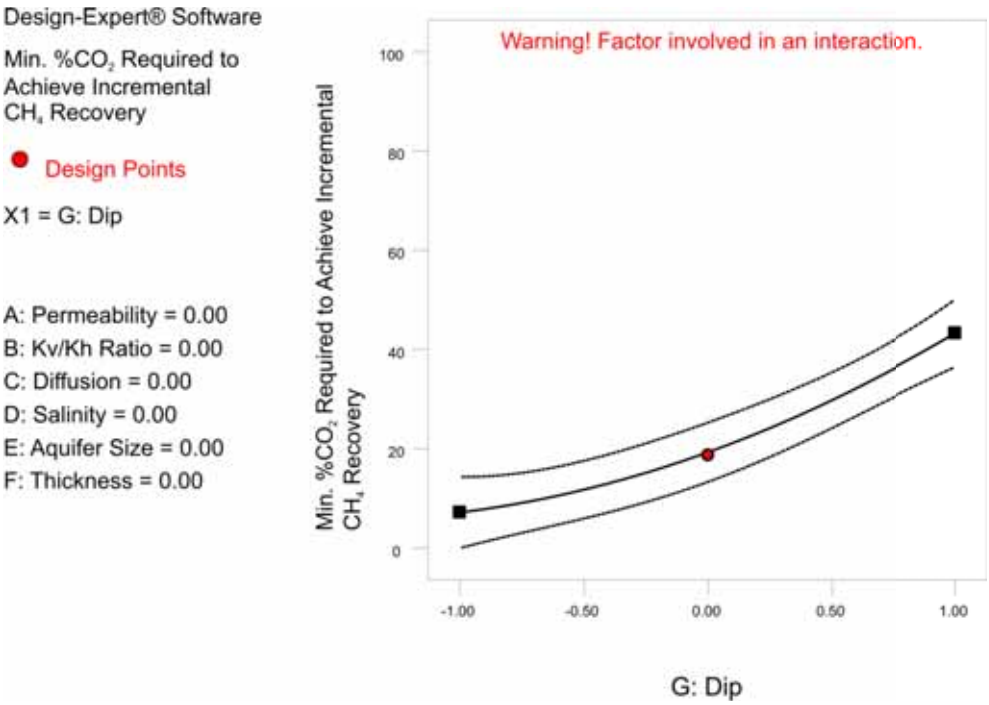


**Figure 5.26: Effect graph for the main effect of formation dip for Response 2**

Table 5-8 indicates that the main effect of the formation dip is by far the most influential coefficient. The effect graph for this coefficient (Figure 5.26) indicates a strong positive trend with increasing formation dip. In other words, incremental recovery will be achieved with a lower minimum producing $CO_2$ concentration in a non-dipping reservoir than a dipping reservoir.

As part of the data collection for Response 2, simulations for each ED run were required for conventional primary depletion scenarios. Consequently, the data to analyse a third response, $CH_4$ recovery efficiency under conventional primary depletion was available. The ANOVA table and effect graphs of the most influential parameters are located in Appendix B. The results from this ED on $CH_4$ recovery under primary depletion also indicated that the main effect of formation dip was the most influential coefficient. The effect graph (Figure 5.27) shows that primary recovery efficiency increases as formation dip increases. The positive effect on primary recovery with increasing formation dip is due to the reservoir geometry and its corresponding effect on the influence of production, as demonstrated in Figure 5.28. In a non-dipping reservoir, the GWC is generally much closer to the producing completions than is typically the case in a dipping reservoir. Consequently, the influence of production is felt at the GWC much sooner and with greater strength. This increases the susceptibility for the coning of water into the production well, which in a non-dipping reservoir can lead to a significant volume of the reservoir remaining unswept once water production begins. The greater distance between the GWC and the producing completions in a dipping reservoir means

that the influence of production felt at GWC is delayed and with reduced strength initially. This ensures a greater sweep of the reservoir once water has reached the production well.

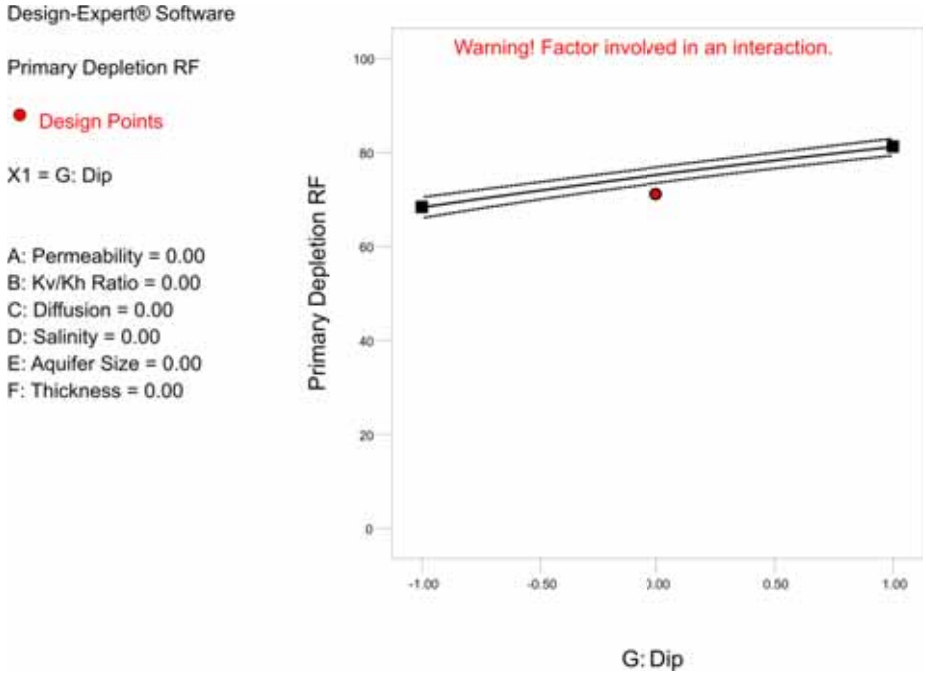


**Figure 5.27: Effect graph of the main effect of formation dip for the third response: $CH_4$ recovery under conventional primary depletion (at water breakthrough)**

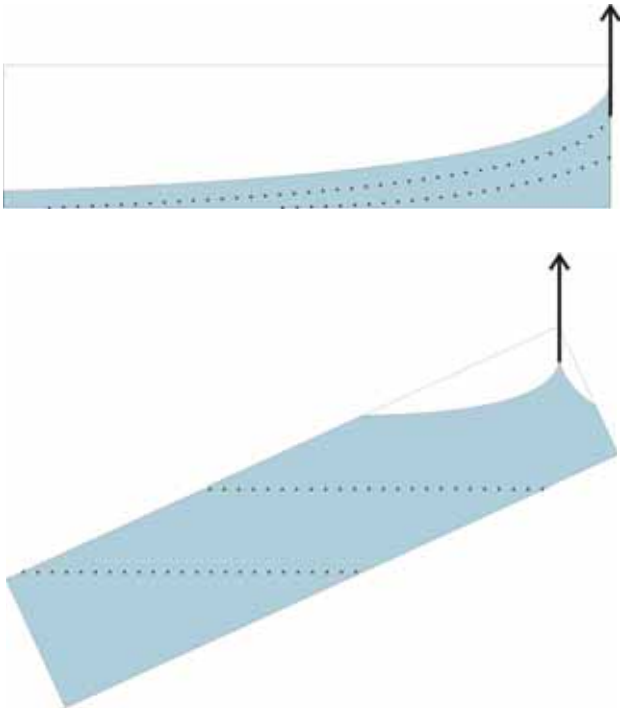

**Figure 5.28: Schematic of the difference in sweep efficiency between (a) non-dipping and (b) dipping reservoirs.**

In terms of the effect of formation dip on the efficiency of the displacement of $CH_4$ by $CO_2$, the effect graph for the main effect of formation dip for Response 1 is shown in Figure 5.29. Although this parameter is involved in more statistically significant interactions (e.g. permeability) the general effect of formation dip is that $CH_4$ recovery efficiency decreases with increasing formation dip.

Coupled with the fact that increasing formation dip leads to a higher primary recovery efficiency, the minimum producing $CO_2$ concentration required to achieve incremental recovery will be greater in a dipping reservoir. Consequently, from this result alone, injection of $CO_2$ should be targeted in non-dipping reservoirs.

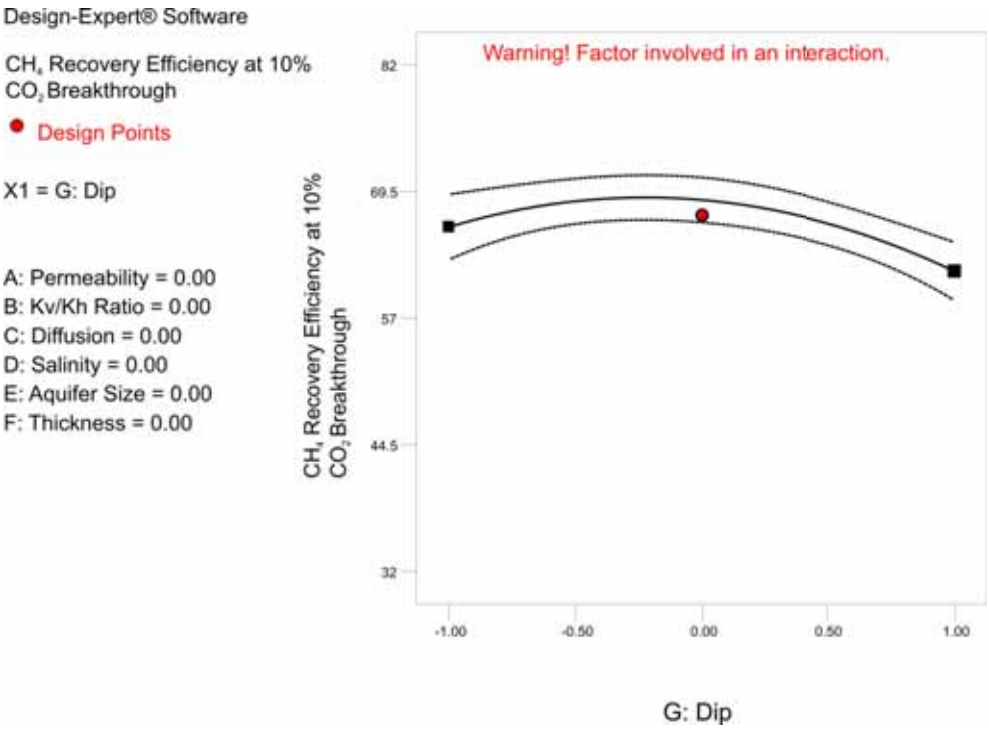


**Figure 5.29: Effect graph for the main effect of formation dip for Response 1**

Permeability – formation dip interaction

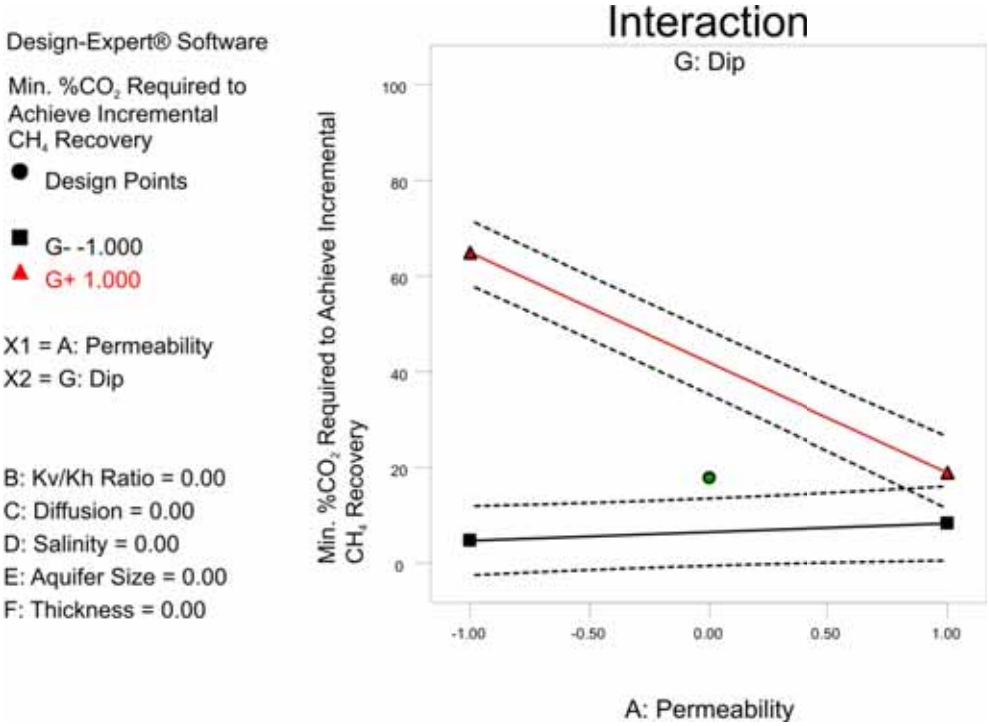


**Figure 5.30: Effect graph for the permeability - formation dip interaction for Response 2**

The extent of the effect of formation dip is however dependent upon other parameters such as the interaction with permeability, the next highest ranking coefficient. The effect graph for this interaction (Figure 5.30) indicates a strong negative trend as permeability increases for a dipping reservoir, with a weak positive trend for a non-dipping reservoir. The strong negative trend for a dipping reservoir is related to the strong influence of permeability on both the displacement of $CH_4$ by $CO_2$ as well as on the primary recovery efficiency. It was shown in Response 1 that viscous dominated displacement attributable to low permeability scenarios resulted in the premature breakthrough of $CO_2$ and a considerably poorer $CH_4$ recovery efficiency in a dipping reservoir. Increasing permeability and allowing gravity to stabilise the displacement improved recovery. The effect of permeability in a dipping reservoir could be considerable in terms of the recovery efficiency achievable at the 10% $CO_2$ limit.

Under primary depletion conditions, low permeability restricts the mobility of the aquifer, limiting the pressure support provided by the aquifer. With a larger pressure reduction possible, a greater primary recovery efficiency can be achieved in low permeability scenarios. Increasing permeability increases the mobility of water, allowing the aquifer to respond to the production of gas, maintaining reservoir pressure and decreasing primary recovery. A higher primary recovery efficiency coupled with considerably earlier $CO_2$ breakthrough times has resulted in low permeability reservoirs requiring a much greater producing $CO_2$ concentration to be handled in order to achieve incremental recovery than is the case for higher permeability reservoirs.

The slight positive trend exhibited for a non-dipping reservoir with increasing permeability is primarily attributable to the effect of permeability under $CO_2$ injection conditions. Under primary depletion conditions, the counteracting influence of the absolute values of horizontal and vertical permeabilities on the susceptibility of water coning results in permeability having a minimal effect on primary $CH_4$ recovery. Recall that at default conditions the vertical permeability is 10% of the horizontal permeability. In general, low horizontal permeability increases the susceptibility for coning to occur. However as vertical permeability is a percentage of the horizontal permeability in this design, low horizontal permeability (at default conditions) also corresponds to low vertical permeability, which mitigates against the coning of fluids. Furthermore, high horizontal permeability, mitigating against coning, corresponds to high vertical permeability. This therefore leads to permeability having a minimal effect on the primary recovery efficiency. Under $CO_2$ injection conditions, it was shown that increasing permeability resulted in earlier $CO_2$ breakthrough and consequently lowered the recovery efficiency. This subsequently correlates to a higher tolerance of $CO_2$ being required to achieve incremental recovery.

Permeability – $k_v/k_h$ ratio interaction

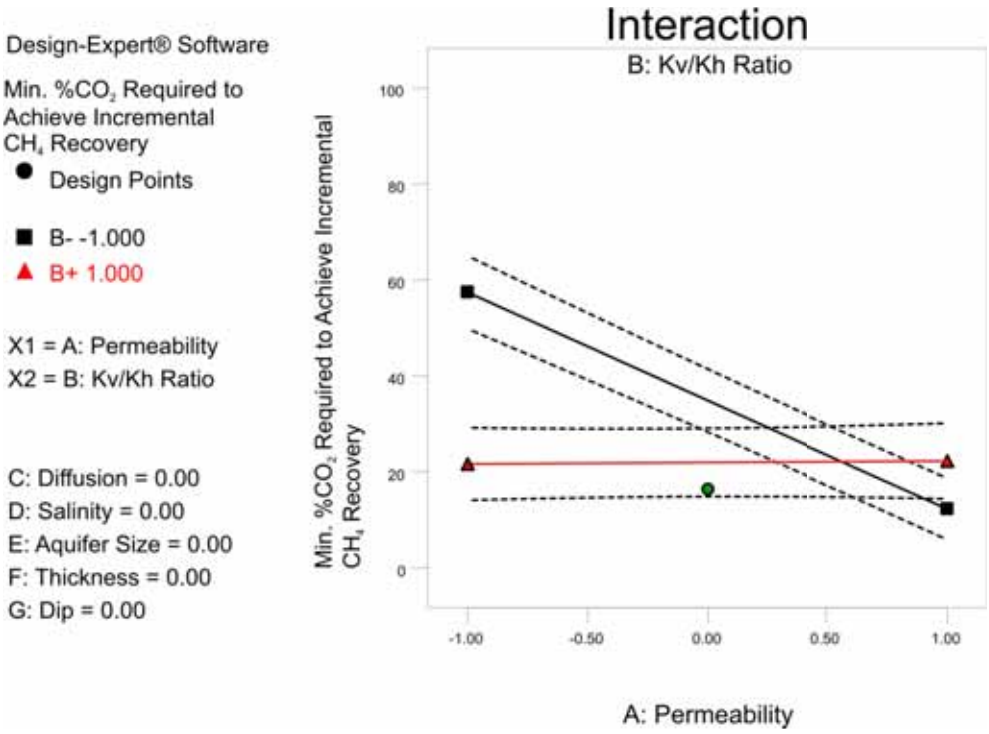


**Figure 5.31: Effect graph for the permeability - $k_v/k_h$ ratio interaction for Response 2**

Figure 5.31 presents the effect graph for the permeability – $k_v/k_h$ ratio interaction, the next highest ranking coefficient in the results of the analysis. Figure 5.31 shows that, at a low level of the ratio increasing permeability reduces the producing $CO_2$ concentration required to enhance gas recovery. Again, this graph is based on the mid level of formation dip, and with the dip being such an influential parameter this effect graph could be different when considered at other levels of formation dip. From the results of Response 1, low permeability scenarios in a dipping reservoir, both in the horizontal and vertical direction, led to an unfavourable displacement profile and premature breakthrough of $CO_2$. Increasing permeability allowed gravity to stabilise the displacement, improving the recovery efficiency at the breakthrough of $CO_2$.

Under primary depletion conditions, low permeability scenarios restrict aquifer influx, increasing the primary recovery that is achievable. Increasing the horizontal permeability (whilst the ratio is maintained at the low level) enhances the mobility of the aquifer, providing greater pressure support and therefore lowering primary recovery. The high primary recovery coupled with the premature breakthrough of $CO_2$ and corresponding low $CH_4$ recovery attributable to low permeability scenarios led to a higher producing $CO_2$ concentration required to achieve incremental recovery than for higher permeability scenarios.

At isotropic permeability conditions, a flat trend is observed in Figure 5.31. With the strong influence of both the horizontal and vertical permeability observed in Response 1, this result was a surprise. Closer investigation of the design runs based at isotropic conditions display opposing trends when plotted with respect to the formation dip (Figure 5.32). Increasing permeability in a non-dipping reservoir produces a positive trend, meaning the producing $CO_2$ concentration will increase with increasing permeability. On the other hand, in a 21-degree dipping reservoir increasing permeability produces a negative trend. It is clear that the effect of isotropic permeability is dependent upon other parameters such as formation dip, and that the variable nature of the effect of isotropic permeability has led to the flat trend observed in Figure 5.31.

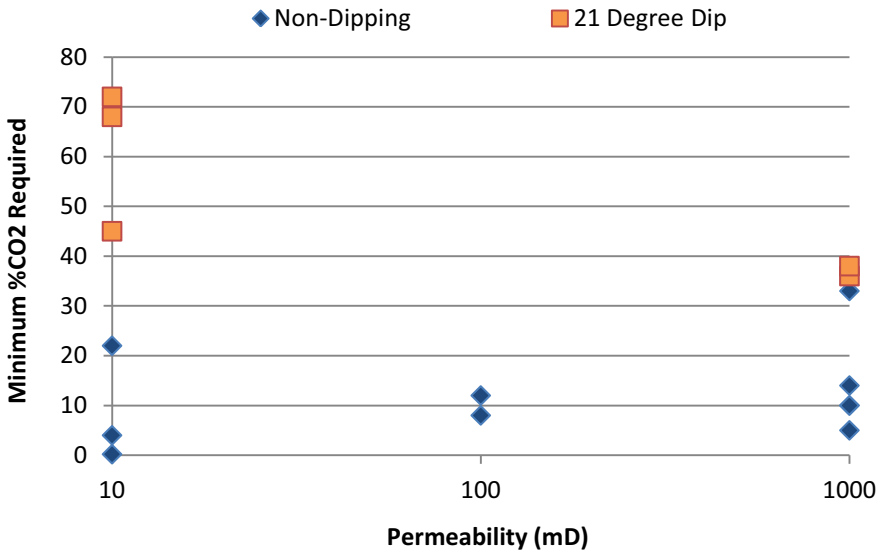


**Figure 5.32: Scatter plot of the results from the ED for Response 2 for a non-dipping and dipping reservoir with respect to isotropic permeability**

Main effect of permeability

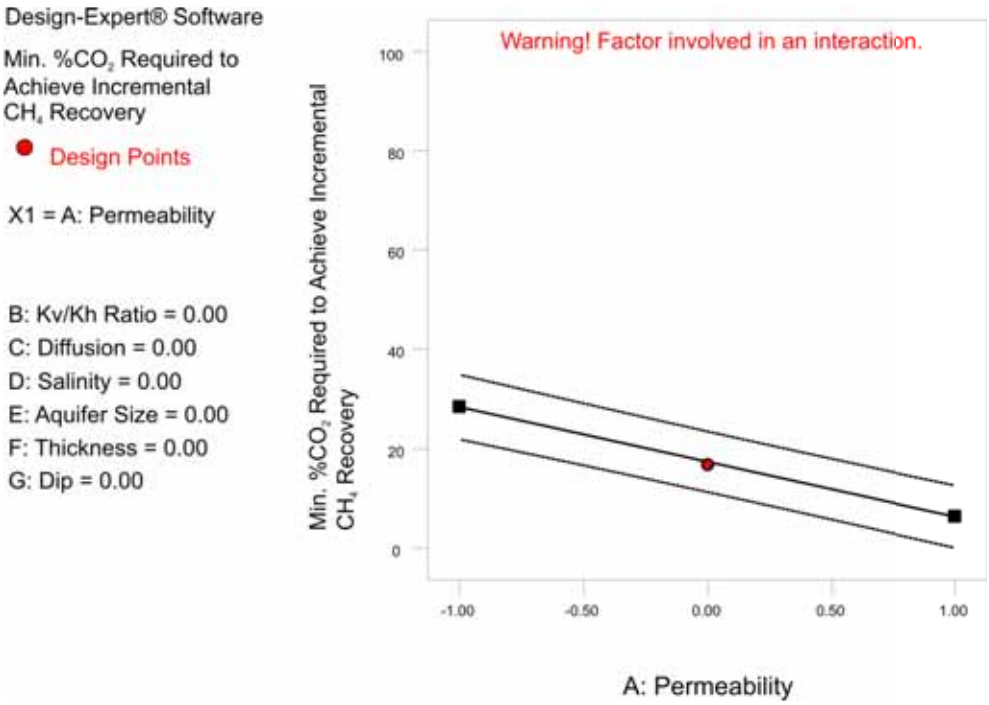


**Figure 5.33: Effect graph for the main effect of permeability for Response 2**

The main effect of permeability displays a negative trend with respect to the minimum percentage of $CO_2$ required to achieve incremental recovery (Figure 5.33). It has been shown in the effect graphs of the permeability – formation dip interaction (Figure 5.30) and the permeability – $k_v/k_h$ ratio interaction that the effect of permeability can have both a positive and negative effect on the producing $CO_2$ concentration. However, it is clear from these two effect graphs that the strongest effect that permeability has is of decreasing the producing $CO_2$ concentration as permeability increases, for the reasons stated in the aforementioned interactions. Consequently, the effect graph for the main effect of permeability shows a negative trend as permeability increases.

One notable parameter that was low on the list of statistically significant coefficients was the aquifer size, both as a main effect as well as when involved in interactions. Under primary depletion conditions, it would be expected that the aquifer size would be one of the more influential parameters in determining the $CH_4$ recovery efficiency. From the ANOVA results for the recovery efficiency under primary depletion conditions (Appendix C), the aquifer size is one of the highest ranking statistically significant parameters, with primary recovery improving with a decrease in the size of the aquifer. With the high ranking of the main effect of the aquifer size in Response 1, and the importance of the aquifer size on the primary recovery it would be expected that the aquifer size would be influential in Response 2. As this is not the case, confidence is gained in the conclusion

from Response 1 that the significance of the main effect of the aquifer size was a product of the design analysis and not a physical reality.

## 5.8 Summary of the Experimental Design

From the results of the analysis of the two responses presented above, some general conclusions can be made as to what reservoir properties will lead to a stable displacement process as well as what types of reservoirs are suited to achieving incremental recovery with the lowest producing $CO_2$ concentration possible.

### 5.8.1 Response 1

The results of Response 1 can be summarised as follows:

- The displacement of $CH_4$ by $CO_2$ can be performed stably in both non-dipping and dipping reservoirs.
- In a non-dipping formation, a stable displacement can be achieved with either viscous or gravity dominated displacement. Consequently the permeability and thickness of the formation are the key parameters in determining the stability of the displacement process. Viscous dominated displacement is characterised by thin and/or low permeability reservoirs, while gravity dominated displacement is characterised by thick and/or high permeability reservoirs.
- The coning of $CO_2$ is the primary concern with the premature breakthrough of $CO_2$ in a non-dipping reservoir.
- In a dipping reservoir, reservoir properties which lead to a gravity stable displacement result in the greatest $CH_4$ recovery at the 10% $CO_2$ breakthrough limit.
- Viscous dominated displacement was shown to be particularly detrimental in dipping reservoirs. Viscous dominated displacement led to an unfavourable displacement profile and resulted in significantly premature breakthrough of $CO_2$ at the production well.
- Although the fluid properties (salinity and the diffusion coefficient) were found to be statistically significant, in comparison to the effects of the reservoir parameters in the design, their effect on the recovery of $CH_4$ at the breakthrough of $CO_2$ was minimal.

### 5.8.2 Response 2

The properties which were found to be the most influential in determining the minimum producing $CO_2$ concentration required to achieve incremental recovery were determined by their impact on the stability of the displacement process between $CO_2$ and $CH_4$ as well as their impact on the primary recovery efficiency. The key conclusions from the analysis of Response 2 were as follows:

- To ensure the minimum producing $CO_2$ concentration required to achieve incremental recovery, the injection of $CO_2$ should be targeted in non-dipping reservoirs. The lower primary recovery efficiencies (as compared to dipping reservoirs) coupled with the ability to achieve a stable $CH_4$ displacement by $CO_2$ ensures incremental recovery can be achieved with the lowest producing $CO_2$ concentration.
- It is possible to achieve a stable displacement in a dipping reservoir (see Response 1), however the higher primary recovery efficiencies attributable, especially in low permeability scenarios, result in much higher producing $CO_2$ concentrations being required to be handled to achieve incremental recovery.
- It was found that the effect of the parameters on the recovery achievable under primary depletion conditions had the greatest influence on determining the minimum producing $CO_2$ concentration required to enhance $CH_4$ recovery. Consequently, any parameter that leads to a lower primary recovery will correspond to a lower producing $CO_2$ concentration being required to achieve incremental recovery.

## 5.9 Follow-up Simulations

All simulations performed in the ED study assumed homogeneous conditions as well as a consistent operational strategy in the form of constant production and injection rates and well locations. These homogeneous models present an idealised situation and could therefore represent an overestimation of the potential to enhance gas recovery using $CO_2$ injection. Additionally, the constant operational strategy employed does not represent optimal conditions whereby $CH_4$ recovery is maximised. Consequently, this section involves an investigation into the effect of simple heterogeneity, as well as determining whether varying the operational strategy could improve metrics for cases where poor performance was shown in the ED study.

### 5.9.1 Impact of Heterogeneity

An important aspect of enhanced hydrocarbon processes is the degree of contact between the injected and in-situ fluids, a measure of this being the volumetric displacement (sweep) efficiency. Factors that strongly influence the degree of contact are the fluid properties, the well pattern and the properties of the reservoir rock. An important factor regarding the properties of the reservoir rock is the degree of heterogeneity. For instance, in EOR operations involving $CO_2$, heterogeneity can create preferential flow paths leading to the premature breakthrough of the injectant. Heterogeneity also leads to reduced contact between the reservoir oil and the injectant which limits the ability to alter the fluid properties. The heterogeneity of the reservoir can therefore be an important factor in the success of an enhanced recovery project.

The models used in the ED study employed homogeneous conditions. This was especially favourable for the models of a non-dipping reservoir involving viscous dominated displacement. The homogeneous nature of the model allowed for the displacement front to uniformly proceed through the reservoir, achieving excellent sweep of the reservoir. The introduction of heterogeneity is likely to cause the uneven advancement of the displacement front, which could significantly affect the sweep efficiency of $CH_4$ by $CO_2$. The effect of heterogeneity was therefore investigated through the placement of a higher permeability layer.

**Non-dipping Reservoir**

Lower permeability (10mD) reservoir with a high permeability (1000mD) layer

In this case, the reservoir is of low permeability (10mD), with a high permeability layer (1000mD), seen in Figure 5.34. The high permeability layer is 10 metres thick and extends across the whole formation in the X and Y plane. All other relevant reservoir properties are equivalent to the mid level of the ED (Table 5-3) as well as the other properties presented in Table 5-1. The high permeability layer is 50 metres from the top of the formation, with injection occurring at the GWC and therefore below this layer.

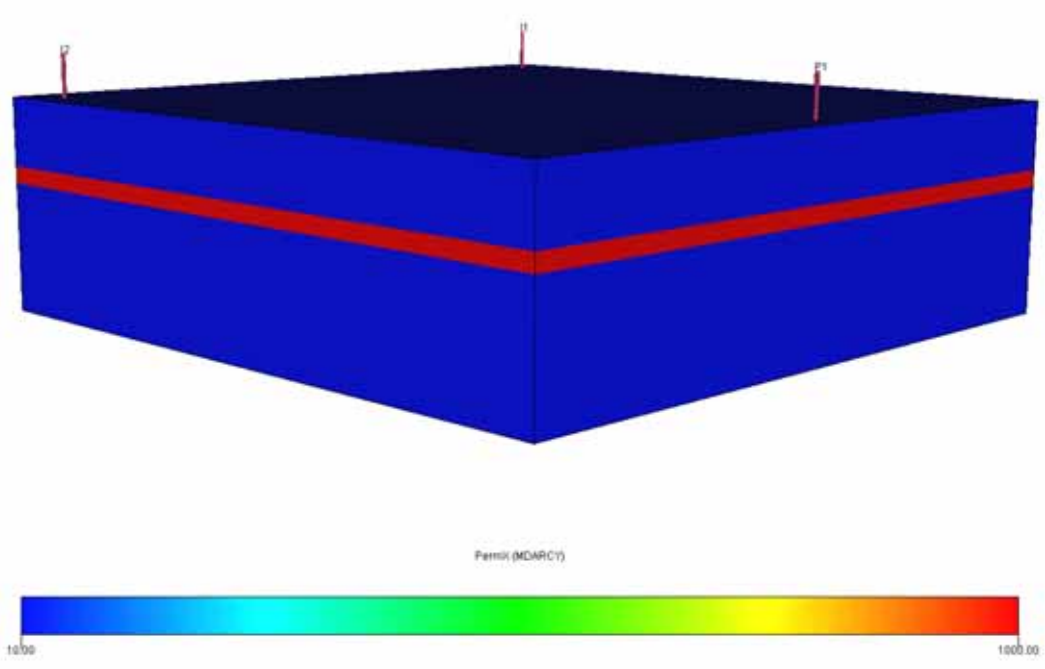


**Figure 5.34: Permeability distribution showing the high permeability layer (1000mD) in a low permeability reservoir (10mD)**

Table 5-9 presents the results of the model described above with a comparison against an equivalent low permeability (10mD), homogeneous model. The presence of the high permeability layer did result in significant uneven advancement of the displacement front, leading to the premature

breakthrough of $CO_2$ at the production well. The success of a viscous dominated displacement in a non-dipping reservoir is completely diminished by the presence of a high permeability layer. A significant issue, observed in Figure 5.35, is that of $CO_2$ coning. In a stable viscous dominated displacement process, the nature of the vertical displacement front eliminates the issue of coning. With the presence of the high permeability layer, $CO_2$ now migrates rapidly towards the area below the production well. The large drawdown required to achieve the specified production rate now promotes the coning of $CO_2$. This significantly impacts on the sweep efficiency and consequently the recovery of $CH_4$ at the breakthrough of $CO_2$. The presence of heterogeneity therefore clearly reduces the benefits of viscous dominated displacement.

**Table 5-9: Results of simulations investigating the impact of a high permeability (1000mD) layer in a low permeability (10mD) reservoir**

| **Case** | Default 10mD Permeability | High Permeability Layer |
|---|---|---|
| **OGIP ($sm^3$)** | $5.63 \times 10^8$ | $5.63 \times 10^8$ |
| **$G_p$ at 10% $CO_2$ Breakthrough ($sm^3$)** | $3.33 \times 10^8$ | $1.73 \times 10^8$ |
| **Recovery Factor at 10% $CO_2$ Breakthrough** | 65.2% | 33.6% |
| **Time to $CO_2$ Breakthrough (days)** | 2620 | 1359 |

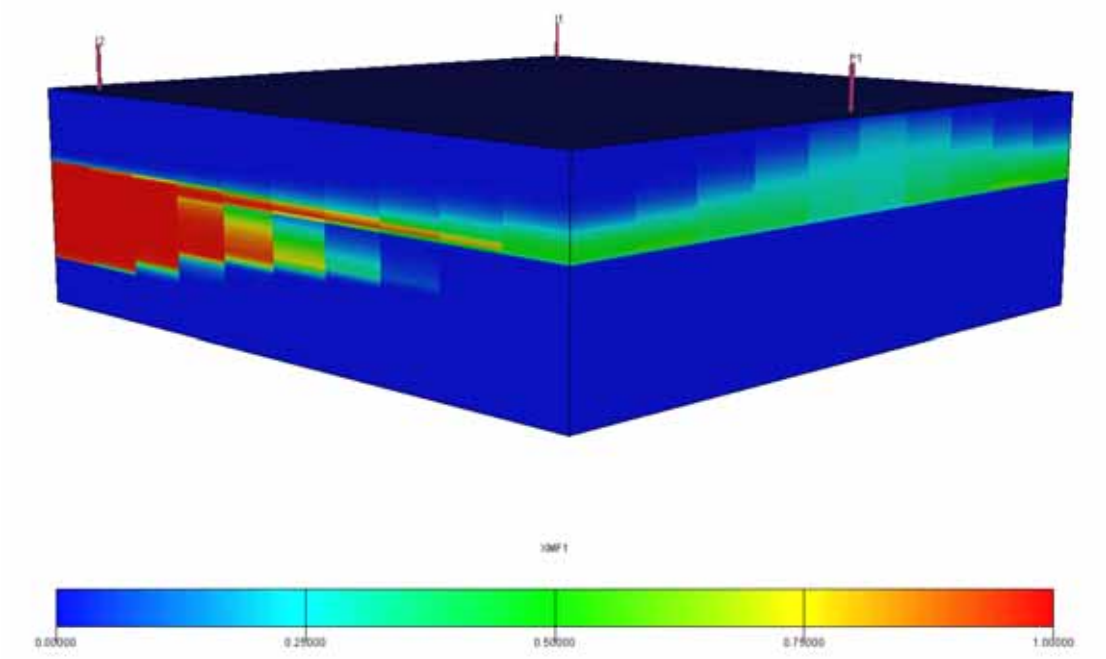

**Figure 5.35: $CO_2$ saturation of the high permeability heterogeneity model displaying the poor sweep efficiency at the 10% $CO_2$ breakthrough limit**

Medium permeability (100mD) reservoir with a high permeability (1000mD) layer

In this case, bulk permeability was increased from 10mD to 100mD, whilst maintaining the high permeability layer at 1000mD. Results for this simulation are presented in Table 5-10 along with the

results of the equivalent 100mD homogeneous model. The effect of the heterogeneity is not as dramatic in this instance, primarily attributable to the stronger influence of gravity due to the higher bulk permeability. The gravity segregation leads to the higher permeability layer being contacted by $CO_2$ at a much later stage in the displacement process. This can be seen in Figure 5.36 whereby the entire lower half of the reservoir has been displaced by $CO_2$, as opposed to Figure 5.35. The negative impact of the heterogeneity is therefore minimised. The results of this simulation suggest that if the primary direction of the displacement process can be altered from horizontal (viscous dominated) to vertical (gravity dominated), the negative impact of the heterogeneity can either be minimised or eliminated. This result also suggests that the impact of heterogeneity is smaller if the range of permeability is smaller.

**Table 5-10: Results of simulations investigating the impact of a high permeability (1000mD) layer in a medium permeability (100mD) reservoir**

| **Case** | Default 100mD Permeability | High Permeability Layer |
|---|---|---|
| **OGIP ($sm^3$)** | $5.63 \times 10^8$ | $5.63 \times 10^8$ |
| **$G_p$ at 10% $CO_2$ Breakthrough ($sm^3$)** | $3.17 \times 10^8$ | $2.98 \times 10^8$ |
| **Recovery Factor at 10% $CO_2$ Breakthrough** | 61.7% | 57.9% |
| **Time to $CO_2$ Breakthrough (days)** | 2486 | 2339 |

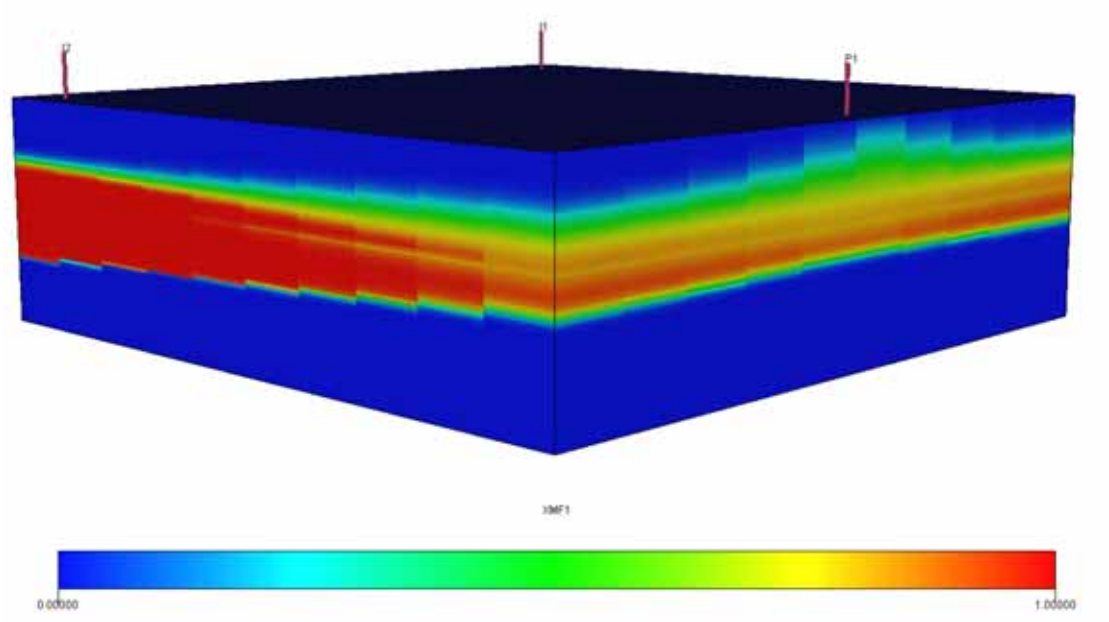


**Figure 5.36: $CO_2$ saturation at the 10% $CO_2$ breakthrough limit for a medium permeability (100mD) reservoir with a high permeability (1000mD) layer**

### 5.9.2 Impact of Operational Strategy

All simulations performed thus far have used constant production and injection rates. From the results of the ED analysis, the viscous to gravity ratio was shown to have a significant influence on

the stability of the displacement process between $CH_4$ and $CO_2$ and consequently the $CH_4$ recovery efficiency. Referring back to the viscous to gravity ratio equation, one parameter is controllable in a field operation, namely the fluid velocity. This naturally can be influenced through the choice of both injection and production rates. The negative impact of heterogeneity previously shown could be minimised by reducing the rates to enable gravity segregation to occur. Varying the rates can also influence the degree of coning. Additionally, other operational strategies, such as the location of the wells, and/or the type of wells used (vertical versus horizontal) can influence the displacement of $CH_4$ by $CO_2$.

This section investigates a selection of scenarios which resulted in early $CO_2$ breakthrough and subsequent low $CH_4$ recovery efficiency. Different operational strategies are applied with the aim of improving the displacement efficiency and hence $CH_4$ recovery at $CO_2$ breakthrough.

Low Permeability, Dipping Formation

The dominance of viscous forces in a dipping formation was shown to have a considerably negative impact on the sweep efficiency and hence $CH_4$ recovery at the breakthrough of $CO_2$. The sweep of the reservoir was improved with gravity dominated displacement. Operationally, this can be achieved through a reduction in the production and injection rates employed.

Injection and production rates were reduced from 5 MMscf/day to 2.5 MMscf/day and 1 MMscf/day. Table 5-11 presents the recovery efficiency at a $CO_2$ breakthrough limit of 10% in addition to the time taken for $CO_2$ to reach the breakthrough limit of 10%. The reduction of rates does improve the sweep efficiency through the reduction in viscous forces, leading to an improvement in the recovery of $CH_4$ at the 10% $CO_2$ breakthrough limit. Increases of around 3% and 6% of the OGIP are achieved for rates of 2.5 MMscf/day and 1 MMscf/day respectively. Figure 5.37 shows the $CO_2$ saturation at the time of 10% $CO_2$ breakthrough for rates equal to 1 MMscf/day. If compared with Figure 5.10 the increased influence of gravity in altering the displacement front can clearly be seen.

An issue with the reduction of rates is the increase in the production schedule. From Table 5-11, it can be seen that the time taken for $CO_2$ breakthrough to occur in the 1 MMscf/day scenario is over 10,000 days longer than for the 5 MMscf/day. While these simulations have not been optimised with respect to typical gas contract timelines, the message from these simulations is that the reduction of rates might not be economically feasible or meet contractual requirements.

**Table 5-11: Results of simulations investigating variable rates in a low permeability (10mD) dipping reservoir**

| **Rate** | 1 MMscf/day | 2.5 MMscf/day | 5 MMscf/day |
|---|---|---|---|
| **OGIP ($sm^3$)** | $5.63 \times 10^8$ | $5.63 \times 10^8$ | $5.63 \times 10^8$ |
| **$G_p$ at 10% $CO_2$ Breakthrough ($sm^3$)** | $3.32 \times 10^8$ | $3.19 \times 10^8$ | $3.03 \times 10^8$ |
| **Recovery Factor at 10% $CO_2$ Breakthrough** | 64.5% | 61.8% | 58.6% |
| **Time to $CO_2$ Breakthrough (days)** | 13056 | 5015 | 2378 |

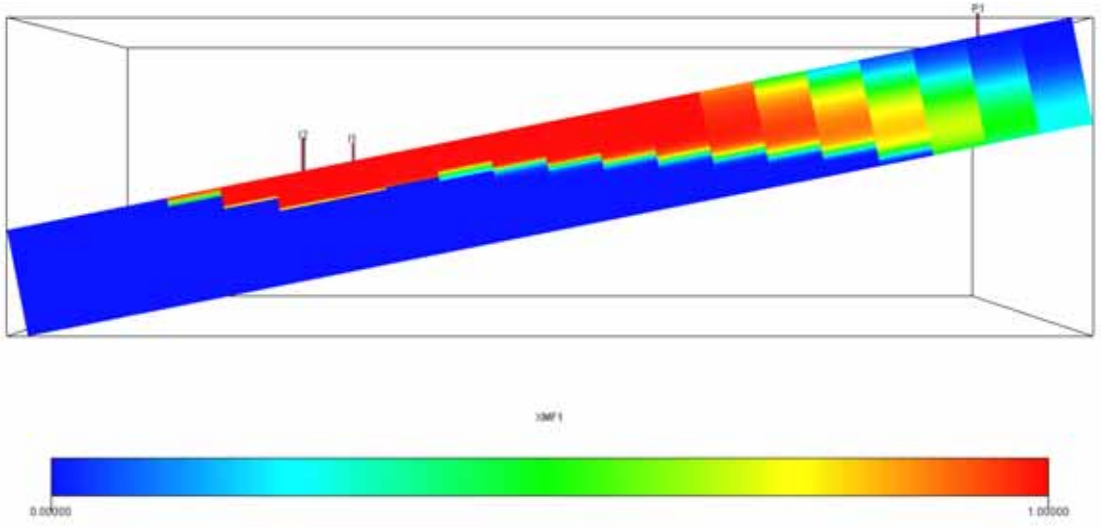

**Figure 5.37: $CO_2$ saturation for a low permeability dipping reservoir with rates equal to 1 MMscf/day**

Another strategy investigated for a low permeability, dipping formation is the location of the injection well completions. Increasing the distance between the injection and production well completions could delay the breakthrough of $CO_2$. Additionally, placement of the injection well completions into the aquifer could enhance the volume of $CO_2$ dissolved into the formation water by increasing the contact between the two fluids potentially delaying the breakthrough of $CO_2$. It was decided to lower the injection well completions into the aquifer (Figure 5.38), whilst maintaining the injection and production rates at the default values.

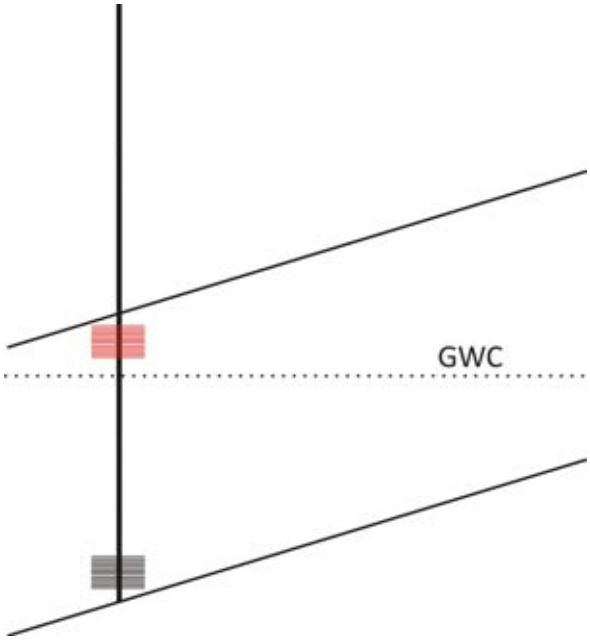


**Figure 5.38: Schematic of the injection well completion location, where red indicates the default location and black represents the altered location**

Table 5-12 presents the results of lowering the completions with comparison to the default case. The breakthrough of $CO_2$ is delayed by just over 300 days, with the benefit being an 8% increase in $CH_4$ recovery at the 10% $CO_2$ breakthrough limit. In addition to increasing the distance between the injection and production well completions, if a comparison is made between the $CO_2$ profiles of the cases presented in Table 5-12 (Figure 5.39 and Figure 5.40), lowering the completions has resulted in a significantly different displacement profile. The strong viscous forces coupled with the lower completions enables the lower section of the reservoir to be swept, which is not the case in the default scenario.

**Table 5-12: Results of simulations investigating the location of completions in a low permeability (10mD) dipping reservoir**

| **Case** | Default Completions | Lower Completions |
|---|---|---|
| **OGIP ($sm^3$)** | $5.63 \times 10^8$ | $5.63 \times 10^8$ |
| **$G_p$ at 10% $CO_2$ Breakthrough ($sm^3$)** | $3.03 \times 10^8$ | $3.43 \times 10^8$ |
| **Recovery Factor at 10% $CO_2$ Breakthrough** | 58.6% | 66.9% |
| **Time to $CO_2$ Breakthrough (days)** | 2378 | 2697 |

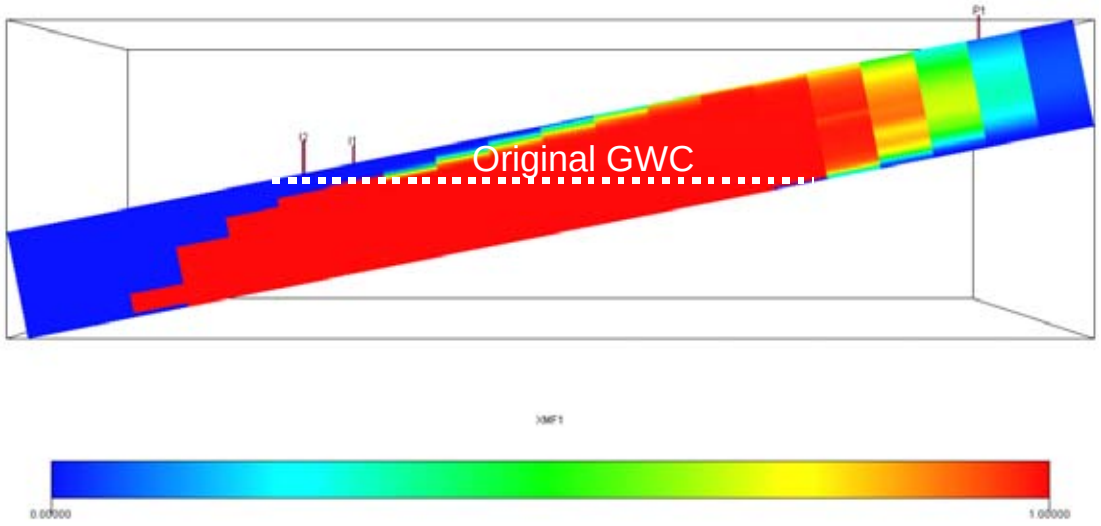


**Figure 5.39: $CO_2$ saturation for the low permeability (10mD) model with injection well completions located at the bottom of the reservoir**

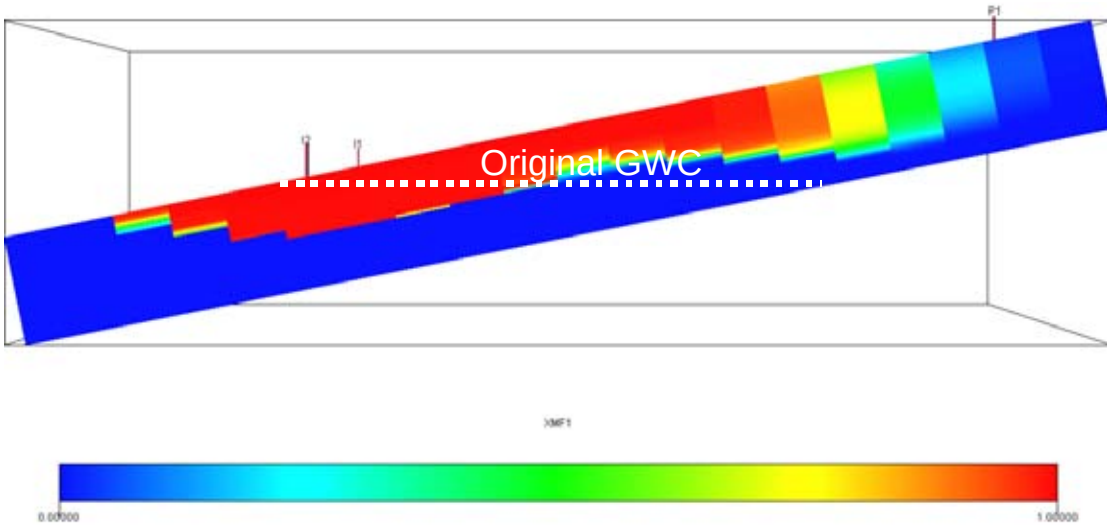


**Figure 5.40: $CO_2$ saturation for the default low permeability (10mD) model with injection well completions located at the top of the reservoir**

These cases have shown that it is possible to improve the displacement efficiency in a low permeability, dipping formation. However due to the higher primary recovery efficiencies possible in these types of formations, the improved recovery efficiency might still not be adequate to make $CO_2$ injection an attractive option over primary depletion.

Thin, Non-dipping Reservoir

It was shown from the results of the ED analysis that gravity dominated displacement in a non-dipping reservoir resulted in the rapid horizontal migration of $CO_2$ towards the area of production. In the case of a thin reservoir, the influence of production in the form of $CO_2$ coning is likely to be an

issue. Improvement in the sweep efficiency could be obtained through either increasing rates in an attempt to achieve a viscous dominated displacement, or reducing rates to limit the susceptibility for $CO_2$ coning. In this section, injection and production rates ranging from 2.5 MMscf/day to 10 MMscf/day are tested, with the results presented in Table 5-13. In this range tested, it is clear that the increase in the strength of viscous forces leads to an improvement in the sweep efficiency at the breakthrough of $CO_2$ as indicated in the comparison of $CO_2$ saturation profiles presented in Figure 5.41 with Figure 5.42. It is noted that further reduction in the injection and production rates would stabilise the gravity dominated displacement by reducing the susceptibility of $CO_2$ coning, but this would have to be considered in conjunction with the increase in the production time.

**Table 5-13: Result of simulations investigating variable rates and the use of horizontal wells in a thin, non dipping reservoir**

| **Case** | 2.5 MMscf/day Rates | 5 MMscf/day Rates | 10 MMscf/day Rates | Horizontal Well |
|---|---|---|---|---|
| **OGIP ($sm^3$)** | $2.81 \times 10^8$ | $2.81 \times 10^8$ | $2.81 \times 10^8$ | $2.81 \times 10^8$ |
| **$G_p$ at 10% $CO_2$ Breakthrough ($sm^3$)** | $1.34 \times 10^8$ | $1.42 \times 10^8$ | $1.52 \times 10^8$ | $1.70 \times 10^8$ |
| **Recovery Factor at 10% $CO_2$ Breakthrough** | 52.4% | 55.5% | 59.5% | 60.5% |
| **Time to $CO_2$ Breakthrough (days)** | 2114 | 1116 | 597 | 1217 |

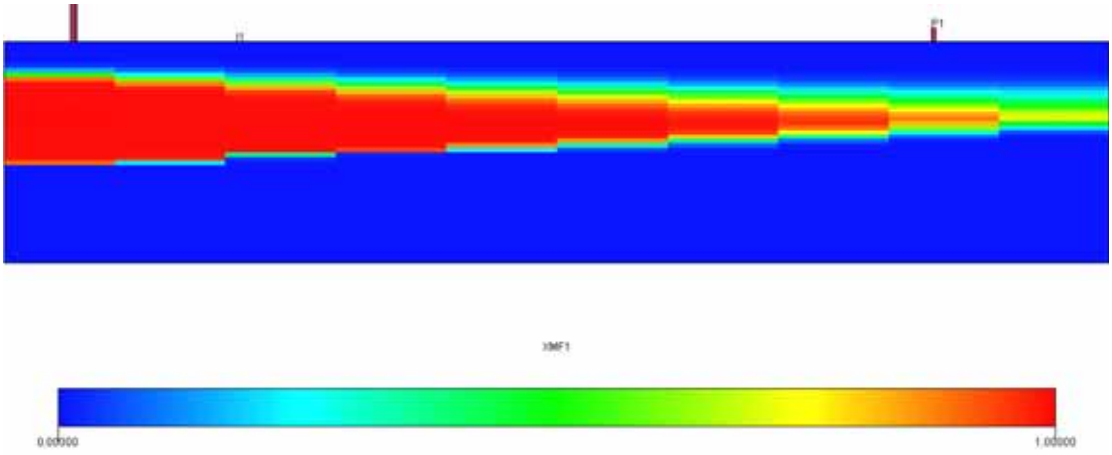


**Figure 5.41: $CO_2$ saturation for rates equal to 2.5 MMscf/day**

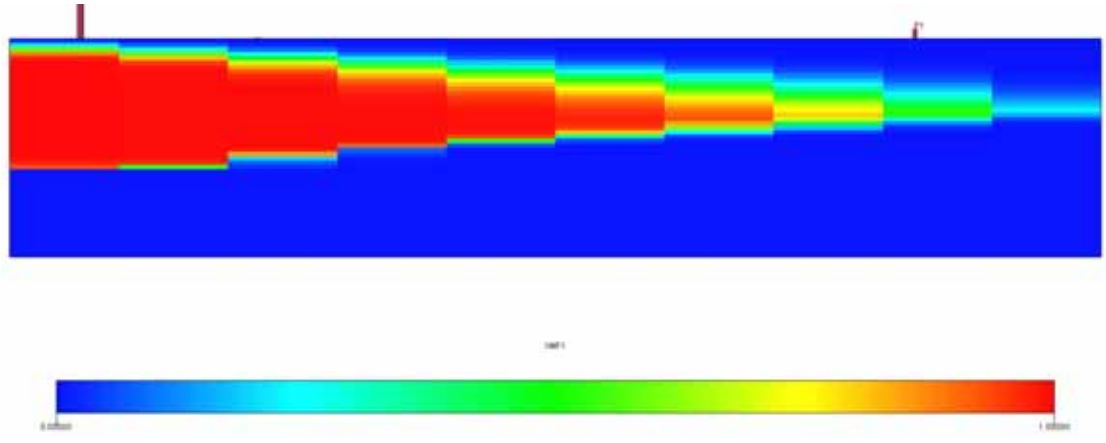

**Figure 5.42: $CO_2$ saturation for rates equal to 10 MMscf/day**

On the other hand, contractual obligations might deem increased rates equally as unfeasible, and so other options would have to be considered. A reduction in localised pressure drawdown required to achieve a specified production rate, critical in the severity of $CO_2$ coning, can be achieved through the use of horizontal wells. The application of horizontal wells has been investigated as a method to improve the sweep efficiency achievable at the default rate of 5 MMscf/day. The production well has been placed at the top, running the length of the formation, while two injection wells have been placed at the GWC at either end of the formation, also running the length of the formation, as seen in Figure 5.43. In addition to reducing the pressure drawdown required to achieve a specified production rate, the use of horizontal wells in this instance will also change the primary direction of displacement from horizontal to vertical. A vertical, gravity stable flood is the aim of this well configuration. Results in Table 5-13 indicate that the breakthrough of $CO_2$ is delayed by 100 days, leading to an increase in $CH_4$ recovery at breakthrough of around 5% OGIP over the default case. It is clear that the alteration of the primary direction of the displacement, coupled with the lower drawdown required to achieve the specified production rate did improve the sweep efficiency. Therefore in situations where rates cannot be altered or where the degree of variation is limited due to contractual requirements, variation in the well type and/or configuration can produce the desired results.

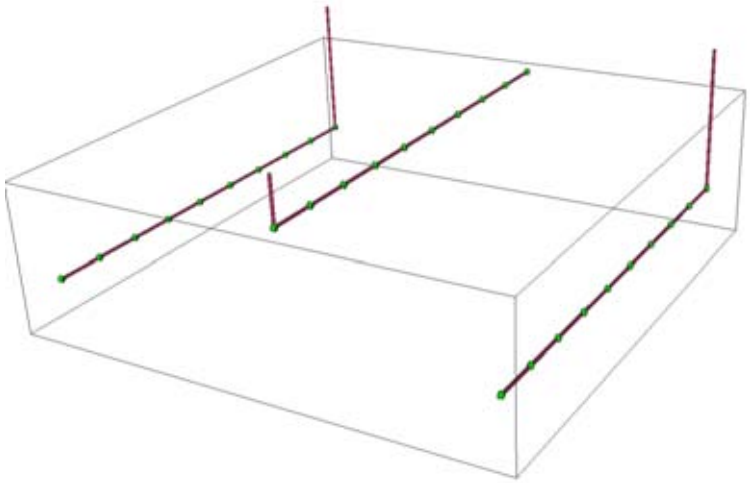

**Figure 5.43: Schematic of horizontal well location. Injection wells located on the edge, with the production well located in the middle of the reservoir**

Application of Horizontal Wells in Heterogeneous, Non-Dipping Formations

The success of the application of horizontal wells in the previous non-dipping scenario was due to the alteration of the dominant direction of flow from horizontal to vertical. A scenario whereby the redirection of the displacement process could be particularly beneficial is when in the presence of heterogeneity. A vertical, gravity stable displacement instead of a horizontal, viscous dominated displacement would completely negate the detrimental impact of the heterogeneity shown previously. Consequently, the use of horizontal wells was applied to the scenario involving low bulk permeability (10mD) with a high permeability layer (1000mD). Recall from Table 5-9 that the recovery efficiency at a breakthrough limit of 10% for this model was a low 33%. With the use of horizontal wells, $CH_4$ recovery at a 10% $CO_2$ breakthrough limit was increased by almost 30% (Table 5-14). Altering the direction of the displacement by achieving a gravity stable displacement has led to a much improved sweep of the reservoir with the negative impact of heterogeneity experienced previously being mitigated (Figure 5.44). A cresting issue is evident in Figure 5.44, which could be solved through a reduction in the rates. This scenario does highlight the potentially significant benefit of using horizontal wells for $CO_2$ EGR operations in layered, non-dipping formations.

**Table 5-14: Results of simulations comparing the use of vertical and horizontal wells**

| **Case** | Vertical Wells | Horizontal Wells |
|---|---|---|
| **OGIP ($sm^3$)** | $5.63 \times 10^8$ | $5.63 \times 10^8$ |
| **$G_p$ at 10% $CO_2$ Breakthrough ($sm^3$)** | $1.73 \times 10^8$ | $3.19 \times 10^8$ |
| **Recovery Factor at 10% $CO_2$ Breakthrough** | 33.6% | 62.1% |
| **Time to $CO_2$ Breakthrough (days)** | 1359 | 2503 |

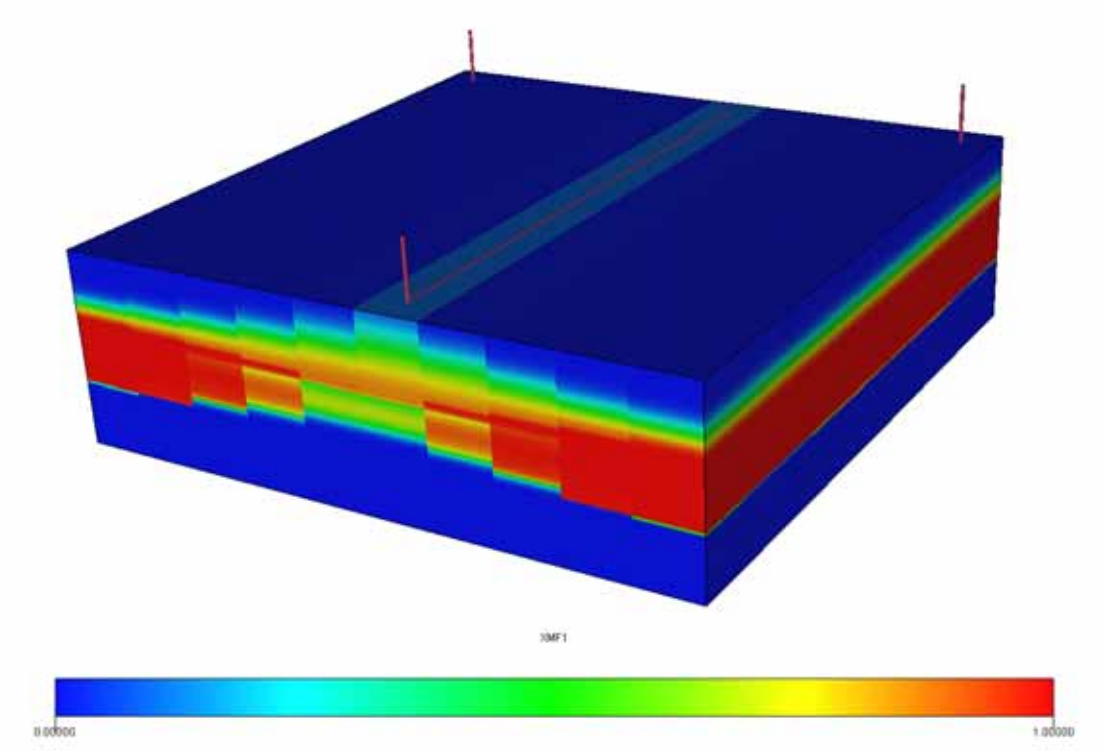

**Figure 5.44: $CO_2$ saturation where injection and production occur through horizontal wells**

Application of Horizontal Wells in Heterogeneous, Dipping Formations

For the sake of brevity, no results will be presented. However the results will be discussed. The application of horizontal wells in a layered, dipping formation is not as successful as in a non-dipping formation. For example, consider the case where the horizontal well direction is perpendicular to the dip direction. The success with using horizontal wells in a non-dipping reservoir was due to the redirection of the displacement process. In a dipping reservoir however, regardless of the type of well employed, the displacement process has both a major horizontal and vertical component as it proceeds towards the production well. This inability to redirect the displacement process severely restricts any benefit in applying horizontal wells in a dipping reservoir. Choosing to direct the horizontal wells parallel to the dip, from the structural high towards the GWC does not make any sense, as water production could be an issue early in the life of the field. In addition, injection of $CO_2$ higher in the structure negates the benefit of the density difference between $CO_2$ and $CH_4$, leading to greater mixing between the two fluids due to density driven flow.

### 5.9.3 Summary

Additional simulations have been performed investigating the effect of heterogeneity in addition to the effect of the operational strategy on the displacement efficiency of $CH_4$ by $CO_2$. Key results from these simulations are as follows:

- Heterogeneity can have a significant negative impact on the sweep efficiency. The presence of a high permeability layer in a low permeability reservoir was shown to decrease $CH_4$ recovery by over 30% of the OGIP.
- With the significance of the viscous to gravity ratio on the efficiency of the displacement process, operational strategies were shown to be an important option to improving the recovery of $CH_4$.
- Production and injection rates can be altered to suit the requirement for either a viscous or gravity dominated displacement. The impact of variable rates on contractual requirements does however have to be considered.
- If flexibility in the rates employed is not an option, variation in the well configuration can achieve the desired results. Well completion locations or the implementation of horizontal wells was shown to improve the results whilst maintaining the rates at the default levels.
- Horizontal wells were shown to be especially beneficial in heterogeneous, non-dipping reservoirs by altering the direction of displacement, and thus negating the negative impact of the heterogeneity present.

# CHAPTER 6

# 6 Study 2: The Effect of Delaying $CO_2$ Injection

## 6.1 Introduction

A common conclusion from the investigations into $CO_2$ EGR in volumetric gas reservoirs was that the incremental recovery of natural gas was improved the longer $CO_2$ injection was delayed. The early injection of $CO_2$ enabled excessive mixing between the resident natural gas and $CO_2$, which with a $CO_2$ production limit applied resulted in a lower recovery of natural gas than when injection is delayed. The early injection of $CO_2$ was also shown to result in a lower recovery efficiency than that achievable under the "do nothing" volumetric depletion case. An effective operational strategy arising from these results was to produce the reservoir to near economic abandonment conditions with $CO_2$ injection to follow in order to re-pressurise the reservoir as well as displace the remaining natural gas towards the production well.

The extent of mixing between $CO_2$ and natural gas is also likely to be of concern in any injection operations involved in water-drive gas reservoirs, but delaying the injection of $CO_2$ in a water-drive reservoir has a major drawback. While such action will limit the time available for mixing, it will also unfortunately allow for the influx of the aquifer to occur, creating a trapped gas saturation. The benefit of delaying injection to limit the extent of mixing is offset by the creation of this trapped gas saturation.

It is however possible to remobilise the trapped gas saturation through the injection of gas. Penetration of the invaded zone by the injected gas could enable reconnection of the trapped gas saturation, forming a continuous gas saturation, enabling flow. However it is uncertain if the injected gas, in this case $CO_2$, will adequately sweep the invaded zone and displace the trapped natural gas. As mentioned in Chapter 2, supercritical $CO_2$ is around 30 – 40% less dense than formation waters, and so gravity segregation will be an issue. Whether it is beneficial to delay the injection of $CO_2$ in order to reduce mixing will be dependent upon the stability of the displacement process in the free gas zone, as well as the ability to sufficiently sweep the invaded zone. Consequently, the effect of viscous and gravity forces, between $CO_2$ and $CH_4$ as well as $CO_2$ and water is expected to be influential on the effectiveness of this strategy. Again using the experimental design methodology, the effect of delaying the injection of $CO_2$, firstly into homogeneous reservoirs and then into heterogeneous reservoirs, is presented in this chapter.

## 6.2 Study 2A: The Injection of $CO_2$ into an Anisotropic, Homogenous Reservoir

The first section of the chapter studies the effect of delaying the injection of $CO_2$ into a homogeneous reservoir. An initial understanding of the key processes involved is desired without adding the complexity of heterogeneity. This will give an understanding of the flow characteristics of the injected $CO_2$ in a uniform environment. The homogeneous models from Study 1 are again employed for use in this investigation.

### 6.2.1 Design, Parameter and Range Selection

**Table 6-1: Parameter and Range Selection for Study 2A**

| Parameter | Low (-1) Level | Mid (0) Level | High (+1) Level |
|---|---|---|---|
| Permeability | 10mD | 100mD | 1000mD |
| $k_v/k_h$ Ratio | 0.01 | 0.1 | 1.0 |
| Thickness | 50m | 100m | 150m |
| Formation Dip | 0° | 11° | 21° |
| Injection Rate* | 100% | 125% | 150% |
| Timing of Injection** | 0% | 20% | 40% |
| * Percent of the production rate | | | |
| ** Injection occurs after the corresponding percent of the OGIP has been produced | | | |

The D-optimal experimental design methodology is once more used in this study. The results of Study 1 showed the significance of viscous and gravity forces on the displacement of $CH_4$ by a denser $CO_2$, especially in comparison to fluid properties such as mixing by diffusion and the salinity of the formation water. In addition to the results found in Study 1, the ability of the injected $CO_2$ to extend into the invaded zone is expected to be a key factor in determining the effect of delaying injection on the recovery of $CH_4$. This will be significantly influenced by the extent of viscous or gravity forces, and so this has led to the selection of parameters and their ranges given in Table 6-1. Note that an injection rate of less than 100% of the production rate was not chosen in this design due to the fact that avoidance of the invasion of the aquifer was sought for the cases involving no delay of $CO_2$ injection. Additionally, cessation of the invasion of the aquifer was sought once $CO_2$ injection commenced for cases where injection was delayed, which could only be achieved injection volumes equalled production volumes at the very least. Table 6-2 presents the design for Study 2A, where it can be seen that the total number of runs is 32.

**Table 6-2: D-Optimal design for Study 2A**

| Run | Permeability | $k_v/k_h$ Ratio | Thickness | Dip | Injection Rate | Timing of Injection |
|---|---|---|---|---|---|---|
| 1 | -1 | -1 | 1 | -1 | 1 | -1 |
| 2 | 1 | 0 | -1 | 1 | -1 | -1 |
| 3 | 1 | -1 | 1 | 0 | -1 | -1 |
| 4 | -1 | 1 | 1 | 1 | 1 | 1 |
| 5 | 1 | -1 | 1 | 1 | 1 | 1 |
| 6 | 1 | 1 | -1 | -1 | -1 | 1 |
| 7 | 1 | 1 | 1 | -1 | 1 | 1 |
| 8 | 1 | -1 | -1 | -1 | -1 | 0 |
| 9 | 0 | 1 | -1 | -1 | -1 | -1 |
| 10 | 1 | -1 | 0 | 1 | 1 | -1 |
| 11 | -0.5 | 0 | 0 | 0 | 0 | 0 |
| 12 | 1 | 1 | -1 | 1 | 1 | 1 |
| 13 | 1 | 1 | 1 | 1 | 1 | -1 |
| 14 | 1 | 1 | 1 | -1 | -1 | -1 |
| 15 | 1 | -1 | -1 | 1 | 0 | 1 |
| 16 | -1 | -1 | -1 | 0 | 1 | 1 |
| 17 | -1 | 1 | 1 | 1 | -1 | -1 |
| 18 | -1 | 0 | -1 | 1 | 1 | -1 |
| 19 | 1 | 1 | -1 | 1 | 0 | -1 |
| 20 | -1 | 1 | 1 | -1 | -1 | 1 |
| 21 | 1 | -1 | 1 | -1 | -1 | 1 |
| 22 | 1 | 1 | 1 | 1 | -1 | 1 |
| 23 | 0 | -1 | -1 | 1 | -1 | -1 |
| 24 | 1 | -1 | -1 | 1 | 1 | 0 |
| 25 | -1 | -1 | -1 | -1 | -1 | -1 |
| 26 | 1 | -1 | -1 | -1 | 1 | -1 |
| 27 | -1 | -1 | 1 | 1 | -1 | 1 |
| 28 | -1 | 1 | -1 | 1 | -1 | 1 |
| 29 | -1 | 1 | -1 | -1 | 1 | 0 |
| 30 | -1 | 1 | -1 | 1 | -1 | 1 |
| 31 | -1 | 1 | 0 | -1 | 1 | -1 |
| 32 | -1 | 1 | -1 | -1 | 1 | 1 |

### 6.2.2 Study 2A Responses

**Response 1: $CH_4$ Recovery at 10% $CO_2$ Breakthrough**

To be consistent with Study 1, a 10% $CO_2$ production limit has been chosen as an indication of the initial breakthrough of $CO_2$. This will demonstrate whether delaying the injection of $CO_2$ can in fact increase $CH_4$ recovery at the initial breakthrough of $CO_2$.

**Response 2: $CH_4$ Recovery at $CO_2$ Limit of 50%**

The average minimum concentration of $CO_2$ required to achieve incremental recovery in Study 1 amounted to around 30%. It was therefore demonstrated that some degree of $CO_2$ production will likely be required in order to achieve incremental recovery. The ability to maximise the incremental

recovery of $CH_4$ will be dependent upon the rate of increase in the production of $CO_2$ after breakthrough. Although a combination of reservoir properties could lead to significantly delayed initial breakthrough of $CO_2$, the rate of increase in $CO_2$ production could be rapid. On the other hand, another combination of properties could lead to early $CO_2$ breakthrough, but the rate of increase in $CO_2$ production could be minor. It will be the maximum allowable concentration of $CO_2$ that can be produced that will determine the possible extent of incremental $CH_4$ recovery. To give an indication of the effect of the input parameters on the rate of increase in $CO_2$ production, a $CO_2$ production limit of 50 mole percent has been applied for this second response.

**Response 3: The Minimum Producing $CO_2$ Concentration Required to Achieve Incremental Recovery**

As in Study 1 this response is used to compare the conventional primary depletion scenario with the $CO_2$ injection scenario, and to determine what parameters lead to a lower producing $CO_2$ concentration being required to achieve incremental recovery.

### 6.2.3 Response 1 Results and Discussion

A graph of the results of each design run for Response 1 is presented in Figure 6.1, indicating a much narrower range of results than the equivalent response from Study 1. Recovery efficiency at the 10% $CO_2$ limit ranges from around 55% to almost 80% of the OGIP. The average of all runs was 65% of the OGIP. The ranking of the statistically significant coefficients is presented in Table 6-3. The six most significant coefficients will be discussed.

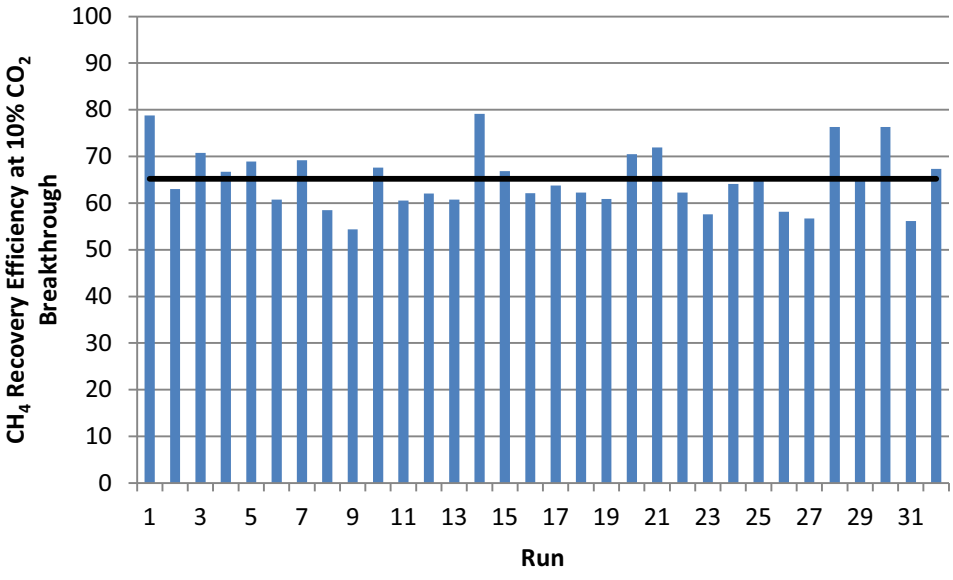


**Figure 6.1: Response 1 results for each design run. The average of all runs is shown as the black line.**

**Table 6-3: Ranking of statistically significant coefficients for Response 1**

| Statistically Significant Coefficient | F Value | p-value Prob > F |
|---|---|---|
| Thickness*Dip | 126.56 | <0.0001 |
| Permeability*Thickness | 122.72 | <0.0001 |
| Thickness | 97.16 | <0.0001 |
| $k_v/k_h$ ratio*Injection Rate | 76.21 | <0.0001 |
| $Dip^2$ | 72.49 | <0.0001 |
| Thickness*Timing of Injection | 64.55 | <0.0001 |
| $k_v/k_h$ ratio | 47.97 | <0.0001 |
| $k_v/k_h$ ratio*Timing of Injection | 44.81 | <0.0001 |
| $Permeability^2$ | 39.88 | <0.0001 |
| Injection Rate*Timing of Injection | 34.44 | <0.0001 |
| $Injection\ Rate^2$ | 30.70 | 0.0001 |
| $k_v/k_h$ ratio*Thickness | 28.52 | 0.0002 |
| Dip | 26.84 | 0.0002 |
| Injection Rate | 16.06 | 0.0017 |
| $Timing\ of\ Injection^2$ | 15.23 | 0.0021 |
| Permeability | 10.37 | 0.0073 |
| Permeability*Timing of Injection | 8.36 | 0.0135 |

With respect to the model diagnostics, the correlation coefficient, $R^2$, and the adjusted $R^2$ coefficient are 0.9824 and 0.09560 respectively. The normal probability plot, shown in Figure 6.2, shows no major deviation from the normality assumption.

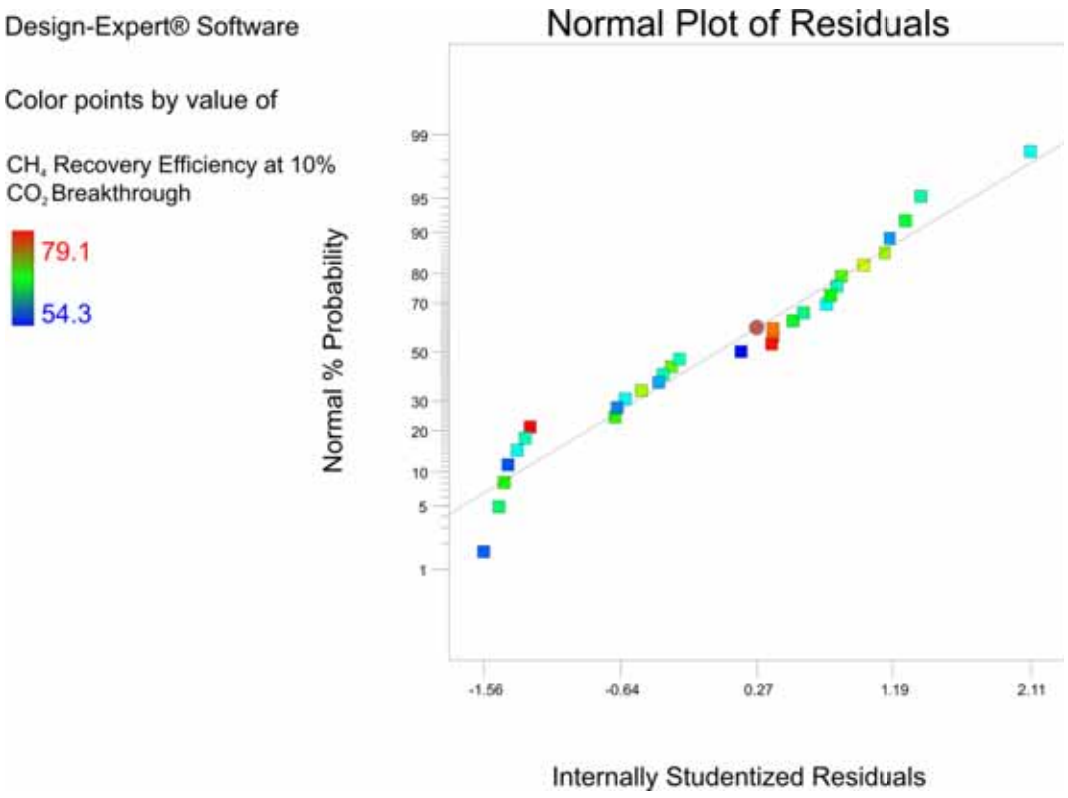


**Figure 6.2: The normal probability plot for Response 1.**

Thickness – formation dip interaction

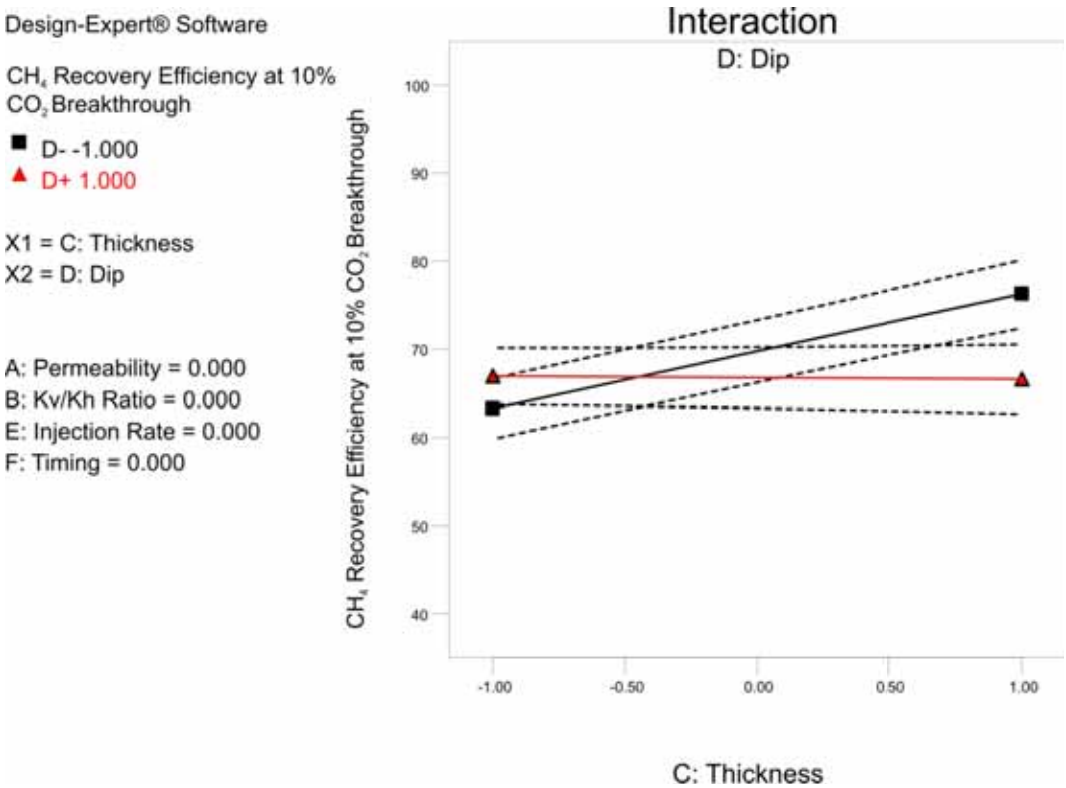


**Figure 6.3: The effect graph for the thickness formation dip interaction for Response 1**

The most statistically significant coefficient, as specified in Table 6-3, is the thickness – formation dip interaction. The effect graph (Figure 6.3) indicates the effect of thickness is especially significant in non-dipping reservoirs, whereas varying thickness has a minimal effect in dipping reservoirs. The positive trend in a non-dipping reservoir is due to a combination of the effect of gravity over-ride, coupled with the influence of production, in the form of CO2 coning, due to variable thickness. Figure 6.4 presents a schematic of a non-dipping reservoir, where injection has occurred after a period of primary production. Unless viscous forces are strong enough to sweep the entire volume invaded by the aquifer, buoyancy will cause over-ride of the invaded zone.

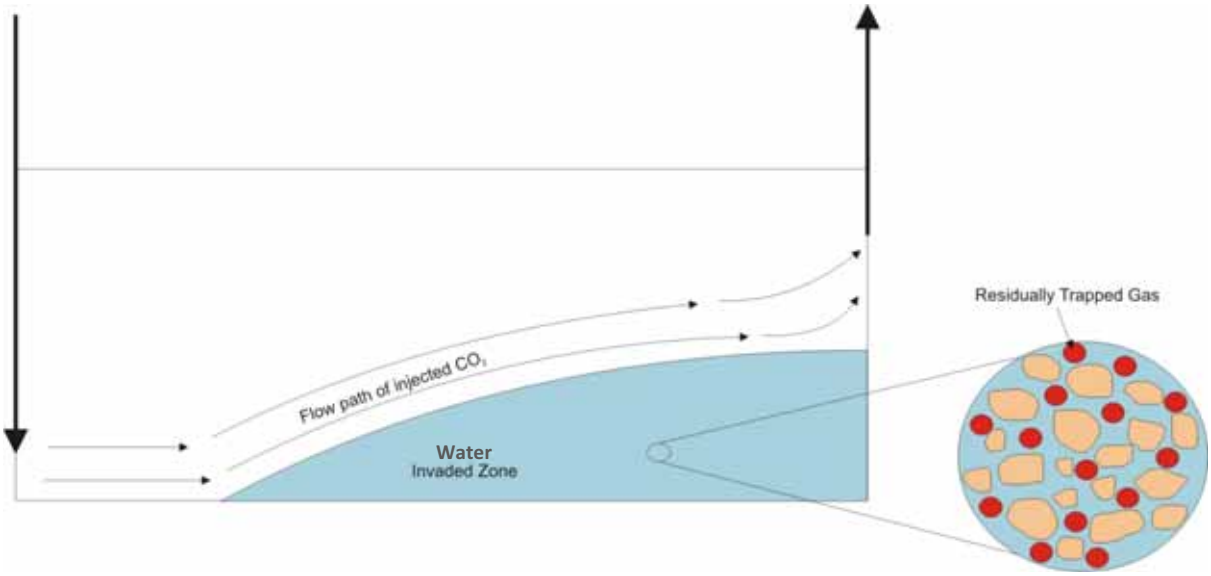


**Figure 6.4: Schematic of the displacement process when the injection of $CO_2$ is delayed in a non-dipping reservoir. The "Invaded Zone" represents the zone invaded by the aquifer.**

The effect of delaying the injection of $CO_2$ is that the thickness of the free gas zone is reduced. This reduction will influence the displacement efficiency of this zone. This reduction is particularly detrimental in thin reservoirs. For example, Figure 6.5 presents a screenshot of a simulation representing a 50 metre thick, non-dipping reservoir with $CO_2$ injection after 20% of the OGIP has been produced. It can be seen that gravity segregation is causing $CO_2$ to under-ride the $CH_4$ column in the free gas zone, and over-ride the invaded zone. The delaying of the injection of $CO_2$ has led to a reduction in the thickness of the free gas zone. Consequently, with $CO_2$ over-riding the invaded zone, it is in closer proximity to the production well completions, with significant coning occurring severely limiting the sweep of the reservoir. Increasing reservoir thickness increases the distance between the current GWC and the producing completions and with constant production rates employed the influence of production will be less severe, limiting $CO_2$ coning. Consequently a positive trend is observed in Figure 6.3.

However, the effect graph for the thickness – formation dip interaction is based on injection occurring after 20% of the OGIP has been produced. Therefore, the efficiency of the displacement in the free gas zone has a greater impact on the recovery efficiency and therefore the trend observed in Figure 6.3. As injection is delayed further, the sweep of the invaded zone becomes increasingly more important. In that regard, as injection is further delayed, increasing reservoir thickness would become increasingly less beneficial in terms of $CH_4$ recovery, and would eventually prove detrimental due to the increase in the influence of gravity and the inability to sweep the invaded zone.

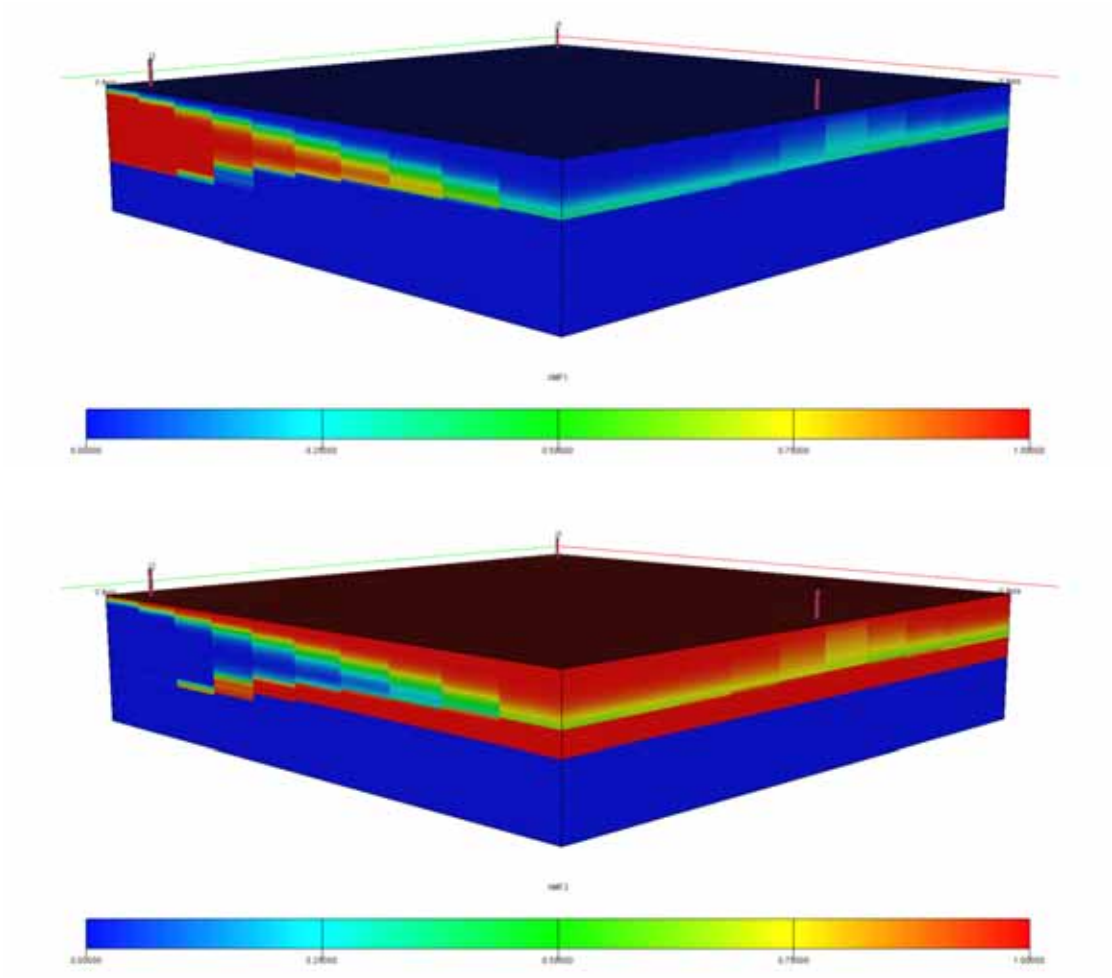

**Figure 6.5: Screenshots of a thin (50m), non-dipping reservoir at the point of 10% $CO_2$ breakthrough showing $CO_2$ saturation (top) and $CH_4$ saturation (bottom). Injection has been delayed.**

In a dipping reservoir a slightly negative trend is observed with increasing thickness. This is analogous to the effect of thickness in a dipping reservoir observed in Study 1. The minimal effect is again due to the similar displacement profiles seen in dipping reservoirs due to the stabilising influence of gravity (in the free gas zone), as seen in Figure 6.6. With a similar efficiency achievable in the free gas zone regardless of thickness, the sweep of the invaded zone now becomes more of an influential factor than was the case in a non-dipping reservoir. Consequently a greater proportion of the invaded zone is swept in the thin scenario due to the stronger viscous forces. As thickness increases, the ever-increasing influence of gravity limits the sweep of the invaded zone. Again, as injection is further delayed, the ability to sweep the invaded zone becomes increasingly more influential and so the negative impact of increasing thickness would be exacerbated.

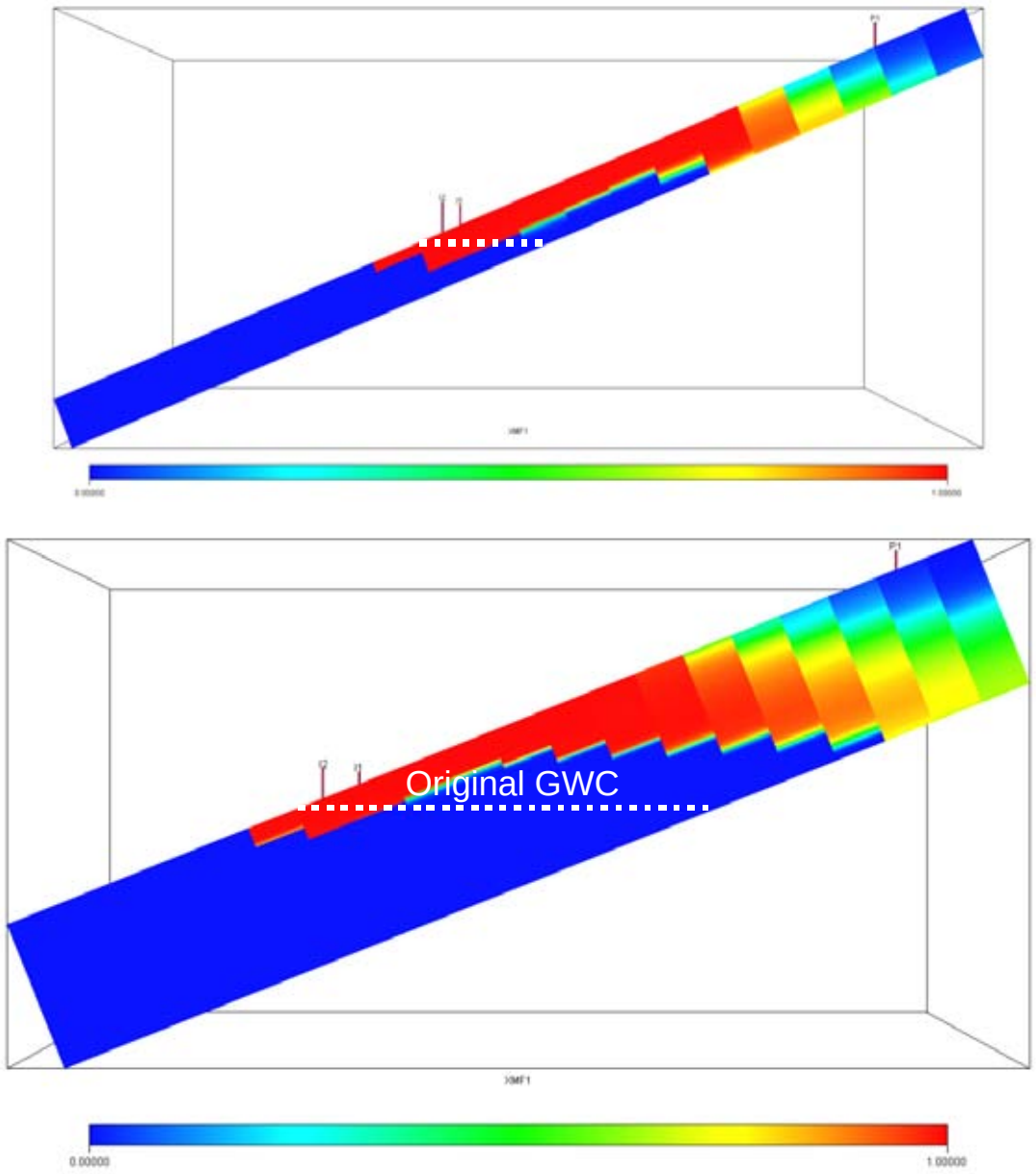


**Figure 6.6: $CO_2$ saturation for a thin (50m) dipping reservoir (top) and a thick (150m) dipping reservoir (bottom), displaying similar displacement profiles in the free gas zone, but with greater over-ride of the invaded zone as thickness increases.**

Permeability – thickness interaction

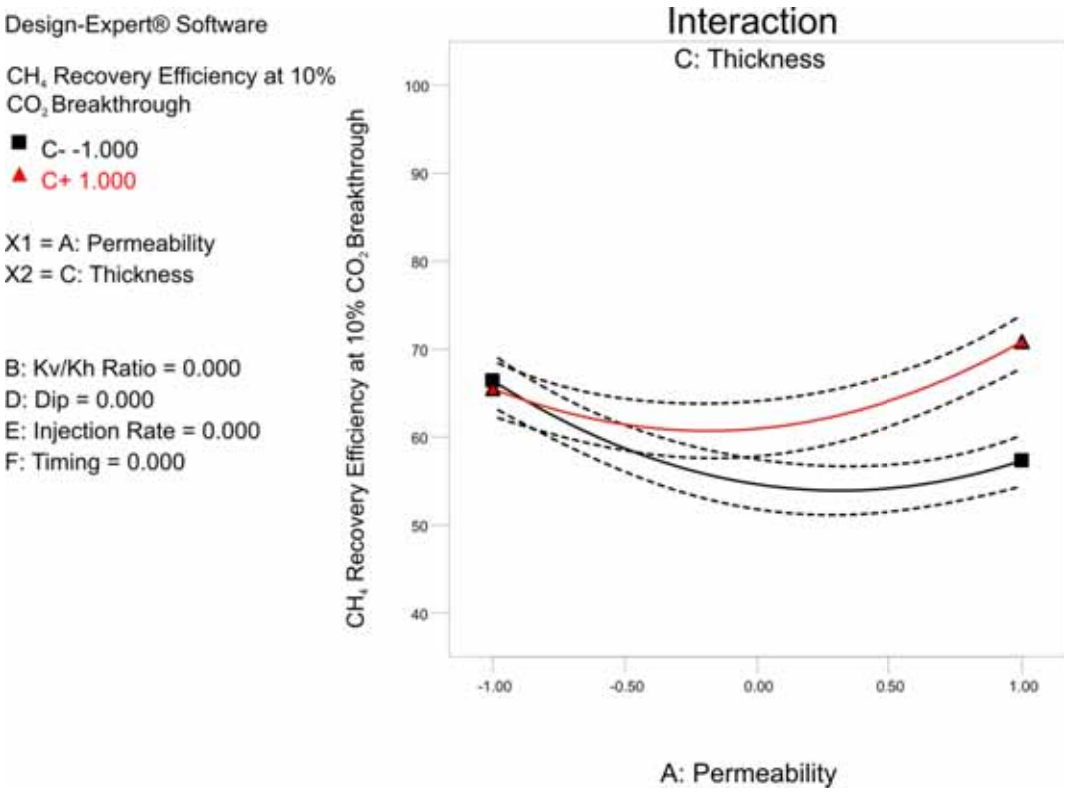


**Figure 6.7: The effect graph for the permeability thickness interaction for Response 1**

The competing effects of viscous and gravity forces on the displacement in the invaded zone and the free gas zone is demonstrated in the effect graph for the permeability – thickness interaction (Figure 6.7). Note that this effect graph is constructed with the timing of injection at the mid level, i.e. after 20% of the OGIP has been produced. For a thin reservoir, although displaying some degree of curvature, the general trend is $CH_4$ recovery decreases as permeability increases. For a thin reservoir, the ability to sweep the invaded zone enables a higher recovery efficiency to be achieved than for higher permeability scenarios. Increasing permeability enhances gravity segregation reducing the ability to sweep residually trapped gas. Additionally, during the period of primary production, the lower permeability restricts the ability of the aquifer to respond to production, allowing for greater pressure reduction. This ensures less moles of $CH_4$ are residually trapped than is the case for higher permeability scenarios.

For a thick reservoir, there is a slight benefit with low permeability scenarios in so far that a greater portion of the invaded zone is able to be swept due to the stronger viscous forces, and that greater pressure reduction is possible for the period of primary production. Increasing reservoir thickness promotes greater gravity segregation which initially is detrimental due to the reduction in the sweep of the invaded zone, but the stability of the displacement process in the free gas zone attributable to

a high permeability, thick reservoir is such that $CH_4$ recovery at the 10% $CO_2$ limit is maximised under these conditions.

Main effect of thickness

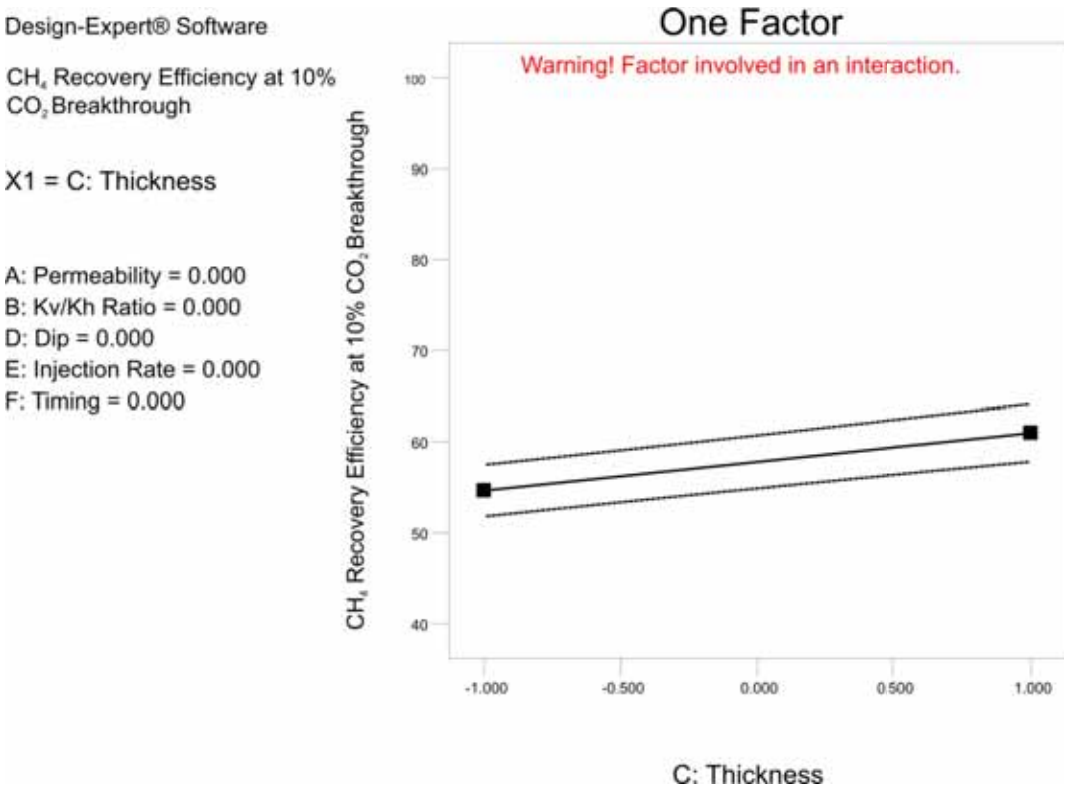


**Figure 6.8: The effect graph for the main effect of thickness for Response 1**

The results of these two interactions involving thickness demonstrate that the extent of the effect is dependent upon the influence of other parameters. However its general effect across all situations tested in the design is positive, as indicated by the effect graph for the main effect of thickness (Figure 6.12). This would however change as injection is further delayed, due to the negative impact of gravity segregation on the ability to sweep the invaded zone. For instance, if the reservoir had been entirely swept by the aquifer, variations in the recovery efficiency would be highly dependent upon the ability to sweep of the invaded zone, which would decrease as thickness increases.

$k_v/k_h$ ratio – injection rate interaction

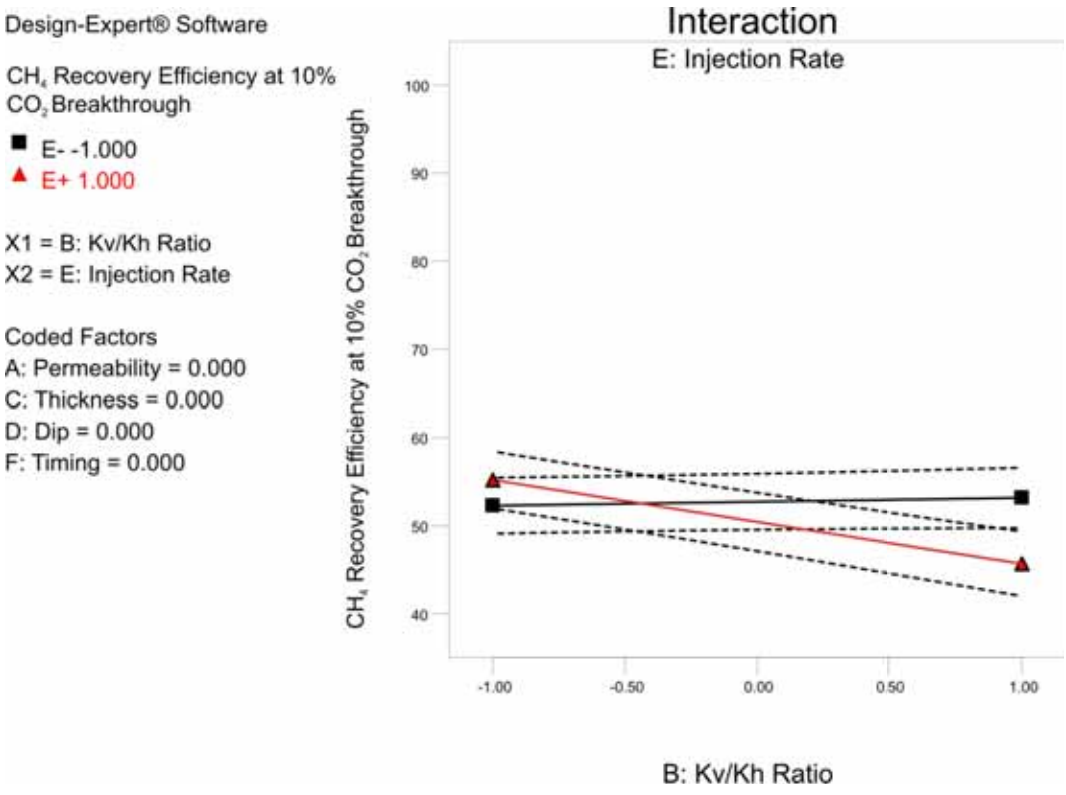


**Figure 6.9: The effect graph for the $k_v/k_h$ ratio injection rate interaction for Response 1**

The effect graph for the $k_v/k_h$ ratio – injection rate interaction (Figure 6.9) indicates a strong negative trend with increasing ratio at a high injection rate. Additionally this graph shows that when vertical permeability is restricted, a higher rate can be beneficial to $CH_4$ recovery. The restriction in vertical flow, directing the injected $CO_2$ horizontally assists in sweeping the reservoir, and if a portion of the reservoir has been invaded by the aquifer, assists in sweeping this zone. Increasing the vertical permeability increases the mobility of the injected $CO_2$ in this direction, which with a higher injection rate, leads to earlier breakthrough of $CO_2$ at the production well, negatively impacting on $CH_4$ recovery.

Main effect of formation dip

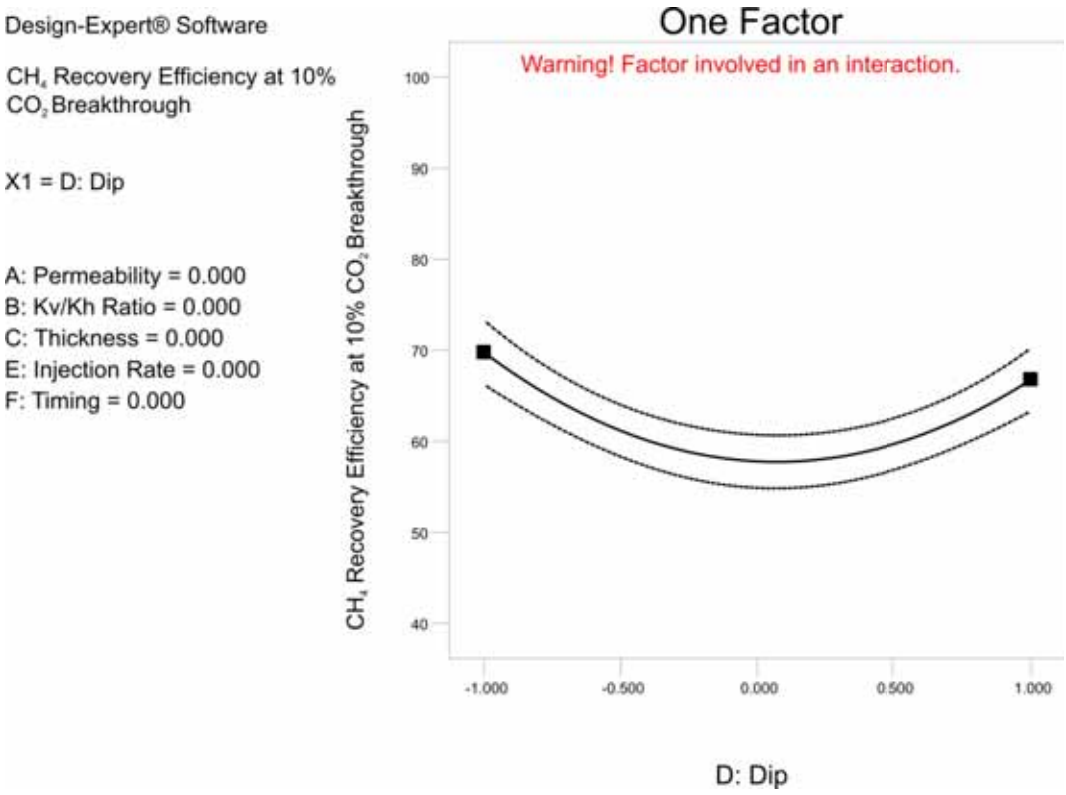


**Figure 6.10: The effect graph for the quadratic effect of formation dip for Response 1**

The significance of the quadratic term for the formation dip parameter indicates that the effect of formation dip exhibits significant curvature, as seen in the effect graph (Figure 6.10). As was the case with the main effect of the aquifer size in Response 1 of Study 1, stand alone simulations were unable to match this result. A graph of the result of each design with respect to the levels of formation dip is presented in Figure 6.11. A key aspect in this graph is the greater spread of results for the non-dipping scenarios versus the dipping scenarios. In a non-dipping reservoir, $CH_4$ recovery can be considerably high (i.e. thick reservoirs) but recovery can also be low (i.e. thin, high permeability reservoirs). The recovery efficiency in a dipping reservoir tends to be relatively similar due to similar displacement profiles attributable to the increased effect of gravity in all cases. It is the fitting of this data, to account for the spread of results for a non-dipping reservoir and the clustering of results in a dipping reservoir, which is believed to result in the curvature displayed.

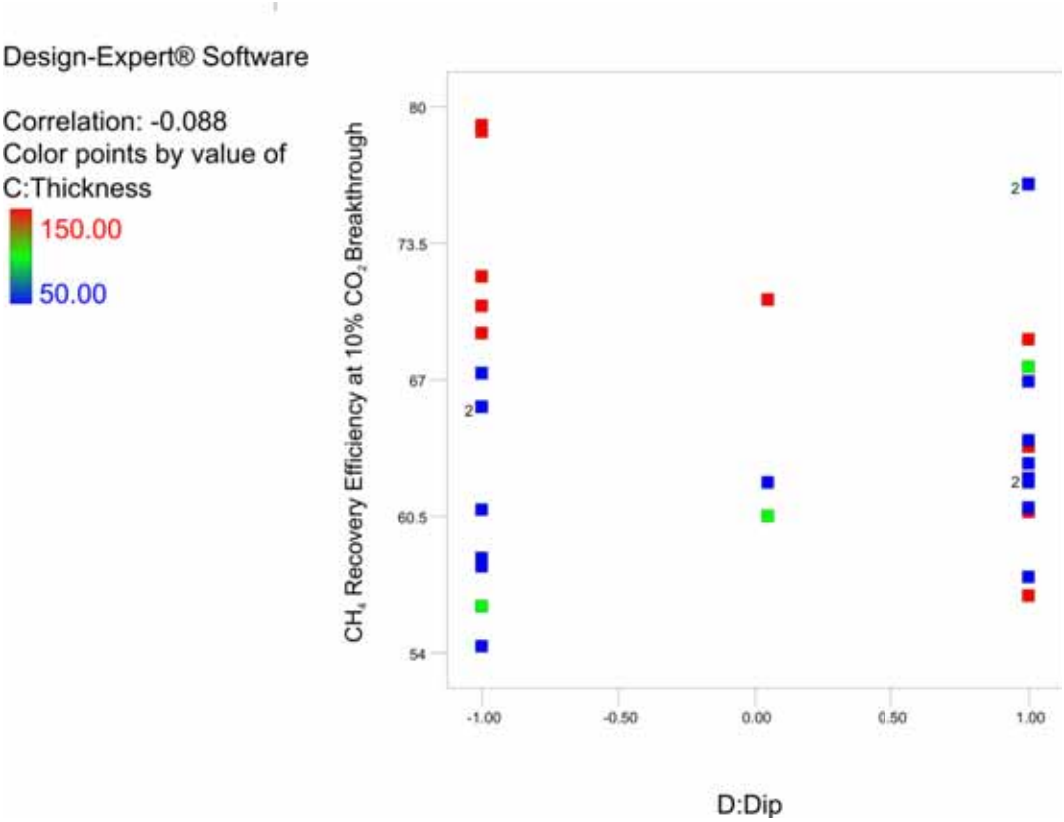


**Figure 6.11: Summary of the results for each run for Response 1 as a function of formation dip and thickness. Note the opposing trends for the levels of thickness as formation dip increases.**

Thickness – timing of injection interaction

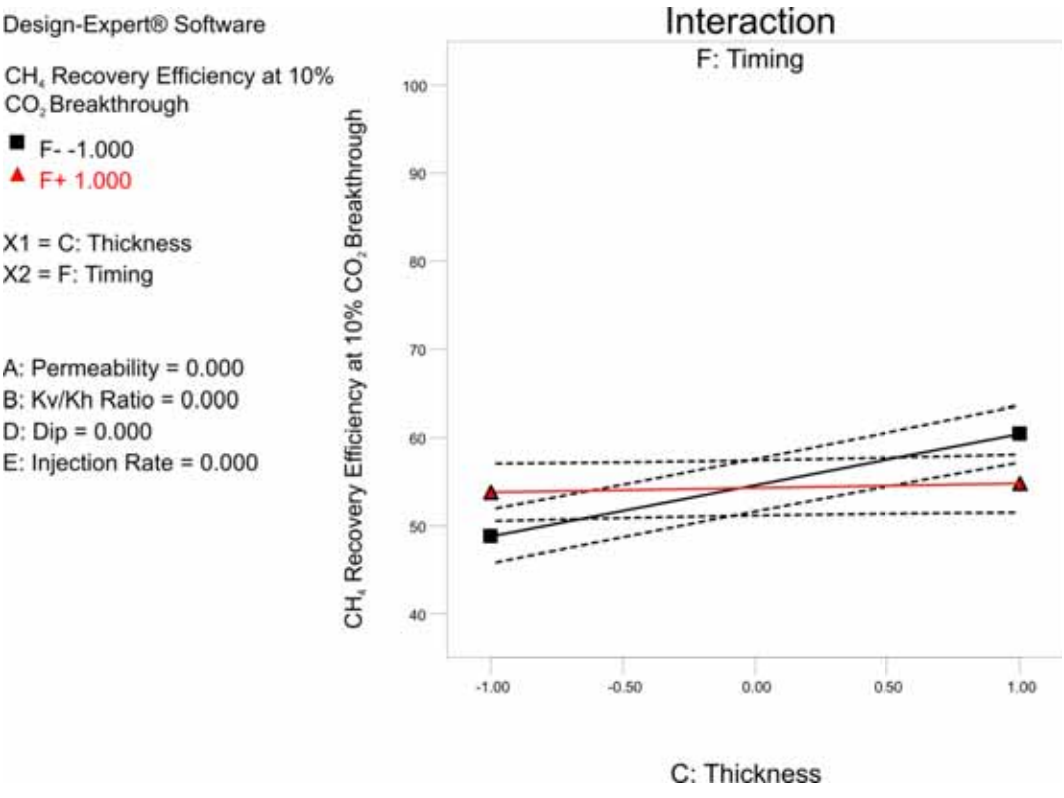


**Figure 6.12: The effect graph for the thickness timing of injection interaction for Response 1**

It was mentioned in the discussion for the main effect of thickness that it is believed that the positive effect of thickness would decrease as injection is delayed. The thickness – timing of injection interaction is also a statistically significant coefficient, and as Figure 6.12, the positive effect of thickness does in fact decrease as the timing of injection is delayed. In the free gas zone, it has been shown that the stability of the displacement process is significantly improved as thickness is increased, primarily in a non-dipping reservoir, hence the strong positive trend shown in Figure 6.12. The effect of gravity is increased with increasing thickness. Gravity serves to stabilise the displacement front, and under conditions of consistent rates employed in this design (as well as Study 1) acts to suppress the coning of $CO_2$. However, as injection is delayed, the sweep of the invaded zone becomes increasingly more important. Whereas gravity segregation is beneficial to the displacement of $CH_4$ by $CO_2$ in the free gas zone, gravity segregation is detrimental to the sweep of residually trapped gas in the invaded zone. This is analogous to the effect of gravity segregation in $CO_2$ EOR operations. Gravity segregation leads to the bypassing of the invaded zone by the injected $CO_2$, leaving the residual saturation unswept. Therefore, as shown in Figure 6.12, the positive effect decreases as injection is delayed. The range of the timing of injection was extended (injection further delayed), the trend would likely be negative as thickness is increased.

Also evident in Figure 6.12 is that for a thin reservoir it is beneficial to delay the injection of $CO_2$, primarily due to the ability to sweep a significant portion of the invaded zone due to the stronger viscous forces. On the other hand, if gravity is the dominant force (at the macroscopic level), for the reasons previously discussed, it is more beneficial to not delay the injection of $CO_2$.

### 6.2.4 Response 2 Results and Discussion

The graph of the results of the individual design runs for Response 2 is presented in Figure 6.13. The recovery efficiencies at an increased $CO_2$ limit of 50% range from 65% to over 90% of the OGIP, however the majority of outcomes lie between mid 70% to mid 80% of the OGIP. Consequently, the average recovery efficiency for all runs is around 80% of the OGIP. These results suggest that if a producing $CO_2$ concentration of up to 50% can be tolerated, recovery in water-drive gas reservoirs can be considerably high, and can be in the region of recovery efficiencies associated with volumetric gas reservoirs.

The ranking of most statistically significant coefficients in determining the recovery efficiency of $CH_4$ at a $CO_2$ limit of 50% is presented in Table 6-4. Clearly noticeable is the dominance of the timing of injection. The remaining, highest ranked coefficients resemble the results of Response 1.

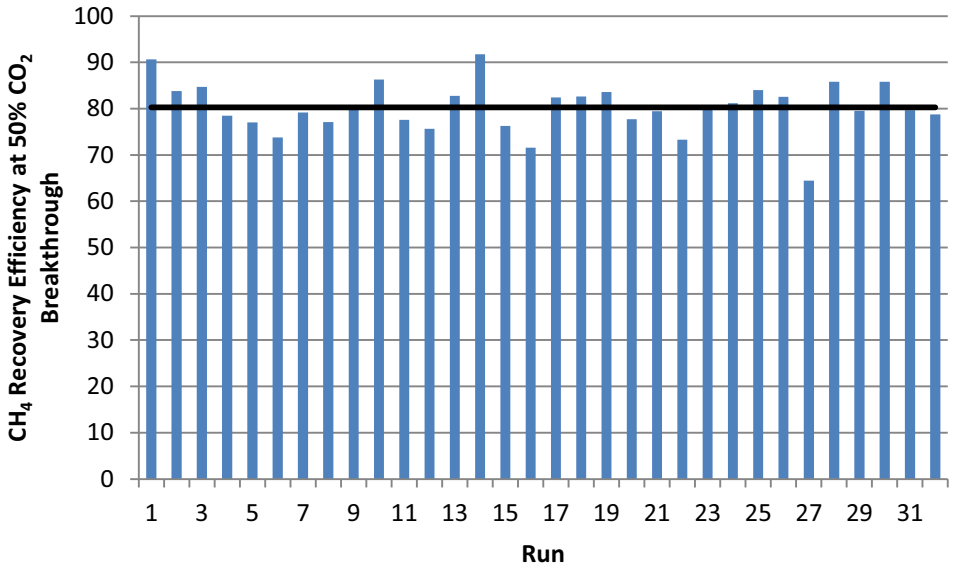


**Figure 6.13: Response 2 results for each design run. The average of all runs is shown as the black line.**

**Table 6-4: Ranking of statistically significant coefficients for Response 2**

| Statistically Significant Coefficients | F Value | p-value Prob > F |
|---|---|---|
| Timing of Injection | 236.57 | <0.0001 |
| Thickness*Dip | 78.91 | <0.0001 |
| Permeability*Thickness | 60.18 | <0.0001 |
| $k_v/k_h$ ratio*Injection Rate | 40.56 | 0.0001 |
| $Dip^2$ | 37.98 | 0.0002 |
| $k_v/k_h$ ratio*Timing of Injection | 29.57 | 0.0004 |
| Thickness | 26.66 | 0.0006 |
| Injection Rate*Timing of Injection | 24.99 | 0.0007 |
| Thickness*Timing of Injection | 24.13 | 0.0008 |
| $k_v/k_h$ ratio*Dip | 22.45 | 0.0011 |
| Permeability* $k_v/k_h$ ratio | 21.57 | 0.0012 |
| Dip | 17.67 | 0.0023 |
| $Injection\ Rate^2$ | 14.22 | 0.0044 |
| Permeability*Timing of Injection | 13.53 | 0.0051 |
| Thickness*Timing of Injection | 10.12 | 0.0112 |
| $k_v/k_h$ ratio*Thickness | 5.23 | 0.0480 |

The regression diagnostics again indicate the model adequately represents the data. The $R^2$ and adjusted $R^2$ coefficients are 0.9859 and 0.9515 respectively. Once more, the normal probability plot, displayed in Figure 6.14, indicates no significant deviation from the normality assumption.

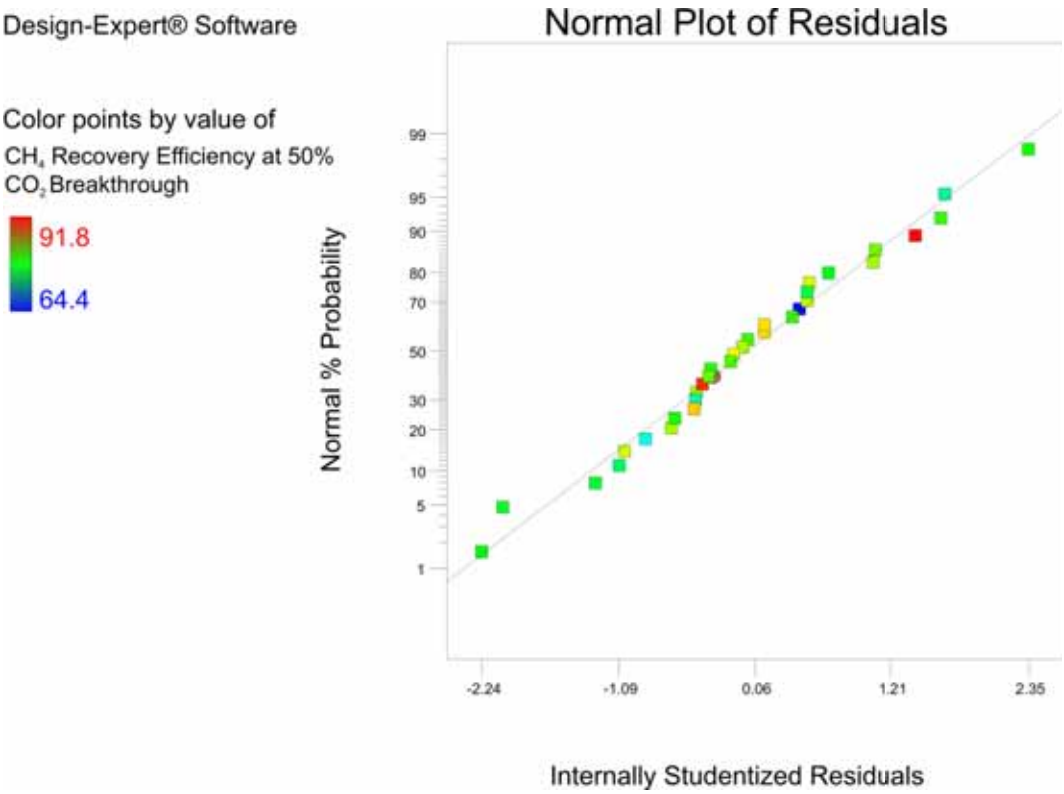


**Figure 6.14: The normal probability plot for Response 2.**

The main effect of the timing of injection

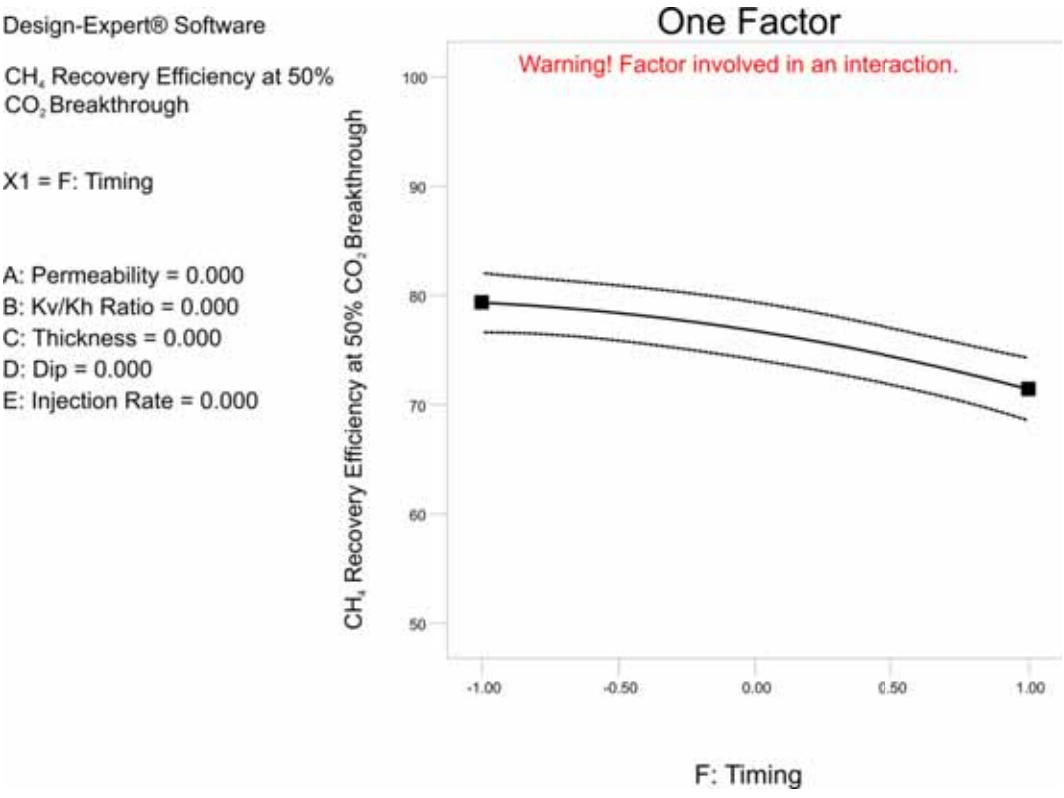


**Figure 6.15: The effect graph for the main effect of timing of injection for Response 2.**

From Table 6-4 it can be seen that the ranking of statistically significant coefficients from the analysis of Response 2 are very similar to that of Response 1, with one significant exception. The effect of the timing of $CO_2$ injection is by far the most influential parameter on $CH_4$ recovery at a $CO_2$ production limit of 50%.

Investigating the main effect of the timing of injection (Figure 6.15), delaying the injection of $CO_2$ has a strong negative effect on the recovery of $CH_4$ at the 50% $CO_2$ production limit. Recall from Response 1 that it was shown that the effect of the timing of injection was dependent upon the thickness of the reservoir, and more generally whether viscous or gravity forces dominated the displacement process. The results from Response 2 however show that delaying the injection of $CO_2$ will always lead to a more rapid increase in the production rate of $CO_2$, and hence lead to a lower $CH_4$ recovery efficiency at the 50% $CO_2$ limit. To give an indication of the effect of timing on the rate of $CO_2$ production, Figure 6.16 presents a comparison of two equivalent models, whereby the timing of $CO_2$ injection has been altered. The time scale has been normalised for each case from the time when $CO_2$ production reaches 10 mole percent to the time when $CO_2$ production reaches 90 mole percent of the production stream. This Figure clearly shows the significantly more rapid rate of increase in $CO_2$ production when injection is delayed. The time taken for $CO_2$ production to increase from 10 – 90 mole percent of the production stream for the delayed injection scenario is around 1,200 days compared to around 3,200 days when injection is not delayed.

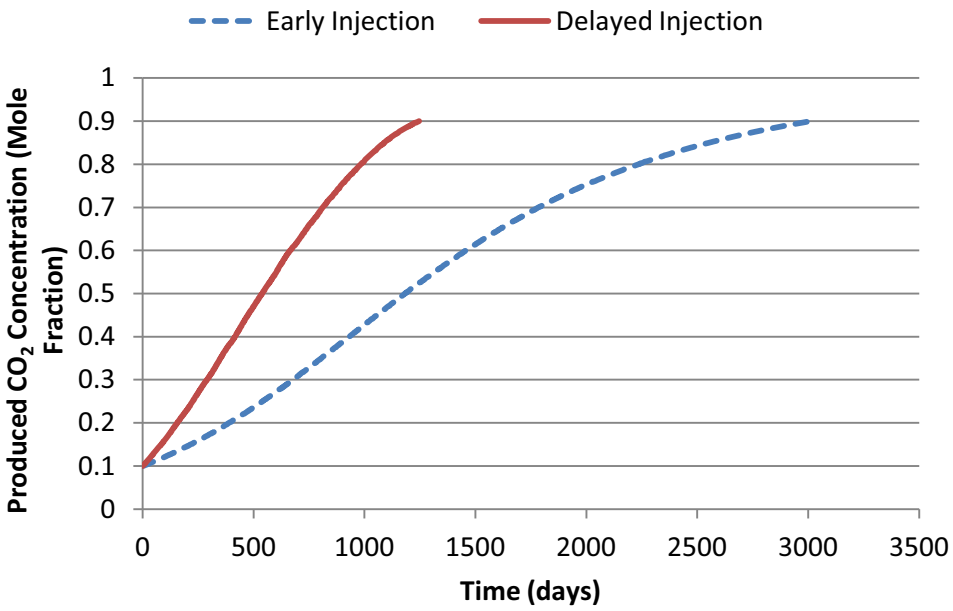


**Figure 6.16: The comparison of producing $CO_2$ concentration profiles where the injection of $CO_2$ has either been delayed or not delayed.**

The more rapid increase in the $CO_2$ production rate as injection is delayed can be attributed to the decrease in the free gas zone and the inability to sweep the invaded zone. For example, consider the situation presented in Figure 6.17. This Figure presents two scenarios where only the timing of injection has been altered. The top screenshot depicts the $CH_4$ saturation for a scenario where injection has occurred at the commencement of production. The bottom screenshot depicts a scenario where injection has occurred after 40% of the OGIP has been produced. It can clearly be seen that for the delayed injection scenario, a significant portion of the invaded zone has remained unswept due to gravity segregation between the $CO_2$ and the aquifer. There is a volume of $CH_4$ that will therefore remain unrecovered (unless operational parameters are altered). Furthermore, delaying the injection and allowing the aquifer to invade is essentially altering the thickness, and hence volume, of the gas reservoir (free gas zone). With the same volume of $CO_2$ being injected into what is essentially a smaller volume reservoir, it would be expected that $CO_2$ production would be more rapid than for a thicker reservoir. Additionally, as depicted in Figure 6.17, the reduction in the free gas zone alters the stability of the displacement process occurring in the free gas zone. It can be seen in the bottom screenshot of Figure 6.17 that once the $CO_2$ has reached the free gas zone, it migrates horizontally along the current GWC towards the production well. Due to the thinness of the reservoir, the coning of $CO_2$ is now a major issue. $CO_2$ coning is evident in the top screenshot also, but as Figure 5.20 showed that, for this particular case of a gravity dominated displacement, increasing reservoir thickness under a constant production rate scenario stabilises the displacement front improving the sweep of the free gas zone. More generally, the alteration of the reservoir thickness through delayed injection, and the subsequent effect on the displacement efficiency (i.e. Study 1) needs to be considered.

The issue with delaying the injection of $CO_2$ is the competing effect of the parameters tested on the efficiency of the displacement in the free gas zone and the invaded zone. A strong gravity dominated displacement, such as a thick non-dipping reservoir, has been shown in Study 1 to result in an efficient displacement process in the free gas zone. However, strong gravity forces will lead to significant gravity segregation between $CO_2$ and water, ensuring poor sweep of the invaded zone if injection is delayed. While stronger viscous forces would allow for a greater portion of the invaded zone to be swept, over the range of values tested for all parameters in this design, delaying the injection of $CO_2$ always leads to a more rapid increase in the production rate of $CO_2$ and therefore lowers the $CH_4$ recovery efficiency at the 50% $CO_2$ limit.

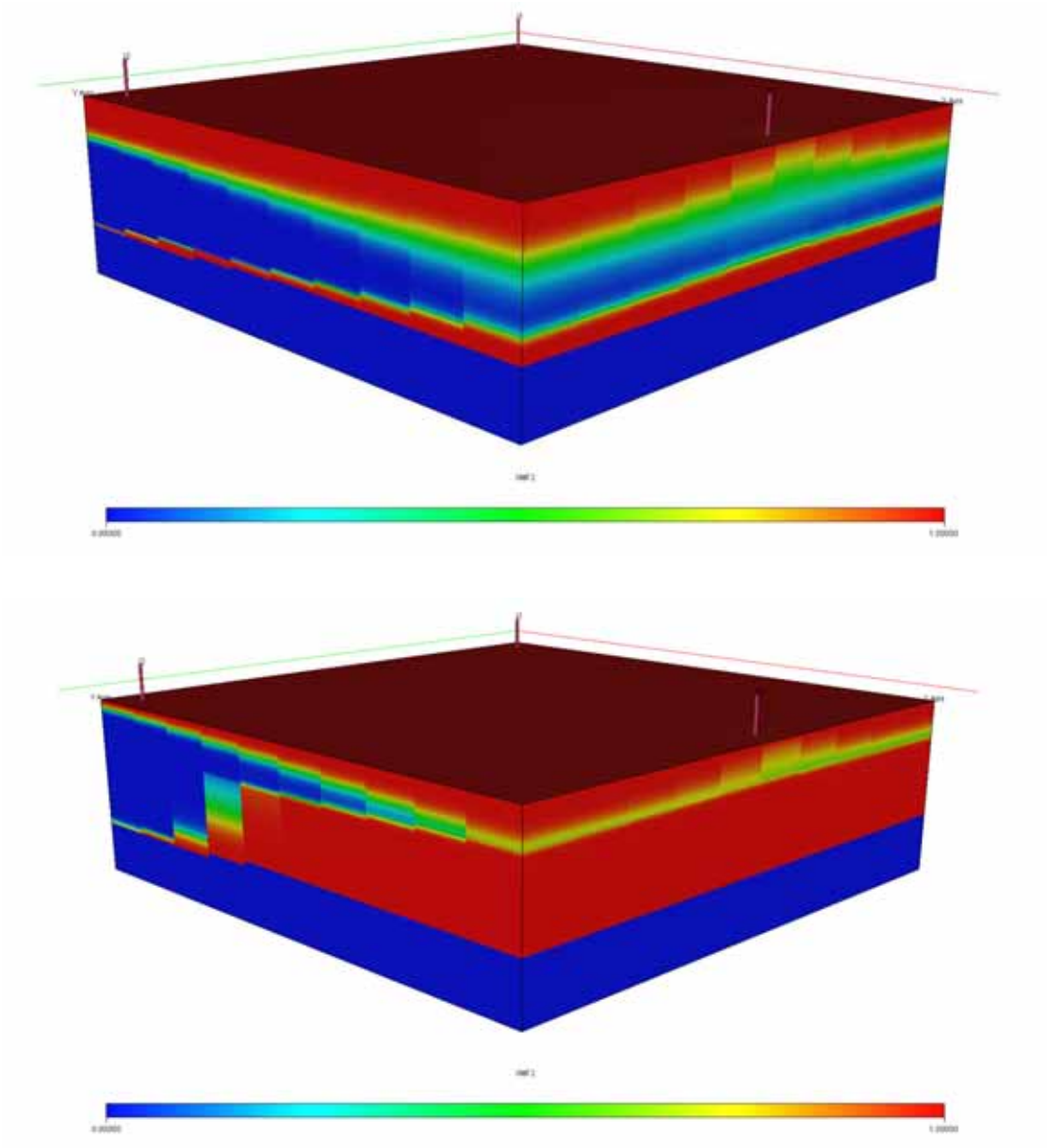

**Figure 6.17: The $CH_4$ saturation for two models where injection has not been delayed (top), and where injection has been delayed (bottom). The reduction in the thickness of the free gas zone (and therefore effectively the reservoir) is clearly visible.**

This result suggests that the extent to which $CO_2$ can be handled will determine the strategy on the timing of $CO_2$ injection. The results from Response 1 showed that delaying the injection of $CO_2$ could be both beneficial and detrimental, depending on the extent of viscous or gravity forces and the corresponding effect on the efficiency of the displacement under the conditions resulting from the choice of the timing of injection. If a higher producing $CO_2$ concentration can be tolerated, the results of Response 2 have shown that the early injection of $CO_2$ will always result in a greater recovery of $CH_4$.

The remaining, highest ranking statistically significant coefficients in the analysis of Response 2 closely mirror the results presented in Response 1. Although the ordering of some of these parameters is slightly different to that seen in Response 1, the most influential coefficients are the same as in Response 1. Similarly, the effect graphs for these coefficients display the same trend as the corresponding coefficient in Response 1. With the timing of injection constant (at the mid level) in these effect graphs, the same processes that result in the initial breakthrough of $CO_2$ at the production well will determine the recovery at the 50% $CO_2$ limit. For example, consider the effect graph for the thickness – formation dip interaction (Figure 6.18), it can again be seen that varying thickness in a dipping reservoir has minimal effect on the recovery of $CH_4$. For a non-dipping reservoir, once again a strong positive trend is apparent with increasing thickness of the formation. The discussions of the effect graphs in Response 1 provide a valid explanation of the trends observed in effect graphs for the next four statistically significant coefficients for Response 2 (Figure 6.18 to Figure 6.21).

Thickness – formation dip interaction

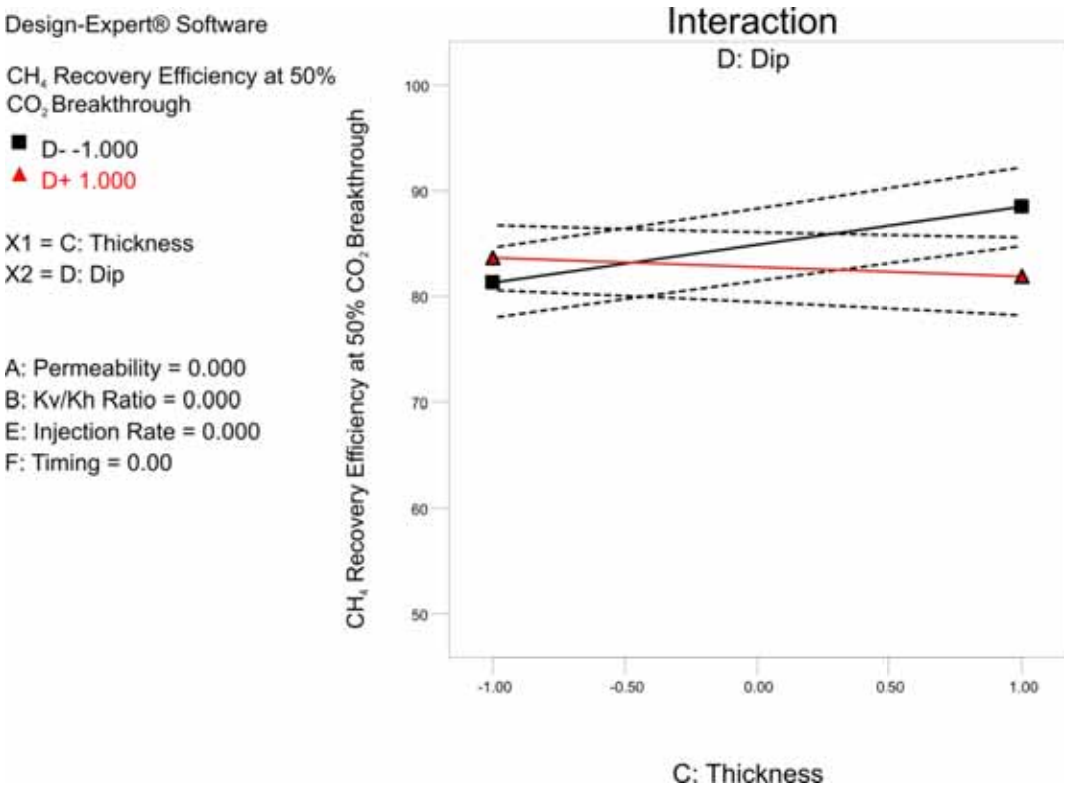


**Figure 6.18: The effect graph for the thickness formation dip interaction for Response 2.**

Permeability – thickness interaction

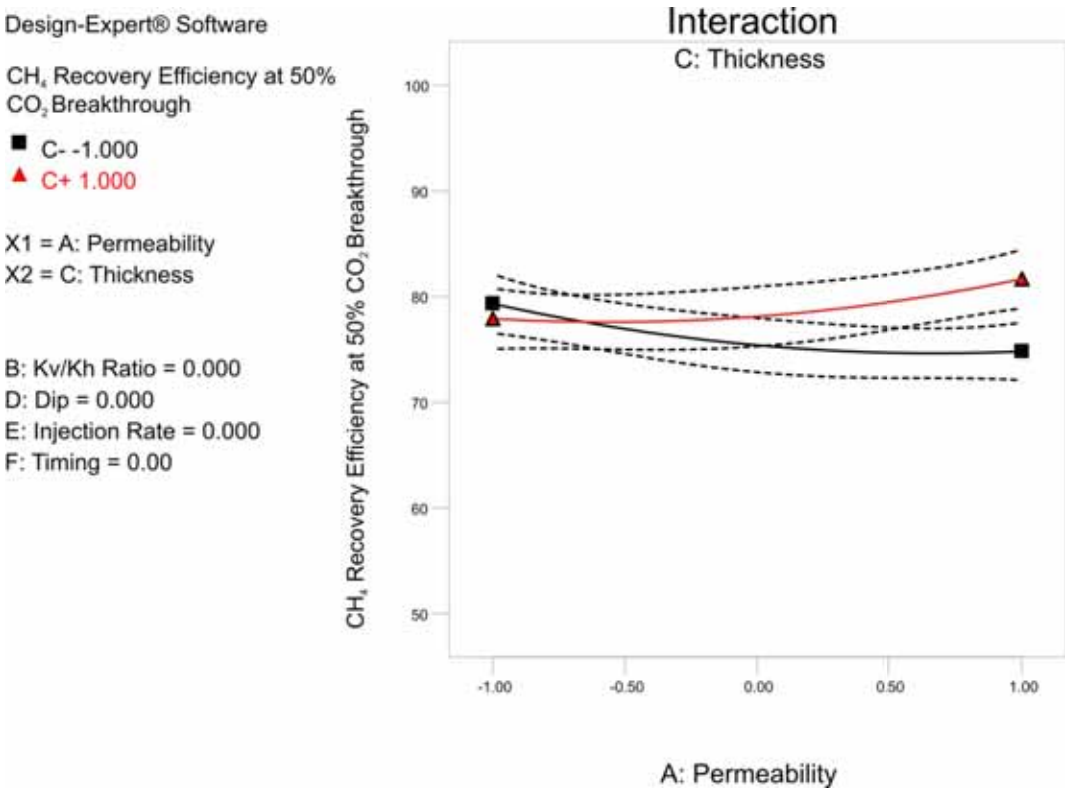


**Figure 6.19: The effect graph for the permeability thickness interaction for Response 2.**

$k_v/k_h$ ratio – injection rate interaction

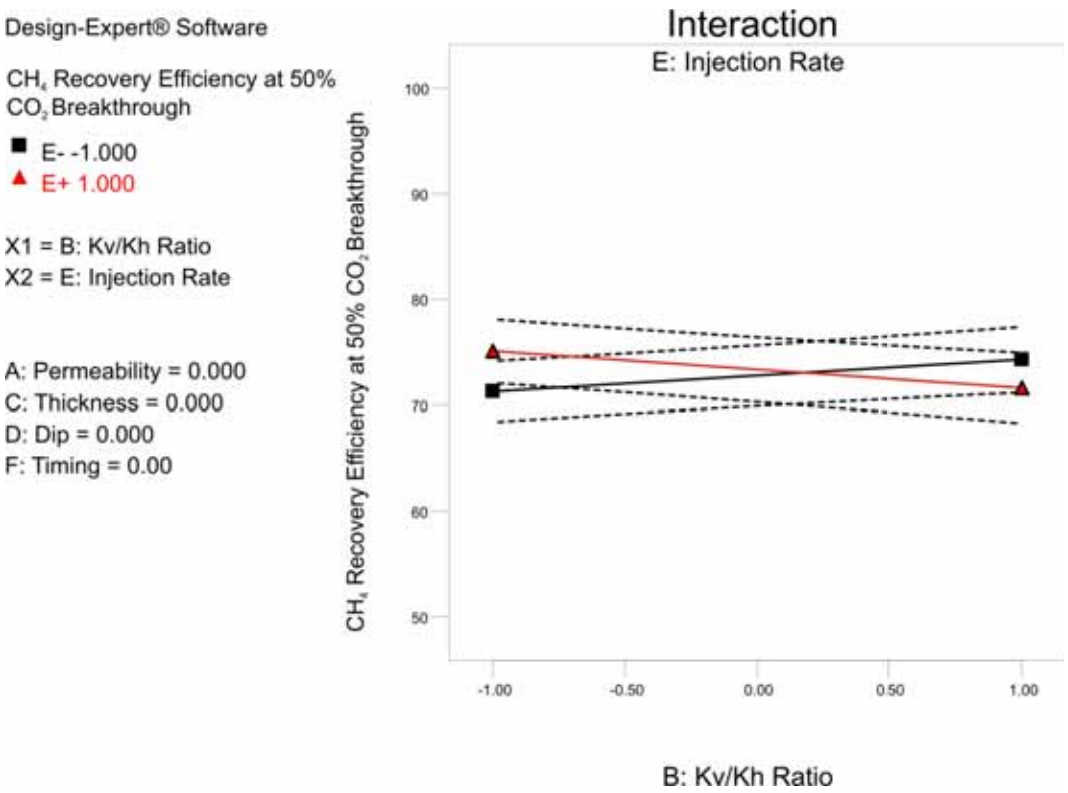


**Figure 6.20: The effect graph for the $k_v/k_h$ ratio injection rate interaction for Response 2.**

Quadratic effect of the formation dip

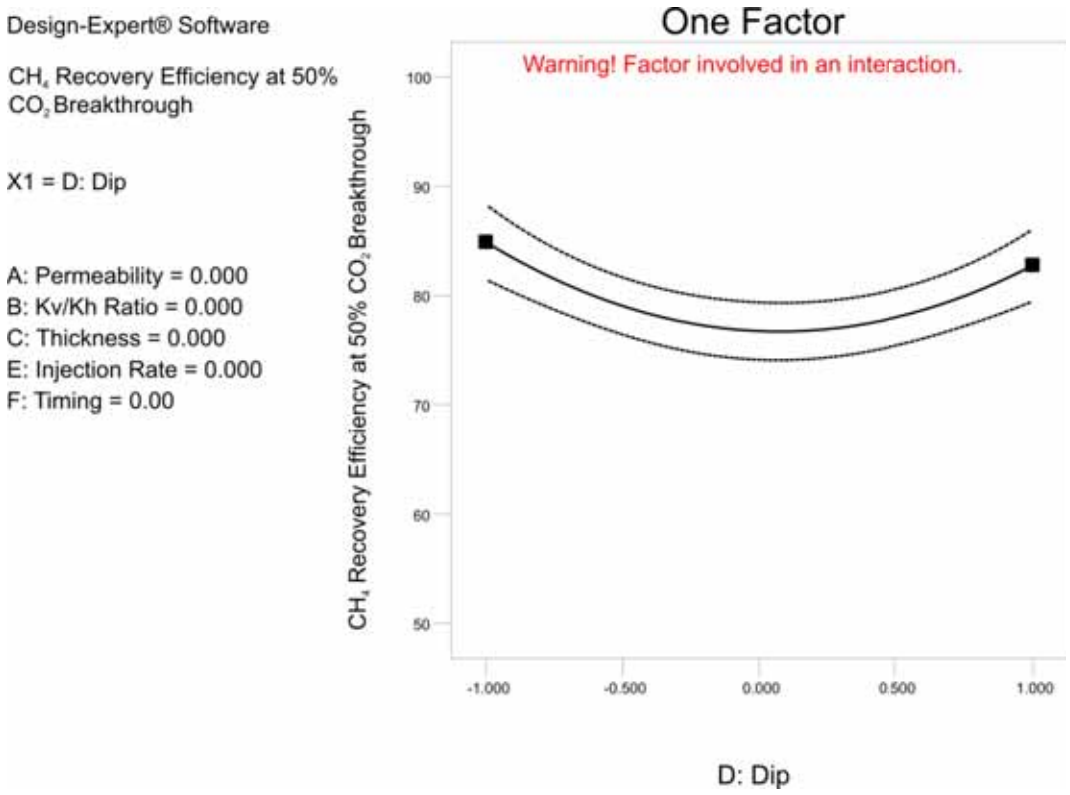


**Figure 6.21: The effect graph for the main effect of formation dip for Response 2.**

### 6.2.5 Response 3: Results and Discussion

A graph of the individual results for each run with respect to Response 3 is presented in Figure 6.22, which again shows a wide range of producing $CO_2$ concentrations required to achieve incremental recovery. The average producing $CO_2$ concentration for all runs is almost 30%.

The ranking of statistically significant coefficients is presented in Table 6-5, indicating the formation dip and permeability, both in the horizontal and vertical direction are the most influential parameters. These parameters are represented in the top six coefficients, mimicking the results of the equivalent response in Study 1.

As was the case in Study 1, through the collection of the data required for Response 3 the analysis of a fourth response, the primary recovery efficiency, can be performed. The results of the primary depletion ED is presented in Appendix C, with the results of this analysis closely matching the results of Response 3. It can therefore be concluded that the same parameters influencing the primary recovery largely determine the minimum concentration of $CO_2$ required to be tolerated in order to achieve incremental recovery.

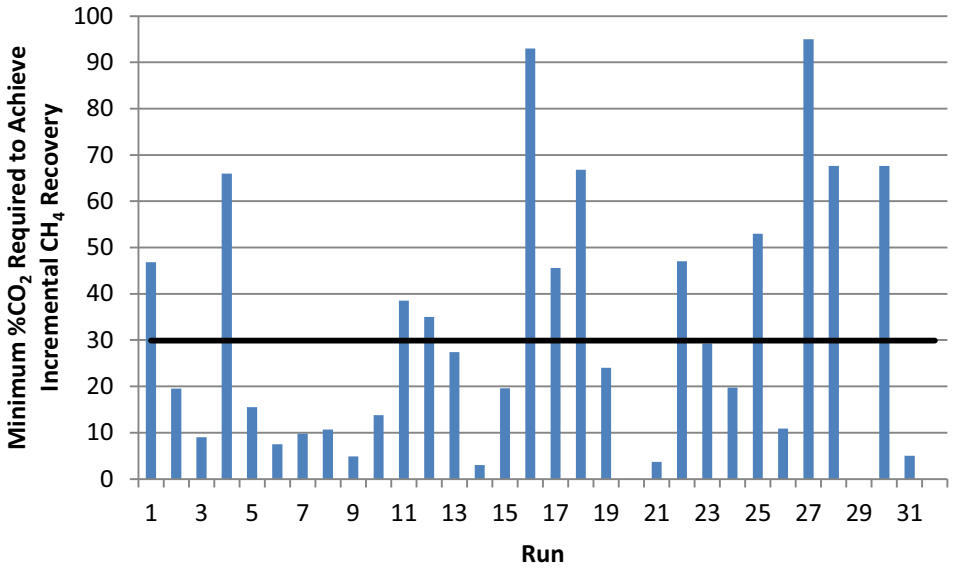


**Figure 6.22: Response 3 results for each design run. The average of all runs is shown as the black line.**

**Table 6-5: ANOVA table for Response 3**

| Statistically Significant Coefficients | F Value | p-value Prob > F |
|---|---|---|
| Dip | 400.95 | <0.0001 |
| Permeability | 248.06 | <0.0001 |
| Permeability*$k_v/k_h$ ratio | 192.89 | <0.0001 |
| $k_v/k_h$ ratio | 72.02 | <0.0001 |
| Permeability*Dip | 57.48 | <0.0001 |
| $k_v/k_h$ ratio*Dip | 49.68 | <0.0001 |
| Dip*Timing of Injection | 19.04 | 0.0006 |
| Timing of Injection | 8.12 | 0.0122 |
| Thickness*Timing of Injection | 7.60 | 0.0147 |
| $k_v/k_h$ ratio*Thickness | 6.76 | 0.0201 |
| $Dip^2$ | 4.58 | 0.0491 |

The regression diagnostics again show the model represents the data adequately, with $R^2$ and the adjusted $R^2$ coefficients of 0.9879 and 0.9749 respectively, and the normal probability plot (Figure 6.23) again showing no major deviation from the normality assumption.

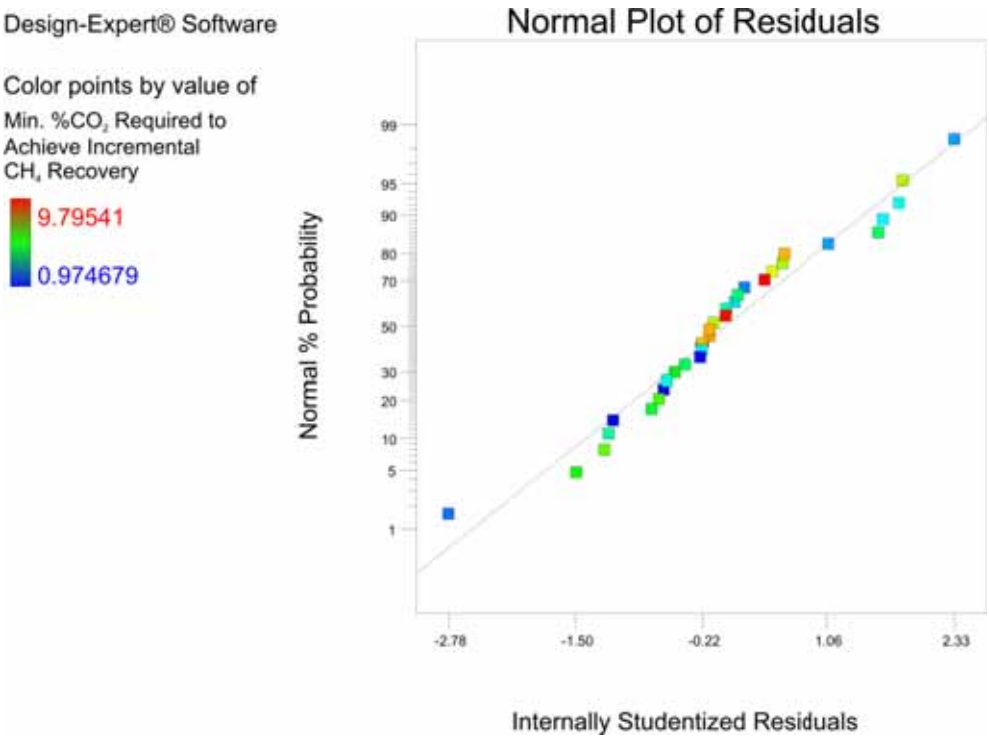


**Figure 6.23: The normal probability plot for Response 3.**

The main effect of formation dip

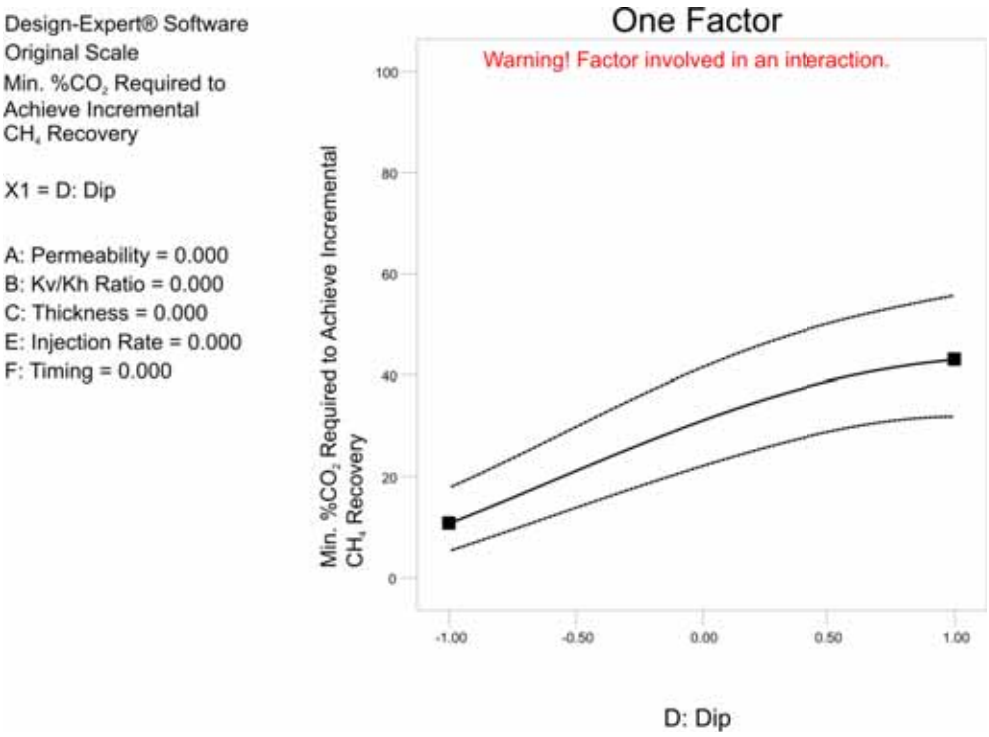


**Figure 6.24: The effect graph for the main effect of formation dip for Response 3.**

Once again, the formation dip is clearly the most statistically significant coefficient, primarily as a main effect. Similar to the result in Study 1, Figure 6.24 indicates the minimum concentration of $CO_2$ required strongly increases with increasing formation dip. This once again suggests that due to the

higher primary recovery generally achievable in a dipping formation, achieving incremental $CH_4$ recovery will require a much greater tolerance of $CO_2$ in the production stream. Consequently, injection should be targeted in non-dipping reservoirs.

The main effect of permeability

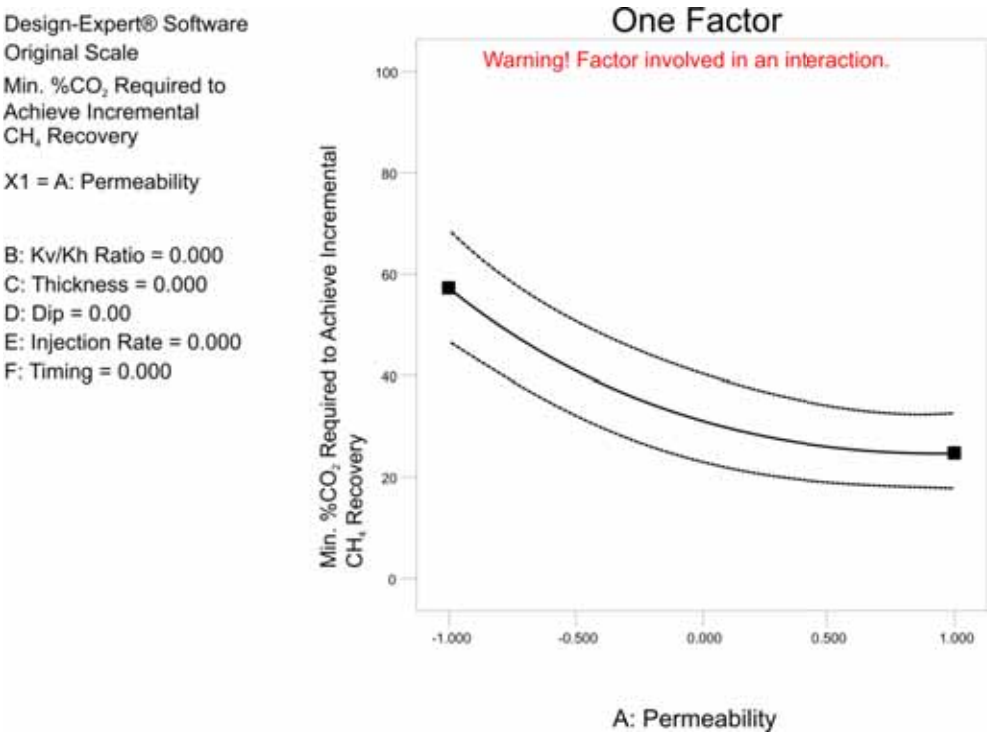


**Figure 6.25: The effect graph for the main effect of permeability for Response 3.**

Additionally, the main effect of permeability (Figure 6.25) suggests that the restriction of the aquifer under primary depletion conditions due to low permeability will enable a high primary recovery efficiency to be achieved. Consequently, if incremental recovery is to be achieved, a higher producing $CO_2$ concentration is required to be tolerated.

In addition to the main effects, the formation dip and permeability are involved in highly ranking statistically significant interactions. Therefore, the exact nature of the effect of these parameters on the response is dependent upon these interactions, as will be shown.

Permeability – $k_v/k_h$ ratio interaction

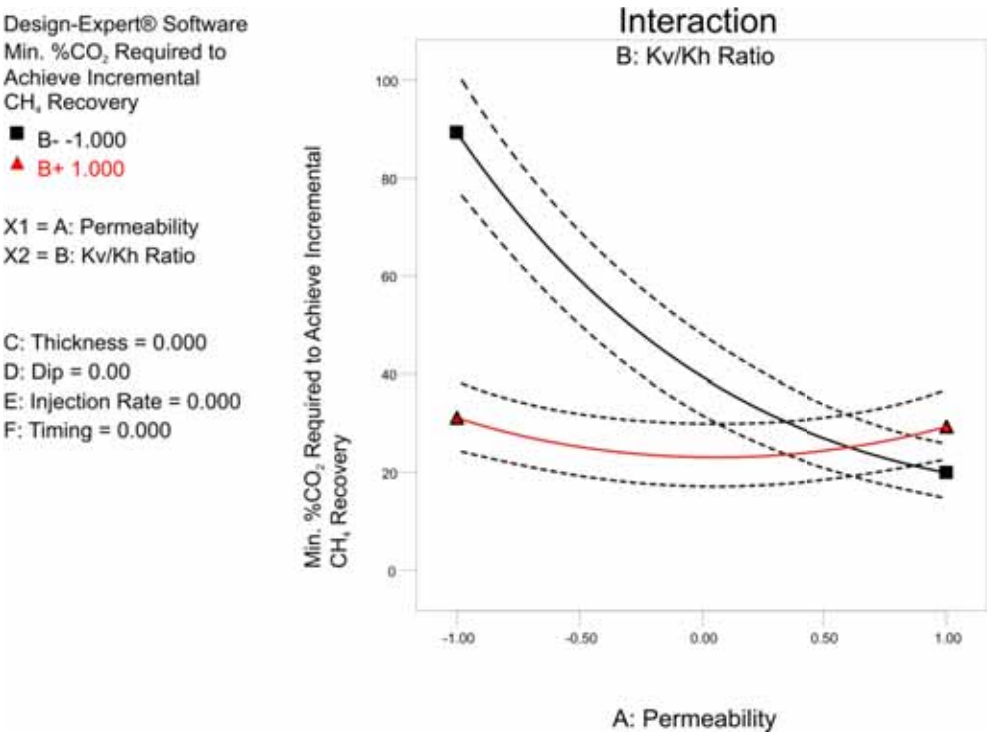


**Figure 6.26: The effect graph for the permeability $k_v/k_h$ ratio interaction for Response 3.**

The effect graph for the permeability – $k_v/k_h$ ratio interaction (Figure 6.26) exhibits a very similar trend to that observed in the equivalent response in Study 1, shown in Figure 5.31. Again the strong negative trend for the low level of $k_v/k_h$ ratio is due to strong reduction in primary recovery due to an increase in the influence of the aquifer associated with greater permeability. The minimal effect at isotropic conditions is due to the variable nature of the effect of changing permeability at isotropic conditions, as described in Response 2 of Study 1.

The main effect of the $k_v/k_h$ ratio

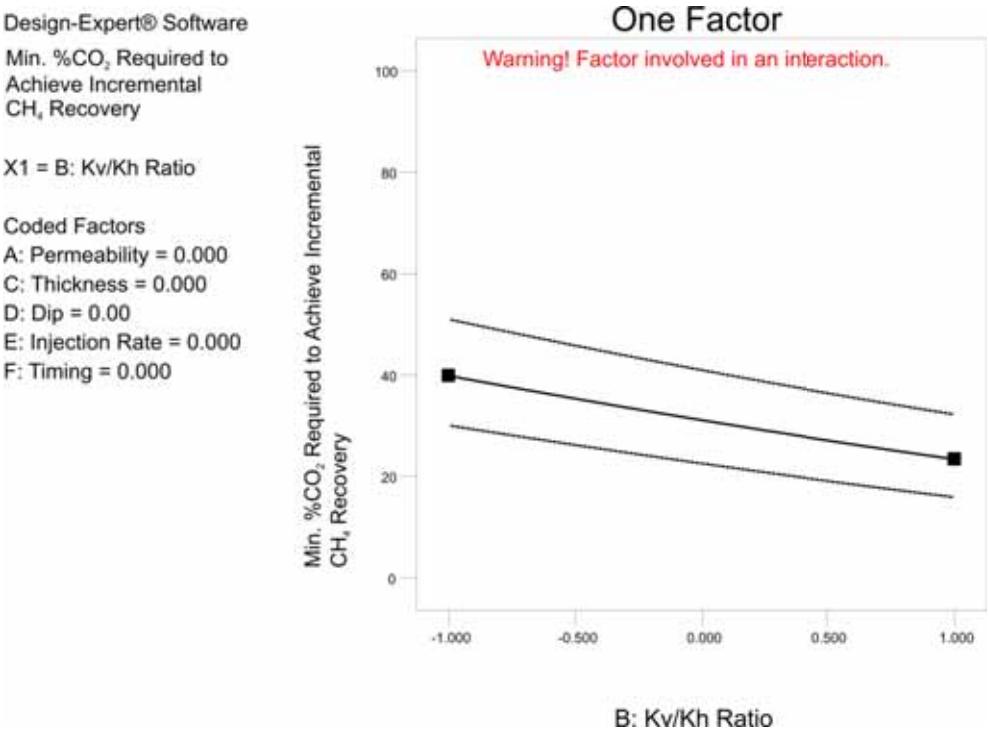


**Figure 6.27: The effect graph for the main effect of $k_v/k_h$ ratio for Response 3.**

The effect graph for the main effect of the $k_v/k_h$ ratio (Figure 6.27) suggests that restriction of the aquifer in the vertical direction under primary depletion conditions will lead to higher primary recovery (low ratio values), and so a higher minimum producing $CO_2$ concentration will be present in order to achieve incremental recovery.

Permeability – formation dip interaction

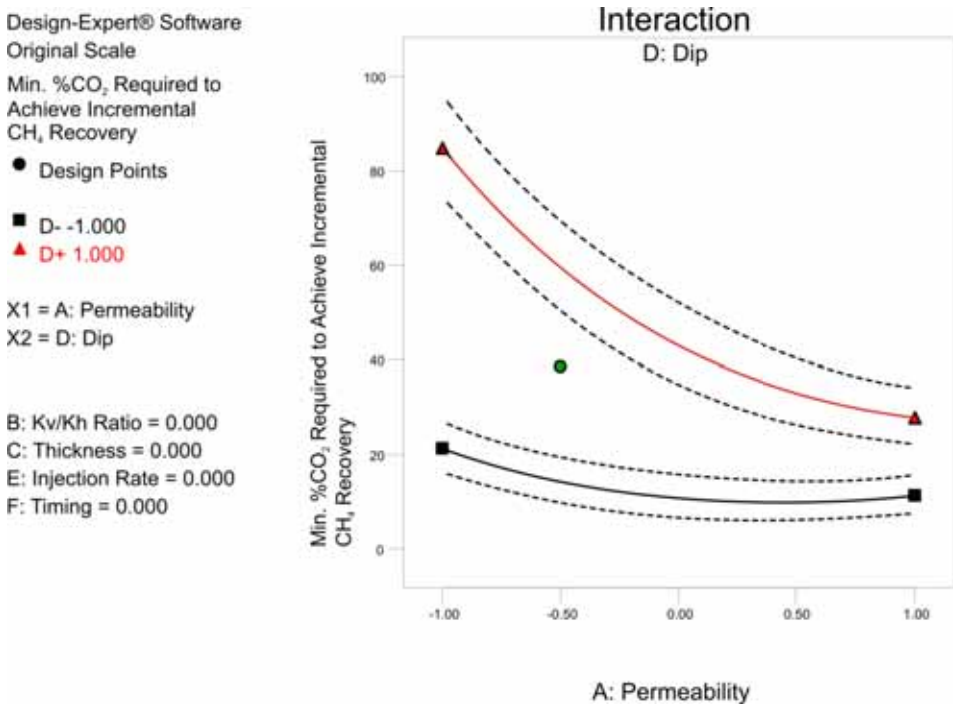


**Figure 6.28: The effect graph for the permeability formation dip interaction for Response 3.**

From the effect graph of the permeability – formation dip interaction (Figure 6.28), it can be seen that the extent of the effect of both permeability and formation dip is significantly dependent upon the other parameter. For example, in a dipping reservoir, increasing permeability has a significant beneficial effect by lowering the minimum producing $CO_2$ concentration required to achieve incremental recovery. Low permeability restricts the mobility of the aquifer allowing for significant pressure reduction to occur. Due to the greater distance between the GWC and the producing completions, the coning of water is not an issue for much of the production life, as opposed to a non-dipping reservoir. Consequently, primary recovery can be considerably high in low permeability, dipping reservoirs. This therefore correlates to a considerable producing $CO_2$ concentration that is required to be handled in order for incremental recovery to occur. An increase in permeability enhances the ability of the aquifer to respond to primary production, providing greater pressure maintenance to the system. Consequently, with a lower primary recovery efficiency, a lower tolerance of $CO_2$ is required to achieve incremental recovery.

The primary recovery efficiency in a low permeability, non-dipping reservoir is restricted by the relatively close proximity, as compared to a dipping reservoir, of the producing completions to the GWC. Although the low permeability allows for greater pressure reduction, it is conducive for the coning of, in this case, water. Consequently, primary recovery is not as great and therefore the effect of increasing permeability in a non-dipping reservoir is not as significant as for a dipping reservoir.

<u>$k_v/k_h$ ratio – formation dip interaction</u>

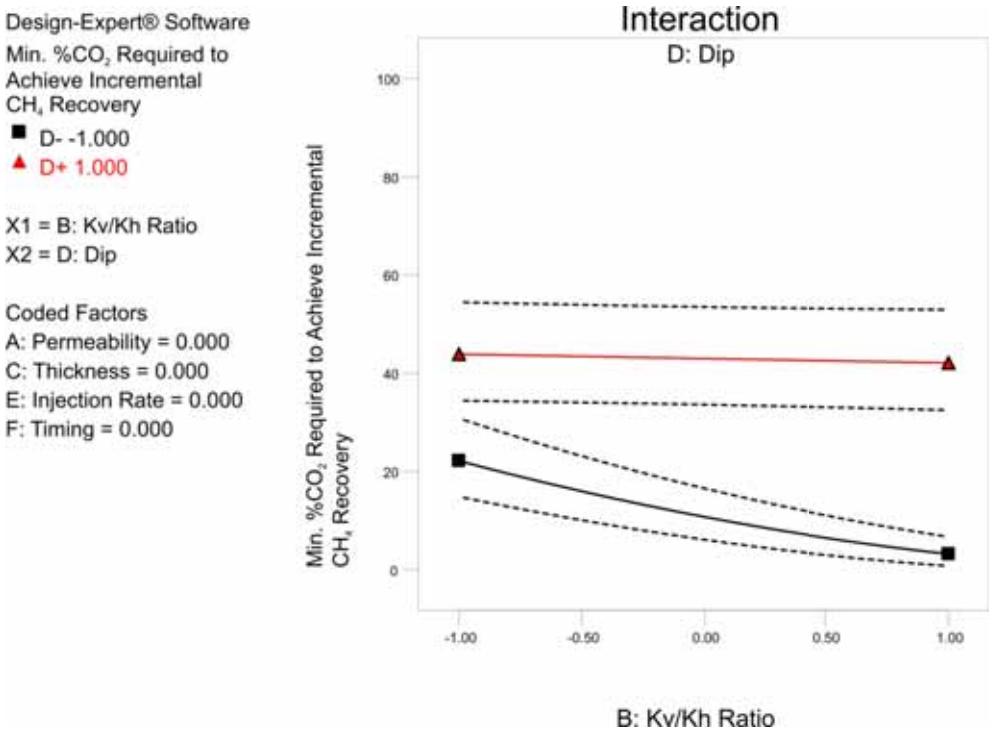


**Figure 6.29: The effect graph for the $k_v/k_h$ ratio formation dip interaction for Response 3.**

The effect of the aquifer on primary depletion is also noted in the effect graph for the $k_v/k_h$ ratio – formation dip interaction (Figure 6.29). Increasing the vertical permeability and consequently the influence of the aquifer has a detrimental effect on the primary recovery efficiency, especially in a non-dipping reservoir, which reduces the minimum concentration of $CO_2$ required to achieve incremental recovery. Again the effect of the aquifer is greater in a non-dipping reservoir, reflected in the steeper slope present in Figure 6.29.

Formation dip – timing of injection interaction

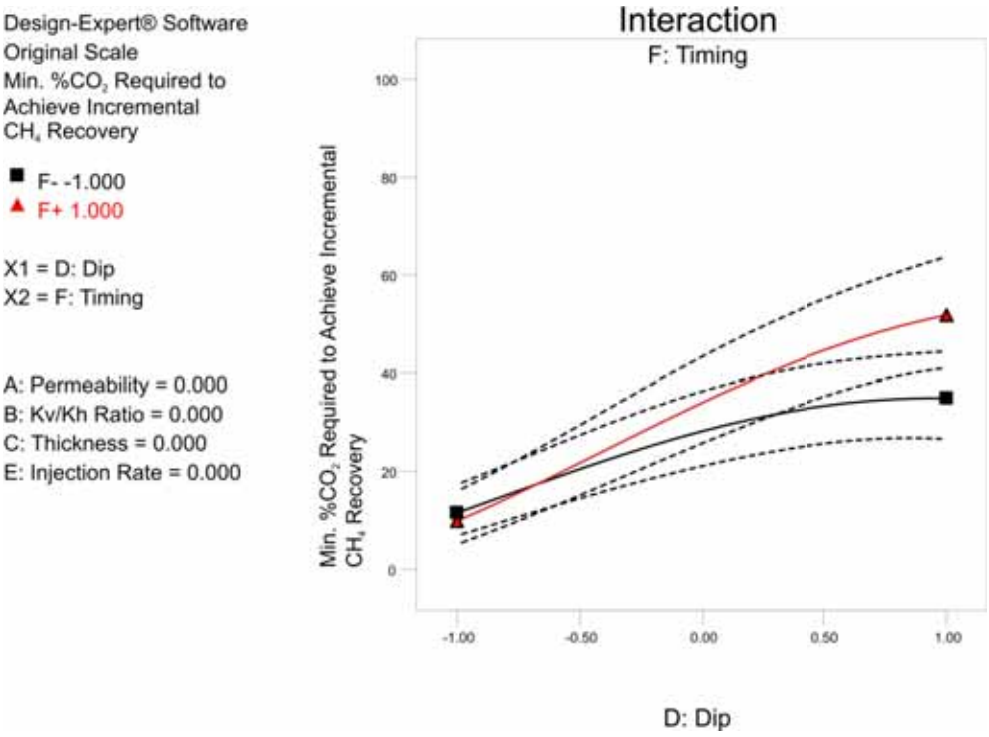


**Figure 6.30: The effect graph for the formation dip timing of injection interaction for Response 3.**

The timing of injection combines in a statistically significant way with the dip of the formation. From Figure 6.30, it can be seen that the effect of timing of injection is minimal in a non-dipping reservoir, but by delaying the injection, the timing of injection becomes increasingly more important. It can be seen in Figure 6.30 that the minimum producing $CO_2$ concentration required in a non-dipping reservoir is of the order of 10%, continually increasing as formation dip increases. Recall from Response 1 that the timing of injection did not have a considerably significant effect on $CH_4$ recovery at a $CO_2$ limit of 10%. With the producing $CO_2$ concentration in Figure 6.30 for a non-dipping reservoir around 10%, it follows that the timing of injection should have no significant effect.

Figure 6.24 showed that the minimum producing $CO_2$ concentration required to achieve incremental recovery is higher in dipping reservoirs compared to non-dipping reservoirs, due to the generally higher primary recovery achievable. With the minimum producing $CO_2$ concentration required in

dipping reservoirs greater than 10%, the rate of increase in the production rate of $CO_2$ is important, i.e. the results of Response 2. The results of Response 2 showed that the rate of increase in the production of $CO_2$ is greater when injection is delayed. Therefore, as Figure 6.30 depicts, delaying the injection of $CO_2$ will result in incremental recovery being achieved with a higher producing $CO_2$ concentration.

### 6.2.6 Summary

The key results of the investigation into the effect of the timing of $CO_2$ injection into a homogeneous reservoir can be summarised as follows:

Response 1:

- The timing of injection did not have a significant direct effect on the $CH_4$ recovery efficiency at the 10% $CO_2$ limit, as indicated by the low ranking of the quadratic effect of the timing of injection parameter.
- The timing of injection did however influence the impact of the other parameters on the recovery efficiency of $CH_4$. The thickness – timing of injection interaction showed that the beneficial nature of an increasing reservoir thickness is continually reduced the longer injection is delayed. While a gravity stable displacement is beneficial for an efficient sweep of the free gas zone, gravity segregation leads to poor sweep of the invaded zone.
- The thickness – timing of injection interaction also showed that, due to the stronger viscous forces and hence the ability to sweep the invaded zone and not over-ride it, delaying the injection of $CO_2$ in thin reservoirs will improve $CH_4$ recovery than if injection is not delayed. Increasing the influence of gravity, in this case by increasing reservoir thickness, reduces the ability to sweep the invaded zone and so it is more beneficial in these instances to not delay the injection of $CO_2$
- Consequently, more generally, if viscous forces are such that a significant proportion of the invaded zone can be swept, it can be beneficial in terms of $CH_4$ recovery efficiency at the 10% $CO_2$ limit to delay the injection of $CO_2$. If gravity is the dominant force, then the injection of $CO_2$ should not be delayed.

Response 2:

- The results of the analysis of Response 2 were almost identical to that of Response 1 except for the clear dominance of the influence of the timing of $CO_2$ injection on the recovery efficiency at the 50% $CO_2$ limit.
- Delaying the injection of $CO_2$ resulted in a considerably more rapid increase in the production rate of $CO_2$ once it had reached the production well.

- The maximum allowable producing $CO_2$ concentration will therefore determine the injection timing strategy. If a high tolerance of $CO_2$ can be handled, such as 50% of the production stream, then there is a clear benefit in not delaying the injection of $CO_2$. If only a minor concentration of $CO_2$ can be handled, then the results of Response 1 would apply, with the timing of injection being dependent upon other reservoir properties.

Response 3:

- The results of Response 3 closely resemble those of the equivalent response from Study 1.
- In order to achieve incremental recovery with the lowest minimum producing $CO_2$ concentration, the injection of $CO_2$ should be targeted in reservoirs which achieve low primary recovery efficiencies, for example high permeability, non-dipping reservoirs.

## 6.3 Study 2B: The Comparison of the Timing of $CO_2$ Injection into a Simple, Heterogeneous Reservoir

The two ED studies presented in this thesis thus far have focussed on investigating the effects of $CO_2$ injection in homogeneous reservoirs. The additional simulations presented in Chapter 5 showed that the introduction of heterogeneity can severely affect the displacement profile, particularly in a non-dipping reservoir. The uneven advancement of the $CO_2$ front led to earlier $CO_2$ breakthrough and accordingly a reduction in the $CH_4$ recovery at the breakthrough of $CO_2$. For the specific case of a non-dipping reservoir, it was shown that an alteration of the prevailing direction of displacement from horizontal to vertical greatly improved the sweep of the reservoir at the $CO_2$ breakthrough limit. This was achieved through the use of horizontal wells, or by reducing production and injection rates when vertical wells are employed. One other method to mitigate against the uneven advancement of $CO_2$ due to heterogeneity could be to delay the injection of $CO_2$. This would allow for a period of $CH_4$ production without the introduction and rapid migration of $CO_2$ towards the production well. The increased saturation of water in the higher permeability zones could also limit the mobility of $CO_2$ along these conduits, potentially delaying the breakthrough of $CO_2$. This study therefore investigates the effect that the timing of injection potentially has on improving the efficiency of the displacement process of $CH_4$ by $CO_2$ in the presence of heterogeneity.

### 6.3.1 Reservoir Model

Heterogeneity is introduced in the model through a single higher permeability layer placed in the middle of the reservoir thickness, similar to the follow-up simulations in Study 1.Aside from the introduction of the higher permeability layer, the reservoir model is equivalent to the models used in the previous studies.

### 6.3.2 Design, Parameter and Range Selection

To be consistent with the other studies performed, a D-optimal design was chosen with five parameters (Table 6-6), resulting in a design with 29 runs (Table 6-7).

**Table 6-6: Design parameters and the corresponding low, mid and high values.**

| Parameter | Low (-1) Level | Mid (0) Level | High (+1) Level |
|---|---|---|---|
| Permeability Multiplier | 0.2 | 0 | 5 |
| Thickness | 50 | 100 | 150 |
| Formation Dip | 0 | 11 | 21 |
| Injection Rate | 100% | 125% | 150% |
| Timing of Injection | 0% | 20% | 40% |

**Table 6-7: D-Optimal design for Study 2B**

| Run | Permeability Multiplier | Thickness | Formation Dip | Injection Rate | Timing of Injection |
|---|---|---|---|---|---|
| 1 | -1 | -1 | -1 | -1 | -1 |
| 2 | 1 | -1 | 1 | -1 | -1 |
| 3 | 1 | 1 | -1 | 1 | -1 |
| 4 | -1 | -1 | 1 | -1 | -1 |
| 5 | 1 | -1 | 1 | 1 | -1 |
| 6 | 1 | -1 | 0 | 1 | 1 |
| 7 | -1 | 1 | -1 | 1 | 1 |
| 8 | 0 | 0 | 0 | 0 | -1 |
| 9 | -1 | -1 | 1 | 1 | 1 |
| 10 | 1 | 1 | 1 | -1 | -1 |
| 11 | 0 | 0 | 0 | -1 | 0 |
| 12 | 1 | 1 | -1 | -1 | 1 |
| 13 | -1 | 1 | 1 | -1 | -1 |
| 14 | 1 | -1 | 0 | 1 | 1 |
| 15 | -1 | 1 | 1 | 1 | -1 |
| 16 | 1 | -1 | -1 | 0 | 1 |
| 17 | 1 | -1 | -1 | -1 | -1 |
| 18 | 0 | 1 | 0 | 0 | 0 |
| 19 | 0 | 1 | 0 | 0 | 0 |
| 20 | -1 | -1 | -1 | 1 | -1 |
| 21 | -1 | 1 | 1 | -1 | 1 |
| 22 | -1 | 1 | -1 | -1 | -1 |
| 23 | 0 | 0 | 0 | -1 | 0 |
| 24 | 1 | -1 | -1 | 1 | -1 |
| 25 | 1 | 1 | 1 | 1 | 1 |
| 26 | 1 | -1 | 1 | -1 | 1 |
| 27 | 1 | 1 | -1 | -1 | -1 |
| 28 | 0 | -1 | -1 | 1 | 1 |
| 29 | -1 | -1 | -1 | -1 | 1 |

It was decided to replace the permeability and $k_v/k_h$ ratio parameters for Study 2B with one parameter, a permeability multiplier. The additional simulations from Study 1 showed that the effect of heterogeneity was particularly detrimental when displacement was dominated by viscous forces. The efficiency of the displacement was improved with the increase in gravity forces. Therefore, rather than testing the effect of specific permeabilities, it was deemed important to test the effect of

the higher permeability layer when displacement was either dominated by viscous or gravity forces. Additionally, varying the permeability of the higher permeability layer separately to the bulk permeability would have added at least another parameter to the design, as well as making analysis more complicated. The higher permeability layer was arbitrarily chosen to be five times larger than the bulk permeability. At the mid level, bulk permeability was maintained at 100mD, making the permeability in the layer equal to 500mD. The $k_v/k_h$ ratio is maintained at 0.10 for all simulations.

The remaining parameters were chosen based on their influence on the magnitude of viscous and gravity forces in the displacement process, with these forces having been shown to be considerably influential in the additional simulations of Study 1 involving heterogeneity. Aside from permeability, the parameters in this study and the ranges chosen are equivalent to those chosen in Study 2A.

### 6.3.3 Study 2B Responses (Metrics)

The responses used in Study 2B are identical to those used in Study 2A, these being:

- $CH_4$ recovery efficiency at a $CO_2$ production limit of 10%
- $CH_4$ recovery efficiency at a $CO_2$ production limit of 50%
- Minimum producing $CO_2$ concentration required to achieve incremental $CH_4$ recovery

### 6.3.4 Response 1 Results and Discussion

The results of each run with respect to Response 1 are presented in Figure 6.31, showing a wide range in recovery efficiencies achievable. The majority of runs however achieve a recovery efficiency in the range of 60 – 70% OGIP. The list of highest ranking statistically significant coefficients is presented in Table 6-8. This list indicates that all parameters are significant to some degree, either as a main effect or when involved in interactions.

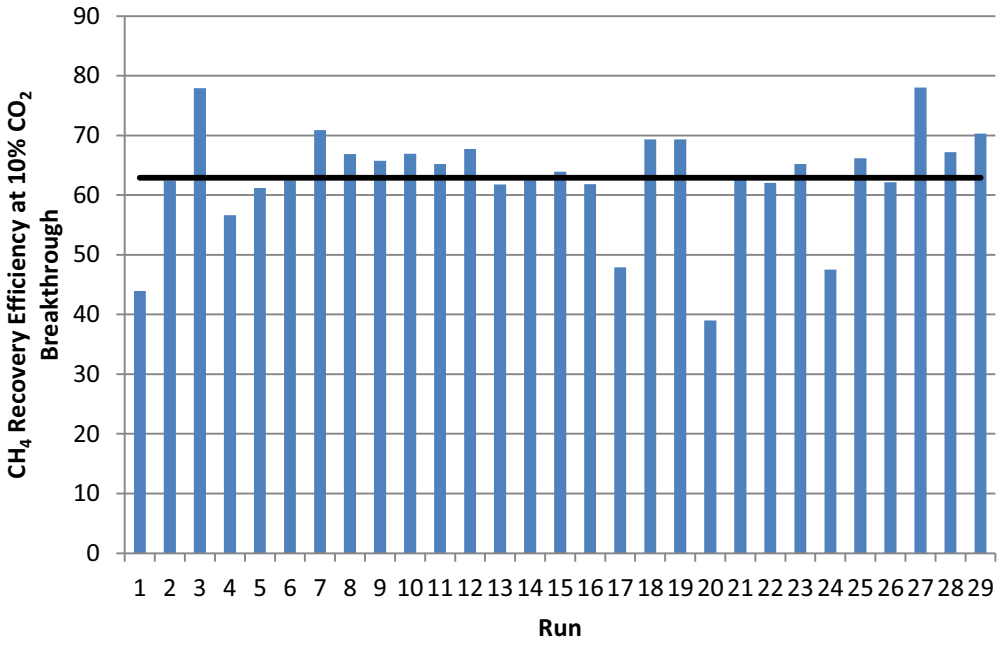


**Figure 6.31: Response 1 results for each design run. The average of all runs is indicated by the black line.**

**Table 6-8: ANOVA table for Response 1**

| Statistically Significant Coefficients | F Value | p-value Prob > F |
|---|---|---|
| Thickness | 64.44 | <0.0001 |
| Thickness*Timing of Injection | 42.97 | <0.0001 |
| Permeability Multiplier*Timing of Injection | 24.62 | 0.0001 |
| Thickness*Dip | 24.34 | 0.0001 |
| Timing of Injection | 21.70 | 0.0003 |
| Dip*Timing of Injection | 13.72 | 0.0019 |
| Permeability Multiplier | 6.29 | 0.0233 |
| Thickness*Injection Rate | 5.61 | 0.0308 |
| Permeability Multiplier*Thickness | 5.09 | 0.0385 |
| Permeability Multiplier*Injection Rate | 4.82 | 0.0432 |

The regression diagnostics are not as high as in previous designs, with the $R^2$ and adjusted $R^2$ coefficients being 0.9363 and 0.8885 respectively. However, this design is primarily used for screening purposes, to test the effect of the input parameters on the chosen response, and not for optimisation or predictive purposes. Consequently, these statistics are acceptable for the purpose of this design. The normal probability plot, presented in Figure 6.32, again shows no major deviation from the normality assumption.

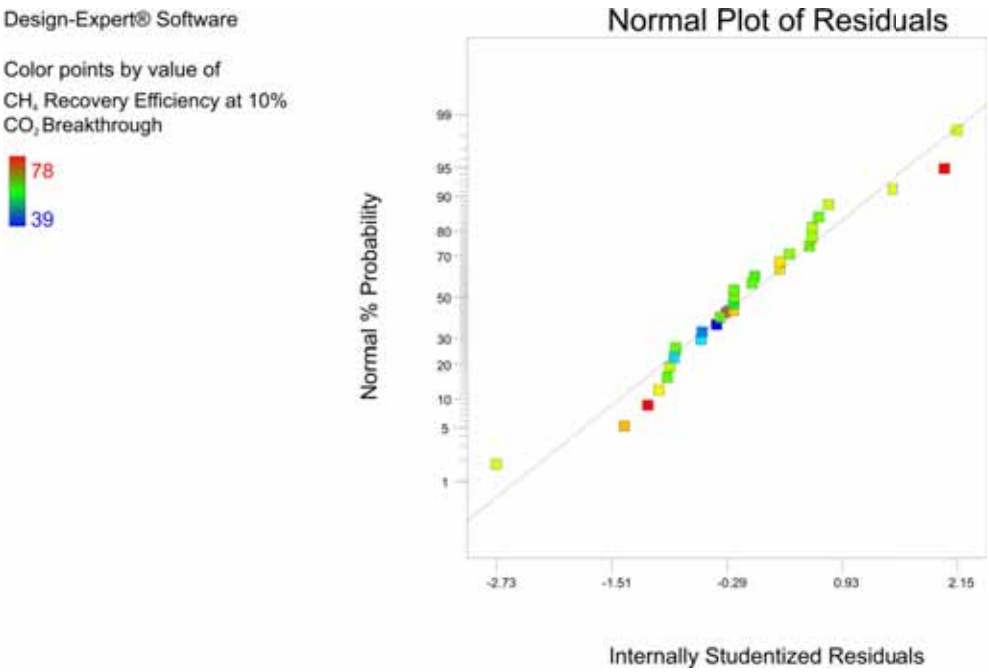


**Figure 6.32: The normal probability plot for Response 1.**

The main effect of thickness

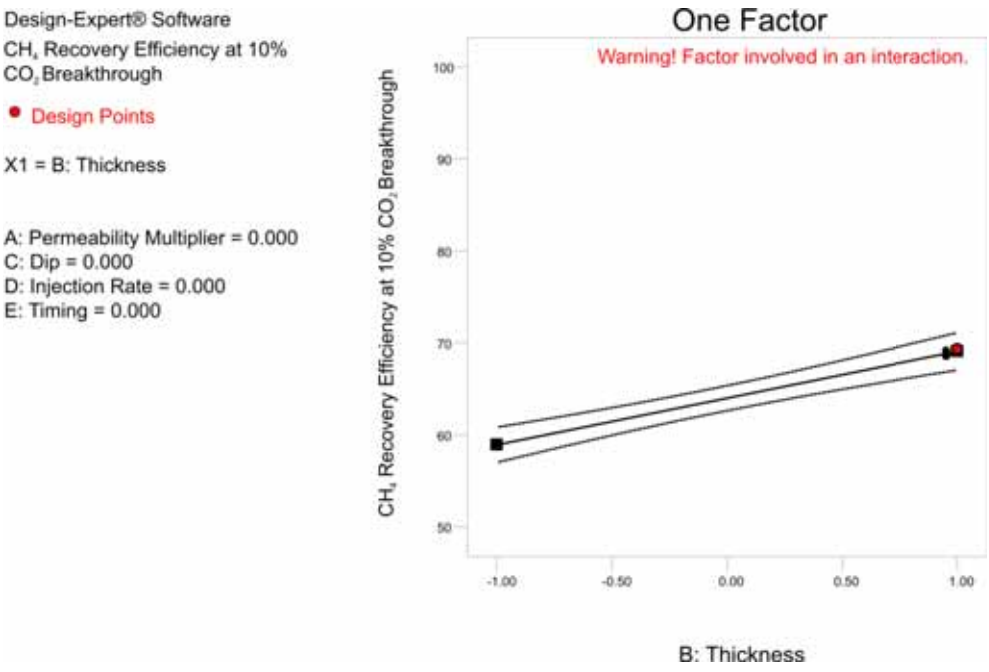


**Figure 6.33: The effect graph for the main effect of thickness for Response 1.**

The highest ranking coefficient in the ANOVA table is the main effect of formation thickness, again displaying a positive trend on the recovery of $CH_4$ at the 10% $CO_2$ limit (Figure 6.33). This result highlights the importance of, in this particular situation, the effects of gravity to assist in mitigating against the unwanted effects of the heterogeneity, that is the uneven advancement of the

displacement front leading to a poor sweep of the reservoir. As this parameter is involved in statistically significant interactions, the effect of thickness will be discussed in association with the influence of these other parameters.

Thickness – timing of injection interaction

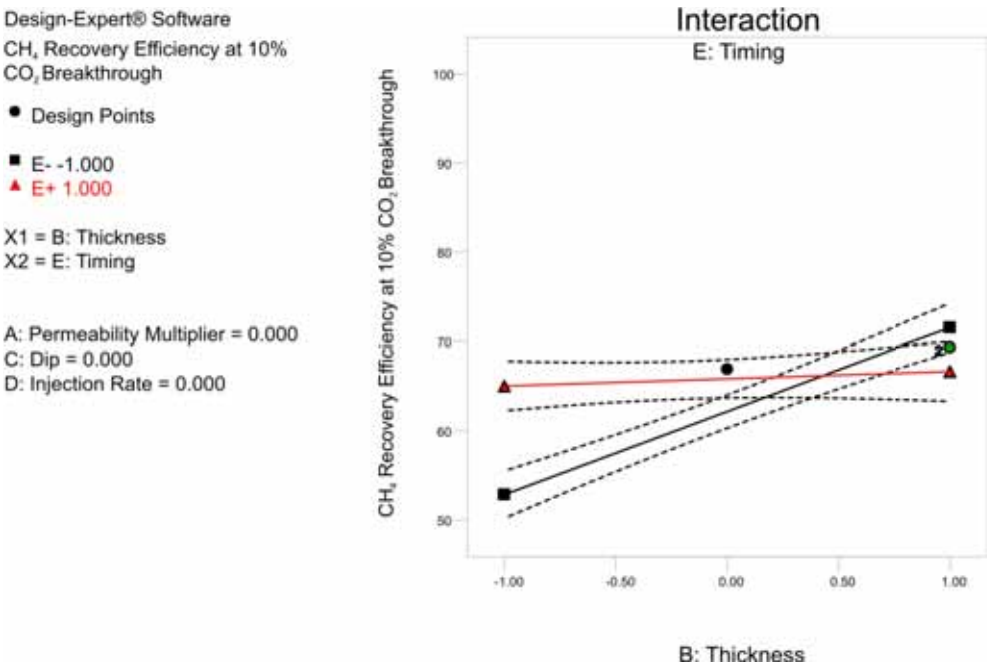


**Figure 6.34: The effect graph for the thickness timing of injection interaction for Response 1.**

The effect graph for this interaction (Figure 6.34) indicates that the positive effect of formation thickness is greatest when injection is not delayed. Viscous dominated flow in heterogeneous reservoirs, especially in non-dipping reservoirs, has been shown to be particularly detrimental to the displacement process due to the uneven advancement of the displacement front as discussed in Chapter 5. As previously noted, stronger viscous forces are associated with thinner reservoirs. Increasing thickness increases the influence of gravity. Gravity segregation between $CH_4$ and $CO_2$ will lead to $CO_2$ under-riding the $CH_4$ column which, as Figure 6.35 highlights, can, in the particular case studied in this chapter, lead to the delayed contact with or the bypassing of the higher permeability layer. In a dipping reservoir, stronger gravity forces will suppress the uneven advancement, stabilising the displacement front as it moves vertically through the reservoir as indicated in Figure 6.36.

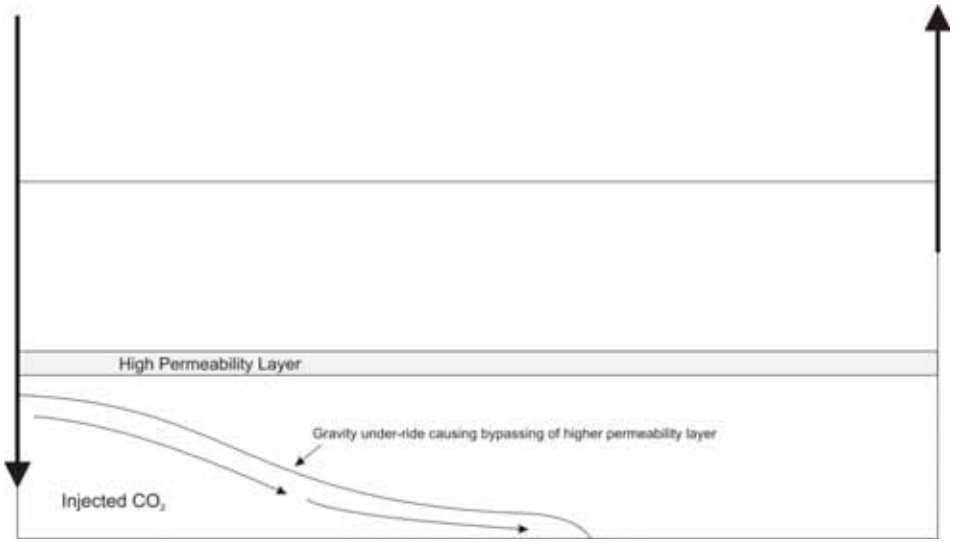


**Figure 6.35: Schematic of the influence of gravity forces on mitigating against the negative effects of the higher permeability layer in a non-dipping reservoir.**

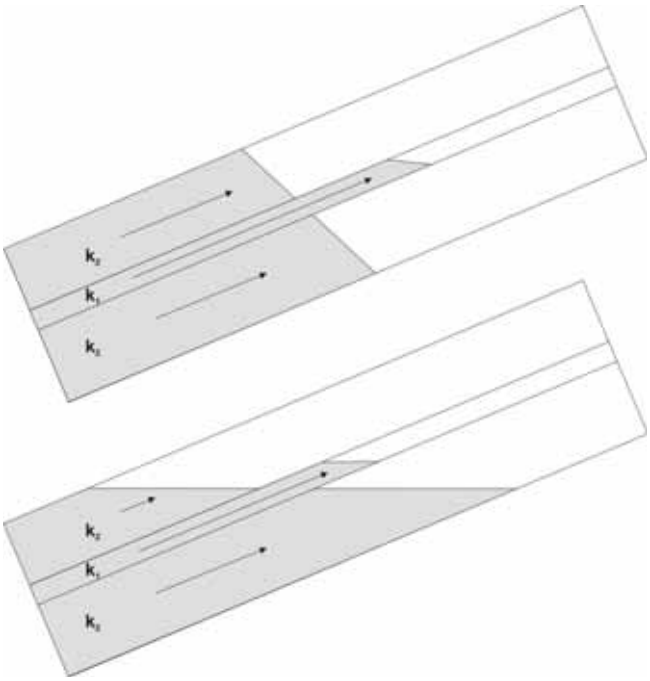

**Figure 6.36: Schematic of the effect of viscous and gravity forces on the displacement in a dipping reservoir. Stronger viscous forces (top) lead to more severe uneven advancement of the displacement front. Increased gravity forces (bottom) act to suppress the uneven advancement.**

Dominant viscous forces can be used to advantage however, in reducing the gravity segregation associated with delayed injection. The mobility of $CO_2$ along the higher permeability layer is restricted due to the increased water saturation present (if the aquifer reaches the higher permeability layer by the time $CO_2$ injection commences). This will mitigate against the uneven advancement of $CO_2$. Additionally, viscous forces enable the injected $CO_2$ to penetrate and sweep the invaded zone, and not simply over-ride it. This enables a portion of the trapped gas to be swept

and displaced towards the production well. These effects are indicated in Figure 6.34 with the significant benefit in delaying the injection of $CO_2$ in thin reservoirs (difference in the levels of the timing of injection for a thin reservoir). As thickness increases, delaying the injection of $CO_2$ loses its appeal. Under delayed injection conditions, increasing thickness and hence the influence of gravity is detrimental to the ability to sweep the invaded zone. In certain circumstances, as indicated in Figure 6.37, gravity segregation can also lead to channelling of $CO_2$ directly towards the high permeability layer. This can therefore result in rapid migration towards the production well, leading to early $CO_2$ breakthrough and poor sweep of the reservoir. It follows that for thick reservoirs, no delay in the injection of $CO_2$ should occur in an effort to maximise $CH_4$ recovery.

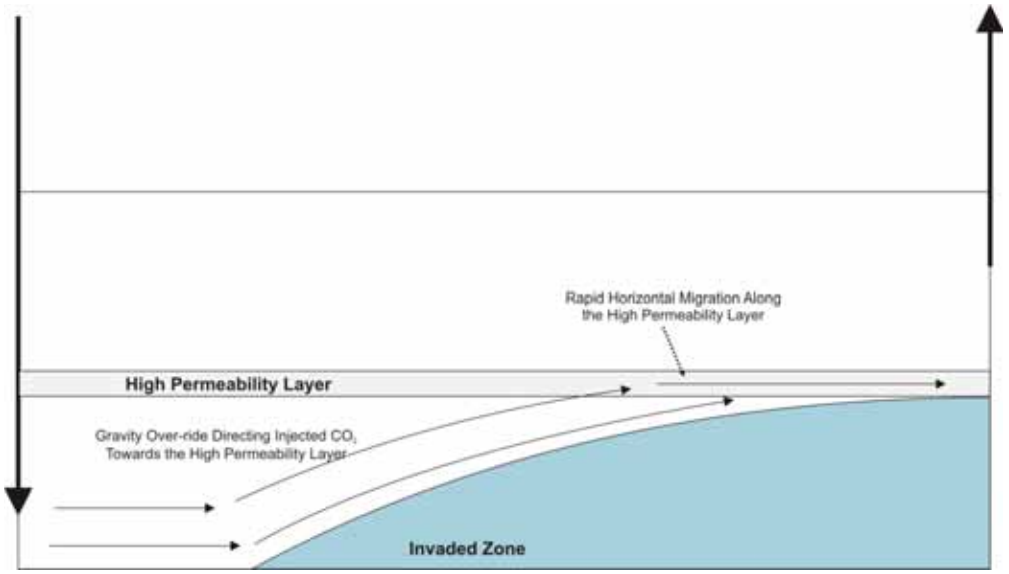


**Figure 6.37: The effect of gravity over-ride in a non-dipping reservoir with heterogeneity. Over-riding of the invaded zone directs the $CO_2$ towards the higher permeability layer.**

Permeability multiplier – timing of injection interaction

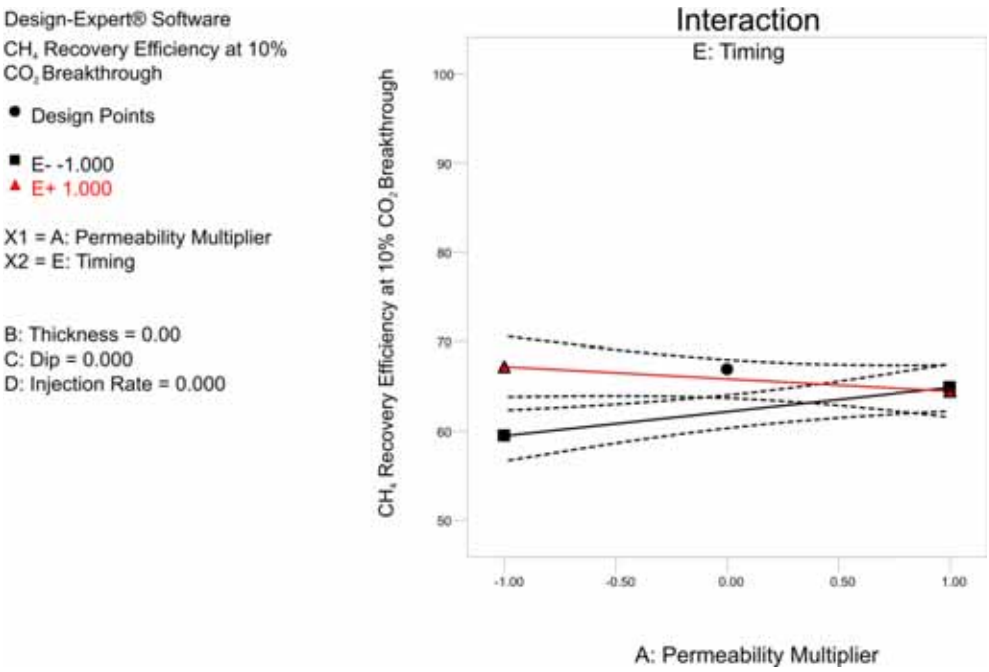


**Figure 6.38: The effect graph for the permeability multiplier timing of injection interaction for Response 1.**

Similar processes to those described in the thickness – timing of injection interaction are also evident in the effect graph for the permeability multiplier – timing of injection interaction (Figure 6.38).If injection is not delayed, increasing permeability, and therefore the influence of gravity, will improve the sweep of the reservoir by mitigating against the effect of the heterogeneity present. If injection is delayed, the minimisation of gravity segregation is key to improving the recovery efficiency achievable. Combining these two effects, Figure 6.38 clearly shows that in low permeability situations delaying the injection of $CO_2$ is the preferred option. Increase permeability, and the beneficial effect of delaying the injection of $CO_2$ is continually reduced.

Thickness – formation dip interaction

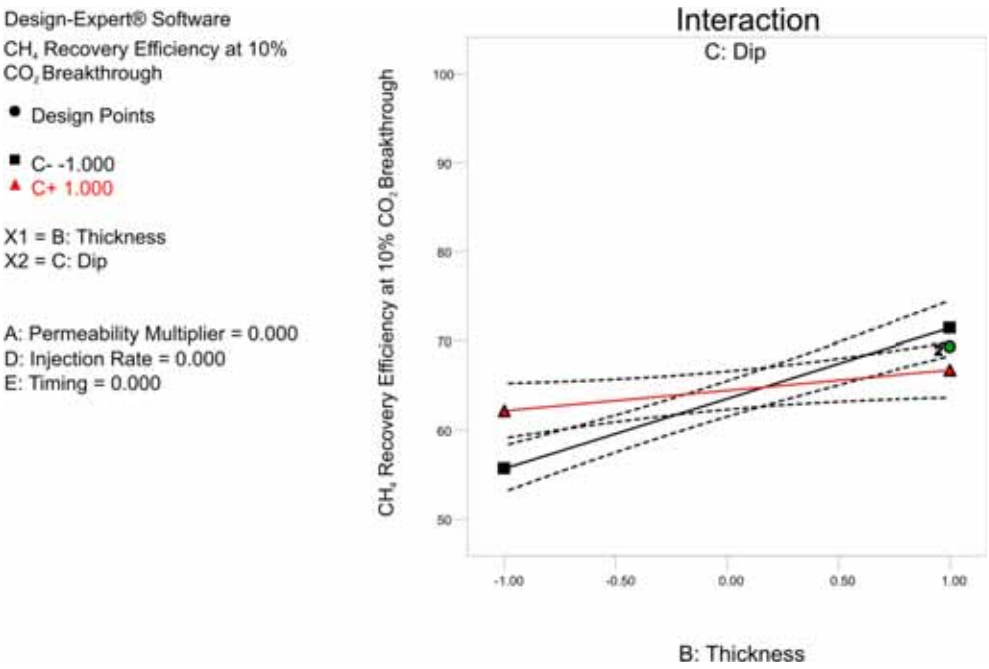


**Figure 6.39: The effect graph of the thickness formation dip interaction for Response 1.**

The importance of thickness on the $CH_4$ recovery efficiency at the 10% $CO_2$ limit has been demonstrated in the previous coefficients discussed. From the effect graph for thickness – formation dip interaction (Figure 6.39) it can be observed that the effect of thickness is greater in a non-dipping reservoir. This is due to the significant alteration of the displacement front achievable by increasing thickness, as shown in Figure 6.40. Under a displacement process dominated by viscous forces, such as in thin reservoirs, maximum contact with the heterogeneity will ensue, leading to the poor sweep of the reservoir observed in Section 5.9.1. With increasing thickness comes a greater influence of gravity on the displacement process, with the reservoir now filling the reservoir from the bottom up. Instead of the displacement occurring horizontally, the direction is altered to predominantly a vertical displacement which ensures the heterogeneity has minimal effect on the sweep of the reservoir.

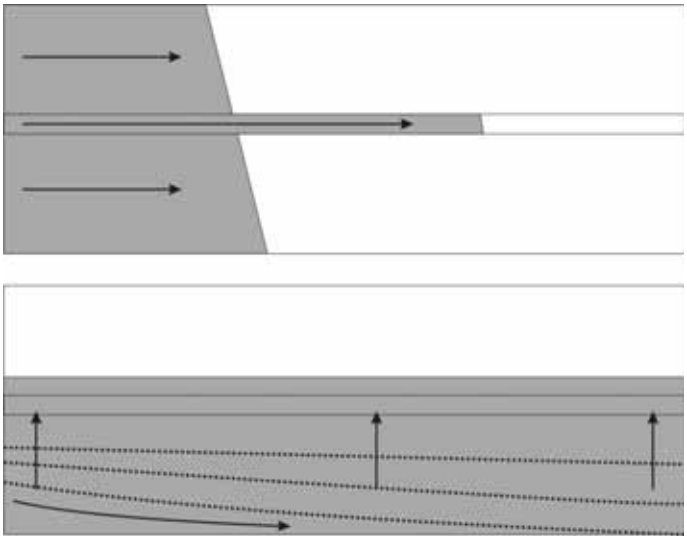

**Figure 6.40: Schematic of the effect of thickness in a non-dipping reservoir. Displacements controlled by viscous forces (top) lead to maximum contact with the heterogeneity, leading to the severe uneven advancement of the displacement front. Increasing thickness and allowing for gravity to influence the displacement (bottom) ensures the reservoir fills from the bottom up (indicated by the dashed lines), negating the effect of the heterogeneity.**

In a dipping reservoir, stronger viscous forces will lead to the uneven advancement of the displacement front, as shown previously in Figure 6.36, however the greater influence of gravity in all cases results in thickness having a reduced impact on the $CH_4$ recovery efficiency when compared to a non-dipping reservoir.

Main effect of the timing of injection

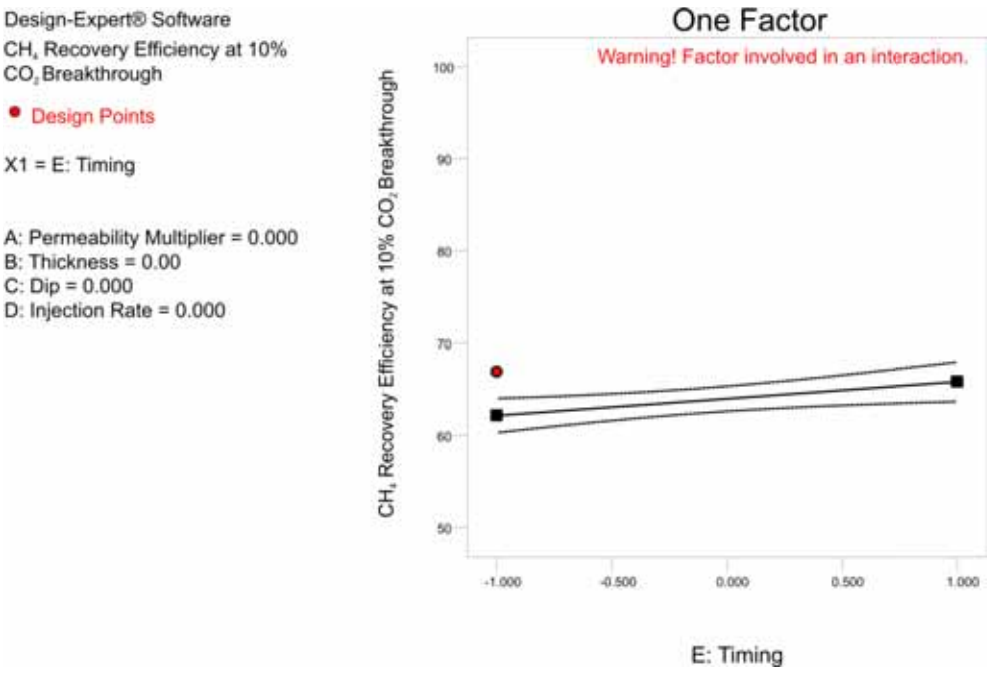


**Figure 6.41: The effect graph for the main effect of timing of injection for Response 1.**

From Figure 6.41, it can be seen that delaying the injection of $CO_2$ improves the recovery of $CH_4$ at the 10% $CO_2$ limit. The presence of heterogeneity promotes the uneven advancement of the displacement front, and so the early injection of $CO_2$ and subsequent early contact with the heterogeneity leads to a poor sweep of the reservoir and premature breakthrough of $CO_2$ at the production well. This is particularly the case with viscous dominated displacement. To avoid the premature breakthrough of $CO_2$, the injection of $CO_2$ should be delayed. delaying the injection allows for a period of primary production without the contamination of $CO_2$, and the increase in water saturation if the aquifer has reached the heterogeneity during the period of primary production will restrict the mobility of $CO_2$, restricting the uneven advancement.

### 6.3.5 Response 2 Results and Discussion

The results for each run regarding the $CH_4$ recovery efficiency at a $CO_2$ breakthrough limit of 50% are presented in Figure 6.42. Similar to Study 2A, as the $CO_2$ limit is increased, the range of recovery efficiencies narrows, with the majority of runs ranging from mid 70% to mid 80% of the OGIP. Table 6-9 presents the ranking of statistically significant coefficients, with the main effect of the timing of injection again by far the most influential coefficient in determining the rate of increase in the $CO_2$ concentration in the production stream.

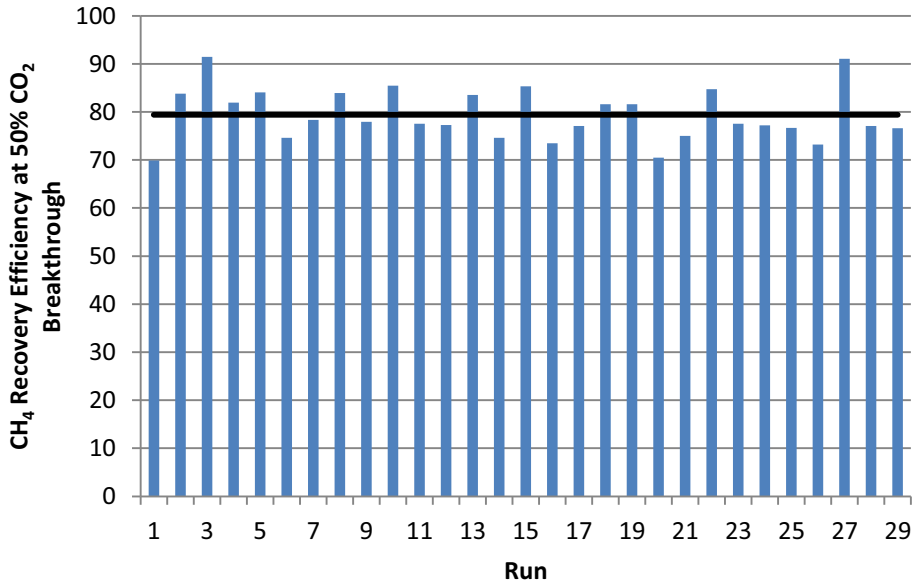


**Figure 6.42: Response 2 results for each design run. The average for all runs is indicated by the black line.**

**Table 6-9: ANOVA table for Response 2**

| Statistically Significant Coefficients | F Value | p-value Prob > F |
|---|---|---|
| Timing of Injection | 118.30 | <0.0001 |
| Thickness | 58.23 | <0.0001 |
| Thickness*Dip | 43.34 | <0.0001 |
| Permeability Multiplier*Timing of Injection | 40.82 | <0.0001 |
| Thickness*Timing of Injection | 39.63 | <0.0001 |
| Dip*Timing of Injection | 15.52 | 0.0011 |
| Injection Rate | 12.43 | 0.0026 |
| Permeability Multiplier*Thickness | 9.41 | 0.0070 |
| Permeability Multiplier | 6.39 | 0.0216 |

The regression diagnostics again show that the model sufficiently represents the data of the experimental design. The $R^2$ and adjusted $R^2$ coefficients are 0.9578 and 0.9305 respectively, while the normal probability plot (Figure 6.43) again shows no major deviation from the normality assumption.

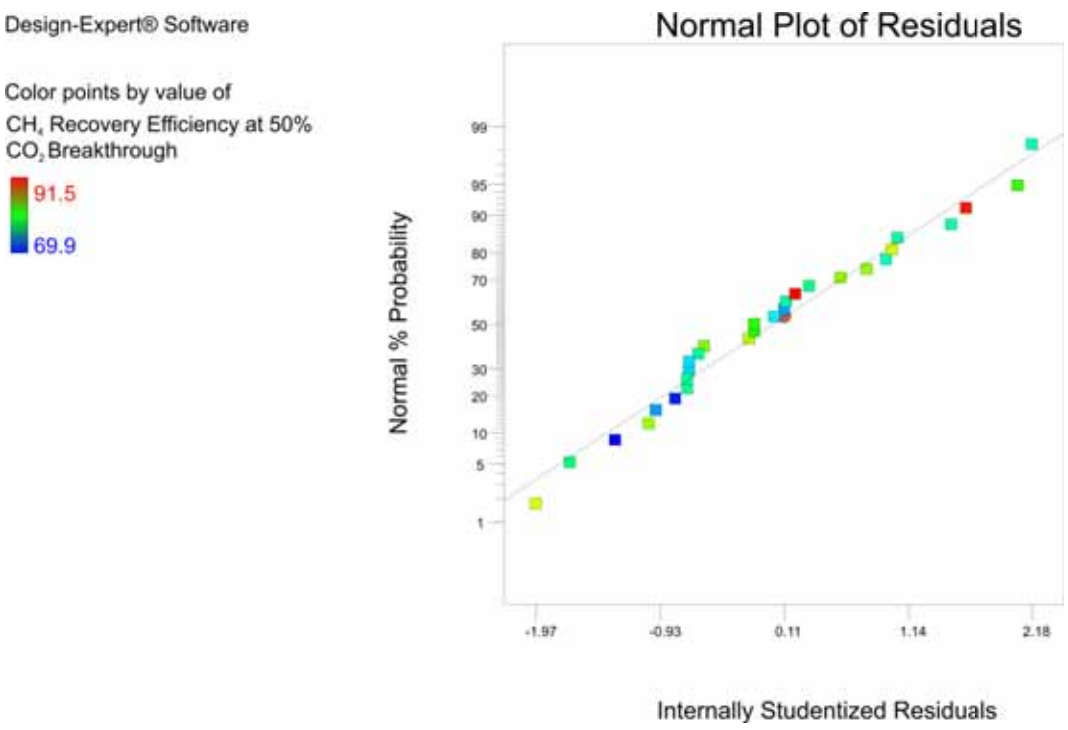


**Figure 6.43: The normal probability plot for Response 2.**

The main effect of the timing of injection

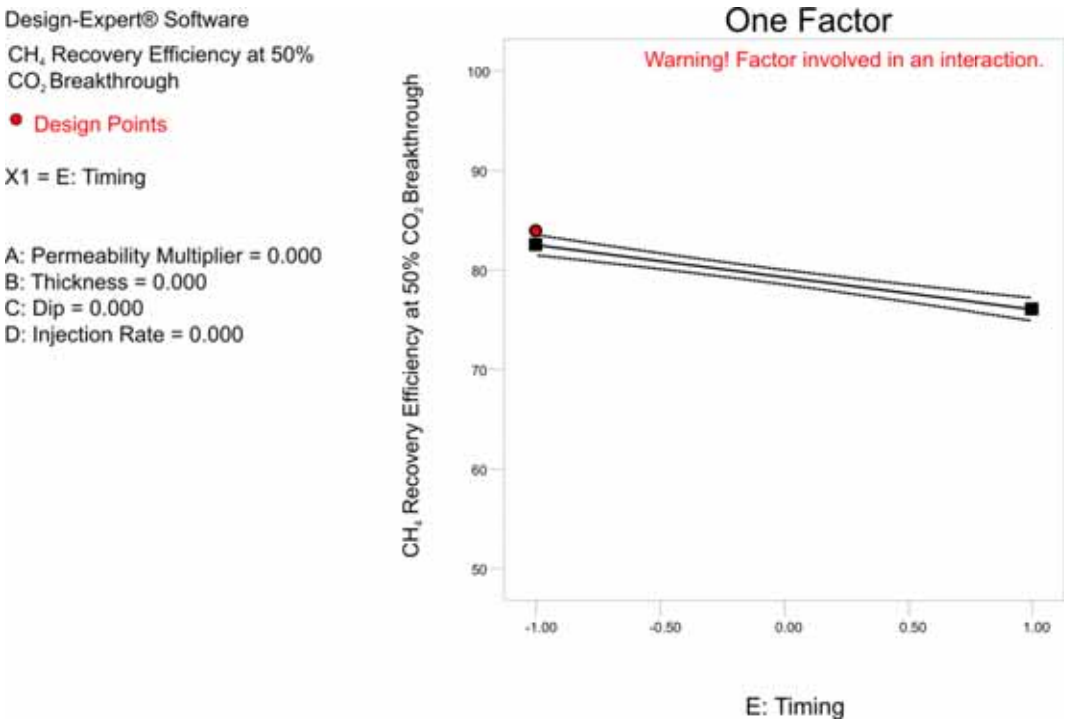


**Figure 6.44: The effect graph for the main effect of timing of injection for Response 2.**

As in Study 2A, the main effect of the timing of $CO_2$ injection is by far the most influential coefficient in determining the $CH_4$ recovery efficiency at a $CO_2$ limit of 50%, and therefore the rate of increase in the production of $CO_2$. Once more delaying the injection of $CO_2$ will lead to a more rapid increase in $CO_2$ production, reducing the recovery efficiency achievable. Despite the results in Response 1 showing that in a number of scenarios it is beneficial to delay the injection of $CO_2$, once $CO_2$ has reached the producer delaying the injection of $CO_2$ will lead to a more rapid increase in the production of $CO_2$. This is again due to the reduction in the volume of the free gas zone by the advancing aquifer, and of the ability for the injected $CO_2$ to sweep the invaded zone, as will be shown in the interactions involving the timing of injection with thickness and the permeability multiplier.

This result does highlight a potential conflict for an operator of a $CO_2$ EGR project in a heterogeneous water-drive gas reservoir. Results from Response 1 showed that in most instances delaying the injection of $CO_2$ improved $CH_4$ recovery at a 10% $CO_2$ limit. On the other hand, increasing the $CO_2$ limit to 50%, the results of Response 2 has shown that delaying the injection of $CO_2$ will clearly lead to a lower $CH_4$ recovery efficiency. Consequently, the primary recovery efficiency and the maximum tolerance of $CO_2$ production now become important issues. If incremental recovery can be achieved prior to the breakthrough of $CO_2$, then the tolerance of $CO_2$ production will determine the strategy employed. If only a minor concentration can be tolerated, then injection should be delayed (aside

from very thick reservoirs). If a higher concentration, say 50% $CO_2$ in the production stream, then injection should clearly not be delayed. However, if incremental recovery cannot be achieved prior to the breakthrough of $CO_2$, then the more rapid increase in the production of $CO_2$ associated with delayed injection leads to the early injection being the preferred option.

The main effect of thickness

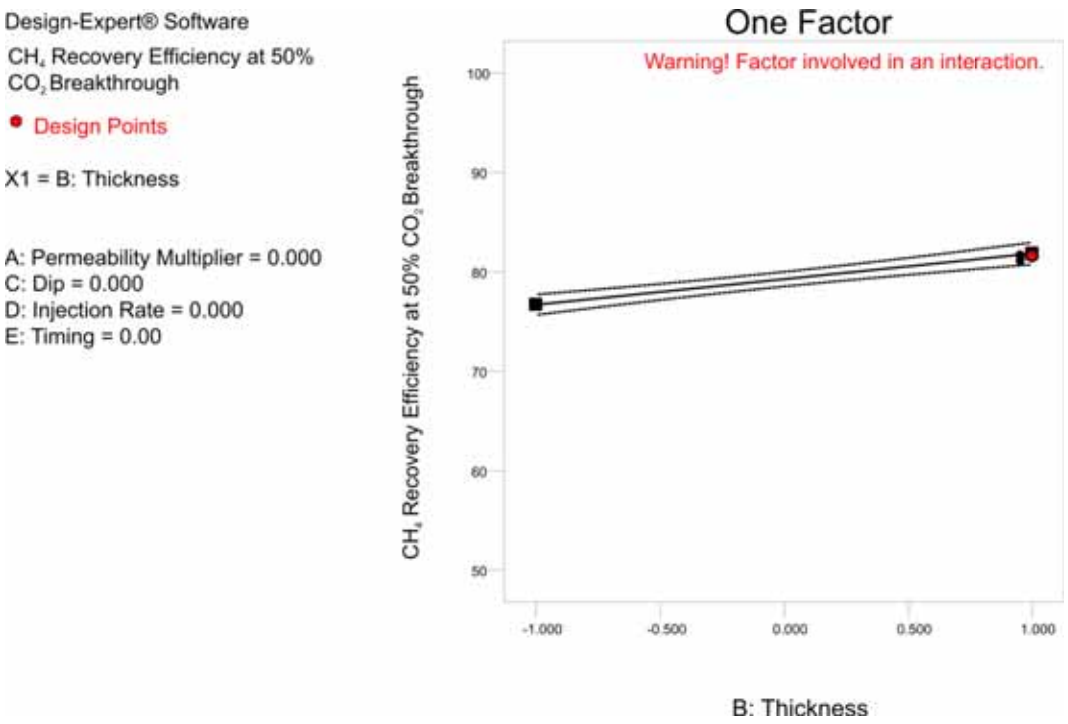


**Figure 6.45: The effect graph for the main effect of thickness for Response 2.**

The main effect of the thickness of the reservoir again indicates that the recovery of $CH_4$ will be improved, on average, with an increase in thickness (Figure 6.45). The extent of this effect is however dependent upon other parameters such as formation dip and the timing of injection, as will be shown in these corresponding effect graphs.

Thickness – formation dip interaction

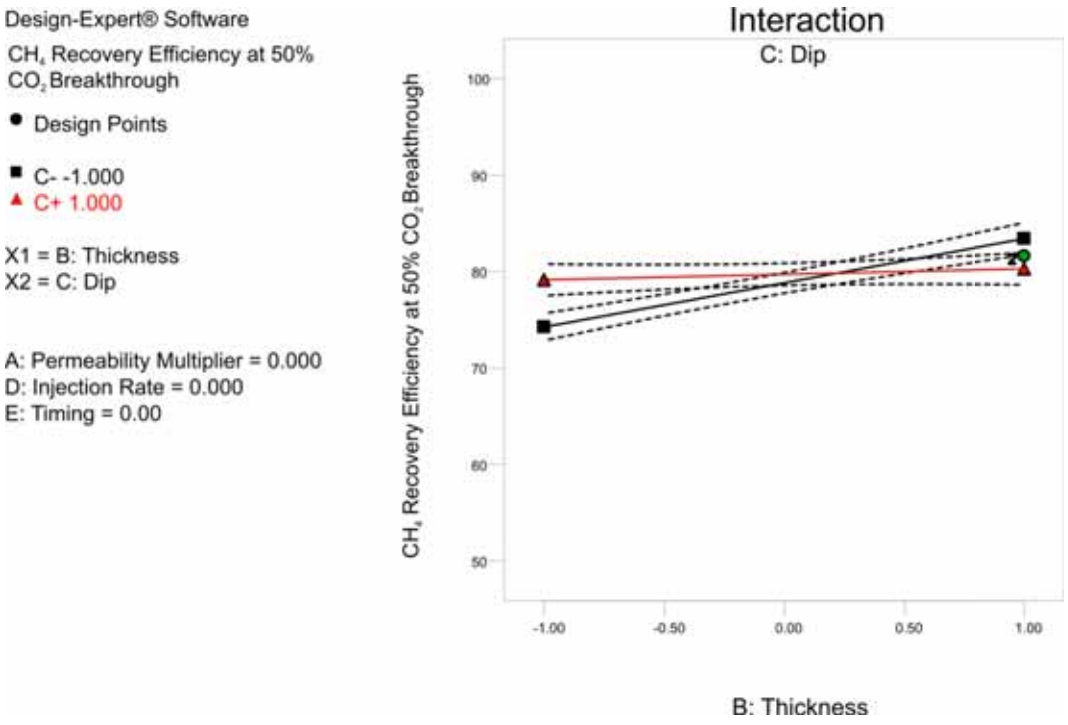


**Figure 6.46: The effect graph for the thickness formation dip interaction for Response 2.**

Mirroring the effect graph for the equivalent interaction in Response 1, the effect of thickness is again more influential in a non-dipping reservoir than a dipping reservoir (Figure 6.46). The balance between viscous and gravity forces is again evident. The stronger viscous forces which led to the channelling of $CO_2$ along the high permeability layer in a thin, non-dipping reservoir have also led to a greater rate of increase in $CO_2$ production. This can be mitigated by increasing the influence of gravity, in this instance by increasing thickness. Again the greater influence of gravity in a dipping reservoir equates to thickness having lesser of an impact. It must be noted that this effect graph is constructed with the timing of injection at the mid level (i.e. after 20% of the OGIP has been produced). It would be expected that as injection is further delayed, the benefit of increasing reservoir thickness would be limited. In the case of a non-dipping reservoir, increasing thickness would increase gravity segregation, and has been described this segregation can lead to channelling directly towards the high permeability layer. This will be seen in the effect graph for the thickness – timing of injection interaction.

Permeability multiplier – timing of injection interaction

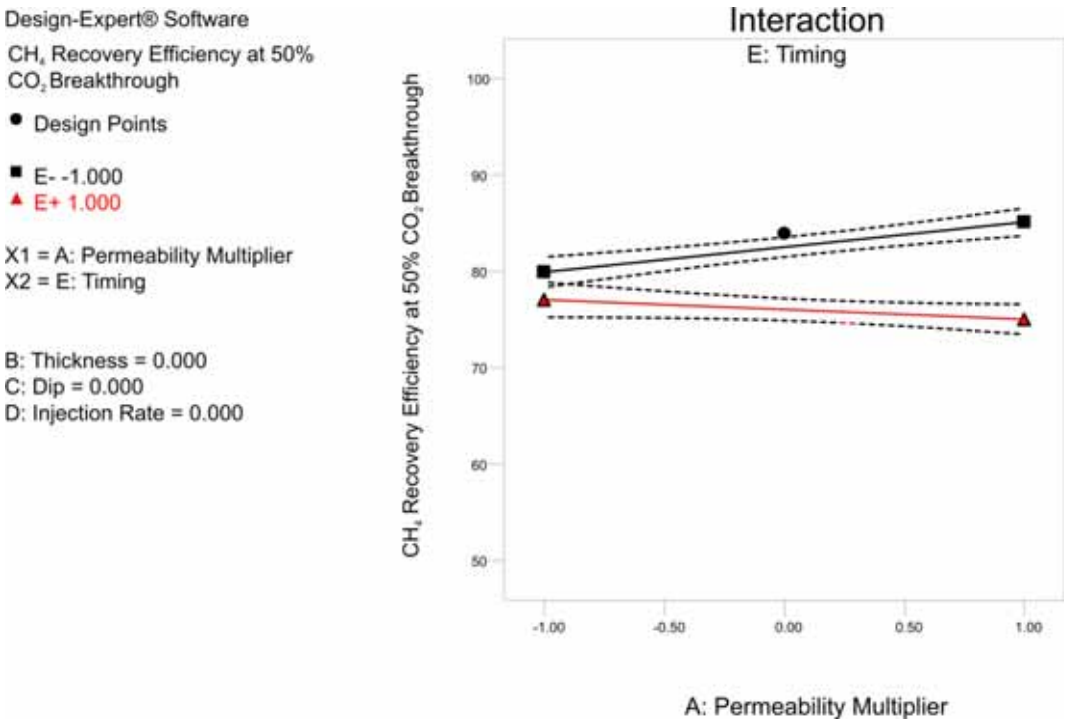


**Figure 6.47: The effect graph for the permeability multiplier timing of injection interaction for Response 2.**

The beneficial and detrimental effect of gravity segregation can be observed in the effect graph for the permeability multiplier – timing of injection interaction, shown in Figure 6.47. When injection is not delayed, increasing the permeability and therefore the influence of gravity leads to an improvement in the sweep of the reservoir by negating the effect of the high permeability layer. Conversely, if injection is delayed, increasing permeability reduces $CH_4$ recovery efficiency at the 50% $CO_2$ limit. High permeability promotes gravity segregation, limiting the ability to sweep the invaded zone. Additionally, a higher permeability increases the mobility of the aquifer and enhances pressure maintenance, with a greater number of moles of $CH_4$ being residually trapped. This therefore correlates to a reduction in the recovery of $CH_4$ as permeability is increased.

The permeability multiplier – timing of injection effect graph also highlights that the effect of the timing of injection is greatest when gravity segregation is at its greatest. Although it is still recommended that injection not be delayed, the beneficial effect of injecting early is minimised when, in this instance, permeability is low. The ability to sweep the invaded zone and the restriction of the aquifer (delayed injection), coupled with the poor displacement profile associated with viscous dominated displacement (early injection) mean the difference in the levels of the timing of injection is considerably less when permeability is low. The excellent sweep of the reservoir (early injection) versus the poor sweep of the invaded zone (delayed injection) associated with gravity segregation lead to the benefit of injecting $CO_2$ early being maximised when permeability is high.

Thickness – timing of injection interaction

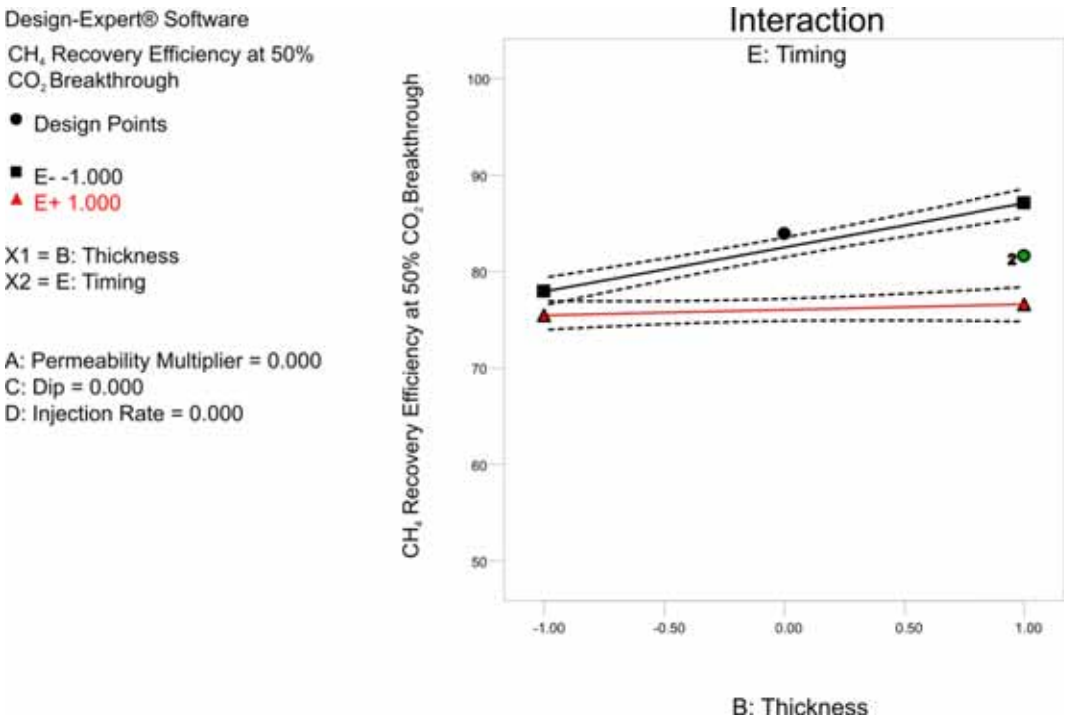


**Figure 6.48: The effect graph for the thickness timing of injection interaction for Response 2.**

For the equivalent reasons that were stated for the permeability multiplier – timing of injection interaction, the benefit of injecting $CO_2$ early in the project life is maximised when reservoir thickness is greater.

Additionally, as mentioned in the thickness – formation dip interaction, the beneficial nature of increasing thickness is reduced the longer the injection of $CO_2$ is delayed. The increase in gravity segregation associated with thicker reservoirs would ensure that a greater volume of the invaded zone would remain unswept. If the injection of $CO_2$ was delayed further, it would be expected that the recovery of $CH_4$ at the 50% $CO_2$ limit would decrease as reservoir thickness increased.

### 6.3.6 Response 3 Results and Discussion

The results for each design run with respect to the minimum producing $CO_2$ concentration required to achieve incremental recovery are presented in Figure 6.49. The range of results is quite wide, varying from essentially zero to over 60%, however the majority of runs fall between 15 – 30 mole percent of $CO_2$ required to achieve incremental recovery. The average of all runs equates to slightly over 20% $CO_2$ required in the production stream to achieve incremental $CH_4$ recovery. Again, the formation dip is the highest ranking statistically significant coefficient as indicated by the list in Table 6-10.

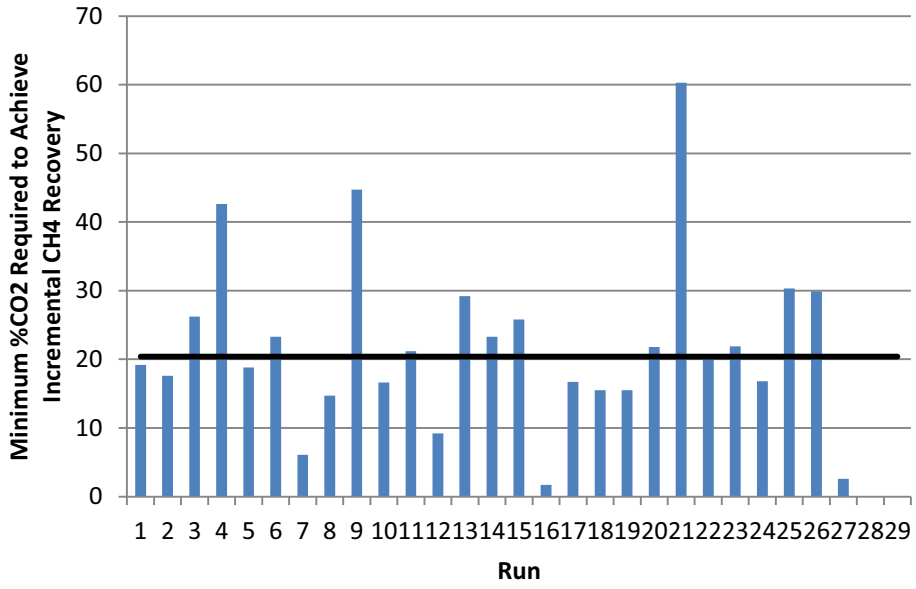


**Figure 6.49: Response 3 results for each design run. The average of all runs is indicated by the black line.**

**Table 6-10: ANOVA table for Response 3**

| Statistically Significant Coefficients | F Value | p-value Prob > F |
|---|---|---|
| Dip | 100.91 | <0.0001 |
| Dip*Timing of Injection | 46.15 | <0.0001 |
| Thickness | 17.25 | 0.0007 |
| Permeability Multiplier*Dip | 15.54 | 0.0011 |
| Dip*Injection Rate | 5.09 | 0.0376 |
| Permeability | 4.86 | 0.0415 |
| Thickness*Timing of Injection | 4.80 | 0.0427 |
| Permeability Multiplier$^2$ | 4.50 | 0.0489 |

The regression dianostics present no concern over the model with $R^2$ and adjusted $R^2$ coefficients of 0.9199 and 0.08681, although they are slightly lower than previous analyses. The normal probability plot (Figure 6.50) shows no major deviation from the normality assumption.

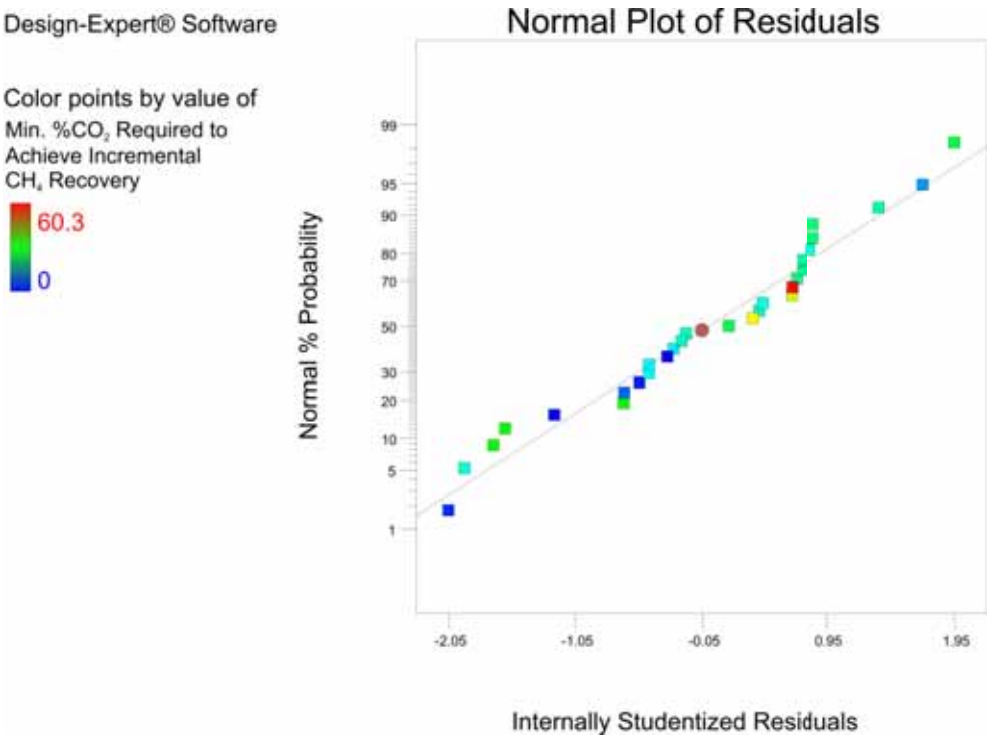


**Figure 6.50: The normal probability plot for Response 3.**

The main effect of formation dip

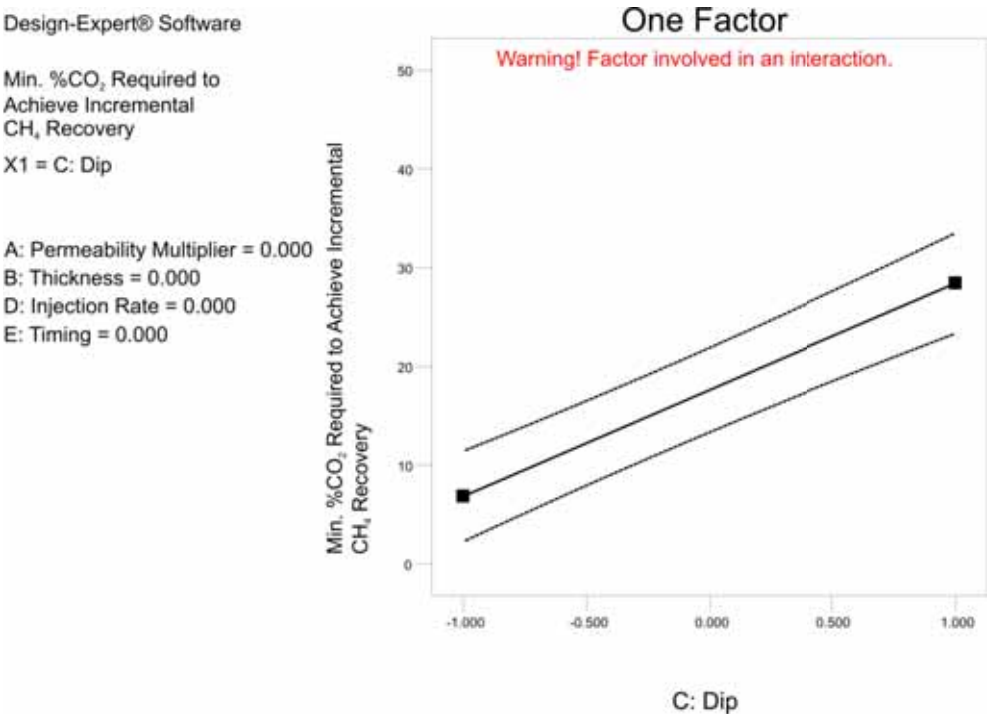


**Figure 6.51: The effect graph for the main effect of formation dip for Response 3.**

As has been the case in all previous studies, the main effect of formation dip is the highest ranking statistically significant coefficient in the analysis of this response. The effect graph for this coefficient

(Figure 6.51) again demonstrates a strong positive trend as formation dip is increased, the reasons for which have been previously discussed.

Formation dip – timing of injection interaction

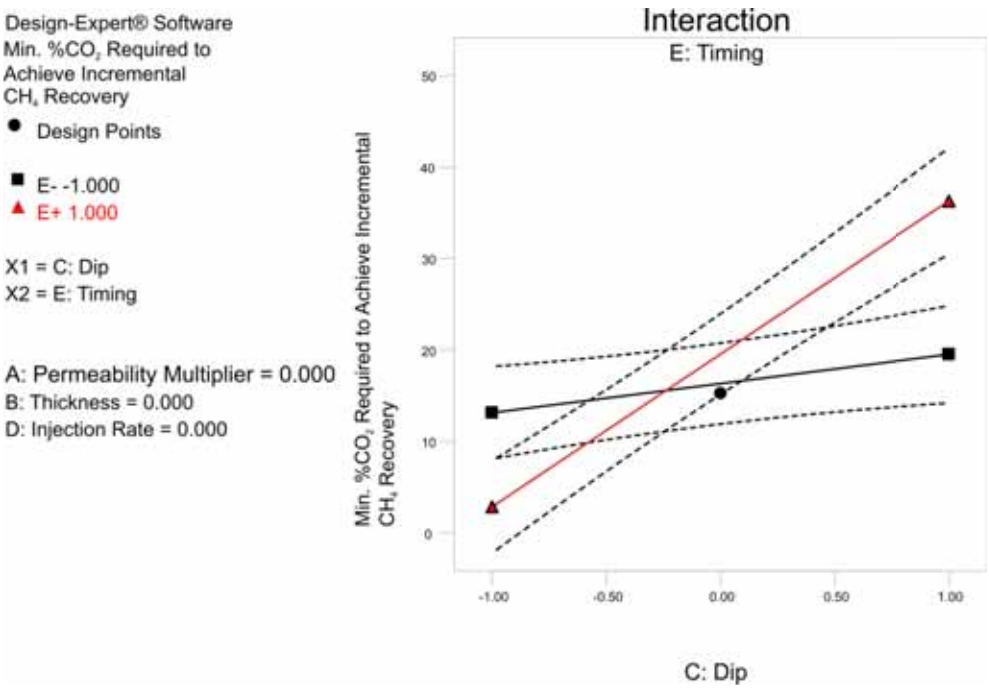


**Figure 6.52: The effect graph for the formation dip timing of injection interaction for Response 3.**

The significance of the timing of $CO_2$ injection in both Response 1 and 2, and the opposing effects it has on the recovery of $CH_4$ at either the 10% or 50% $CO_2$ production limit had led to the significance of the effect of this parameter in conjunction with the dip of the formation, in determining the minimum producing $CO_2$ concentration required to achieve incremental recovery. As shown in Figure 6.52, the effect of the timing of injection is dependent upon the formation dip. Incremental recovery can be achieved with a lower minimum producing $CO_2$ concentration in a non-dipping reservoir if injection is delayed. Table 6-11, whereby the result of two simulations where only the timing of injection has been altered is presented, suggests why. The primary recovery efficiency for both simulations amounted to 63.2% of the OGIP. Note that the recovery efficiency at the 10% $CO_2$ limit is similar to that of the primary recovery efficiency (63.2%). Consequently, the results of Response 1 will be influential in determining the effect of the timing of injection on the producing $CO_2$ concentration required to achieve incremental recovery. Results from Response 1 showed that delaying the injection of $CO_2$ led to an improvement in $CH_4$ recovery, seen in Table 6-11. It follows that delaying the injection in a non-dipping reservoir will lead to a lower minimum producing $CO_2$ concentration required to achieve incremental recovery.

**Table 6-11: Comparison of results between equivalent non-dipping models, investigating the difference between the timing of injection.**

| **Timing Scenario** | Early Injection | Delayed Injection |
|---|---|---|
| **Recovery Factor at 10% $CO_2$ Breakthrough Limit** | 58.6% | 66.9% |
| **Recovery Factor at 50% $CO_2$ Breakthrough Limit** | 81.5% | 76.7% |
| **Minimum %$CO_2$ Required to Achieve Incremental Recovery** | 14.2% | 3.2% |

This result is not however a definitive statement that the injection of $CO_2$ should be delayed in a non-dipping reservoir. This result is only an indication as to the scenario which will achieve incremental recovery with the lowest minimum producing $CO_2$ concentration. Any further $CH_4$ production beyond this point will be incremental recovery, however the extent of this recovery will be dependent upon the rate of increase in $CO_2$ production, and the maximum $CO_2$ concentration that can be tolerated. Note the recovery efficiency at the 50% $CO_2$ limit for the two cases presented in Table 6-11. Due to the more rapid increase in $CO_2$ production associated with delayed injection (Response 2), the recovery efficiency at the 50% $CO_2$ limit for the delayed injection scenario is less than if injection occurred early.

The decision on the timing of injection in a dipping reservoir is more straightforward. The effect graph shows that incremental recovery can be achieved with a considerably lower minimum producing $CO_2$ concentration if injection is not delayed. Table 6-12 presents results of two further simulations whereby the timing of injection has been altered in a 21° dipping model. As mentioned previously, primary recovery in a dipping reservoir is generally greater than for a non-dipping reservoir. The primary recovery for both models amounted to 71.2% of the OGIP. Referring to Table 6-12, it can be seen that the recovery efficiency at the 50% $CO_2$ limit is in the range of the primary recovery. Consequently, the rate of increase in $CO_2$ production is going to determine the minimum producing $CO_2$ concentration required to achieve incremental recovery. The results of Response 2 subsequently become influential. It was demonstrated that delaying the injection of $CO_2$ will always result in a more rapid increase in the $CO_2$ production rate. It therefore follows that incremental recovery will be achieved with a lower producing $CO_2$ concentration if the injection of $CO_2$ is not delayed. Having said that, the result of the main effect of formation dip still stands, and that the injection of $CO_2$ into a non-dipping reservoir will achieve incremental recovery with a lower producing $CO_2$ concentration than would be the case for a dipping reservoir.

**Table 6-12: Comparison of results between equivalent dipping models, investigating the difference between the timing of injection.**

| **Timing Scenario** | Early Injection | Delayed Injection |
|---|---|---|
| **Recovery Factor at 10% $CO_2$ Breakthrough Limit** | 65.5% | 65.4% |
| **Recovery Factor at 50% $CO_2$ Breakthrough Limit** | 84.3% | 74.7% |
| **Minimum %$CO_2$ Required to Achieve Incremental Recovery** | 17.3% | 27.5% |

The main effect of the permeability multiplier and the permeability multiplier – formation dip interaction

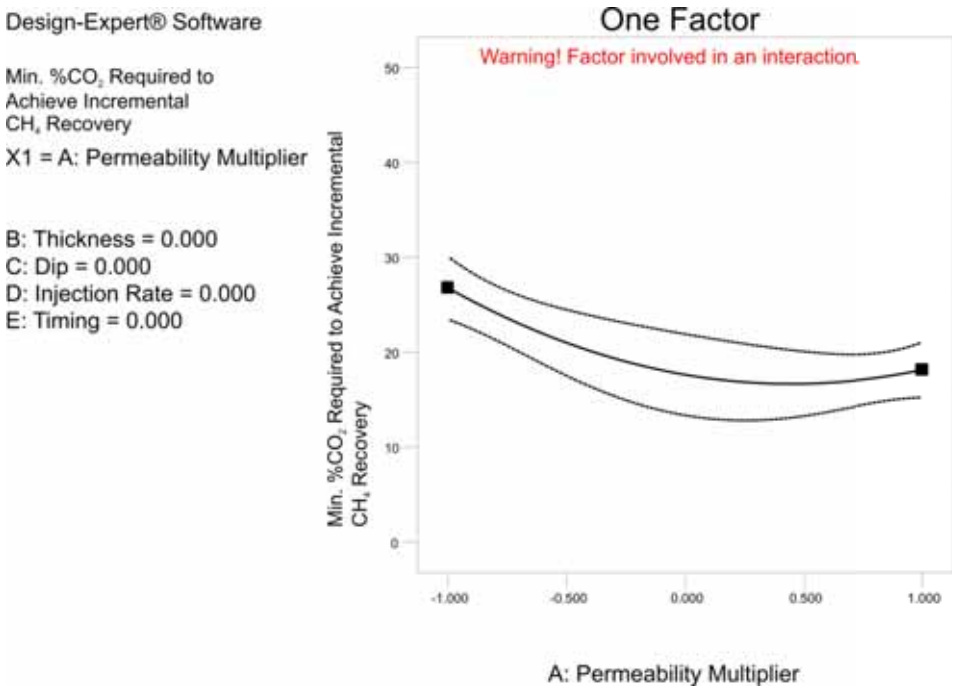


**Figure 6.53: The effect graph for the main effect of the permeability multiplier for Response 3.**

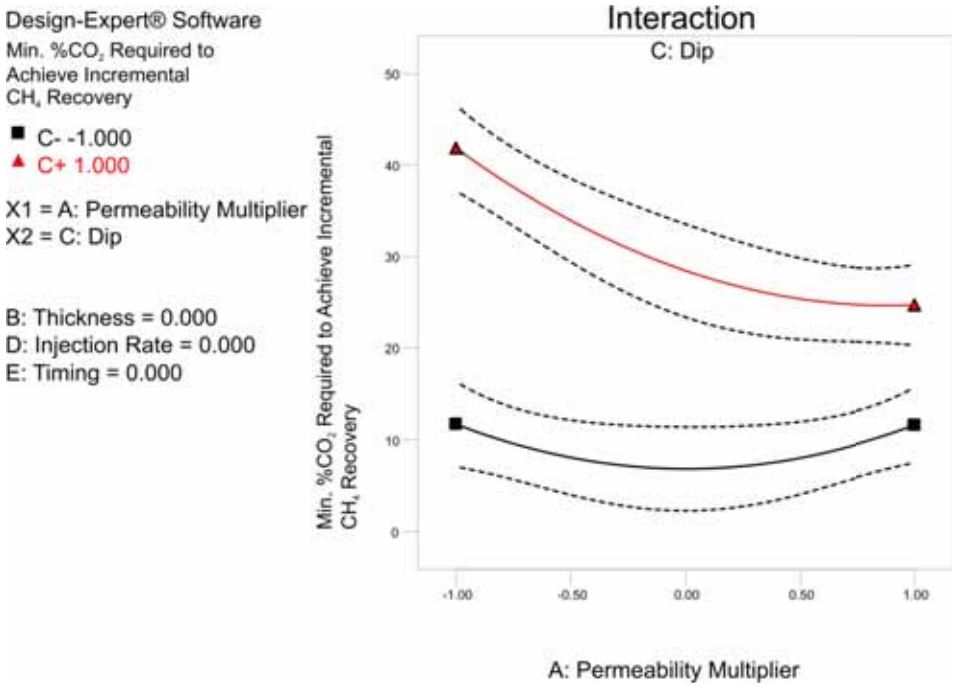


**Figure 6.54: The effect graph for the permeability multiplier formation dip interaction for Response 3.**

The other mildly significant coefficients from the analysis of Response 3 are the main effect of permeability (Figure 6.53) in addition to the permeability – formation dip interaction (Figure 6.54). These effects are identical to the equivalent coefficients from Study 2A and so the discussion of these effects can be found in Section 6.2.5.

The results of this study show that recommendations cannot be made on the results of one response. Consideration of the effect of parameters on all three responses needs to take place in order to make appropriate recommendations. This was shown with injection of $CO_2$ into a non-dipping reservoir. Delayed injection was shown to result in incremental recovery being achieved with the lowest minimum producing $CO_2$ concentration. Based on this result alone, the recommendation would be to delay the injection of $CO_2$. However, as Response 2 showed, the rate of increase in $CO_2$ production was considerably greater if injection was delayed. Consequently, if a producing $CO_2$ concentration of 50% could be tolerated, delaying the injection of $CO_2$ could result in a considerably lower recovery efficiency than if injection was not delayed.

### 6.3.7 Summary

The results of the analysis of the timing of $CO_2$ injection in the presence of simple heterogeneity can be summarised as follows:

Response 1:

- Viscous dominated displacement in the presence of heterogeneity leads to the uneven advancement of the displacement front when the injection of $CO_2$ occurs early, leading to the premature breakthrough of $CO_2$ and a reduction in $CH_4$ recovery. This detrimental effect is more severe in non-dipping reservoirs.
- Consequently, it was shown that delaying the injection of $CO_2$ is beneficial in improving the recovery of $CH_4$ at the initial breakthrough of $CO_2$. This was especially true in cases involving strong viscous forces, enabling a significant portion of the invaded zone to be swept by the injected $CO_2$.
- The benefit of delaying the injection of $CO_2$ reduces as the influence of gravity increases. Gravity segregation will limit the ability to sweep the invaded zone, and can actually lead to preferential flow directly towards the higher permeability layers leading to poor sweep of the free gas zone as well.
- Gravity dominated displacement is beneficial if injection of $CO_2$ occurs early. The effect of gravity either suppresses the uneven advancement (dipping reservoirs), or can minimise or eliminate contact with the high permeability layer (non-dipping reservoirs).

Response 2:

- Similar to Study 2A, delaying the injection of $CO_2$ results in a considerably more rapid increase in the $CO_2$ production rate than if injection was to occur early. Consequently, $CH_4$ recovery is maximised at the 50% $CO_2$ limit if injection is not delayed.
- The benefit of early $CO_2$ injection was greater in conditions where gravity has a dominant influence, such as high permeability and/or thick reservoirs.

Response 3:

- The formation dip was the most influential parameter, with injection into non-dipping reservoirs always achieving incremental recovery with the lowest minimum producing $CO_2$ concentration as compared to a dipping formation.
- The effect of the timing of $CO_2$ injection was dependent upon the dip of the formation. In a non-dipping reservoir, incremental recovery could be achieved with a lower producing $CO_2$ concentration if injection was delayed. In a dipping reservoir, the generally higher primary recovery efficiency meant that the rate of increase in $CO_2$ production was influential with the early injection of $CO_2$ resulting in a lower minimum producing $CO_2$ concentration achieving incremental recovery.
- The caveat with the effect of the timing of injection into a non-dipping reservoir is that the result for Response 3 needs to be considered with the maximum producing $CO_2$ concentration allowed. Although incremental recovery with a lower producing $CO_2$ concentration is achieved by delaying the injection, the more rapid increase in the $CO_2$ production rate associated with delayed injection (Response 2) can lead to a lower total incremental recovery being achieved.

# CHAPTER 7

# 7 Case Study: The Naylor Gas Field, Otway Basin, Victoria

The research conducted to this point has investigated the process of injecting $CO_2$ to enhance natural gas recovery in simplified numerical models. Realistic situations are often considerably more complex (i.e. permeability heterogeneity) and so conclusions drawn from simple models do not necessarily correlate to the real world. It is therefore an aim of this chapter to determine whether the conclusions drawn from the previous studies of this thesis can be matched to results of this investigation of $CO_2$ EGR in a actual case study. The model used for the case study is the depleted and abandoned Naylor gas field. As part of this study, operational parameters will be investigated and optimised in an effort to maximise the recovery of $CH_4$ with respect to the producing $CO_2$ concentration.

## 7.1 Field Location and Background

The Naylor field is a small, produced and abandoned gas field located in the onshore Otway Basin of central Victoria, Australia (Figure 7.1). The field was discovered by Santos in 2001 and subsequently developed. The only well drilled, Naylor-1, intersected natural gas in three separate zones – Waarre C, A1 and A2. Due to the small nature of the field, economic considerations required cost to be minimised. The well was completed as a 3½" mono-bore, with only a basic wire-line log suite gathered. No other testing was conducted.

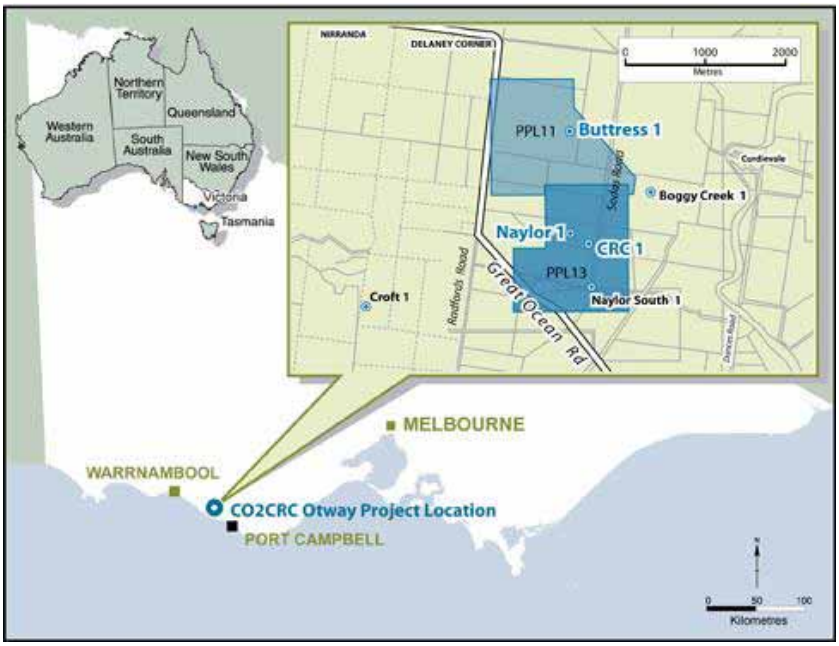


**Figure 7.1: Location of the Naylor field in south-western Victoria, Australia.**

The Waarre C and A formations were interpreted to be isolated zones, with the sealing barrier comprising the Waarre B formation. Development subsequently focused on the Waarre C formation, which is the main producing hydrocarbon interval regionally (Spencer & Pedalina 2006).

Geologically, the Waarre C section of the Naylor field is interpreted to be an incised valley fill/braided fluvial system. The field is bounded by three faults, and is connected to a large aquifer (Spencer & Pedalina 2006). The geometry of the reservoir is shown in Figure 7.2, which also displays the location of the production well, Naylor-1. Basic properties of the Naylor Field are given in Table 7-1.

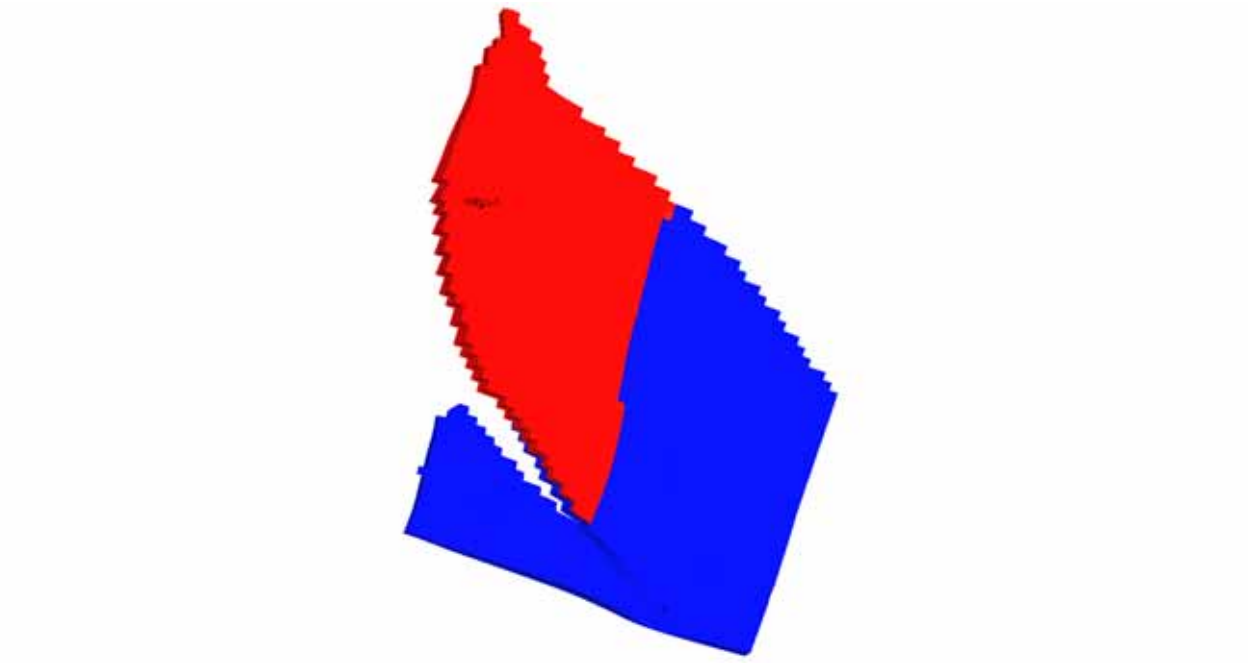

**Figure 7.2: Plan view of the model of the Naylor field. The gas reservoir (red) is enclosed by three bounding faults.**

**Table 7-1: Basic properties of the Naylor field.**

| | |
|---|---|
| Reservoir Geometry (2P) | 404,680 $m^2$ |
| OGIP (2P) | 147 x $10^6$ $m^3$ (5.2 Bscf) |
| Gas Composition (mol %) | N2 = 2.25 |
| | $CO_2$ = 1.05 |
| | C1 = 87.43 |
| | C2 = 4.84 |
| | C3 = 2.15 |
| | C4+ = 2.28 |
| Average Porosity | 17.8% |
| Connate Water Saturation | 9% |
| Average Permeability | 500 – 1000mD* |
| Initial Pressure | 192.5 Bars (2830 psia) |
| Thickness | 25 m |
| Reservoir Temperature | 85°C (185°F) |
| Drive Mechanism | Water Drive |

The production rate was of a variable nature, as indicated in Figure 7.3, ranging between 2 – 13 MMscf/day. Cumulative production amounted to 95.2 x $10^6$ $m^3$ (3.3 Bcf), which based upon the 2P OGIP calculation equates to around 65% of the OGIP. Economic considerations did not allow for the installation of water handling facilities and consequently production ceased at the onset of water production.

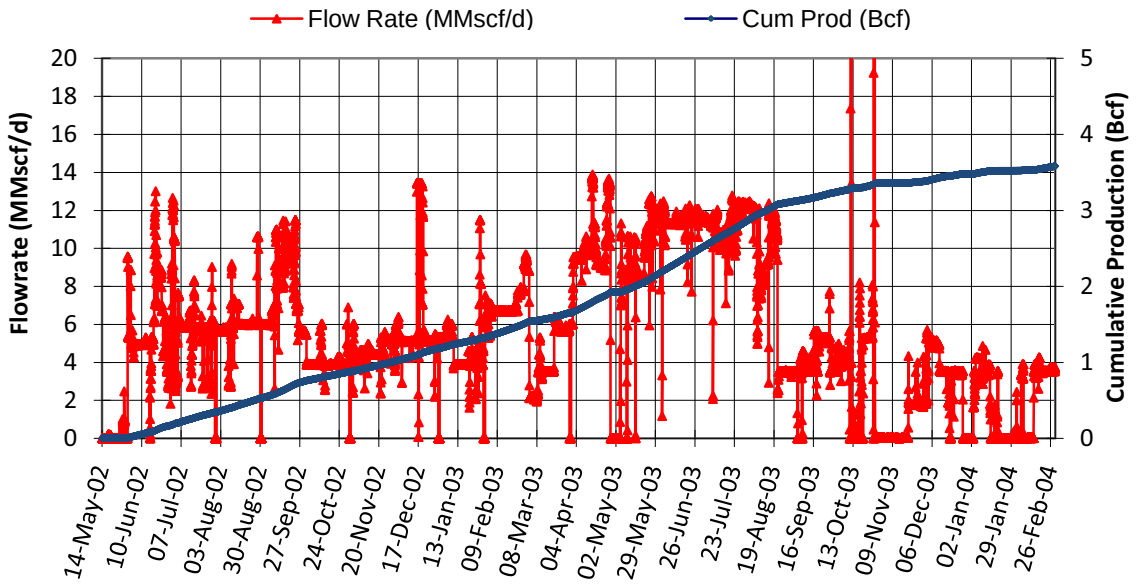


**Figure 7.3: Historical gas production rate for the Naylor field.**

Following the production of the natural gas resource from the Naylor field, control of the field turned to the Co-operative Research Centre for Greenhouse Gas Technologies (CO2CRC) for use as a pilot scale $CO_2$ storage project. The project aimed to demonstrate the safe transport and storage of $CO_2$ under Australian conditions. The specific aims of the project were:

Operational

- To safely produce and transport $CO_2$ from the Buttress field, and store in the depleted Naylor gas field.

Technical

- To effectively model and monitor the sub-surface behaviour of the injected $CO_2$.
- To verify the successful containment of $CO_2$ within the storage formation.
- To develop, test and deploy new and enhanced monitoring and verification (M&V) technology.

Communication

- To effectively communicate with stakeholders, the local community and the wider general public about CCS, and in particular the successful progress of the Otway Basin Pilot Project (OBPP).
- To provide data and information for the development of a regulatory regime for CCS.

Specifically, the project involved the production of a $CO_2$-rich (79% $CO_2$, 21% $CH_4$) gas from the nearby Buttress field, with transportation to the Naylor field via a 2.25km stainless steel pipe. During an 18 month period, over 65,000 tonnes of the $CO_2$ rich gas was injected into the Waarre C formation through a new injection well, CRC-1. Monitoring of the $CO_2$ plume occurred with tools installed in the original production well, Naylor-1, located 300 metres updip from CRC-1. The predicted time of $CO_2$ breakthrough at the Naylor-1 well was estimated at between 4 – 9 months, subject to uncertainty in the geological models and relative permeability data, the product of minimal data gathered by the previous operator of the field. Breakthrough of $CO_2$ at the Naylor-1 well occurred after 150 days, within the predicted time frame, confirming the uncertainty range established through the reservoir characterisation and modelling of $CO_2$ flow within the Naylor field.

The case study performed within this chapter is investigating the potential for enhancement of natural gas recovery through the injection of $CO_2$ with respect to the original development of the Naylor field. No comparison is made with the OBPP results, and whether EGR could have been a feature of this $CO_2$ storage operation.

## 7.2 Reservoir Model Characterisation

As part of the development of the OBPP, and to assess the suitability and risk of the Waarre C formation for $CO_2$ injection and storage, an industry standard, geological model was constructed by researchers at the CO2CRC. Nineteen realisations were developed based upon four geological cases (Spencer & Pedalina 2006). A most-likely case model was selected from Case 3 which represented the interpreted geological deposition, the braided fluvial stream, which was successfully history matched in order to perform predictive modelling for $CO_2$ storage (J. Xu 2006). This model was therefore selected for this study. Note that the collection of data and the commencement of this study occurred prior to the collection of additional data and the re-interpretation and updating of the geological and dynamic models as part of the OBPP following the drilling of CRC-1. With consideration of the number of simulations performed in this study, and the time required to re-complete these simulations, the additional data was not incorporated into this study.

The geological model employs a corner-point Cartesian grid, incorporating grid dimensions of 71 x 70 x 55. Grid sizes equate to about 20 x 20 x 1.2 metres, which through a grid sensitivity study was shown to sufficiently represent the heterogeneity of the reservoir, whilst providing sufficient resolution to model the processes involved in the injection of $CO_2$ into a reservoir where $CH_4$ and water are present.

As mentioned previously, the reservoir is bounded by three sealing faults. These faults are represented in the model as no flow boundaries.

Porosity values were calculated from wire-lines logs run in the Naylor-1 and Naylor South-1 wells. The porosity for the model was subsequently populated using the Sequential Gaussian Simulation (SGS) technique. The SGS technique involves the random population of the model based upon a specific distribution (Olea 1999), which in this case is based upon a braided fluvial system. The porosity distribution has a mean of 0.1385 with a standard deviation of 0.0543. No core was obtained from Naylor-1, resulting in no permeability data with which to directly estimate the reservoir permeability distribution. In order to populate the model with permeability data, a porosity-permeability correlation was developed from data obtained from core from the Waarre C formation in neighbouring wells (Spencer & Pedalina 2006). The mean permeability in this model is 1105mD. Due to the absence of core from the Waarre C section of the Naylor field, no direct relative permeability measurements were available. As part of the history matching process, hypothetical relative permeability curves were developed for the model using Pirson's correlation (Pirson 1958), as shown in Figure 7.4.

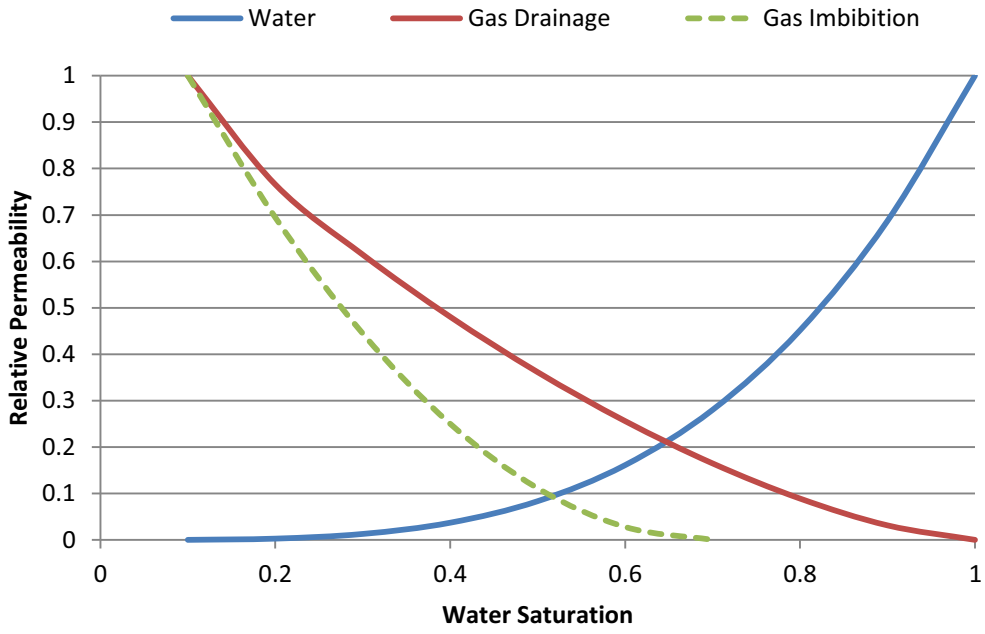


**Figure 7.4: Relative permeability data used for the dynamic model.**

A major uncertainty in the history matching process was the size and corresponding strength of the aquifer. A successful history match was obtained with the use of dual, numerical aquifers positioned as illustrated in Figure 7.5.

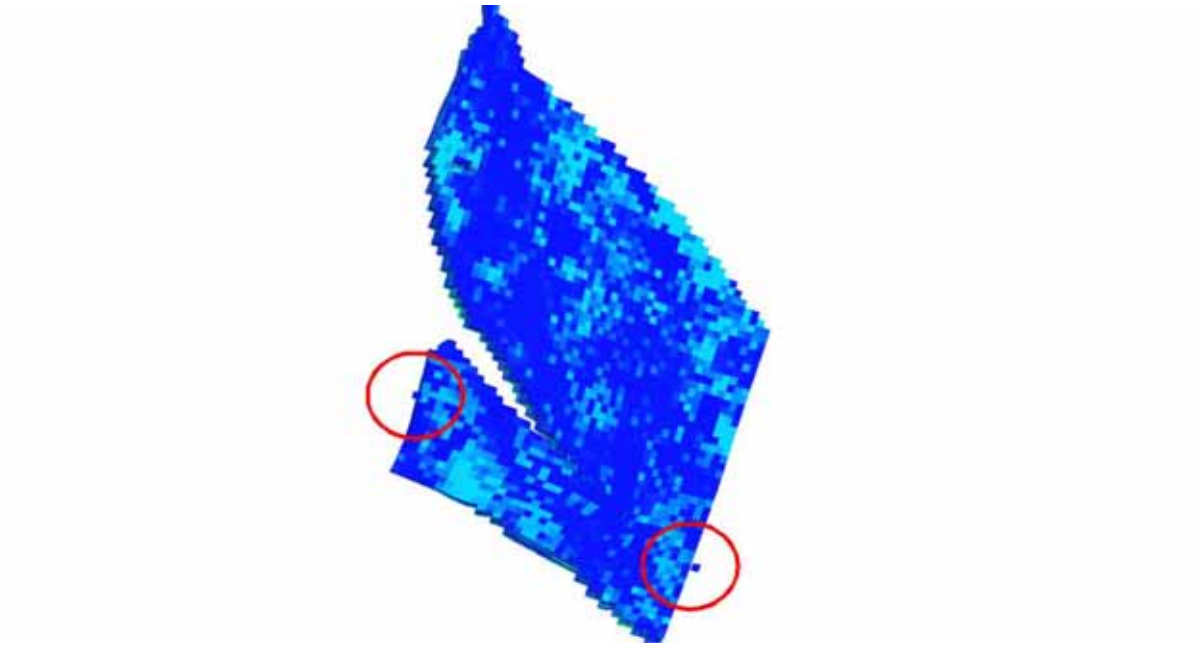

**Figure 7.5: Location of the numerical aquifers used to history match the historical production.**

With consideration of the simulation run time (ranging from 2 – 10 hours), only three components were considered in the model, $CH_4$, $C_2H_6$, and $CO_2$. Incorporating all components of the Naylor gas composition (Table 7-1) would have increased the simulation run time substantially. Initial reservoir gas composition incorporated into the model was therefore 90% $CH_4$ and 10% $C_2H_6$. Fluid properties were then developed using Schlumberger's PVTi program (Schlumberger 2007).

In order to compare the results of this study with the original development, the existing production well, Naylor-1, was used as the production well for all simulations. The location of CRC-1 is not used in this study, with this well being located within the original gas zone, as illustrated in Figure 7.6. To maximise the contact and sweep of the reservoir, the injection well is placed at least on the edge of the gas zone.

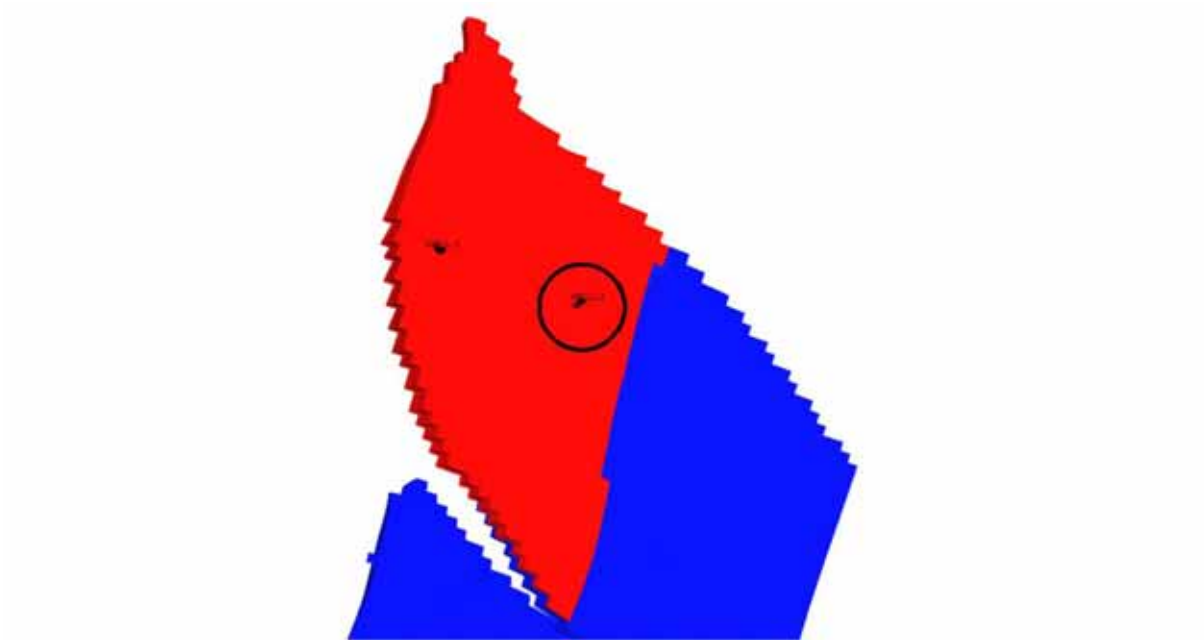

**Figure 7.6: Location of the CRC-1 well drilled by the CO2CRC for use in a $CO_2$ storage pilot project.**

## 7.3 Initial Investigations

The properties presented in Table 7-1 give an indication, based on the results of the previous studies in this thesis, to the results that could be expected from injecting $CO_2$ into the Naylor field. The average reservoir permeability is high, with a mean permeability from the model of 1105 mD. Additionally, the reservoir is thin, at 25 metres. Figure 7.7 presents a cross-section of the reservoir. A formation dip of less than five degrees was calculated from the top left of the structure to the edge of the GWC as seen in Figure 7.7, and so it is expected that the results representing a non-dipping reservoir from the previous studies will apply. It was shown in Chapter 5 and Chapter 6 that the breakthrough of $CO_2$ at the production well in a non-dipping reservoir can be considerably early if the reservoir is thin with high permeability. The high permeability promotes gravity segregation and rapid horizontal migration towards the production well whereby the coning of $CO_2$ was shown to limit the sweep of the reservoir. Viscous dominated displacement was shown to be an effective displacement mechanism, however this was only the case in a homogeneous reservoir. With heterogeneity present, the effectiveness of a viscous dominated displacement in a non-dipping reservoir was severely impacted by the uneven advancement of the displacement front leading to premature $CO_2$ breakthrough and consequently poor sweep of the reservoir.

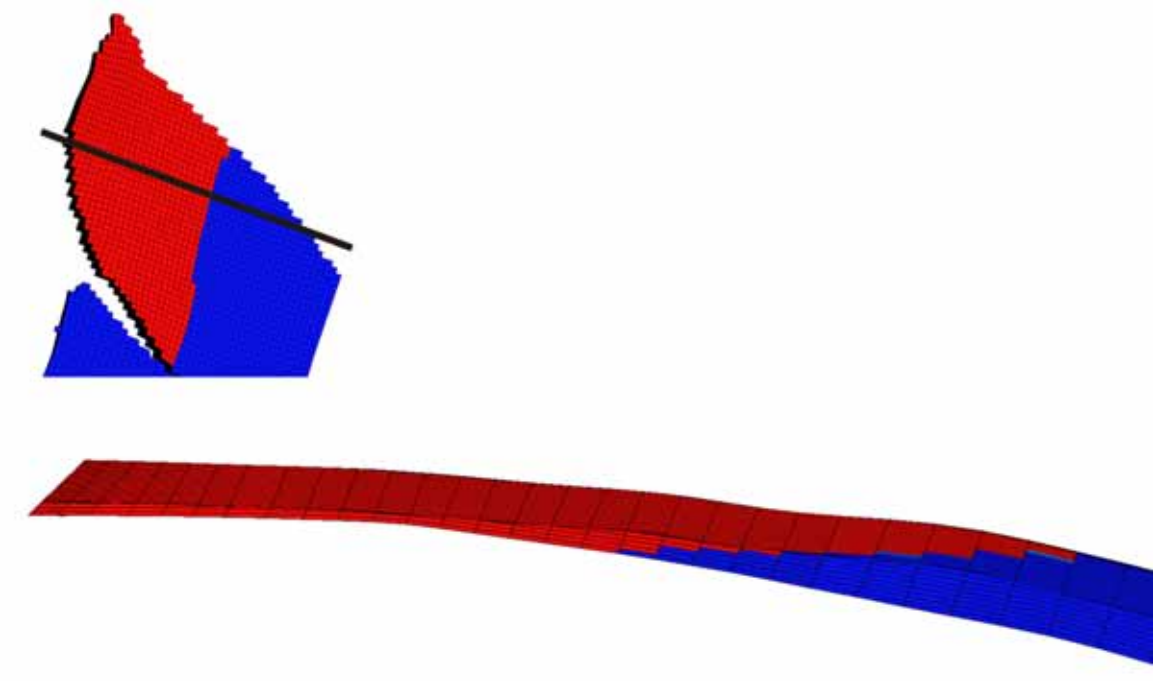

**Figure 7.7: Cross-section of the reservoir showing the flat nature of the gas zone.**

It was concluded from Study 1 that the sweep of a thin, high permeability, non-dipping reservoir can be poor due to gravity segregation, rapid horizontal migration towards the production well and the influence of production causing coning of $CO_2$. Sweep could be improved by either reducing production rates to allow for gravity to stabilise the displacement front, reducing the susceptibility for $CO_2$ coning, or by increasing rates in order to achieve viscous dominated displacement. Figure 7.8 presents a cross-section of the reservoir displaying the horizontal permeability. This cross-section indicates significant heterogeneity in the model, in particular the large range of permeabilities present. In the free gas zone, permeability ranges from as low as 4 mD to as high as 6000 mD. The large range of permeabilities present in the reservoir will make a stable viscous dominated displacement very difficult if not impossible to achieve.

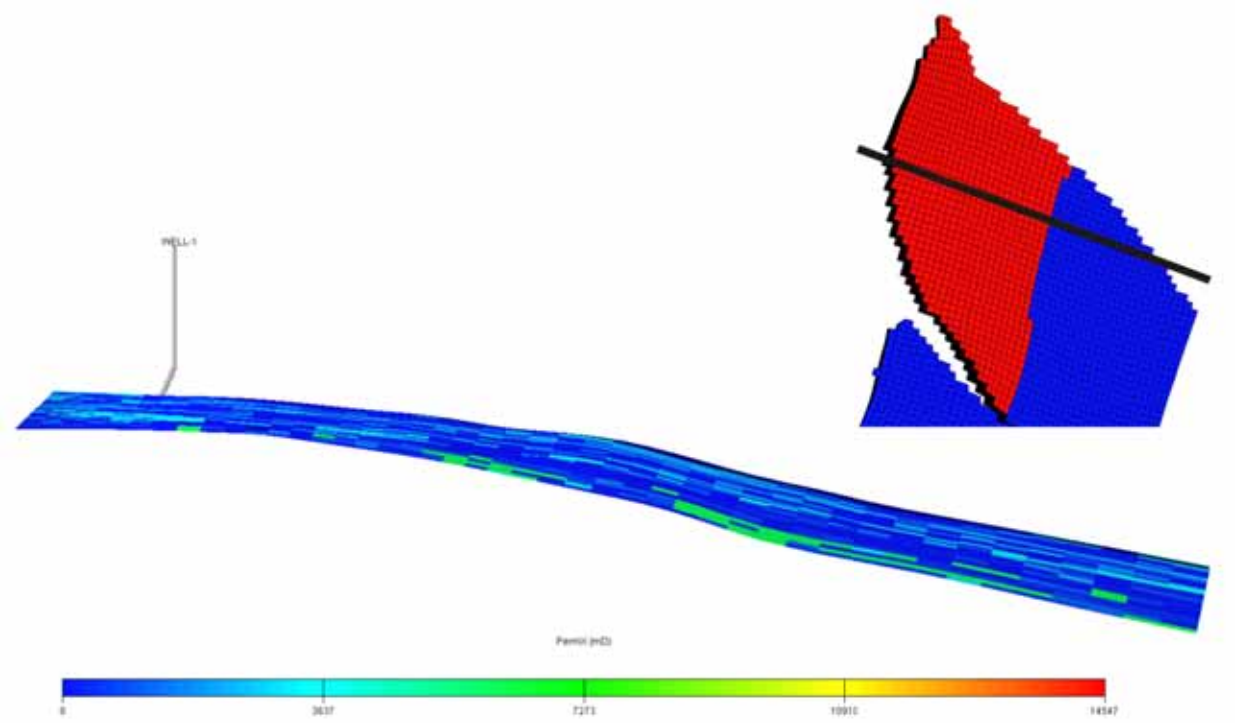

**Figure 7.8: Cross-section of the reservoir displaying the permeability heterogeneity present in the model.**

The uneven displacement of the natural gas by $CO_2$ is therefore expected to be a key feature in this case study, and so techniques which can mitigate against uneven displacement will be key to maximising the recovery of natural gas. Operational parameters such as the injection and production rates, well location, and the timing of injection are expected to be influential in achieving an efficient displacement process.

An initial investigation was performed to gain a preliminary understanding of fluid movement in the Naylor field, and to perform an initial test on how varying operational parameters will affect the sweep of the reservoir. Firstly, the injection well location was investigated. Due to the heterogeneity of the reservoir, the well location could significantly influence the sweep of the reservoir. Figure 7.9 displays a plan view of the Naylor field with the top surface location of each of the five injection well locations tested. The first three locations were chosen to be just beyond the edge of the gas zone. The fourth and fifth locations are further into the aquifer. It was shown in Chapter 5 that lowering the injection well completions further into the aquifer could delay the breakthrough of $CO_2$ and improve $CH_4$ recovery, albeit for a low permeability reservoir. The high permeability of the Naylor model is expected to cause rapid migration of the injected $CO_2$ along the GWC towards the production well, and so injection into the water leg has the potential to restrict $CO_2$ mobility for a period of time, potentially delaying the breakthrough of $CO_2$.

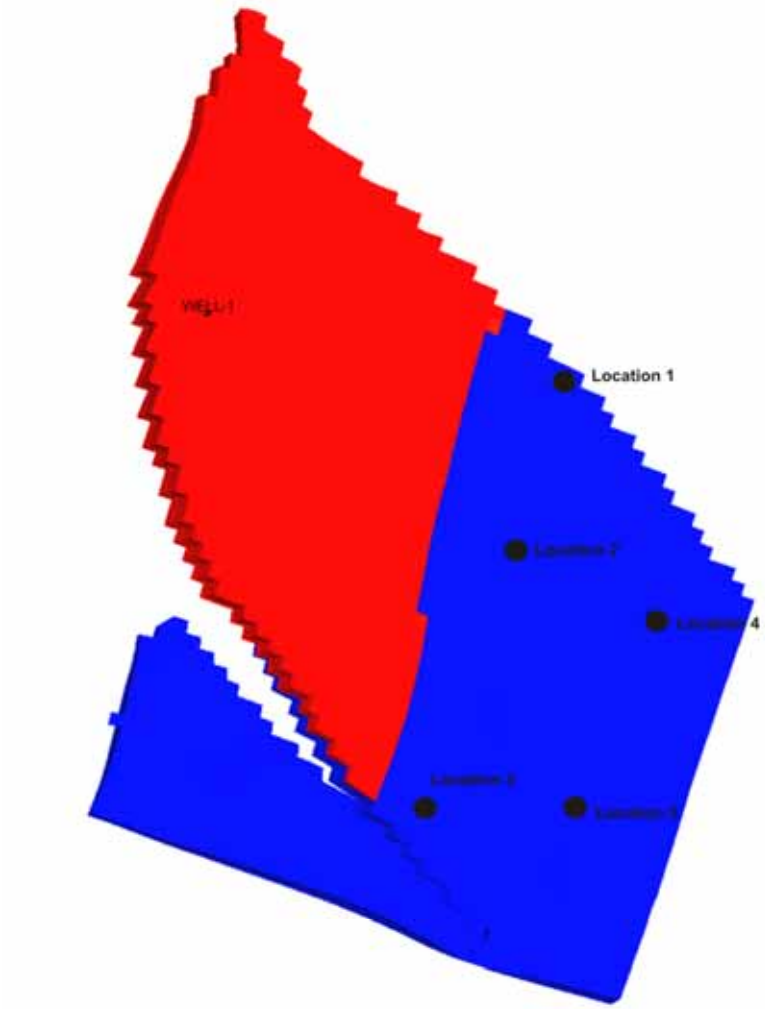


**Figure 7.9: Plan view of the reservoir indicating the location of the five injection wells.**

Equivalent injection and production rates are used in these simulations, and are equal for all locations. The production rate is taken from the average of the monthly average production rates for the period of production from the Waarre C formation for the Naylor field (188,000 $m^3$/day). No delay in the injection of $CO_2$ occurs for all cases.

Table 7-2 presents the results of the five simulations performed, with these results based upon the three responses used in Study 2. In terms of natural gas recovery at the 10% $CO_2$ limit, only minor variability is seen, with recovery being greater in the northern part of the reservoir (location 1, 2 and 4), as opposed to the southern part (location 3 and 5). The same trend is observed for recovery at a $CO_2$ limit of 50% with the difference in results between the north and south of the reservoir increasing. The greatest variability is however seen for the minimum $CO_2$ concentration required to achieve incremental recovery. Note that the primary recovery is the recovery achievable with a rate of 188,000 $m^3$/day and not the historical recovery efficiency. Despite the closer proximity of the injection wells in the north of the reservoir to the production well, these cases demonstrated a

better sweep of the reservoir and a more gradual increase in the $CO_2$ production rate. It therefore appears that there is greater heterogeneity present in the south of the reservoir, or there is a high permeability conduit leading to the channelling of $CO_2$ directly towards the production well. This heterogeneity does not appear to have a significant impact on the initial breakthrough of $CO_2$, but once the $CO_2$ has reached the production well, the greater channelling in the south of the reservoir causes a more rapid increase in the $CO_2$ production rate. The injection well location could therefore have a significant impact on the displacement process and the ability to maximise natural gas recovery whilst minimising $CO_2$ production.

**Table 7-2: The results from the testing of the injection well location.**

| **Well Location** | Location 1 | Location 2 | Location 3 | Location 4 | Location 5 |
|---|---|---|---|---|---|
| **Recovery Efficiency at 10% $CO_2$ Limit** | 53.6% | 54.4% | 52.2% | 54.1% | 52.7% |
| **Recovery Efficiency at 50% $CO_2$ Limit** | 74.8% | 74.9% | 70.5% | 73.9% | 69.4% |
| **Min. %$CO_2$ Concentration** | 33.0% | 34.0% | 44.7% | 37.8% | 47.7% |

As mentioned previously, this model has considerable heterogeneity, with a wide range of permeabilities. This range of permeabilities is expected to make stable viscous dominated displacement unfeasible. Previous results have shown that under gravity dominated displacement, the reduction of the influence of production, achieved in those particular cases by increased thickness, will reduce the severity of any coning of $CO_2$, greatly improving the sweep of the reservoir at the breakthrough of $CO_2$. Operationally, this can be achieved by altering the production and injection rates. Table 7-3 presents the results of four simulations where the production and injection rates have been altered. Injection and production rates at surface conditions are again equivalent in each case.

**Table 7-3: The results of the testing of the injection and production rates.**

| **Rates ($sm^3$/day)** | 100,000 | 150,000 | 200,000 | 250,000 |
|---|---|---|---|---|
| **Recovery Efficiency at 10% $CO_2$ Limit** | 58.4% | 54.4% | 52.2% | 51.2% |
| **Recovery Efficiency at 50% $CO_2$ Limit** | 79.3% | 76.0% | 73.1% | 70.8% |
| **Min. %$CO_2$ Concentration** | 28.0% | 33.8% | 38.3% | 46.2% |

The injection well in this instance is located in the middle of the reservoir in the vicinity of Location 2 in Figure 7.9. The results presented in Table 7-3 show that increasing the injection and production rates has a clear detrimental effect on the recovery of natural gas at both $CO_2$ production limits. As expected, the higher rates employed do not lead to a stable, viscous dominated displacement. Severe channelling along the higher permeability conduits is the resulting effect, as seen in Figure 7.10. This Figure compares two cross-sections where injection and production rates are 100,000 $m^3$/day and 250,000 $m^3$/day. Both screenshots display $CO_2$ concentration at the time when the producing $CO_2$ concentration has reached 5 mole percent for each respective case. Visually, the effect of the rates employed on the sweep is evident, particularly in the area around the production

well. A much greater concentration of $CO_2$ is present at the top of the structure for the lower rate scenario, indicating a more effective sweep of the reservoir than is the case for the higher rate scenario. Although the uneven advancement of $CO_2$ is apparent in both circumstances, greater gravity segregation, attributable to the lower rates, has led to $CO_2$ sweeping the natural gas from the bottom up which has been shown to be an efficient displacement process. On the other hand, stronger viscous forces attributable to higher rates in conjunction with the large range of permeabilities has led to the channelling of $CO_2$ along the higher permeability conduits, particularly at the top of the structure. As can be seen from the screenshot, this had led to a significant section of the reservoir remaining unswept at the breakthrough of $CO_2$. Consequently, lower rates have been shown to mitigate against the effect of heterogeneity, improving the efficiency of the displacement process. Further reductions in the rates employed could further enhance the stability of the displacement, however these reductions would need to be optimised with respect to the economics of the project.

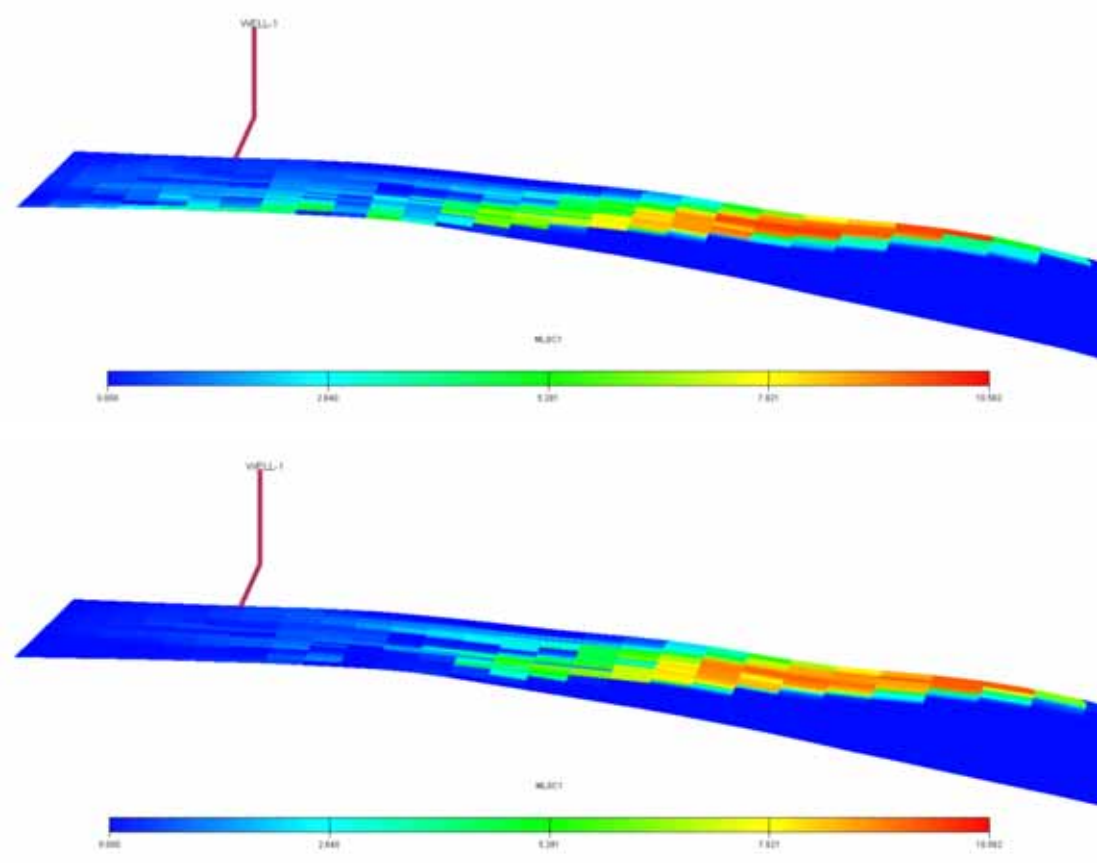

**Figure 7.10: Comparison of $CO_2$ concentration for a production/injection rate of 100,000 sm3/day (top) and 250,000 sm3/day (bottom) when the producing $CO_2$ concentration reaches 5 mole percent.**

It is important to note that the result of the variable injection and production rates is for that one particular location only, and is not necessarily representative of all locations in the model. It is therefore important to test the effect of operational parameters at a number of different locations

in the reservoir model. Again, the ED methodology is used to test a number of parameters concurrently and efficiently. Adding to this study, the resulting surrogate (proxy) equation will be used to optimise the chosen responses of the design, in order to maximise $CH_4$ recovery whilst minimising the producing $CO_2$ concentration.

## 7.4 Experimental Design Study

The aim of this study is to collectively test the effect of a number of operational parameters while also developing a surrogate equation that will enable the optimisation of these parameters to maximise natural gas recovery whilst minimising $CO_2$ production. The design parameters and corresponding ranges are presented in Table 7-4 while the design is presented in Table 7-5. To enable comparison of results with the previous studies, the same responses have been chosen for this study.

**Table 7-4: Parameters and the corresponding levels for the experimental design.**

| Parameter | Low (-1) Level | Mid (0) Level | High (+1) Level |
|---|---|---|---|
| Model Grid X Location | 30 | 35 | 40 |
| Model Grid Y Location | 17 | 33 | 49 |
| Timing of Injection* | 0% | 20% | 40% |
| Production Rate ($sm^3$/day) | 100000 | 150000 | 200000 |
| Injection Rate** | 100% | 125% | 150% |
| * Injection occurs after corresponding percent of the OGIP has been produced | | | |
| ** Percent of the production rate | | | |

**Table 7-5: Experimental design runs indicating parameter level combinations.**

| Run | X Location | Y Location | Timing of Injection (% of OGIP Produced) | Production Rate ($sm^3$/day) | Injection Rate (% of Production Rate) |
|---|---|---|---|---|---|
| 1 | 39 | 17 | 40 | 150000 | 150 |
| 2 | 30 | 17 | 40 | 133333.3 | 116.67 |
| 3 | 39 | 17 | 0 | 200000 | 100 |
| 4 | 40 | 49 | 0 | 100000 | 100 |
| 5 | 30 | 49 | 40 | 200000 | 150 |
| 6 | 40 | 38 | 0 | 200000 | 150 |
| 7 | 40 | 49 | 40 | 100000 | 150 |
| 8 | 33 | 17 | 0 | 100000 | 100 |
| 9 | 39 | 17 | 0 | 100000 | 150 |
| 10 | 40 | 49 | 40 | 200000 | 100 |
| 11 | 36 | 49 | 0 | 200000 | 116.67 |
| 12 | 30 | 17 | 40 | 200000 | 100 |
| 13 | 30 | 49 | 40 | 100000 | 100 |
| 14 | 30 | 17 | 0 | 200000 | 150 |
| 15 | 30 | 17 | 40 | 100000 | 150 |
| 16 | 30 | 49 | 0 | 150000 | 150 |
| 17 | 40 | 49 | 20 | 200000 | 150 |
| 18 | 40 | 38 | 0 | 200000 | 150 |
| 19 | 30 | 38 | 0 | 100000 | 116.67 |
| 20 | 39 | 17 | 40 | 200000 | 100 |
| 21 | 35 | 33 | 20 | 150000 | 100 |
| 22 | 39 | 17 | 40 | 100000 | 100 |
| 23 | 40 | 49 | 40 | 100000 | 100 |
| 24 | 30 | 49 | 40 | 200000 | 150 |
| 25 | 30 | 38 | 0 | 200000 | 100 |

The benefits of implementing the experimental design methodology are particularly apparent in this study. Five parameters have been chosen for investigation, all at three levels. If the one at a time strategy was to be employed, this would require $3^5$, or 243, simulations to be run in order to investigate the entire design space. With each simulation run time varying from between 2 – 10 hours, the time resources necessary to complete this study would be significant. The implementation of a D-Optimal design required only 25 simulations to be performed to acquire consistent information, a considerable saving in time resources.

The initial simulations performed on the Naylor model highlighted the significance of the correct choice of the operational strategy. The heterogeneity in the reservoir was shown to impact both the well location and the choice of rates. The placement of the injection well in the south of the reservoir led to a more rapid breakthrough of $CO_2$, potentially due to the channelling of $CO_2$ along a high permeability conduit. The results of studies performed in previous chapters have shown that both viscous and gravity dominated displacement can produce favourable results in the displacement of $CH_4$ by $CO_2$ in thin, non-dipping reservoirs. However, as was seen in the results of the initial investigation, the feasibility of viscous dominated displacement is reduced by the presence

of heterogeneity. A uniform displacement front was not possible with $CO_2$ preferentially flowing along the higher permeability streaks. Furthermore, higher permeability streaks in the upper section of the reservoir can provide conduits directly towards the producing completions. It was however noted that this result was for one location in the model, and does not necessarily represent what would occur in other locations in the reservoir. Consequently, both the well location and the injection and production rates have been chosen as parameters for the design. It was shown in Study 2B that the timing of $CO_2$ injection can have contrasting effects on the recovery of natural gas in the presence of heterogeneity. Delaying the injection of $CO_2$ was shown to be beneficial in maximising natural gas recovery at the initial breakthrough of $CO_2$. However, once $CO_2$ had reached the production well, a more rapid increase in the production of $CO_2$ occurred when injection was delayed. This result was apparent in a model with only simple heterogeneity. The more complex heterogeneity present in the Naylor model is expected to exacerbate the effect of the timing of $CO_2$ injection, and so this parameter has also been included in the design.

This study uses one vertical well for the injection of $CO_2$. Due to the small size of the Naylor field, it was decided that using two injection wells would, in reality, be prohibitively expensive. Additionally the use of horizontal wells was considered economically and technically unfeasible. The use of horizontal wells in non-dipping reservoirs is more beneficial in thicker reservoirs. The thin nature of the Naylor field, and the extra cost associated with horizontal wells precluded the implementation of horizontal wells in this instance.

### 7.4.1 Results and discussion for Response 1: Natural Gas Recovery Efficiency at a 10% $CO_2$ Breakthrough Limit

A graph of the results of each of the design runs is presented in Figure 7.11. Natural gas recovery over the runs tested range from 49% to almost 65% of the OGIP. This large range highlights the significant influence the operational parameters chosen for this design can have on the recovery of natural gas and therefore the viability of a $CO_2$ EGR project.

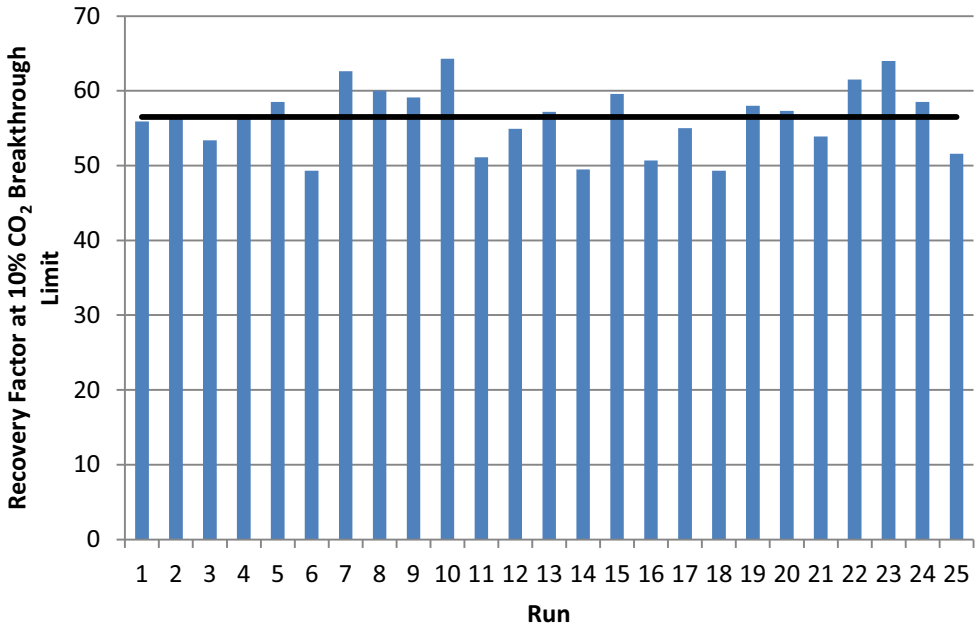


**Figure 7.11: The result for individual design runs with regard to Response 1. The average of all runs is shown in black.**

Table 7-6 presents the ranking of statistically significant coefficients in determining the natural gas recovery achievable at the 10% $CO_2$ limit. This Table indicates that all of the input parameters have a statistically significant effect, however the production rate and the timing of $CO_2$ injection are clearly the most influential parameters.

**Table 7-6: Ranking of statistically significant coefficients from the analysis of Response 1.**

| Statistically Significant Coefficients | F Value | p-value Prob > F |
|---|---|---|
| Timing of Injection | 361.38 | <0.0001 |
| Production Rate | 358.52 | <0.0001 |
| Y Location*Timing of Injection | 106.73 | <0.0001 |
| Timing of Injection*Production Rate | 81.28 | <0.0001 |
| Y Location*Production Rate | 73.01 | <0.0001 |
| X Location | 68.44 | <0.0001 |
| X Location*Timing of Injection | 32.57 | 0.0007 |
| Injection Rate | 31.27 | 0.0008 |
| X Location*Injection Rate | 25.51 | 0.0015 |
| Production Rate*Injection Rate | 21.51 | 0.0024 |
| Production Rate$^2$ | 18.28 | 0.0037 |
| X Location$^2$ | 17.60 | 0.0041 |
| Injection Rate$^2$ | 9.21 | 0.0190 |
| Timing of Injection*Injection Rate | 8.53 | 0.0223 |

Regression diagnostics were excellent, with $R^2$ and adjusted $R^2$ coefficients of 0.9961 and 0.9865 respectively. Additionally, the normal probability plot once more showed no major deviation from the normality assumption (Figure 7.12).

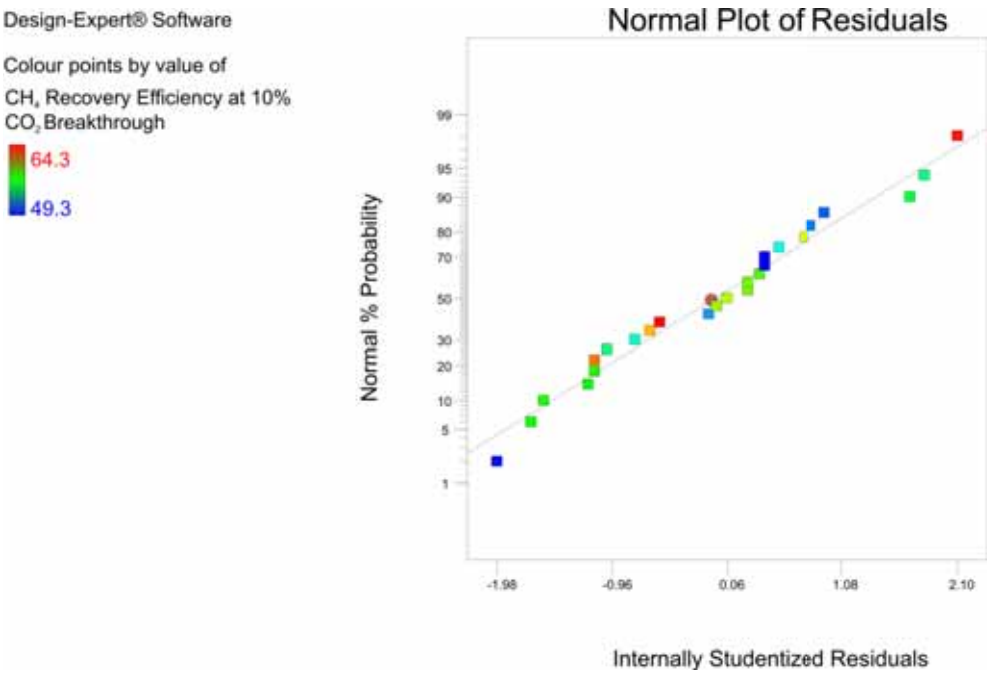


**Figure 7.12: The normal probability plot for the analysis of Response 1.**

Main effect of the timing of injection

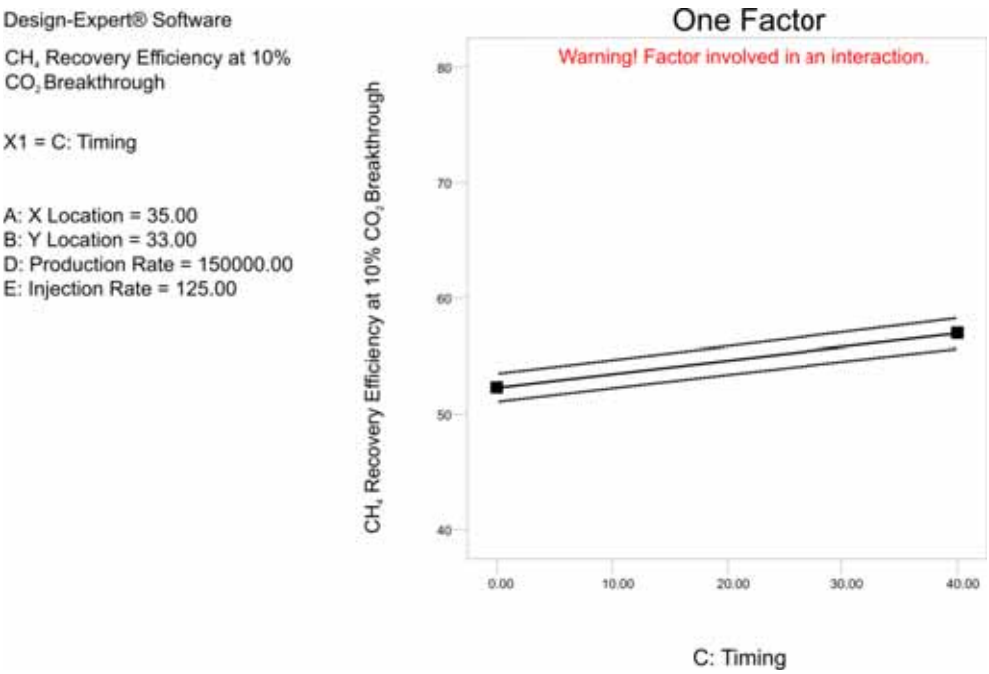


**Figure 7.13: Effect graph for the main effect of the timing of $CO_2$ injection.**

Figure 7.13 indicates that delaying the injection of $CO_2$ will improve the recovery of natural gas at the 10% $CO_2$ limit. From the analysis of the equivalent response in Study 2B, it was found that delaying the injection of $CO_2$ in the presence of heterogeneity improved $CH_4$ recovery. With greater heterogeneity present in this model as compared to that used in Chapter 6, it was expected that the

timing of injection would also have a significant effect. This heterogeneity leads to channelling of $CO_2$ along the high permeability zones, negatively impacting on the sweep of the reservoir. As found in Study 2B, delaying the injection of $CO_2$ allows for a period of primary production without the contamination of $CO_2$, and the increased water saturation in gas zone restricts the mobility of $CO_2$ along higher permeability zones.

The main effect of the production rate

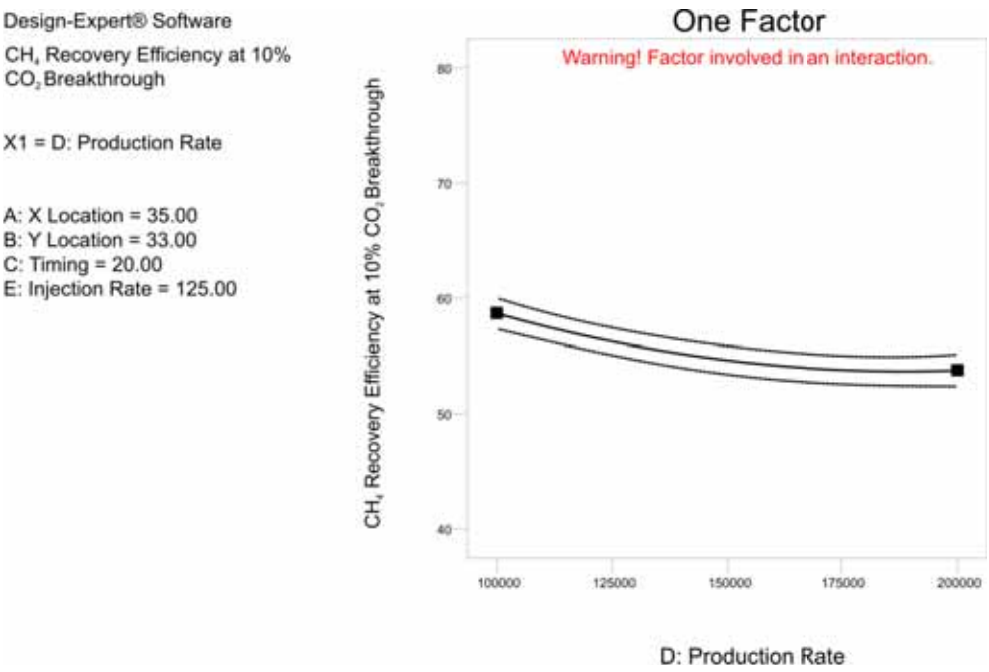


**Figure 7.14: Effect graph for the main effect of the production rate.**

The effect graph for the main effect of the production rate (Figure 7.14) confirms that attempting to achieve a viscous dominated displacement process in a heterogeneous reservoir will lead to significant uneven advancement of the displacement front, reducing the sweep efficiency of the displacement process and reducing natural gas recovery. Allowing gravity segregation to occur aids in mitigating against the effect of the heterogeneity present, as found in Study 2B. A more efficient sweep of the reservoir is achievable resulting in an improvement in the recovery of natural gas at the 10% $CO_2$ production limit.

Y location – timing of injection interaction

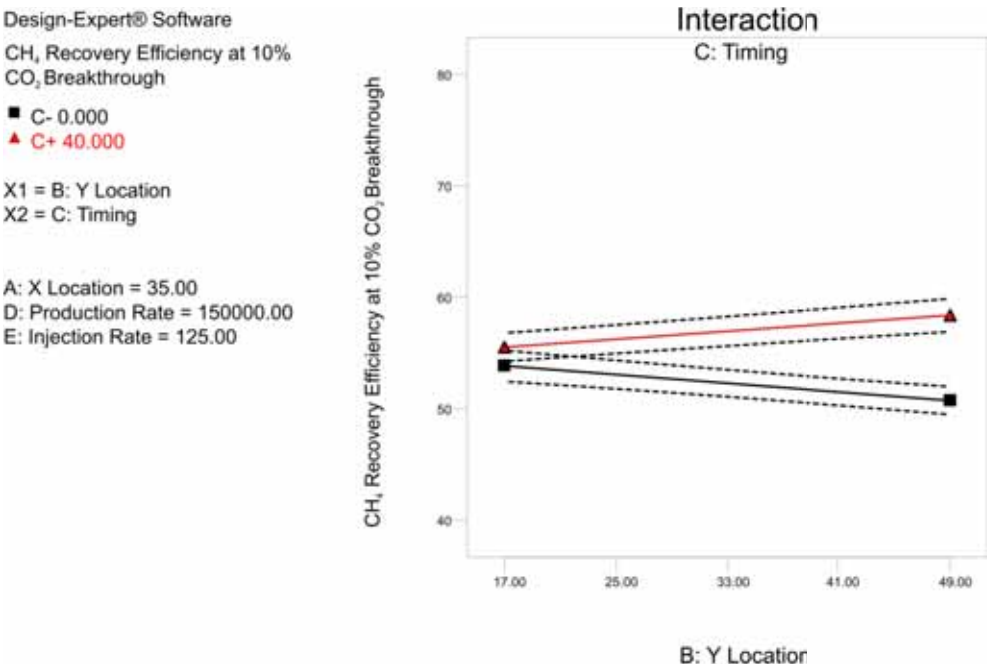


**Figure 7.15: Effect graph for the interaction between the timing of $CO_2$ injection and the Y location of the injection well.**

Figure 7.15 shows that delaying the injection of $CO_2$ is particularly beneficial with the injection well located in the south of the reservoir. As was concluded from the initial investigations from Section 7.3, the early injection of $CO_2$ with the injection well located in the south of the reservoir (Y location = 49) results in premature $CO_2$ breakthrough, and consequently a lower recovery. Inspection of the model between the southern injector and the producer indicates the presence of a laterally continuous high permeability layer in the lower part of the cross-section (Figure 7.16). The early injection of $CO_2$ leads to channelling of $CO_2$ along this layer directly towards the production well resulting in poor sweep of the reservoir at the breakthrough of $CO_2$. Even though the distance between the injector and producer is smaller with the injection well located in the north (Y location = 17), a greater sweep of the reservoir results.

However, as demonstrated in Figure 7.15, delaying the injection of $CO_2$ will maximise natural gas recovery with the injector located in the south of the reservoir. Allowing the aquifer to advance into the gas zone increases the water saturation in the high permeability layer, and as depicted in Figure 7.17, gravity segregation assists in mitigating against the effect of this layer.

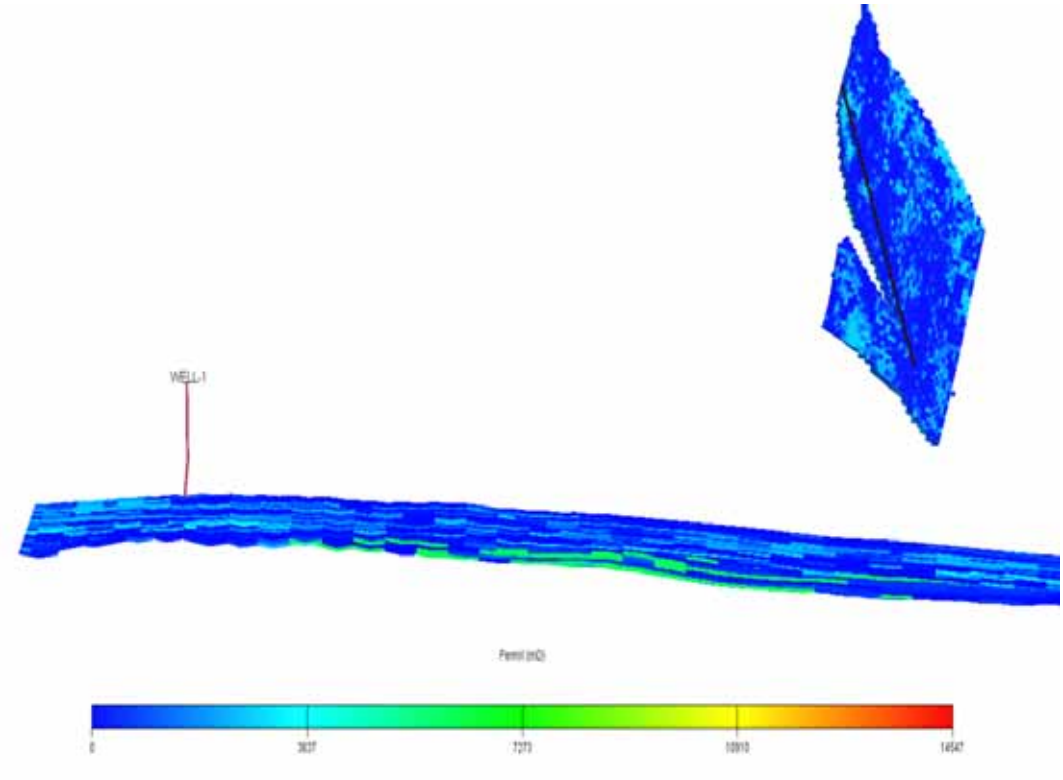


**Figure 7.16: Cross-section from the production well to the injection well located in the south of the reservoir. The continuous higher permeability streak can be seen in green in the lower section of the cross-section.**

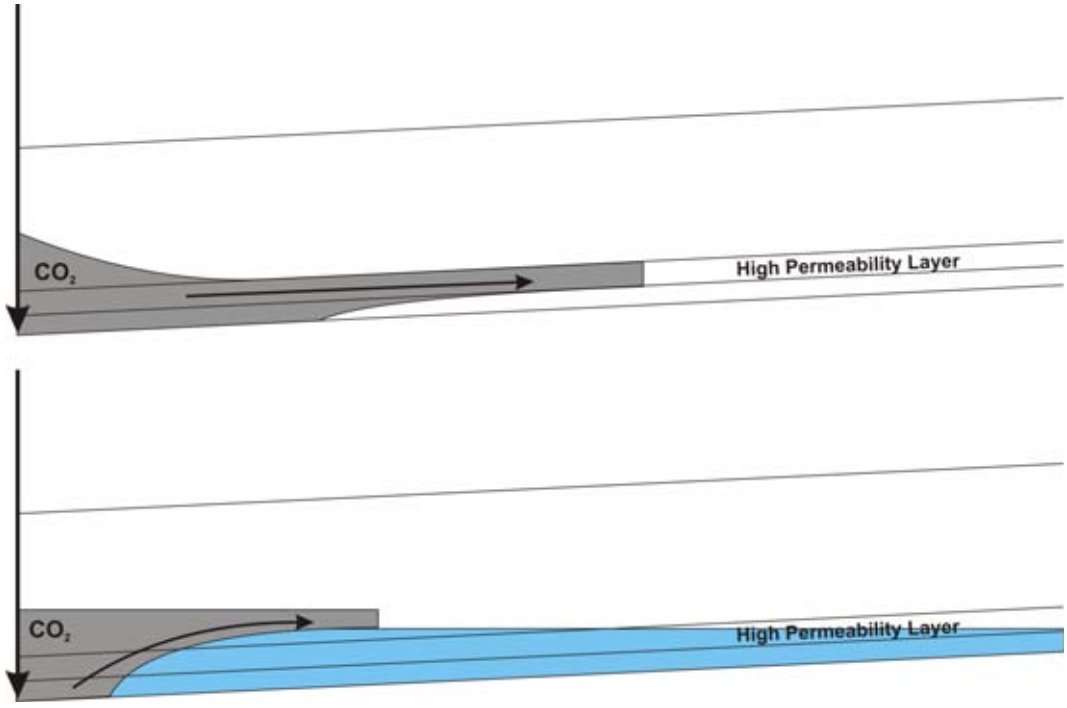


**Figure 7.17: Schematic of the effect of the high permeability layer when (a) injection is not delayed (top) and (b) injection is delayed (bottom) where the invaded zone is represented in blue. If injection is delayed, gravity segregation leads to the bypassing of the high permeability layer.**

Timing of injection – production rate interaction

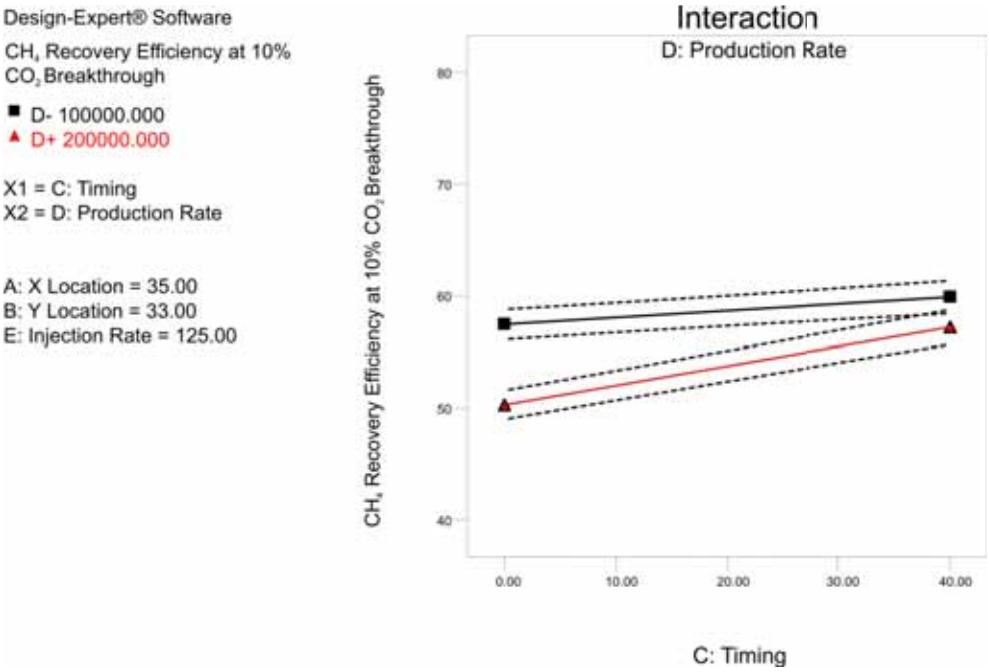


**Figure 7.18: Effect graph for the interaction between the timing of $CO_2$ injection and the production rate.**

Figure 7.18 illustrates the detrimental effect of stronger viscous forces, attributable in this instance to higher production and therefore injection rates, when the injection of $CO_2$ is not delayed. While stronger viscous forces are beneficial in allowing a greater volume of the invaded zone to be swept as injection is delayed, over the range of injection timing tested, lower rates will always achieve greater natural gas recovery at the 10% $CO_2$ limit. it can be seen in the effect graph that the ability to displace natural gas residually trapped in the invaded zone becomes increasingly more important as injection is delayed, indicated by the steeper slope of the high level of the production rate. If injection was to be delayed further than that tested in the design, it would be expected that a greater recovery of natural gas would result from the implementation of higher rates.

Y location – production rate interaction

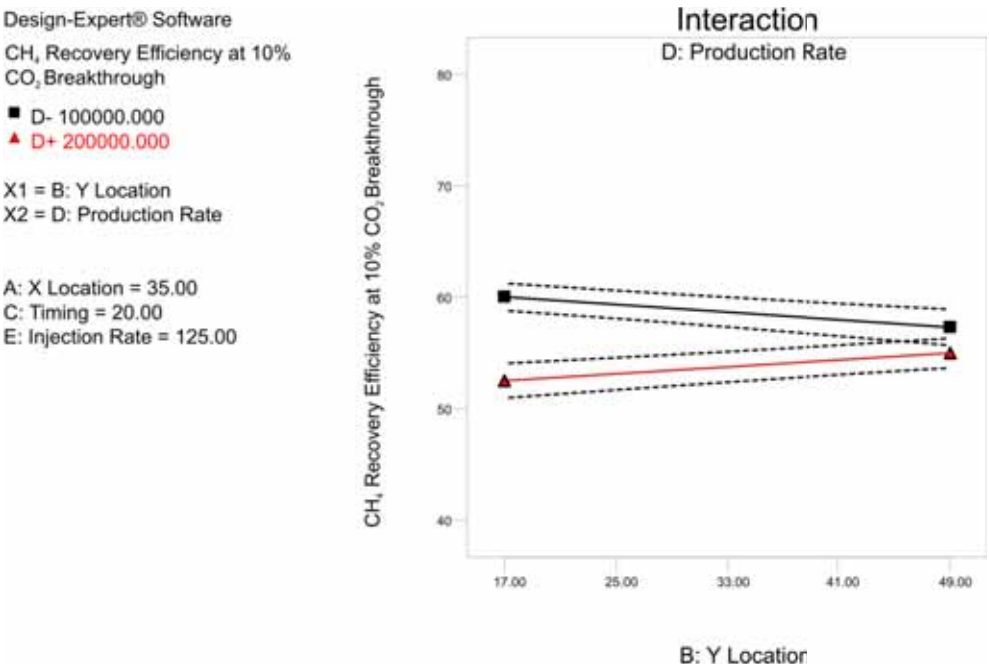


**Figure 7.19: Effect graph for the interaction between the Y location of the injection well and the production rate.**

It is clear from the effect graph for the Y location – production rate interaction (Figure 7.19) that the effect of the production rate is greater with the well located in the north, rather than the south. The presence of greater heterogeneity between the southern injection well and the producer, in the form of the high permeability streak, compared with the northern injector is likely the reason behind this effect. Regardless of the injection rate employed, when injected in the south of the reservoir $CO_2$ will rapidly migrate along this high permeability streak towards the production well. The greater permeability homogeneity in the north of the reservoir consequently leads to the sweep of $CO_2$ being dictated to a greater extent by the choice of rates rather than by the permeability. Lowering the rates allows for gravity to stabilise the displacement process, limiting the detrimental effect of the heterogeneity present.

A noticeable aspect in Figure 7.19 is that locating the injector in the north of the reservoir (Y location = 17) achieves maximum $CH_4$ recovery. It is important to note that this effect graph is constructed with the timing of injection equal to the mid level (i.e. after 20% of the OGIP has been produced). From the effect graph of the Y location – timing of injection effect graph (Figure 7.15) that the optimal choice of the Y location of the injector is dependent on the timing of injection. If injection is not delayed, injection should occur in the north of the reservoir (Y location = 17), while the injector should be located in the south if injection occurs after 40% of the OGIP has been produced. It is clear from Figure 7.19 that after 20% of the OGIP has been produced, it is still advantageous to inject in the north of the reservoir. However, the main effect of the timing of injection indicated $CH_4$ recovery

is maximised when injection occurs after 40% of the OGIP has been produced, and so the injector should be located in the south of the reservoir. The effect graph for the Y location – production rate interaction indicates that the effect of varying the production rate will not be as significant with the injector located in the south of the reservoir.

Main effect of the X location

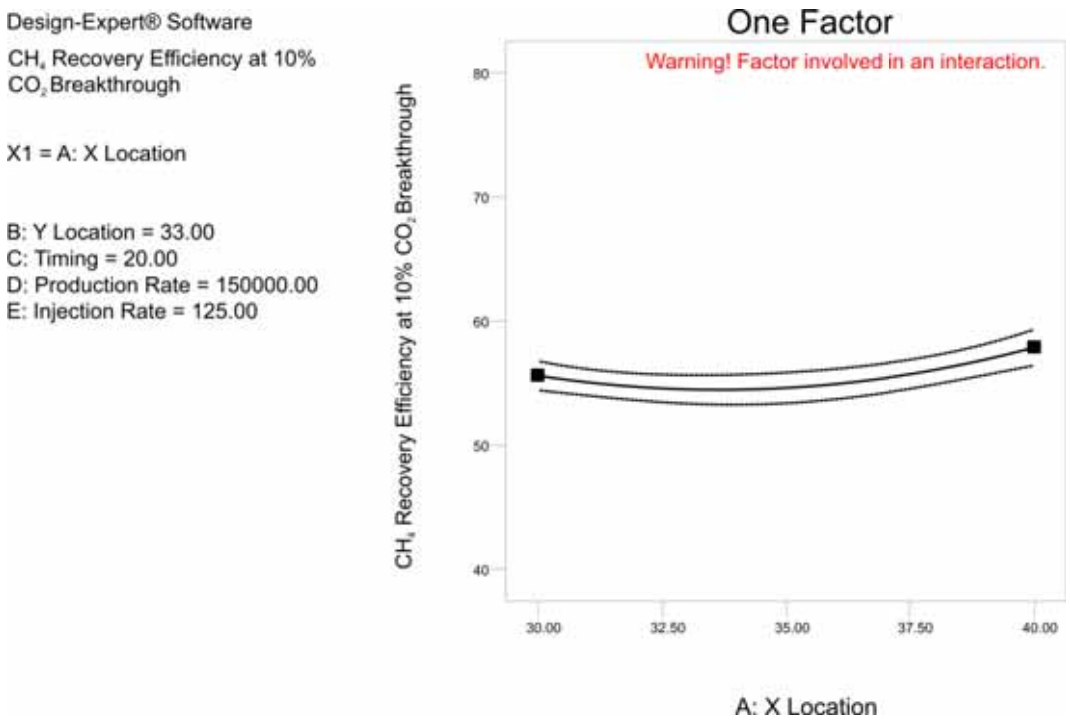


**Figure 7.20: Effect graph for the main effect of the X location of the injection well.**

The last statistically significant coefficient that will be discussed is the main effect of the X-location. The effect graph exhibits some degree of curvature (Figure 7.20), but the general effect is that locating the injection well further into the aquifer will improve natural gas recovery at the breakthrough of $CO_2$. Injection further into the aquifer will temporarily restrict the mobility of the $CO_2$, delaying the breakthrough of $CO_2$ and improving recovery.

Summarising the results of the discussed effect graphs, to maximise natural gas recovery at the initial breakthrough of $CO_2$, the choice of operational parameters should be:

- Delay the injection of $CO_2$
- Lower the production (and injection rate)
- Locate the injection well in the south of the reservoir
- Locate the injection well further into the aquifer

As part of the analysis, a regression model was developed representing the input data (from which the effect graphs are constructed) which can be used as a surrogate to reservoir simulation. As mentioned in Chapter 4, a primary aim of implementing the ED methodology in oil and gas studies is to build a meaningful probability distribution using a subset of all possible combinations of input parameters. The resultant surrogate, or proxy, equation can therefore be used in place of reservoir simulation for predictive or optimisation purposes, saving considerable time and money provided the proxy equation is representative of the solution space.

Equation 7.1 presents the proxy equation from the analysis of Response 1. Using the Excel Solver tool, this Equation was optimised to obtain the parameter level combination which maximises $CH_4$ recovery at the 10% $CO_2$ level, presented in Table 7-7. The optimisation process confirmed that injection should be delayed with the injector located in the south of the reservoir and further into the aquifer. Injection and production rates should be low to mitigate against the effects of heterogeneity. This combination of parameters levels achieves a natural gas recovery efficiency of 64.3%.

$$CH_4\ RF\ at\ 10\%\ CO_2 = 54.61 + 1.14A - 0.062B + 2.33C - 2.46D - 0.82E + 0.31AB + 0.73AC - 0.65AE + 1.50BC + 1.30BD + 0.26BE + 1.12CD + 0.38CE - 0.64DE + 2.12A^2 + 1.59D^2 - 1.30E^2 \quad (7.1)$$

Where A is the grid X location, B is the grid Y location, C is the timing of injection, D is the production rate, and finally E is the injection rate. Note that these letters represent the same parameters in the following equations in this Chapter (Equation 7.2 and Equation 7.3).

**Table 7-7: The parameter level combination in coded form (-1, 0, +1) which optimises Response 1.**

| X-location (A) | Y-location (B) | Timing of $CO_2$ injection (C) | Production Rate (D) | Injection Rate (E) | Recovery Efficiency at 10% $CO_2$.Breakthrough Limit |
|---|---|---|---|---|---|
| 1 | 1 | 1 | -1 | -0.073 | 64.3% |

Comparison of the optimised recovery efficiency with the historical recovery shows that the optimised recovery is some 8 x $10^6$ $sm^3$ short of the historical gas production (95.2 x $10^6$ $sm^3$). Note that the OGIP as calculated from the simulation model (135.6 x $10^6$) is smaller than the volume stated in Table 7-1 (147 x $10^6$ $m^3$). From this point the reference OGIP will be based upon the simulated OGIP. The simulated primary depletion based on a production rate of 100,000 $sm^3$/day achieved a primary recovery of 96.9 x $10^6$ $sm^3$ at the breakthrough of water. Consequently, the recovery from the optimised $CO_2$ injection case is also not sufficient to achieve incremental recovery over the simulated primary depletion case with a producing $CO_2$ concentration of less than 10%.

To ensure the proxy equation can be confidently applied as a surrogate to numerical simulation, a verification of the predictive capability of the equation must be performed. To do so, additional runs at levels which are not part of the design are simulated. In this study, 10 additional simulations were performed, with the results with respect to Response 1 shown in Table 7-8.

**Table 7-8: The comparison of the error between predicted and simulated (calculated) results for Response 1.**

| Confirmation Run | X Local | Y Local | Timing | Production Rate | Injection Rate | Predicted RF at 10% $CO_2$ Limit | Calculated RF at 10% $CO_2$ Limit | % Error |
|---|---|---|---|---|---|---|---|---|
| 1 | 30 | 17 | 0 | 100,010 | 123% | 62.3 | 59.4 | 4.7 |
| 2 | 35 | 30 | 40 | 200,000 | 150% | 54.3 | 55.3 | 1.8 |
| 3 | 40 | 40 | 20 | 150,000 | 125% | 58.0 | 53.4 | 7.9 |
| 4 | 40 | 20 | 15 | 100,000 | 135% | 61.9 | 59.3 | 4.2 |
| 5 | 35 | 20 | 35 | 175,000 | 125% | 54.6 | 53.0 | 2.9 |
| 6 | 31 | 26 | 23 | 140,000 | 110% | 55.7 | 54.7 | 1.8 |
| 7 | 35 | 17 | 0 | 100,000 | 100% | 59.8 | 60.2 | 0.7 |
| 8 | 35 | 17 | 0 | 200,000 | 100% | 51.4 | 53.5 | 4.1 |
| 9 | 30 | 17 | 0 | 100,000 | 100% | 61.2 | 60.0 | 2.0 |
| 10 | 30 | 17 | 0 | 100,000 | 150% | 60.9 | 58.7 | 3.6 |

The comparison of predicted results for Response 1 show good agreement with the simulated results (Table 7-8). The maximum error exhibited in these 10 additional runs for Response 1 was just short of 8% (Run 3), however the remaining nine runs have an error of less than 5%. The Root Mean Square Error (RMSE), which is the square root of the variance of the residuals, gives an indication of the absolute fit of the model to the data. It is an absolute fit as the units of the RMSE are the same as the response variable. The RMSE of the results of the confirmation runs for Response 1 is 2.27%. With recovery efficiencies for the first response ranging from 50 – 60%, the average error in the prediction is less than 5%.

### 7.4.2 Results and discussion of Response 2: Natural Gas Recovery Efficiency at a 50% $CO_2$ Breakthrough Limit

The outcome from Response 1 was that incremental recovery would only be achievable with a $CO_2$ concentration greater than 10 mole percent. As incremental recovery is not able to be achieved prior to the breakthrough of $CO_2$, the rate of increase in $CO_2$ production is now integral in determining the potential to achieve incremental recovery with the lowest possible producing $CO_2$ concentration.

The average natural gas recovery efficiency at the 50% $CO_2$ limit increases by almost 20% from the average recovery at the 10% $CO_2$ limit to 73.4% as shown in Figure 7.21. The range of results is again large, with the difference between the lowest and highest recovery efficiencies equating to around 13% of the OGIP. The majority of runs however achieve a recovery efficiency in the range of 70 – 80% of the OGIP.

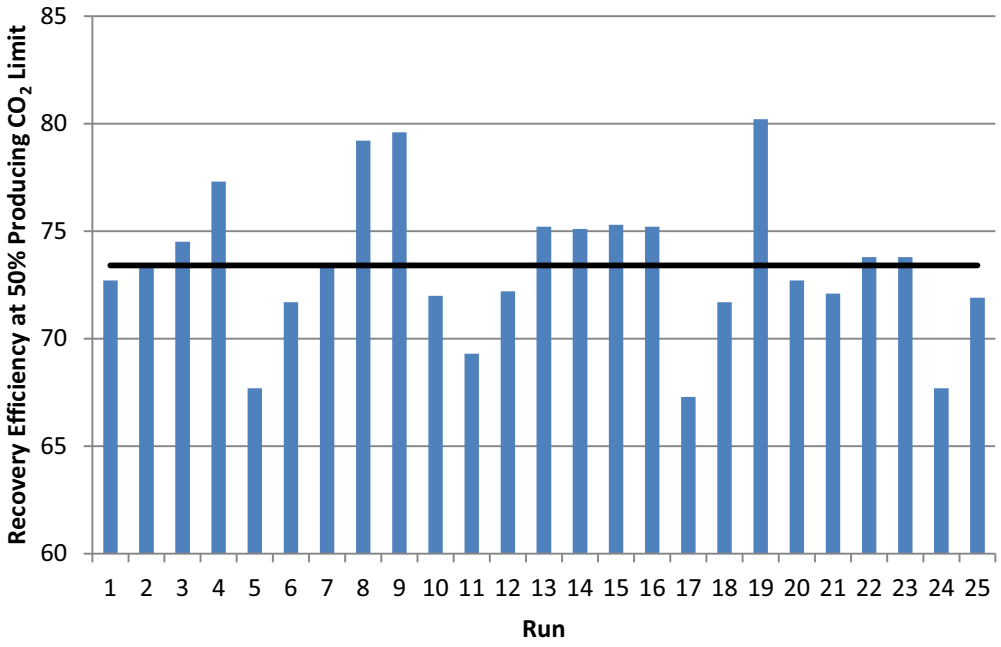


**Figure 7.21: The result for individual design runs with regard to Response 2. The average of all runs is shown in black.**

The ranking of statistically significant coefficients for Response 2 (Table 7-9) shows similar results to that of Response 1, except that the main effect of the production rate is by far the most influential coefficient.

**Table 7-9: Ranking of statistically significant coefficients from the analysis of Response 2.**

| Statistically Significant Coefficients | F Value | p-value Prob > F |
|---|---|---|
| Production Rate | 537.59 | <0.0001 |
| Timing of Injection | 283.74 | <0.0001 |
| Y Location | 89.94 | <0.0001 |
| Timing of Injection*Production Rate | 67.47 | <0.0001 |
| X Location*Production Rate | 29.48 | 0.0004 |
| Y Location*Production Rate | 23.69 | 0.0009 |
| Timing of Injection$^2$ | 23.01 | 0.0010 |
| Y Location*Timing of Injection | 19.24 | 0.0018 |
| X Location*Timing of Injection | 11.52 | 0.0080 |
| Timing of Injection*Injection Rate | 9.73 | 0.0123 |
| Production Rate*Injection Rate | 9.35 | 0.0136 |
| Y Location*Injection Rate | 6.18 | 0.0346 |

The $R^2$ and adjusted $R^2$ coefficients are 0.9935 and 0.9828 again suggesting that the regression model adequately represents the data. The normal probability plot (Figure 7.22) shows no major deviation from the normality assumption.

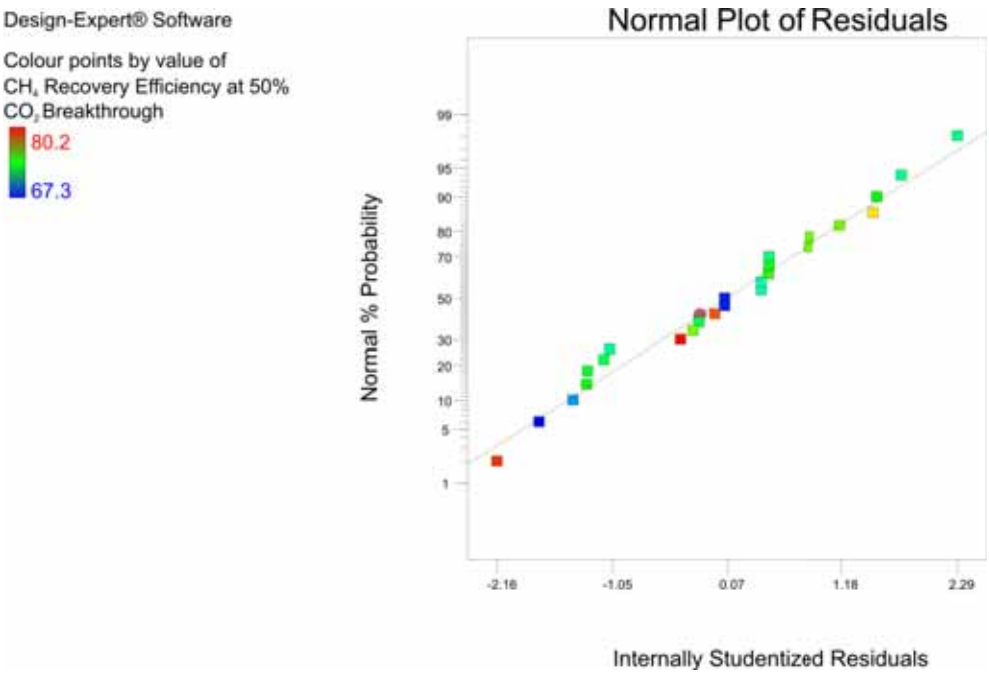


**Figure 7.22: The normal probability plot from the analysis of Response 2.**

The main effect of the production rate

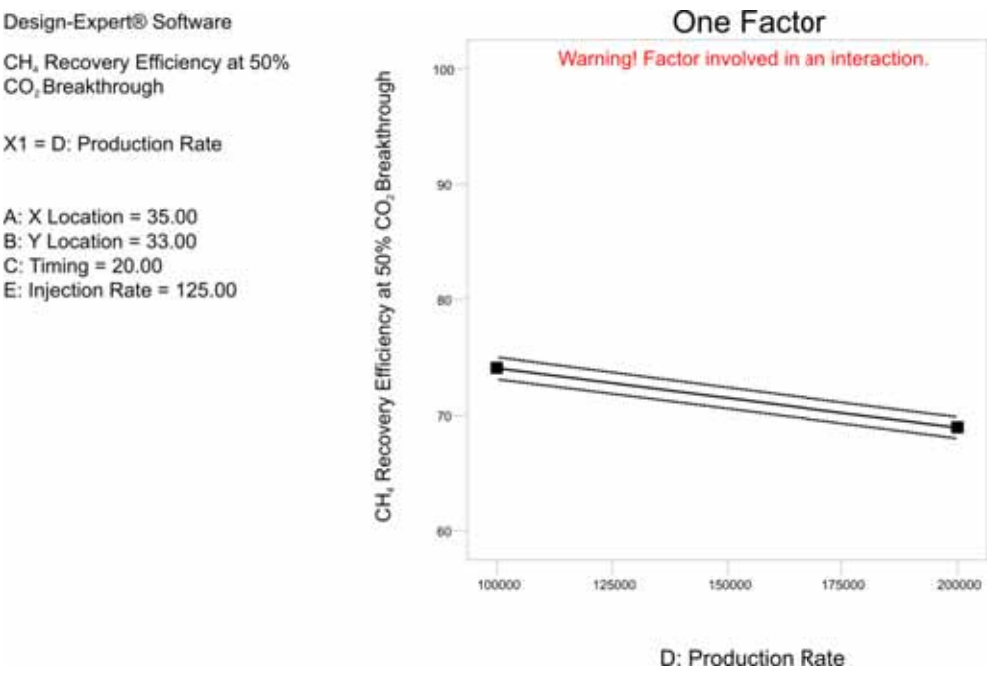


**Figure 7.23: The effect graph for the main effect of the production rate for Response 2.**

Once more, increasing the production rate has a negative impact on recovery (Figure 7.23). As previously mentioned, higher rates lead to more viscous dominated displacement, which in the presence of heterogeneity leads to the uneven advancement of the front. This preferential flow along the high permeability layers leads to both the early breakthrough of $CO_2$ as well a faster rate of

increase in $CO_2$ production. Lowering the rates, allowing gravity to stabilise the displacement will decrease the rate of increase in $CO_2$ production, thereby improving natural gas recovery.

The main effect of the timing of injection

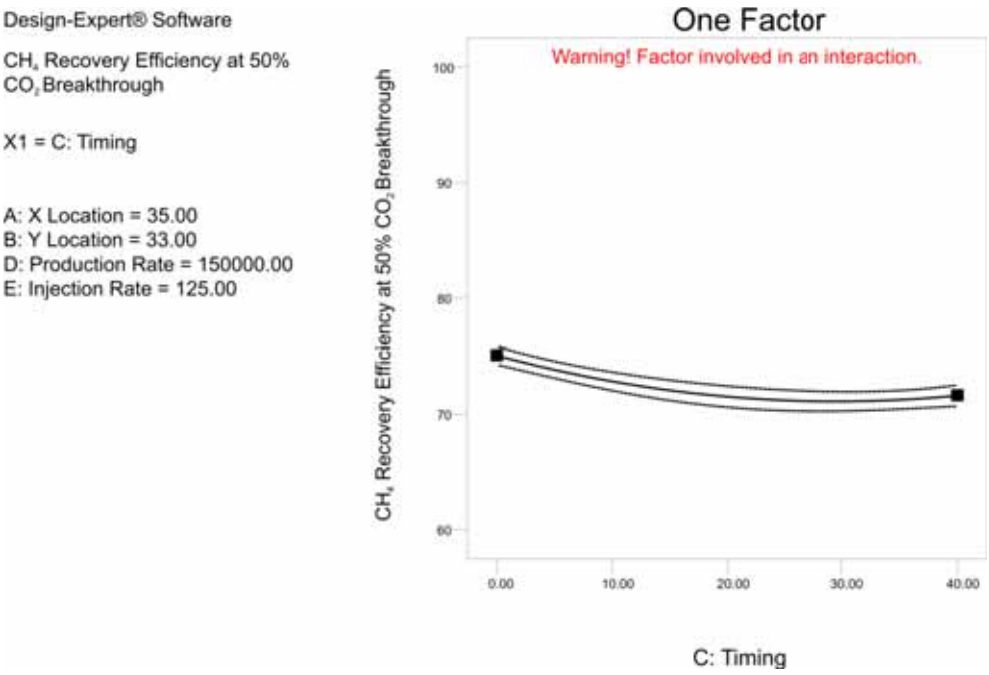


**Figure 7.24: The effect graph for the main effect of the timing of $CO_2$ injection for Response 2.**

In a result reflecting that found in Study 2B, the timing of $CO_2$ injection has the opposite effect on natural gas recovery at the 50% $CO_2$ limit than it does at the 10% $CO_2$ limit (Response 1). While delaying the injection of $CO_2$ might delay the initial breakthrough of $CO_2$ at the production well, it will result in a more rapid increase in the production of $CO_2$ (Figure 7.24). With incremental recovery in this particular instance only achievable with a producing $CO_2$ concentration of greater than 10%, this is a particularly important coefficient. For instance, in Response 1 Figure 7.15 indicated that if injection is to be delayed, the injector should be located in the south of the reservoir. However, if injection is not delayed, natural gas recovery at the 10% $CO_2$ limit would be maximised with the injector located in the north of the reservoir.

The main effect of the Y location

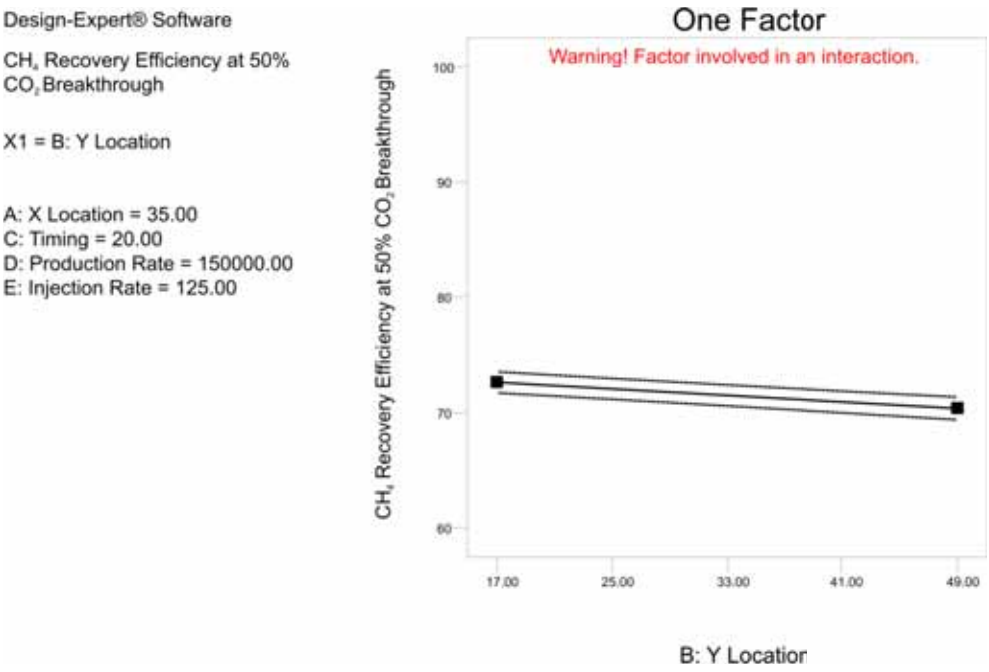


**Figure 7.25: The effect graph for the main effect of the Y location for Response 2.**

The effect graph for the main effect of the Y location for Response 2 (Figure 7.25) shows that recovery at the 50% $CO_2$ limit will be maximised with the injector located in the north of the reservoir. Therefore, while the result of Response 1 suggested that natural gas recovery at the 10% $CO_2$ limit will be maximised with the injector in the south of the reservoir, the more rapid increase in $CO_2$ production attributable to delayed injection means that this option will result in a lower natural gas recovery once the producing $CO_2$ concentration has reached 50%. The optimisation of Response 1 showed that incremental recovery cannot be achieved with a producing $CO_2$ concentration of less than 10%, and so more weight is given to the results of Response 2. Therefore, while locating the injector in the north of the reservoir might not achieve the highest recovery efficiency at the 10% $CO_2$ limit, it will result in a more gradual increase in the production of $CO_2$ and therefore maximise recovery at the 50% $CO_2$ limit.

Timing of injection – production rate interaction

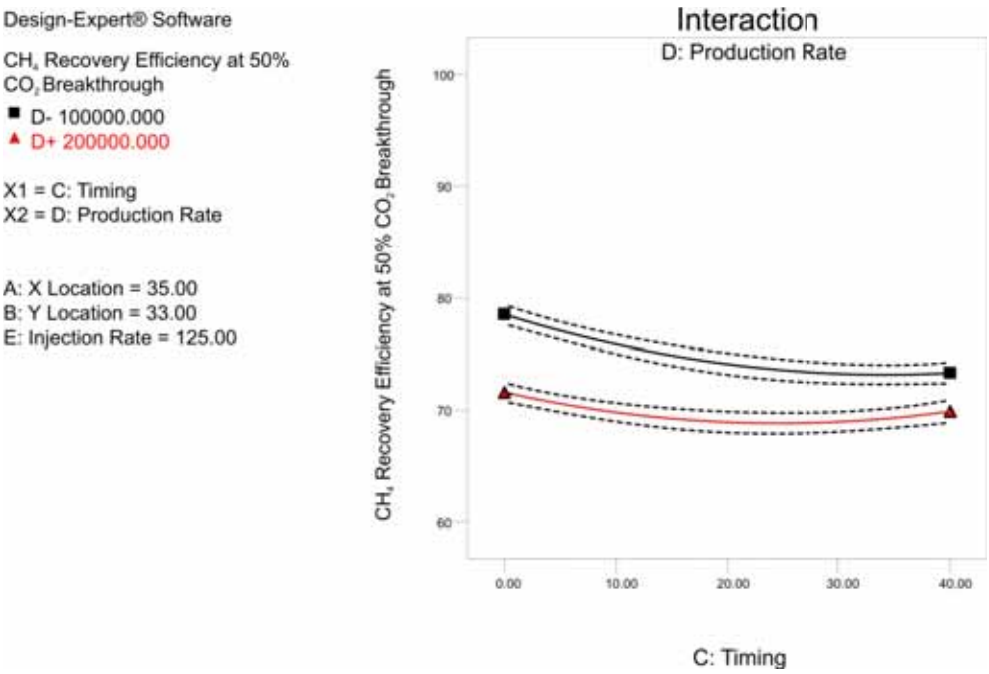


**Figure 7.26: The effect graph for the interaction between the timing of $CO_2$ injection and the production rate for Response 2.**

Figure 7.26 shows that commencing the injection of $CO_2$ early and implementing lower rates will maximise natural gas recovery at the 50% $CO_2$ limit, mimicking the trends of the respective effect graphs for the main effects of the production rate (Figure 7.23) and the timing of injection (Figure 7.24). The effect graph for the interaction of these parameters does however indicate the benefit of higher rates in improving the sweep of the invaded zone through the narrowing of the difference in recovery efficiencies between the levels of the production rates. Although over the range of injection timings tested, lower rates will maximise natural gas recovery at the 50% $CO_2$ limit.

Summarising the results of the second response, maximising natural gas recovery at a $CO_2$ production limit of 50 mole percent is achieved by:

- Lowering the injection and production rates as much as economically possible
- Injecting $CO_2$ at the commencement of natural gas production
- Locating the injection well in the north-east of the reservoir

Based upon the proxy equation developed (Equation 7.2) from the analysis of the design for Response 2, the parameter levels which maximise the recovery of natural gas at the $CO_2$ limit of 50% are shown in Table 7-10. Note the parameters in Equation 7.2 (A, B, C, D, E) are the same as in Equation 7.1.

$$CH_4\ RF\ at\ 50\%\ CO_2 = 71.51 - 0.26A - 1.14B - 1.73C - 2.59D - 0.19E + 0.37AC + 0.63AD + 0.47BC - 0.63BD - 0.29BE + 0.88CD - 0.35CE - 0.36DE + 1.01A^2 + 1.82C^2 \qquad (7.2)$$

**Table 7-10: The parameter level combination in coded form (-1, 0, +1) which optimises the natural gas recovery for Response 2.**

| X-location (A) | Y-location (B) | Timing of $CO_2$ injection (C) | Production Rate (D) | Injection Rate (E) | Recovery Efficiency at 50% $CO_2$ Breakthrough Limit |
|---|---|---|---|---|---|
| -1 | -1 | -1 | -1 | 1 | 82.6% |

From the effect graphs it appears that, although the relative effect of the statistically significant coefficients might be large (Table 7-9), the absolute effect on the recovery efficiency of natural gas is minor. For instance, the difference between the maximum and minimum recovery efficiencies for the high and low levels of the production rate is just over 5% of the OGIP (Figure 7.23). However, when combining the effects of all of the statistically significant coefficients, the total effect on the recovery efficiency can be quite large. Optimisation of the proxy equation (Equation 7.2) to maximise recovery achieved a recovery efficiency of 82% at the 50% $CO_2$ limit (Table 7-10). However, if the optimisation process is conducted in reverse to minimise the recovery at the 50% $CO_2$ limit, a recovery efficiency of just 66% is achieved (Table 7-11). This equates to a difference of 16% between the maximum and minimum recovery efficiencies achievable. Although the individual effect of each parameter might be minor, the combination of parameters can significantly influence the performance of the process. This result highlights the importance of performing a study of this nature in order to determine the impact of operational parameters so that the correct decisions can be made in order to maximise the natural gas recovery.

**Table 7-11: The parameter level combination in coded form that minimises the natural gas recovery for Response 2.**

| X-location (A) | Y-location (B) | Timing of $CO_2$ injection (C) | Production Rate (D) | Injection Rate (E) | CH4 Recovery Efficiency at 50% $CO_2$ Breakthrough Limit |
|---|---|---|---|---|---|
| -0.224 | 1 | 0.223 | 1 | 1 | 66.2% |

A recovery efficiency of 82% equates to a production volume of 112 x $10^6$ sm3. This is some 17 x $10^6$ $sm^3$ greater than the historical production, and 15 x $10^6$ $sm^3$ greater than the simulated primary recovery achievable with a production rate of 100,000 $sm^3$/day.

The predictive capability of the proxy equation for Response 2 improves on that exhibited by Response 1 (Table 7-12). The predicted values for all of the confirmation runs have an error percentage of less than 4%. Consequently, the RMSE for the confirmation runs is a low 1.86%, which is particularly good considering the recovery efficiencies range from 70 – 80%. The predictive capability of the proxy equation for Response 2 is therefore excellent.

**Table 7-12: The comparison of the error between predicted and simulated (calculated) results for Response 2.**

| Confirmation Run | X Local | Y Local | Timing | Production Rate | Injection Rate | Predicted RF at 50% $CO_2$ Limit | Calculated RF at 50% $CO_2$ Limit | % Error |
|---|---|---|---|---|---|---|---|---|
| 1 | 30 | 17 | 0 | 100,010 | 123% | 81.7 | 79.9 | 2.2 |
| 2 | 35 | 30 | 40 | 200,000 | 150% | 69.3 | 69.6 | 0.4 |
| 3 | 40 | 40 | 20 | 150,000 | 125% | 71.8 | 71.3 | 0.7 |
| 4 | 40 | 20 | 15 | 100,000 | 135% | 75.6 | 78.0 | 3.2 |
| 5 | 35 | 20 | 35 | 175,000 | 125% | 71.2 | 73.6 | 3.4 |
| 6 | 31 | 26 | 23 | 140,000 | 110% | 73.1 | 75.5 | 3.3 |
| 7 | 35 | 17 | 0 | 100,000 | 100% | 78.7 | 79.2 | 0.6 |
| 8 | 35 | 17 | 0 | 200,000 | 100% | 73.7 | 75.0 | 1.8 |
| 9 | 30 | 17 | 0 | 100,000 | 100% | 81.0 | 79.3 | 2.1 |
| 10 | 30 | 17 | 0 | 100,000 | 150% | 82.6 | 79.6 | 3.6 |

### 7.4.3 Results and Discussion of Response 3: Minimum Production Stream $CO_2$ Concentration Required to Achieve Incremental Natural Gas Recovery.

The results from the design runs (Figure 7.27) demonstrate a wide range (25 – 55%) of possible minimum producing $CO_2$ concentrations required to achieve incremental natural gas recovery. While the average of all runs stands at 38.9 mole percent, the lowest producing $CO_2$ concentration established in the design was 25%. Therefore, it can be expected that the lowest producing $CO_2$ concentration required to achieve incremental recovery will be around 25%. The most statistically significant coefficients in determining this producing $CO_2$ concentration is presented in Table 7-13.

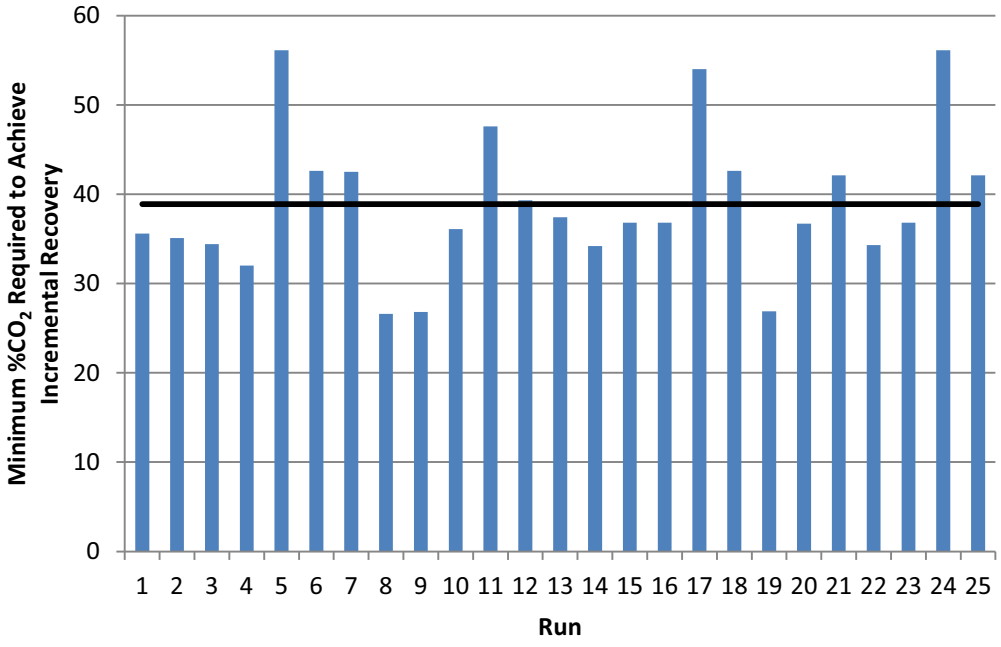


**Figure 7.27: The result for individual design runs with regard to Response 3. The average of all runs is shown in black.**

**Table 7-13: Ranking of statistically significant coefficients from the analysis of Response 3.**

| Statistically Significant Coefficients | F Value | p-value Prob > F |
|---|---|---|
| Production Rate | 305.05 | <0.0001 |
| Y Location | 234.54 | <0.0001 |
| Timing of Injection | 209.13 | <0.0001 |
| Timing of Injection*Production Rate | 107.48 | <0.0001 |
| Injection Rate | 42.13 | <0.0001 |
| Timing of Injection$^2$ | 39.12 | <0.0001 |
| X Location*Timing of Injection | 34.42 | 0.0002 |
| X Location*Production Rate | 34.30 | 0.0002 |
| Y Location*Timing of Injection | 22.27 | 0.0008 |
| X Location$^2$ | 16.50 | 0.0023 |
| Y Location*Injection Rate | 14.52 | 0.0034 |
| Timing of Injection*Injection Rate | 8.74 | 0.0144 |
| Production Rate$^2$ | 7.17 | 0.0232 |
| X Location | 5.57 | 0.0399 |

Inspection of the residuals from the initial analysis of Response 3 (Figure 7.28 and Figure 7.29) pointed to the fact that the residuals did not obey the requirement of normality. Recall that there should be no obvious pattern in the graphs of the residuals if the normality assumption is met. A clear conical pattern is however obvious from the graph of residuals versus predicted response values (Figure 7.29).

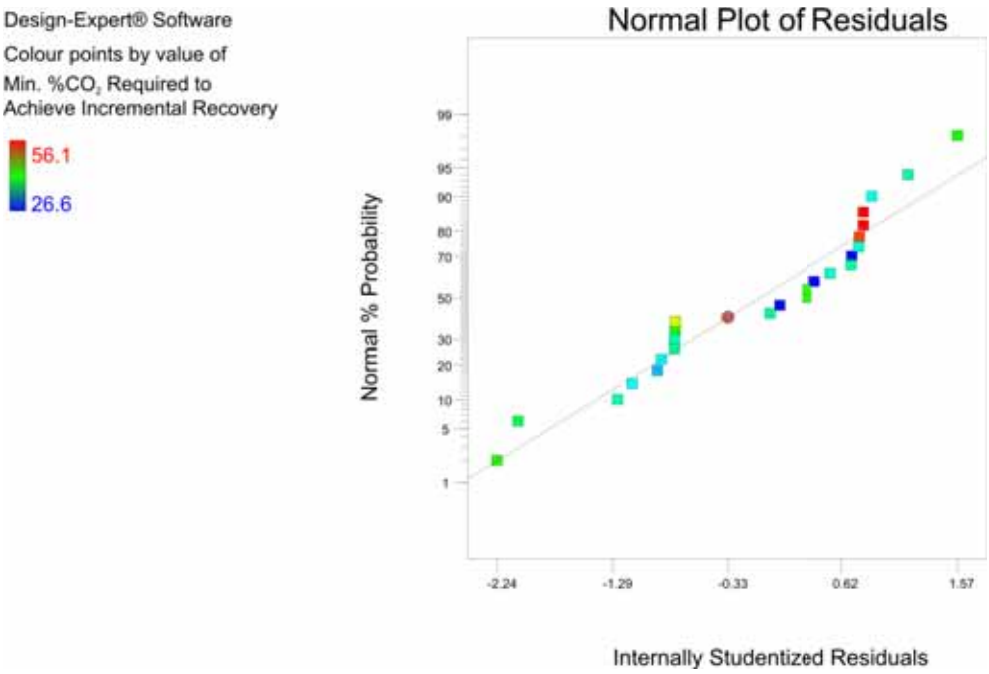


**Figure 7.28: The normal probability plot displaying the deviation from the normality assumption, requiring a transformation.**

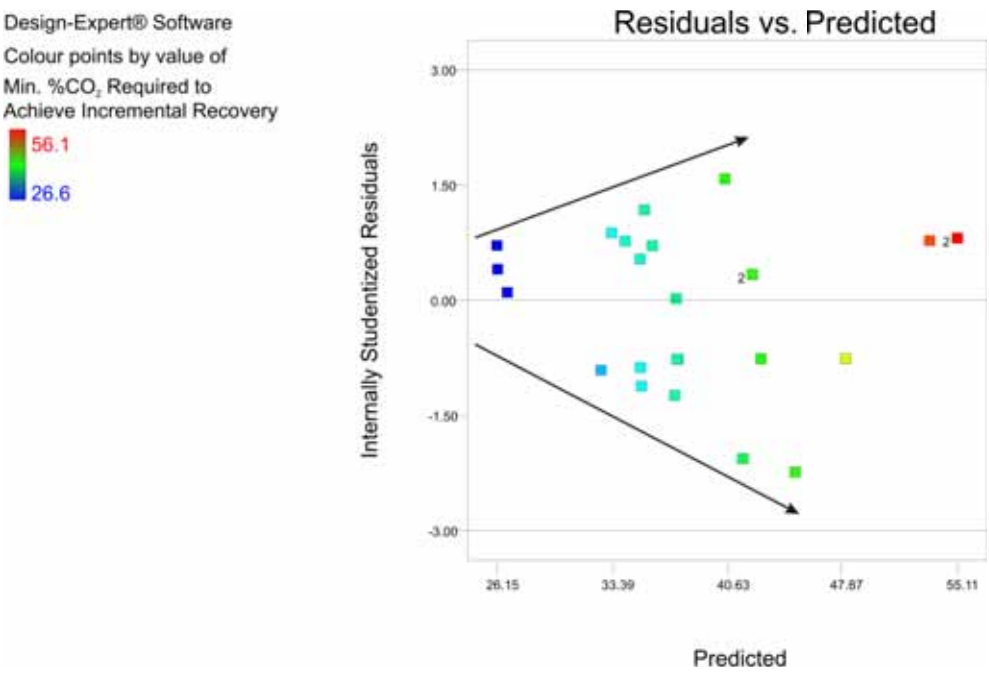


**Figure 7.29: A graph of the residuals versus the predicted values, with the funnel pattern indicating non-constant variance.**

To obtain residuals with constant variance, thus fulfilling the assumption of normality, a transformation of the response data of the form $y^* = y^{\lambda}$ is required, where $y^*$ is the transformed data and $\lambda$ is the transformation parameter. For example, $\lambda = ½$ means use the square root of the original response. As indicated by the Box-Cox plot (Figure 7.30), a tool which aids in determining the most appropriate transformation to apply to the data, a lambda of -0.69 will produce optimal results. The transformation that will achieve a lambda closest to -0.69 is the inverse square root transformation ($\lambda = -0.5$). Inspection of the resulting normal probability plot (Figure 7.31), as well as the residuals versus predicted response graph (Figure 7.32) indicates that this transformation achieved the desired outcome, this being residuals with a constant variance and there being no observable pattern in the residuals graphs. The $R^2$ and adjusted $R^2$ coefficients resulting from the transformation are 0.9923 and 0.9815 respectively. The results presented in Table 7-13 are based upon the transformed data.

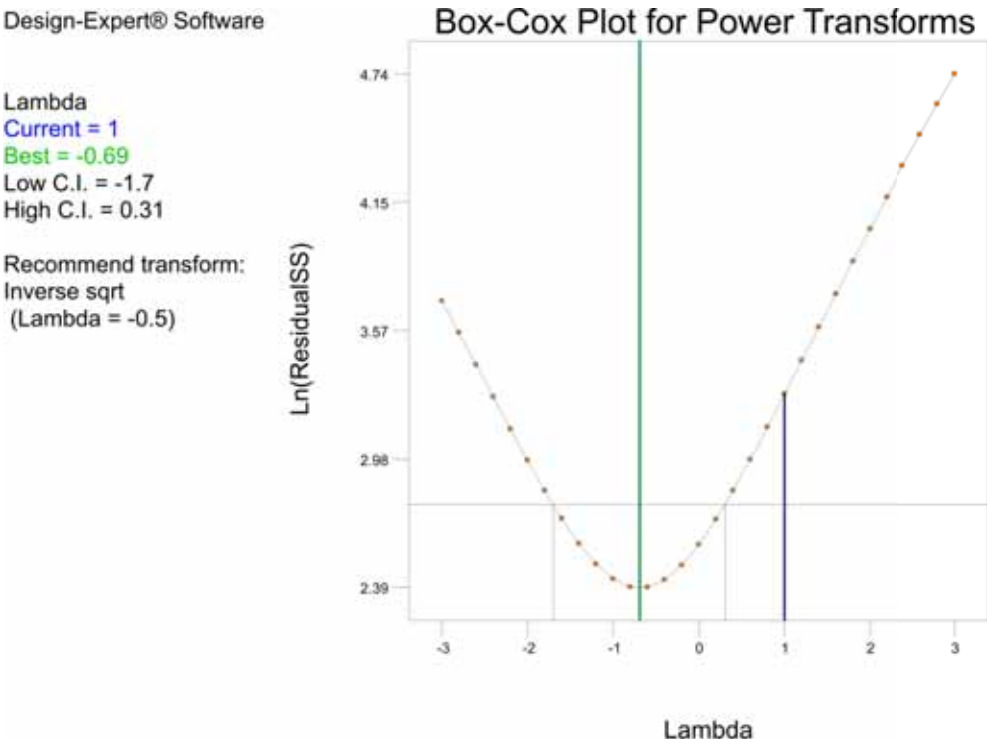


**Figure 7.30: Box-Cox diagnostic plot indicating a transform would improve the fit of the regression model to the input data.**

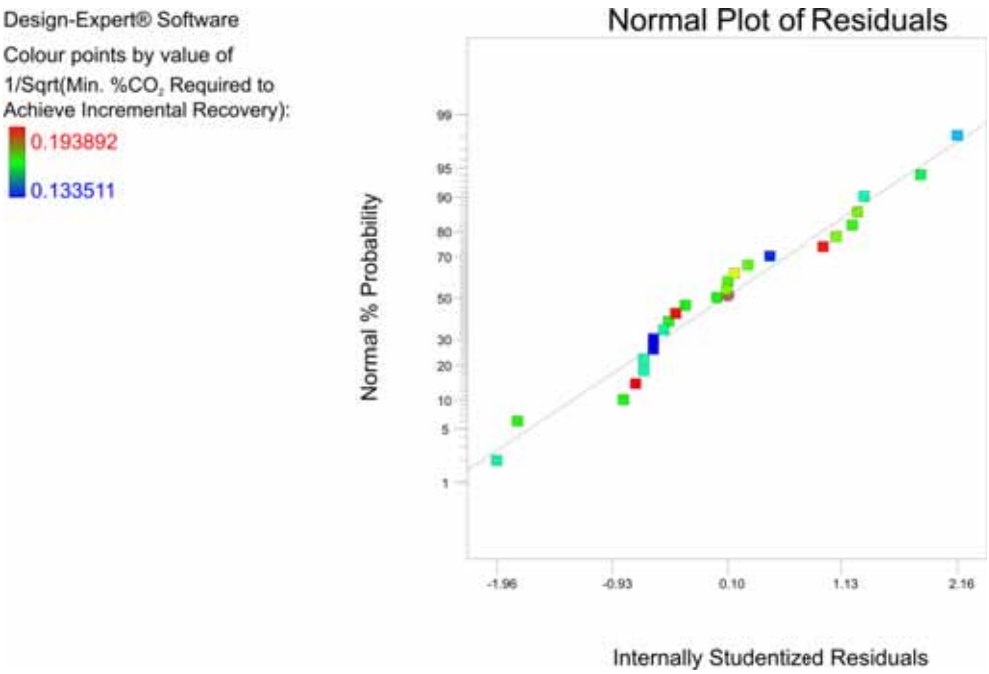


**Figure 7.31: The normal probability plot after the transformation to the data has been applied.**

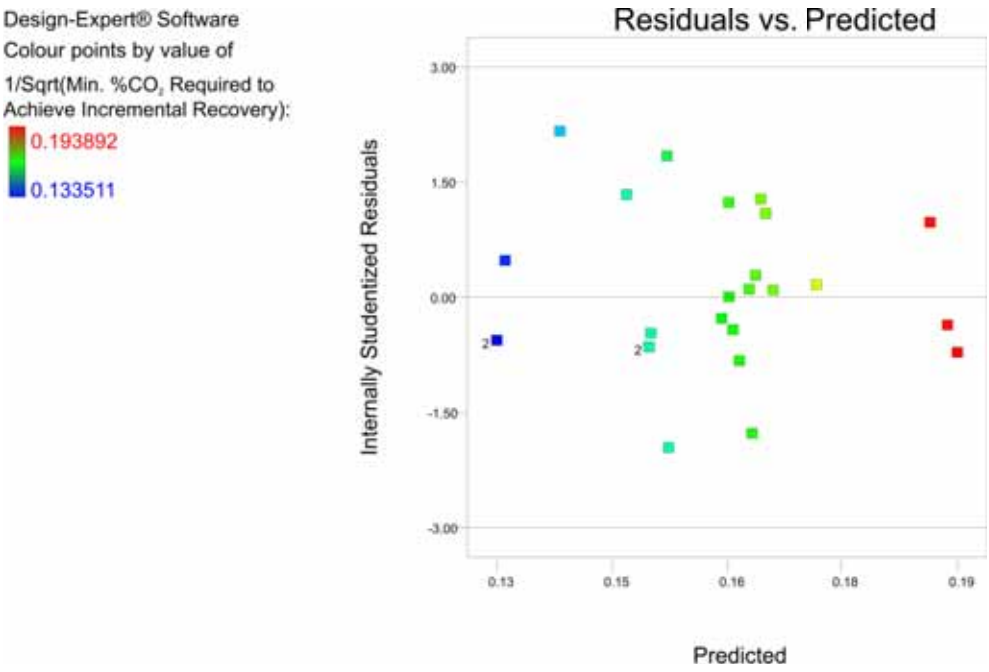


**Figure 7.32: The plot of residuals versus the predicted values after the transformation to the data has been applied, displaying no obvious pattern.**

The main effect of the production rate

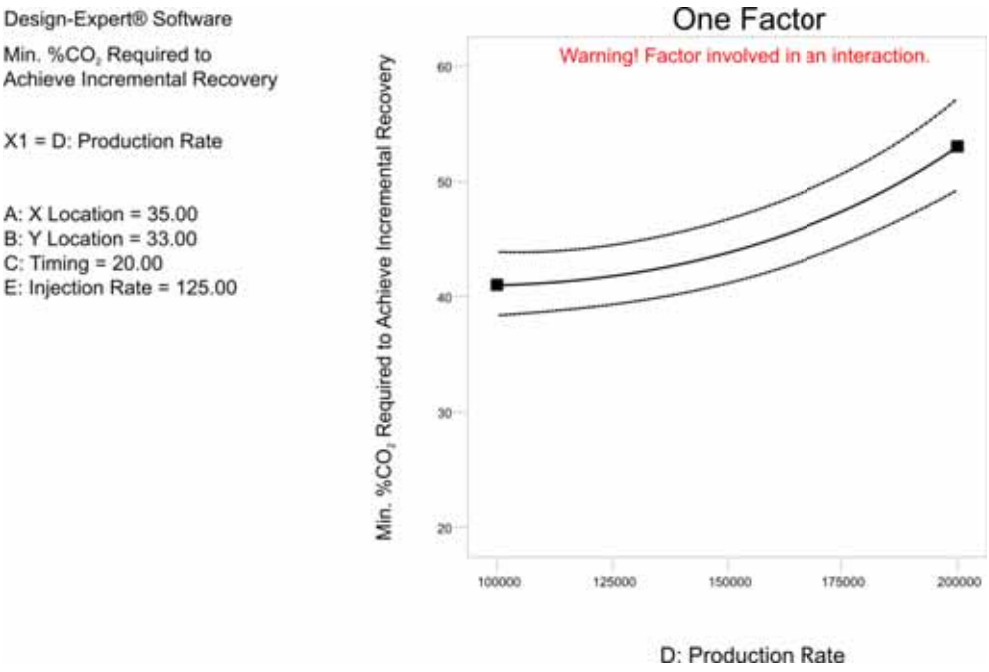


**Figure 7.33: The effect graph for the main effect of the production rate for Response 3.**

The results from the analysis of Response 3 (Table 7-13) indicate that, similar to Response 2, the main effects of the production rate, the Y-location of the injection well, and the timing of $CO_2$ injection are the most influential coefficients.

The results presented thus far have shown that lower production and injection rates have led to both an improvement in the recovery of natural gas at the 10% $CO_2$ limit as well as the 50% $CO_2$ limit. Lower rates therefore improve the sweep of the reservoir prior to the breakthrough of $CO_2$, and lead to a more gradual increase in the production of $CO_2$ once it has reached the production well.

The effect of the production rate levels tested in the ED on the primary recovery efficiency is presented in Table 7-14. This Table shows that higher rates also limit the recovery of natural gas under primary depletion conditions. Over the range of production rates tested, the theory of accelerated gas production is not applicable, with the aquifer able to respond to production in a timely manner, and the heterogeneity present in the reservoir causing the same uneven advancement as has been the case in natural gas – $CO_2$ displacements. Therefore, even with a higher primary recovery efficiency, the improvement in the stability of the natural gas – $CO_2$ displacement results in the employment of lower rates leading to incremental recovery being achieved with a lower production $CO_2$ concentration.

**Table 7-14: Primary recovery efficiencies for production rates employed in the experimental design**

| Production Rate ($sm^3$/day) | Primary Recovery Efficiency at Water Breakthrough |
|---|---|
| 100,000 | 71.4% |
| 133,000 | 70.1% |
| 150,000 | 69.7% |
| 200,000 | 68.7% |

The main effect of the Y location

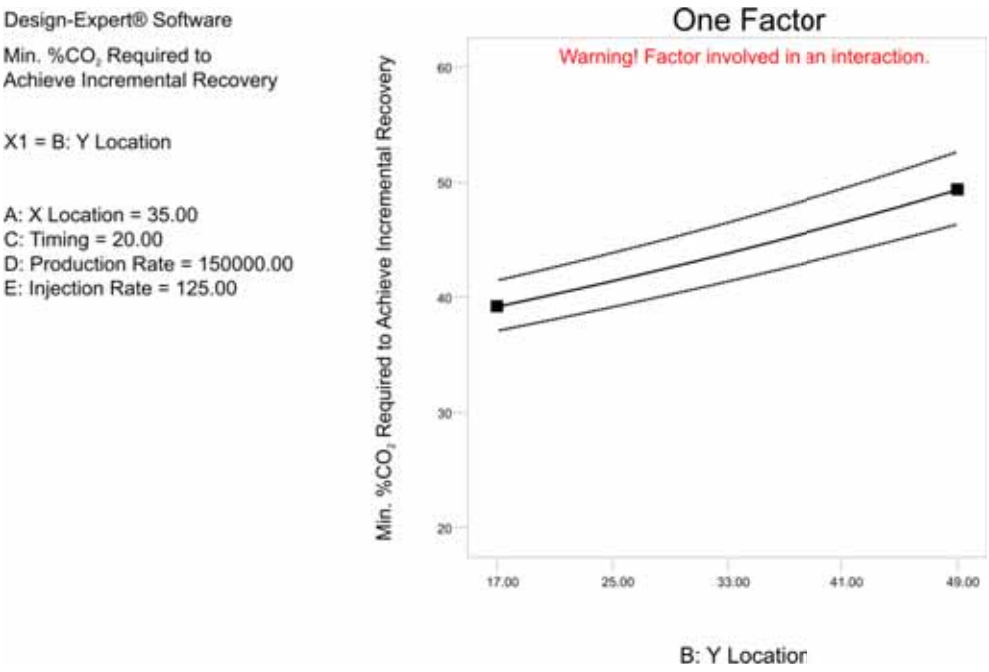


**Figure 7.34: The effect graph for the main effect of the Y location of the injection well for Response 3.**

Figure 7.34 shows that incremental recovery will be achieved with a lower producing $CO_2$ concentration if the injection well is located in the north of the reservoir. The results of Response 1 showed that incremental recovery could only be achieved with a producing $CO_2$ concentration greater than 10%. Additionally, the results from Response 2 showed that rate of increase in $CO_2$ production was less if the injection well was located in the north of the reservoir. It follows that this would correlate to incremental recovery being achieved with a lower producing $CO_2$ concentration with the well located in the north.

The main effect of the timing of injection

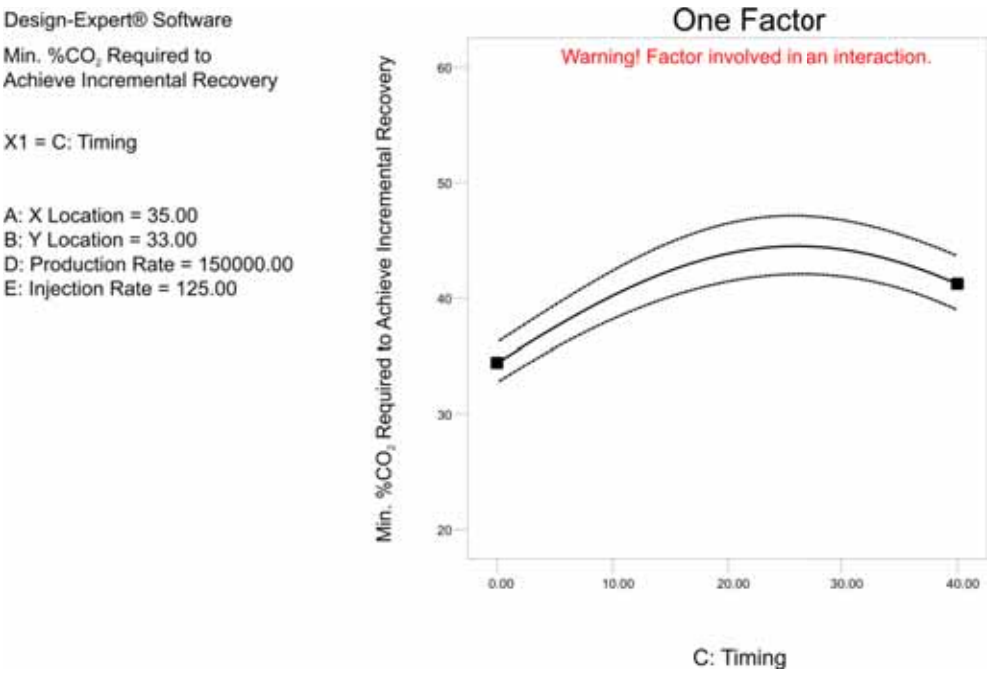


**Figure 7.35: The effect graph for the main effect of the timing of $CO_2$ injection for Response 3.**

Again, with incremental recovery only able to be achieved with a $CO_2$ concentration of greater than 10%, and with the rate of increase in the production of $CO_2$ more gradual with injection commencing early, it follows that the early injection of $CO_2$ will result in incremental recovery being achieved with a lower producing $CO_2$ concentration (Figure 7.35). The cause of the curvature in Figure 7.35 can be better explained in the effect graph for the timing of injection – production rate interaction (Figure 7.36).

Timing of injection – production rate interaction

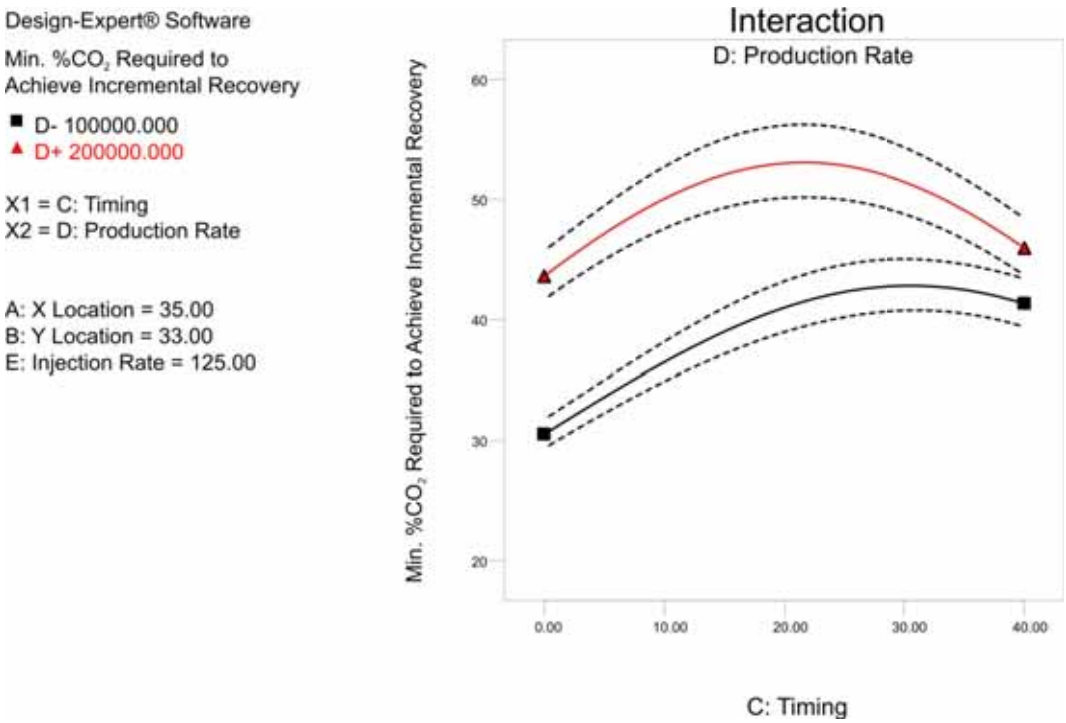


**Figure 7.36: The effect graph for the interaction between the timing of $CO_2$ injection and the production rate for Response 3.**

From Figure 7.36 it can be seen that the degree of curvature as the injection of $CO_2$ is delayed is greater for the higher production rate scenario. This result is suggesting that as the injection of $CO_2$ is further delayed, the sweep of the invaded zone is becoming increasingly more important, with higher rates better able to sweep the invaded zone of residually trapped gas. Once more, it would be expected that if the timing of injection was further delayed (beyond the range tested in this design), then incremental recovery would be achieved with a lower producing $CO_2$ concentration utilising higher rates.

However, although the effect of timing at the high level of the production rate produced an interesting result, over the range tested, implementing higher rates will always lead to higher producing $CO_2$ concentrations and is therefore not the optimal choice. Commencing the injection of $CO_2$ early while implementing lower production and injection rates will lead to incremental recovery being achieved with the lowest minimum concentration of $CO_2$.

Summarising the results of the analysis of Response 3, incremental natural gas recovery can be achieved with the lowest minimum producing $CO_2$ concentration if:

- The production and injection rates are low
- The injection well is located in the north of the reservoir

- The injection of $CO_2$ commences at the start of natural gas production

From the optimisation of the proxy model (Equation 7.3) minimising the concentration of $CO_2$ in the production stream in order to achieve incremental recovery is achieved with the input parameters at the levels presented in Table 7-15.

$$1/\sqrt{Min.CO2\ Required\ to\ EGR} = 0.15 + 0.001302A - 0.008689B - 0.00734C - 0.009411D - 0.0036E + 0.003117AC + 0.003319AD + 0.002751BC - 0.00217BE + 0.005388CD - 0.001602CE + 0.008075A^2 + 0.012C^2 - 0.004298D^2 \quad (7.3)$$

**Table 7-15: The parameter level combination in coded form that optimises Response 3.**

| X-location (A) | Y-location (B) | Timing of $CO_2$ injection (C) | Production Rate (D) | Injection Rate (E) | Minimum %$CO_2$ Required for EGR |
|---|---|---|---|---|---|
| -1 | -1 | -1 | -1 | 1 | 23.9% |

An interesting outcome from the optimisation of Response 3 is that the same combination of parameter levels will both maximise natural gas recovery at the 50% $CO_2$ limit, whilst minimising the producing $CO_2$ concentration required to achieve incremental recovery. Optimisation of Response 3 shows that incremental recovery can be achieved in the Naylor field with a minimum producing $CO_2$ concentration of 23.9 mole percent.

The predictive capability of the proxy equation for Response 3 does not show the same accuracy as the previous responses. However, as Table 7-16 indicates, the error percentage between the predicted and simulated values can be quite significant. In one case, the error between the predicted and simulated value is 21%. Furthermore, the RMSE is 4.45% which, with simulated $CO_2$ concentrations as low as 26%, can represent significant errors in the values calculated by the proxy equation. The requirement of a transformation in order to adequately fit the model to the data of the experimental design could be the cause for the reduction in the predictive capability of this proxy equation in comparison to the other equations. The original model from the analysis of the ED was unable to adequately fit the experimental data, and so a square root transformation was required. While this transformation improved the fit of the model to the experimental data, the results of the confirmation runs demonstrate that this does not necessarily correlate to the model accurately predicting the outcome of untested locations in the design space. Despite the lack of precision in the predictive capability of the proxy equation for Response 3, it does correctly predict the levels of the parameters that will achieve the lowest minimum producing $CO_2$ concentration. For instance, comparison of confirmation runs 1 and 2 indicates that injecting $CO_2$ in the north of the reservoir at lower rates will achieve incremental recovery with a lower producing $CO_2$ concentration

than injecting in the south with higher rates. With the expectation that the proxy equation will indicate the levels of the parameters that will achieve the lowest minimum producing $CO_2$ concentration while not precisely predicting the exact concentration of $CO_2$, the proxy equation sufficiently serves its purpose.

**Table 7-16: The comparison of the error between the predicted and simulated (calculated) results for Response 3.**

| Confirmation Run | X Local | Y Local | Timing | Production Rate | Injection Rate | %$CO_2$ for EGR Estimated | %$CO_2$ for EGR Calculated | % Error |
|---|---|---|---|---|---|---|---|---|
| 1 | 30 | 17 | 0 | 100,010 | 123% | 23.7 | 26.4 | 11.4 |
| 2 | 35 | 30 | 40 | 200,000 | 150% | 48.3 | 47.0 | 2.7 |
| 3 | 40 | 40 | 20 | 150,000 | 125% | 40.8 | 45.7 | 12.0 |
| 4 | 40 | 20 | 15 | 100,000 | 135% | 33.7 | 28.0 | 16.9 |
| 5 | 35 | 20 | 35 | 175,000 | 125% | 42.2 | 38.2 | 9.5 |
| 6 | 31 | 26 | 23 | 140,000 | 110% | 38.4 | 30.2 | 21.4 |
| 7 | 35 | 17 | 0 | 100,000 | 100% | 27.1 | 27.0 | 0.4 |
| 8 | 35 | 17 | 0 | 200,000 | 100% | 37.8 | 33.1 | 12.4 |
| 9 | 30 | 17 | 0 | 100,000 | 100% | 23.7 | 27.1 | 14.4 |
| 10 | 30 | 17 | 0 | 100,000 | 150% | 23.6 | 27.5 | 16.5 |

### 7.4.4 Optimisation of the Responses

The results from the analysis of the three responses showed that incremental recovery could only be achieved with a producing $CO_2$ concentration of greater than 10%. Therefore more importance was placed on the results of Response 2 rather than Response 1. These two responses had contradictory conclusions. The conclusions from Response 1 indicated that natural gas recovery at the 10% $CO_2$ limit would be maximised with delayed injection, and the injector located in the south of the reservoir. On the other hand, the conclusions from Response 2 indicated that injection should not be delayed, with injection to occur in the north of the reservoir. The optimisation process for Response 3 showed that the same parameter level combination that maximised natural gas recovery at the 50% $CO_2$ limit (Response 2) also led to incremental recovery being achieved with the lowest minimum producing $CO_2$ concentration (Response 3). As the same parameter level combination led to the optimisation of both Response 2 and Response 3, this was taken to be the optimal combination for the development of the $CO_2$EGR process in the Naylor field.

Confirmation run number 10 for each response (Table 7-8, Table 7-12, and Table 7-16) presents the comparison between predicted and simulated results for each response using the parameter level combination in Table 7-10 and Table 7-15. This is summarised in Table 7-17. Good agreement between the predicted and calculated results for the first two responses is evident, each with an error of 3.6%. The error is considerably larger for the third response at 16.5%, however the result does represent one of the lowest minimum producing $CO_2$ concentrations simulated.

**Table 7-17: Comparison of calculated and predicted results for the optimised model**

| | |
|---|---|
| **Response 1 Predicted** | 60.9% |
| **Response 1 Calculated (Simulated)** | 58.7% |
| **Response 2 Predicted** | 82.6% |
| **Response 2 Calculated** | 79.6% |
| **Response 3 Predicted** | 23.6% |
| **Response 3 Calculated** | 27.5% |

Comparing the results of the optimised scenario with the results of the primary depletion of the reservoir, incremental recovery will be achieved with a minimum producing $CO_2$ concentration of 27%. The incremental recovery achievable at a $CO_2$ limit of 50% is just over 8% of the OGIP. This equates to an increase in recovery of 11 x $10^6$ $sm^3$ of natural gas.

## 7.5 Composition of the Injection Gas

A previous investigation into the effect of the type of gas used in a gas-gas displacement found that the injection of a flue gas improved $CH_4$ recovery at a particular breakthrough limit when compared with the use of a pure gas (Turta et al. 2007). The flue gas involved contained only a small fraction of $CO_2$ (14%) with the remainder of the gas comprised of nitrogen (76%). It was concluded that the discrepancy in results between the gases was due to the different solubilities of the injection gas components and the tolerance of these components in the production stream. $CO_2$ has a greater solubility in water than nitrogen. Consequently, a greater volume of $CO_2$ will dissolve into the water, delaying the breakthrough in comparison to the breakthrough of nitrogen. The tolerance for nitrogen in pipeline gas is generally greater than for $CO_2$, and so production will not cease when nitrogen has initially reached the production well. This prolonged period of production prior to the breakthrough of $CO_2$ improved the recovery over that achievable when pure $CO_2$ was used.

The source of gas used for the $CO_2$ storage pilot project operated by the CO2CRC in the depleted Naylor field is not a pure stream. The gas composition is 79% $CO_2$ and 21% $CH_4$. Based upon the conclusions of the aforementioned study, the injection of an impure (flue) gas stream has the potential to delay the breakthrough of $CO_2$ and improve the recovery profile when compared to the injection of pure $CO_2$. The use of a flue gas might also be more economically attractive, provided it does not contain other unwanted contaminants which would require additional processing, either prior to injection or of the production stream in order to meet pipeline specifications.

It was decided that a comparison between an impure source of $CO_2$ and a pure source of $CO_2$ would be made at the same parameter level combination as the optimised model (Table 7-10 and Table 7-15). A comparison of the $CO_2$ production profiles for both cases is presented in Figure 7.37.

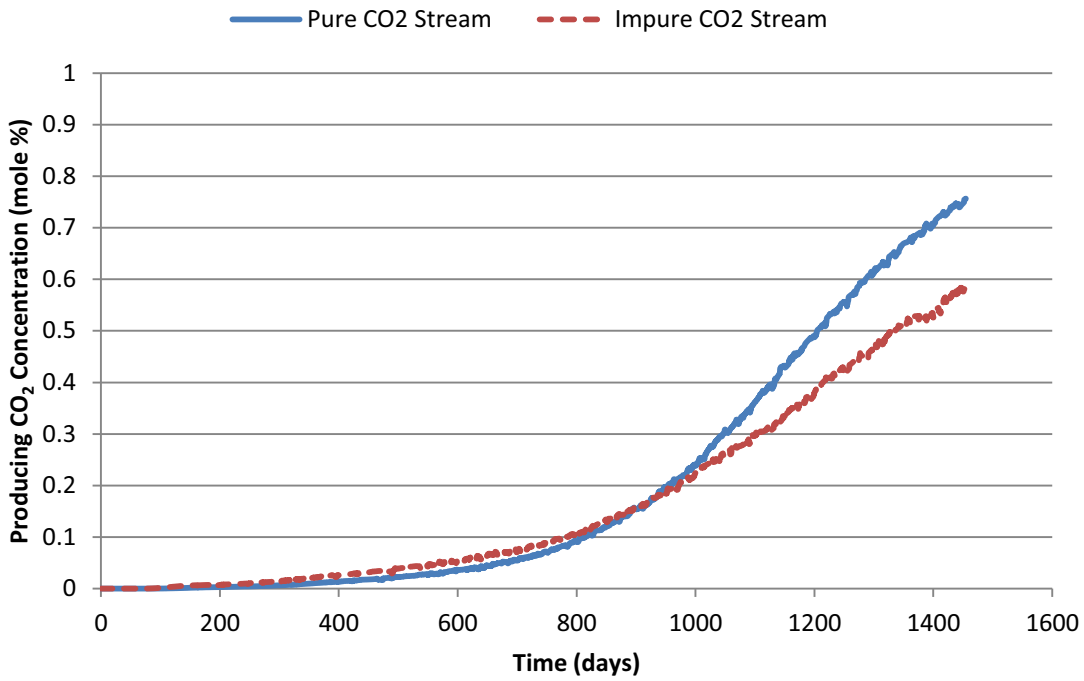


**Figure 7.37: A comparison of the $CO_2$ production profiles where the injection gas composition is being tested.**

It is interesting to note from the comparisons of the $CO_2$ production profiles that the injection of the impure $CO_2$ source actually results in the premature breakthrough of $CO_2$. Consequently, the natural gas recovery at the 10% $CO_2$ limit is actually less when a pure source is utilised. The early breakthrough of $CO_2$ in this case is believed to be due to greater volumetric injection rate at reservoir conditions coupled with the greater Darcy velocity of the injected stream. The different compressibilites of $CH_4$ and $CO_2$ mean that for the same surface volume of gas, at reservoir conditions the $CO_2$ will occupy a smaller volume than $CH_4$. At reservoir conditions, the volume of gas injected for the impure stream is more than for the pure $CO_2$ stream. This equates to higher injection pressures, and so greater energy being input into the reservoir. Additionally, the Darcy velocity and mobility of the impure stream are greater than the pure $CO_2$ stream. From Darcy's law, the Darcy velocity is inversely proportional to the viscosity of the fluid. The presence of $CH_4$ reduces the viscosity of the injection gas. The enhanced mobility of the injected fluid leads to more rapid migration and earlier breakthrough at the production well.

However, despite the earlier breakthrough of $CO_2$ at the production well, the reduced volume of $CO_2$ being injected coupled with the injection of $CH_4$ into the reservoir (increasing the in place volume of natural gas) results in a lower rate of increase in $CO_2$ production. This is beneficial in lowering the minimum producing $CO_2$ concentration required to achieve incremental recovery (25 mole percent of $CO_2$), whilst also increasing the recovery at the 50% $CO_2$ limit (85%).

As mentioned, this has the potential to improve the economics of the project. In the case of the Naylor field, this would allow for the injection of the gas from the Buttress field without any processing to remove the $CH_4$ component. In general, the positive results shown here could allow for the use of natural accumulations of $CO_2$ or the use of a flue gas stream from an industrial process without the increase in cost due to processing to purify the stream. $CO_2$ is an expensive commodity, and so any means of reducing the cost of the injection stream will greatly improve the prospects of utilising $CO_2$ to enhance natural gas recovery in water-drive gas reservoirs.

## 7.6 Summary of Results

The results of the analysis of $CO_2$ injection into the Naylor field closely match what was expected based upon the knowledge gained from the analyses presented in previous chapters. Viscous dominated displacement was expected to be an inefficient process due to the presence of heterogeneity. Allowing the force of gravity to dominate the displacement did in fact mitigate against the unwanted effects of the heterogeneity, improving the metrics studied. Specifically, the results can be summarised as follows:

- With the significant degree of heterogeneity present, the early injection of $CO_2$ did lead to the uneven advancement of $CO_2$ resulting in the premature breakthrough at the production well. The early injection of $CO_2$ in the south of the reservoir was shown to be particularly detrimental with respect to Response 1 (recovery efficiency at the 10% CO2 breakthrough limit).
- Mirroring the results of Study 2B, delaying the injection of $CO_2$ was shown to improve natural gas recovery at the 10% $CO_2$ breakthrough limit. Optimisation of Response 1 showed that maximum recovery was achieved with injection located in the south of the reservoir.
- The optimisation process for Response 1 did however show that incremental recovery could not be achieved with an initial producing $CO_2$ concentration of less than 10 mole percent.
- The rate of increase in the $CO_2$ production rate was now important with the analysis of Response 2 again showing that delaying the injection of $CO_2$ resulted in a more rapid increase in the production of $CO_2$. To maximise recovery at the 50% $CO_2$ limit, injection should not be delayed. This led to the recommendation that the injection of $CO_2$ should therefore occur in the north of the reservoir.
- Additionally, to maximise the beneficial effects of gravity in mitigating against the influence of heterogeneity, the production and injection rates employed should be as low as economically possible.

- The optimisation of Response 3 was achieved with the identical parameter level combination which maximised natural gas recovery at the 50% $CO_2$ limit (Response 2).
- The results of Response 3 showed that incremental recovery could only be achieved with a producing $CO_2$ concentration greater than 10%. Consequently the optimisation of Responses 2 and 3 were given more weight than for Response 1.
- The optimisation of Response 2 and Response 3 showed incremental recovery being achieved with a minimum producing $CO_2$ concentration of 27%, with incremental recovery at the 50% $CO_2$ limit amounting to 8% of the OGIP over the corresponding primary depletion case.
- Injection of an impure $CO_2$ source (79% $CO_2$, 21% $CH_4$) was shown to improve the metrics of Responses 2 and 3, with an incremental recovery of 13% of OGIP at the 50% $CO_2$ limit, with the minimum producing $CO_2$ concentration required to achieve incremental recovery dropping by 2% to 25 mole percent. However, the injection of the impure $CO_2$ stream actually led to an earlier breakthrough of $CO_2$ at the production well.

# CHAPTER 8

# 8 Screening Criteria

Screening criteria have been used for decades to assist in the selection of oil reservoirs for the application of various enhanced recovery methods (Taber 1983; Doe et al. 1987; Diaz et al. 1996; Graham et al. 1996; Taber et al. 1997b; Taber et al. 1997a; Thomas 1998; Henson et al. 2002; Shaw & Bachu 2002; Mohammed-Singh et al. 2006). The most notable of these criteria is the set by Taber *et al* published in 1997 (Taber et al. 1997b; Taber et al. 1997c). As EGR through the injection of $CO_2$ has received very little attention in the literature a primary aim of this thesis is to produce a set of guidelines highlighting the reservoir and/or fluid properties that are more suited to the successful application of $CO_2$ EGR in water-drive gas reservoirs. These guidelines can therefore be used as a screening criteria with which to determine if a chosen reservoir would be suitable for $CO_2$ injection, warranting further investigation.

These criteria only address the technical aspect of injecting $CO_2$ to enhance natural gas recovery based upon the results of the simulations performed in this study. Incorporating economic analyses is outside of the scope of the study, and has not been considered. Gas reservoirs are typically developed under long-term contracts of 20+ years and as such their development usually has to honour strict contractual obligations. For example, the requirement to produce a particular daily volume of natural gas could have limitations on any increase in production and injection rates which might be required to achieve a stable, viscous dominated displacement. The consideration of an economic analysis could therefore alter the recommendations of this Chapter.

## 8.1 Criteria for an Efficient Displacement of $CH_4$ by $CO_2$

The screening criteria describe the conditions whereby a stable displacement of $CH_4$ by $CO_2$ will occur. The screening criteria can be presented in two parts, the first part describing the favourable properties for a non-dipping reservoir and the second for a dipping reservoir. It has been shown that delaying the injection of $CO_2$ results in a more rapid increase in the $CO_2$ production rate once $CO_2$ has reached the production well, limiting the potential to maximise incremental recovery if a $CO_2$ production limit is applied. The criteria presented in this section refer to the ideal characteristics if injection is commenced at the start of the natural gas production. The effect of the timing of injection will be discussed in Section 8.2.

### 8.1.1 Fluid properties

A criteria key to all situations is the requirement for the injection of supercritical $CO_2$. The key to minimising the potential mixing between $CO_2$ and natural gas is to maximise the difference between the properties of the two fluids, specifically density and viscosity. This is achieved through the injection of supercritical $CO_2$. This correlates to an initial reservoir pressure of greater than 1071 psi. In terms of reservoir depth, the same criterion applied to the sequestration of $CO_2$ would apply. Reservoir depth should therefore be greater than 800 metres (Metz et al. 2005).

### 8.1.2 Non-dipping reservoirs

In a non-dipping reservoir homogeneity is preferred. The presence of heterogeneity can lead to the uneven displacement of natural gas by $CO_2$, resulting in the premature breakthrough of $CO_2$and leading to a poor sweep of the reservoir. Heterogeneity is particularly detrimental in displacement processes involving strong viscous forces.

If the reservoir is homogeneous, the permeability and reservoir thickness are not critical. It is possible to achieve an efficient displacement through either a viscous or gravity dominated displacement process.

In a gravity dominated displacement, the injected $CO_2$ fills the reservoir from the bottom, resulting in a vertical displacement of $CH_4$ by $CO_2$ towards the production well(s). The primary issue with a gravity dominated displacement process in a non-dipping reservoir is $CO_2$ coning. Assuming constant production rates, coning of fluids is mitigated by increasing permeability and thickness. Consequently, thick, high permeability reservoirs are an ideal candidate for $CO_2$ EGR. Implementation of $CO_2$ EGR in thick, high permeability reservoirs allows greater flexibility in the choice of rates. The reduction in the susceptibility of coning will allow higher rates to be implemented.

If the reservoir is thin, the preference is for a lower permeability reservoir. High permeability will increase the influence of gravity, leading to gravity segregation and rapid horizontal migration towards the production well. The coning of $CO_2$ becomes an issue in thin reservoirs. To minimise or eliminate $CO_2$ coning, rates have to be lowered which could be unfeasible economically. Viscous dominated displacement processes can lead to an efficient sweep of a non-dipping reservoir, as highlighted in the $CO_2$ EOR screening criteria outlined by Taber *et al* (1997).

To minimise the degree of $CO_2$ coning that can occur, the vertical permeability should be low, especially under a gravity dominated displacement process.

The presence of heterogeneity in a non-dipping reservoir can be detrimental to a displacement process, especially under viscous dominated displacement conditions. The heterogeneity will cause the uneven advancement of $CO_2$, leading to the premature breakthrough of $CO_2$ and a poor sweep of the reservoir. To mitigate against the unfavourable effects of heterogeneity, the direction of the displacement should be altered from primarily horizontal to vertical. Gravity should therefore have a strong influence in the displacement process in a heterogeneous reservoir. In terms of uncontrollable factors, this is achieved with a thick and/or high permeability reservoir. Additionally, in terms of controllable factors, this can be achieved by a reduction in the injection and production rates employed, or by employing horizontal wells.

### 8.1.3 Dipping reservoirs

In a dipping reservoir, the efficient displacement of natural gas by $CO_2$ can only be achieved with a gravity stable displacement. This corresponds to a reservoir which has high horizontal and vertical permeability and is thick. Viscous dominated displacement processes in dipping reservoirs has been shown to lead to a poor sweep of the reservoir. This relates to low horizontal and vertical permeability and/or thin reservoirs. A dipping reservoir can be thin however, ideally, permeability should be high to ensure a gravity stable displacement. Heterogeneity in a dipping reservoir is not as critical as is the case in a non-dipping reservoir due to the greater influence on the displacement process, however to ensure maximum efficiency in the displacement of $CH_4$ by $CO_2$, it is recommended that the reservoir be homogeneous.

A summary of the ideal criteria is presented in Table 8-1.

**Table 8-1: Summary of key criteria to maximise the efficiency of the displacement of $CH_4$ by $CO_2$.**

| | | Depth | Thickness | Permeability |
|---|---|---|---|---|
| Non-dipping reservoir (preferred) | Homogeneous (preferred) | > 800 metres | Not critical. | Not critical.<br>If reservoir is thin, low permeability preferred |
| | Heterogeneous | > 800 metres | Thick | High permeability<br>Narrow permeability range |
| Dipping reservoir | Homogeneous and Heterogeneous | > 800 metres | Thick | High permeability |

The above recommendations are for the ideal reservoir conditions in which to conduct the displacement of natural gas by $CO_2$. Under these conditions, an operator has greater flexibility in the choice of operational parameters. For instance, for a non-dipping reservoir with heterogeneity, more options will be available for the development of the field if the reservoir is thick. The choice of injection and production rates will not be as critical, as a gravity stable displacement can be achieved with a wider range of rates. Additionally, results from Study 1 showed that the implementation of

horizontal wells is more beneficial in thicker reservoirs. For an equivalent case in a thin reservoir, the options are more limited. Horizontal wells were shown to be less effective in thin reservoirs. Furthermore, the range of production and injection rates that can be implemented to achieve a gravity stable displacement is limited. In order to achieve a gravity stable flood, the rates might have to be considerably low, which could put pressure on the economic viability of the project. It is possible to achieve a technically efficient displacement in reservoirs with less than ideal characteristics, however the impact of these characteristics on the choice of the operational strategy could prove costly with regards to the economic viability of the project.

## 8.2 The Effect of the Timing of $CO_2$ Injection

The above recommendations are based upon the injection of $CO_2$ commencing at the start of natural gas production. In all the scenarios studied in this thesis, incremental recovery could not be achieved prior to the breakthrough of $CO_2$. The extent of incremental recovery achievable is therefore a strong function of the maximum allowable producing $CO_2$ concentration and therefore the rate of increase in $CO_2$ production. It has been shown that delaying the injection of $CO_2$ is detrimental to maximising incremental recovery, as it leads to a more rapid increase in the $CO_2$ production once $CO_2$ has reached the production well. Consequently, if a $CO_2$ production limit is applied to a project, this faster increase in $CO_2$ production will put a constraint on the incremental recovery of natural gas.

However, if a reservoir has undergone a period of primary production, the ideal criteria will be based upon whether the displacement process is to target the remaining free gas zone, the invaded zone or both. The issue with targeting both the free gas and invaded zones is that the characteristics that can lead to an efficient sweep of one zone will not correlate to an efficient sweep of the other zone. For example, it has been shown that a gravity stable displacement in a thick, high permeability reservoir can lead to an excellent sweep of the free gas zone. However, these properties will lead to strong gravity segregation between $CO_2$ and water. This will lead to a poor sweep of residual gas present in the invaded zone. Properties which lead to strong viscous forces will ensure gravity segregation is limited, and that the injected $CO_2$ can penetrate and sweep the invaded zone of the residually trapped gas saturation.

It is therefore recommended that the injection of $CO_2$ should target one of the zones. If a reservoir has already undergone a period of primary production, a strategy could be to continue primary depletion until water breakthrough, ensuring a minimal free gas zone is present at this stage. $CO_2$ injection could then follow, with a focus on ensuring maximum sweep of the invaded zone to maximise the recovery of the trapped gas saturation. Properties which negate the effect of gravity

(i.e. viscous dominated displacement) will assist in maximising the sweep, which in turn maximises the recovery of natural gas.

## 8.3 Key Criteria to Maximise the Benefit of $CO_2$ Injection over Primary Depletion

The previous criteria have given an indication as to the properties which will lead to an efficient displacement process. However, these properties do not necessarily correspond to conditions which will maximise the benefit of the injection of $CO_2$ over conventional primary depletion in water-drive gas reservoirs. Conditions which lead to an efficient natural gas – $CO_2$ displacement could also correspond to a high primary recovery efficiency, and so injection of $CO_2$ in that situation would not be a recommended option.

Due to the lower primary recovery efficiencies achievable, the injection of $CO_2$ should target non-dipping reservoirs as opposed to dipping reservoirs. The influence of the aquifer is typically not as strong in a dipping reservoir, and so greater pressure reduction is achievable improving primary natural gas recovery. Even though stable natural gas-$CO_2$ displacement can be achieved in a dipping reservoir, this higher primary recovery equates to a higher $CO_2$ concentration needing to be handled to achieve incremental recovery.

In terms of the primary depletion, there is no particular non-dipping reservoir that is better suited to the injection of $CO_2$. While low permeability might restrict the mobility of the aquifer, allowing for greater pressure reduction, low horizontal permeability is conducive to the formation of water coning. The coning of water can severely limit the sweep of the reservoir, resulting in a significant volume of bypassed gas. Higher horizontal permeability might be beneficial in mitigating against the formation of water coning, but it enhances the mobility of the aquifer enabling the aquifer to respond to gas production quickly, maintaining reservoir pressure. The same can be said for the effect of reservoir thickness. Under a constant production rate, greater pressure reduction is achievable in a thinner reservoir. However, there is a greater susceptibility for the coning of water. Increasing reservoir thickness will mitigate against the coning of water, but will limit the extent of pressure reduction. It is therefore primarily the efficiency of the natural gas – $CO_2$ displacement process that determines the extent of the benefit of injecting $CO_2$ in maximising the recovery of natural gas over that achievable under conventional primary depletion.

While a dipping reservoir is not the preferred option for $CO_2$ injection (as opposed to a non-dipping reservoir), specifying the conditions which maximise the benefit of $CO_2$ injection on the recovery of natural gas over that achievable under primary depletion is more straightforward. Due to the

restriction in the mobility of the aquifer, a much higher primary recovery can be achieved in low permeability (both horizontal and vertical) scenarios. The geometry of the reservoir ensures that the coning of water is not as great an issue as is the case in a non-dipping reservoir. Under $CO_2$ injection conditions, low permeability scenarios were shown to result in a significantly poorer reservoir sweep. Consequently, a high primary recovery in conjunction with poor reservoir sweep under $CO_2$ injection conditions leads to low permeability scenarios in dipping reservoirs not being ideal candidates for $CO_2$ injection. With increasing permeability comes an increased ability for the aquifer to respond to gas production under primary conditions, hence lowering primary recovery. Combining this poor primary recovery with the improvement that increased permeability has on the displacement of natural gas by $CO_2$ (gravity stable flood), indicates that high permeability scenarios are the ideal candidates.

# CHAPTER 9

# 9 Conclusions and Future Work

## 9.1 Conclusions

In this thesis, an investigation into the injection of $CO_2$ into a water-drive gas reservoir is presented. The primary concern with the injection of $CO_2$ is the extent of mixing between the injectant and the resident natural gas. This thesis has therefore focussed on determining the effect of a number of controllable and uncontrollable factors on the efficiency of the displacement process and the ability to produce uncontaminated natural gas, with comparisons to the recovery efficiency achievable under conventional primary depletion conditions.

Study 1 involved an investigation into the injection of $CO_2$ at the commencement of $CH_4$ production, with the aim to minimise any influx of the aquifer into the reservoir. Reservoir and fluid properties deemed to have a potential impact on the stability of the displacement process were chosen for investigation through the use of the experimental design methodology. The effect of these parameters was tested on two responses, the $CH_4$ recovery efficiency at a 10% $CO_2$ production limit, and the minimum producing $CO_2$ concentration required to achieve incremental recovery. The key results from the analysis of the experimental design were:

- The efficiency of the displacement process, and therefore the recovery of $CH_4$ at a 10% $CO_2$ limit were strongly influenced by the viscous to gravity ratio. The properties that determine the relative strength of these forces (viscous or gravity) were the most influential parameters.
- In a non-dipping reservoir, an efficient displacement can be achieved through both a viscous or gravity dominated displacement. If gravity is the dominate force, the coning of $CO_2$ into the production well is a vital component in determining the sweep efficiency at the 10% $CO_2$ limit. With dominant viscous forces, an efficient horizontal displacement process occurs, analogous to the preferred displacement process for a $CO_2$ EOR project in a non-dipping reservoir.
- In a dipping reservoir, an efficient sweep can only be achieved through a gravity stable displacement process. Viscous dominated displacement was shown to lead to the poor sweep of the reservoir and the early breakthrough of $CO_2$.
- The minimum producing $CO_2$ concentration required to achieve incremental recovery was largely determined by the effect the input parameters had on the conventional primary

recovery efficiency. Parameter levels which led to a low primary recovery efficiency also led to incremental recovery being achieved with the lowest producing $CO_2$ concentrations.

- Consequently, with non-dipping reservoirs generally achieving lower primary recovery efficiencies than dipping reservoirs due to the stronger influence of the aquifer, injection of $CO_2$ should be targeted in non-dipping reservoirs.
- The effect of the salinity of the aquifer and the diffusion coefficient were found to be statistically significant, however their effect on the ED responses relative to the reservoirs properties such as permeability, thickness and formation dip, was found to be considerably less.

Following the ED in Study 1, an investigation into the effects of heterogeneity as well as the impact of operational strategies on the stability of the displacement process was performed. The key results were as follows:

- Heterogeneity can have a significant negative impact on the efficiency of the displacement process. The presence of heterogeneity can lead to significant channelling of $CO_2$, leading to the early breakthrough of $CO_2$ and consequently a poor sweep of the reservoir.
- The presence of heterogeneity is particularly detrimental in non-dipping reservoirs, and where a displacement process is characterised by strong viscous forces.
- Due to the significance of the viscous to gravity ratio on the efficiency of the displacement process, operational strategies can have a significant impact.
- Production and injection rates can be altered to suit the requirement of either a viscous or gravity dominated displacement. For example, it was shown that viscous dominated displacement in a dipping reservoir led to a poor sweep of the reservoir. In this instance, injection and production rates could be lowered in an attempt to achieve a gravity stable displacement.
- If flexibility in the selection of rates is not an option (e.g. contractual requirements), it was shown that alterations to the well configuration/design can achieve the desired results. For example, the application of horizontal wells in non-dipping heterogeneous reservoirs was shown to be particularly beneficial due to the alteration of direction of the displacement from horizontal to vertical, thus negating the impact of the heterogeneity.

Study 2A and 2B involved an investigation into the timing of $CO_2$ injection and whether delaying the injection of $CO_2$ could improve the recovery of $CH_4$ at specified $CO_2$ production limits. The experimental design methodology was again employed, and involved a study of a homogeneous (Study 2A) as well as a heterogeneous (Study 2B) reservoir. In addition to the timing of injection,

parameters which influence the viscous and gravity forces were included in the investigation. In addition to the effect of the displacement between $CO_2$ and $CH_4$, the viscous and gravity forces between $CO_2$ and the aquifer are expected to strongly influence the displacement process if injection is delayed. The key results of this study were:

- In a homogeneous reservoir, delaying the injection of $CO_2$ did not have a significant effect on the recovery of $CH_4$ at a $CO_2$ production limit of 10%.
- The timing of injection determined the influence of the other parameters on the sweep of either the free gas zone or the invaded zone. As the injection of $CO_2$ is delayed, the influence of the other parameters (thickness, dip, and horizontal and vertical permeability) on the ability to sweep the invaded zone becomes increasingly more important. While properties which lead to a gravity stable displacement is beneficial in efficiently displacing natural gas in the free gas zone, these properties will lead to gravity segregation between $CO_2$ and water, and consequently lead to an inability to sweep the invaded zone.
- The timing of injection did have a significant impact on the recovery of $CH_4$ at a $CO_2$ production limit of 50%. The rate of increase in $CO_2$ production was considerably faster if the injection was delayed, reducing the recovery of $CH_4$ at the 50% $CO_2$ limit.
- The maximum allowable producing $CO_2$ concentration will subsequently determine the timing of injection strategy. If a high concentration of $CO_2$ can be tolerated, there is a clear benefit in commencing the injection early.
- The primary recovery efficiency was again largely responsible for determining minimum producing $CO_2$ concentration required to achieve incremental recovery. Formation dip was again the most influential parameter, with injection recommended to be targeted in non-dipping reservoirs.
- In a heterogeneous reservoir, the primary concern is the uneven advancement of the displacement front leading to the early breakthrough of $CO_2$, especially in viscous dominated displacement.
- Viscous dominated displacement in association with the early injection of $CO_2$ is particularly detrimental in non-dipping reservoirs. The stronger impact of gravity in a dipping reservoir reduces the uneven advancement, improving the sweep of the reservoir.
- Consequently it was shown that delaying the injection of $CO_2$ improves the recovery of $CH_4$ at the 10% $CO_2$ breakthrough limit.
- The benefit of delaying the injection of $CO_2$ diminishes as gravity forces increase. In a non-dipping reservoir, gravity dominated displacement can result in delaying/minimising contact

with the higher permeability layer improving the sweep of the reservoir, while in a dipping reservoir gravity acts to suppress the uneven advancement.

- Delaying the injection of $CO_2$ does however result in a considerably more rapid increase in the production of $CO_2$, as was found for a homogeneous reservoir.
- The choice of the maximum allowable producing $CO_2$ concentration is therefore particularly important. A low limit corresponds to a recommendation for injection to be delayed, while a high tolerance for $CO_2$ production leads to the recommendation that injection not be delayed.

The final study (Chapter 7) involved $CO_2$ injection into a model of the Naylor field. The case study had two aims. The first was to test whether the conclusions from the investigations on the simple models correlate to a more complex, more realistic scenario. The second was to optimise controllable factors in order to maximise the recovery of natural gas with the lowest producing $CO_2$ concentration possible, with a comparison to the historical recovery and the simulated recovery under primary depletion conditions. The key results were as follows:

- The Naylor field is a thin, high permeability reservoir with significant heterogeneity. This field is therefore not an ideal candidate for $CO_2$ EGR, but there is still potential to enhance recovery.
- The significant heterogeneity present led to significant uneven advancement of the displacement front with the injection of $CO_2$ occurring early. In a result mirroring that of Study 2B, the early injection of $CO_2$ resulted in a lower recovery efficiency at the 10% $CO_2$ limit than when injection was delayed. The early injection was particularly detrimental at higher rates.
- Optimisation of the proxy equation for Response 1 (recovery efficiency at a 10% $CO_2$ breakthrough limit) recommended that the injection of $CO_2$ should be delayed, with the well located in the south of the reservoir.
- The optimisation did not however achieve a recovery efficiency at the 10% $CO_2$ limit greater than both the historical recovery or the simulated primary recovery. Incremental recovery could therefore only be achieved with a producing $CO_2$ concentration greater than 10%.
- Once more, delaying the injection of $CO_2$ resulted in a more rapid increase in the $CO_2$ production rate, resulting in a lower recovery efficiency at a $CO_2$ production limit of 50%.
- Optimisation of Response 2 (recovery efficiency at a 50% $CO_2$ limit) indicated that the injection of $CO_2$ should occur in the north of the reservoir, and with low production and

injection rates. Lower rates ensured the negative effect of the heterogeneity was mitigated by allowing gravity to stabilise the displacement process.

- Optimisation of Response 3 (minimum producing $CO_2$ concentration required to achieve incremental recovery) was achieved with the same parameter level combination as Response 2.
- With incremental recovery unable to be achieved with a producing $CO_2$ concentration lower than 10%, more emphasis is therefore placed on the results of the second and third responses.
- Optimisation of Response 2 and 3 showed that incremental recovery would be achieved with a minimum producing $CO_2$ concentration of 27%, with a recovery efficiency at a 50% $CO_2$ limit of 79.6% of the OGIP. This corresponded to an incremental recovery of 17 x $10^6$ $sm^3$ over the historical production.
- Testing of the use of an impure source of $CO_2$ showed an improvement in the rate of increase in the production of $CO_2$ and therefore the recovery of natural gas at the 50% $CO_2$ limit was achieved over the use of a pure source of $CO_2$. The improvement in results using an impure source of $CO_2$ could have significant benefits in terms of the economics of a $CO_2$ EGR project.

In brief, the injection of $CO_2$ has been shown to successfully displace natural gas whilst minimising the residual trapping caused by the aquifer. Technically, the most ideal candidate for injection is one which will achieve a low primary recovery efficiency and where a stable, efficiency displacement of natural gas by $CO_2$ can be achieved. In the research conducted, this equated to a thick, non-dipping reservoir. The extent of incremental recovery achievable with the injection of $CO_2$ is only limited by the producing $CO_2$ concentration that can be economically handled.

## 9.2 Future Work

This study has focussed on the impact of injecting $CO_2$ into water-drive gas reservoirs in an attempt to eliminate/minimise residual gas trapping and displace natural gas towards the production wells. Specifically, this study has involved only the technical aspect of $CO_2$ injection into gas reservoirs as well as solely focussing on dry gas. Future work on the topic could include:

- Investigation of the economic viability of injecting $CO_2$ into natural gas reservoirs with an active water-drive. The continual research into the separation of $CO_2$ from gas streams linked with $CO_2$ sequestration is providing new and improved methods of separation with the aim to reduce costs. Reduction in the costs of $CO_2$ separation both prior to injection ($CO_2$

source) as well as from the production stream could prove beneficial to the economics of any potential $CO_2$ EGR project.

- Optimisation of the technical aspects of $CO_2$ EGR in water-drive gas reservoirs with the typical development of a natural gas field. Natural gas fields are typically developed through the establishment of long term contracts which require a specified volume of gas to be continuously delivered on a daily basis over extended periods, typically 20 years. This limitation on the potential rates that can be employed could have an influence on the ability to achieve either a viscous or gravity dominated displacement.

- Investigation of the enhancement of natural gas recovery in water-drive gas reservoirs coupled with $CO_2$ sequestration. The drivers for an EGR project might either coincide or conflict with the drivers of a $CO_2$ sequestration project. A conflicting scenario is $CO_2$ EOR and sequestration. A $CO_2$ EOR project aims to enhance oil recovery while minimising the volume of $CO_2$ injected, while a $CO_2$ sequestration project aims to inject and store as great a volume of $CO_2$ as possible.

- Investigation of the mixing of $CO_2$ and natural gas, both by molecular diffusion and advection in various porous media. Minimal experimental data was found in the literature with respect to the mixing of $CO_2$ and natural gas in porous media. While this thesis found that mixing by diffusion did not have as significant effect as other parameters, this was based upon a numerical analysis. Quantifying the mixing of $CO_2$ and natural gas at reservoir conditions through experimental studies in various porous media would provide important data for use in numerical simulation studies.

# References

Aanonsen, S. et al., 1995. Optimizing Reservoir Performance Under Uncertainty with Application to Well Location. In *Proceedings of SPE Annual Technical Conference and Exhibition*. SPE Annual Technical Conference and Exhibition.

Abdi, H., 2009. *Experimental Design and Analysis for Psychology*, Oxford University Press, New York.

Abou-Kassem, J., Farouq Ali, S. & Islam, M., 2006. Petroleum Reservoir Simulation - A Basic Approach.

Agarwal, R., Al-Hussainy, R. & Jr., H., 1965. The Importance of Water Influx in Gas Reservoirs. *Journal of Petroleum Technology*, 17(11).

Ahmed, T., 2000. *Reservoir engineering handbook*, Gulf Pub. Co. Houston Tex.

Al Salhi, M. et al., 2005. Structured Uncertainty Assessment for Fahud Field through the Application of Experimental Design and Response Surface Methods. In *Proceedings of SPE Middle East Oil and Gas Show and Conference*. SPE Middle East Oil and Gas Show and Conference.

Al-Hashami, A., Ren, S. & Tohidi, B., 2005. CO2 Injection for Enhanced Gas Recovery and Geo-Storage: Reservoir Simulation and Economics. In *Proceedings of SPE Europec/EAGE Annual Conference*. SPE Europec/EAGE Annual Conference.

Amorim, T. & Moczydlower, B., 2007. Validating the Use of Experimental Design Techniques in Exploratory Evaluations. In *Proceedings of Latin American & Caribbean Petroleum Engineering Conference*. Latin American & Caribbean Petroleum Engineering Conference.

Ancell, K. & Manhart, T., 1987. Secondary Gas Recovery From a Water-Drive Gas Reservoir: A Case Study. In *Proceedings of SPE Annual Technical Conference and Exhibition*. SPE Annual Technical Conference and Exhibition.

Bachu, S. & Adams, J.J., 2003. Sequestration of CO2 in Geological Media in Response to Climate Change: Capacity of Deep Saline Aquifers to Sequester CO2 in Solution. *Energy Conversion and Management*, 44(20), pp.3151-3175.

Bethel, F. & Calhoun, C., 1953. Capillary Desaturation in Unconsolidated Beads. *Trans., AIME*, 198, pp.197-202.

Blok, K. et al., 1997. Hydrogen Production from Natural Gas, Sequestration of Recovered CO2 in Depleted Gas Wells and Enhanced Natural Gas Recovery. *Energy*, 22(2-3), pp.161-168.

Box, G.E.P. & Behnken, D.W., 1960. Some New Three Level Designs for the Study of Quantitative Variables. *Technometrics*, 2(4), pp.455-475.

Box, G.E.P., Hunter, W. & Hunter, J., 1978. *Statistics for Experimenters : An Introduction to Design, Data Analysis, and Model Building*, Wiley, New York.

Box, G.E.P. & Wilson, K.B., 1951. On the Experimental Attainment of Optimum Conditions. *Journal of the Royal Statistical Society. Series B (Methodological)*, 13(1), pp.1-45.

Boyd, W., Christian, L. & Danielsen, C., 1982. Secondary Gas Recovery From a Watered-Out Reservoir. In *Proceedings of SPE Annual Technical Conference and Exhibition*. SPE Annual Technical Conference and Exhibition.

Brady, T., 2002. Friendswood Field - A Case Study in Reservoir Management. In *Proceedings of SPE Annual Technical Conference and Exhibition*. SPE Annual Technical Conference and Exhibition.

Brinkman, F., 1981. Increased Gas Recovery From a Moderate Water Drive Reservoir. *Journal of Petroleum Technology*, 33(12).

Burwell, E. & Jacobson, I., 1975. Concurrent Gasification and Retorting of Oil Shale - A Dual Energy Source. In *Proceedings of SPE Rocky Mountain Regional Meeting*. SPE Rocky Mountain Regional Meeting.

Cagle, T., 1990. Performance of Secondary Gas Recovery Operations: North Alazan H-21 Reservoir. In *Proceedings of SPE Annual Technical Conference and Exhibition*. SPE Annual Technical Conference and Exhibition.

Carreras, P., Johnson, S. & Turner, S., 2006. Tahiti Field: Assessment of Uncertainty in a Deepwater Reservoir Using Design of Experiments. In *Proceedings of SPE Annual Technical Conference and Exhibition*. SPE Annual Technical Conference and Exhibition.

Carreras, P., Turner, S. & Wilkinson, G., 2006. Tahiti: Development Strategy Assessment Using Design of Experiments and Response Surface Methods. In *Proceedings of SPE Western Regional/AAPG Pacific Section/GSA Cordilleran Section Joint Meeting*. SPE Western Regional/AAPG Pacific Section/GSA Cordilleran Section Joint Meeting.

Chang, Y., Coats, B. & Nolen, J., 1998. A Compositional Model for CO2 Floods Including CO2 Solubility in Water. *SPE Reservoir Evaluation & Engineering*, 1(2).

Cheong, Y. & Gupta, R., 2005. Experimental Design and Analysis Methods for Assessing Volumetric Uncertainties. *SPE Journal*, 10(3).

Cheong, Y., Gupta, R. & Vijayan, K., 2005. Managing Uncontrollable and Controllable Uncertainties using EDA Methods: A Fluvial Reservoir Case Study. In *Proceedings of SPE Asia Pacific Oil and Gas Conference and Exhibition*. SPE Asia Pacific Oil and Gas

Conference and Exhibition.

Chesney, T., Lewis, R. & Trice, M., 1982. Secondary Gas Recovery From a Moderately Strong Water Drive Reservoir: A Case History. *Journal of Petroleum Technology*, 34(9).

Chierici, G., Ciucci, G. & Long, G., 1963. Experimental Research on Gas Saturation Behind the Water Front in Gas Reservoirs Subjected to Water Drive. In *Proc. Sixth World Pet. Cong.* Frankfurt am Main.

Clemens, T. & Wit, K., 2002. CO2 Enhanced Gas Recovery Studied for an Example Gas Reservoir. In *Proceedings of SPE Annual Technical Conference and Exhibition*. SPE Annual Technical Conference and Exhibition.

Cobianco, S. et al., 1999. How To Manage Drill-In Fluid Composition To Minimize Fluid Losses During Drilling Operations. In *Proceedings of SPE/IADC Middle East Drilling Technology Conference*. SPE/IADC Middle East Drilling Technology Conference.

Cook, P., 2005. Optimizing the Blowdown of Wizard Lake. In *Proceedings of SPE International Improved Oil Recovery Conference in Asia Pacific*. SPE International Improved Oil Recovery Conference in Asia Pacific.

Corre, B. et al., 2000. Integrated Uncertainty Assessment For Project Evaluation and Risk Analysis. In *Proceedings of SPE European Petroleum Conference*. SPE European Petroleum Conference.

Craig, F. et al., 1957. A Laboratory Study of Gravity Segregation in Frontal Drives. *Trans., AIME*, 210, pp.275-282.

Crowell, D., Dean, G. & Loomis, A., 1966. *Efficiency of Gas\line Displacement from a Water-Drive Reservoir*, USBM.

Culberson, O. & McKetta, J., 1951. The Solubility of Methane in Water at Pressures to 10,000 psia. *Trans., AIME*, 192, pp.223-226.

Dake, L., 2001. *Fundamentals of Reservoir Engineering*, Elsevier, Amsterdam.

Dake, L., 2001. Practice of Reservoir Engineering (Revised Edition). Available at: http://www.knovel.com/web/portal/browse/display?_EXT_KNOVEL_DISPLAY_bookid=2184.

Damsleth, E., Hage, A. & Volden, R., 1992. Maximum Information at Minimum Cost: A North Sea Field Development Study With an Experimental Design. *Journal of Petroleum Technology*, 44(12).

Delclaud, J., 1991. Laboratory Measurements of the Residual Saturation. In *Second European Core Analysis Symposium*. London, pp. 431-451.

Diaz, D. et al., 1996. Screening Criteria for Application of Carbon Dioxide Miscible Displacement in Waterflooded Reservoirs Containing Light Oil. In *Proceedings of SPE/DOE Improved Oil Recovery Symposium*. SPE/DOE Improved Oil Recovery Symposium.

Ding, M. & Kantzas, A., 2004. Estimation of Residual Gas Saturation From Different Reservoirs. In *Proceedings of Canadian International Petroleum Conference*. Canadian International Petroleum Conference.

Doe, P., Carey, B. & Helmuth, E., 1987. The 1984 Natl. Petroleum Council Study on EOR: Chemical Processes. *Journal of Petroleum Technology*, 39(8).

Egeland, T., Holden, L. & Larsen, E., 1992. Designing Better Decisions. In *Proceedings of European Petroleum Computer Conference*. European Petroleum Computer Conference.

van Elk, J. & Guerrera, L., 2000. Improved Uncertainty Management in Field Development Studies through the Application of the Experimental Design Method to the Multiple Realisations Approach. In *Proceedings of SPE Asia Pacific Oil and Gas Conference and Exhibition*. SPE Asia Pacific Oil and Gas Conference and Exhibition.

Ennis-King, J. & Paterson, L., 2002. Engineering Aspects of Geological Sequestration of Carbon Dioxide. In *Proceedings of SPE Asia Pacific Oil and Gas Conference and Exhibition*. SPE Asia Pacific Oil and Gas Conference and Exhibition.

Esmaiel, T., Fallah Bolandtaba, S. & van Kruijsdijk, C., 2005. Reservoir Screening and Sensitivity Analysis of Waterflooding with Smart Wells through the Application of Experimental Design. In *Proceedings of SPE Middle East Oil and Gas Show and Conference*. SPE Middle East Oil and Gas Show and Conference.

Feng, W. & White, C., 2002. Designed Simulation for a Detailed 3D Turbidite Reservoir Model. In *Proceedings of SPE Gas Technology Symposium*. SPE Gas Technology Symposium.

Firoozabadi, A., Olsen, G. & Golf-Racht, T., 1987. Residual Gas Saturation in Water-Drive Gas Reservoirs. In *Proceedings of SPE California Regional Meeting*. SPE California Regional Meeting.

Fisher, R., 1973. *Statistical Tables for Biological, Agricultural, and Medical Research* 14th ed., Hafner Pub. Co, New York.

Fisher, R., 1971. *Design of Experiments* 9th ed., Macmillan.

Fishlock, T. et al., 1988. Experimental Studies on the Waterflood Residual Gas Saturation and Its Production by Blowdown. *SPE Reservoir Engineering*, 3(2).

Flett, M., Gurton, R. & Taggart, I., 2004. The Function of Gas-Water Relative Permeability

Hysteresis in the Sequestration of Carbon Dioxide in Saline Formations. In *Proceedings of SPE Asia Pacific Oil and Gas Conference and Exhibition*. SPE Asia Pacific Oil and Gas Conference and Exhibition.

Friedmann, F., Chawathe, A. & Larue, D., 2001. Assessing Uncertainty in Channelized Reservoirs Using Experimental Designs. In *Proceedings of SPE Annual Technical Conference and Exhibition*. SPE Annual Technical Conference and Exhibition.

Geffen, T. et al., 1952. Efficiency of Gas Displacement from Porous Media by Liquid Flooding. *Trans., AIME*, 195, pp.29-38.

van Genuchten, M.T., 1980. A Closed-form Equation for Predicting the Hydraulic Conductivity of Unsaturated Soils. *Soil Science Society of America Journal*, 44(5), pp.892-898.

Gerbacia, W., 1978. THE EVALUATION OF SURFACTANT SYSTEMS FOR OIL RECOVERY USING STATISTICAL DESIGN PRINCIPLES AND ANALYSIS. In *Proceedings of SPE Symposium on Improved Methods of Oil Recovery*. SPE Symposium on Improved Methods of Oil Recovery.

Ghaderi, S., Azadeh, M. & Bamdad, S., 2005. Analyzing the Electricity Consumption Using Experimental Design Technique. *American Journal of Applied Sciences*, 2(10), pp.1464-1470.

Ghomian, Y., Pope, G. & Sepehrnoori, K., 2008. Hysteresis and Field-Scale Optimization of WAG Injection for Coupled CO. In *Proceedings of SPE Symposium on Improved Oil Recovery*. SPE Symposium on Improved Oil Recovery.

Graham, R. et al., 1996. Enhanced Oil Recovery By Gas Injection: Proposed Screening Criteria. In *Proceedings of Annual Technical Meeting*. Annual Technical Meeting.

Green, D. & Willhite, G., 1998. *Enhanced oil recovery*, Richardson TX: Henry L. Doherty Memorial Fund of AIME Society of Petroleum Engineers.

Heins, R. & Friz, T., 1967. The Effect of Low Temperature on Some Physical Properties of Rock. In *Proceedings of Drilling and Rock Mechanics Conference*. Drilling and Rock Mechanics Conference.

Henson, R., Todd, A. & Corbett, P., 2002. Geologically Based Screening Criteria for Improved Oil Recovery Projects. In *Proceedings of SPE/DOE Improved Oil Recovery Symposium*. SPE/DOE Improved Oil Recovery Symposium.

Jacques, D. & Bourland, B., 1983. A Study of Solubility of Strontium Sulfate. *Society of Petroleum Engineers Journal*, 23(2).

Jerauld, G., 1997. Prudhoe Bay Gas/Oil Relative Permeability. *SPE Reservoir Engineering*, 12(1).

Jikich, S. et al., 2003. Enhanced Gas Recovery (EGR) with Carbon Dioxide Sequestration: A Simulation Study of Effects of Injection Strategy and Operational Parameters. In *Proceedings of SPE Eastern Regional Meeting*. SPE Eastern Regional Meeting.

Johnson, J., Oelkers, E. & Helgeson, H., 1992. SUPCRT92: A Software Package for Calculating the Standard Molal Thermodynamic Properties of Minerals, Gases, Aqueous Species, and Reactions from 1 to 5000 bar and 0 to 1000C. *Computers & Geosciences*, 18(7), pp.899-947.

Jones, A. et al., 1997. Rapid Assessment of Pattern Waterflooding Uncertainty in a Giant Oil Reservoir. In *Proceedings of SPE Annual Technical Conference and Exhibition*. SPE Annual Technical Conference and Exhibition.

Juanes, R. et al., 2006. Impact of relative permeability hysteresis on geological CO2 storage. *Water Resources Research*, 42(12).

Kabir, C. et al., 2002. Developing New Fields Using Probabilistic Reservoir Forecasting. In *Proceedings of SPE Annual Technical Conference and Exhibition*. SPE Annual Technical Conference and Exhibition.

Kalla, S. & White, C., 2007. Efficient Design of Reservoir Simulation Studies for Development and Optimization. *SPE Reservoir Evaluation & Engineering*, 10(6).

Katz, D.L. et al., 1966. How Water Displaces Gas from Porous Media. *Oil and Gas Journal*, pp.55-60.

Keelan, D. & Pugh, V., 1975. Trapped-Gas Saturations in Carbonate Formations. *Society of Petroleum Engineers Journal*, 15(2).

Keelan, D., 1976. A Practical Approach to Determination of Imbibition Gas-Water Relative Permeability. *Journal of Petroleum Technology*, 28(2).

Kumar, A. et al., 2005. Reservoir Simulation of CO2 Storage in Deep Saline Aquifers. *SPE Journal*, 10(3).

Land, C., 1968. Calculation of Imbibition Relative Permeability for Two- and Three-Phase Flow From Rock Properties. *Society of Petroleum Engineers Journal*, 8(2).

Lazic, Z., 2004. *Design of Experiments in Chemical Engineering a Practical Guide*, Wiley-VCH, Weinheim.

Lee, L. et al., 2006. Application of Model-Based Uncertainty Analysis. In *Proceedings of Abu Dhabi International Petroleum Exhibition and Conference*. Abu Dhabi International Petroleum Exhibition and Conference.

Lemmon, E., McLinden, M. & Friend, D., 2010. Thermophysical Properties of Fluid Systems.

Available at: http://webbook.nist.gov [Accessed January 13, 2010].

Lutes, J. et al., 1977. Accelerated Blowdown of a Strong Water-Drive Gas Reservoir. *Journal of Petroleum Technology*, 29(12).

Mamora, D. & Seo, J., 2002. Enhanced Gas Recovery by Carbon Dioxide Sequestration in Depleted Gas Reservoirs. In *Proceedings of SPE Annual Technical Conference and Exhibition*. SPE Annual Technical Conference and Exhibition.

McKay, B., 1977. Laboratory Studies of Gas Displacement from Sandstone Reservoirs Having Strong Water Drive. *APEA Journal*, pp.189-194.

van der Meer, L. et al., 2005. K12-B: A Test Site for CO2 Storage and Enhanced Gas Recovery. In *Proceedings of SPE Europec/EAGE Annual Conference*. SPE Europec/EAGE Annual Conference.

Metz, B. et al. eds., 2005. *IPCC special report on carbon dioxide capture and storage*, Cambridge University Press for the Intergovernmental Panel on Climate Change, Cambridge.

Mohammed-Singh, L., Singhal, A. & Sim, S., 2006. Screening Criteria for Carbon Dioxide Huff 'n' Puff Operations. In *Proceedings of SPE/DOE Symposium on Improved Oil Recovery*. SPE/DOE Symposium on Improved Oil Recovery.

Moltz, A., 1993. Modeling a Repressured Waterdrive Gas Reservoir. *Journal of Petroleum Technology*, 45(4).

Montevechi, J.A.B. et al., 2007. Application of design of experiments on the simulation of a process in an automotive industry. In *Proceedings of the 39th conference on Winter simulation: 40 years! The best is yet to come*. Washington D.C.: IEEE Press, pp. 1601-1609.

Montgomery, D., 2001. *Design and Analysis of Experiments* 5th ed., John Wiley, New York.

Montgomery, D., Peck, E. & Vining, G., 2006. *Introduction to Linear Regression Analysis* 4th ed., Wiley-Interscience, Hoboken N.J.

Muskat, M., 1981. *Physical Principles of Oil Production* 2nd ed., International Human Resources Development Corp, Boston.

Myers, R., 2009. *Response Surface Methodology : Process and Product Optimization using Designed Experiments.* 3rd ed., Hoboken N.J.: Wiley.

Myers, R., 1990. *Classical and Modern Regression with Applications* 2nd ed., Duxbury/Thompson Learning, Pacific Grove CA.

Nattwongasem, D. & Jessen, K., 2009. Residual Trapping of CO2 in Aquifers During the

Counter-Current Flow. In *Proceedings of SPE Annual Technical Conference and Exhibition*. SPE Annual Technical Conference and Exhibition.

Nghiem, L. et al., 2009. Optimization of Residual Gas and Solubility Trapping for $CO^2$ Sequestration in Saline Aquifers. In *Proceedings of SPE Reservoir Simulation Symposium*. SPE Reservoir Simulation Symposium.

NIST, 1992. *NIST Database 14 Mixture Property Database*,

Oldenburg, C., 2003. Carbon Sequestration in Natural Gas Reservoirs: Enhanced Gas Recovery and Natural Gas Storage. In *Proc. TOUGH Symposium 2003*. Berkeley, USA.

Oldenburg, C. & Benson, S., 2001. Carbon Sequestration with Enhanced Gas Recovery: Identifying Candidate Sites for Pilot Study. In *Proc. of NETL First National Conference on Carbon Sequestration*. Pennsylvania, USA.

Oldenburg, C. et al., 2003. Mixing of CO2 and CH4 in Gas Reservoirs: Code Comparison Studies. In *Greenhouse Gas Control Technologies - 6th International Conference*. Oxford: Pergamon, pp. 443-448.

Oldenburg, C., Pruess, K. & Benson, S., 2001. Process Modeling of CO2 Injection into Natural Gas Reservoirs for Carbon Sequestration and Enhanced Gas Recovery. *Energy & Fuels*, 15(2), pp.293-298.

Olea, R., 1999. *Geostatistics for Engineers and Earth Scientists*, Kluwer Academic, Boston.

Papay, J., 1999. Improved Recovery of Conventional Natural Gas. Part 1: Theoretical Discussion of Recovery Methods. *Erdoel, Erdgas, Kohle*, 6, pp.302-308.

Papay, J., 1999. Improved Recovery of Conventional Natural Gas. Part 2: Results of a Pilot Test. *Erdoel, Erdgas, Kohle*, 7-8, pp.354-355.

Peake, W., Abadah, M. & Skander, L., 2005. Uncertainty Assessment using Experimental Design: Minagish Oolite Reservoir. In *Proceedings of SPE Reservoir Simulation Symposium*. SPE Reservoir Simulation Symposium.

Pirson, S., 1958. *Oil Reservoir Engineering*, McGraw-Hill.

Pruess, K., 2004. Code intercomparison builds confidence in numerical simulation models for geologic disposal of CO2. *Energy*, 29(9-10), pp.1431-1444.

Pruess, K. & Garcia, J., 2002. Multiphase Flow Dynamics During CO2 Disposal into Saline Aquifers. *Environmental Geology*, 42(2-3), pp.282-295.

Pruess, K. & Garcia, J., 2005. *Solutions of test problems for disposal of CO2 in saline aquifers*, Lawrence Berkeley National Laboratory.

Pruess, K. et al., 2002. *Intercomparison of Numerical Simulation Codes for Geologic Disposal of CO2*, Lawrence Berkeley National Laboratory.

Pruess, K. et al., 2001. *Intercomparison of Simulation Models for CO2 Disposal in Underground Storage Reservoirs*, Lawrence Berkeley National Laboratory.

Randolph, P. & Wible, J., 1986. Co-Production of the N.E. Hitchcock Field, Galveston, Texas. In *Proceedings of SPE Unconventional Gas Technology Symposium*. SPE Unconventional Gas Technology Symposium.

Rogers, L., 1984. Test of Secondary Gas Recovery by Coproduction of Gas and Water From Mt. Selman Field, TX. In *Proceedings of SPE Unconventional Gas Recovery Symposium*. SPE Unconventional Gas Recovery Symposium.

Sayegh, S.G. & Najman, J., 1987. Phase Behavior Measurements of CO2-SO2-Brine Mixtures. *The Canadian Journal of Chemical Engineering*, 65(2), pp.314-320.

Schlumberger, 2007. *PVTi*, Houston, TX, USA: Schlumberger Information Solutions Inc.

Sciortino, A., 2002. Experimental design and model parameter estimation for locating a dissolving dense nonaqueous phase liquid pool in groundwater. *Water Resources Research*, 38(5).

Secklehner, S., Arzmüller, G. & Clemens, T., 2010. Tight Ultra-deep Gas Field Production Optimisation - Development Optimisation and CO2 Enhanced Gas Recovery Potential of the Schoenkirchen Uebertief Gas Field, Austria. In *Proceedings of SPE Deep Gas Conference and Exhibition*. SPE Deep Gas Conference and Exhibition.

Seo, J. & Mamora, D., 2003. Experimental and Simulation Studies of Sequestration of Supercritical Carbon Dioxide in Depleted Gas Reservoirs. In *Proceedings of SPE/EPA/DOE Exploration and Production Environmental Conference*. SPE/EPA/DOE Exploration and Production Environmental Conference.

Setzmann, U. & Wagner, W., 1991. A New Equation of State and Tables of Thermodynamic Properties for Methane Covering the Range from the Melting Line to 625 K at Pressures up to 100 MPa. *Journal of Physical and Chemical Reference Data*, 20(6), pp.1061-1155.

Shaw, J. & Bachu, S., 2002. Screening, Evaluation, and Ranking of Oil Reservoirs Suitable for CO2-Flood EOR and Carbon Dioxide Sequestration. *Journal of Canadian Petroleum Technology*, 41(9).

Shock, E., Helgeson, H. & Sverjensky, D., 1989. Calculation of the Thermodynamic and Transport Properties of Aqueous Species at High Pressures and Temperatures: Standard Partial Molal Properties of Inorganic Neutral Species. *Geochimica et Cosmochimica Acta*, 53(9), pp.2157-2183.

Sigmund, P., 1976. Prediction of Molecular Diffusion At Reservoir Conditions. Part 1- Measurement And Prediction of Binary Dense Gas Diffusion Coefficients. *Journal of Canadian Petroleum Technology*.

Sim, S. et al., 2008. Enhanced Gas Recovery: Factors Affecting Gas-Gas Displacement Efficiency. In *Proceedings of Canadian International Petroleum Conference*. Canadian International Petroleum Conference.

Span, R. & Wagner, W., 1996. A New Equation of State for Carbon Dioxide Covering the Fluid Region from the Triple-Point Temperature to 1100 K at Pressures up to 800 MPa. *Journal of Physical and Chemical Reference Data*, 25(6), pp.1509-1596.

Spencer, L. & Pedalina, F., 2006. *Otway Basin Pilot Project, Naylor Field, Waarre Formation Unit C; Reservoir Static Models*, CRC for Greenhouse Gas Technologies, Canberra. CO2CRC.

Spiteri, E. et al., 2005. Relative-Permeability Hysteresis: Trapping Models and Application to Geological CO2 Sequestration. In *Proceedings of SPE Annual Technical Conference and Exhibition*. SPE Annual Technical Conference and Exhibition.

Spycher, N. & Reed, M., 1988. Fugacity Coefficients of H2, CO2, CH4, H2O and of H2O- CO2-CH4 Mixtures: A Virial Equation Treatment for Moderate Pressures and Temperatures Applicable to Calculations of Hydrothermal Boiling. *Geochimica et Cosmochimica Acta*, 52(3), pp.739-749.

Standing, M., 1974. *Notes of Relative Permeability Relationships*, Division of Petroleum Engineering and Applied Geophysics, Norwegian Institute of Technology, University of Trondheim.

Stat-Ease, 2008. *Design-Expert*, Minneapolis, MN, USA: Stat-Ease Inc.

Stegemeier, G., 1977. Mechanisms of Entrapment and Mobilization of Oil in Porous Media. In *Improved Oil Recovery by Surfactant and Polymer Flooding*. New York City: Academic Press.

Suzanne, K. et al., 2003. Experimental Relationships Between Residual Gas Saturation and Initial Gas Saturation in Heterogeneous Sandstone Reservoirs. In *Proceedings of SPE Annual Technical Conference and Exhibition*. SPE Annual Technical Conference and Exhibition.

Taber, J., 1969. Dynamic and Static Forces Required To Remove a Discontinuous Oil Phase from Porous Media Containing Both Oil and Water. *Society of Petroleum Engineers Journal*, 9(1).

Taber, J., 1983. Technical Screening Guides for the Enhanced Recovery of Oil. In *Proceedings of SPE Annual Technical Conference and Exhibition*. SPE Annual Technical Conference and Exhibition.

Taber, J., Martin, F. & Seright, R., 1997. EOR Screening Criteria Revisited - Part 1: Introduction to Screening Criteria and Enhanced Recovery Field Projects. *SPE Reservoir Engineering*, 12(3).

Taber, J., Martin, F. & Seright, R., 1997. EOR Screening Criteria Revisited—Part 2: Applications and Impact of Oil Prices. *SPE Reservoir Evaluation & Engineering*, 12(3).

Tek, M., 1989. *Underground Storage of Natural Gas : Theory and Practice*, Kluwer Academic Publishers, Dordrecht Boston.

Thomas, B., 1998. Proposed Screening Criteria For Gas Injection Evaluation. *Journal of Canadian Petroleum Technology*, 37(11).

Torrest, R., 1982. Aspects of Slurry and Particle Settling and Placement for Viscous Gravel \line Packing (AQUAPAC). In *Proceedings of SPE Annual Technical Conference and Exhibition*. SPE Annual Technical Conference and Exhibition.

Turta, A. et al., 2007. Basic Investigations on Enhanced Gas Recovery by Gas-Gas Displacement. In *Proceedings of Canadian International Petroleum Conference*. Canadian International Petroleum Conference.

Vincent, G., Corre, B. & Thore, P., 1999. Managing Structural Uncertainty in a Mature Field for Optimal Well Placement. *SPE Reservoir Evaluation & Engineering*, 2(4).

Vincent, G., Corre, B. & Thore, P., 1999. Managing Structural Uncertainty in a Mature Field for Optimal Well Placement. *SPE Reservoir Evaluation & Engineering*, 2(4).

Wagmann, D. et al., 1982. The NBS Tables of Chemical and Thermodynamic Propertiies. *Journal of Physical and Chemical Reference Data*, 11, supplement no. 2.

White, C. & Royer, S., 2003. Experimental Design as a Framework for Reservoir Studies. In *Proceedings of SPE Reservoir Simulation Symposium*. SPE Reservoir Simulation Symposium.

White, C. et al., 2001. Identifying and Estimating Significant Geologic Parameters With Experimental Design. *SPE Journal*, 6(3).

Wiebe, R. & Gaddy, V.L., 1940. The Solubility of Carbon Dioxide in Water at Various Temperatures from 12 to 40° and at Pressures to 500 Atmospheres. *Journal of the American Chemical Society*, 62(4), pp.815-817.

Willhite, G., 1986. *Waterflooding*, Society of Petroleum Engineers, Richardson TX.

Xu, J., 2006. *Otway Basin Pilot Project: Naylor-1 History Matching*, CRC for Greenhouse Gas Technologies, Canberra. CO2CRC.

# Appendix A – Regression Analysis

The data compiled from the completion of the experimental runs as stipulated by the experimental design is analysed using regression analysis. Regression involves approximating an observed, empirical output or response using an estimated output. This estimated output is based on a relationship between the output and one or more input variables. The most widely used method to fit a model to a dataset is the linear regression method (linear least squares regression) (NIST, 1992).

## A.1 Linear Regression Models

To introduce linear regression models, consider a first order linear regression model:

$$y = \beta_0 + \beta_1 x_1 + \beta_2 x_2 + \varepsilon \quad \text{(A.1)}$$

This is a multiple linear regression model with two independent variables, $x_1$ and $x_2$. The independent variables are also called predictor variables or regressors. This model describes a plane in the $x_1$, $x_2$ plane with the intercept of the plane being $\beta_0$.

The term linear applies because the above models are linear functions of the unknown parameters $\beta_j$ regardless of the shape of the response surface that it generates (not necessarily linear in the $x_j$).

In general a response variable *y* can be related to *k* regressor variables.

$$y = \beta_0 + \beta_1 x_1 + \beta_2 x_2 + \cdots \beta_k x_k + \varepsilon \quad \text{(A.2)}$$

The model above is called a multiple linear regression model with *k* regressor variables. The parameters $\beta_j$, $j = 0, 1, \ldots, k$, are called regression coefficients. The parameter $\beta_j$ represents the expected change in response y per unit change in $x_j$ when all of the remaining variables, $x_i$ $(i \neq j)$, are held constant.

The method to estimate the coefficients $\beta_j$ is called least squares estimation. The following will demonstrate how to generate the least squares estimators ($b_j$, $j = 0, 1, \ldots, k$) which represent the regression coefficients ($\beta_j$, $j = 0, 1, \ldots, k$) using the least squares methodology.

Suppose we have a linear regression model as shown in equation A.3,

$$y_i = \beta_0 + \sum_{j=1}^{k} \beta_j x_{ij} + \varepsilon_i, \qquad i = 1, 2, \ldots, n \tag{A.3}$$

where $y_i$ = Observed response

$x_{ij}$ = Observed regressor variable

$\beta_j$ = Regression coefficients

$\varepsilon_i$ = Error term for each observation

$n$ = Number of observations.

The method of least squares assigns $\beta$'s so that the sum of squares of the errors $\varepsilon_i$ is minimised. The least squares function is

$$L = \sum_{i=1}^{n} \varepsilon_i^2$$

$$= \sum_{i=1}^{n} \left(y_i - \beta_0 - \sum_{j=1}^{k} \beta_j x_{ij}\right)^2 \tag{A.4}$$

The function L is to be minimised with respect to $\beta_0, \beta_1, \ldots, \beta_k$.

The least squares estimators, say $b_0, b_1, \ldots, b_k$, must satisfy

$$\left.\frac{\partial L}{\partial \beta_0}\right|_{b_0, b_1, \ldots, b_k} = -2 \sum_{i=1}^{n} \left(y_i - b_0 - \sum_{j=1}^{k} b_j x_{ij}\right) = 0 \tag{A.5a}$$

and

$$\left.\frac{\partial L}{\partial \beta_j}\right|_{b_0, b_1, \ldots, b_k} = -2 \sum_{i=1}^{n} \left(y_i - b_0 - \sum_{j=1}^{k} b_j x_{ij}\right) x_{ij} = 0 \qquad j = 1, 2, \ldots, k \tag{A.5b}$$

A simpler form is to express these equations in matrix notation. Equation A.2 in matrix notation is

$$\mathrm{y} = \mathrm{X}\beta + \varepsilon \tag{A.6}$$

where

$$y = \begin{bmatrix} y_1 \\ y_2 \\ \vdots \\ y_n \end{bmatrix} \quad X = \begin{bmatrix} 1 & x_{11} & \cdots & x_{1k} \\ 1 & x_{21} & \cdots & x_{2k} \\ \vdots & \vdots & \ddots & \vdots \\ 1 & x_{n1} & \cdots & x_{nk} \end{bmatrix} \quad \beta = \begin{bmatrix} \beta_0 \\ \beta_1 \\ \vdots \\ \beta_k \end{bmatrix} \quad \varepsilon = \begin{bmatrix} \varepsilon_0 \\ \varepsilon_1 \\ \vdots \\ \varepsilon_n \end{bmatrix}$$

*y* is an (n x 1) vector of the observations, *X* is an (n x p) matrix of the levels of the independent variables, *β* is a (p x 1) vector of regression coefficients, and *ε* is an (n x 1) vector of random errors. Note *X´* is the transpose of *X*.

It is desired to find the vector of least squares estimators, *b*, that minimises

$$L = \sum_{i=1}^{n} \varepsilon_i^2 = \varepsilon'\varepsilon = (y - X\beta)'(y - X\beta) \qquad (A.7)$$

Expanding *L*

$$L = y'y - \beta'X'y - y'X\beta + \beta'X'X\beta \qquad (A.8)$$

which may be expressed as

$$L = y'y - 2\beta'X'y + \beta'X'X\beta \qquad (A.9)$$

as *β'X'y* is a (1 x 1) matrix, or scalar, and its transpose *(β'X'y)' = y'Xβ* is the same scalar.

The least squares estimator must satisfy

$$\left.\frac{\partial L}{\partial \beta}\right|_b = -2X'y + 2X'Xb = 0 \qquad (A.10)$$

which simplifies to

$$X'Xb = X'y \qquad (A.11)$$

which is the matrix form of equation A.5.

The least squares estimator of β is found by multiplying both sides with the inverse of X'X.

$$\mathrm{b} = (\mathrm{X}'\mathrm{X})^{-1}\mathrm{X}'\mathrm{y} \tag{A.12}$$

The fitted regression model is

$$\hat{\mathrm{y}} = \mathrm{Xb} \tag{A.13}$$

In scalar notation, the fitted model is

$$\hat{y}_i = b_0 + \sum_{i=1}^{k} b_j x_{ij} \tag{A.14}$$

The difference between the actual observation $y_i$ and the corresponding fitted value $\hat{y}_i$ is the residual,

$$e_i = y_i - \hat{y}_i \tag{A.15}$$

The (n x 1) vector of the residuals is denoted by

$$\mathrm{e} = \mathrm{y} - \hat{\mathrm{y}} \tag{A.16}$$

## A.2 Hypothesis Testing in Multiple Regression

Certain tests of hypothesis about the model parameters are useful in measuring the significance of the model. In other words, hypothesis testing is used to determine whether there is a linear relationship between the response variable, *y*, and the regressor variables, $x_{ij}$. These tests require that the residuals (error), *e*, in the model be normally and independently distributed with a mean of zero and a variance $\sigma^2$ ($\varepsilon \sim \mathrm{NID}(0, \sigma^2)$). The observations as a result of this assumption are normally and independently distributed with a mean $\beta_0 + \sum_{j=1}^{k} \beta_j x_{ij}$ and variance $\sigma^2$.

**Test for Significance of Regression**

The test for significance of regression is performed to establish whether there is a linear relationship between the response variable y and the subset of the regressor variables $x_1, x_2, \ldots, x_k$.

The appropriate hypotheses are

$$H_0: \beta_1 = \beta_2 = \cdots = \beta_k = 0 \tag{A.17}$$

$$H_1: \beta_j \neq 0 \tag{A.18}$$

Rejection of $H_0$ implies that at least one regressor variable contributes significantly to the model. The testing procedure involves using analysis of variance partitioning of the total sum of squares $SS_T$ into the sum of squares due to the model ($SS_R$) and the sum of squares due to the residual ($SS_E$).

$$SS_T = SS_R + SS_E \tag{A.19}$$

The sum of squares due to the residual is defined as

$$SS_E = y'y - b'X'y \tag{A.20}$$

And the sum of squares due to the regression is defined as

$$SS_R = b'X'y - \frac{\left(\sum_{i=1}^{n} y_i\right)^2}{n} \tag{A.21}$$

Therefore the total sum of squares is defined as

$$SS_T = y'y - \frac{\left(\sum_{i=1}^{n} y_i\right)^2}{n} \tag{A.22}$$

The test procedure for $H_0$:$\beta_1 = \beta_2 = \ldots. = \beta_k = 0$ is to compute

$$F_0 = \frac{SS_R/k}{SS_E/(n-k-1)} = \frac{MS_R}{MS_E} \tag{A.23}$$

and to reject $H_0$ if

$$F_0 > F_{\alpha,\mathrm{k},\mathrm{n}-\mathrm{k}-1} \tag{A.24}$$

Note MS is the mean square. The value of $F_{\alpha,k,n-k-1}$ can be obtained from an F-distribution table, and $\alpha$ is known as the significance level. In words, for a significance level $\alpha$, the hypothesis that the regression model is not significant can be rejected at the $\alpha$-level if $F_0 > F_{crit} = F_{\alpha,\ k,\ n-k-1}$. Significance levels of 0.10, 0.05, 0.01 are used to determine the critical values $F_{crit}$, obtained from the F distribution table, where decreasing significance levels indicate increasing confidence for the model.

An analysis of variance (ANOVA) table (Table A-1) is commonly used to summarise the test of significance of the model.

**Table A-1: An analysis of variance (ANOVA) table**

| Source of Variation | Sum of Squares | Degrees of Freedom | Mean Square | $F_0$ | Significance or Error Probability P |
|---|---|---|---|---|---|
| Regression Model | $SS_R$ | $i$ | $MS_R = SS_R/i$ | $MS_R/MS_E$ | $= P(H_0:F_0 \leq F_{crit})$ |
| Residual (Error) | $SS_E$ | $n$-1-$i$ | $MS_E = SS_E/(n$-1-$i)$ | | |
| Total | $SS_T$ | $n$-1 | | | |

A common statistic to measure the adequacy of the fit of the model is the coefficient of multiple determination, $R^2$, defined as

$$R^2 = \frac{SS_R}{SS_T} = 1 - \frac{SS_E}{SS_T} \tag{A.25}$$

$R^2$ is a measure of the amount of variability reduction of $y$ obtained using the regressor variables $x_1$, $x_2$,…., $x_k$ in the model. It is a measure of how well the regression line fits the data. $R^2$ is in the range of 0 to 1 with a value of 1 indicating that the regression model fits perfectly with the data points. One precaution does however exist with the coefficient of multiple determination. A large value of $R^2$ does not however necessarily imply that the regression model is suitable since adding a variable to the model will always increase $R^2$ regardless of whether the variable is statistically significant or not.

The introduction of another statistic, the adjusted $R^2$, as an alternative aims to solve this problem. The adjusted $R^2$ statistic is defined as

$$R^2_{adj} = 1 - \frac{SS_E/(n-p)}{SS_T/(n-1)} = 1 - \frac{(n-1)}{(n-p)}(1 - R^2) \tag{A.26}$$

In general the $R^2_{adj}$ statistic doesn't automatically increase as variables are added to the model. If the variable added is not statistically significant, this will reduce the fit of the regression model, decreasing the $R^2_{adj}$ statistic. When $R^2$ and $R^2_{adj}$ differ dramatically, there is a good chance that non-significant variables have been included in the model.

**Tests on Individual Regression Coefficients**

Tests on individual regression coefficients are useful in determining the value of each regressor variable in the regression model, therefore testing the significance of each variable. The addition/subtraction of variables from the model can either increase or decrease the effectiveness of the model in fitting the data. It therefore forms the basis of model optimisation.

The hypothesis testing of the significance of individual regression coefficients ($\beta_j$) are

$$H_0: \beta_j = 0 \quad \text{(A.27)}$$

$$H_1: \beta_j \neq 0 \quad \text{(A.28)}$$

If $H_0$: βj = 0 is not rejected, this indicates that $x_j$ can be deleted from the model. A t-statistic is used as the test statistic for this hypothesis

$$t_0 = \frac{b_j}{\sqrt{\sigma^2 C_{ij}}} \quad \text{(A.29)}$$

where $C_{ij}$ is the diagonal element of $(X'X)^{-1}$ corresponding to $b_j$. The null hypothesis $H_0$:$\beta_j$ = 0 is rejected if

$$|t_0| > t_{\alpha/2,n-k-1} \quad \text{(A.30)}$$

Once more, the value for $t_{\alpha/2,\ n\text{-}k\text{-}1}$ can be obtained from a t-distribution table. For instance, for α=0.05, it would be said that there is a 5% error probability that the corresponding coefficient is not significant. Note that this is a partial or marginal test as the regression coefficient $b_j$ depends on all of the other regressor variables $x_i (i \neq j)$ that are in the model. These coefficients can change significantly with a different set of regressor variables.

In summary, the test for significance of regression will determine the applicability of the model as a whole to replicate the results of the experimental runs, and its usefulness in predicting untested areas of the design space. The test on the individual regression coefficients will determine the effect of each coefficient (main effect or interaction) in the model and whether that coefficient significantly influences the response (i.e. whether permeability significantly influences oil recovery).

**Regression Model Diagnostics**

An important part of the regression analysis is checking the adequacy of the model in replicating the data. Aside from the $R^2$ and $R^2_{adj}$ statistics, the primary diagnostic tool is residual analysis. If the model is adequate, then the residuals should be structureless (i.e. contain no obvious pattern). Graphical analysis of the residuals is one of the easiest and most effective methods of residual analysis. Recall the normality assumption, where the residuals in the model are to be normally and independently distributed with a mean of zero and a constant but unknown variance $\sigma^2$. A useful method to check if this assumption is valid is the construction of a normal probability plot using the residuals. Figure A.1 presents a normal probability plot.

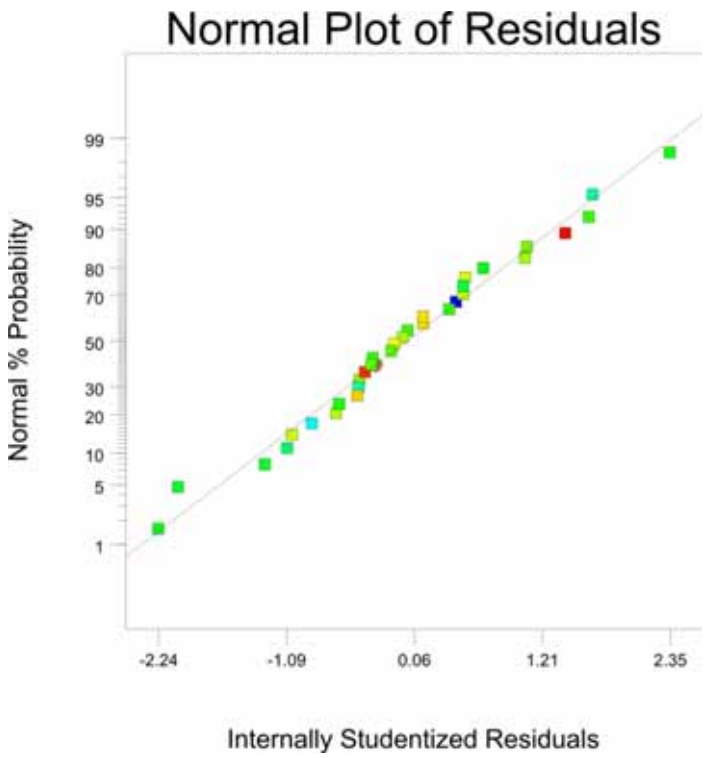


**Figure A.1: Normal probability plot of the studentized residuals**

Under the normality assumption, the residuals in the plot should fall on the straight line. In reality, the residuals do not strictly lie on the straight line, however these moderate departures from normality are acceptable, as is the case in Figure 4. Significant departures from normality, as is the case in Figure A.2, are of concern, and need to be further investigated in order to try and determine the possible causes of model inadequacy. Common departures from normality are observed by definite patterns in the residuals such as an 'S-shape' curve. One method which can potentially improve the analysis is the use of a transformation, discussed below.

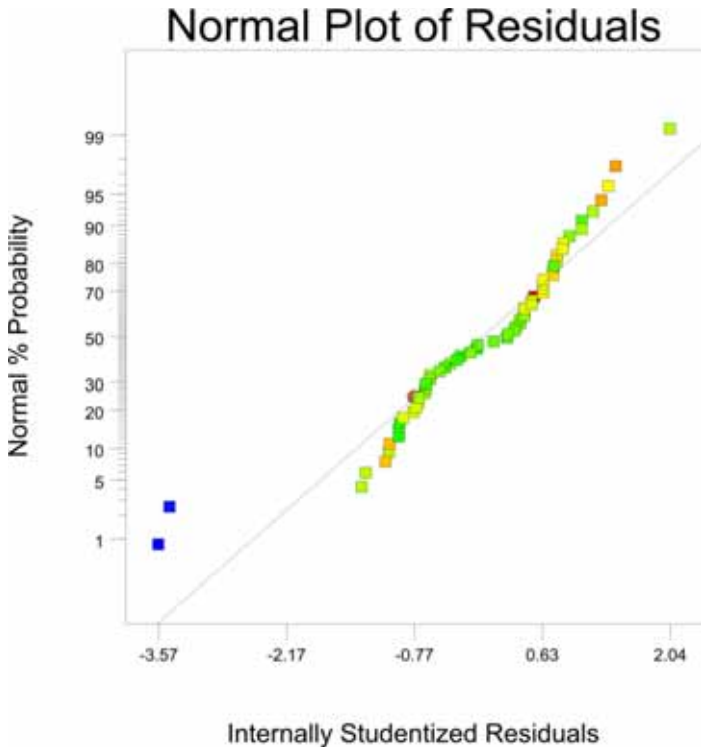


**Figure A.2: Normal probability plot which departs from the normality assumption**

Other graphical methods include plots of the residuals versus the fitted values ($y_{ij}$), and the residuals versus experimental design run. The plot of residuals versus the fitted values tests for the assumption of constant variance. The plot should be structureless if this assumption is held. The plot of residuals versus experimental design run aids in determining if there is any correlation amongst the residuals, such as a period of positive residuals followed by a period of negative residuals. Again the plot should be structureless. If a pattern is observed in any of these plots, again a transformation can be used in an attempt to achieve a better fit of the model to the data and satisfy the assumptions.

**Transformations**

When the various regression assumptions are violated, model transformation can be used to alter the residuals so that they follow a normal distribution, stabilise the response variance (achieve constant variance) and to achieve a better fit of the model to the data. Some common transformations are as follows

| | | |
|---|---|---|
| Square root | $y' = \sqrt{y + k}$ | (A.31) |
| Natural log | $y' = \ln (y + k)$ | (A.32) |
| Inverse square root | $y' = \frac{1}{\sqrt{y+k}}$ | (A.33) |
| Inverse | $y' = \frac{1}{y+k}$ | (A.34) |
| Power | $y' = (y + k)^{\lambda}$ | (A.35) |

In addition to the residual plots, there are a number of other model diagnostics that can be used in regression analysis. These diagnostic tools will only be briefly mentioned here, for more complete descriptions refer to references such as (Raymond Myers 1990; D. Montgomery 2001; D.C. Montgomery *et al*. 2006; R. Myers 2009). These diagnostics include scaled residuals such as standardized and studentized residuals, which are useful for determining outliers, with these outliers potentially having a high influence on the analysis of the model. Prediction error sum of squares (PRESS) is also another form of residual scaling. If there is a large difference between the ordinary residual and the PRESS residual then this indicates that this is a point where the model fits the data well, but a model without this points predicts poorly. As such, the PRESS residual can be used to compute an approximate $R^2$ for prediction ($R^2_{prediction}$) which gives an indication of the predictive capability of the regression model (an important aspect of using ED and regression analysis in the oil and gas industry).

## A.3 References

Montgomery, D., 2001. *Design and Analysis of Experiments* 5th ed., John Wiley, New York.

Montgomery, D., Peck, E. & Vining, G., 2006. *Introduction to Linear Regression Analysis* 4th ed., Wiley-Interscience, Hoboken N.J.

Myers, R., 2009. *Response Surface Methodology : Process and Product Optimization using Designed Experiments.* 3rd ed., Hoboken N.J.: Wiley.

Myers, R., 1990. *Classical and Modern Regression with Applications* 2nd ed., Duxbury/Thompson Learning, Pacific Grove CA.

# Appendix B – ANOVA Tables

## B.1 Study 1

**Table B-1: ANOVA table for Response 1: $CH_4$ recovery efficiency at a 10% $CO_2$ breakthrough limit**

| Source | Sum of Squares | df | Mean Square | F Value | p-value Prob > F |
|---|---|---|---|---|---|
| Model | 4403.05 | 26 | 169.35 | 90.13 | < 0.0001 |
| A-Permeability | 59.91 | 1 | 59.91 | 31.88 | < 0.0001 |
| B-$k_v/k_h$ Ratio | 0.36 | 1 | 0.36 | 0.19 | 0.6667 |
| C-Diffusion | 139.23 | 1 | 139.23 | 74.1 | < 0.0001 |
| D-Salinity | 59.41 | 1 | 59.41 | 31.62 | < 0.0001 |
| E-Aquifer Size | 188.03 | 1 | 188.03 | 100.07 | < 0.0001 |
| F-Thickness | 195.59 | 1 | 195.59 | 104.09 | < 0.0001 |
| G-Dip | 115.9 | 1 | 115.9 | 61.68 | < 0.0001 |
| AB | 337.51 | 1 | 337.51 | 179.63 | < 0.0001 |
| AD | 127.32 | 1 | 127.32 | 67.76 | < 0.0001 |
| AF | 71.26 | 1 | 71.26 | 37.93 | < 0.0001 |
| AG | 832.74 | 1 | 832.74 | 443.19 | < 0.0001 |
| BC | 104.44 | 1 | 104.44 | 55.59 | < 0.0001 |
| BD | 12.81 | 1 | 12.81 | 6.82 | 0.0205 |
| BE | 181.77 | 1 | 181.77 | 96.74 | < 0.0001 |
| BF | 32.2 | 1 | 32.2 | 17.14 | 0.001 |
| BG | 247.62 | 1 | 247.62 | 131.79 | < 0.0001 |
| CE | 40.71 | 1 | 40.71 | 21.67 | 0.0004 |
| CF | 58.7 | 1 | 58.7 | 31.24 | < 0.0001 |
| DE | 78.06 | 1 | 78.06 | 41.54 | < 0.0001 |
| EF | 91.32 | 1 | 91.32 | 48.6 | < 0.0001 |
| EG | 49.92 | 1 | 49.92 | 26.57 | 0.0001 |
| FG | 189.29 | 1 | 189.29 | 100.74 | < 0.0001 |
| $C^2$ | 35.25 | 1 | 35.25 | 18.76 | 0.0007 |
| $D^2$ | 92 | 1 | 92 | 48.96 | < 0.0001 |
| $F^2$ | 123.46 | 1 | 123.46 | 65.71 | < 0.0001 |
| $G^2$ | 31.31 | 1 | 31.31 | 16.67 | 0.0011 |
| Residual | 26.31 | 14 | 1.88 | | |
| Lack of Fit | 26.31 | 11 | 2.39 | | |
| Pure Error | 0 | 3 | 0 | | |
| Cor Total | 4429.35 | 40 | | | |
| | | | | | |
| Std. Dev. | 1.3707 | | R-Squared | 0.9941 | |
| Mean | 62.6906 | | Adj R-Squared | 0.9830 | |
| C.V. % | 2.2118 | | Pred R-Squared | 0.9345 | |
| PRESS | 290.2744 | | Adeq Precision | 43.8636 | |

**Table B-2: ANOVA table for Response 2: Minimum producing $CO_2$ concentration required to achieve incremental recovery**

| Source | Sum of Squares | df | Mean Square | F Value | p-value Prob > F |
|---|---|---|---|---|---|
| Model | 31373.26 | 23 | 1364.05 | 68.19 | < 0.0001 |
| A-Permeability | 2862.67 | 1 | 2862.67 | 143.10 | < 0.0001 |
| B-$k_v/k_h$ Ratio | 1170.08 | 1 | 1170.08 | 58.49 | < 0.0001 |
| C-Diffusion | 51.55 | 1 | 51.55 | 2.58 | 0.1258 |
| D-Salinity | 20.35 | 1 | 20.35 | 1.02 | 0.3266 |
| E-Aquifer Size | 280.41 | 1 | 280.41 | 14.02 | 0.0015 |
| F-Thickness | 888.79 | 1 | 888.79 | 44.43 | < 0.0001 |
| G-Dip | 9671.56 | 1 | 9671.56 | 483.48 | < 0.0001 |
| AB | 2988.93 | 1 | 2988.93 | 149.42 | < 0.0001 |
| AC | 353.14 | 1 | 353.14 | 17.65 | 0.0005 |
| AF | 242.67 | 1 | 242.67 | 12.13 | 0.0027 |
| AG | 4003.32 | 1 | 4003.32 | 200.13 | < 0.0001 |
| BC | 93.57 | 1 | 93.57 | 4.68 | 0.0443 |
| BE | 685.86 | 1 | 685.86 | 34.29 | < 0.0001 |
| BG | 659.66 | 1 | 659.66 | 32.98 | < 0.0001 |
| CD | 76.59 | 1 | 76.59 | 3.83 | 0.0661 |
| CF | 156.40 | 1 | 156.40 | 7.82 | 0.0119 |
| EF | 128.42 | 1 | 128.42 | 6.42 | 0.0208 |
| EG | 262.34 | 1 | 262.34 | 13.11 | 0.0020 |
| FG | 170.95 | 1 | 170.95 | 8.55 | 0.0091 |
| $B^2$ | 445.86 | 1 | 445.86 | 22.29 | 0.0002 |
| $E^2$ | 197.13 | 1 | 197.13 | 9.85 | 0.0057 |
| $F^2$ | 134.63 | 1 | 134.63 | 6.73 | 0.0183 |
| $G^2$ | 90.67 | 1 | 90.67 | 4.53 | 0.0473 |
| Residual | 360.07 | 18 | 20.00 | | |
| Lack of Fit | 360.07 | 15 | 24.00 | | |
| Pure Error | 0.00 | 3 | 0.00 | | |
| Cor Total | 31733.33 | 41 | | | |
| | | | | | |
| Std. Dev. | 4.4726 | | R-Squared | 0.9887 | |
| Mean | 30.7577 | | Adj R-Squared | 0.9742 | |
| C.V. % | 14.1293 | | Pred R-Squared | 0.9119 | |
| PRESS | 2795.5031 | | Adeq Precision | 28.7079 | |

## B.2 Study 2A

**Table B-3: ANOVA table for Response 1: $CH_4$ recovery efficiency at a 10% $CO_2$ breakthrough limit**

| Source | Sum of Squares | df | Mean Square | F Value | p-value Prob > F |
|---|---|---|---|---|---|
| Model | 1298.138 | 18 | 72.11877 | 37.22892 | < 0.0001 |
| A-Permeability | 20.09535 | 1 | 20.09535 | 10.37356 | 0.0073 |
| B-$k_v/k_h$ Ratio | 92.93159 | 1 | 92.93159 | 47.97285 | < 0.0001 |
| C-Thickness | 188.2121 | 1 | 188.2121 | 97.15827 | < 0.0001 |
| D-Dip | 51.98551 | 1 | 51.98551 | 26.83579 | 0.0002 |
| E-Injection Rate | 31.11213 | 1 | 31.11213 | 16.0606 | 0.0017 |
| F-Timing | 0.506749 | 1 | 0.506749 | 0.261592 | 0.6183 |
| AC | 237.7375 | 1 | 237.7375 | 122.7241 | < 0.0001 |
| AF | 16.19858 | 1 | 16.19858 | 8.361978 | 0.0135 |
| BC | 55.24935 | 1 | 55.24935 | 28.52064 | 0.0002 |
| BE | 147.6371 | 1 | 147.6371 | 76.21275 | < 0.0001 |
| BF | 86.80786 | 1 | 86.80786 | 44.81168 | < 0.0001 |
| CD | 245.1597 | 1 | 245.1597 | 126.5556 | < 0.0001 |
| CF | 125.0355 | 1 | 125.0355 | 64.54545 | < 0.0001 |
| EF | 66.70606 | 1 | 66.70606 | 34.43479 | < 0.0001 |
| $A^2$ | 77.25458 | 1 | 77.25458 | 39.88011 | < 0.0001 |
| $D^2$ | 140.4296 | 1 | 140.4296 | 72.49213 | < 0.0001 |
| $E^2$ | 59.46416 | 1 | 59.46416 | 30.6964 | 0.0001 |
| $F^2$ | 29.49515 | 1 | 29.49515 | 15.22589 | 0.0021 |
| Residual | 23.24605 | 12 | 1.937171 | | |
| Lack of Fit | 23.24605 | 11 | 2.113277 | | |
| Pure Error | 0 | 1 | 0 | | |
| Cor Total | 1321.384 | 30 | | | |
| | | | | | |
| Std. Dev. | 1.391823 | | R-Squared | 0.982408 | |
| Mean | 65.12903 | | Adj R-Squared | 0.95602 | |
| C.V. % | 2.137024 | | Pred R-Squared | 0.876748 | |
| PRESS | 162.8626 | | Adeq Precision | 23.82503 | |

**Table B-4: ANOVA table for Response 2: $CH_4$ recovery efficiency at a 50% $CO_2$ breakthrough limit**

| Source | Sum of Squares | df | Mean Square | F Value | p-value Prob > F |
|---|---|---|---|---|---|
| Model | 899.4664 | 22 | 40.88484 | 28.62798 | < 0.0001 |
| A-Permeability | 0.770137 | 1 | 0.770137 | 0.539258 | 0.4814 |
| B-$k_v/k_h$ Ratio | 0.259661 | 1 | 0.259661 | 0.181817 | 0.6798 |
| C-Thickness | 38.07425 | 1 | 38.07425 | 26.65998 | 0.0006 |
| D-Dip | 25.23575 | 1 | 25.23575 | 17.67033 | 0.0023 |
| E-Injection Rate | 1.941298 | 1 | 1.941298 | 1.359317 | 0.2736 |
| F-Timing | 337.8572 | 1 | 337.8572 | 236.5711 | < 0.0001 |
| AB | 30.80451 | 1 | 30.80451 | 21.56963 | 0.0012 |
| AC | 85.94485 | 1 | 85.94485 | 60.17946 | < 0.0001 |
| AF | 19.31755 | 1 | 19.31755 | 13.52635 | 0.0051 |
| BC | 7.468057 | 1 | 7.468057 | 5.22921 | 0.0480 |
| BD | 32.06158 | 1 | 32.06158 | 22.44985 | 0.0011 |
| BE | 57.92706 | 1 | 57.92706 | 40.56112 | 0.0001 |
| BF | 42.22919 | 1 | 42.22919 | 29.56931 | 0.0004 |
| CD | 112.6957 | 1 | 112.6957 | 78.9107 | < 0.0001 |
| CE | 14.44702 | 1 | 14.44702 | 10.11595 | 0.0112 |
| CF | 34.46037 | 1 | 34.46037 | 24.12951 | 0.0008 |
| DE | 5.384106 | 1 | 5.384106 | 3.770007 | 0.0841 |
| EF | 35.69235 | 1 | 35.69235 | 24.99215 | 0.0007 |
| $A^2$ | 3.351801 | 1 | 3.351801 | 2.346965 | 0.1599 |
| $D^2$ | 54.23404 | 1 | 54.23404 | 37.97523 | 0.0002 |
| $E^2$ | 20.30701 | 1 | 20.30701 | 14.21917 | 0.0044 |
| $F^2$ | 4.617759 | 1 | 4.617759 | 3.233402 | 0.1057 |
| Residual | 12.85328 | 9 | 1.428142 | | |
| Lack of Fit | 12.85328 | 8 | 1.60666 | | |
| Pure Error | 0 | 1 | 0 | | |
| Cor Total | 912.3197 | 31 | | | |
| | | | | | |
| Std. Dev. | 1.195049 | | R-Squared | 0.985911 | |
| Mean | 80.24688 | | Adj R-Squared | 0.951473 | |
| C.V. % | 1.489216 | | Pred R-Squared | 0.801095 | |
| PRESS | 181.4654 | | Adeq Precision | 26.34822 | |

**Table B-5: ANOVA table for Response 3: Minimum producing $CO_2$ concentration required to achieve incremental recovery**

| Source | Sum of Squares | df | Mean Square | F Value | p-value Prob > F |
|---|---|---|---|---|---|
| Model | 201.0619 | 16 | 12.56637 | 76.41407 | < 0.0001 |
| A-Permeability | 40.79433 | 1 | 40.79433 | 248.0638 | < 0.0001 |
| B-$k_v/k_h$ Ratio | 11.84383 | 1 | 11.84383 | 72.02042 | < 0.0001 |
| C-Thickness | 0.731135 | 1 | 0.731135 | 4.445913 | 0.0522 |
| D-Dip | 65.93715 | 1 | 65.93715 | 400.9533 | < 0.0001 |
| E-Injection Rate | 0.136259 | 1 | 0.136259 | 0.82857 | 0.3771 |
| F-Timing | 1.336075 | 1 | 1.336075 | 8.124457 | 0.0122 |
| AB | 31.72108 | 1 | 31.72108 | 192.8908 | < 0.0001 |
| AD | 9.452905 | 1 | 9.452905 | 57.48161 | < 0.0001 |
| BC | 1.112104 | 1 | 1.112104 | 6.762529 | 0.0201 |
| BD | 8.170147 | 1 | 8.170147 | 49.68136 | < 0.0001 |
| BE | 0.632623 | 1 | 0.632623 | 3.846877 | 0.0687 |
| CE | 1.250025 | 1 | 1.250025 | 7.6012 | 0.0147 |
| DF | 3.130598 | 1 | 3.130598 | 19.03667 | 0.0006 |
| $A^2$ | 0.669806 | 1 | 0.669806 | 4.072984 | 0.0618 |
| $C^2$ | 0.641645 | 1 | 0.641645 | 3.901741 | 0.0669 |
| $D^2$ | 0.753589 | 1 | 0.753589 | 4.582454 | 0.0491 |
| Residual | 2.466764 | 15 | 0.164451 | | |
| Lack of Fit | 2.466764 | 14 | 0.176197 | | |
| Pure Error | 0 | 1 | 0 | | |
| Cor Total | 203.5286 | 31 | | | |
| | | | | | |
| Std. Dev. | 0.405526 | | R-Squared | 0.98788 | |
| Mean | 4.943814 | | Adj R-Squared | 0.974952 | |
| C.V. % | 8.202686 | | Pred R-Squared | 0.925195 | |
| PRESS | 15.22503 | | Adeq Precision | 29.30117 | |

## B.3 Study 2B

**Table B-6: ANOVA table for Response 1: $CH_4$ recovery efficiency at a 10% $CO_2$ breakthrough limit**

| Source | Sum of Squares | df | Mean Square | F Value | p-value Prob > F |
|---|---|---|---|---|---|
| Model | 2056.553 | 12 | 171.3794 | 19.603 | < 0.0001 |
| A-Permeability Multiplier | 54.94474 | 1 | 54.94474 | 6.284779 | 0.0233 |
| B-Thickness | 563.3735 | 1 | 563.3735 | 64.44071 | < 0.0001 |
| C-Dip | 1.004385 | 1 | 1.004385 | 0.114885 | 0.7391 |
| D-Injection Rate | 1.231053 | 1 | 1.231053 | 0.140812 | 0.7124 |
| E-Timing | 189.711 | 1 | 189.711 | 21.69984 | 0.0003 |
| AB | 44.46939 | 1 | 44.46939 | 5.086571 | 0.0385 |
| AD | 42.17372 | 1 | 42.17372 | 4.823984 | 0.0432 |
| AE | 215.2489 | 1 | 215.2489 | 24.62096 | 0.0001 |
| BC | 212.7042 | 1 | 212.7042 | 24.32988 | 0.0001 |
| BD | 49.0142 | 1 | 49.0142 | 5.606423 | 0.0308 |
| BE | 375.6733 | 1 | 375.6733 | 42.97089 | < 0.0001 |
| CE | 119.971 | 1 | 119.971 | 13.72272 | 0.0019 |
| Residual | 139.8801 | 16 | 8.742508 | | |
| Lack of Fit | 139.8801 | 13 | 10.76001 | | |
| Pure Error | 0 | 3 | 0 | | |
| Cor Total | 2196.433 | 28 | | | |
| | | | | | |
| Std. Dev. | 2.956773 | | R-Squared | 0.936315 | |
| Mean | 62.92414 | | Adj R-Squared | 0.888551 | |
| C.V. % | 4.698949 | | Pred R-Squared | 0.759662 | |
| PRESS | 527.887 | | Adeq Precision | 20.30061 | |

**Table B-7: ANOVA table for Response 2: $CH_4$ recovery efficiency at a 50% $CO_2$ breakthrough limit**

| Source | Sum of Squares | df | Mean Square | F Value | p-value Prob > F |
|---|---|---|---|---|---|
| Model | 695.8054 | 11 | 63.25503289 | 35.10037 | < 0.0001 |
| A-Permeability Multiplier | 11.52323 | 1 | 11.523233 | 6.39427 | 0.0216 |
| B-Thickness | 104.9342 | 1 | 104.9341661 | 58.22822 | < 0.0001 |
| C-Dip | 1.85838 | 1 | 1.858379694 | 1.031219 | 0.3241 |
| D-Injection Rate | 22.39446 | 1 | 22.39446187 | 12.42674 | 0.0026 |
| E-Timing | 213.1847 | 1 | 213.1846732 | 118.2967 | < 0.0001 |
| AB | 16.95083 | 1 | 16.95083071 | 9.406057 | 0.0070 |
| AE | 73.56168 | 1 | 73.5616784 | 40.81955 | < 0.0001 |
| BC | 78.15703 | 1 | 78.15703185 | 43.36953 | < 0.0001 |
| BD | 5.608511 | 1 | 5.608510589 | 3.112176 | 0.0957 |
| BE | 71.41722 | 1 | 71.41722298 | 39.62959 | < 0.0001 |
| CE | 27.97313 | 1 | 27.97313081 | 15.52236 | 0.0011 |
| Residual | 30.63602 | 17 | 1.80211868 | | |
| Lack of Fit | 30.63602 | 14 | 2.188286969 | | |
| Pure Error | 0 | 3 | 0 | | |
| Cor Total | 726.4414 | 28 | | | |
| | | | | | |
| Std. Dev. | 1.34243 | | R-Squared | 0.957827 | |
| Mean | 79.41724 | | Adj R-Squared | 0.930539 | |
| C.V. % | 1.690351 | | Pred R-Squared | 0.825865 | |
| PRESS | 126.4989 | | Adeq Precision | 22.45786 | |

**Table B-8: ANOVA table for Response 3: Minimum producing $CO_2$ concentration required to achieve incremental recovery**

| Source | Sum of Squares | df | Mean Square | F Value | p-value Prob > F |
|---|---|---|---|---|---|
| Model | 4586.631 | 11 | 416.9664 | 17.7557 | < 0.0001 |
| A-Permeability Multiplier | 405.0795 | 1 | 405.0795 | 17.24952 | 0.0007 |
| B-Thickness | 0.232238 | 1 | 0.232238 | 0.009889 | 0.9219 |
| C-Dip | 2369.714 | 1 | 2369.714 | 100.9096 | < 0.0001 |
| D-Injection Rate | 2.616621 | 1 | 2.616621 | 0.111424 | 0.7426 |
| E-Timing | 69.35235 | 1 | 69.35235 | 2.953235 | 0.1039 |
| AC | 365.0101 | 1 | 365.0101 | 15.54324 | 0.0011 |
| AD | 114.1741 | 1 | 114.1741 | 4.861881 | 0.0415 |
| BE | 112.6901 | 1 | 112.6901 | 4.798687 | 0.0427 |
| CD | 119.4635 | 1 | 119.4635 | 5.087122 | 0.0376 |
| CE | 1083.756 | 1 | 1083.756 | 46.14964 | < 0.0001 |
| $A^2$ | 105.6354 | 1 | 105.6354 | 4.498278 | 0.0489 |
| Residual | 399.2199 | 17 | 23.48352 | | |
| Lack of Fit | 399.2199 | 14 | 28.51571 | | |
| Pure Error | 0 | 3 | 0 | | |
| Cor Total | 4985.851 | 28 | | | |
| | | | | | |
| Std. Dev. | 4.84598 | | R-Squared | 0.919929 | |
| Mean | 20.37276 | | Adj R-Squared | 0.868119 | |
| C.V. % | 23.78657 | | Pred R-Squared | 0.7384 | |
| PRESS | 1304.3 | | Adeq Precision | 18.27708 | |

## B.4 Naylor Field Case Study

**Table B-9: ANOVA table for Response 1: $CH_4$ recovery efficiency at a 10% $CO_2$ breakthrough limit**

| Source | Sum of Squares | df | Mean Square | F Value | p-value Prob > F |
|---|---|---|---|---|---|
| Model | 477.9948 | 17 | 28.11734 | 104.2698 | < 0.0001 |
| A-X Location | 18.45464 | 1 | 18.45464 | 68.43684 | < 0.0001 |
| B-Y Location | 0.05418 | 1 | 0.05418 | 0.200919 | 0.6675 |
| C-Timing of Injection | 97.45018 | 1 | 97.45018 | 361.3824 | < 0.0001 |
| D-Production Rate | 96.67682 | 1 | 96.67682 | 358.5145 | < 0.0001 |
| E-Injection Rate | 8.432601 | 1 | 8.432601 | 31.2713 | 0.0008 |
| AB | 1.272798 | 1 | 1.272798 | 4.720021 | 0.0664 |
| AC | 8.781494 | 1 | 8.781494 | 32.56513 | 0.0007 |
| AE | 6.879354 | 1 | 6.879354 | 25.51127 | 0.0015 |
| BC | 28.78001 | 1 | 28.78001 | 106.7272 | < 0.0001 |
| BD | 19.68694 | 1 | 19.68694 | 73.00667 | < 0.0001 |
| BE | 0.942572 | 1 | 0.942572 | 3.495416 | 0.1037 |
| CD | 21.91765 | 1 | 21.91765 | 81.27901 | < 0.0001 |
| CE | 2.299174 | 1 | 2.299174 | 8.526215 | 0.0223 |
| DE | 5.801 | 1 | 5.801 | 21.51232 | 0.0024 |
| $A^2$ | 4.74633 | 1 | 4.74633 | 17.6012 | 0.0041 |
| $D^2$ | 4.928227 | 1 | 4.928227 | 18.27574 | 0.0037 |
| $E^2$ | 2.482119 | 1 | 2.482119 | 9.204643 | 0.0190 |
| Residual | 1.887616 | 7 | 0.269659 | | |
| Lack of Fit | 1.887616 | 5 | 0.377523 | | |
| Pure Error | 0 | 2 | 0 | | |
| Cor Total | 479.8824 | 24 | | | |
| | | | | | |
| Std. Dev. | 0.519287 | | R-Squared | 0.996067 | |
| Mean | 56.348 | | Adj R-Squared | 0.986514 | |
| C.V. % | 0.921572 | | Pred R-Squared | 0.904581 | |
| PRESS | 45.7897 | | Adeq Precision | 34.68673 | |

**Table B-10: ANOVA table for Response 2: $CH_4$ recovery efficiency at a 50% $CO_2$ breakthrough limit**

| Source | Sum of Squares | df | Mean Square | F Value | p-value Prob > F |
|---|---|---|---|---|---|
| Model | 279.3343 | 15 | 18.62229 | 92.32618 | < 0.0001 |
| A-X Location | 1.207637 | 1 | 1.207637 | 5.987262 | 0.0369 |
| B-Y Location | 18.14043 | 1 | 18.14043 | 89.9372 | < 0.0001 |
| C-Timing | 57.22958 | 1 | 57.22958 | 283.7347 | < 0.0001 |
| D-Production Rate | 108.4328 | 1 | 108.4328 | 537.5917 | < 0.0001 |
| E-Injection Rate | 0.500713 | 1 | 0.500713 | 2.482454 | 0.1496 |
| AC | 2.323274 | 1 | 2.323274 | 11.51841 | 0.0080 |
| AD | 5.945094 | 1 | 5.945094 | 29.47478 | 0.0004 |
| BC | 3.879818 | 1 | 3.879818 | 19.23549 | 0.0018 |
| BD | 4.778664 | 1 | 4.778664 | 23.69182 | 0.0009 |
| BE | 1.246714 | 1 | 1.246714 | 6.180999 | 0.0346 |
| CD | 13.60916 | 1 | 13.60916 | 67.47193 | < 0.0001 |
| CE | 1.962324 | 1 | 1.962324 | 9.728873 | 0.0123 |
| DE | 1.885947 | 1 | 1.885947 | 9.350212 | 0.0136 |
| $A^2$ | 1.219239 | 1 | 1.219239 | 6.044784 | 0.0362 |
| $C^2$ | 4.641514 | 1 | 4.641514 | 23.01185 | 0.0010 |
| Residual | 1.815309 | 9 | 0.201701 | | |
| Lack of Fit | 1.815309 | 7 | 0.25933 | | |
| Pure Error | 0 | 2 | 0 | | |
| Cor Total | 281.1496 | 24 | | | |
| | | | | | |
| Std. Dev. | 0.449111 | | R-Squared | 0.993543 | |
| Mean | 73.396 | | Adj R-Squared | 0.982782 | |
| C.V. % | 0.611902 | | Pred R-Squared | 0.895682 | |
| PRESS | 29.32888 | | Adeq Precision | 35.15457 | |

**Table B-11: ANOVA table for Response 3: Minimum producing $CO_2$ concentration required to achieve incremental recovery**

| Source | Sum of Squares | df | Mean Square | F Value | p-value Prob > F |
|---|---|---|---|---|---|
| Model | 0.006397 | 14 | 0.000457 | 91.71476 | < 0.0001 |
| A-X Location | 2.78E-05 | 1 | 2.78E-05 | 5.57135 | 0.0399 |
| B-Y Location | 0.001168 | 1 | 0.001168 | 234.5351 | < 0.0001 |
| C-Timing | 0.001042 | 1 | 0.001042 | 209.1332 | < 0.0001 |
| D-Production Rate | 0.00152 | 1 | 0.00152 | 305.0477 | < 0.0001 |
| E-Injection Rate | 0.00021 | 1 | 0.00021 | 42.13221 | < 0.0001 |
| AC | 0.000171 | 1 | 0.000171 | 34.4203 | 0.0002 |
| AD | 0.000171 | 1 | 0.000171 | 34.29549 | 0.0002 |
| BC | 0.000111 | 1 | 0.000111 | 22.2701 | 0.0008 |
| BE | 7.23E-05 | 1 | 7.23E-05 | 14.51659 | 0.0034 |
| CD | 0.000535 | 1 | 0.000535 | 107.4813 | < 0.0001 |
| CE | 4.35E-05 | 1 | 4.35E-05 | 8.741327 | 0.0144 |
| $A^2$ | 8.22E-05 | 1 | 8.22E-05 | 16.49525 | 0.0023 |
| $C^2$ | 0.000195 | 1 | 0.000195 | 39.11831 | < 0.0001 |
| $D^2$ | 3.57E-05 | 1 | 3.57E-05 | 7.172341 | 0.0232 |
| Residual | 4.98E-05 | 10 | 4.98E-06 | | |
| Lack of Fit | 4.98E-05 | 8 | 6.23E-06 | | |
| Pure Error | 0 | 2 | 0 | | |
| Cor Total | 0.006447 | 24 | | | |
| | | | | | |
| Std. Dev. | 0.002232 | | R-Squared | 0.992272 | |
| Mean | 0.162818 | | Adj R-Squared | 0.981453 | |
| C.V. % | 1.370874 | | Pred R-Squared | 0.942933 | |
| PRESS | 0.000368 | | Adeq Precision | 34.95193 | |

# Appendix C – Experimental Design Data for Primary Depletion Responses for Study 1, 2A and 2B

## C.1 Study 1

**Table C-1: ANOVA table for the analysis of the primary depletion response for Study 1**

| Source | Sum of Squares | df | Mean Square | F Value | p-value Prob > F |
|---|---|---|---|---|---|
| Model | 6.89E+10 | 15 | 4.59E+09 | 19.50039 | < 0.0001 |
| A-Permeability | 3.01E+09 | 1 | 3.01E+09 | 12.79033 | 0.0013 |
| B-Kv/Kh Ratio | 2.12E+09 | 1 | 2.12E+09 | 9.00255 | 0.0057 |
| C-Diffusion | 4.46E+08 | 1 | 4.46E+08 | 1.894554 | 0.1800 |
| D-Salinity | 1789993 | 1 | 1789993 | 0.007598 | 0.9312 |
| E-Aquifer Size | 3.49E+09 | 1 | 3.49E+09 | 14.80308 | 0.0007 |
| F-Thickness | 80240827 | 1 | 80240827 | 0.340616 | 0.5643 |
| G-Dip | 1.93E+10 | 1 | 1.93E+10 | 82.0673 | < 0.0001 |
| AB | 6.31E+09 | 1 | 6.31E+09 | 26.79872 | < 0.0001 |
| AF | 6.28E+08 | 1 | 6.28E+08 | 2.667439 | 0.1140 |
| AG | 3.27E+09 | 1 | 3.27E+09 | 13.89822 | 0.0009 |
| BE | 4.24E+09 | 1 | 4.24E+09 | 18.00517 | 0.0002 |
| BG | 7.42E+09 | 1 | 7.42E+09 | 31.48516 | < 0.0001 |
| CD | 1.2E+09 | 1 | 1.2E+09 | 5.088011 | 0.0324 |
| EG | 2.77E+09 | 1 | 2.77E+09 | 11.75919 | 0.0020 |
| FG | 2.4E+09 | 1 | 2.4E+09 | 10.16874 | 0.0036 |
| Residual | 6.36E+09 | 27 | 2.36E+08 | | |
| Lack of Fit | 6.36E+09 | 24 | 2.65E+08 | | |
| Pure Error | 0 | 3 | 0 | | |
| Cor Total | 7.53E+10 | 42 | | | |
| | | | | | |
| Std. Dev. | 15348.47 | | R-Squared | 0.915494 | |
| Mean | 103870 | | Adj R-Squared | 0.868547 | |
| C.V. % | 14.77662 | | Pred R-Squared | 0.764939 | |
| PRESS | 1.77E+10 | | Adeq Precision | 15.05903 | |

NB: A power transformation was required to adequately fit the model to the data. The results presented are based on that transformation.

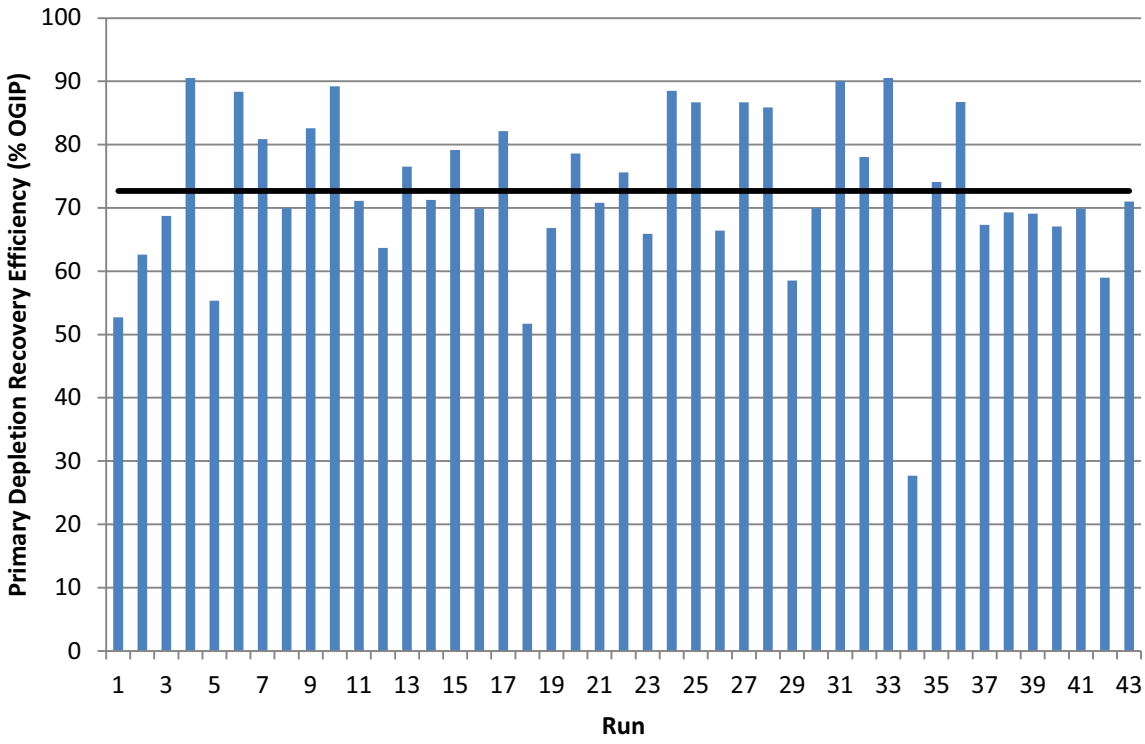


**Figure C.1: Results of each design run for the primary depletion response for Study 1**

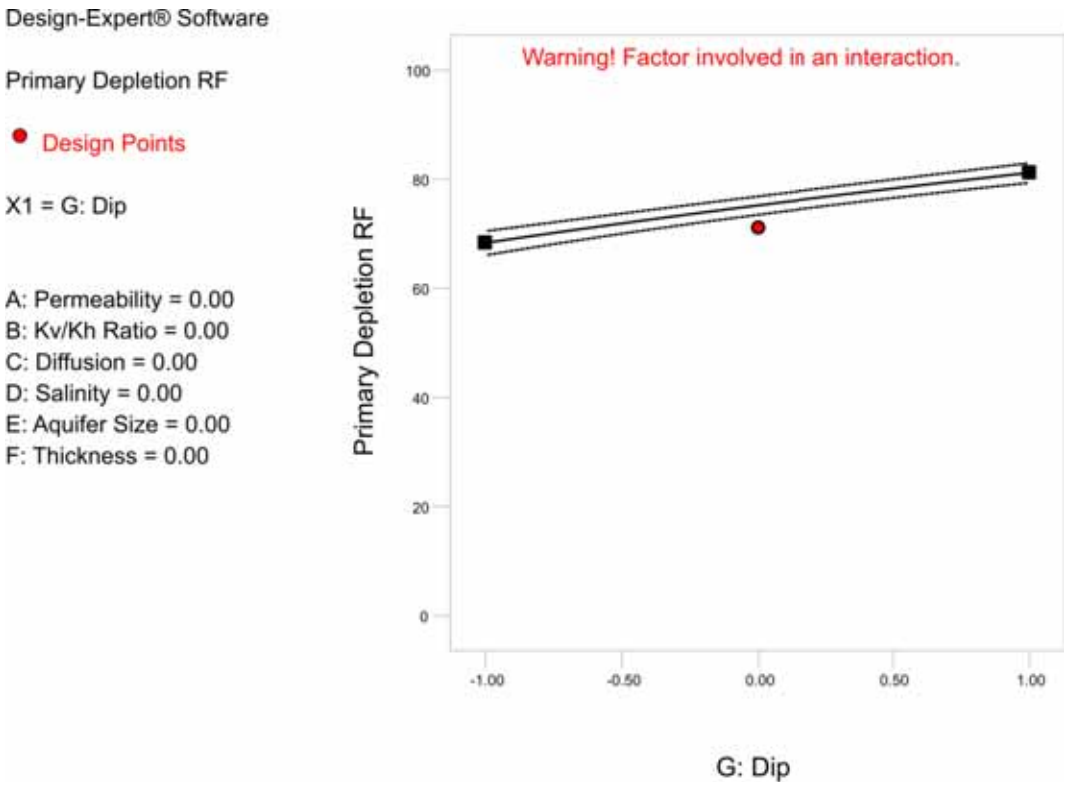


**Figure C.2: Effect graph for the main effect of formation dip**

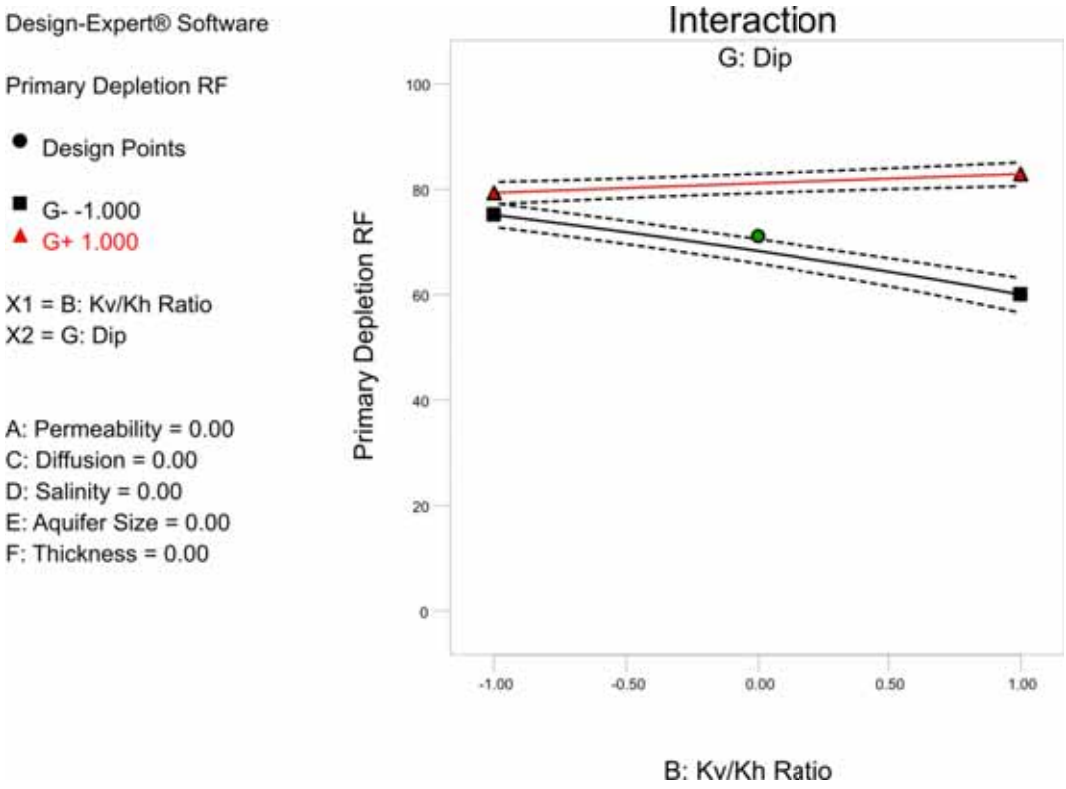


**Figure C.3: Effect graph for the kv/kh ratio formation dip interaction**

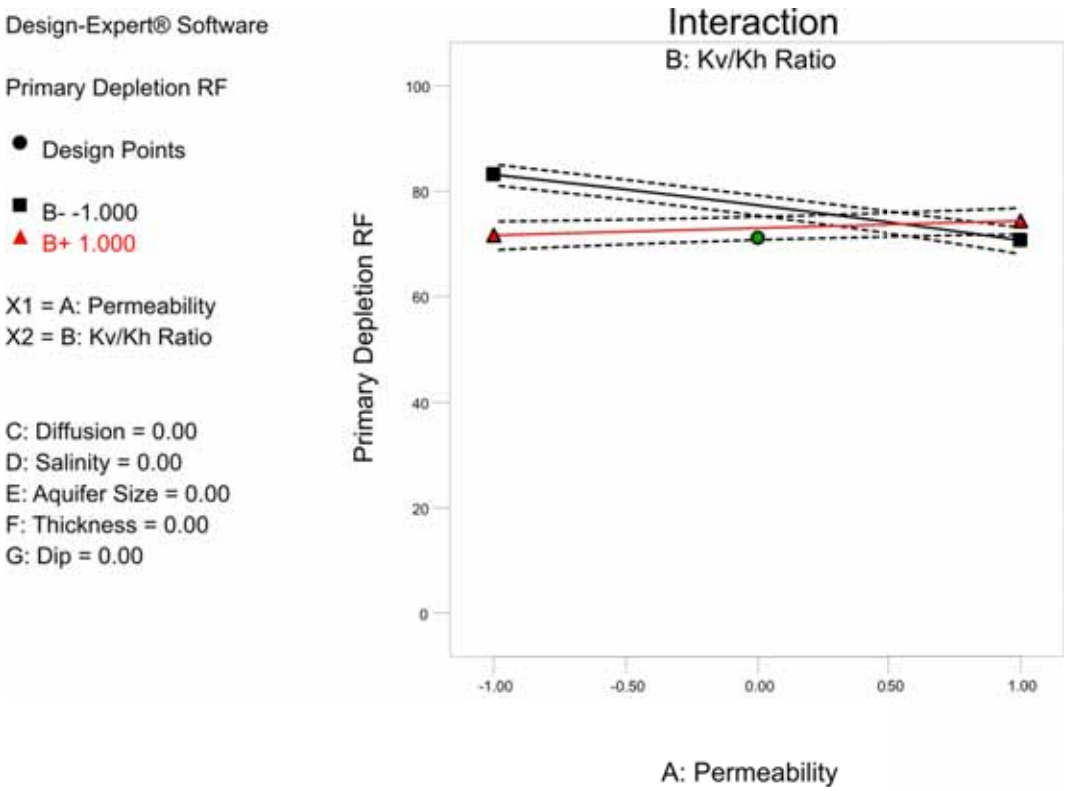


**Figure C.4: Effect graph for the permeability kv/kh ratio interaction**

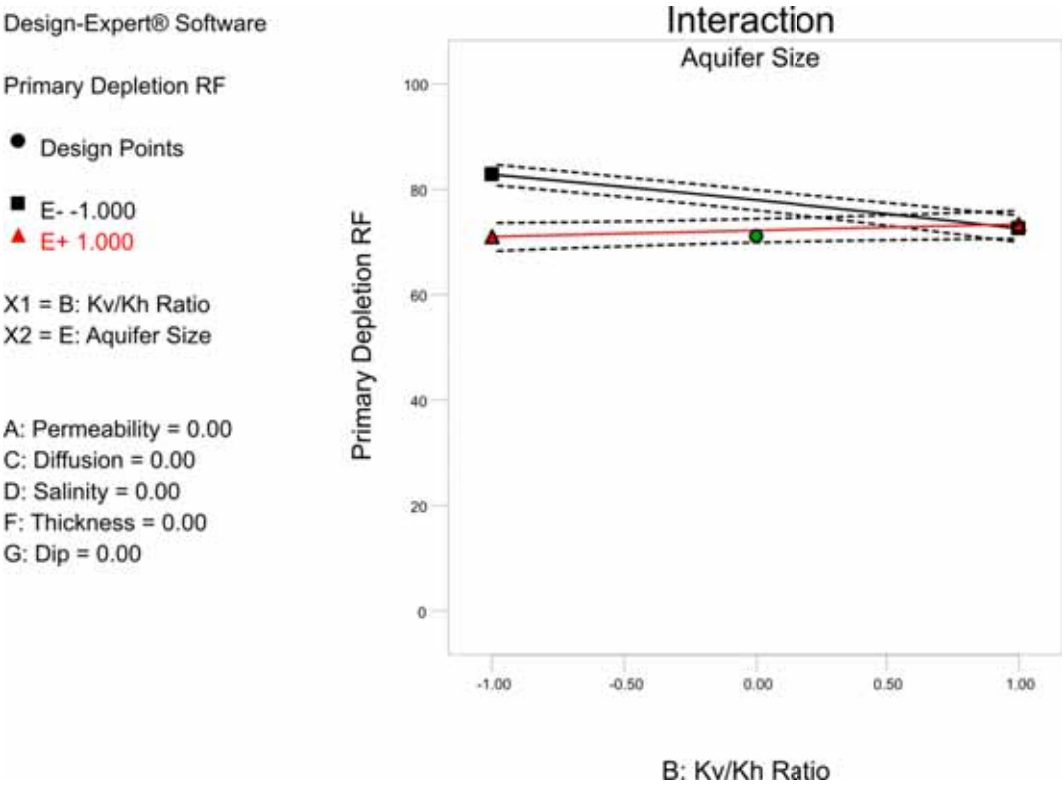


**Figure C.5: Effect graph for the kv/kh ratio aquifer size interaction**

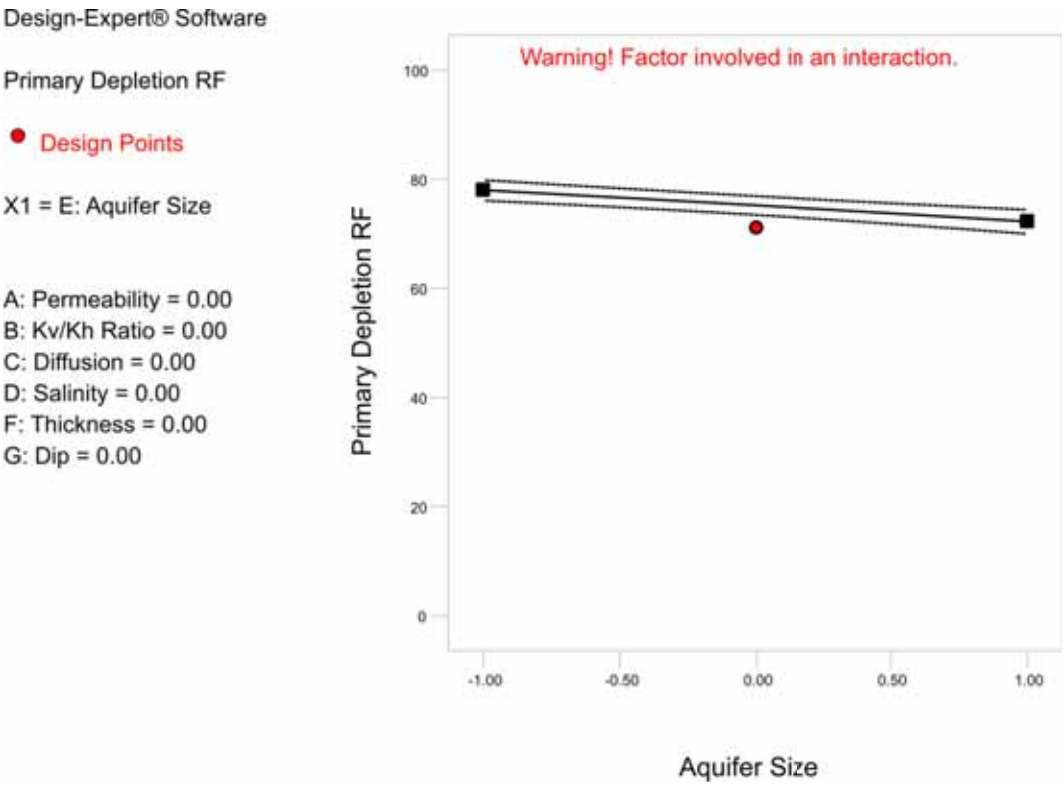


**Figure C.6: Effect graph for the main effect of the aquifer size**

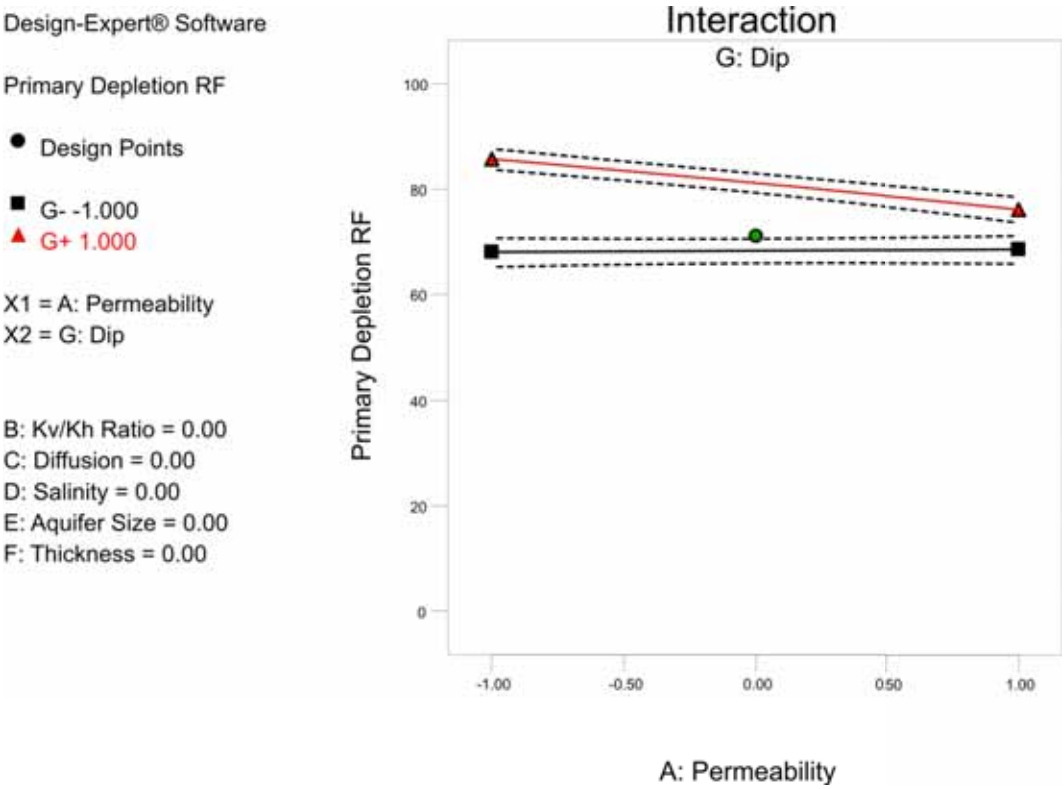


**Figure C.7: Effect graph for the permeability formation dip interaction**

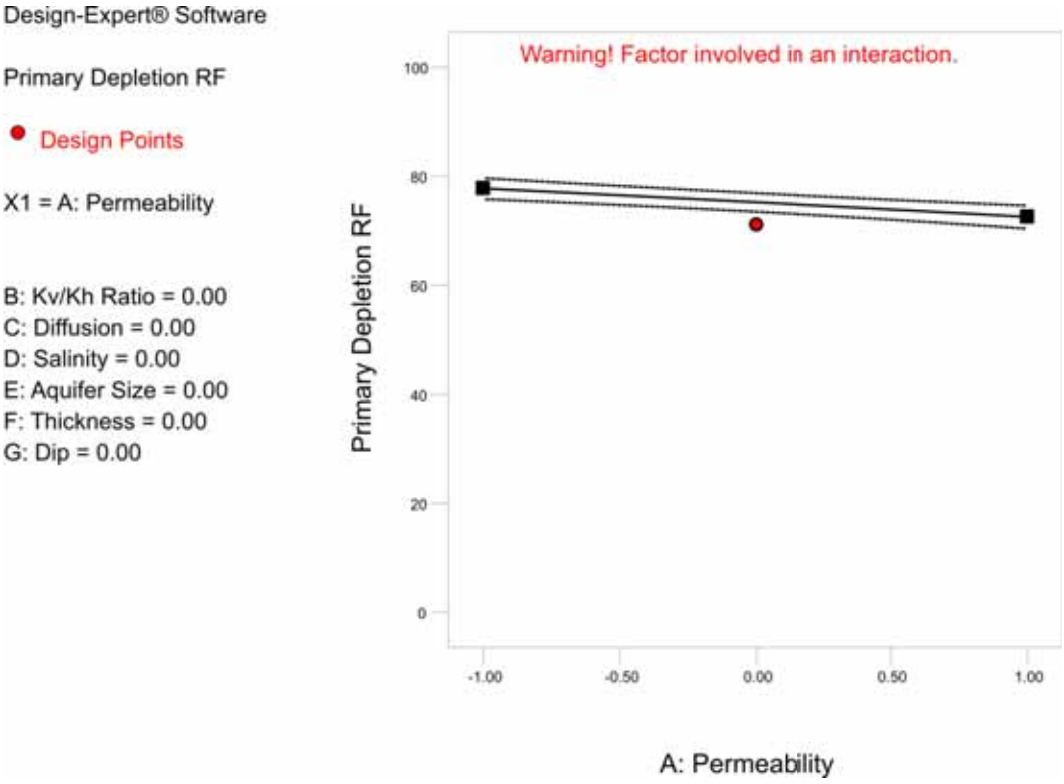


**Figure C.8: Effect graph for the main effect of permeability**

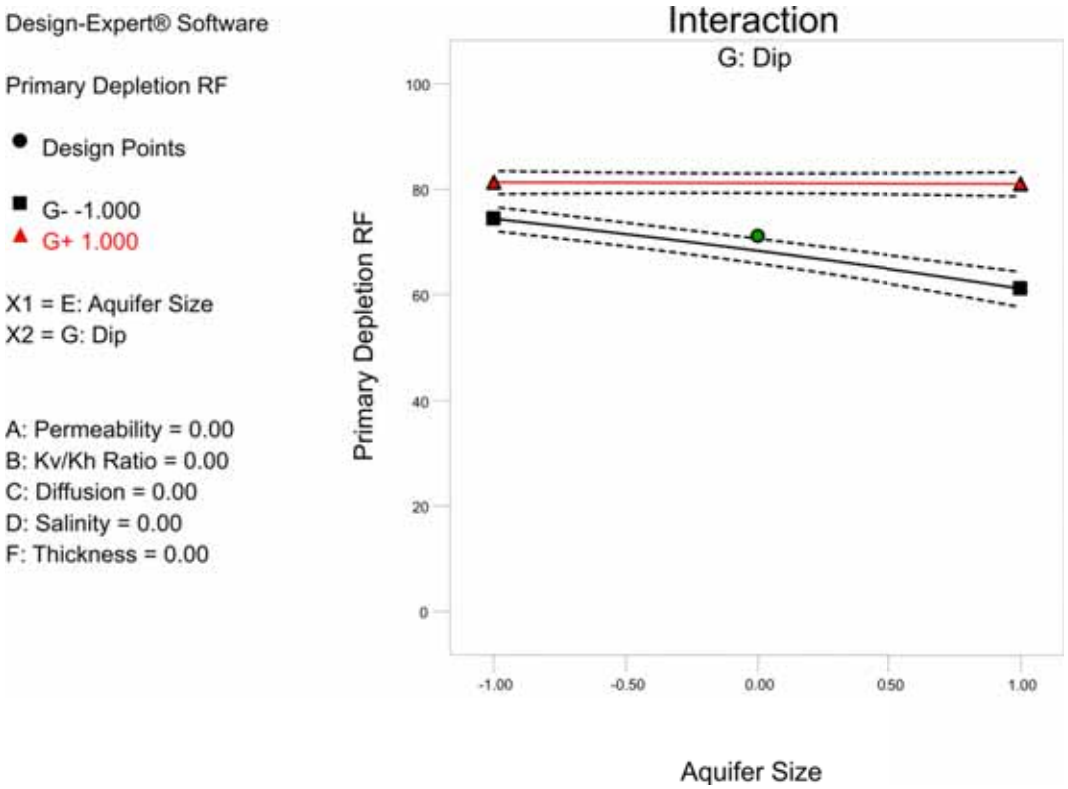


**Figure C.9: Effect graph for the aquifer size formation dip interaction**

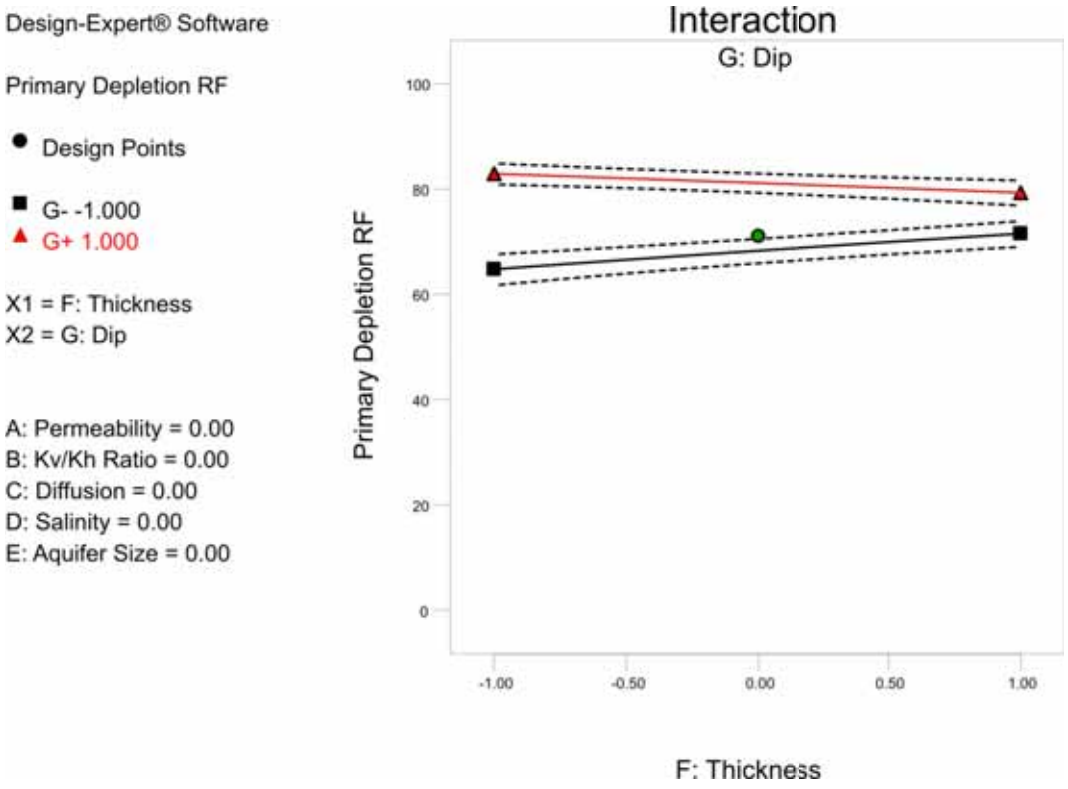


**Figure C.10: Effect graph for the thickness formation dip interaction**

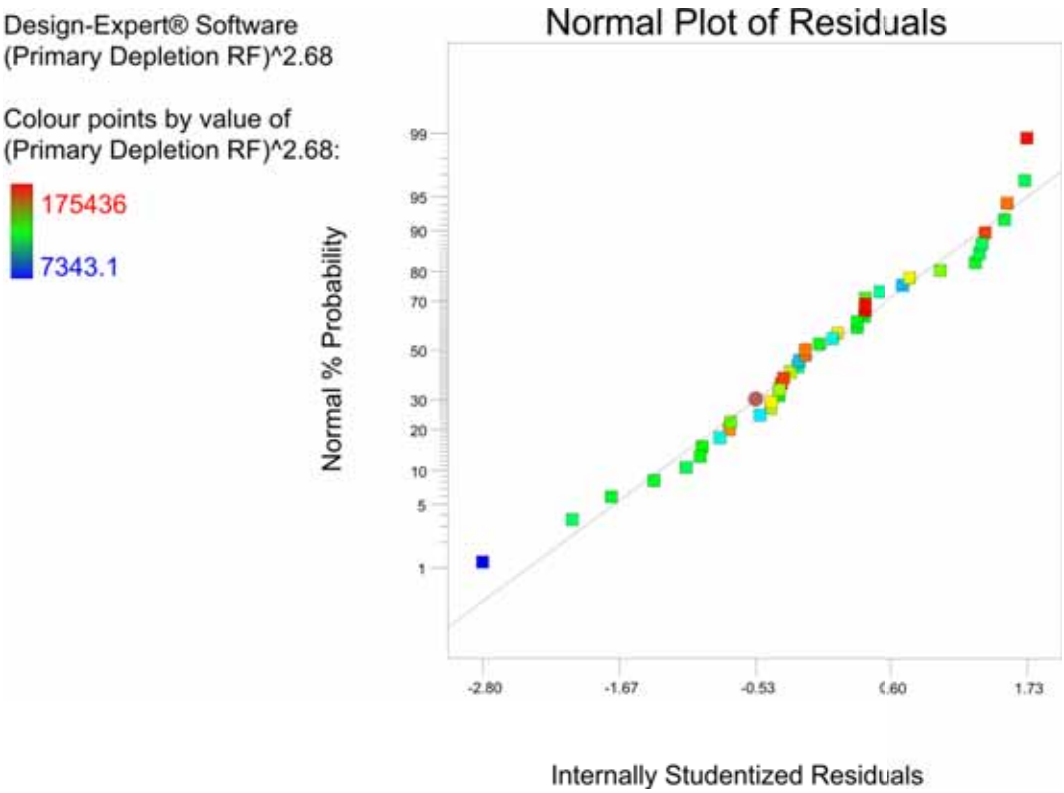


**Figure C.11: Transformed normal probability plot for the primary depletion response for Study 1**

# C.2 Study 2A

**Table C-2: ANOVA table for the analysis of the primary depletion response for Study 2A**

| Source | Sum of Squares | df | Mean Square | F Value | p-value Prob > F |
|---|---|---|---|---|---|
| Model | 7336.993 | 21 | 349.3806 | 108.4288 | < 0.0001 |
| A-Permeability | 529.4782 | 1 | 529.4782 | 164.3213 | < 0.0001 |
| B-Kv/Kh Ratio | 447.5074 | 1 | 447.5074 | 138.882 | < 0.0001 |
| C-Thickness | 152.7832 | 1 | 152.7832 | 47.41562 | < 0.0001 |
| D-Dip | 1121.686 | 1 | 1121.686 | 348.1105 | < 0.0001 |
| E-Injection Rate | 30.19659 | 1 | 30.19659 | 9.371382 | 0.0120 |
| F-Timing | 46.77481 | 1 | 46.77481 | 14.51636 | 0.0034 |
| AB | 474.2687 | 1 | 474.2687 | 147.1872 | < 0.0001 |
| AD | 387.8223 | 1 | 387.8223 | 120.359 | < 0.0001 |
| AE | 53.01143 | 1 | 53.01143 | 16.45187 | 0.0023 |
| AF | 107.939 | 1 | 107.939 | 33.4984 | 0.0002 |
| BC | 56.24529 | 1 | 56.24529 | 17.45548 | 0.0019 |
| BD | 227.0205 | 1 | 227.0205 | 70.45483 | < 0.0001 |
| BE | 150.5591 | 1 | 150.5591 | 46.72537 | < 0.0001 |
| BF | 14.82169 | 1 | 14.82169 | 4.599848 | 0.0576 |
| CD | 586.5775 | 1 | 586.5775 | 182.0418 | < 0.0001 |
| CE | 287.5515 | 1 | 287.5515 | 89.24036 | < 0.0001 |
| DE | 116.2357 | 1 | 116.2357 | 36.07324 | 0.0001 |
| DF | 47.18839 | 1 | 47.18839 | 14.64471 | 0.0033 |
| $A^2$ | 169.1953 | 1 | 169.1953 | 52.50902 | < 0.0001 |
| $D^2$ | 183.1492 | 1 | 183.1492 | 56.83957 | < 0.0001 |
| $F^2$ | 21.5879 | 1 | 21.5879 | 6.699713 | 0.0270 |
| Residual | 32.22213 | 10 | 3.222213 | | |
| Lack of Fit | 32.22213 | 9 | 3.580237 | | |
| Pure Error | 0 | 1 | 0 | | |
| Cor Total | 7369.215 | 31 | | | |
| | | | | | |
| Std. Dev. | 1.795052 | | R-Squared | 0.995627 | |
| Mean | 69.42279 | | Adj R-Squared | 0.986445 | |
| C.V. % | 2.585682 | | Pred R-Squared | 0.932155 | |
| PRESS | 499.9632 | | Adeq Precision | 43.05691 | |

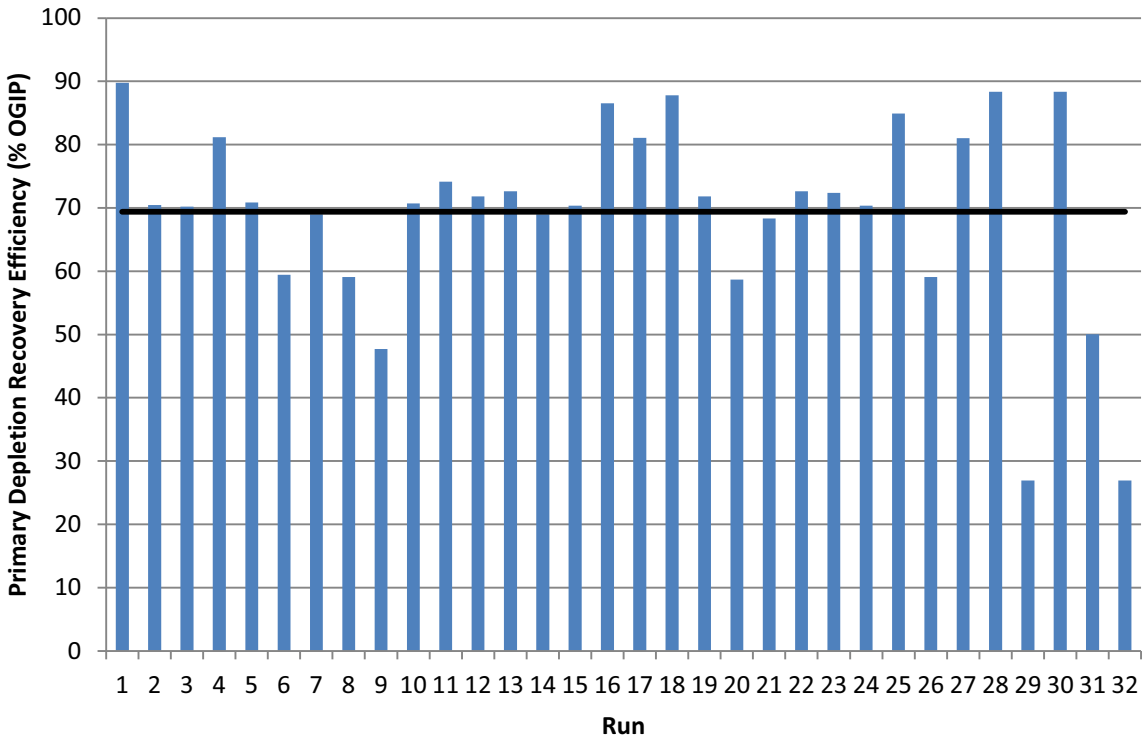


**Figure C.12: The results for each design run for the primary depletion response for Study 2A**

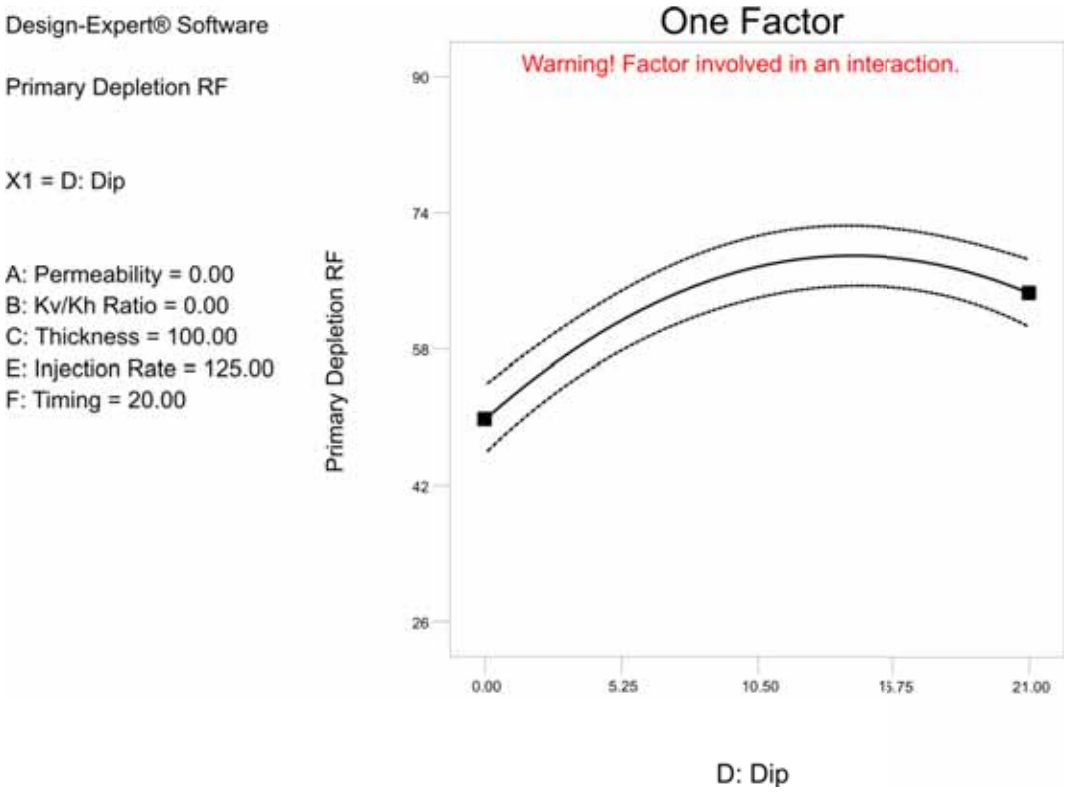


**Figure C.13: Effect graph for the main effect of formation dip**

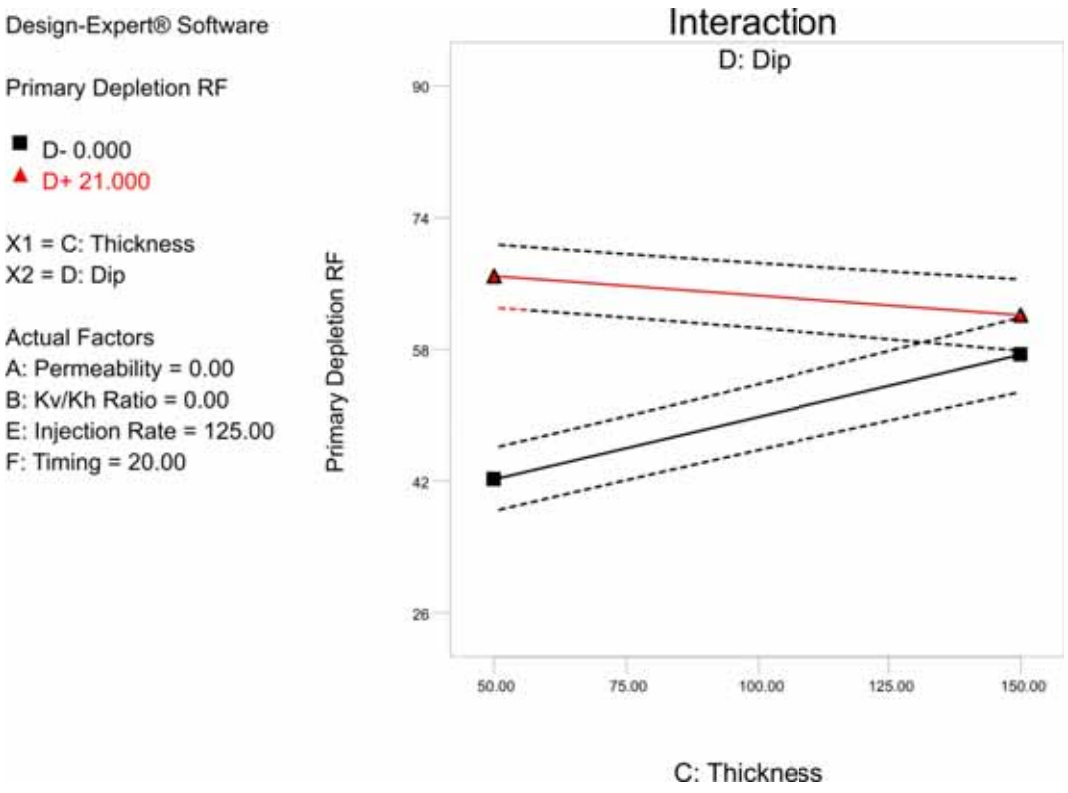


**Figure C.14: Effect graph for the thickness formation dip interaction**

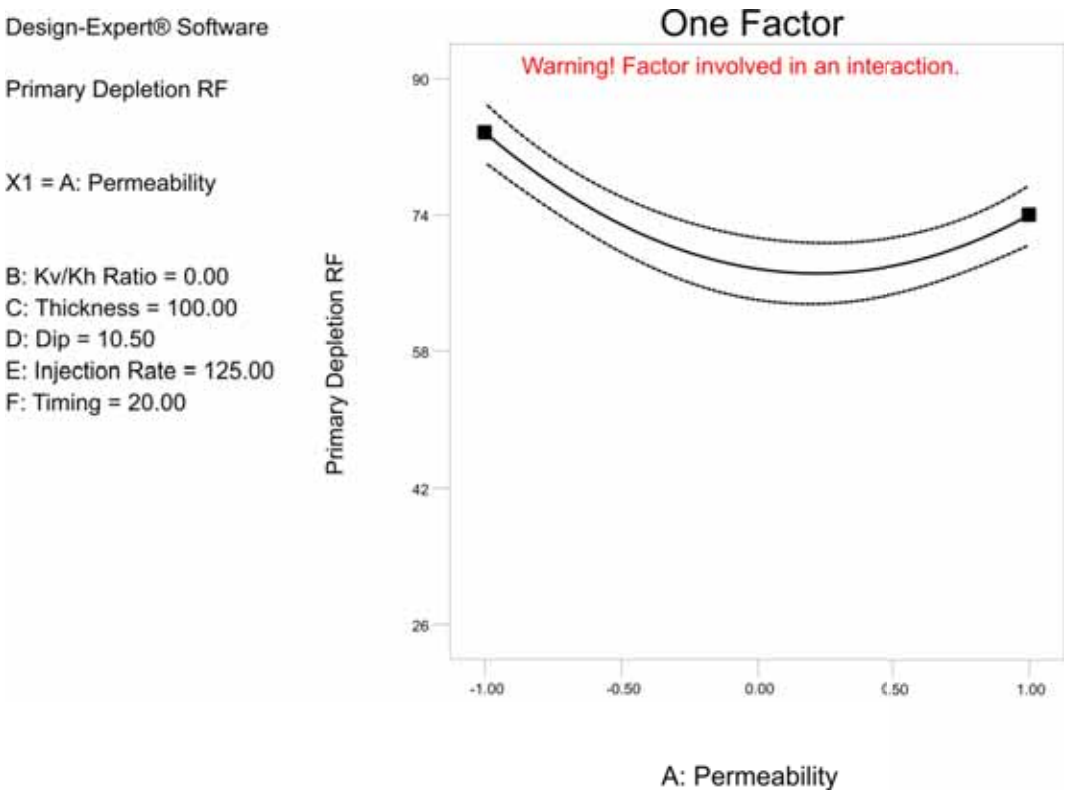


**Figure C.15: Effect graph for the main effect of permeability**

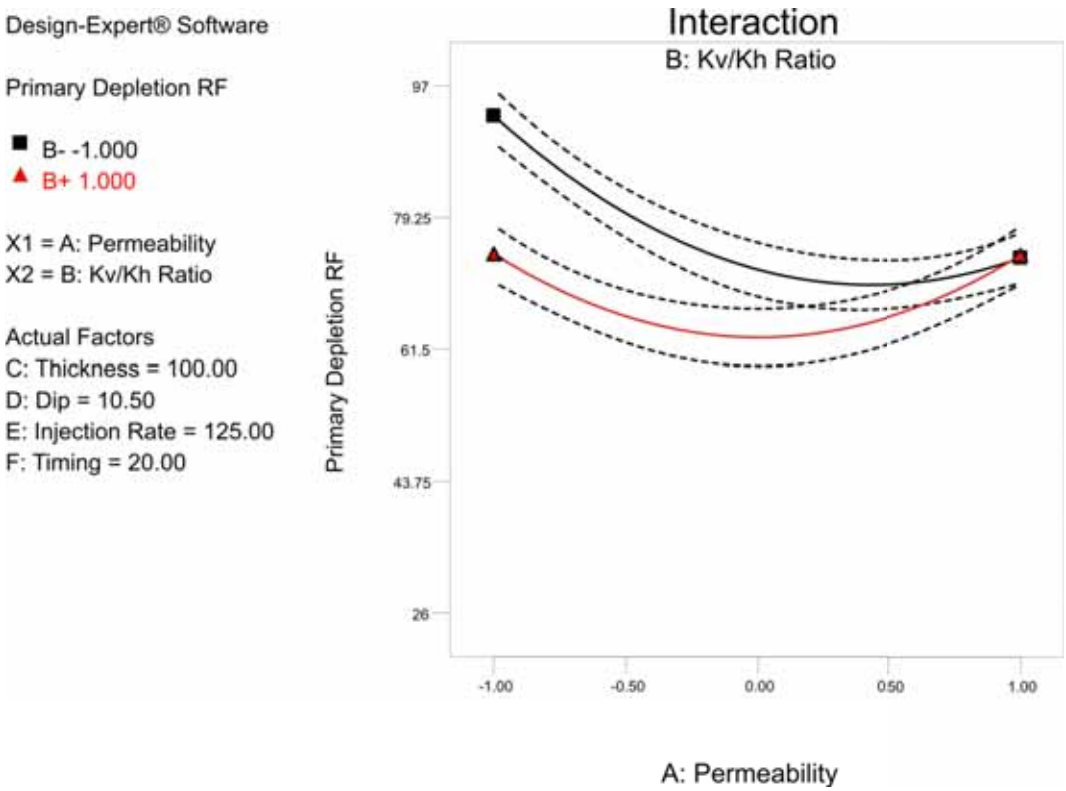


**Figure C.16: Effect graph for the permeability kv/kh ratio interaction**

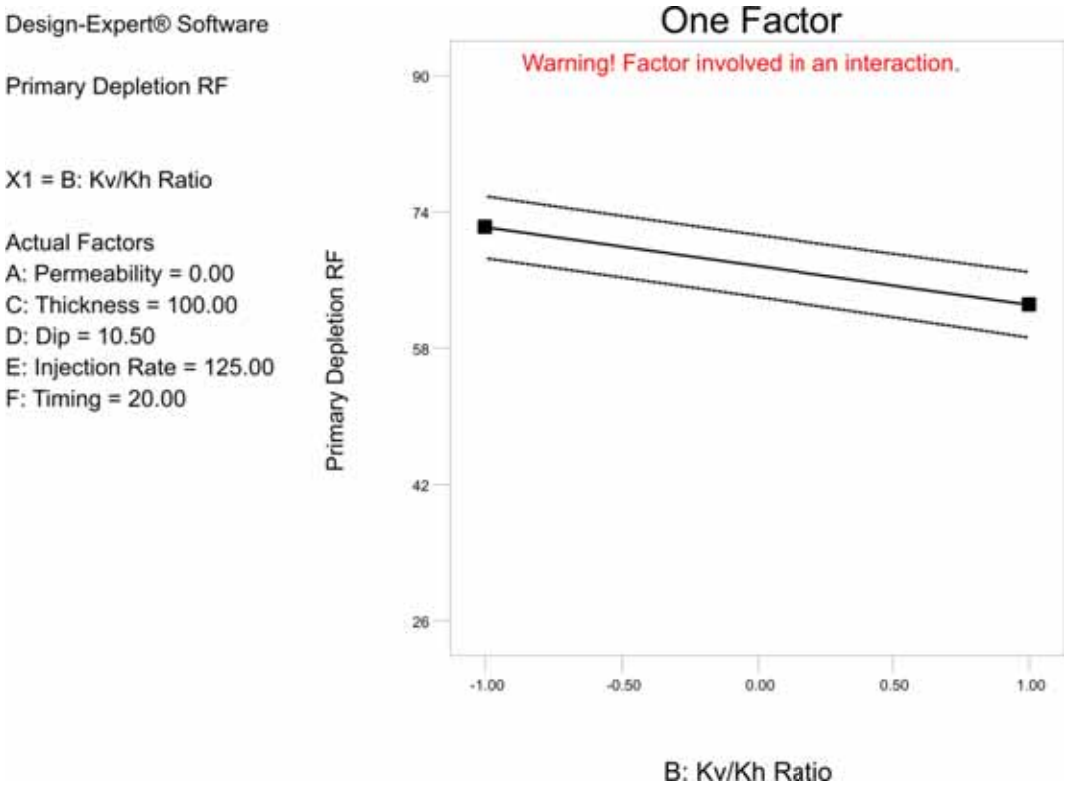


**Figure C.17: Effect graph for the main effect of the kv/kh ratio**

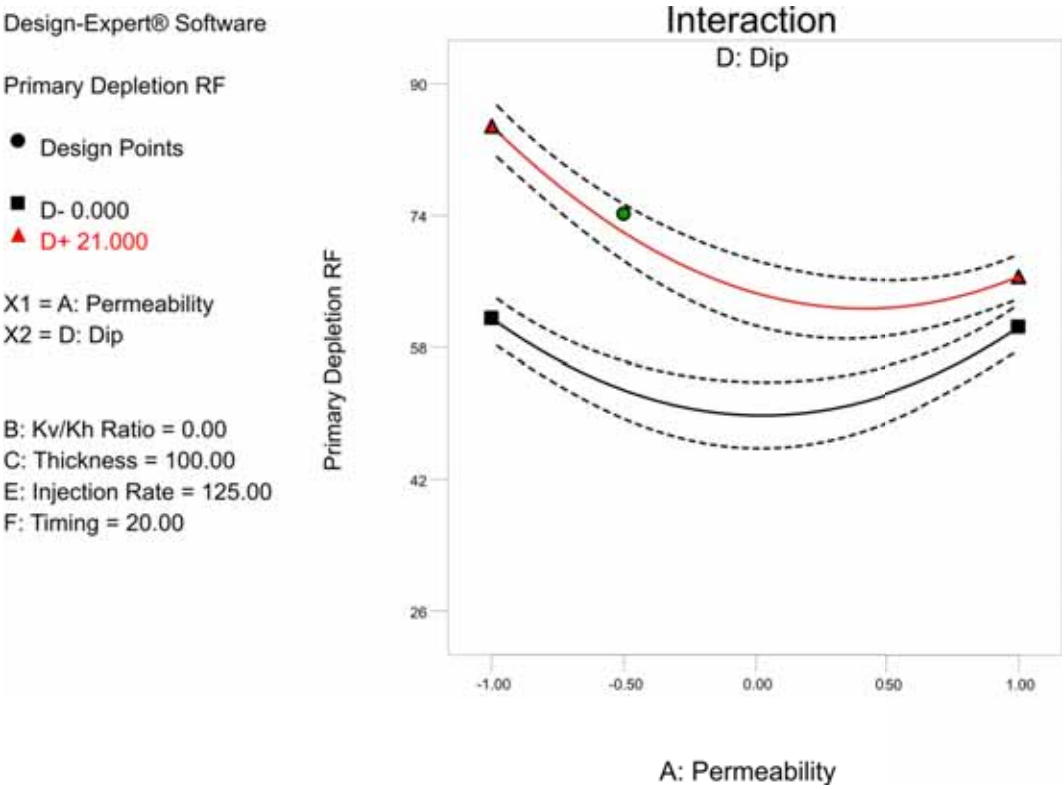


**Figure C.18: Effect graph for the permeability formation dip interaction**

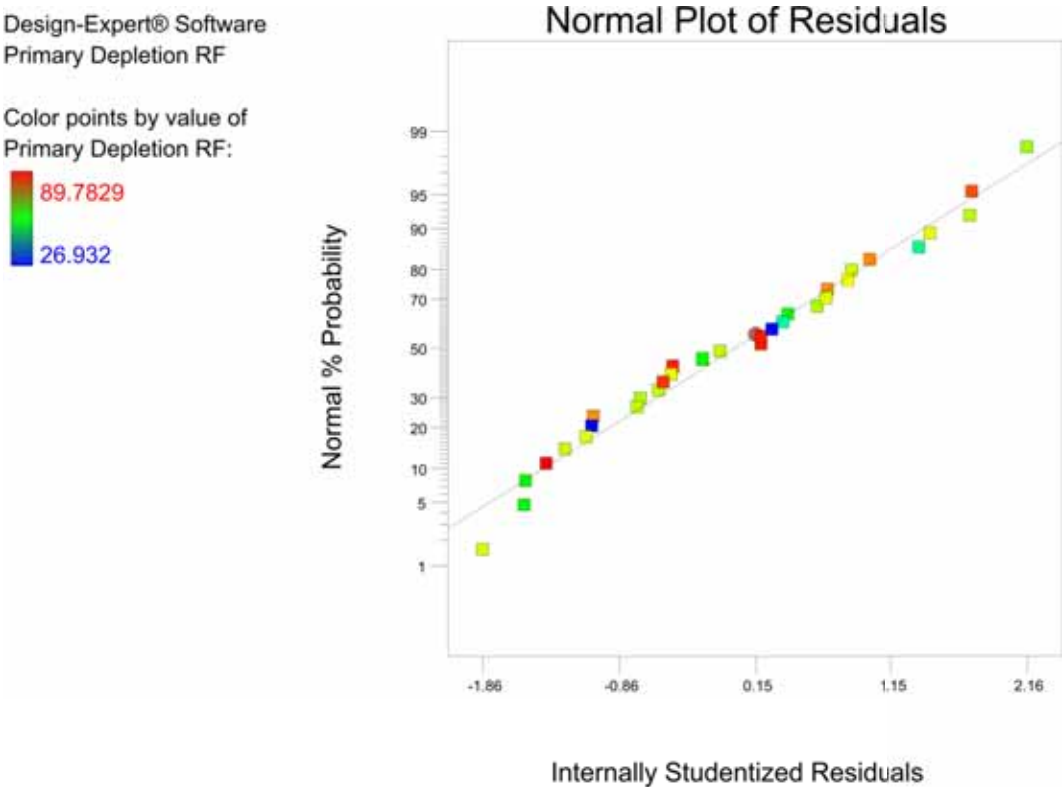


**Figure C.19: The normal probability plot for the primary depletion response for Study 2A**

# C.3 Study 2B

**Table C-3: ANOVA table from the analysis of the primary depletion response for Study 2B**

| Source | Sum of Squares | df | Mean Square | F Value | p-value Prob > F |
|---|---|---|---|---|---|
| Model | 1757.314 | 11 | 159.7558 | 93.87763 | < 0.0001 |
| A-Permeability Multiplier | 22.3868 | 1 | 22.3868 | 13.1552 | 0.0021 |
| B-Thickness | 263.5276 | 1 | 263.5276 | 154.8573 | < 0.0001 |
| C-Dip | 765.55 | 1 | 765.55 | 449.8617 | < 0.0001 |
| D-Injection Rate | 5.511749 | 1 | 5.511749 | 3.23888 | 0.0897 |
| E-Timing | 2.543347 | 1 | 2.543347 | 1.494552 | 0.2382 |
| AC | 86.35535 | 1 | 86.35535 | 50.74517 | < 0.0001 |
| BC | 208.8945 | 1 | 208.8945 | 122.7531 | < 0.0001 |
| DE | 24.83101 | 1 | 24.83101 | 14.5915 | 0.0014 |
| $A^2$ | 11.34368 | 1 | 11.34368 | 6.665909 | 0.0194 |
| $B^2$ | 7.60802 | 1 | 7.60802 | 4.470716 | 0.0496 |
| $C^2$ | 26.72371 | 1 | 26.72371 | 15.70371 | 0.0010 |
| Residual | 28.92967 | 17 | 1.701745 | | |
| Lack of Fit | 28.92967 | 14 | 2.066405 | | |
| Pure Error | 0 | 3 | 0 | | |
| Cor Total | 1786.244 | 28 | | | |
| | | | | | |
| Std. Dev. | 1.30451 | | R-Squared | 0.983804 | |
| Mean | 67.07554 | | Adj R-Squared | 0.973325 | |
| C.V. % | 1.944836 | | Pred R-Squared | 0.956771 | |
| PRESS | 77.21788 | | Adeq Precision | 30.79708 | |

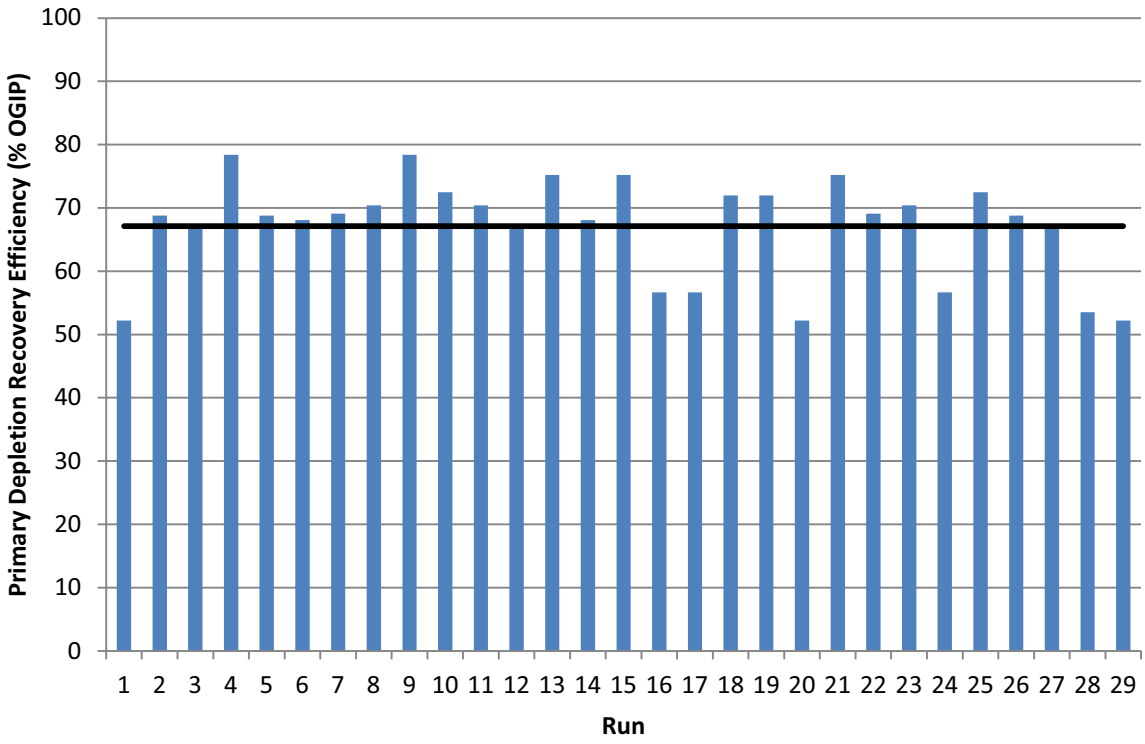


**Figure C.20: The results of each design run for the primary depletion response for Study 2B**

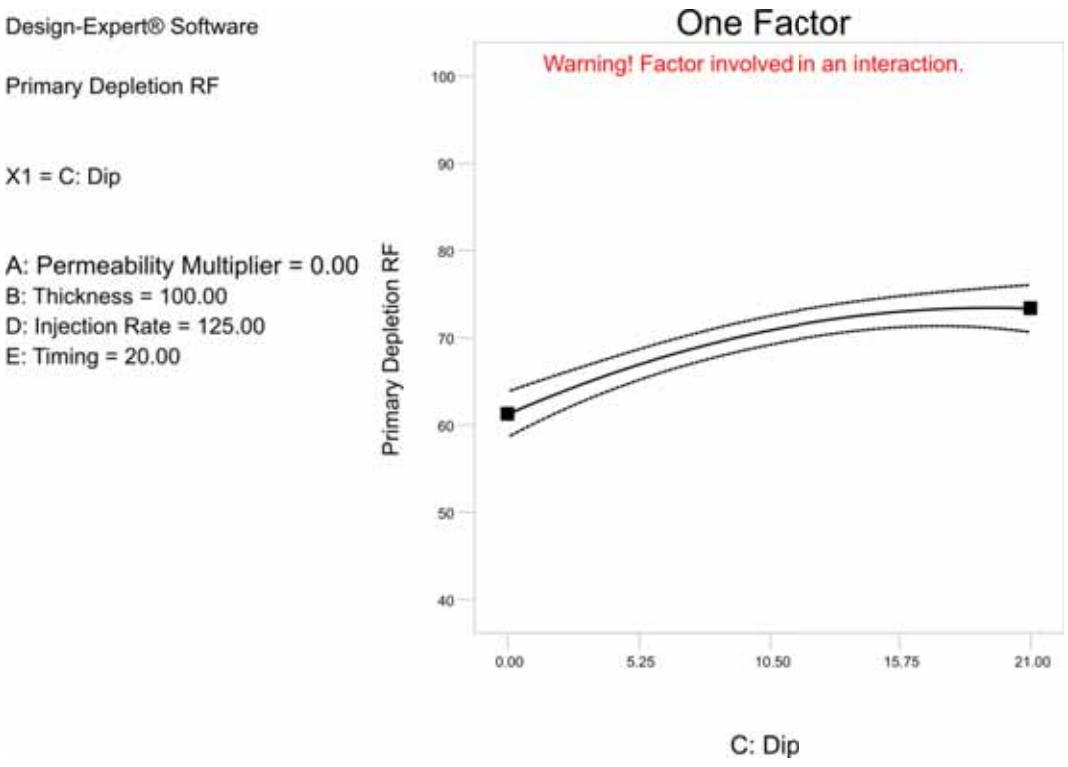


**Figure C.21: Effect graph for the main effect of formation dip**

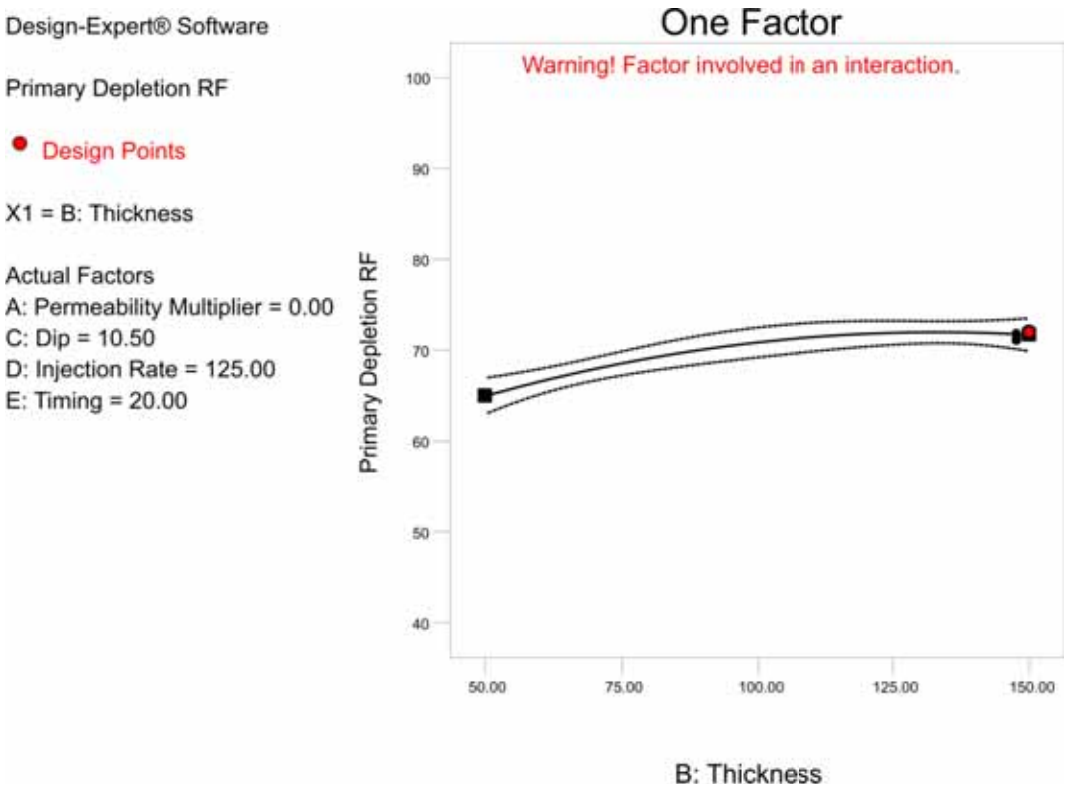


**Figure C.22: Effect graph for the main effect of thickness**

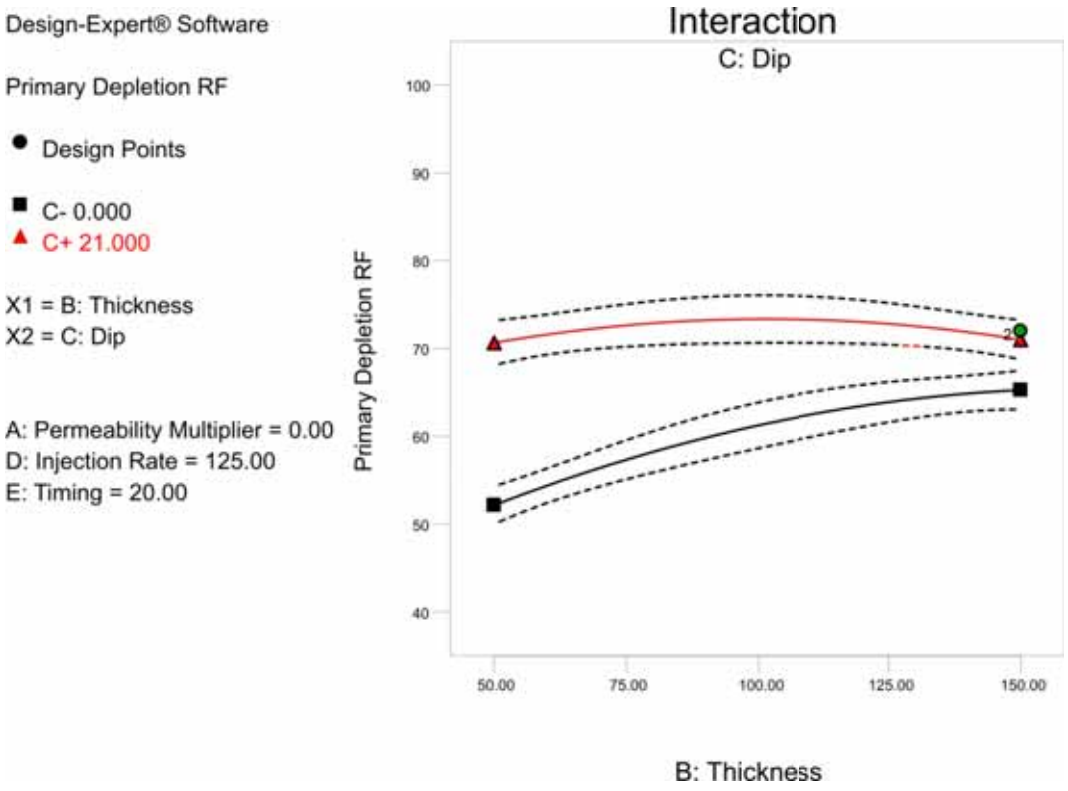


**Figure C.23: Effect graph for the thickness formation dip interaction**

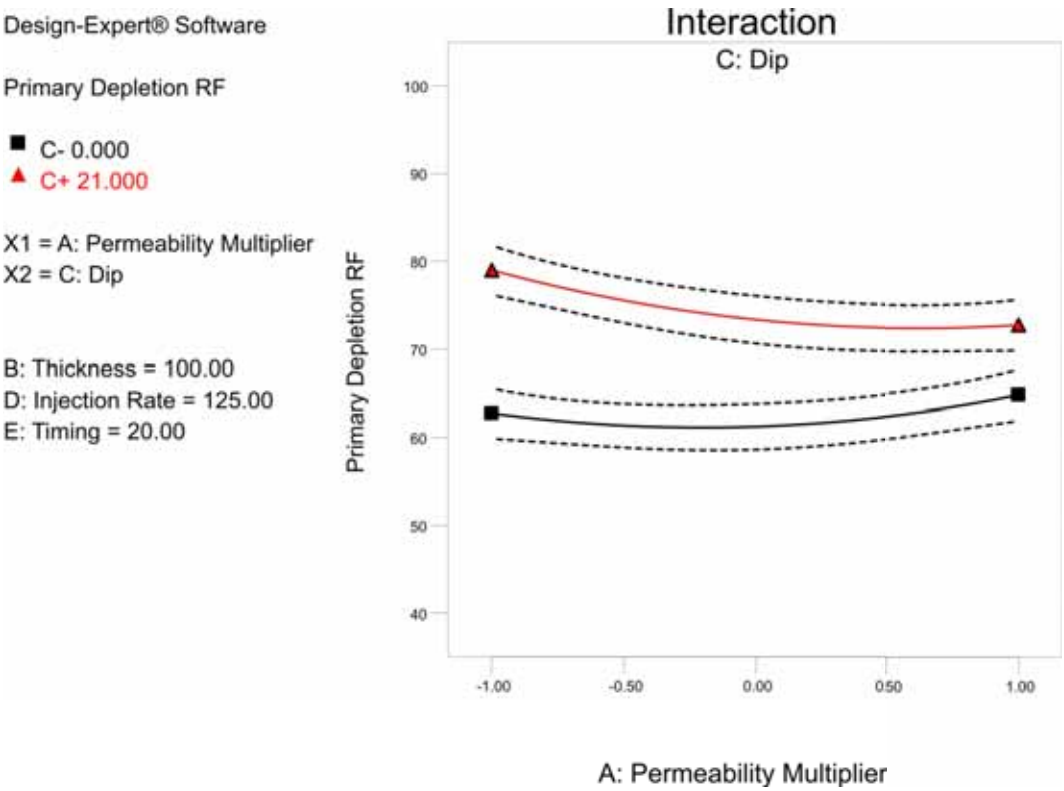


**Figure C.24: Effect graph for the permeability multiplier formation dip interaction**

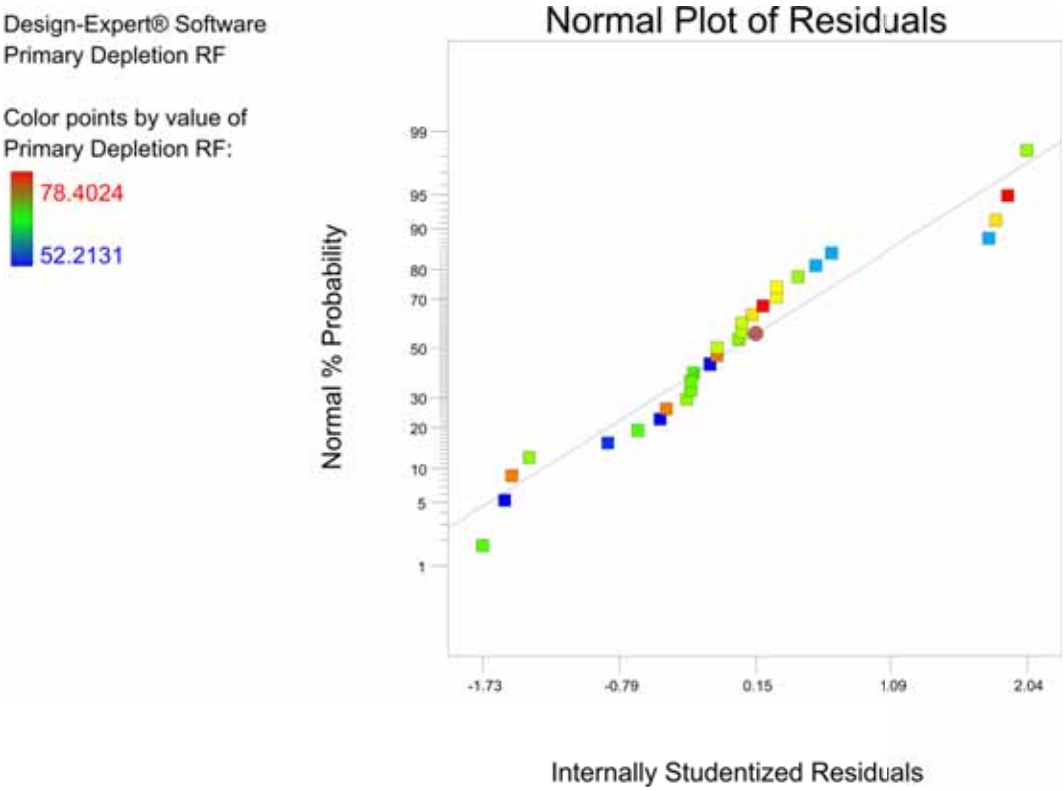


**Figure C.25: The normal probability plot for the primary depletion response for Study 2B. Note that based upon the other diagnostics from the analysis (ANOVA table) this normal probability plot was deemed acceptable despite the more pronounced S-shape.**